THE APPLICATION OF FLOW CHEMISTRY TO THE SYNTHESIS OF PHARMACEUTICALLY PRIVILEGED HETEROCYCLES

Blake Jamie Mark Baker[†, ‡]

PhD Thesis

2019

† GSK Medicines Research Centre, Gunnels Wood Road, Stevenage, Hertfordshire, SG1 2NY

‡ Department of Pure & Applied Chemistry, University of Strathclyde, 295 Cathedral Street, Glasgow, G1 1XL

GSK CONFIDENTIAL INFORMATION – DO NOT COPY

Author Declaration

This thesis is the result of the author's original research. It has been composed by the author and has not been previously submitted for examination which has led to the award of a degree.

The copyright of this thesis belongs to the author under the terms of the United Kingdom Copyright Acts as qualified by University of Strathclyde Regulation 3.50. Due acknowledgement must always be made of the use of any material contained in, or derived from, this thesis.

Signed: Date:

Acknowledgements

Firstly, I would like to acknowledge my gratitude to my two PhD supervisors, Darren Poole at GlaxoSmithKline plc, and William Kerr at the University of Strathclyde. Without your guidance and support I would not have been able to develop the work herein. I would specifically like to thank Darren for day-to-day advice in the lab, and his wealth of experience. Your advice has undoubtedly helped in times when I may have been unsure in the future direction of my work, or otherwise found myself in a panic, so thank you!

I would also like to thank both William Kerr and Harry Kelly for accepting me onto the programme, and thereby granting me a number of career-developing opportunities. As part of the PhD programme, I greatly appreciated working in Prof. William Kerr's research group and loved my time in Glasgow. I'd like to thank past and present members of the group, and Billy himself, for making me feel so welcome.

Additionally, I am grateful to my colleagues (both past and present) within the Flexible Discovery Unit at GSK's site in Stevenage. I have been fortunate to work with many talented individuals who have helped me in times of need, or areas of inexperience, and motivated me to push myself to be the best scientist I can be.

Specifically, I would like to thank Stephen Richards for his assistance regarding NMR spectroscopy investigations, and the continuous flow experts at GSK (especially Lee Edwards) for allowing me to access the required flow equipment to make this work possible, and helping me to understand how best to use it.

I would like to thank the other PhD students in my cohort for making my degree a fun and engaging experience, especially my close friend Dec, let's go for a drink when we've both finished, it's been a while coming!

My postgraduate work contract was extended for a couple of months and I am tremendously grateful to Vipul Patel for securing funding for my last couple of months at GSK. Thank you, you have made the already daunting process of writing a thesis less horrifying than it otherwise would have been!

Finally, I would like to thank my family and my partner, Heather. Without your support I would not be where I am today. My parents have always impressed on me the importance of a strong work ethic, especially in my academic studies, and I hope I have made you proud now that I have (finally!) reached their end. H, you have always managed to cheer me up after science has gone wrong, as it often does. I am eternally grateful for your support and can't wait for our adventures post-PhD!

GSK CONFIDENTIAL INFORMATION – DO NOT COPY

Table of contents

GSK CONFIDENTIAL INFORMATION – DO NOT COPY

GSK CONFIDENTIAL INFORMATION – DO NOT COPY

Abbreviations

Chemicals

Ac	Acetyl
ACH	Acetone cyanohydrin
Ar	Aryl
BINOL	1,1'-Bi-2-naphthol
Bt	Benzotriazolyl
BTTP (or BTPP)	*tert*-Butylimino-tri(pyrrolidino)phosphorane
Bz	Benzyl
^{c}Hex	Cyclohexyl
DBU	1,8-Diazabicyclo[5.4.0]undec-7-ene
DCM	Dichloromethane
DDT	Dichlorodiphenyltrichloroethane
DIPEA	Diisopropylethylamine (or Hunig's base)
DMA	Dimethylacetamide
DMAP	4-*N*,*N*-Dimethylaminopyridine
DMF	Dimethylformamide
DMSO	Dimethylsulfoxide
Dppf	1,1'-Bis(diphenylphosphino)ferrocene
EDC	Ethylene dichloride (or 1,2-dichloroethane)
Et	Ethyl
Hetero-Ar	Heteroaromatic
IPA	Isopropanol (or 2-propanol)
Me	Methyl
NBP	*N*-Butyl-2-pyrrolidone (or Tamisolve®)
^{n}Bu	Normal (non-branched) butyl
NIS	*N*-Iodosuccinimide
NMP	*N*-Methyl-2-pyrrolidone
PFA	Perfluoroalkoxy alkane

Ph	Phenyl
Poly-Lys YOx	Polylysine yttrium oxide
PTFE	Polytetrafluoroethylene
RockPhos	Di-*tert*-butyl (2′,4′,6′-triisopropyl-3-meth oxy-6-methyl -[1,1′-biphenyl]-2-yl)phosphine
RockPhos Pd G3	[(2-Di-*tert*-butylphosphino-3-methoxy-6-methyl-2′,4′,6′-tri isopropyl-1,1′-biphenyl)-2-(2-aminobiphenyl)]palladium (II)methanesulfonate
RuPhos	2-Dicyclohexylphosphino-2′,6′-diisopropoxybiphenyl
RuPhos Pd G2	Chloro(2-dicyclohexylphosphino-2′,6′-diisopropoxy-1,1′-bi phenyl)[2-(2′-amino-1, 1′-biphenyl)]palladium(II)
SL-J009-1 Pd G3	((*R*)-1-[(Sp)-2-(Dicyclohexylphosphino)ferrocenyl]ethyl di-*tert*-butyl phosphine)[2-(2′-amino-1,1′-biphenyl)] palladium(II)methanesulfonate
T3P	Propanephosphonic acid anhydride
TBME	*Tert*-butyl methyl ether
^{t}Bu	*Tert*-butyl
TEMPO	2,2,6,6-Tetramethyl-1-piperidinyloxy
TFA	Trifluoroacetic acid
TFT	α,α,α-Trifluorotoluene
THF	Tetrahydrofuran
Ts	*p*-Toluene sulfonyl
XantPhos Pd G3	[(4,5-Bis(diphenylphosphino)-9,9-dimethyl xanthene)-2-(2′-amino-1, 1′-biphenyl)]palladium(II) methanesulfonate

Techniques, measurements and parameters

°C	Degrees Celsius
δ	Chemical shift (measured in parts per million (ppm))
µCi	Microcurie (10^{-6} Curie (Ci))
µg	Microgram (10^{-6} grams (g))
Å	Angstrom (10^{-10} metres (m))
AMP	Artificial membrane permeability (measured in nm s^{-1} (nanometres per second))
AMU	Atomic mass unit (also called Dalton, with symbol u or Da)

Aq. soln.	Aqueous solution
AUC	Area under curve
CAD	Charged aerosol detection
ChromLogD	Chromatographic distribution coefficient
CLND	Chemiluminescent nitrogen detection
cLogP	Computational partition coefficient
cm^{-1}	Wavenumbers
COSY	Correlation spectroscopy
CRISPR-Cas9	Clustered regularly interspaced short palindromic repeats-CRISPR associated protein-9
CV	Cyclic voltammetry
ee	Enantiomeric excess
ESI	Electrospray ionisation
g	Grams
GC-MS	Gas chromatography-mass spectrometry
h	Hours
HA	Heavy atoms
HBA	Hydrogen bond acceptors
HBD	Hydrogen bond donors
HMBC	Heteronuclear multiple-bond correlation spectroscopy
HRMS	High resolution mass spectrometry
ID	Internal diameter
IFT	Interfacial tension
IR	Infra-red (spectroscopy)
KF	Karl Fischer (analysis)
LCMS	Liquid chromatography-mass spectrometry
LLE_{AT}	Attenuated lipophilic ligand efficiency
M	Molarity (in mol dm^{-3})
m/z	Mass-to-charge ratio
MDAP	Mass-directed auto purification

mg	Milligrams (10^{-3} g)
MHz	Megahertz (10^{6} Hertz (Hz))
min	Minutes
mmol	Millimoles (10^{-3} moles (mol))
MPO	Multi-parameter optimisation
MS-CETSA	Mass spectrometry coupled-cellular thermal shift assay
MW	Microwave
NMR	Nuclear magnetic resonance (spectroscopy)
NOESY	Nuclear Overhauser effect spectroscopy
PCR	Polymerase chain reaction
PFI	Property forecast index
pIC_{50}	Negative logarithm of the half-maximal inhibitory concentration (IC_{50})
pKa	Negative logarithm of the acid dissociation constant (*Ka*)
PPB	Plasma protein binding
Re	Reynolds number
s	Seconds
SA	Surface area
TLC	Thin-layer chromatography
TOF	Time-of-flight (measurement used in MS analysis)
TPSA	Topological polar surface area (measured in angstroms squared ($Å^2$))
UPLC	Ultra performance liquid chromatography
UV	Ultraviolet (light)
v/v	Volume per volume concentration
wt.	Percent by mass (weight)

Other abbreviations

ACTs	Artemisinin-based combination therapies
CD55	Complement decay-accelerating factor (protein)
CYT*bc1*	Cytochrome *bc1* protein complex

dec.	Material decomposed (upon heating, at the noted temperature)
DHFR	Dihydrofolate reductase
DHODH	Dihydroorotate dehydrogenase
DHPS	Dihydropteroate synthase
DNA	Deoxyribonucleic acid
ELD	Electronic line diagram
ETC	Electron transport chain
FID	Flame ionisation detector
G6PD	Glucose-6-phosphate dehydrogenase
GBBR	Groebke-Blackburn-Bienaymé reaction
GLP-1	Glucagon-like peptide-1
GPCR	G protein-coupled receptor
GSK	GlaxoSmithKline
hERG	Human ether-à-go-go related gene
HIV	Human immunodeficiency virus
HSA	Human serum albumin
HTS	High-throughput screening
IFA	Indirect fluorescent antibody
IgG	Immunoglobin G
IMCRs	Isocyanide-based multicomponent reactions (MCRs)
iRBCs	Infected red blood cells
IV	Intravenous
KAHRP	*Plasmodium falciparum* knob-associated histidine-rich protein
LED	Light-emitting diode
lit.	Literature reference (for melting point (mp) analysis)
LTF	Little Things Factory® GmbH
MCR	Multicomponent reaction
MVI	Malaria Vaccine Initiative
NADPH	Nicotinamide adenine dinucleotide phosphate

NCEs	New chemical entities
NK	Natural killer (cells)
PATH	Program for Appropriate Technology in Health
Pf. (or *P. falc.*)	Plasmodium falciparum
PfATP4	*P. falc.* Adenosine triphosphatase 4
PfCRT	*P. falc.* Chloroquine resistance transporter
PfEF2	*P. falc.* Translation elongation factor 2
PfEMP1	*P. falc.* Erythrocyte membrane protein 1
PfPI3K	*P. falc.* Phosphatidylinositol-3 kinase
PfPI4K	*P. falc.* Phosphatidylinositol-4-OH kinase
PfPNP	*P. falc.* Purine nucleoside phosphorylase
PRR	Parasite reduction ratio
PVM	Parasitophorous vacuole membrane
RDT	Rapid diagnostic test
rt	Room temperature
SAR	Structure-activity relationship
SCID	Severe combined immunodeficiency
S_NAr	Nucleophilic aromatic substitution
SOMO	Singly occupied molecular orbital
SPA	Scintillation proximity assay
TIMS	Tool for Interactive Monomer Selection
TLR9	Toll-like receptor 9
WHO	World Health Organisation

GSK CONFIDENTIAL INFORMATION – DO NOT COPY

Abstract

This thesis describes the development and use of flow methods in the synthesis of medicinally privileged heterocycles.

As a developing technology, advances in the understanding and technological hardware involved within flow chemistry have resulted in its widespread employment throughout the chemical sector. Specifically, factors including the ease of in-line analysis and streamlining of multi-step syntheses, as well as benefits offered in safety control, heating efficiency, reagent addition control, uniformity of performance and facile upscaling, and the reduced footprint of reactors in comparison to traditional batch methods have appreciably added to the value and applicability of this technique, especially in large scale synthetic procedures.

Despite this, the majority of early stage research and discovery chemistry still relies on the use of batch reactions. As a result, and in a drive to utilise state-of-the-art technology within our laboratory in order to redefine drug discovery practices, this work presents the use of flow chemistry within two distinct, and highly relevant applications.

Imidazoheterocycles are motifs of foremost importance to the medicinal chemistry community, being present in clinical candidates and probes for a number of health indications. As a result, an effective and reliable synthetic preparation for their access and isolation would be invaluable. The first chapter involves the use of a combination of commercial flow apparatus to develop a chemical methodology for the efficient, sustainable, scalable and robust synthesis of aminated imidazoheterocycles *via* the Groebke-Blackburn-Bienaymé multicomponent reaction. Advantages of this process include the requirement for a reaction (residence) time of only 50 minutes, the tolerance of a wide-range of functionality in all starting materials, and the facile scalability in flow, as demonstrated on multi-gram scale.

A smaller, bespoke microfluidic system was then applied for the second chapter, where the use of flow equipment was validated in an ongoing programme within our laboratories, to rapidly generate a small library of diaminoquinazolines as potential antimalarials, following on from work at GSK's infectious disease site in Tres Cantos, Madrid.

Computational design elements were used to select small molecule targets based on frequently considered physicochemical parameters, and a tandem S_NAr method was employed to produce decorated heterocyclic products in a short overall reaction time. This process represents a substantial acceleration in the synthesis of these compounds, facilitating far-reaching future work involving rapid drug design and access, and the potential for streamlining the preparative methods between small and large scale chemistry within early stage discovery, especially within the pharmaceutical industry.

1. Introduction

1.1 Flow Chemistry

As a result of the developments in early combinatorial chemistry and chemical engineering, the use of continuous flow reaction apparatus within chemical research has become increasingly common over the past few decades.[1] Indeed, a Web of Science search of the topic "flow chemistry" shows a substantial increase in the amount of journal articles published over the last 25 years (**Graph 1.1**).[2]

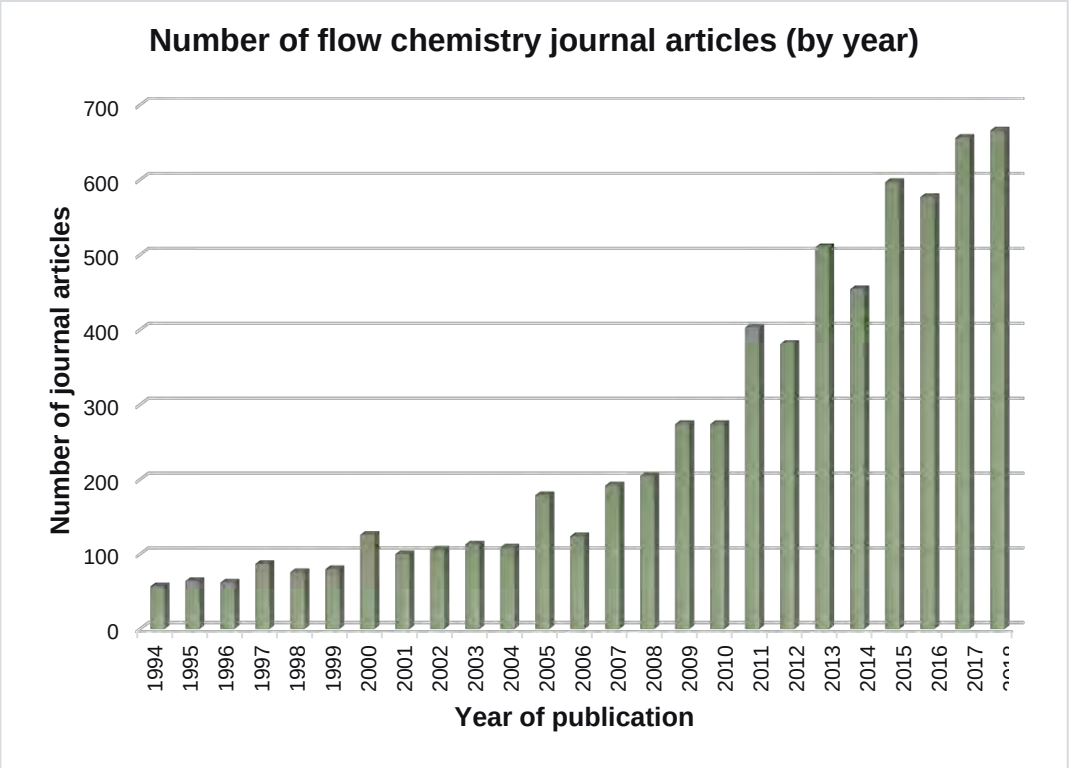

Graph 1.1: Web of Science data regarding the number of journal articles published since 1994 which involve the term "flow chemistry". Data relating to organic chemistry, medicinal chemistry, multidisciplinary chemistry and chemical engineering journals are displayed.

Recently, the increasing volume of commercial suppliers for flow equipment, and the accessibility of step-by-step protocols for the assembly of such equipment have simplified education for the traditionally uninformed chemist, and have meant that flow synthesis has become a well-established and affordable technique with a diverse array of applications.[3]

Flow chemistry involves performing chemical reactions within a series of connected channels containing reaction solutions, which are propelled in a unidirectional manner along the channels by continuous pumping systems. Some examples of the chemical reactors now available include heated loop reactors, microchip reactors for small scale chemistry, tube reactors, and flow chemistry apparatus designed for performing electrochemistry and

photochemistry reactions, all allowing for the continuous processing of novel synthetic methodologies.

The use of flow equipment in synthesis has a variety of benefits when compared to traditional batch-based methods. Firstly, since only a small amount of the overall reaction mixture is within the tubing or reaction chamber at any one time, and due to the increased surface area:volume ratio provided, especially in small scale flow reactors, heat transfer is very rapid. As a result, flow reactions can be heated very effectively, and exothermic reactions can be performed safely, often without the prerequisite of cryogenic conditions, which become progressively difficult to maintain with respect to increasing reactor size.[4]

For example, Murray *et al*. described the use of a peristaltic pumping system for the safe handling of multiple organometallic reagents (such as **2**) in flow.[5] The procedure, using stable fluoropolymer tubing, demonstrates the use of Grignard reagents, organolithium reagents and organocuprates in synthetic transformations usually requiring more intensive cryogenic conditions in batch. All reactions were performed continuously on a multi-gram scale, and the method offered numerous benefits over the analogous batch procedures, such as improved yields, faster reaction times, and reduced amounts of observed by-products. An example of one such reaction is shown in **Scheme 1.1**.

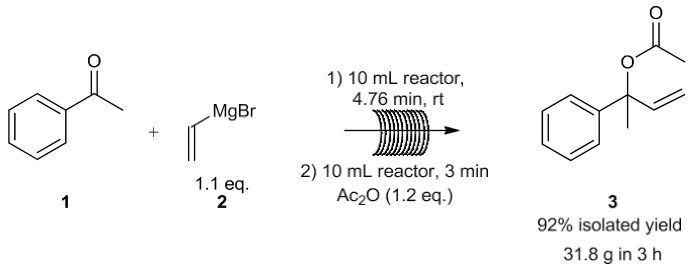

Scheme 1.1: Example of a Grignard addition to ketone 1, and subsequent acetylation reaction performed in continuous flow under ambient conditions to generate adduct 3.[5]

As well as controlling dangerous reactions easily, flow systems are usually pressurised, meaning that performing reactions at temperatures far above the boiling points of solvents is well tolerated, allowing a significant acceleration of reaction procedures. In equivalent batch methods, superheating conditions are usually limited to microwave reactions for small scale applications, or the expensive use of autoclaves for larger scale chemistry.

The use of highly pressurised microreactors means that reactions which are usually limited to reaction times of multiple hours to days can now be performed safely in minutes or less. This greatly facilitates reaction optimisation and improves efficiency.

For example, though offering a simple, one-step process to generate immensely useful functionality, the uncatalysed conversion of carboxylic acids to nitriles requires temperatures

of over 300 °C, far outside of the range of traditional batch reactors, in order to have any synthetic utility. Nevertheless, within a stainless-steel capillary reactor, and using supercritical acetonitrile solvent, nitriles (**4-7**) were afforded in excellent yields, in only 25 minutes (**Scheme 1.2**). The reaction proceeded cleanly and tolerated a range of functionality, including the use of aromatic, heteroaromatic and aliphatic carboxylic acids.[6]

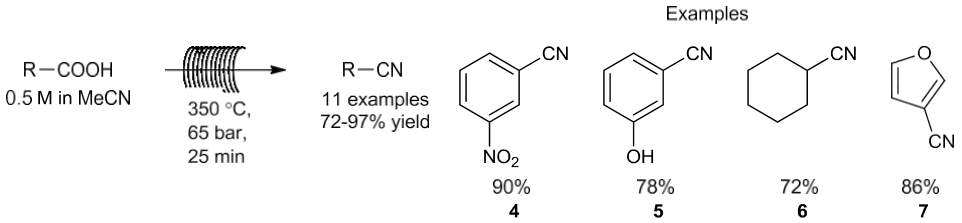

Scheme 1.2: The uncatalysed conversion of carboxylic acids into nitriles, and some representative examples and yields from the flow procedure.[6]

Another benefit concerns the rapid optimisation of reactions in flow, which can be attained through the use of quantitative in-line analysis and purification. Using modern technology, reaction monitoring using NMR,[7] IR,[8] UV,[9] MS or Raman methods are possible,[10,11] and the direct observation of reactions is also a possibility as a result of high-tech camera surveillance.[12,13]

Reaction telescoping is also made more straightforward with the use of in-line liquid/liquid extraction and separation techniques, immobilised reagents and reaction scavengers.[14,15]

Some of these benefits are elegantly demonstrated together in the multi-step flow synthesis of oxomaritidine, **10**, a cytotoxic alkaloid (**Scheme 1.3**).[16] The paper describes a 7-step synthesis, which has been performed in one continuous flow process. The procedure uses various packed reactor columns containing a mixture of immobilised reagents, catalysts, catch and release agents and scavengers to perform the synthetic steps without the requirement for aqueous work-up procedures or column chromatography at any point. This afforded a cumulative 40% yield of the isolated natural product in over 90% purity in under 1 day.[16]

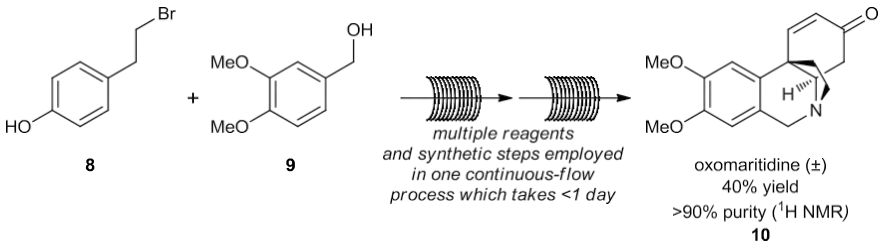

Scheme 1.3: Flow synthesis of oxomaritidine (10), an alkaloid natural product synthesised in a multi-step continuous flow procedure.

Under batch conditions, the synthesis of oxomaritidine using the same multi-step sequence, with polymer-supported reagents, required an overall manipulation time of around 4 days.[17] This represents a huge efficiency gain in the use of flow technology to quickly synthesise a structurally complex natural product.

1.2 Bespoke flow applications

Despite a plethora of potential benefits that flow chemistry has to offer over batch methods, batch chemistry still predominates early stage research in medicinal chemistry. Nevertheless, two distinct flow applications have found common use within industry.

Continuous flow hydrogenation and ozonolysis technologies such as the H-Cube™ and the O-Cube™, respectively, both from Thales Nano® (**Figure 1.1**) facilitate the use of otherwise dangerous reagents, even on large scale. Furthermore, a new alternative to the O-Cube™, the Ice-Cube™ is currently sold by Thales Nano® for ozonolysis reactions.

Figure 1.1: The H-Cube™ (left) and O-Cube™ (right) machines from Thales Nano®, used for safe continuous flow hydrogenation and ozonolysis reactions, respectively.[18,19]

Hydrogenation is an extremely important reaction within chemical synthesis. It is used to introduce saturation into organic compounds and complete various reductions or defunctionalisation reactions. Unfortunately, batch hydrogenation procedures require the storage and use of potentially explosive hydrogen cylinders and pyrophoric catalysts, as well as long reaction times, due to the limited interactions between the heterogenous mixture of reaction catalyst, substrate solution and hydrogen gas.

The H-Cube™ permits highly efficient hydrogenation reactions in a safe and scalable manner up to temperatures of 150 °C and pressures of 100 bar. The hydrogen used is generated through the electrolysis of water, and 60 mL/min of high-pressure hydrogen can be generated through this method. The use of this hydrogen generator, as well as a packed bed reactor containing a hydrogenation catalyst, enables rapid hydrogenation processes using this system.

The H-Cube™ has been used by Viviano *et al.* to generate a small library of 1,4-benzodiazepin-5-ones, which are privileged motifs within medicinal chemistry

(**12**, **Scheme 1.4**). Under continuous flow conditions, a selective hydrogenation/cyclisation process could be performed in under 1 h residence time in excellent yields.[20]

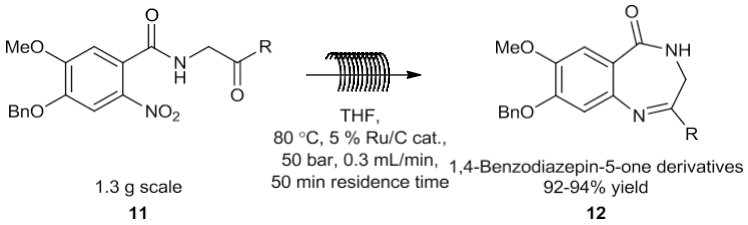

Scheme 1.4: A continuous flow hydrogenation procedure to generate medicinally-relevant 1,4-benzodiazepin-5-one derivatives in excellent yields.

Under equivalent catalytic conditions in batch, only undesired by-products were observed. In non-catalytic procedures, the desired materials could be synthesised, but in greatly reduced yields (51-77%), and using far more laborious, and less sustainable methods.

Ozonolysis is another potentially dangerous but useful reaction. The use of ozone carries respiratory risks, and ozonide intermediates generated during the ozonolysis reaction are often highly explosive. In the original O-Cube™, ozone was produced continually up to 20 mL/min from molecular oxygen at temperatures of -25 °C to ambient conditions. A more recent reactor (The Ice-Cube™) has since been developed which allows access to temperatures down to -70 °C, and up to 80 °C. Nevertheless, using the original reactor, ozonolysis could be performed and the subsequent intermediates quenched in a facile manner in continuous flow to produce a range of valuable oxidised products (**Scheme 1.5**).[21]

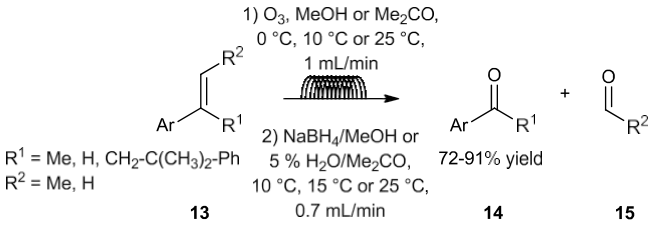

Scheme 1.5: The continuous flow ozonolysis of various styrenes to generate aryl aldehydes and ketones, 14.

1.3 Scaling up and scaling out in continuous flow

The scale of continuous flow processes can be modified in a manner of ways. “Scaling up” refers to increasing the capability of a flow setup, usually by increasing the size of the reactor, or simply in running the continuous setup for longer. Alternatively, “scaling out” involves using parallel flow reactors to perform the same reaction on larger demand and can be especially useful in combining multiple microfluidic devices.

1.4 Microfluidic and mesofluidic flow equipment

Broadly speaking, standard lab scale flow reactors are considered to be either microfluidic (having an internal diameter of 10-500 μm inside the reactor tubing) or mesofluidic (also called minifluidic; with an internal diameter of 500 μm–several mm).[22] The choice of the type of flow reactor used in a synthetic procedure is dependent on the quantity of product material required, as well as particular engineering considerations such as pressure requirements, downstream reaction solution handling requirements, and any chemical instability with the constituents of the flow reactor.

In comparison to larger reactors, microfluidic devices provide advantages in the following ways:

- Improved thermal transfer. Due to the increased surface area:volume ratio (also called specific area) of microfluidic reactors, the heat transfer capacity observed for microfluidic devices (typically 5000-50000 m^2m^{-3} surface area (SA):volume ratio) is usually greater than for mesofluidic reactors (100-10000 m^2m^{-3}).[22] By comparison, a 250 mL round bottom flask has a specific area of ~ 80 m^2m^{-3}.[23]
- Improved mass transfer. As a result of this high specific area, mixing is also more efficient in flow reactors containing smaller internal diameters of reaction tubing, despite the changing flow regimes observed when considering different sizes of tubing (see **Section 1.5 Residence times, flow rates and fluid dynamics**). Mixing can also be controlled more efficiently, as a result of "stacking" parallel laminar flow channels to minimise reagent contact and side-product formation, where desired.[23]

However, mesofluidic flow systems provide access to much more material, as even in cases where parallelisation of microfluidic reactors is employed, only small volumes of products can be generated in comparison.

Microfluidic reactors are also prone to blockage, as a result of their small channel diameter. In such an event, they can also be very difficult to clean, since they are usually fabricated through specific printing procedures and cannot be dismantled easily without breaking.[22]

Finally, pressure drops are very common in small scale reactors, which are limited to relatively low flow rates of reaction solutions.[24] Therefore, thermal and mass transfer advantages for microreactors are most applicable in the production of small volumes of material.

1.5 Residence times, flow rates and fluid dynamics

The flow rate determines the rate at which a reaction solution passes through a flow reactor. When the volume of the flow reactor is divided by the flow rate, this determines the residence time (the length of time that the reaction solution spends within the flow reactor, **Equation 1.1**).

GSK CONFIDENTIAL INFORMATION – DO NOT COPY

$$\text{Residence time (in minutes)} = \frac{\text{Volume of flow reactor/reaction chamber (in μL or mL)}}{\text{Flow rate (μL/ min or mL/min)}}$$

Equation 1.1: Relationship between the flow rate, residence time and volume of the flow reactor. The residence time within the reaction chamber alone can be calculated, since a flow reactor includes both the reaction chamber, which may be subjected to reaction conditions (*i.e.* thermal heating, microwave irradiation, photo-irradiation etc) and the surrounding tubing, within which conditions are relatively unreactive. Residence times of seconds or faster may be required, especially when employing superheated conditions.

The type of flow present within a flow reactor is significantly affected by the diameter of the tubing present. This relationship can be understood by use of the Reynold's number (Re), a dimensionless parameter which predicts the interactions present between parallel reaction streams.

The Reynolds number can be determined through the use of **Equation 1.2**.[25]

$$\text{Re} = \frac{\text{Inertial forces}}{\text{Viscous forces}} = \frac{\rho v L}{\mu}$$

Equation 1.2: Equation to calculate the Reynolds number, a dimensionless parameter describing liquid-liquid interfacial kinetics between parallel streams within a flow reactor. Within the equation, ρ = density of the liquid (in kg/m), L = the channel diameter (in m), v = the velocity of the reaction solution (in m/s) and μ = viscosity of the liquid (kg/m/s).

The Reynolds number can be thought of as a ratio between the inertial forces (the momentum of the fluid, proportional to its velocity and density) and the viscous forces (the resistance of a fluid to flowing, as a result of frictional shear forces between layers) acting on a pumping liquid in a pipe. At low values of Re (< 2100), mixing between parallel streams occurs predictively by diffusion, and a uniform flow rate and pressure is sustained within the pipe. However, at large values of Re (> 4000) turbulence overcomes any drag present within the system, and the flow regime present in the system suffers from irrational changes of flow pressure and velocity as mixing becomes chaotic (**Figure 1.2**).[25] Reynold's number values between these two extremes display an intermediate form of mixing, known as "transient" mixing, and a Re value of 2040 (± 10) represents an accurate prediction of the critical point at which the onset of sustained turbulence occurs.[26]

GSK CONFIDENTIAL INFORMATION – DO NOT COPY

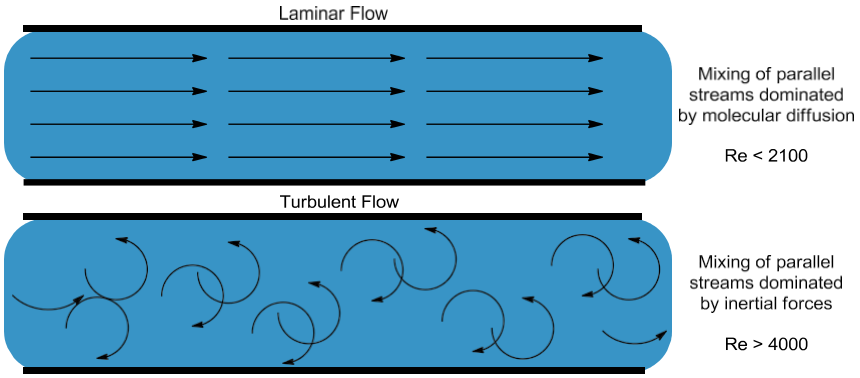

Figure 1.2: Figure describing the relationship between the Reynolds number and the mixing present within the reactor. At values of Re < 2100, laminar flow is observed, and mixing occurs by diffusion. At values > 4000, inertial forces dominate, and interfacial mixing becomes chaotic between parallel streams in the reactor.[27]

Microfluidic devices typically display laminar flow without intervention, although various developments have been made in order to introduce turbulent flow (known as macromixing) into small scale flow reactions.[28-32] As flow reactors increase in size, their mixing naturally becomes increasingly turbulent. Batch reactions display a combination of micromixing and macromixing through mechanical agitation.[23]

This is especially important in small scale devices, as relying on diffusion alone to produce one uniform reaction concentration takes a relatively long time in reactions requiring residence times of seconds. Typically, between parallel streams, the diffusion time required for a molecule, *A*, is given through **Equation 1.3**.[23]

$$t = \frac{x^2}{D_{AB}}$$

Equation 1.3: Equation to calculate the time (*t*) taken for a molecule (*A*) to diffuse over a path length (*x*) through a solution of molecule B. D_{AB} describes the molecular diffusivity of the system.

Once a uniform reaction concentration has been attained within the solution, a steady state is achieved. However, the fluid inside a flow reactor experiences friction against the inner wall of the tubing. As a result, the solution passing through the tube travels fastest towards the centre of the tubing, giving rise to a bell-shaped curve in the establishment and subsequent loss of steady state conditions during the course of a flow reaction (**Graph 1.2**).

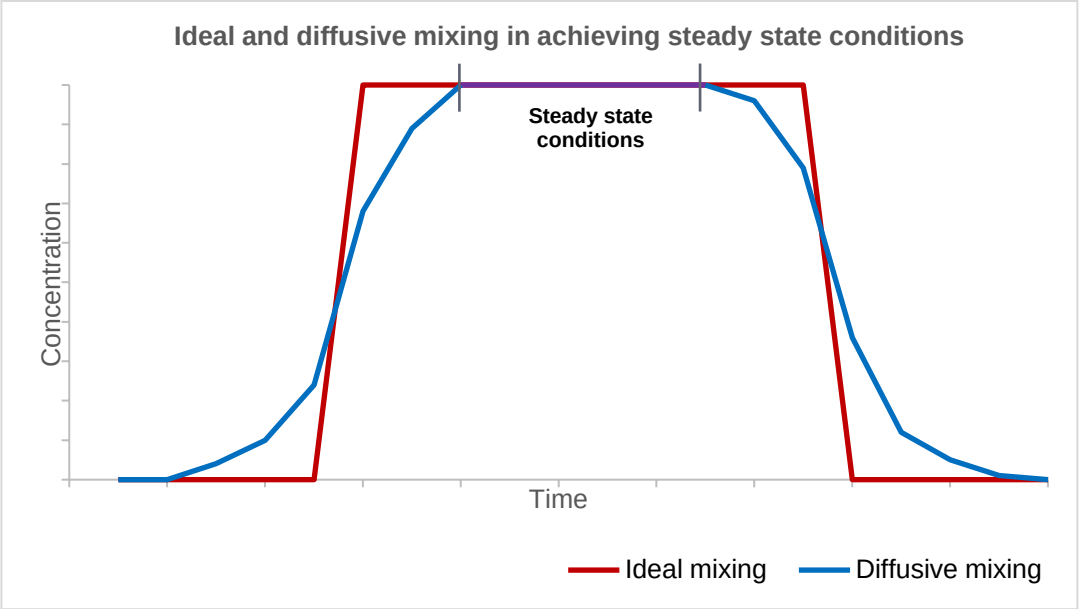

Graph 1.2: Representation of ideal mixing (no friction observed; red) and a more realistic picture of diffusive mixing (blue) in establishing steady state conditions within a flow reactor.[27]

Therefore, work using flow chemistry either involves the collection of all of the crude reaction material, to provide the overall reaction efficiency, or otherwise collection for a set period of time at steady state. This method of collection can be used to determine the production capability of a flow setup, especially within large scale applications.

1.6 Description of flow equipment and operations used

The flow equipment used in the work within this programme is summarised below. All diagrams and schematics of the flow systems used can be found in the ***Experimental*** section (**Section 6, Figures 6.1-6.9**).

Mesofluidic equipment is used for ***Chapter 1***, employing a Vapourtec® RS-200™ reactor to perform flow reactions efficiently, and in scales affording up to several grams (or more) of desired products. This apparatus was chosen as a result of both equipment accessibility, as well as the ease of scalability in comparison to microfluidic devices.

For both projects described, a Syrris Asia® syringe pump was used to propel reaction solutions through the flow tubing. Syringe pumps give access to accurate low flow rates suitable to the applications required herein. Different sizes of syringe can be applied during use of the pump dependent on the flow rate needed. For ***Chapter 1***, Asia® green syringes (2 sets of 250 µL + 500 µL volume syringes) were used, which can facilitate a flow rate between 5 µL to 1.25 mL/min/channel. In ***Chapter 2***, Asia® yellow syringes (2 sets of 50 µL + 100 µL volume syringes) were used, which can pump a flow rate of between 1 µL and 250 µL/min/channel.

The syringe pump performs as shown below:

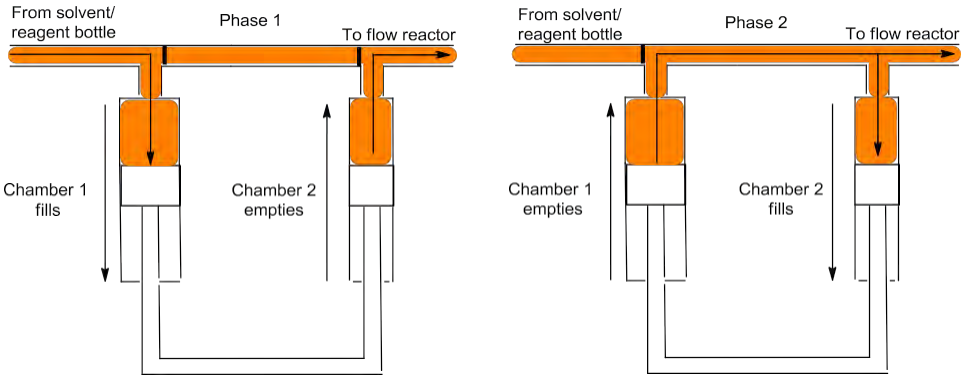

Figure 1.3: The pumping mechanism used by the Syrris Asia® syringe pump. During pumping, two phases are present. In the first, the larger syringe fills with a solution of reagent(s) as the (already filled) smaller one discharges its contents downstream into the flow reactor. During the second phase, the larger syringe empties, with half of the volume of reagent solution entering the second, smaller syringe, and the remainder of the solution being pumped into the flow reactor. This continuous process introduces pulse dampening in comparison to other cyclic pumping systems, such as HPLC and peristaltic pumps, to ensure that steady pumping is maintained, even at low flow rates.[33,34]

For ***Chapter 2***, heated reactions were performed within 2 x Little Things Factory® (LTF) microreactor chips. The reactor chips both have a channel diameter of 500 µm. The LTF-MS™ chip (115 x 60 x 6 mm; 0.2 mL volume) was used for the reaction heated to 90 °C, whilst the LTF-VS™ chip (115 x 60 x 6 mm; 1.1 mL volume) was used for the second, hotter reaction step.[35] For diagrams and schematics, see ***Experimental,*** **Section 6.1.19 Flow reactions (malaria work)**.

For both bodies of work, the tubing used within the flow reactors had an internal diameter (ID) of 1/16 or 1/32 inches (1.59 mm or 0.794 mm), as detailed within the ***Experimental*** section.

2. Chapter 1: Extension of the GBBR: a green, robust, scalable and efficient continuous flow process to synthesise 3-aminoimidazoheterocycles

2.1 Multicomponent reactions (MCRs)

Multicomponent reactions are defined as reactions which combine three or more starting materials within a single convergent process to generate a specific product. Within synthesis, the use of MCRs is highly desirable for many reasons:

- Usually they are performed in high yields, with minimal by-product formation (often only water is generated as a by-product).
- Since most of the atoms in the starting materials are incorporated into the product, multicomponent reactions are highly atom efficient.[36]
- In a single step, highly complex structures can be constructed, with a potentially appreciable increase in the synthetic efficiency involved in a process.
- Since all starting components can be varied, compound libraries can be readily assembled using multicomponent reactions.

This variation in starting components has led to the development of various secondary multicomponent reactions, where named multicomponent reactions can be adapted with functional changes in reaction components.[37]

Nevertheless, in optimising multicomponent reactions, careful control of the kinetics involved in bond forming reactions between all of the reactants must be considered in order to preferentially generate the desired product. In some cases, different postulated reaction intermediates can result in the formation of the same product through different reaction pathways.[38]

Within the forthcoming section, only examples of MCRs which generate iminium intermediates will be considered, as these are most closely relevant to the field of work presented herein.

2.2 The Strecker reaction

The first multicomponent reaction to be officially reported was the Strecker reaction in 1850 (**Scheme 2.1**).[39] The Strecker reaction involves the synthesis of *α*-amino acids from carbonyl compounds through the intermediate generation of an *α*-aminonitrile (**19**). The *α*-amino acid moiety is ubiquitous in medicinal chemistry, and amino acids are frequently used as chiral catalysts.[40,41]

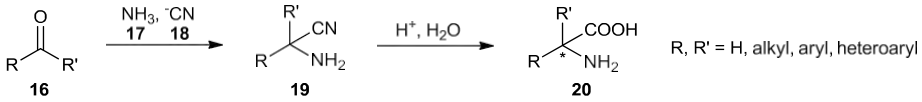

Scheme 2.1: The Strecker reaction, combines aldehyde or ketone (16), amine and nitrile components to generate *α*-amino acid derivatives (20) following hydrolysis under acidic conditions.

The reaction has been performed in an enantioselective manner on numerous occasions. Chemoenzymatic methods to *α*-amino acids have proven successful, though the generation of non-natural amino acids through this process is challenging.[42] Alternatively, various enantioselective catalysts have been designed for the Strecker reaction, although, due to their complexity, the use of catalysts can be limited by poor scalability. Additionally, within these processes, the hydrolysis step of the *α*-aminonitrile can result in racemisation.[43]

Nevertheless, in one such series of approaches, various urea and thiourea organocatalysts were identified from a parallel library screening. First-generation catalyst **21** (**Figure 2.1**) can be used in solution or when bound to a polystyrene resin (**22**), without the loss of reactivity (96-98% yield maintained) or enantioselectivity (92-93% *ee* maintained) after at least ten reaction cycles.[44] The catalysts were found to influence stereocontrol at low catalyst loading, by making various non-covalent interactions to the activated iminium intermediate and inducing steric crowding around the catalyst-iminium complex.[45,46] As a result, refinement of the initial catalyst design led to the development of catalyst **23**, offering improved enantioselectivity for sterically demanding substrates.[45] A more recent development has led to the simplified catalyst structure **24**, which retains exquisite enantioselectivity (> 20 examples, 73-99% *ee*), but requires fewer steps to synthesise, and is more useful in large scale applications.[47]

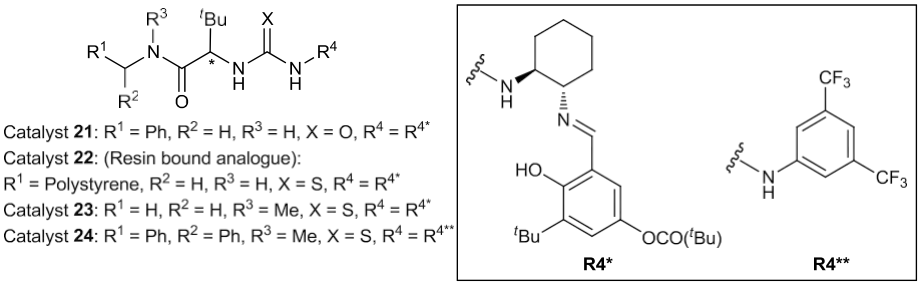

Figure 2.1: Thiourea and urea organocatalysts (21-24) developed by Jacobsen and co-workers for the asymmetric Strecker reaction.[44,45,47]

Though giving access to highly privileged amino acid structures, the original conditions for the Strecker reaction required the use of superstoichiometric amounts of hydrogen cyanide, a highly potent neurotoxin.[48] Newer variants of the cyanide source, including trimethylsilyl cyanide (TMSCN) and acetone cyanohydrin (ACH) have frequently been used in synthesis,

though these reagents generate hydrogen cyanide *in situ*, and hence still suffer from severe safety precautions accompanying their use.[40]

As a result, safer modern alternatives have been sought to counteract this problem. For example, Yan *et al.* have developed a scalable process employing an asymmetric cation binding ligand (**25**) to strongly co-ordinate to potassium cyanide, solubilise the reagent within the organic solution (toluene) to prevent exposure, increase anion reactivity and induce an asymmetric transition state to control the enantioselectivity of the reaction (**Scheme 2.2**).[49]

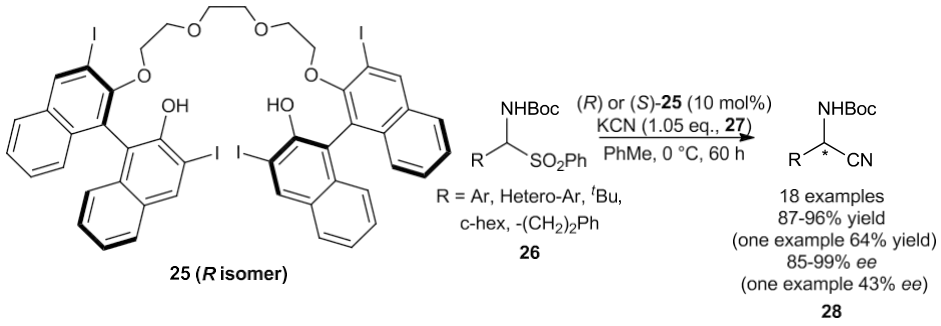

Scheme 2.2: The organocatalytic asymmetric Strecker reaction using a chiral bis-hydroxypoly ether BINOL derivative, 25.

In the procedure, an *α*-amido sulfone **26** is used as a stable synthetic imine precursor, both to generate the imine *in situ*, and in supporting the chiral cage structure generated between **25**, the *α*-amido sulfone **26** and the cyanide source, potassium cyanide **27**. The suggested reaction mechanism is shown in **Scheme 2.3**.

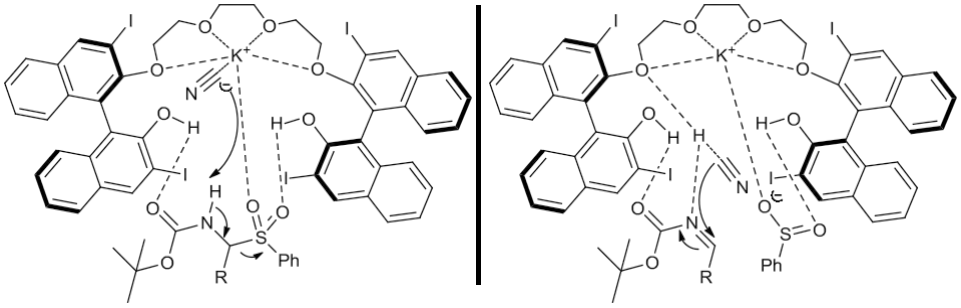

Scheme 2.3: Postulated transition state for the organocatalytic asymmetric Strecker reaction.[49] A small excess (1.05 eq) of KCN is used in the reaction, as it is required as both a base and a source of the nucleophilic cyanide ion.

Using this procedure, a one-pot process from the *α*-amido sulfone to the hydrochloric acid salt of the analogous *α*-amino acid could be performed, and the catalyst could be recycled through a simple phase separation/solvent evaporation process. This one-pot method was used to generate a range of unnatural D-amino acids in excellent enantioselectivity on gram scale.[49]

2.3 The Mannich reaction

The Mannich reaction was first reported in 1912, and involves the synthesis of *β*-aminocarbonyl compounds.[50] Again, an imine intermediate is generated in the reaction, before nucleophilic attack from an enolate (formed from **32**) furnishes the desired product (**33**, **Scheme 2.4**). *β*-Aminocarbonyl compounds (or Mannich bases) made in the reaction have a wide variety of application within medicinal chemistry and drug design.[51]

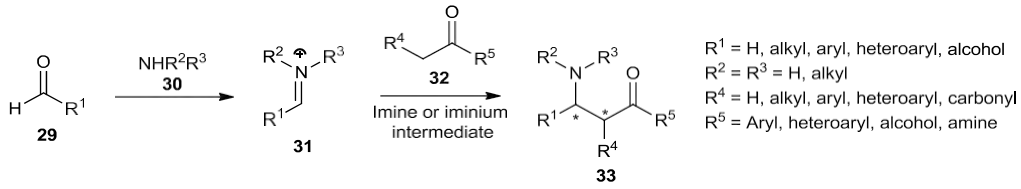

Scheme 2.4: Another multicomponent reaction, the Mannich reaction generates *β*-aminocarbonyl compounds (33) from the nucleophilic addition of an enolate to an imine intermediate.

The reaction is usually performed at low temperatures, since the products are often thermally unstable, and the promotion of side-reactions is observed under conditions using elevated temperatures.[52]

Various efforts to increase the efficiency and sustainability of the Mannich reaction have been made, including a one-pot, solvent-free, mild and efficient process utilising bis-(piperazine-1,4-diium)hexachlorobismuthate(III) chloride monohydrate catalyst **37** at 3 mol% catalyst loading. A representative example is shown in **Scheme 2.5**, affording the desired Mannich adduct **38** in moderate (55%) yield, and an inherently high diastereomeric ratio (96:4 by ^{1}H NMR analysis). The catalyst could be recycled, with only a small drop in activity after ten uses (95% to 84% yield for the same substrate).[53]

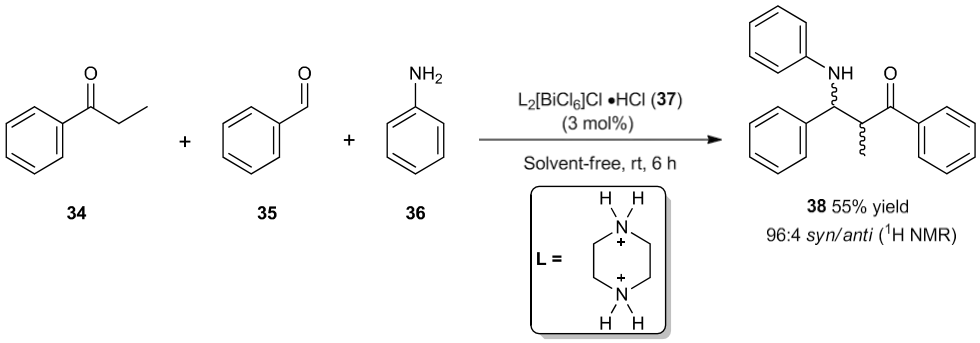

Scheme 2.5: Example substrate from a solvent-free Mannich reaction under bismuth catalysis.

The Mannich reaction has been performed under enantioselective and diastereoselective control with a myriad of catalysts, with the precise reaction mechanism depending on the catalytic system utilised to achieve the transformation.

A typical example is shown in **Scheme 2.6**. A BINOL-derived phosphoric acid catalyst **39** achieves stereocontrol of the Mannich reaction to selectively afford *anti*-addition of ketones to various aldimines with high diastereoselectivity and enantioselectivity, even with very low catalyst loading (as low as 0.5 mol% in some cases). **Scheme 2.6** shows an example combining cyclohexanone (**40**) with the aldimine intermediate formed through the condensation of 4-chlorobenzaldehyde **41** with aniline **42**.[54]

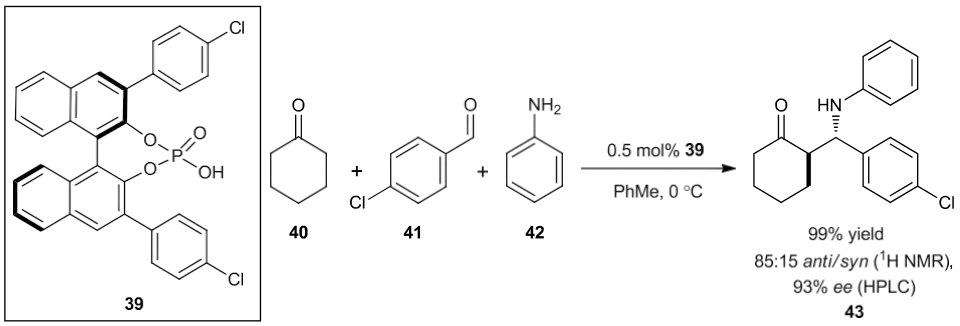

Scheme 2.6: An asymmetric Mannich reaction utilising a chiral BINOL-derived phosphoric acid.

Finally, amino acids are regularly used as chiral organocatalysts for the asymmetric Mannich reaction. Typically, when (*S*)-proline and related pyrrolidine derivates with acidic *α*-functionality are used in the Mannich reaction, *syn*-products are afforded preferentially.[55-58]

In a seminal paper, Zhang *et al*. have reviewed the use of 3-pyrrolidinecarboxylic acid **44** and similar *β*-amino acid catalysts in controlling the stereochemistry involved in the Mannich reaction.[59] Importantly, when utilising an (*R*)-acidic residue in the 3-position of the pyrrolidine, stereocontrol of the addition could be reversed with respect to the use of (*S*)-proline, with near perfect enantio- and diastereoselectivity.[59] **Figure 2.2** shows some example *anti*-Mannich products (**45-50**) made from the use of *anti*-selective catalyst **44**.

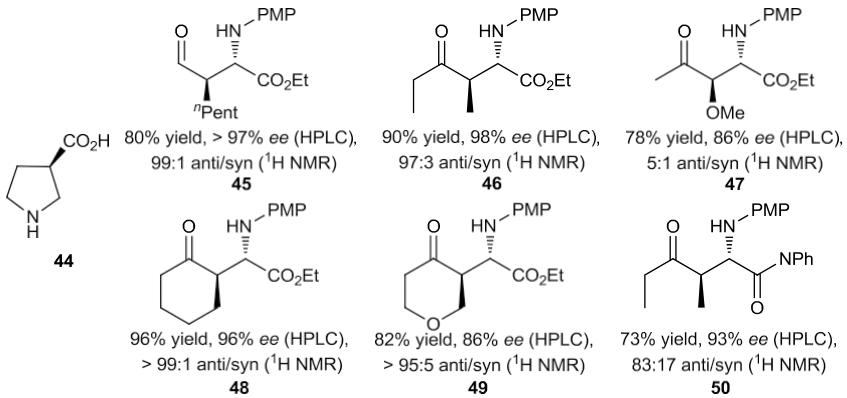

Figure 2.2: Some example *anti*-Mannich products afforded from the catalytic use of (*R*)-3-pyrrolidine carboxylic acid, 44.

Iminium intermediates such as those present within the Strecker and Mannich reactions can be attacked by various nucleophiles, giving access to a wide array of products. Indeed, in a modification to the Mannich reaction, non-enolate derived carbon nucleophiles can be used to generate functionalised amines.

The Petasis (boron Mannich) reaction uses activated boronic acids or boronate esters (**53**) to facilitate nucleophilic attack on the imine intermediate (**Scheme 2.7**).[60] The reaction generally requires the use of carbonyl reagents (**51**) with an *α*-functionality which can coordinate to (and activate) the boron species.[61]

Scheme 2.7: General scheme describing the Petasis (boron Mannich) reaction

Various asymmetric approaches to the Petasis (boron Mannich) reaction have been employed, including the use of chiral *α*-hydroxyaldehydes and chiral catalysts for the asymmetric generation of *α*-amino alcohols.[62,63]

2.4 Isocyanides and isocyanide-based multicomponent reactions (IMCRs)

A common subset of multicomponent reactions is isocyanide-based multicomponent reactions (IMCRs). Isocyanides (also called isonitriles) are hugely versatile reagents in organic synthesis.[64] The isocyanide functionality constitutes a carbon-nitrogen triple bond arranged in reverse order to a nitrile, which can also be represented in an alternative resonance form, as a carbenoid reagent, with a lone pair on the terminal carbon atom (**55** and **56**, **Figure 2.3**).

According to high-level valence bond calculations, the major resonance form is actually the carbene form, with the triple bond character of isocyanides being a result of strong delocalisation to the terminal carbon from the neighbouring nitrogen atom.[65] As a result, isocyanides can be thought of as either highly stabilised carbenoid reagents, or heteroatomic analogues of alkynes, depending on whether dissecting their chemical reactivity or electronic properties.[64]

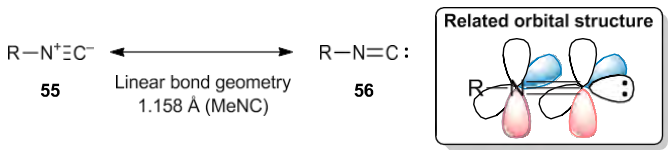

Figure 2.3: Resonance forms of the isocyanide functional group (left), and its related orbital structure (right).

Isocyanides retain close to a formal linear geometry, and similarly positioned π-orbitals to analogous alkynes.[64,66] However, the presence of the nitrogen heteroatom increases the polarisation of the triple bond. In isocyanides, only 26% of the electron density present within the N≡C bond is located on the carbon atom.[64]

Infra-red (IR) analysis of isocyanides has found a distinctive stretch at around 2130 cm^{-1}, similar to carbon monoxide (2143 cm^{-1}).[67] This likeness has led to the development of metal-isocyanide binding complexes, with the functional group able to participate in synergic π-backbonding from the metal centre.[68]

Though rare in nature, some isocyanides exist within isolated natural products. The first isocyanide-containing natural product to be isolated was the antibiotic xanthocillin (**57**, **Figure 2.4**), whose chemical structure was identified in 1956.[69,70] Xanthocillin was isolated from the *Penicillium notatum* fungus, and a range of its derivatives have since been found to have potential anti-cancer application as thrombopoietin receptor agonists.[71] Since then, a number of isocyanide-containing natural products have been identified in marine and terrestrial sources, such as marine sponges, molluscs, fungi and bacteria.[72,73]

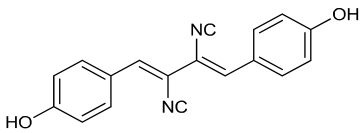

57

Figure 2.4: Xanthocillin, an isocyanide-containing natural product, isolated from the *Penicillium notatum* fungus.

A unique characteristic which belongs to most isocyanides is their foul-smelling and noxious nature. The smell is so bad that isocyanides have, in fact, been used within non-lethal weapons.[74] The first synthesis of an isocyanide was in 1859, from the reaction of allyl iodide **58** and silver cyanide **59**.[75] Currently, the most common method for the preparation of isocyanides is through the dehydration of formamides, which has been performed with a variety of dehydrating agents.[76-78] The formamide is usually made from the relevant amine precursor (**61**), but can also be synthesised from aldehyde or ketone reagents (**62**) *via* a Leuckart-Wallach reaction with formamide and formic acid.[79]

Other ways of synthesising isocyanides include the carbylamine reaction, which produces isocyanides **67** from amines through the use of a dichlorocarbene, and the deprotonation of oxazoles (**68**) and benzoxazoles (**70**) with strong bases.[80,81] All of these methods of preparation are shown in **Scheme 2.7**.

GSK CONFIDENTIAL INFORMATION – DO NOT COPY

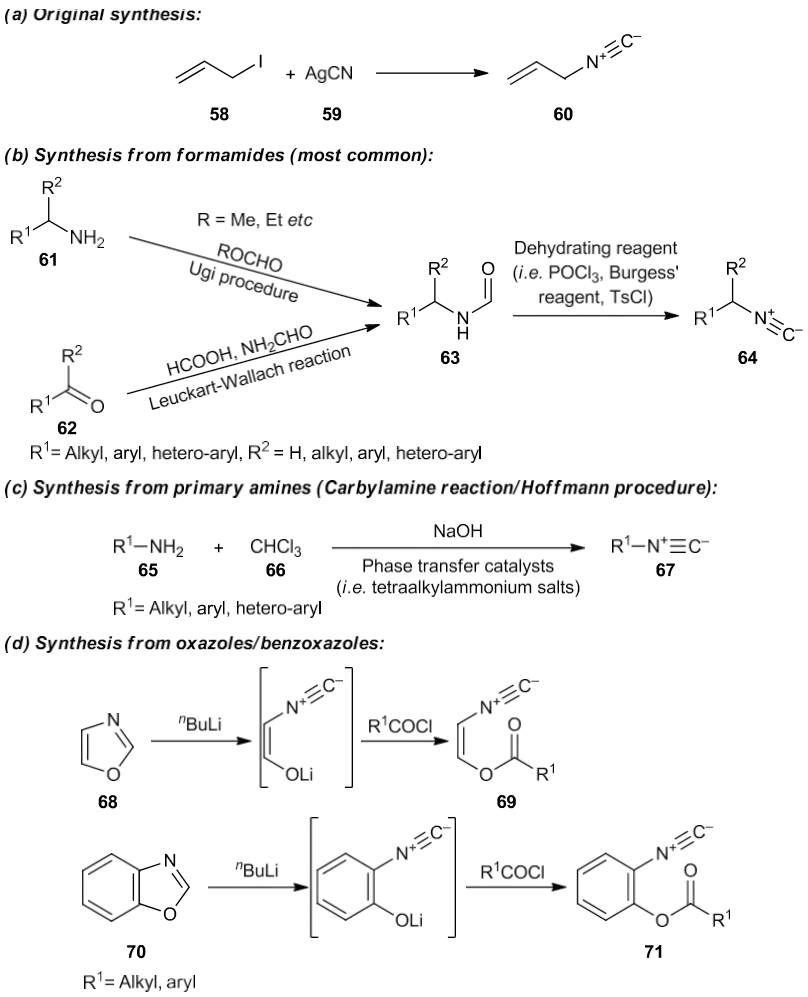

Scheme 2.7: Synthetic methods for the preparation of isocyanides.

Within organic synthesis, exploitation of the dual reactivity of the isocyanide terminal carbon (having both nucleophilic and electrophilic character) can be observed through a plethora of 1,1-radical reactions and cycloadditions.

For example, Curran *et al*. used isocyanides such as **73** in a range of radical cascade reactions to generate cyclopentane-fused quinolones (**74**).[82] These annulation strategies afforded a range of privileged structures, such as a precursor to camptothecin, a natural product with anti-cancer applications (Compound **78**, **Scheme 2.8**).[83]

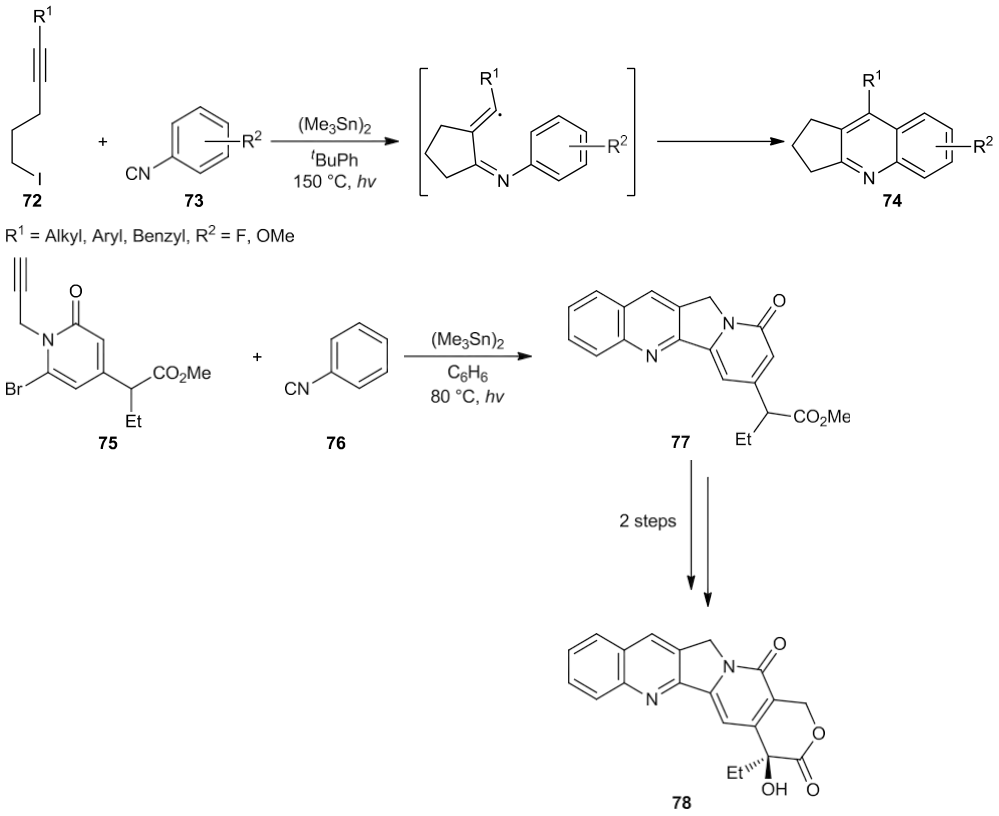

Scheme 2.8: Example of a [4+1] radical cascade reaction, and its application in the synthesis of camptothecin, 78.

Outside of radical reactions, isocyanides readily participate in multicomponent reactions to generate heterocycles and complex structures. The use of isocyanides within MCRs can also offer alternatives to more dangerous or difficult synthetic procedures.

For example, *α*-aminonitrile products (comparable to those formed during the Strecker reaction, *vide supra*) can be afforded through the combination of trityl isocyanide **81** with the iminium intermediate made from the condensation of various anilines with carbonyl reagents.

Following a subsequent *in situ* acidic deprotection of the trityl group, the desired products can be attained smoothly, without requiring the use of toxic cyanide sources (**Scheme 2.9**).[84]

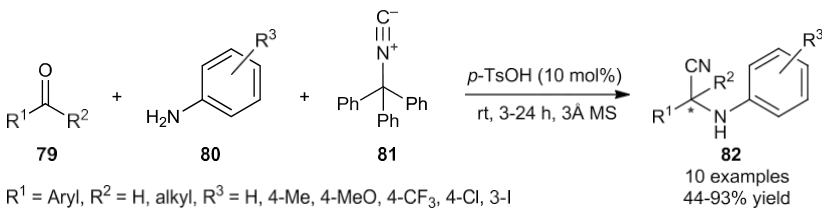

Scheme 2.9: The application of trityl isocyanide (81) in a Strecker-type reaction to afford *α*-aminonitrile products (82) without the use of toxic cyanide reagents.

As discussed above, the main synthetic use of isocyanides is observed within isocyanide-based multicomponent reactions (IMCRs), a common subset of MCRs which have been thoroughly explored within the synthesis of pharmaceuticals and natural products.[85]

2.5 The Passerini reaction

The first IMCR, the Passerini reaction was discovered in 1921.[86,87] The Passerini reaction combines aldehyde (or ketone), carboxylic acid and isocyanide starting materials to generate *α*-acyloxy carboxamide products, **87**. An alternative variant of the Passerini reaction has also been developed using titanium tetrachloride ($TiCl_4$) to produce *α*-hydroxy amides, through the metal-mediated combination of an isocyanide and a ketone (or aldehyde) reagent.[88]

Generally, high concentrations of each of the starting materials is favourable for formation of the desired product, and low temperature reaction conditions are used to mitigate against the formation of undesired side-products.

The mechanism has been the subject of much debate.[89-91] Early kinetic experiments were found to be first order in relation to each of the three reaction components.[90] The mechanism is thought to be non-ionic. This hypothesis is supported by the fact that the Passerini reaction is accelerated in non-polar solvents.[92] A plausible reaction mechanism which satisfies both of these observations is shown in **Scheme 2.10**.[92]

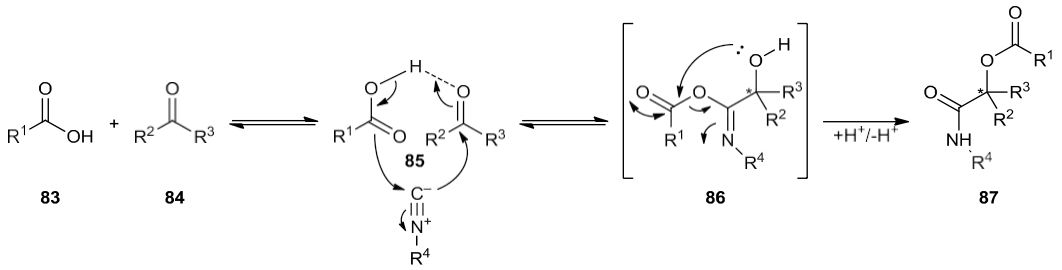

Scheme 2.10: Plausible non-ionic mechanism for the Passerini reaction which supports experimental findings.

During the reaction, following the formation of a H-bonded ternary complex between the carboxylic acid **83** and a further carbonyl-derived reagent **84**, a reversible 1,1-addition of the isocyanide to both reagents, through the terminal carbon, generates intermediate **86**, which is not isolable, and through an intramolecular transacylation rearrangement and subsequent tautomerisation, readily becomes *α*-acyloxy carboxamide product **87**.

However, in a more recent publication, using formic acid, formaldehyde and methyl isocyanide as simple reactants, Maeda *et al*. have presented a quantum chemical study of all potential Passerini reaction pathways.[93] Interestingly, their findings explain that the actual reaction mechanism must occur in a way differing to the one shown in **Scheme 2.10**, since the intermediate **86** rearranges too quickly to be observed experimentally, and yet the expected

reaction coordinate for the above pathway contains transition states with energy barriers too high to explain this (160.1 kJ mol^{-1}, 147.5 kJ mol^{-1} and 124.2 kJ mol^{-1}).[93,94]

No feasible mechanism utilising only three molecules was found which satisfied experimental findings, based on observed energy values. In fact, an extra formic acid molecule was found to be hugely influential in lowering the energy of the reaction pathway. The mechanism shown in **Scheme 2.11** was consequently suggested for the model reaction studied.

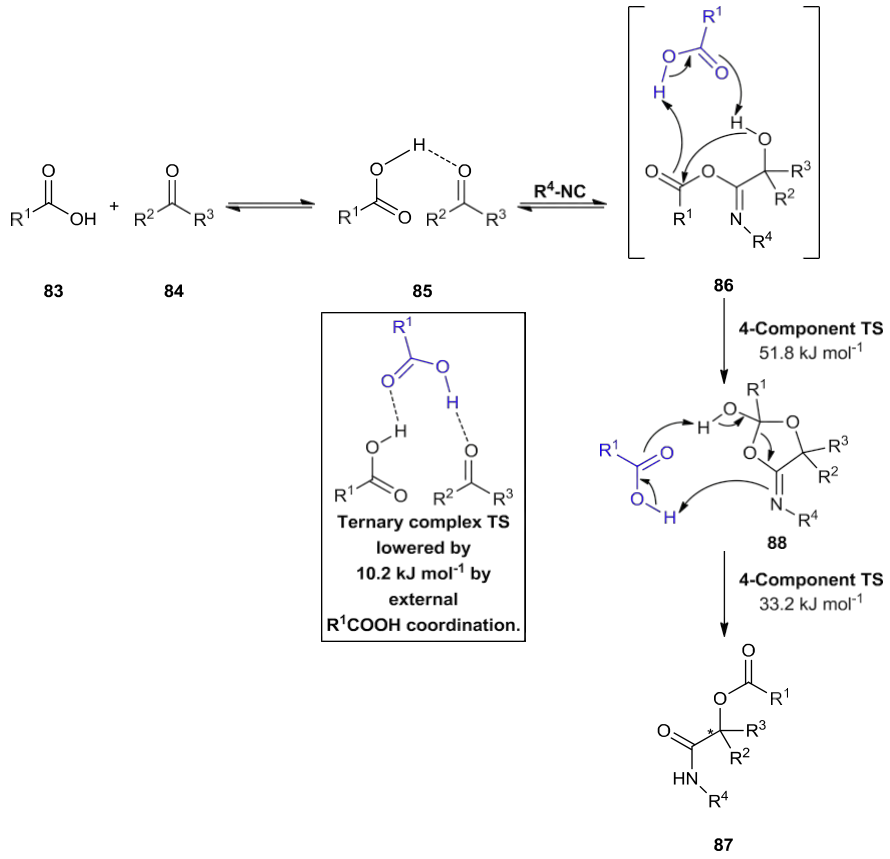

Scheme 2.11 Passerini reaction mechanism as determined through quantum chemical analysis. The involvement of an extra carboxylic acid molecule (blue) substantially lowers the transition state energies for the reaction pathway.

The reaction mechanism in **Scheme 2.11** involves the initial formation of the H-bonded cluster, **85**, in accordance with **Scheme 2.10**. Additionally, the subsequent reaction between the isocyanide and **85** affords **86** as previously established. Yet, although not critical, further coordination to another molecule of the carboxylic acid at this stage is predicted to lower the transition state energy by 10.2 kJ mol^{-1}.[93]

The main mechanistic differences, however, arise during the final bond rearrangement steps. The carboxylic acid was predicted to act as both a H-bond acceptor and donor for **86** to facilitate the intramolecular transacylation reaction, *via* formation of 2-hydroxy-4-imino

acetal **88**. Tautomerisation and the succeeding ring-opening of **88**, again by using the acid component as a proton shuttle, then affords the desired product **87**.[93]

These two steps hence both involve 4-component transition states, and have energetic barriers which are substantially reduced (51.8 kJ mol^{-1} and 33.2 kJ mol^{-1}, respectively compared to 160.1 kJ mol^{-1}, 147.5 kJ mol^{-1} and 124.2 kJ mol^{-1}) in comparison to the reaction pathway not involving another molecule of the carboxylic acid.[93]

Various enantioselective approaches to the Passerini reaction have been attempted. These include stereochemical induction using chiral auxiliaries and chiral isocyanides, with varying degrees of success.[95-98]

Nevertheless, chiral catalysis has proven useful in introducing stereochemical control to Passerini-like reactions. The first published method used the Lewis basic chiral bis-phosphoramide catalyst, **94**. When using 5 mol% of the catalyst, along with stoichiometric silicon tetrachloride ($SiCl_4$), the addition of isocyanide reagents to aldehydes was performed enantioselectively to produce *α*-hydroxycarboxamide products (**92**, **Scheme 2.12**).[99] Heating of the reaction mixture in the presence of methanol and base facilitated the isolation of the analogous *α*-hydroxymethyl esters **93** in enantiomeric excess of 64% to > 98% (*S*:*R*).

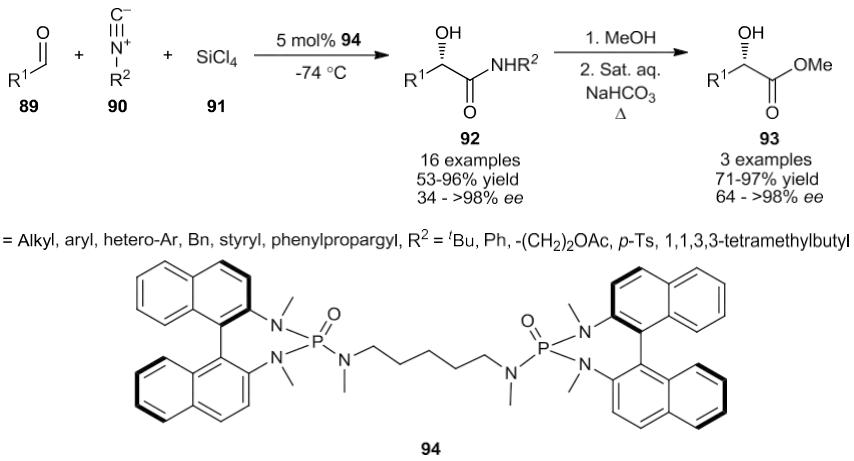

Scheme 2.12: The first published chiral Lewis base catalyst for a Passerini-like reaction.

More recently, an aluminium salen Lewis acid complex **100** has been used in a general enantioselective approach to the Passerini reaction.[100] Unlike earlier developments, the procedure tolerates non-chelating aldehydes, and also the presence of the carboxylic acid component in the reaction.[101] The method provides access to *α*-acyloxycarboxamides in good to excellent enantioselectivity (*ee* = 63 to > 99%).

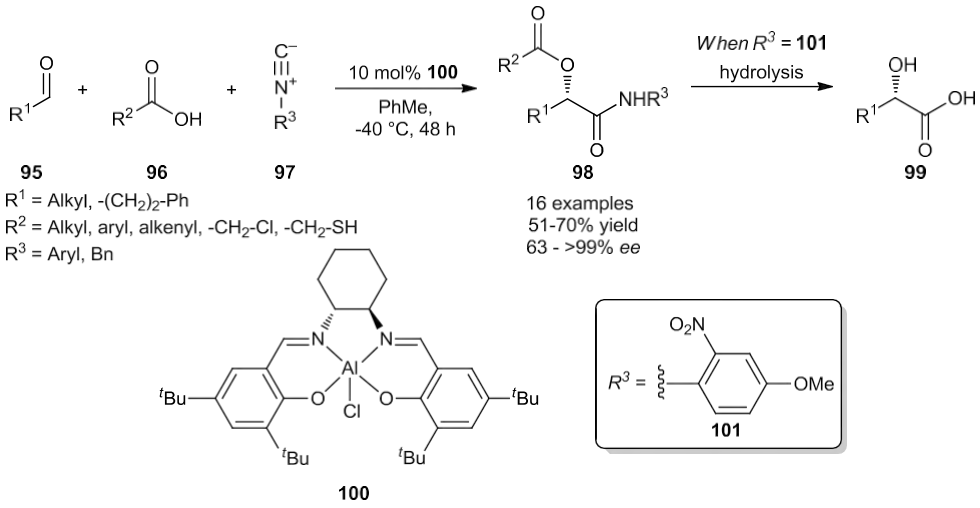

Scheme 2.13: Enantioselective Passerini reaction using an aluminium salen chiral complex, 100. When a convertible isocyanide (101) was used, the authors imply that this procedure affords potential access to chiral *α*-hydroxyacids (99).

In this process, through the use of a convertible isocyanide such as **101**, chiral *α*-hydroxyacids can be acquired following hydrolysis under basic conditions. Convertible isocyanides (also called “universal isocyanides”) are reactive components which can be utilised in isocyanide containing reactions, such as IMCRs, and subsequently enable the derivatisation of formed products.[102] This hence further enhances the synthetic utility of isocyanide reagents in generating compound libraries.

Unfortunately, the synthetic method shown in **Scheme 2.13** was unsuccessful when using aromatic aldehydes, and only delivered a racemic product in the use of a sterically encumbered aldehyde reagent, pivaldehyde. Zhang *et al.* later reported the enantioselective Passerini reaction through the use of chiral phosphoric acids as catalysts, which overcomes both of these issues (**Scheme 2.14**).[103]

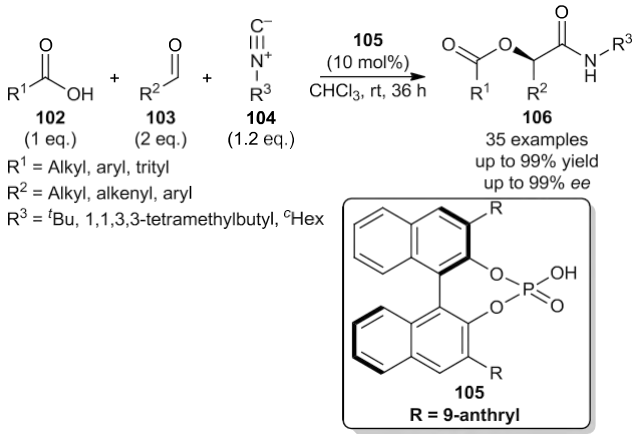

Scheme 2.14: The enantioselective Passerini reaction reported by Zhang *et al.*[103]

Good to excellent enantioselectivity is observed in a large substrate scope, and the reaction has been performed successfully on gram scale, making the access to enantiopure Passerini products facile, even on large scale.

2.6 The Ugi reaction

Following on from the discovery of the Passerini reaction, Ivar Ugi introduced a related four-component reaction in 1959, which was later named the Ugi reaction.[104] The traditional Ugi reaction combines amine, carboxylic acid, aldehyde and isocyanide components to generate *α*-amido carboxamides (**111**), in an analogous aza-equivalent to the reaction shown in **Scheme 2.10**. The simplified mechanism for the 4-component Ugi reaction is shown in **Scheme 2.15**.

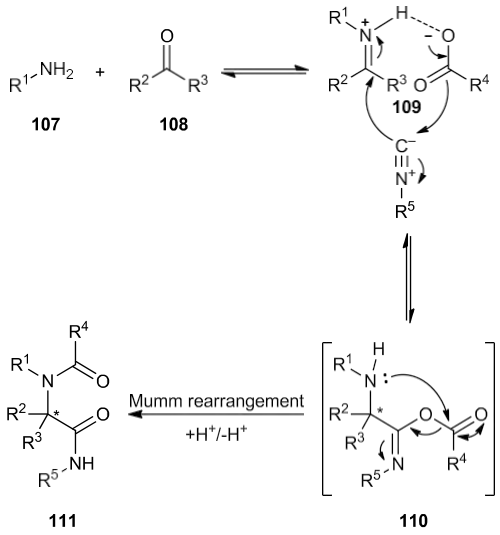

Scheme 2.15: Reaction mechanism for the original Ugi 4-component reaction. The isocyanide attacks a pre-formed iminium intermediate. Following an intramolecular transamidation from 110 (known as a Mumm rearrangement), and resultant proton transfer, α-amido carboxamide products (111) are afforded.

The reaction mechanism proceeds in a comparable way to the Passerini reaction overall. However, the H-bonded complex is this time formed between the acid component and the iminium species, made from the condensation of the amine and carbonyl reagents under acidic conditions.

Following the *α*-addition of the isocyanide into the ternary complex, the desired products are furnished following an intramolecular transamidation reaction (also known as a Mumm rearrangement).[105,106] Again, the precise reaction mechanism has been a subject of debate. The order of the addition has been hypothesised as either taking place through an initial coupling of the imine intermediate with the carboxylic acid component or the isocyanide component (***reaction paths a*** and ***b***, respectively, **Scheme 2.16**).[107,108] ***Reaction path a*** requires an ensuing isocyanide insertion to form intermediate **110**.

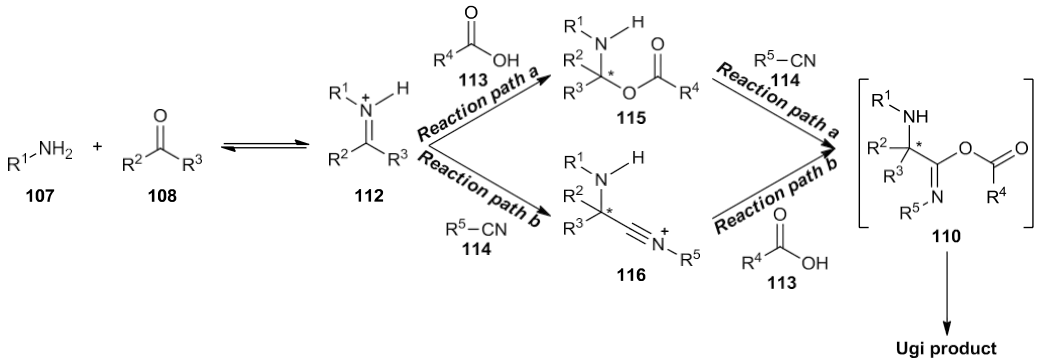

Scheme 2.16: Potential pathways for the Ugi reaction. Ivar Ugi's originally suggested mechanism, involving the formation of nitrilium intermediate 116, prior to nucleophilic attack from the carboxylate ion, is the most likely according to experimental findings and computational calculations.

Computational data, as well as experimental findings from the use of ESI-MS/MS analysis, support the reaction mechanism proceeding *via* the formation of nitrilium intermediate **116**, and thus *via* ***reaction path* b** in the rate-determining step of the reaction.[107,108] The other steps involved in the reaction are well established, since isolation of the (pre-Mumm rearrangement) 2-aminoimidic anhydride intermediate (**110**) has been accomplished, and imine formation was observed rapidly, even in the presence of the other reaction components.[108,109]

Based on these findings, as well as the acceleration of the reaction in polar protic solvents, the reaction is believed to proceed through the aforementioned mechanism, with the carboxylate addition into the nitrilium ion happening readily since the reactants form an ion-pair in solution.[107] As observed in the Passerini reaction, high concentrations of the reactants and low temperatures favour the selective formation of the Ugi products and reduce side-product formation. Pre-formation of the iminium intermediate also helps to reduce any undesired side-reactions observed.

Due to the possible variations in each of the reaction components, as well as the relevance of the afforded products and their derivatives in medicinal chemistry and organic synthesis, the Ugi reaction has been explored extensively in many synthetic methodologies, natural product syntheses, pharmaceutical applications and library syntheses.[91,110]

The Ugi reaction has been performed in flow for various investigative studies. For example, Petasis (boron Mannich) and Ugi reactions have been performed in tandem within a microfluidic reactor.[111] This complex combined reaction gives access to multidimensional libraries of dipeptide products (**121**), as outlined in **Scheme 2.17**.[111,112] Performing the procedure within two connected microreactors resulted in massively accelerated reaction optimisation, with minimal physical manipulation of the equipment. Compared to a combined reaction time of ~3 days in batch, less than 20 minutes was required for each MCR when performed in flow.[111]

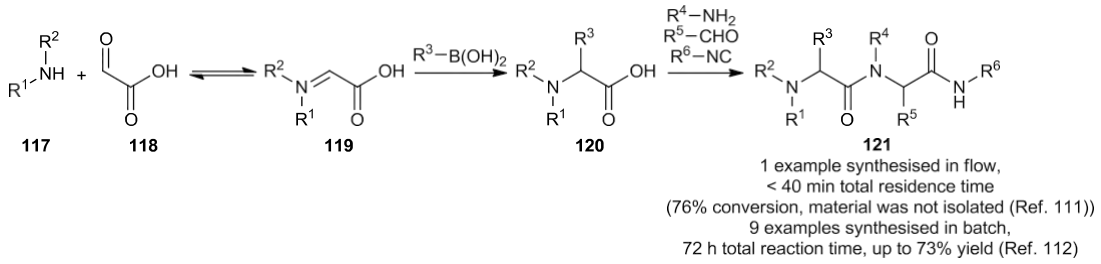

Scheme 2.17: General scheme for the tandem Petasis (boron Mannich) and Ugi reaction procedures. The reaction series gives access to a large array of heavily functionalised dipeptide products (121).

Furthermore, other series of reactions were targeted by Sharma *et al.* In a novel flow approach, the *in situ* preparation of isocyanides from formamides, and their subsequent utility in either Passerini or Ugi reactions could be performed, with minimal exposure to the malodorous isocyanide reagents (**Scheme 2.18**).[113]

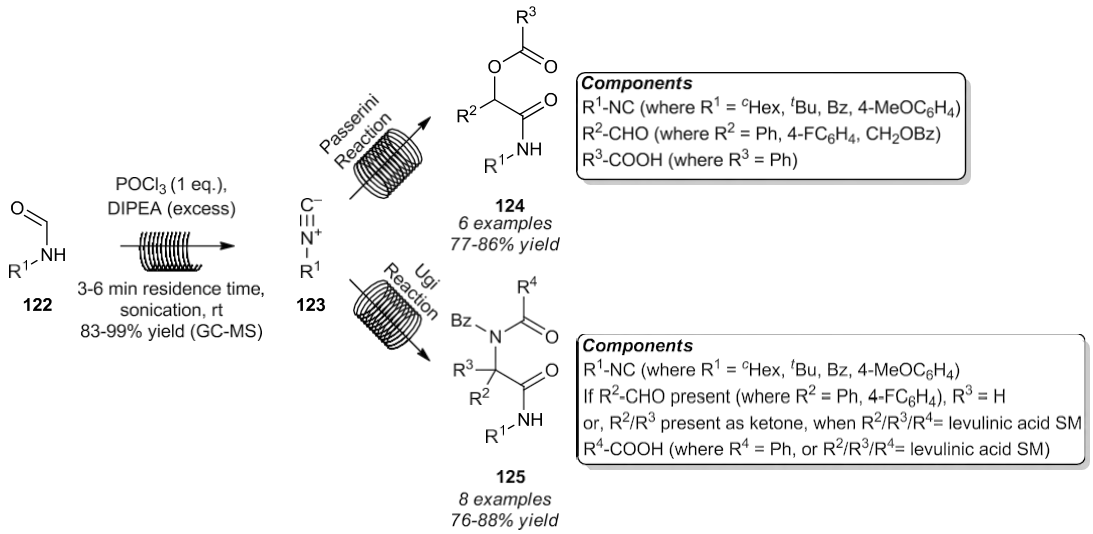

Scheme 2.18: The *in situ* tandem formation/reaction sequence of isocyanides in flow. Isocyanides (123) were prepared from formamide reagents (122), prior to their use in either Passerini or Ugi reactions.

In a very recent publication, the issue of exquisitely controlling the enantioselective control of the Ugi reaction may have finally been resolved. Following developing highly enantioselective catalysts for the Passerini reaction, Zhang *et al*. have once again used chiral phosphoric acid catalysis, this time to selectively synthesise chiral *α*-amido carboxamides.[114] Over 40 examples are demonstrated for each enantiomer, with broad substrate scope tolerance and yields (up to 96% for both enantiomers), as well as outstanding enantioselectivity (up to 99% *ee* for one isomer (**131**) and up to 94% *ee* for the other (**132**), **Scheme 2.19**).

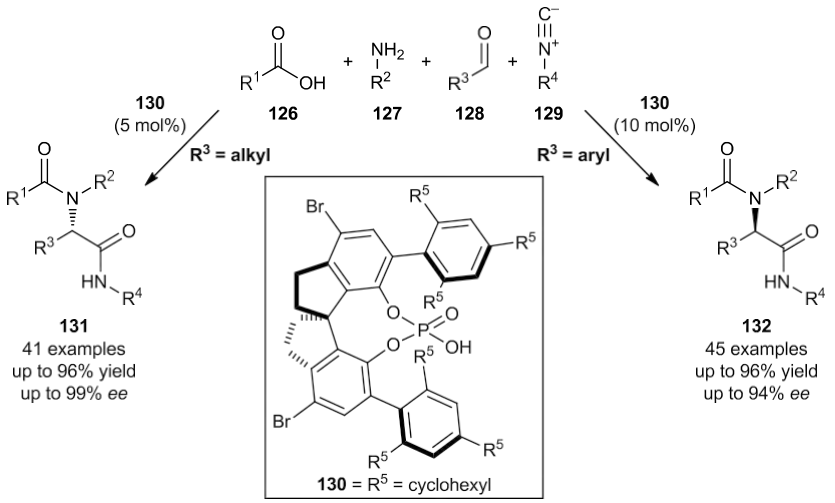

Scheme 2.19: Enantioselective Ugi reaction. The Ugi reaction has recently been performed on an extensive substrate scope under mild conditions using chiral phosphoric acid organocatalyst, 130.

The authors explain that stereocontrol originates from 4 key points in the design of the chiral phosphoric acid (**130**). Firstly, the structure of the chiral phosphoric acid determines the shape of the chiral pocket in which the iminium intermediate resides. The enhanced acidity of the phosphoric acid catalyst in comparison to the carboxylic acid component means that catalyst-mediated iminium activation is favoured over the uncatalysed background reaction. In the use of aryl aldehydes, the enantioselectivity of catalyst **130** was studied by DFT calculations, and the aryl functionality was determined (by also using crystallographic methods) to sit in the pocket between cyclohexyl substituents on the catalyst and form important non-covalent bonding interactions within the reagent-catalyst complex. As a result of this interaction, the use of aryl aldehydes in the reaction procedure affords the opposite enantiomer to that favoured with alkyl aldehyde starting materials. When alkyl aldehydes are used, steric effects of the catalyst are the predominant factor involved in stereoinduction.

Another result of the activation of the iminium intermediate is an increase in its electrophilicity in relation to the carbonyl component prior to condensation. This allows the reactions to be performed without the necessity of prior formation of the imine intermediate, which would otherwise be required to prevent the formation of the undesired Passerini side-product.

Moreover, the proficiency of the catalysts is further enhanced through their ability to also act as H-bond acceptors. This ensures their complexation with the carboxylic acid component and resultantly increases the nucleophilicity of the acid component, again favouring the Ugi reaction pathway.

The scope of the Ugi reaction can be increased to include secondary amines through the use of an aminoborane additive (**Scheme 2.20**).[115] In this procedure, the carboxylic acid component is not required, and the work is formally described as a three-component reaction.

Aminoborane **134** is used to synthesise an activated iminium intermediate (**137**) in the reaction, which is subsequently attacked by the isocyanide.

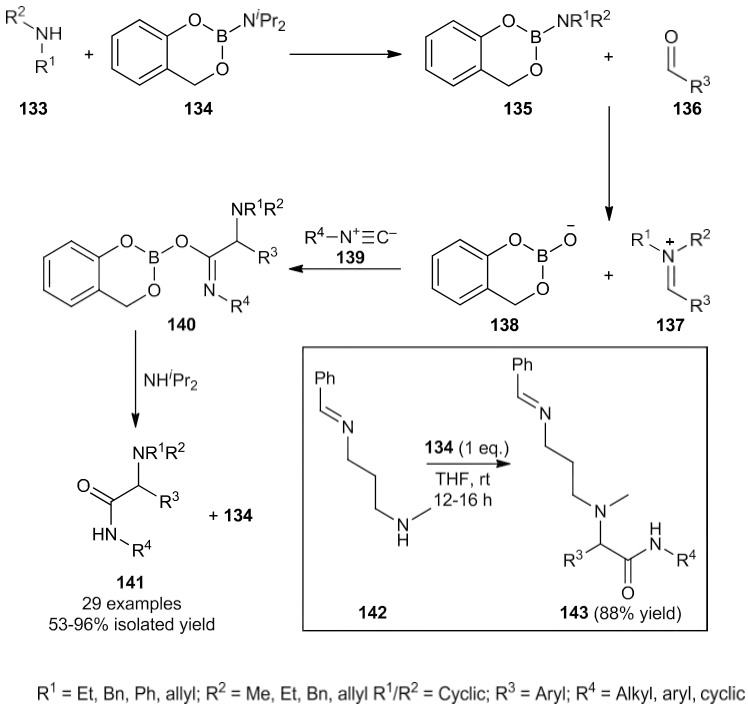

Scheme 2.20: The formation of *α*-amino carboxamides *via* the 3-component Ugi reaction with addition of an aminoborane (134).

The nitrilium intermediate is then attacked by the boronoxide generated (**138**). A subsequent aminolysis affords the desired product and regenerates the active aminoborane additive. As a result of the non-acidic conditions used in the reaction, even a secondary amine (such as in product **143**) with distant imine functionality is tolerated, with the Ugi reaction occurring regioselectively on the iminium ion generated from use of the aminoborane (**Scheme 2.20**).

List and co-workers later proved that the same products could be generated through the catalytic use of phenyl phosphinic acid. In this case, the formed nitrilium intermediate is attacked from water in the reaction system, likely extruded from the initial condensation of the amine and carbonyl reagents.[116]

The nitrilium Ugi intermediate can be intercepted with a plethora of potential nucleophiles, in both an intramolecular and intermolecular fashion. In fact, substitution of the ‘acid’ component leads to a multitude of synthetic opportunities.

These reactions are frequently known as Ugi-like multicomponent reactions, as a result of similarities shared in some of their reaction components, and initial mechanistic steps. Some examples of acid components used in Ugi-like multicomponent reactions to attack nitrilium ions are shown in **Scheme 2.21**.[91,117-119]

GSK CONFIDENTIAL INFORMATION – DO NOT COPY

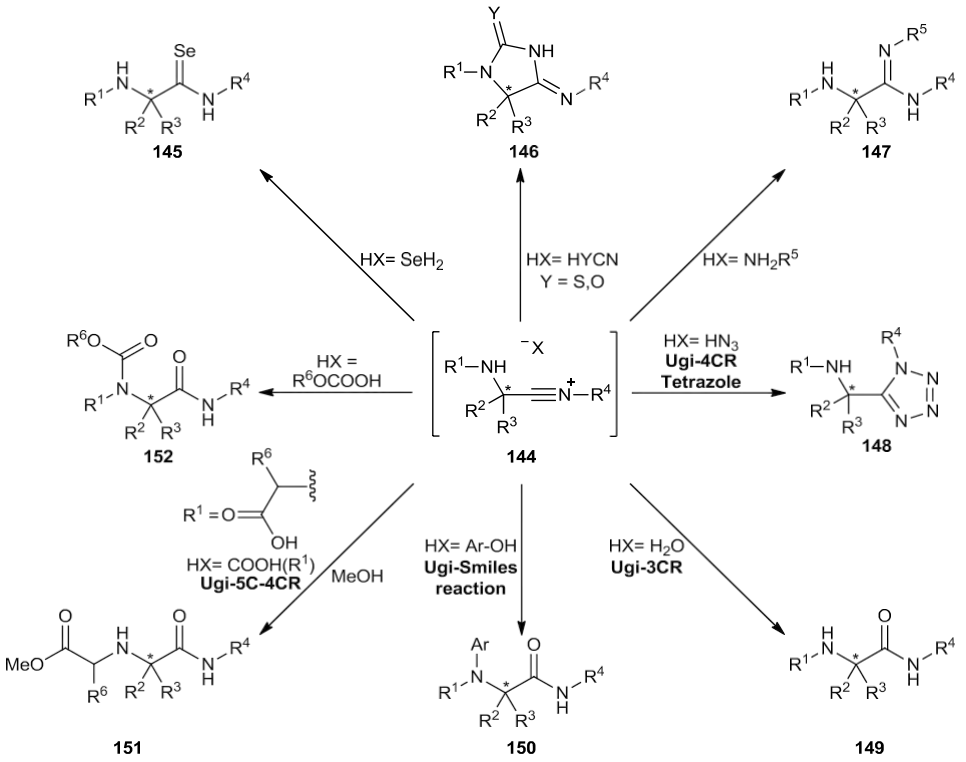

Scheme 2.21: Some products made from Ugi-like multicomponent reactions made through variation of the acid component.

If the iminium intermediate is instead formed from the condensation of an aldehyde component with an aromatic amidine reagent, the resultant isocyanide addition leads to the formation of aminated heterocycles. This reaction is known as the Groebke-Blackburn-Bienaymé reaction (GBBR) and will be the focus of the first chapter of the work presented herein.

2.7 The Groebke-Blackburn-Bienaymé reaction (GBBR) and other syntheses of aminated imidazoheterocycles

The Groebke-Blackburn-Bienaymé reaction (GBBR) is another type of Ugi-like multicomponent reaction and was discovered towards the end of the 20th century by three independent research groups.[120-122]

The GBBR combines aromatic amidine (**153**), aldehyde (**154**) and isocyanide (**155**) components in a single process to generate 3-aminoimidazoheterocycles (**156**), such as 3-aminoimidazo[1,2-*a*]pyridines, 3-aminoimidazo[1,2-*a*]pyrazines and 3-aminoimidazo[1,2-*a*]pyrimidines (**Scheme 2.22**).

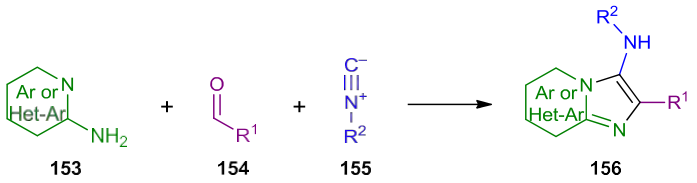

153 154 155 156

Scheme 2.22: General scheme for the GBBR. The combination of amidine, aldehyde and isocyanide reagents generates 3-aminoimidazoheterocyclic products. The scheme is colour coded to indicate how the compound is assembled.

The products of the GBBR are extremely relevant within medicinal chemistry. For instance, the GBBR has been utilised in the synthesis of compounds which demonstrate use in indications including cancer, inflammation, bacterial infections, HIV, cancer-induced osteoporosis, Alzheimer's disease and diabetes.[123-129]

Moreover, fused imidazoheterocyclic ring systems are ubiquitous within medicinal chemistry. The cardiotonic Olprinone, the antimalarial probe KA1407, and Zolpidem, a frequently prescribed anti-xylotic agent, are all examples of bioactive molecules containing imidazoheterocyclic motifs within their core structure.[130-132]

Importantly, aminated derivatives of imidazoheterocycles, such as those afforded from the GBBR have also begun to see commercial application. Compounds **157** and **158** (**Figure 2.5**) have been patented for anti-inflammatory and GLP-1 fusion peptide component uses, respectively.[133,134] As such, there is a demand for useful preparative methods of amino-imidazoheterocycles for the medicinal chemistry community.

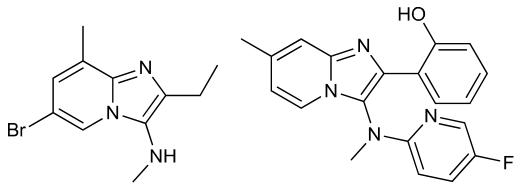

157 158

Figure 2.5: Examples of 3-aminoimidazoheterocycles patented for use in medicinal chemistry applications.

Following on from the initial discovery of the GBBR, many developments have been made in the area. The GBBR has been catalysed by a range of Lewis and Brønsted acids, it has been performed under microwave irradiation and by using ionic liquids as both solvents and catalysts for the reaction.[120-122,135-138]

In 2001, universal rink-isonitrile resin was applied for the GBBR.[139] This solid-supported reagent facilitated the effective production of 3-aminoimidazo[1,2-*a*]pyridine products with traceless cleavage of the resin. The generated products were cleaved in a reaction with acyl

chloride reagents to form 3-acylaminoimidazo[1,2-*a*]pyridine derivates in a facile, one-pot process.

A more recent development by Vidyacharan *et al.* has focused on performing the GBBR in solvent and catalyst-free conditions (**Scheme 2.23**).[140] The reaction combines amidine, aldehyde and isocyanide reagents in a one-pot procedure to afford GBBR products in high yield. Although beneficial from a sustainability standpoint, the reaction procedure has limited scalability, requires a reaction temperature of 160 °C, and is very restricted in regard to the suitable starting materials, since a lack of solvent dictates that at least one of the reagents is required as a liquid, and the reaction mixture should form a solution *in situ*.

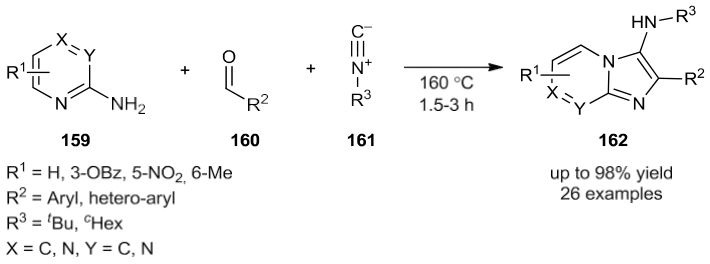

Scheme 2.23: General scheme for the solvent and catalyst-free conditions for the GBBR.

Two flow procedures for the GBBR have been published in the literature. The aim of the first is to control the regioselectivity observed in the reaction of 2-aminopyrimidines in the GBBR.[141] The use of 2-aminopyrimidines as the amidine reagent can generate two regioisomers, as a result of whether the imine intermediate is formed on the endocyclic or exocyclic nitrogen prior to cyclisation (**Scheme 2.24**).

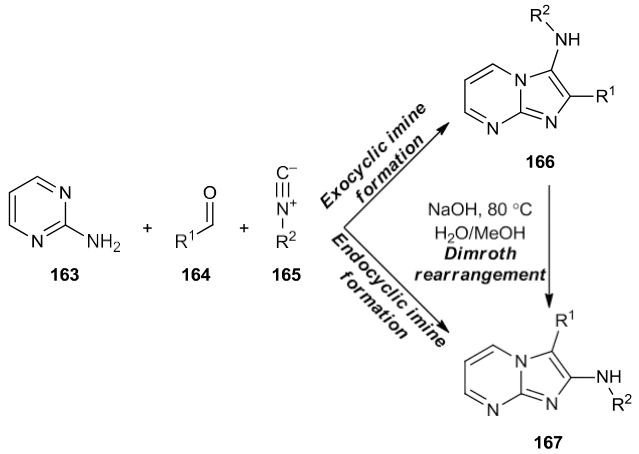

Scheme 2.24: General scheme for the possible products from the Groebke-Blackburn-Bienaymé reaction between 2-aminopyrimidines, aldehydes and isocyanides. Interconversion from the 3-aminoimidazo [1,2-*a*]pyrimidine product (166) to the 2-amino[1,2-*a*]imidazopyrimidine side-product (167) can be achieved through a Dimroth rearrangement with sodium hydroxide at 80 °C.[142]

In this publication, through optimisation of the catalyst ($ZrCl_4$), and temperature of the reaction, the authors report a regioselective method for the synthesis of 3-aminoimidazo[1,2-*a*]pyrimidines.[141] Moderate yields (up to 61%) are observed throughout this study, including a few examples of products with (usually unattainable) alkyl substituents in the 2-position of the imidazoheterocycle. However, once again these materials were isolated in low yields (27% and 32%).

Though allowing access to some novel materials, albeit with variable yields, the methodology only employs 2-aminopyridimine reagents as the amidine component for the reaction, thereby limiting the robustness of the procedure. Additionally, the reactions are performed by utilising both a metal catalyst ($ZrCl_4$), and a solvent mixture containing dichloromethane. Therefore, the use of these conditions could pose sustainability issues when executing the reaction on large scale, due to the significant amount of metallic and halogenated waste which would be generated. These waste materials often require specific treatment protocols, which may be expensive, and require substantial time and energy to implement.

Various catalysts have been explored as a way to control the regioselectivity of the reaction, and it has also been reported that a Dimroth rearrangement of the 3-aminoimidazo[1,2-*a*]pyrimidine product can afford the other isomer (**Scheme 2.24**).[142]

The second flow procedure, by Reutlinger *et al*. employs microfluidic chips (~16 mm in size) to quickly optimise the GBBR for small scale application.[143] The products generated here are identified as potential G protein-coupled receptor (GPCR) ligands. The reactions were rapid, being heated (or superheated) for only a few seconds, although the scope is very limited and variable yields were afforded. Moreover, the application of the approach may be limited in large scale syntheses, due to the explosive nature of perchloric acid at high temperatures,[144] and since alternative flow equipment would also have to be utilised (**Scheme 2.25**). Poor yields are typically observed in the publication, and greatly inhibit its potential use as a general process for performing the GBBR in flow.

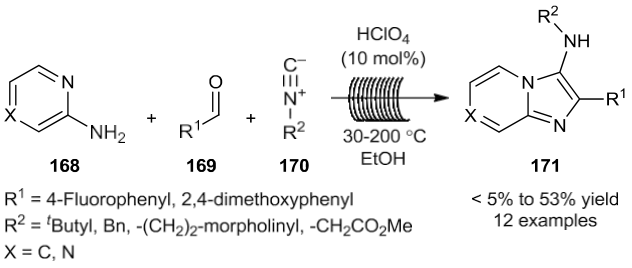

Scheme 2.25: General scheme for the microfluidic synthesis of 3-aminoimidazo[1,2-*a*]pyridines and3-aminoimidazo[1,2-*a*]pyrazines as G protein-coupled receptor (GPCR) ligands.

Despite these drawbacks, the publication demonstrates the benefit of using microfluidic flow chemistry in early stage library syntheses, since a range of medicinally-relevant derivatives could be produced in short timescales.

A similar general approach has been applied in ***Chapter 2: A telescoped, continuous flow synthesis of diaminoquinazoline antimalarials*.**

Aside from the GBBR, various other methods also exist for the synthesis of the 3-amino imidazoheterocycles similar to those attained from the GBBR process. For example, Ramesha *et al.* reported the synthesis of such targets through the coupling of 2-aminopyridine, benzyl alcohol and isocyanide reagents in the presence of the oxidative mixture of propylphosphonic anhydride (T3P) in dimethyl sulfoxide (DMSO).[145]

During the course of the reaction, an *in situ* oxidation of the alcohol reagent generates a benzylic aldehyde, which consequently reacts through a GBBR process to generate the desired products.

Use of this protocol may provide access to an extended number of GBBR products, where the relevant aldehyde precursors are not readily available. However, the procedure introduces extra complexity in comparison to the GBBR method alone, and has a limited substrate scope, having only been demonstrated on a few isocyanide reagents, and benzyl and *α*-heteroaromatic substituted primary alcohols.

In a related publication, the aldehyde reagent can also be substituted for benzyl halide or benzyl tosylate precursors. In a similar suggested mechanism to that described for alcohol reagents, the aldehyde reactants required for the GBBR are produced *in situ* from benzyl halides or benzyl tosylates *via* a Kornblum oxidation.[146] A general scheme for this method is shown in **Scheme 2.26**.

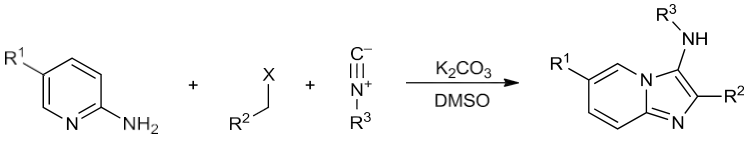

172 **173** **174** **175**

R^1 = H, Me, Br
R^2 = CH_2-aryl
R^3 = Alkyl, Bn
X = Br, Cl, OTs

88-96% yield
20 examples

Scheme 2.26: Formation of 3-aminoimidazo[1,2-*a*]pyridines through the MCR of a benzyl halide or tosylate, 2-aminopyridine and an isocyanide.

Excellent yields are afforded in all cases, and both electron-withdrawing groups and electron-donating groups are well tolerated on the halide (or tosyl) reagent. However, only aminopyridine reagents have been utilised as the amidine component of the reaction.

Alternative synthetic strategies have also been sought for the generation of libraries of 3-aminoimidazoheterocycles. An example procedure by Katritzky and co-workers forms 3-aminoimidazoheteroaromatic compounds through the reaction of either 2-aminopyridines, 2-aminopyrimidines or 4-aminopyrimidines, with 1,2-bis(benzotriazolyl)-1,2-(dialkylamino) ethane reagents (**177**, **Scheme 2.27**).[147]

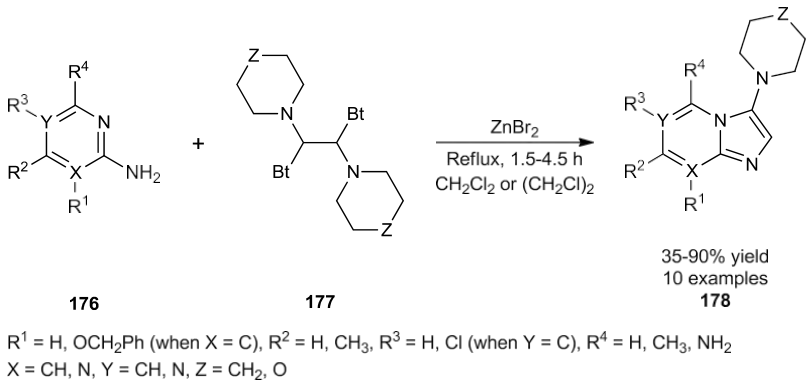

Scheme 2.27: The synthesis of 3-aminoimidazoheterocycles by Katritzky *et al.* using a $ZnBr_2$ catalysed cyclisation with a bis(benzotriazolyl)diaminoethane reagent (177).

While the reaction facilitates the synthesis of tertiary amine products not accessible by the GBBR, it also has the prerequisite for the synthesis of **177** and poor atom economy, since half of the reagent is not utilised in the reaction.

Another synthetic route uses molecular iodine and DMSO to oxidise aryl ketones (**179**) into 1,2-dicarbonyl reagents. A subsequent condensation with 2 molecules of a 2-aminopyridine reagent, and a resulting cyclisation then leads to 2-aryl-3-aminoimidazo[1,2-*a*]pyridine derivatives.[148]

Unfortunately, despite not requiring the use of metal catalysts, the reaction is limited, as only aminopyridine reagents were employed as successful nucleophiles and both aminopyridine reagents involved in the reaction are identical, limiting product scope exclusively to bis-substituted 2-aminopyridine derivatives (**Scheme 2.28**).

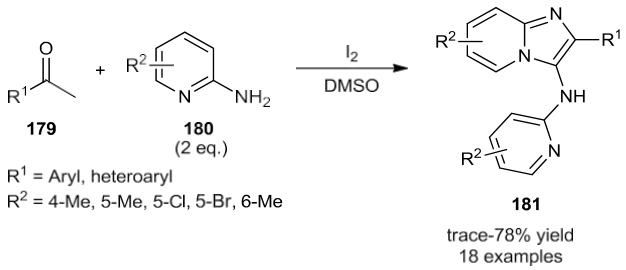

Scheme 2.28: Oxidative coupling of aryl aldehydes with 2-aminopyridines to synthesise 2-aryl-3-(pyridine-2-ylamino)imidazo[1,2-*a*]pyridines.

In another publication, a one-pot, two-step process to afford *N*-(imidazo[1,2-*a*]pyridin-3-yl) sulfonamides has been reported. Here, aryl glyoxylates (**182**) first react reversibly with primary sulfonamide reagents (**183**) to form aminals **184**. Following nucleophilic attack from 2-aminopyridine reagents and a consequential ring closure, a range of sulfonylated 3-aminoimidazo[1,2-*a*]pyridine products are delivered (**186**, **Scheme 2.29**).[149]

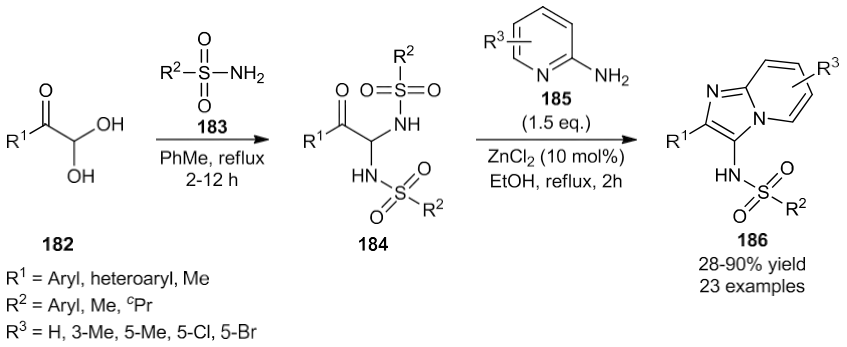

Scheme 2.29: Preparative method for the synthesis of *N*-(imidazo[1,2-*a*]pyridin-3-yl) sulfonamides.

Electron-rich sulfonamides performed best within this procedure, which gives direct access to sulfonylated derivatives of products similar to those obtained by the GBBR. However, observed yields are substantially decreased when using alkyl glyoxylates and the reaction suffers from a limited substrate scope around the amidine reagent.

β-Lactam carbenes may also be employed to generate 2-carbonyl-3-aminoimidazo[1,2-*a*] pyridines, which could be used as fluorescent probes (**Scheme 2.30**).[150] 2-Pyridinyl isonitrile reagents (**189**) are combined *via* the use of a *β*-lactam carbene. Following a cyclisation, *β*-lactam ring opening under acidic conditions, and a 1,5-*H* shift, the desired products were afforded in 41-84% yields.

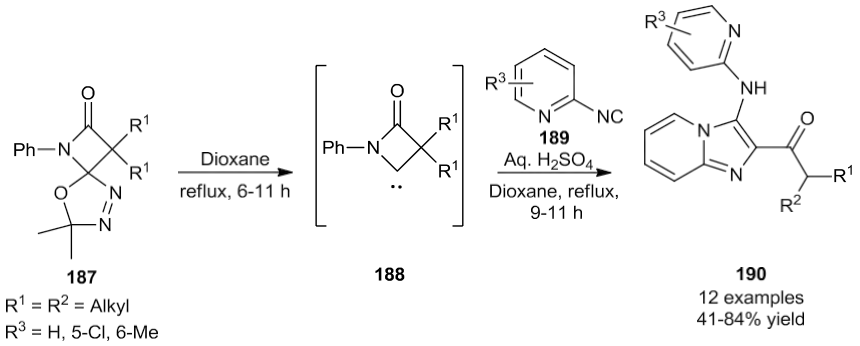

Scheme 2.30: Synthesis of 2-carbonyl-3-aminoimidazo[1,2-*a*]pyridines from *β*-lactam carbenes regents.

Potentially useful 2-carbonyl derivatives are synthesised from this procedure, however, the prior synthesis of the *β*-lactam carbene precursor is required and only 2-isocyanopyridine and two structurally similar isocyanides were employed as part of this reported process.

A different synthetic approach was adopted by Charette and co-workers, who divulged the cyclisation of *α*-aminopyridinyl amides using triflic anhydride in the presence of 2-methoxypyridine (**Scheme 2.31**).[151] The method allows for the production of 3-aminoimidazoheterocycles which can be unsubstituted at the 2-position, which is seldom seen in publications describing the Groebke-Blackburn-Bienaymé reaction.

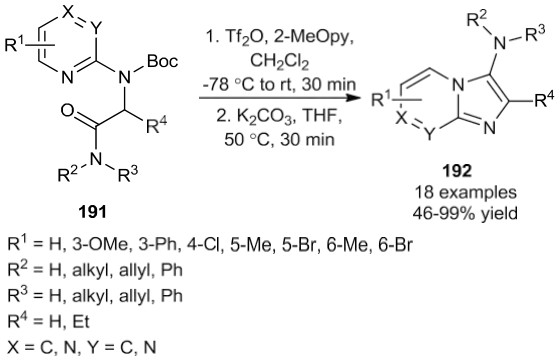

Scheme 2.31: The synthesis of 3-aminoimidazoheterocycles from the cyclisation of *α*-aminopyridinyl amides.

Tertiary amine products are easily made in the reaction illustrated in **Scheme 2.31**, which are not possible from the GBBR. On the other hand, several synthetic steps are required for preparation of the *α*-aminopyridinyl amide starting materials, meaning the process is less suitable to library syntheses.

A comparable cyclisation technique has more recently been applied to different 4-substituted 2-(*α*-carboxamide)aminopyrimidine reagents to regioselectively form either the resultant 5- or 7-substituted imidazo[1,2-*a*]pyrimidine cyclised products.[152]

Finally, Adiyala *et al*. reported the synthesis of imidazo[1,2-*a*]pyridines from the reaction of *α*-keto vinyl azides (**193**) with 2-aminopyridines (**194**, **Scheme 2.32**).[153] The reaction gives a one-pot procedure for the synthesis of products equivalent to those produced in the GBBR, but requires the addition of a reducing agent, as the equivalent 3-iminoimidazo[1,2-*a*]pyridines are otherwise observed.

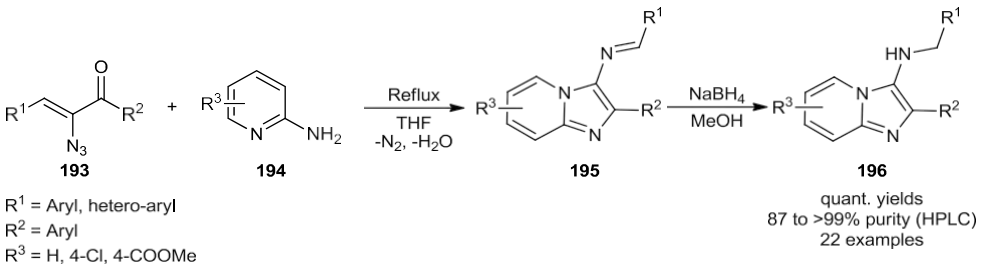

Scheme 2.32: The synthesis of 3-aminoimidazo[1,2-*a*]pyridines from *α*-keto vinyl azides.

Nevertheless, the reaction boasts excellent yields and does not require purification other than solvent removal. As well as the additional reduction step, problems facing the commercial application of the process include the synthesis and use of potentially explosive azide starting materials, especially on large scale, and the requirement for aryl substituents on the *α*-keto vinyl azides reagents to prevent degradation and by-product formation.

The proposed mechanism for the formation of intermediate **195** deserves comment, and two potential pathways to describe the mechanism are shown in **Scheme 2.33**. Following the condensation of **193** and **194** to form the unsaturated imine intermediate **197**, nitrogen expulsion is observed during the concomitant azirine formation to produce **198**. At this point, the authors argue that a reaction pathway comprising either a ring-closure (mediated by the pyridine nitrogen), followed by an aziridine ring-opening and product rearomatisation (***reaction path a***), or the formation of nitrilium ion **200**, subsequent intramolecular cyclisation and rearomatisation of the product (***reaction path b***) could result in the desired material, **195**.

GSK CONFIDENTIAL INFORMATION – DO NOT COPY

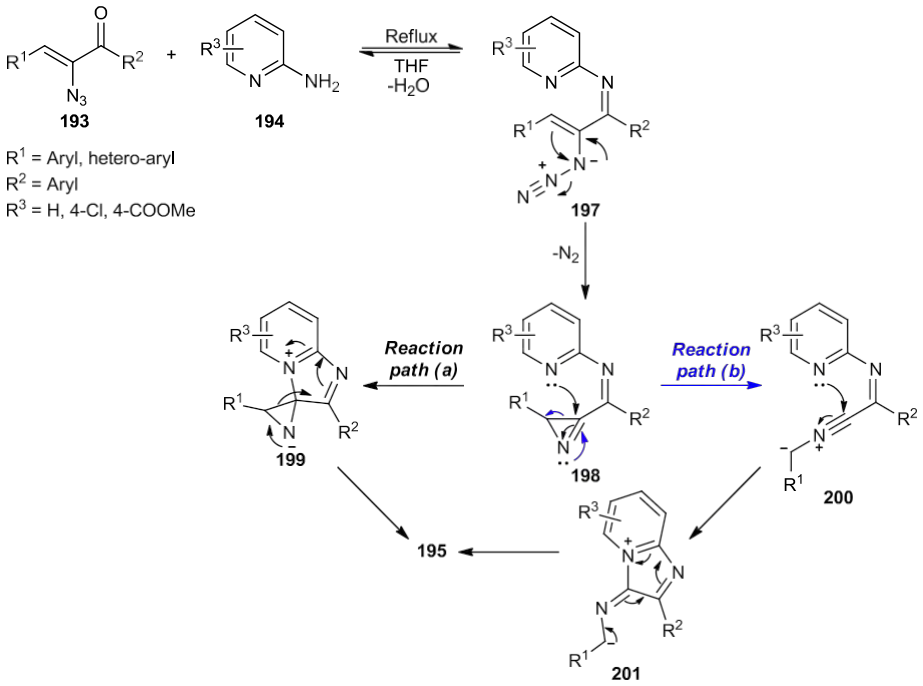

Scheme 2.33: The postulated mechanism for the formation of intermediate 195 from *α*-keto vinyl azides (193).

In conclusion, an assortment of methods exist for the synthesis of 3-amino imidazoheterocycles. However, the GBBR method remains the most promising and potentially widely effective as a result of its convergent nature, which is amenable to library syntheses. As well as this, the products are generated in a single synthetic step, and a range of functionality is tolerated in the reaction components. Though the reaction uses malodorous isocyanide reagents, it often does not require the pre-assembly of starting materials, except in specific applications, and it does not require the use of other inherently dangerous reagents.

2.8 Project aims – Chapter 1: Extension of the GBBR: a green, robust, scalable and efficient continuous flow process to synthesise 3-aminoimidazoheterocycles.

Considering the current literature surrounding GBBR methodology, various important limitations of the reaction were recognised. These include:

- The lack of scalability. Reported examples of the GBBR involve a combination of either long reaction times, metal catalysts or other potentially undesirable acid catalysts (such as perchloric acid), chlorinated solvents or other solvents with toxicity risks and/or microwave-mediated superheating. These issues make the procedures unreliable for large scale chemistry from both sustainability and efficiency perspectives. Therefore, the use of flow chemistry may facilitate the establishment of a rapid and sustainable synthetic procedure which is also scalable to demand.
- The substrate scope of the GBBR. As highlighted, various developments surrounding the GBBR procedure have been reported. Nevertheless, substrate scopes for the reaction often do not cover distinct types of each component. Moreover, the inclusion of formaldehyde and alkyl aldehyde reagents in the GBBR is seldom seen, likely due to by-product formation and generally poor yields.[122,123,141,154-156] In fact, glyoxylic acid is often used as a formaldehyde equivalent in the reaction.[157-159] A general strategy which effectively overcomes these reactivity issues would be highly valuable.
- Variable yields. When changing the reactivity of the reaction components by altering substituents or introducing more heteroatoms into the aromatic components, reduced yields are often observed. This work aims to formulate a flow-based method which provides highly varied GBBR products in practical yields for research and discovery purposes.
- Handling precautions relating to the isocyanide. Despite the versatility of the isocyanide functionality, their malodorous nature often makes them impractical in synthetic use. Ideally, the use of flow chemistry can address this problem by limiting exposure to the isocyanide reagent. Ideally, the preparative method described would also not include a formal work-up procedure, further lessening contact to the isocyanide component.

As a result, the work described herein targets these limitations through the development of a robust, efficient, sustainable and scalable flow synthesis of 3-aminoimidazoheterocycles *via* a Groebke-Blackburn-Bienaymé multicomponent reaction.

3. Results and discussion – Chapter 1: Extension of the GBBR: a green, robust, scalable and efficient continuous flow process to synthesise 3-aminoimidazoheterocycles.

3.1 GBBR optimisation

Initial optimisation of the Groebke-Blackburn-Bienaymé reaction between 2-aminopyridine (**202**), benzaldehyde (**203**) and *tert*-butyl isocyanide (**204**) to generate *N*-(*tert*-butyl)-2-phenylimidazo[1,2 a]pyridin-3-amine (**205**, **Scheme 3.1**) was performed using a Radleys® Carousel 12 Plus™ reaction setup. This method was used to evaluate the effectiveness of the sixteen different solvent and catalyst combinations shown in **Table 3.1**. The reactions were heated at 50 °C over 21 h before being analysed by LCMS. As expected, excellent conversion was observed, but long reaction times were required in all cases.

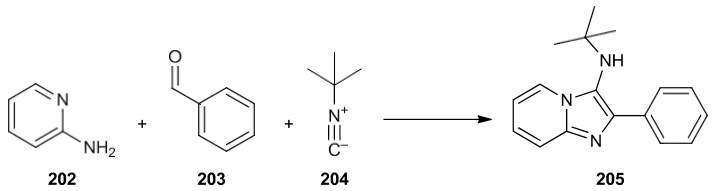

Scheme 3.1 Groebke-Blackburn-Bienaymé reaction between 2-aminopyridine (202), benzaldehyde (203) and *tert*-butyl isocyanide (204) reagents, used for the synthesis of *N*-(*tert*-butyl)-2-phenylimidazo[1,2-*a*] pyridin-3-amine (205).

Entry	Solvent	Catalyst[a]	Solubility of solvent/catalyst mixture	Estimated Conversion
1	Methanol	HCl[b]	Homogenous solution	97%
2	Methanol	$Sc(OTf)_3$	Partially soluble mixture	97%
3	Methanol	$ZrCl_4$	Partially soluble mixture	97%
4	Methanol	$HClO_4$[c]	Homogenous solution	98%
5	Acetonitrile	HCl[b]	Product precipitation observed	94%
6	Acetonitrile	$Sc(OTf)_3$	Partially soluble mixture	98%
7	Acetonitrile	$ZrCl_4$	Partially soluble mixture	91%
8	Acetonitrile	$HClO_4$[c]	Homogenous solution	96%
9	Toluene	HCl[b]	Insoluble mixture	92%
10	Toluene	$Sc(OTf)_3$	Partially soluble mixture	> 99%
11	Toluene	$ZrCl_4$	Partially soluble mixture	95%
12	Toluene	$HClO_4$[c]	Partially soluble mixture	96%
13	2-MeTHF	HCl[b]	Insoluble mixture	92%
14	2-MeTHF	$Sc(OTf)_3$	Partially soluble mixture	97%
15	2-MeTHF	$ZrCl_4$	Partially soluble mixture	93%
16	2-MeTHF	$HClO_4$[c]	Homogenous solution	96%

Table 3.1: Initial optimisation of the GBBR procedure between 2-aminopyridine (202), benzaldehyde (203) and *tert*-butyl isocyanide (204) in 1:1:1 stoichiometry. All reactions were performed at 50 °C, at 0.35 M concentration with respect to the amidine reagent. Conversion estimates were taken after 21 h reaction time by LCMS AUC analysis, (a) 10 mol% catalyst loading was used in all cases, (b) 4 M HCl solution in dioxane (c) 70% wt. aq. soln.

Gratifyingly, the use of mineral acid catalysis (HCl/$HClO_4$) showed similar activity to standard metal catalysts most frequently used within the GBBR. An early consideration was given to

the solubility of the reaction mixtures when combining different solvents and catalysts, since the aim was to eventually adapt the methodology for use within a flow reactor, where precipitates can result in blockages.

As a result, and due to the unsustainability of metal catalysis, especially on large scale, all solvent/catalyst combinations apart from **Entries 1, 4, 8** and **16** were preliminarily eliminated from further consideration. Curiously, **Entry 5** was present as a homogenous reaction solution during the course of the reaction, but precipitation of the formed product was observed upon cooling to ambient temperature. As such, these conditions would also be unsuitable for transition into a standard flow chemistry system. **Entry 10** offered quantitative conversion in 21 h, and so would be considered further, though the insolubility of the reaction mixture again makes the reaction conditions undesirable.

As a result of these initial investigations, a variety of reactions were performed using a few selected conditions, and by varying the heating method and temperature applied to the reaction, in order to accelerate the GBBR process. As such, the experimental conditions described in **Table 3.2** demonstrate the steps taken to achieve this.

Entry	Heating Source	Temperature (°C)	Solvent	Catalyst[a]	Reaction/ Residence Time	SM consumption[b] (Isolated yield)
1[c]	Thermal	50	Toluene	$Sc(OTf)_3$	24 h	> 99%[d]
2[c]	Thermal	50	MeOH	$HClO_4$	24 h	92%
3[c]	Thermal	50	MeCN	HCl[e]	24 h	77%
4[c]	Thermal	50	EtOH	HCl[e]	24 h	91%
5[c]	MW	130	EtOH	HCl[e]	50 min	93% (84%)
6[c]	MW	130	EtOH	HCl[e,f]	50 min	75%
7[c]	MW	130	EtOH	No catalyst	50 min	36%
8[g]	MW	130	EtOH	HCl[e]	50 min	> 99%
9[g]	MW	130	EtOH	HCl[h]	50 min	> 99%
10[g]	Flow	130	EtOH	HCl[h]	50 min	97% (96%)

Table 3.2: Further optimisation of the GBBR procedure between 2-aminopyridine (202), benzaldehyde (203) and *tert*-butyl isocyanide (204), and its subsequent transition to flow. (a) 10 mol% catalyst loadings used unless stated, (b) SM consumption measured by HPLC analysis, (c) 1:1:1 stoichiometry, (d) heterogenous mixture made, (e) 4 M solution in dioxane, (f) 100 mol% catalyst, (g) 1:2:2 stoichiometry (h) 1.25 M solution in ethanol.

Starting material consumption was determined using a quantitative HPLC method against measured concentration gradients for amidine starting materials. For more information, see **Section 7.1 Appendix 1, procedure for attaining conversion estimates from HPLC concentration gradients.**

Once again, **Entry 1** confirmed that pre-established conditions using toluene and scandium(III) trifluoromethanesulfonate as the solvent and catalyst mixture for the reaction facilitated the complete consumption of 2-aminopyridine in 24 h. Nevertheless, the insolubility of the reaction mixture, as well as the undesirable environmental problems associated with using both metal

catalysts and toluene, a potentially genotoxic solvent, meant that the conditions were not pursued further.[160]

In agreement with a previous result (**Entry 4, Table 3.1**), perchloric acid proved to be an efficient catalyst for the transformation (**Entry 2**). Perchloric acid was investigated since it was reported in Bienaymé's original publication.[122] However, although demonstrating efficient formation of **205**, since the reaction mixture was to be superheated within the flow setup, hydrochloric acid-mediated catalysis was preferred, due to the explosive risks associated with using perchloric acid at elevated temperatures.[144]

Methanol proved more effective than acetonitrile as a reaction solvent, as a result of both the increased solubility of the reaction mixture, and higher conversion results obtained (**Entries 1 and 5**, **Table 3.1** and **Entry 3, Table 3.2**). A solvent switch to ethanol (**Entry 4**) maintained the observed reactivity, and presented the benefit of using a sustainable solvent, according to its green metrics and the environmental advantage of producing the solvent from renewable feedstocks.[161,162]

Having optimised sustainable conditions for the GBBR procedure, the reaction was performed in the microwave to investigate reaction conditions above the boiling point of the solvent. Running the reaction at 130 °C resulted in 93% consumption of **202** in only 50 minutes, and an isolated yield of 84% of the desired material was afforded following purification (**Entry 5**).

Entries 6 and **7** showed that the catalyst was required for acceleration of the reaction, as when catalyst was omitted, only a starting material consumption of 36% was observed. Moreover, stoichiometric addition of the HCl catalyst was also accompanied with a reduction in efficiency of the reaction, presumably due to protonation of the amidine component.

Despite the high conversions observed at this point, more forcing conditions were tested in **Entries 8-10** in case other, less reactive starting materials were found in the future to not go to completion. As such, a stoichiometry of 1:2:2 (amidine:aldehyde:isocyanide) was subsequently applied. Introduction of these conditions generated the desired material in quantitative conversion (**Entry 8**).

Finally, changing the source of hydrochloric acid from a 4 M HCl solution in dioxane to a 1.25 M HCl solution in ethanol (**Entry 9**) preserved the excellent reaction profile, and meant that a sustainable one-solvent reaction mixture could be utilised in the process, and the toxicological issues associated with the use of 1,4-dioxane could be avoided.[163]

Performing the analogous flow reaction using these optimised conditions led to the near-quantitative production of **205**, which was purified in 96% yield following only passing the reaction solution through an Isolute® 5 g aminopropyl cartridge with 20 mL methanol and

drying the reaction mixture under vacuum (For information on the flow setup used throughout this work, see **Section 6.1.16 Flow Reactions (GBBR work)**).

3.2 Substrate scope – Aryl aldehydes

With optimised conditions in hand, the substrate scope of the reaction was first explored using 2-aminopyridines (**206**) with various aryl and hetero-aryl aldehydes (**207**) with different isocyanide reagents (**208**, **Scheme 3.2**). Again, the same HPLC method was utilised to measure starting material consumption in the reaction.

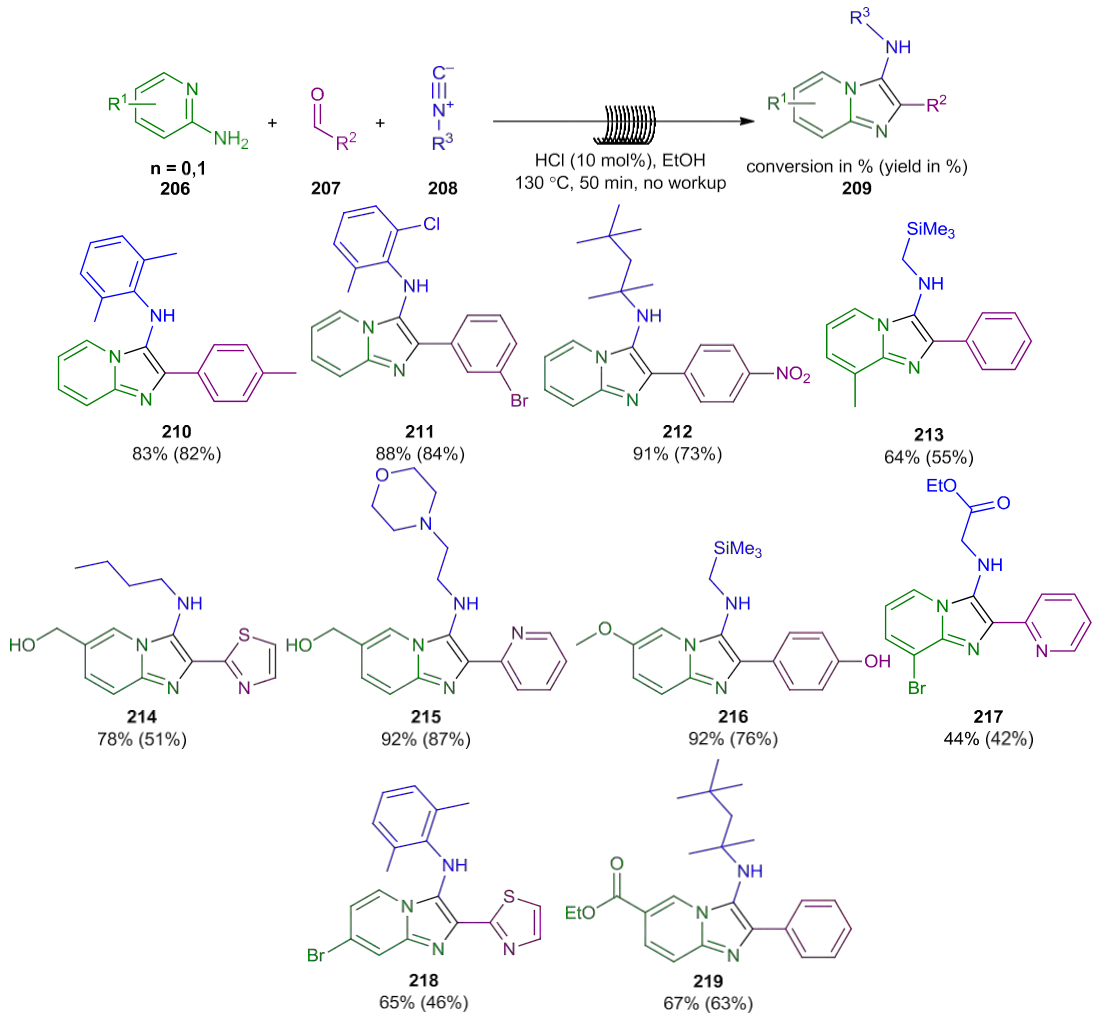

Scheme 3.2: Substrate scope of the GBBR methodology in flow for 2-aminopyridines (206), utilising different isocyanides (208) with aryl and heteroaryl aldehydes (207). 10 mol% catalyst loading was used in all cases, with a reaction stoichiometry of 1:2:2 amidine:aldehyde:isocyanide. In each case, HPLC measurements of the consumption of the amidine starting material is shown outside of the brackets, and isolated yields for the products are shown inside the brackets.

As shown, a variety of aryl and heteroaryl aldehydes were well tolerated under the reaction conditions. In all cases, a residence time of 50 minutes was applied, and no work-up procedure was required. Following the reaction, solvent removal under reduced pressure and a

subsequent purification by flash column chromatography afforded products **210**-**219** in moderate to very good yields, proving that different substitution patterns and substituents could be successfully incorporated into GBBR procedure.

Alkyl, aryl and laterally functionalised isocyanides could be utilised successfully. Remarkably, product **213** was generated cleanly in the reaction, with the trimethylsilylmethyl amine group intact under the mildly acidic conditions applied in the flow reaction. Ethyl ester functionalities were stable to the conditions and were tolerated in both the isocyanide and amidine reagents, as demonstrated in products **217** and **219**. Bromide substituents also endured the reaction conditions, affording products **217** and **218** in moderate yields. These compounds may react in cross-coupling reactions for potential downstream manipulation.

The reaction conditions were then applied to other amidine components, in order to probe the generality of the conditions (**220**, **Scheme 3.3**).

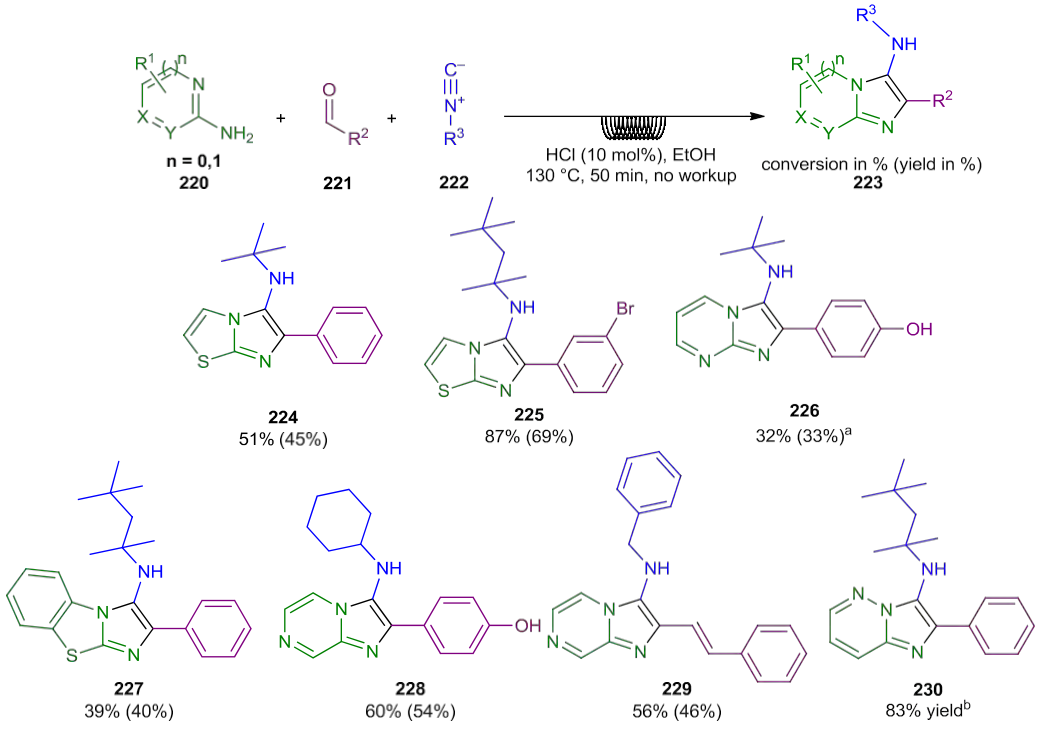

Scheme 3.3: Substrate scope of the GBBR methodology in flow when reacting amidine components other than 2-aminopyridines with aryl and heteroaryl aldehydes and different isocyanides. 10 mol% Catalyst loading was used in all cases, with a reaction stoichiometry of 1:2:2 amidine:aldehyde:isocyanide. In each case, starting material consumptions are shown outside of the brackets, and isolated yields for the products are shown inside the brackets. (a) > 10:1 regioselectivity for the desired product observed by NOESY NMR (See Section 7.2 Appendix 2 - NMR data of regioisomeric mix for compounds 226 and 248). (b) Reaction performed in the microwave.

Products derived from 2-aminothiazole (**224**, **225**), 2-aminobenzothiazole (**227**), 2-aminopyrimidine (**226**) and 2-aminopyrazine (**228**, **229**) were all successfully afforded in synthetically workable yields (33-69%).

Products containing amine derivatives resulting from the use of 1,1,3,3-*tert*-butylisocyanide (**212**, **219**, **225**, **227** and **230**) or benzylisocyanide (**229**) also offer further possibility for the derivatisation of GBBR products, as the latent amine functionality can be acquired following acid-mediated dealkylation or benzyl deprotection strategies.[121,164,165] Finally, the use of *trans*-cinnamaldehyde was well tolerated to facilitate the synthesis of interesting compound **229**, with conjugation between the imidazo[1,2-*a*]pyrazine and phenyl ring systems.

Following completion of the flow methodology, it was later realised that 2-aminopyridazines had not been tested within the scope of the reaction. Fortunately, although the flow instrumentation was no longer available to hand at the time, compound **230** could still be furnished through the use of equivalent conditions under microwave irradiation. Though this method lacks scalability, it still demonstrates an efficient and sustainable way to perform the GBBR and exemplifies the possibility of using aminopyridazines as the amidine component within the flow procedure.

3.3 Substrate scope – Formaldehyde and alkyl aldehydes

As highlighted earlier, one current issue with the GBBR centres around the use of formaldehyde and alkyl aldehyde reagents. Often, the use of these reagents results in low yields of products and/or the formation of multiple side-products.

With this in mind, formylating reagents were initially sought for the current GBBR procedure to allow the formation of 2-C unsubstituted 3-aminoimidazo[1,2-*a*]heterocycles. Microwave reactions were attempted using 1,3-dioxolane (**231**), 1,3,5-trioxane (**232**) and dimethoxymethane (**233**) as formaldehyde equivalents, under varying conditions.

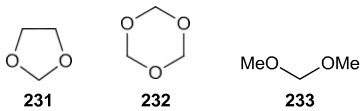

231 **232** **233**

Figure 3.1: Unsuccessful formaldehyde equivalents attempted in the GBBR procedure.

Unfortunately, in all cases, the desired product was not observed. However, under microwave irradiation using the standard reaction conditions described above, the desired 2-unsubstituted 3-aminoimidazo[1,2-*a*]pyridine (**235**) could be synthesised cleanly in 56% yield (**Scheme 3.4**) using only 37% wt. aqueous formaldehyde solution (**234**) in a reaction with 2-aminopyridine (**202**) and *tert*-butylisocyanide (**204**).

Subsequently performing the reaction under flow conditions and using only a slight excess of the formaldehyde afforded **235** in an 82% isolated yield following purification.

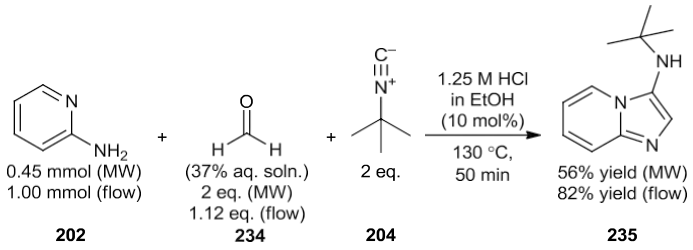

Scheme 3.4: The synthesis of *N*-(*tert*-butyl)imidazo[1,2-*a*]pyridin-3-amine (235), initially under MW conditions and resultantly under optimised flow conditions.

These conditions were subsequently applied to substituted 2-aminopyridine reagents to afford compounds **240** and **241** (**Scheme 3.5**) in excellent yields. Moreover, under the standard conditions reported above, alkyl aldehydes could also be applied in the GBBR process, furnishing compounds **242**-**247** in a facile manner.

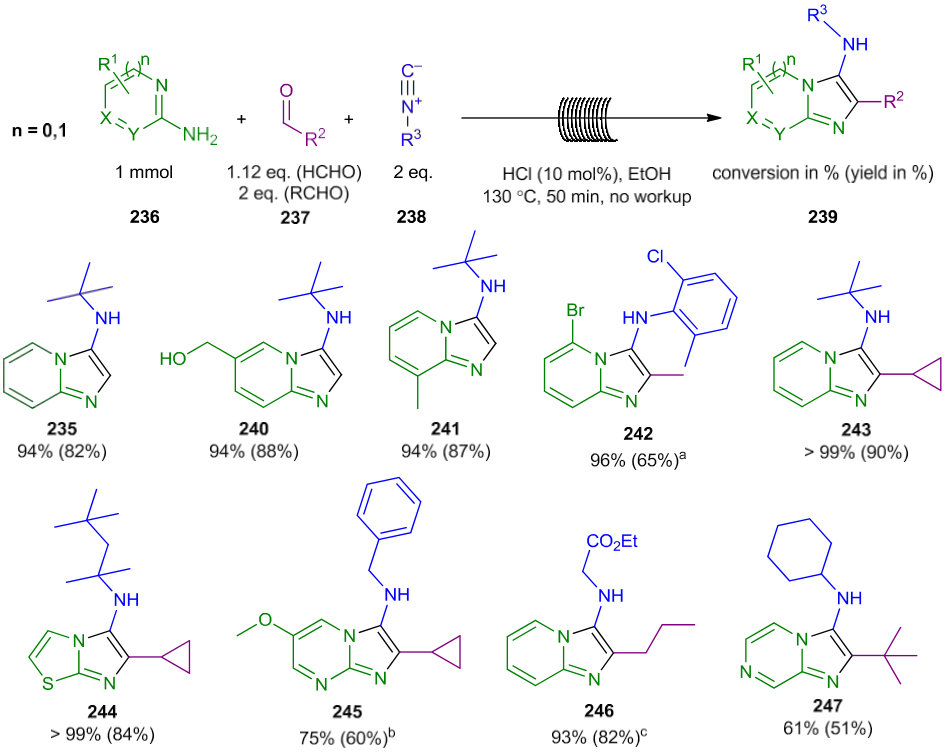

Scheme 3.5: Substrate scope used for formaldehyde and alkyl aldehydes in the flow-based GBBR method. (a) 3 eq. acetaldehyde used in the reaction, (b) only regioisomer observed by ^{15}N HMBC analysis, (c) reaction also performed in batch using literature conditions (Ref. 169), 8% yield observed, multiple side-products observed, one successfully isolated.

As demonstrated, the reaction is readily applicable to afford a range of GBBR products derived from the use of formaldehyde and alkyl aldehyde reagents. Primary, secondary and tertiary alkyl aldehydes are all tolerated well and in good to excellent yields.

Moreover, the reaction conditions have been demonstrated using 2-aminopyridines (**235**, **240**-**243**, **246**), 2-aminothiazole (**244**), 2-aminopyrimidine (**245**) and 2-aminopyrazine (**247**) as the amidine component, highlighting the general utility of the methodology.

For compound **242**, the conditions used were adapted slightly, to circumvent acid-mediated polymerisation otherwise observed when employing acetaldehyde under standard conditions.[166] Use of 3 eq. of the aldehyde, and changing the way that the starting material solutions were prepared prior to the reaction helped to selectively avoid polymerisation.

This represents another benefit of using the flow procedure in comparison to published GBBR methods. For all other scope examples reported here, the experimental method, as detailed in **General synthetic procedures - General procedure D: flow GBBR method using alkyl aldehydes**, involves making a stock solution of the amidine, aldehyde and acid catalyst in ethanol for one line of the flow reactor and a solution of the isocyanide in ethanol for the other. This helps to keep the isocyanide separate and minimises exposure to the malodorous chemical.

However, for compound **242**, the second input stock solution contained both the aldehyde and isocyanide components, as to avoid the polymerisation observed from directly combining the aldehyde and acid catalyst. Thus, **242** was successfully produced using this approach.

Though not the formal aim of this study, regioisomeric control was considered in products derived from the use of 2-aminopyrimidines (leading to products **226** and **245**). As previously mentioned, different regioisomeric products can arise from the use of 2-aminopyrimidines in the GBBR, and various studies have focused on controlling the regioselectivity of the reaction.[141,152,167,168] For compound **226**, a regioselectivity of >10:1 was observed for the desired 3-aminoimidazo[1,2-*a*]pyrimidine isomer over the undesired 2-aminoimidazo[1,2-*a*]pyrimidine (**248**, **Figure 3.2**) by NOESY NMR analysis (See **Section 7.2 Appendix 2 - NMR data of regioisomeric mix for compounds 226 and 248** for relevant NMR data and the method used for structure elucidation of the regioisomeric productmixture).

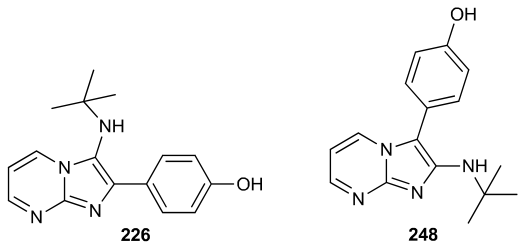

Figure 3.2: The desired (left, 226) and undesired (right, 248) products formed from the reaction between 2-aminopyrimidine (163), 4-hydroxybenzaldehyde and *tert*-butyl isocyanide (204). A ratio of over 10:1 is observed by NOESY NMR analysis for compound 226 without any functional group conferring bias for either regioisomer (See Section 7.2 Appendix 2 - NMR data of regioisomeric mix for compounds 226 and 248 for relevant data).

Furthermore, adding an electron-donating substituent to the 2-aminopyrimidine (as in **245**) further favours this regioselectivity due to an effect of increasing the nucleophilicity of the exocyclic nitrogen, thereby accelerating formation of the desired imine intermediate involved in the GBBR (**Figure 3.3**). In this case, the desired 3-aminoimidazo[1,2-*a*]pyrimidine product was the only regioisomer observed by 2D NMR analysis (See **Section 7.3 Appendix 3 – NMR data for compound 245** for the method used for structure elucidation of compound **245**).

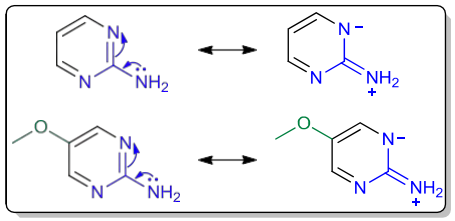

σ_P substitution with an electron-donating group (OMe, green) increases the electron density in the guanidine functional group (blue). As a consequence, the exocyclic nitrogen is more nucleophilic, and therefore reacts more readily in the GBBR than the endocyclic nitrogen atoms.

Figure 3.3: Effect of the methoxy substituent on the GBBR regioselectivity when using 2-aminopyrimidines.

In order to compare the reported synthesis to previous literature methods, compound **246** was also synthesised using the preparative method described in a recent patent (**Scheme 3.6**).[169]

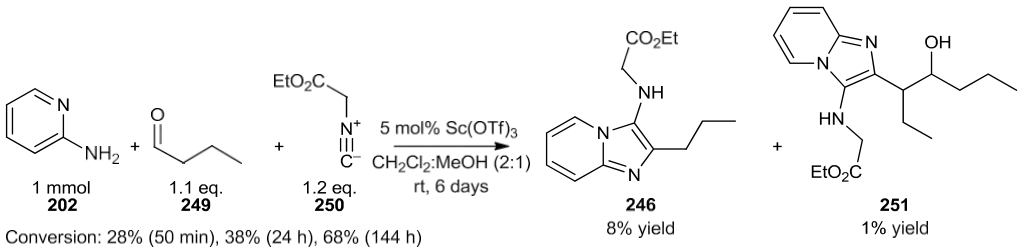

Conversion: 28% (50 min), 38% (24 h), 68% (144 h)

Scheme 3.6: Inefficient formation of product 246 under reported GBBR conditions found within the patent literature. A small amount of unexpected side-product 251 was also isolated, highlighting the fact that alkyl aldehyde inclusion in previously reported literature conditions are typically low-yielding, unclean reactions.

As expected, only a very low isolated yield of the desired product was afforded, even after a greatly extended reaction time. Additionally, various side-products were formed in the reaction, despite it being performed under ambient conditions. A small amount of one such side-product, **251** was isolated, and a postulated mechanism for its formation is shown in **Scheme 3.7**. The structure of **251** was elucidated by various NMR analyses, as described in **Section 7.4 Appendix 4 - NMR data for by-product, compound 251**.

Alternatively, the intermediate imine **252** may be formed from the condensation of 2-aminopyridine with the aldol by-product formed between 2 molecules of **249**.

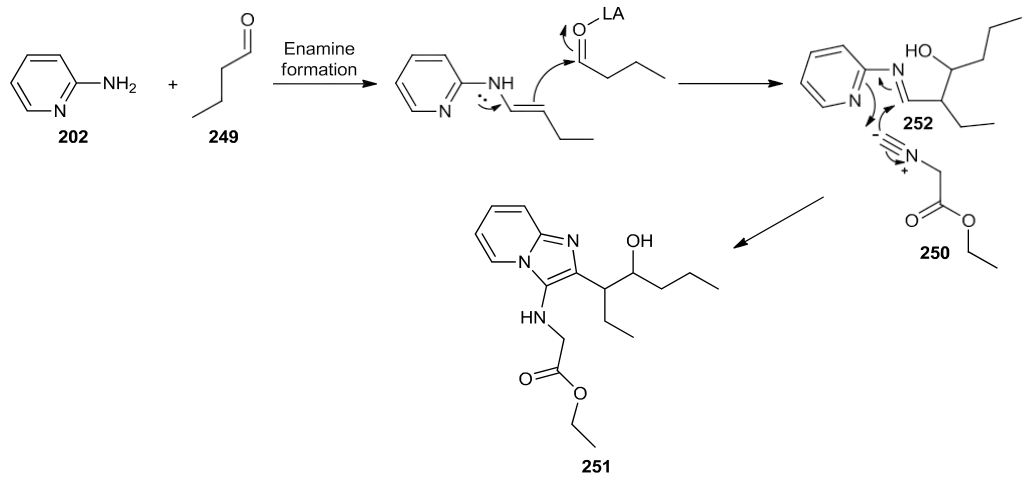

Scheme 3.7: Postulated mechanism for the formation of side-product 251, under GBBR conditions used in patent literature. NMR data used for the elucidation of the structure of 251 is provided in Section 7.4 Appendix 4 – NMR data for by-product, compound 251.

As a result of the outputs from this programme to this stage, the flow-based GBBR procedure is far more suitable towards application with an extended substrate scope, which includes formaldehyde and alkyl aldehyde reagents. Use of the continuous flow process was proven to be more efficient than patented GBBR literature conditions and facilitates access to C2-alkyl substituted imidazoheterocycles in a single-step process, as exemplified, in particular, by the synthesis of compound **246**.

3.4 Substrate scope – Low-yielding and unsuccessful examples

A number of substrates were observed to undergo low yielding or unsuccessful reactions. These examples were explored individually, as described below.

To explore the reactivity of 2-aminooxazoles in the GBBR, 5-phenyloxazol-2-amine (**255**) was synthesised from 2-phenylacetaldehyde (**253**) in two steps (**Scheme 3.8**).

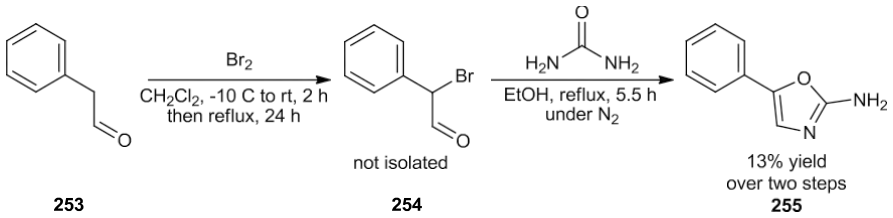

Scheme 3.8: Method used for the formation of 5-phenyl-oxazol-2-amine (255).

However, when added to the other GBBR components, compound **255** exhibited low solubility in ethanol, and was found to be unstable under the reaction conditions. As such, the formation of the desired product (**256**) from the reaction between **255**, benzaldehyde (**203**) and *tert*-butyl isocyanide (**204**) was never observed (**Scheme 3.9**).

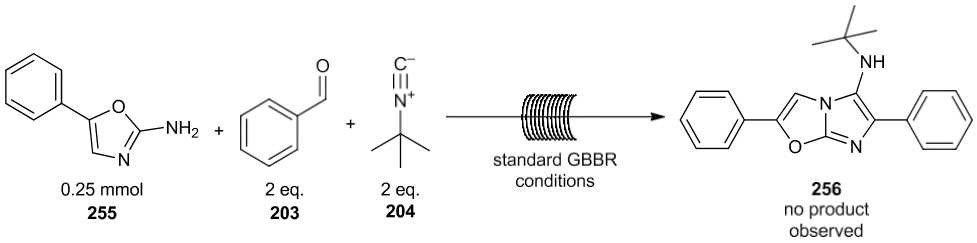

Scheme 3.9: The unsuccessful reaction between 5-phenyl-oxazol-2-amine (255), benzaldehyde (203) and *tert*-butyl isocyanide (204) in an attempt to generate compound 256.

Furthermore, various commercially sourced reaction components were also poor substrates for the flow-based GBBR procedure (**Figure 3.4**).

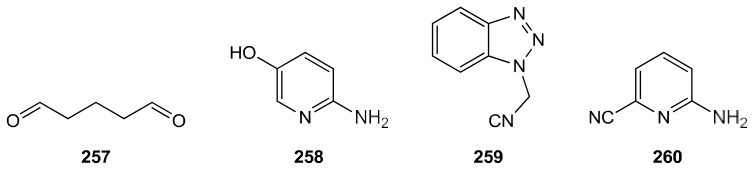

Figure 3.4: Unsuccessful components tested in the flow GBBR process.

Early approaches to develop dimers was attempted, through the use of dialdehyde **257**. Unfortunately, dimerisation could never be seen under the standard reaction conditions, and GBBR procedures utilising **257** seemed to stall after formation of the iminium intermediate. As such, more forcing conditions may be required to successfully execute this strategy.

A variety of components also showed insufficient solubility in ethanol. When 5-hydroxy-2-aminopyridine (**258**) or benzotriazole isocyanide (**259**) were used as the amidine or isocyanide component, respectively, the stock SM solutions made were present as heterogenous mixtures. Since the reactions are performed using flow chemistry, heterogenous mixtures are problematic, as they can lead to tubing blockages and excessive pressure spikes.

Therefore, reactions using these reagents were not investigated further. Nevertheless, solvent substitution may facilitate the dissolution of the starting materials which are otherwise insoluble in ethanol and could be investigated if a specific component was required for library syntheses.

Finally, reactions involving 6-aminopicolinonitrile (**260**) proved difficult to achieve and were subsequently abandoned. This result was unsurprising, since cyanide reagents are known to readily participate in cycloaddition reactions, and can be prone to acid-mediated hydrolysis.[170,171] Hence, the desired reaction was inefficient, and many side-products were observed through the analysis of crude reaction mixtures which used **260**.

Similar issues to those seen with problematic starting materials also affected some products of the GBBR process. For instance, compound **261** (**Figure 3.5**) was generated using the flow GBBR procedure, but subsequently crystallised within the reaction tubing. As result, the reaction did not proceed to completion as pumping in the flow system halted due to pressure constraints.

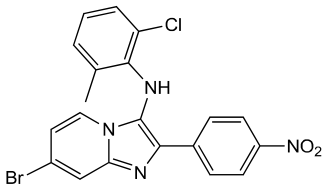

261

Figure 3.5: Compound 261, which was formed in flow using the GBBR procedure, but subsequently crystallised within the tubing.

Imidazo[1,2-*a*]pyridine **265** was successfully synthesised using standard conditions, but only with a low yield of 9%. This highlights some of the forcing limitations of the reaction, since the relevant reaction used to produce **265**, as shown in **Scheme 3.10**, involves the combination of both an electron-deficient amidine and a highly sterically hindered aldehyde reagent, which both unfavourably contribute to the lowered reaction efficiency observed. As such, more forcing conditions or longer reactions times may allow for the synthesis of compounds developed from more challenging substrates.

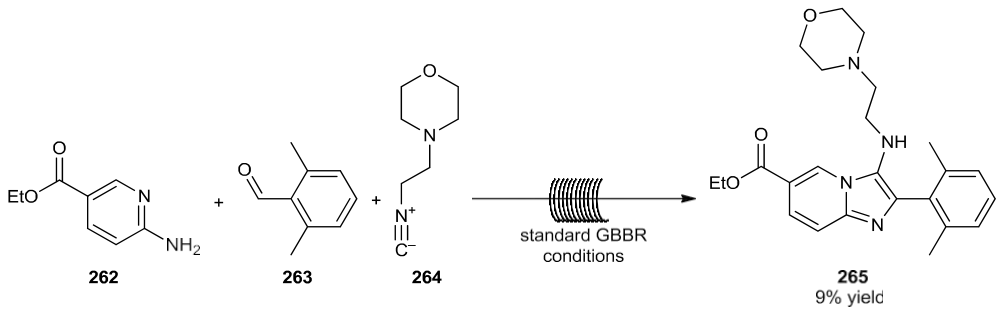

262 **263** **264** **265**
9% yield

Scheme 3.10: Low-yielding synthesis of compound 265, using the flow-based GBBR method.

Conversely, some of the more reactive scope examples competed in side-reactions, resulting in a complex reaction profile. Product **266** (**Figure 3.6**) was produced in a 34% yield using standard GBBR conditions, although a considerable number of by-products were observed within the crude mixture.

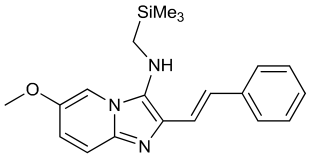

266

Figure 3.6: imidazo[1,2-*a*]pyridine 266, which was formed in 34% yield using the flow GBBR process, but also displayed an undesirable reaction profile by LCMS analysis.

3.5 Scale-up reaction and subsequent dealkylation

Having proven the applicability of the reported process on standard small scale lab scale syntheses (up to ~ 1 g), another benefit of flow methodology was demonstrated in the scale-up synthesis of a GBBR product.

Compound **269** was formed through the combination of 5-bromo-2-aminopyridine (**267**), formaldehyde (**234**, 37% wt. solution in H_2O) and 1,1,3,3-tetramethylbutylisocyanide (**268**, **Scheme 3.11**). The reaction was performed by doubling the volume of the heated reactor loop inside the bespoke flow reactor (see ***Experimental*, Section 6.1.16 Flow Reactions (GBBR work)** for more information) and continually running the flow reaction for 9 hours in a single pass manner.

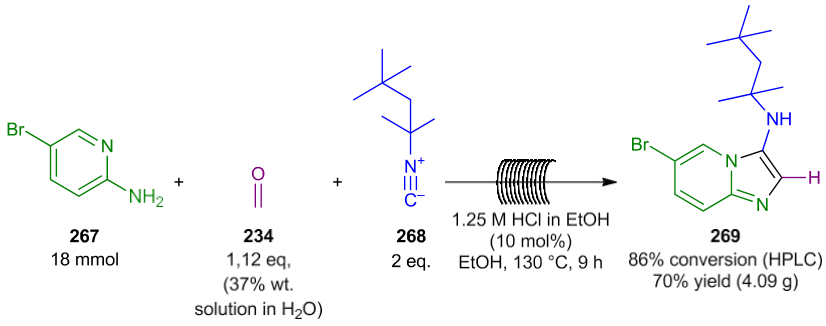

Scheme 3.11: Scale-up synthesis of 6-bromo-*N*-(2,4,4-trimethylpentan-2-yl)imidazo[1,2-*a*]pyridin-3-amine, 269, using the flow GBBR process with formaldehyde.

Consequently, the reaction was performed at this point in the study on an 18 mmol scale with respect to the amidine starting material. Using the standard conditions for the coupling of formaldehyde (**234**) with the other reaction components, the desired material could be generated in a 70% yield (~4 g) following purification.

It should be noted that the reaction work-up was especially clean, with purification only required to remove the residual amidine starting material from the mixture. Chromatographic purification was initially unsuccessful, as the amidine starting material and desired product co-eluted under the eluent conditions examined (40% to 60% TBME in cyclohexane). However, a subsequent anti-solvent cold crystallisation using MeCN/H_2O was effective in isolating the desired material and suggests that column purification would not be required in the scale-up example, making the process even more suitable for large scale application.

Furthermore, the scalability of the process is not limited. The starting materials and product were observed to be soluble in ethanol at up to five times the concentration of the reaction (0.5 M). Moreover, by further increasing either the volume of the flow reactor, the length of time for continuous processing of the reaction, or the introduction of parallel synthesis, the achievable scale of the reaction using this procedure could be increased, to suit on-demand synthesis, for instance, of active pharmaceutical ingredients containing products derived from the GBBR.

The same reaction was also performed in batch, using the standard GBBR conditions found in the patent literature, which were employed for the inefficient batch synthesis of **246** described earlier (**Scheme 3.6**).[169] Despite achieving a similar isolated yield in the formation of **269**, the reaction required *c.* 20 h to attain a high HPLC consumption of the amidine starting material.

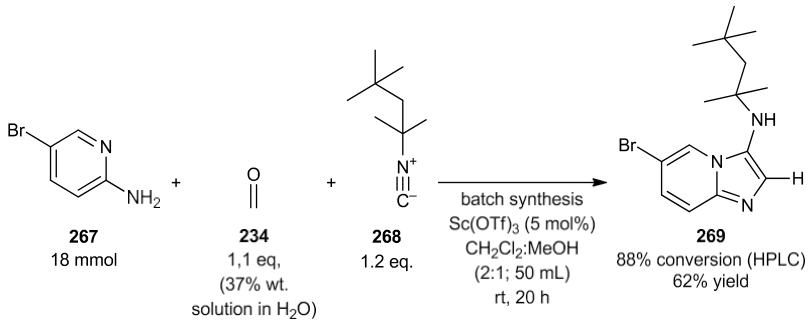

Scheme 3.12: Batch synthesis of 269 under GBBR conditions found within the patent literature. Though the product could be attained in good yield, an extended reaction time was required to achieve a similar SM consumption to the flow procedure, and the batch process used unsustainable conditions.

Additionally, the efficiency of the reaction is inversely proportional to the size of the reaction vessel, as a result of the surface area to volume ratio of the system. Therefore, mixing will become increasingly inefficient in larger scale batch reactions, again favouring use of the flow procedure rather than batch reactors for large scale applications of the Groebke-Blackburn-Bienaymé reaction. Furthermore, the industrial use of both metal catalysis and chlorinated solvents on large scale is unsustainable and costly, hence avoiding these issues would be highly advantageous.

Once GBBR product **269** had successfully been synthesised, an acid-mediated dealkylation procedure could be applied to afford advanced intermediate **270** in quantitative yield, without the use of column purification (**Scheme 3.13**).

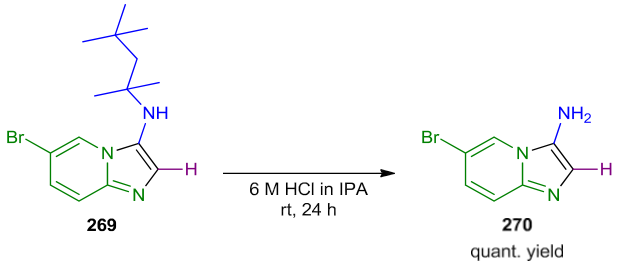

Scheme 3.13: Dealkylation of GBBR product 269 under acidic conditions to afford difunctionalised advanced GBBR derivative, 270.

Isocyanide **268** has previously been reported as a GBBR reaction component which is sensitive to dealkylation following the MCR.[164,165] However, the optimal conditions found to dealkylate **269** here used 6 M HCl in isopropanol (IPA). Use of these conditions afforded the desired material in a facile manner after 24 h, following trituration in diethyl ether and a subsequent filtration and a solvent swap to methanol/water. After the polar reaction solution was passed through an Isolute® 2 g aminopropyl cartridge, and the solvent was removed under reduced pressure, the desired material was acquired in quantitative yield.

As a result, advanced intermediate **270**, which contains both a bromide and amine functionality for further derivatisation, could be synthesised quickly, and on large scale using the method developed within this programme.

3.6 Tandem isocyanide formation/Groebke-Blackburn-Bienaymé reaction process

Following on from the success of performing the reaction on a plethora of substrate examples, as well as on multigram scale, further work was sought to potentially perform a tandem reaction procedure in flow, comprising both the formation of the isocyanide reagent and the *in situ* Groebke-Blackburn-Bienaymé reaction.

The synthetic strategy was supported by previous work from Sharma *et al*. which demonstrated a tandem flow-based procedure to synthesise isocyanides in flow prior to their use in both Passerini and Ugi MCRs (as shown earlier in **Scheme 2.18**).[113] These methods benefit from generating the variety of products available through MCRs without the handling issues associated with malodorous isocyanide reagents.

In an attempt to achieve the tandem synthetic GBBR approach, the general scheme described in **Scheme 3.14** was targeted. It was thought that a dehydration reaction of formamide reagent **271** (with $POCl_3$) would deliver *tert*-butylisocyanide (**204**). At this point, it would likely be necessary to introduce an *in situ* workup procedure, as both the water released from the

dehydration reaction, as well as the amount of hydrochloric acid released in the use of the dehydrating reagent would both be likely to affect the efficiency of the subsequent GBBR process.

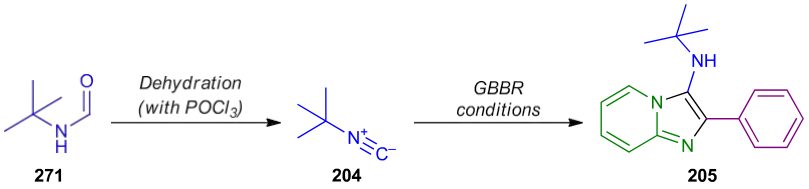

Scheme 3.14: General scheme for the formation of compound 205 through the tandem formation of *tert*-butylisocyanide (204) from its corresponding formamide (271), and the *in situ* use of 204 in a flow GBBR procedure.

Furthermore, the efficiency of the phase separation would have to be considered. The Zaiput® Sep-10 liquid-liquid phase separator (See ***Experimental*, Section 6.1.18 Flow reactions (Tandem reactions)** for more information) allows for liquid-liquid separation using either a hydrophobic or hydrophilic semi-permeable membrane, with adaptable pore size. It was hoped that optimisation of the membrane (and flow rate) used would lead to the clean formation and separation of the isocyanide reagent.

In order to probe the feasibility of the tandem reaction, standard GBBR conditions employing 2-aminopyridine (**202**), benzaldehyde (**203**) and *tert*-butylisocyanide (**204**) were used. It was anticipated early on that the use of ethanol as the reaction solvent would not be well tolerated in the tandem procedure due to its miscibility in water. Furthermore, as well as being immiscible with water, the solvent needs to be suitable for both steps, and able to solubilise any intermediates or by-products formed in either reaction, in order to prevent precipitation within the flow reactor.

As such, a first exploratory attempt at the tandem reaction was made in batch using the conditions adapted from the earlier discussed work by Sharma *et al.* (**Scheme 2.18**).[113] The reaction was performed in ethyl acetate using Hunig's base (**272**), and a colour change from colourless to dark red accompanied the consumption of the phosphorus oxychloride during the 2 h dehydration of **271**. However, following the addition of other GBBR components to the reaction mixture, and irradiation in the microwave, no desired material was observed.

As a result, the two steps were considered separately. Batch GBBR conditions were applied to 2-aminopyridine (**202**), benzaldehyde (**203**) and *tert*-butyl isocyanide (**204**) using ethyl acetate as solvent, and 95% conversion was seen by LCMS analysis after microwave irradiation for 50 minutes (**Scheme 3.15**). As a result, the optimal GBBR conditions developed earlier (as discussed in **Table 3.1** and **Table 3.2**) were readily applicable to other solvent systems.

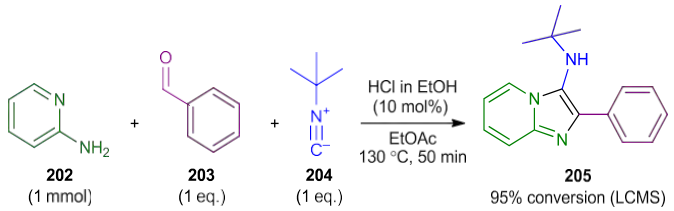

Scheme 3.15: GBBR conditions in ethyl acetate, to check the viability of the reaction conditions in another solvent.

Next, the dehydration reaction was attempted in ethyl acetate using phosphorus oxychloride. *N*,*N*-Diisopropylethylamine (**272**) was used as a base in the reaction, both to aid in the formation of the isocyanide, as well as to quench the acid generated from the use of the dehydration agent. Unfortunately, precipitation was observed in the reaction, likely as a result of the alkyl ammonium chloride salt by-product (**274**) formed during the course of the reaction (**Scheme 3.16**).

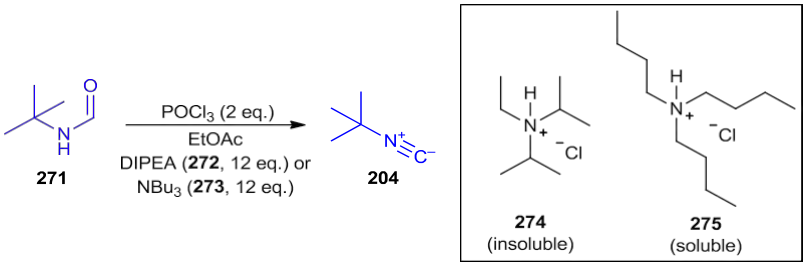

Scheme 3.16: Dehydration reaction in ethyl acetate, and the resultant solubility of trialkyl ammonium chloride by-products formed through the use of DIPEA (272) and tributylamine (273) bases.

Indeed, when the reaction was repeated, instead using tributylamine (**273**) as the amine source, no precipitation was observed. Therefore, a sufficiently lipophilic amine was required in the tandem flow procedure to prevent precipitation of the reaction materials.

Using these conditions for the dehydration reaction, the tandem procedure was again attempted in batch. Following the one-pot isocyanide formation, and subsequent MW GBBR sequence, the desired material was formed in ~20% conversion by LCMS analysis, indicating that the tandem reaction may be feasible under optimised conditions (**Scheme 3.17**).

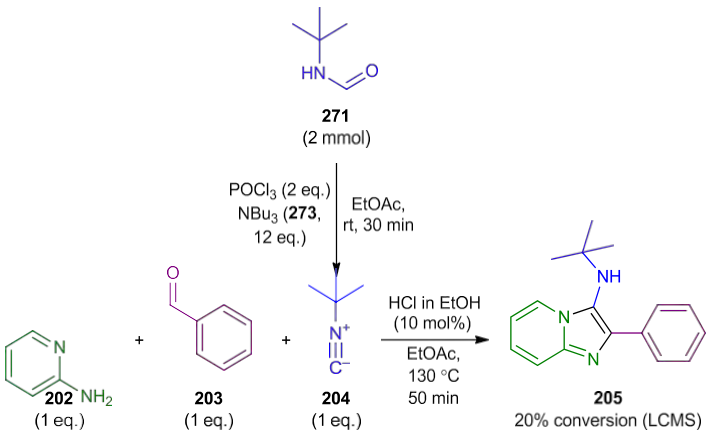

Scheme 3.17: Tandem isocyanide formation/GBBR sequence performed in batch. The GBBR step was performed using microwave irradiation.

In order to more closely monitor the isocyanide formation step in the reaction, IR analysis at different reaction time points was considered. However, the excess of the basic component used in the reaction meant that the trialkylamine component dominated the infra-red spectrum, and no useful reaction information could be determined.

Consequently, GC-MS analysis was instead utilised as a technique to measure both formamide consumption, and isocyanide formation. Quantitative analysis for these measurements could, in theory, be attained through the use of an internal standard, and as such, concentration gradients of both formamide-naphthalene and isocyanide-naphthalene solutions were generated as references (See **Section 7.5 Appendix 5 – GC-MS concentration gradients with respect to naphthalene internal standard at different relative molar ratios**). The retention times for the solvent and base used in the reaction were also recorded.

Even when using GC-MS as an analysis technique, it was obvious that accurate estimates of conversion could only be attained after separation of the alkyl ammonium and $POCl_3$ derivatives formed as by-products in the reaction.

Thus, the reaction was transitioned into flow, using the Zaiput® liquid-liquid separator to perform the separation following the dehydration reaction. Along with acquiring GC-MS analysis of the crude reaction mixtures, Karl Fischer (KF) analyses of both the organic and aqueous streams emanating from the Zaiput® separator were obtained using a Mettler Toledo V10S Compact Volumetric KF Titrator machine.

Initially, a hydrophobic PTFE membrane (1.0 nm pore size) was used to facilitate the separation. Water, saturated aq. brine solution and 1.0 M aq. HCl solution were considered as

the aqueous phase for the separation. However, all conditions still resulted in the separated organic phase containing at least ~3% wt. water in the reaction mixture following separation.

This inefficient separation proved to be critical, as performing the GBBR procedure in batch using a solvent mixture of ethyl acetate with 3% wt. water attained only ~20% conversion to the desired product by LCMS analysis, suggesting inhibition of the reaction by water, presumably due to reversible hydrolysis of the imine intermediate.

Other solvents were therefore sought to increase the efficiency of the separation. By increasing the inherent interfacial tension (IFT) between the phases, the separation should be more efficient without manipulating the pore size of the membrane.[172] As a result, α,α,α-trifluorotoluene (TFT) was selected as the organic phase for performing the reaction going forward, due to its high IFT with water, and preferred levels of sustainability and increased polarity in comparison to toluene.[173]

At this point, the currently optimised separation conditions using a 2 mL/min flow rate of the organic solution, a hydrophobic PTFE membrane with 1 nm pore size, and a 0.1 mL/min flow rate of water was attempted on neat TFT, and the collected organic phase following liquid-liquid separation contained only 0.65% water by weight according to Karl Fischer analysis.

In order to ensure this level of water retention was tolerated within the reaction conditions, the GBBR procedure shown in **Scheme 3.18** was attempted using anhydrous *α,α,α*-trifluorotoluene which was doped with 0.65% wt. water. LCMS analysis of the resultant product mixture showed that a good conversion (64%) was still observed. As such, both of the steps involved in the process should, in theory, be possible using TFT as a solvent.

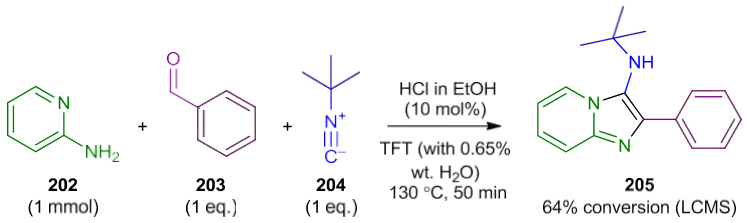

Scheme 3.18: GBBR method performed in TFT doped with 0.65% water by weight. Only a small amount of water was observed in neat TFT following passing the solvent through the liquid-liquid phase separator with water. Performing the MCR using anhydrous TFT which was doped with an equivalent amount of water still led to the formation of the desired product in good conversion, suggesting the tandem procedure was possible using this solvent.

However, despite successfully forming the desired product, the GBBR mixture was present as a biphasic solution. To try and improve the miscibility between the two phases, different sources of acid were tested in batch for the GBBR method. In all cases, the acid solution was never miscible with TFT, and hence standard conditions using HCl in ethanol were maintained.

Unfortunately, the tandem reaction in flow was still not fruitful. Optimal conditions for the separation were very difficult to achieve since a sufficiently low flow rate was required in the Zaiput® module to achieve an acceptable level of separation, and therefore the selective diffusion of phosphorus oxychloride (and its derivatives) and the alkyl ammonium salt into the aqueous layer. On the other hand, extremely slow flow rates would both render the tandem reaction too inefficient to be of practical use, and lead to the degradation of the formed isocyanide reagent under the harsh conditions.

With these issues in mind, various alterations were made to the process, including changing the pore size and nature of the membrane used in the phase separator, using excess amine base in the separation, and employing 4-toluenesulfonyl chloride as a milder dehydrating agent. None of these modifications to the reaction conditions could afford the desired product from the tandem reaction sequence, as residual base was often retained in the organic phase, affecting the subsequent GBBR process, and the tosyl chloride reagent required a greatly extended residence time to generate the isocyanide intermediate, thereby negating its use as a dehydrating reagent, since the isocyanide intermediate was observed to degrade over time.

Regrettably, conditions for the successful tandem flow procedure to generate isocyanide reagents, and their subsequent use in an *in situ* GBBR method were never found. However, earlier experimental findings strongly suggest that the tandem procedure could be realistic under the correctly optimised conditions, and by using the appropriate apparatus to facilitate the steps involved. In this case, the tandem procedure was not pursued further due to the focus on other priorities, and the seemingly insurmountable barriers found when using the currently explored reaction conditions.

3.7 GBBR product derivatisation

3.7.1 Sandmeyer-like difluoromethylation reaction

The next, related area to be researched was the synthesis of imidazoheterocyclic derivatives *via* reactions on the products afforded from the GBBR. Originally, a derivatisation procedure to make fluorinated analogues was considered, using published conditions for a one-pot diazotisation and subsequent Sandmeyer reaction to install a difluoromethyl group.[174] The general scheme for this prospective method is shown in **Scheme 3.19**.

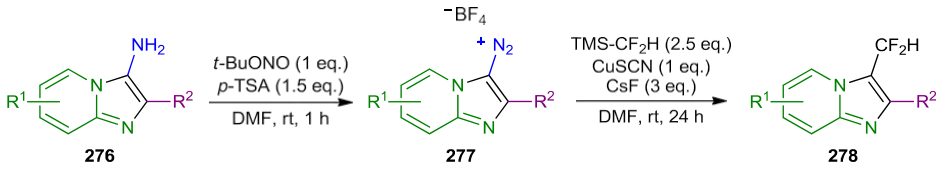

Scheme 3.19: General scheme for the tandem formation of the diazonium salt (277), and subsequent Sandmeyer-type reaction to generate difluoromethyl imidazoheterocyclic derivatives (278).

The introduction of a small fluorine moiety such as a difluoromethyl group can offer similar polarity and size to hydroxyl functionality, yet it has increased lipophilicity over the analogous alcohol-containing compounds. As a result, the introduction of such difluoromethyl groups into biologically active compounds may be attractive in drug discovery, due to the possibility of varying physicochemical properties of the molecule.[174]

In order to achieve this, GBBR product **280** was first synthesised, and dealkylated under previously optimised conditions to afford the latent amine **281**. It was thought that the use of an electron-rich 3-aminoimidazo[1,2-*a*]pyridine would favour the initial diazonium intermediate formation, and thus likely be more successful in affording the desired derivative.

A batch-based (MW) synthesis of **280** efficiently generated the desired product, and the acidic dealkylation procedure which followed gave access to **281** in quantitative yield under ambient conditions (**Scheme 3.20**).

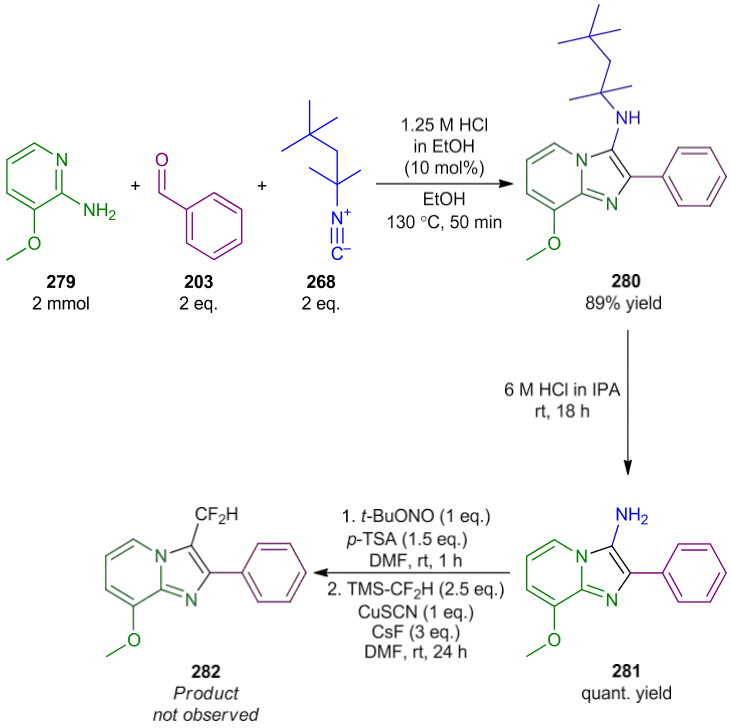

Scheme 3.20: Attempted synthesis of difluoromethyl derivative 282 through a GBBR, deprotection and diazotisation/Sandmeyer synthetic sequence.

With the desired synthetic intermediate in hand, **281** was subjected to the one-pot conditions for a tandem diazotisation/Sandmeyer reaction process. Unfortunately, the desired product was never successfully synthesised. Formation of the diazonium intermediate was observed by LCMS analysis, and protodediazotisation was also noted, but addition of the difluoromethyl group could not be accomplished. This is despite the extended reaction time employed for the

procedure with respect to the published conditions.[174] As such, the reaction was not pursued further.

3.7.2 Decarboxylative *sp*^{3} C-N coupling by dual copper and photoredox catalysis

Rather than activate and remove the amine functionality present within the dealkylated GBBR derivatives, another considered approach was to functionalise these units with alkyl electrophiles. If possible, this would greatly extend the scope of GBBR-type products available, to include those which would require the use of isocyanides in the GBBR which are unstable or unattainable by traditional means of formation.

Therefore, the use of recent conditions reported by MacMillan and co-workers which allowed for the selective monofunctionalisation of an assortment of nitrogen nucleophiles by decarboxylative cross coupling was an attractive proposition.[175]

In order to test this methodology, compound **244** was initially dealkylated under acidic conditions to afford **283** in *c.* 90% purity under the standard conditions (**Scheme 3.21**). Product **283** was used in the reaction without further purification, as it was found to degrade after prolonged periods, even at cold temperatures.

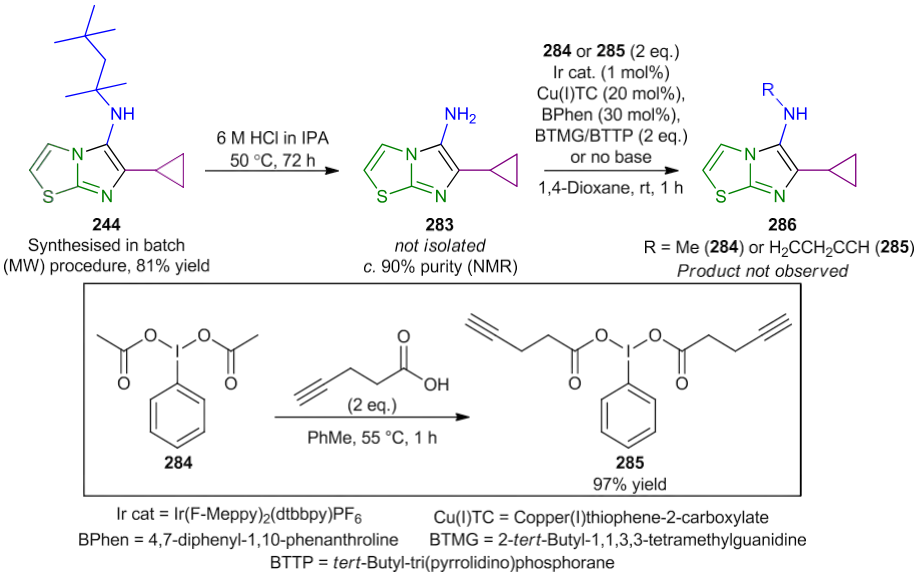

Scheme 3.21: Attempted synthesis of compound 286 using a decarboxylative C-N coupling strategy combining copper and photoredox catalysis.

Using the procedure described in the publication, the alkyl-radical iodonium precursor **285** was synthesised cleanly in high yield. However, the combination of molecules **283** and **285** under decarboxylative *sp*^{3} C-N coupling conditions did not lead to the isolation of the desired product (**286**). Moreover, no desired product was observed even when commercial iodonium complex **284** was employed in the reaction, or when different light sources or bases were used.

The instability of compound **283** could have been the issue affecting the success of the coupling reaction. However, as no product formation was ever observed in any of the attempts to synthesise alkylated derivatives, further optimisation of the methodology was not completed.

3.7.3 The synthesis of semi-saturated imidazoheterocycles

Alternative reagents to the isocyanide were also considered for the synthesis of other GBBR-like heterocycles. Following deprotonation, ylides formed from sulfonium salts are known to display both nucleophilic and electrophilic behaviour, as a consequence of their α-acidity, and neighbouring sulfide leaving group. This has previously led to their use in cyclisation methods such as the Corey-Chaykovsky reaction of sulfonium salts with carbonyl compounds, imines or enones to form epoxides, aziridines or cyclopropanes, respectively.[176]

With this in mind, it was thought that the reactivity of the sulfonium ylide could potentially be intercepted by the GBBR imine intermediate. In this case, cyclisation using a 2-aminopyridine amidine component would form the 2,3-dihydroimidazo[1,2-*a*]pyridine compound (**290**) shown in the general scheme detailed in **Scheme 3.22**.

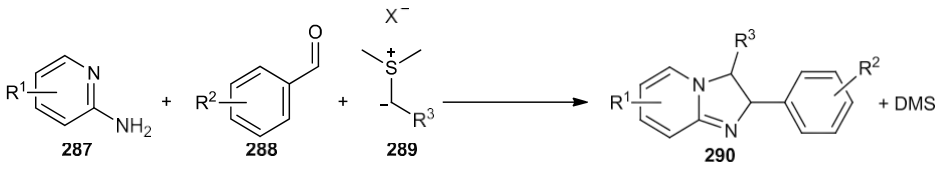

Scheme 3.22: General concept for the condensation reaction of an amidine, an aromatic aldehyde and a sulfonium ylide.

To begin with, the cyclisation was attempted using 2-aminopyridine (**202**), benzaldehyde (**203**) and trimethylsulfonium bromide (**291**). Potassium *tert*-butoxide was the base selected to deprotonate the sulfonium salt in solution. The reaction was performed in a few different solvents, namely tetrahydrofuran (THF), *tert*-butanol and acetonitrile and the desired product was not observed in any case. In fact, acetonitrile was deprotonated during the procedure, and following an aldol-type addition into the benzaldehyde reagent, cinnamonitrile (**292**) was afforded (**Scheme 3.23**).

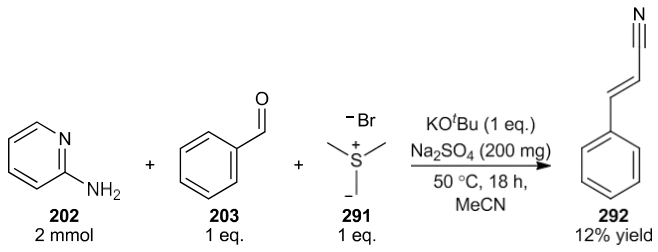

Scheme 3.23: The formation of cinnamonitrile (292) when using the reaction conditions in acetonitrile.

It was thought that perhaps the trimethylsulfonium bromide was insufficiently acidic to be deprotonated by the potassium *tert*-butoxide base in solution. Therefore, a more acidic sulfonium ion (**293**, **Figure 3.7**), with a neighbouring electron-withdrawing group was chosen, to try and drive the deprotonation procedure.

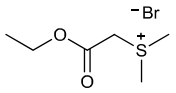

293

Figure 3.7: (2-Ethoxy-2-oxoethyl)dimethylsulfonium bromide (293).

Unfortunately, in all cases, the desired cyclisation product was not isolated, and the most efficient conditions only showed the presence of a material with the same expected m/z ion as compound **292** in negligible amounts. Indeed, the use of higher reaction temperatures (up to 130 °C), stronger, phosphazene bases (BTTP) and drying agents such as sodium sulfate could not direct the reaction pathway towards the desired products successfully. The use of 2-aminophenol (**294**) as an amidine equivalent also did not lead to formation of the analogous oxazine product (**295**, **Scheme 3.24**), suggesting sulfonium salts may not be useful synthetic equivalents for isocyanide reagents in the GBBR-type process.

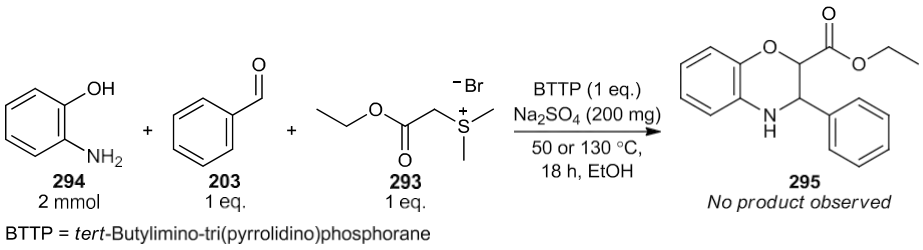

Scheme 3.24: The unsuccessful cyclisation reaction between 2-aminophenol (294), benzaldehyde (203) and (2-ethoxy-2-oxoethyl)dimethylsulfonium bromide (293).

3.7.4 Photoredox-mediated derivatisation of C2-unsubstituted GBBR products

Finally, since one of the benefits of the reported procedure involves the use of formaldehyde to form C2-unsubstituted products, derivatisation at this position was targeted as a potential way to generate complex coupled products in a few synthetic steps.

Nicewicz and co-workers recently reported the regioselective functionalisation of nitrogen heterocycles with pyrazole using photoredox catalysis.[177] The work used computational calculations to determine the site most likely to undergo radical cross coupling, and in many cases, a single regioisomer is observed.

In the publication, a few examples of imidazoheterocycles are utilised. Imidazo[1,2-*b*] pyridazines (**296**-**299**), imidazo[1,2-*a*]pyrimidine (**300**) and imidazo[1,2-*a*]pyridine (**301**) are

explored using the methodology. In all cases, a single regioisomeric product is observed, and adducts which all contain the pyrazole functionality in the 3-position are seen.

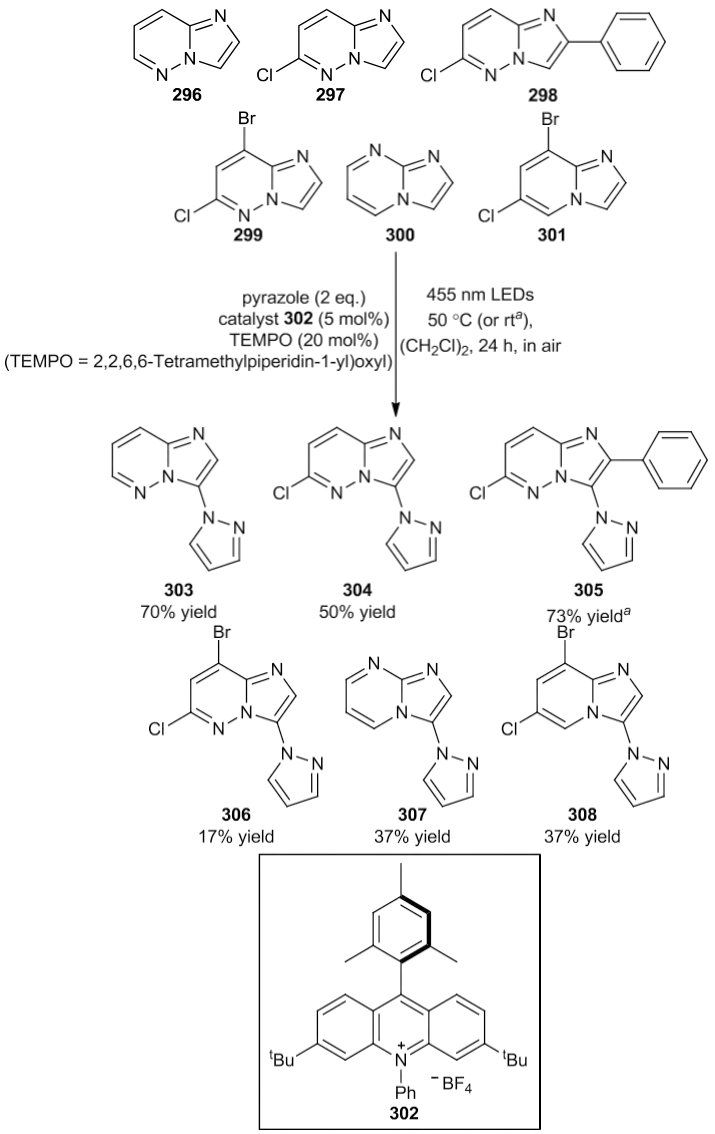

Scheme 3.25: Imidazoheterocyclic examples functionalised within the work reported from Nicewicz and co-workers.

With this in mind, it was postulated that use of the conditions on the C2-unsubstituted products described in the GBBR process could afford functionalised derivatives in another position, since the amine appendage is blocking the otherwise most reactive site and affecting the distribution of electron density within the molecule.

The conditions were thus applied to compound **235** (**Scheme 3.26**). Gratifyingly, under photoredox activation at 50 °C, product **309** was afforded, albeit in a modest yield. The reaction appeared to be clean, but inefficient, since starting materials were the only other materials present in the composition of the reaction mixture. Functionalised product **309** was

successfully isolated as a single regioisomeric product. As a result, this method allows for the synthesis of otherwise inaccessible heterocyclic derivatives in a facile manner. Moreover, combining the GBBR and photoredox reactions allows access to these materials in two synthetic steps from commercially available materials.

Interestingly, no evidence to suggest functionalisation in any other position of the imidazo[1,2-*a*]pyridine, was observed, with the remaining mass balance of the reaction mixture only comprising unreactive starting materials.

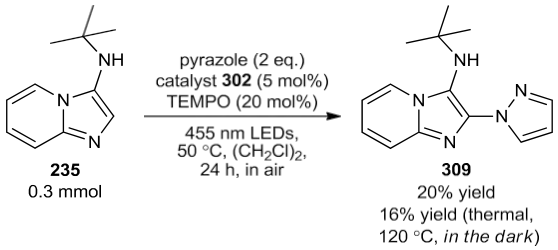

Scheme 3.26: Photoredox catalysed functionalisation of C2-unsubstituted GBBR product 235.

Since the reaction was successful, the precise mechanism was investigated further. Cyclic voltammetry was performed on **235** and found that it was sensitive to two single electron oxidations within the tested voltage range (0 to 2 V). This data is shown in **Section 7.6 Appendix 6 – Cyclic voltammetry data for compound 235**. As photoredox catalyst **302** has an E^*_{RED} of +2.15 V vs SCE, this supports an argument for a single electron transfer to the photoexcited catalyst (**310**) to generate the heteroaryl radical cation (**311**).

Nucleophilic addition of pyrazole (**312**) then forms a coupled radical cation (**313**) which may be attacked by molecular oxygen. A subsequent elimination of hydrogen peroxide then accompanies removal of the C2-hydrogen atom and the desired product is formed. TEMPO (**314**) may also be used in order to facilitate oxidation of **313** and can be recycled by the radical anion of hydrogen peroxide which is present as a result of the reduction of molecular oxygen by the reduced acridinium photocatalyst (**315**). This putative reaction mechanism is described in **Scheme 3.27** and is modified from an initial proposal made by the Nicewicz group.[178]

However, the reaction was also performed in the absence of light under more forcing conditions, and the desired product was afforded in a slightly lower yield (**Scheme 3.26**). As such, the reaction mechanism may not require photoexcitation or may work through a slightly different mechanism, potentially as a result of thermal excitation of the catalyst.

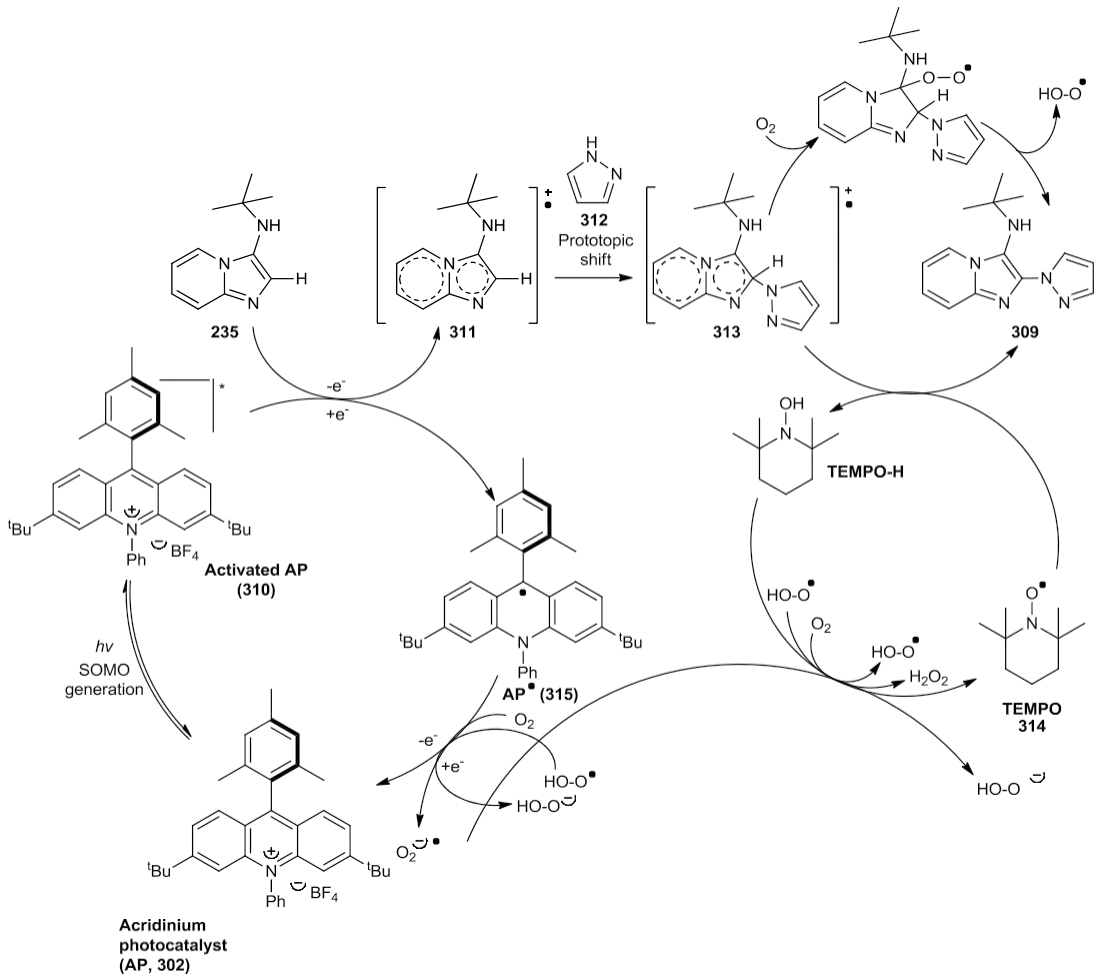

Scheme 3.27: Putative mechanism for the photoredox-mediated coupling of 235 with pyrazole. Modified from the mechanistic scheme proposed by Romero *et al*.[178]

This procedure offers interesting future developments into potential coupling products which can be derived through the derivatisation of GBBR products. If not for a lack of scope within the programme to further elaborate the reaction, differing reaction conditions would have been investigated, including those coupling a variety of functionalities following the formation of the heteroaryl radical cation. This therefore represents an interesting route for late-stage derivatisation of compounds which may be of significant importance to the medicinal chemistry community, which are difficult to access *via* more traditional methods.

3.8 Chapter 1 conclusions

In conclusion, an efficient, robust, sustainable and scalable procedure for the Groebke-Blackburn-Bienaymé reaction has been developed. The method gives access to a plethora of imidazoheterocyclic products, with a large amount of diversity in all components used in this convergent multicomponent reaction approach.

GSK CONFIDENTIAL INFORMATION – DO NOT COPY

The reaction has been developed to be performed most effectively under flow conditions and has been tailored to include the use of usually difficult formaldehyde and alkyl aldehyde reagents. Moreover, adaptations to the flow procedure can be easily made to account for issues otherwise observed with acid-sensitive reagents.

The process has been shown to be adaptable to the production of the desired products on large scale and avoids the use of hazardous solvents and metal catalysts which are undesirable, increasingly so when scaled. Efforts were also made towards implementing a tandem procedure for the synthesis and the *in situ* generation and use of isocyanide reagents within a flow system. Unfortunately, this goal was not achieved under the limits of the utilised flow equipment, but early experiments suggest that the process may be possible when performed under the appropriate conditions. An applicable microwave based method was also formulated for the GBBR.

This reaction was applied in multiple examples and allows for the clean formation of latent amine-containing molecules following a subsequent dealkylation procedure, which was also devised, to afford a difunctionalised advanced intermediate for further manipulation in a facile process.

Finally, various methods of derivatisation of the products afforded from the GBBR process were explored. Though issues were encountered in many of these potential methodologies, the photoredox-mediated coupling of a C2-unsubstituted GBBR product was fruitful and offered regioselective and direct access to a pyrazole adduct in a simple manner. The combination of these two synthetic steps can therefore produce significantly complex molecules in only two steps from commercial reagents.

3.9 Future work for Chapter 1

Future work utilising the GBBR methodology may be based on applying the procedure towards the synthesis of active pharmaceutical products containing the desired functionality. Furthermore, the products accessed may also be used as heterocyclic ring replacement tools for similar bicyclic heterocycles (**Figure 3.8**). For instance, an active medicinal chemistry programme involving target molecules with benzimidazole or indole scaffolds in their structure may benefit from novel SAR developments through their substitution with a similar bicyclic heterocycle such as an imidazo[1,2-*a*]pyridine.

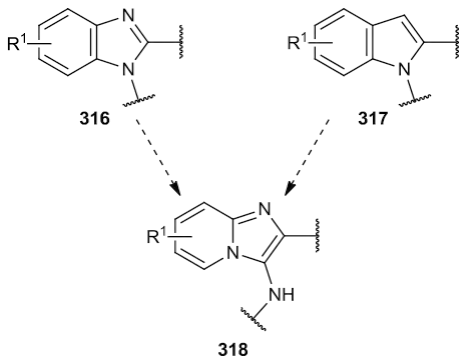

Figure 3.8: Representation of the potential use of imidazo[1,2-*a*]pyridine functionality (318) as a heterocyclic replacement tool for similar heterocycles such as benzimidazoles (316) or indoles (317).

In terms of derivatisation, future endeavours around the photoredox-catalysed coupling may offer the potential for the greatest success out of the explored options described earlier. The Nicewicz group have published extensively in this area, including conditions which allow for the late-stage regioselective functionalisation of heterocycles with nitrile and amine functionalities, for instance.[178,179] Development around this methodology for the regioselective functionalisation of C2-unsubstituted GBBR products may allow for the efficient generation of a range of 2-substituted derivatives, which may have potential use within synthetic and medicinal chemistry applications, and which cannot be accessed *via* the GBBR, or other methods discussed above.

4. Chapter 2: A telescoped, continuous flow synthesis of diaminoquinazoline antimalarials

4.1 Malaria

Malaria is a deadly tropical disease caused by 6 species of eukaryotic single-celled *Plasmodium* parasites in humans. The *World Malaria Report*, which publishes key facts and developments relating to the disease annually, shows that an estimated 219 million cases of malaria were reported worldwide in 2017.[180] Though this represents a reduction of ~20 million cases since 2010, no significant recent progress in reducing the amount of reported cases was found over the three years preceding the 2017 study.[180]

Moreover, 435,000 deaths from the disease were reported in 2017, and the majority (61%) of these cases were children under 5. Pregnant women are particularly susceptible to malaria due to specific receptors on the parasites, which recognise placental vasculature and increase the risk of adverse effects on the foetus, and miscarriage. Immunocompromised patients, or those co-infected with other malarial strains, or other pathogens, are also at an increased risk of severe complications and death.[181]

Of reported malaria cases worldwide in 2017, 92% occurred within African countries, and of these cases, 99.7% of them derived from a single parasitic species, *Plasmodium falciparum.*[180] The representative worldwide geographical distribution of malaria is shown in **Figure 4.1**.

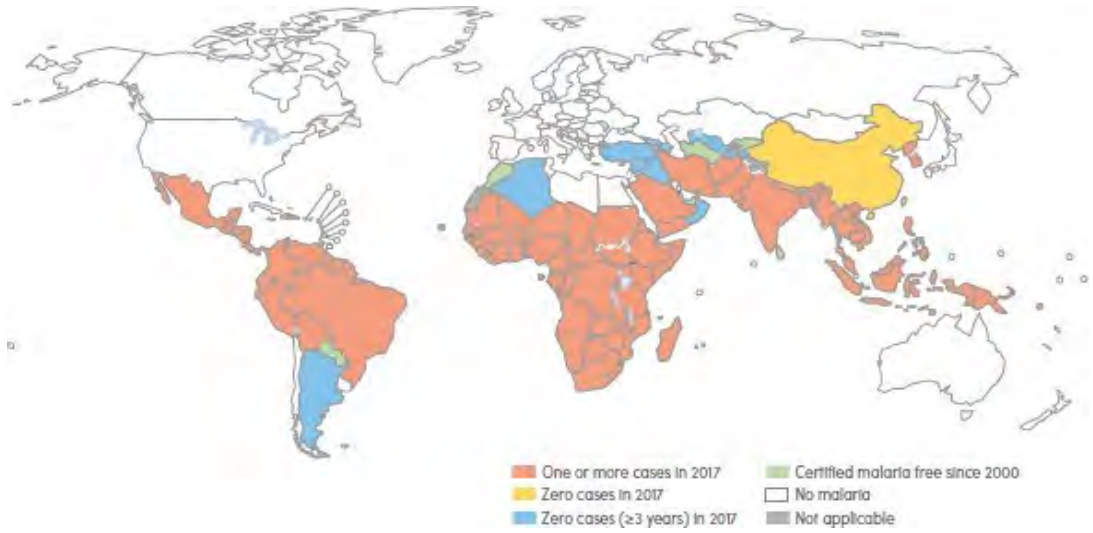

Figure 4.1: Worldwide distribution of reported malaria cases.[182]

Plasmodium parasites, namely *Plasmodium falciparum* (the most lethal species globally), *Plasmodium vivax* (the most prevalent species within the Americas), *Plasmodium ovale* (actually two species, *P. ovale curtisi* and *P. ovale wallikeri*), *Plasmodium malariae* and *Plasmodium knowlesi* (usually responsible for the infections of Macaque monkeys in

Southeast Asia) induce the symptoms of malaria, after entry to the body, following the blood meal of an infected female *Anopheles* mosquito on a human host.[181]

Malarial cases can either be asymptomatic, uncomplicated or severe. Asymptomatic patients have parasites circulating in their bloodstream but have not yet developed symptoms from the infection. In malaria-endemic regions, many individuals may be year-round asymptomatic carriers of the disease, where the parasitaemia is maintained at equilibrium levels by their immune system. Uncomplicated malaria manifests itself through various non-specific flu-like symptoms such as nausea, fever, sweating, rapid temperature changes and anaemia. If untreated or aggressive, malaria can become severe in nature. In these cases, the increasing parasitaemia can cause severe anaemia. Furthermore, infected erythrocytes can also block blood vessels due to their typically hardened membranes.[183] The combination of these two symptoms observed in severe malaria often result in organ failure and death.[181]

4.2 Parasite life cycle

The typical life cycle of a plasmodium parasite population is depicted in **Figure 4.2**. During mating between anopheline mosquitoes, the male transfers a large amount of the steroid hormone 20-hydroxyecdysone to the female mosquito. The presence of this hormone has been connected to ideal conditions for the development and protection of *Plasmodium* parasites within the mosquito hosts.[184]

In order for sporozoites (mobile cellular forms of the parasite) to develop within the gut of the mosquito host, favourable conditions for both survival of the parasite and the mosquito are required. *Anopheles* mosquitoes typically lay their eggs in fresh or brackish bodies of water. These eggs then take a few days to hatch, before larvae mature over a 9-12 day period.[185]

Resultantly, the climate has a significant impact on the survival of the mosquitoes. If excessive rainfall is seen, or the climate is too dry to support an optimal hatching environment, the longevity of the mosquitoes will be insufficient to facilitate parasite transmission.

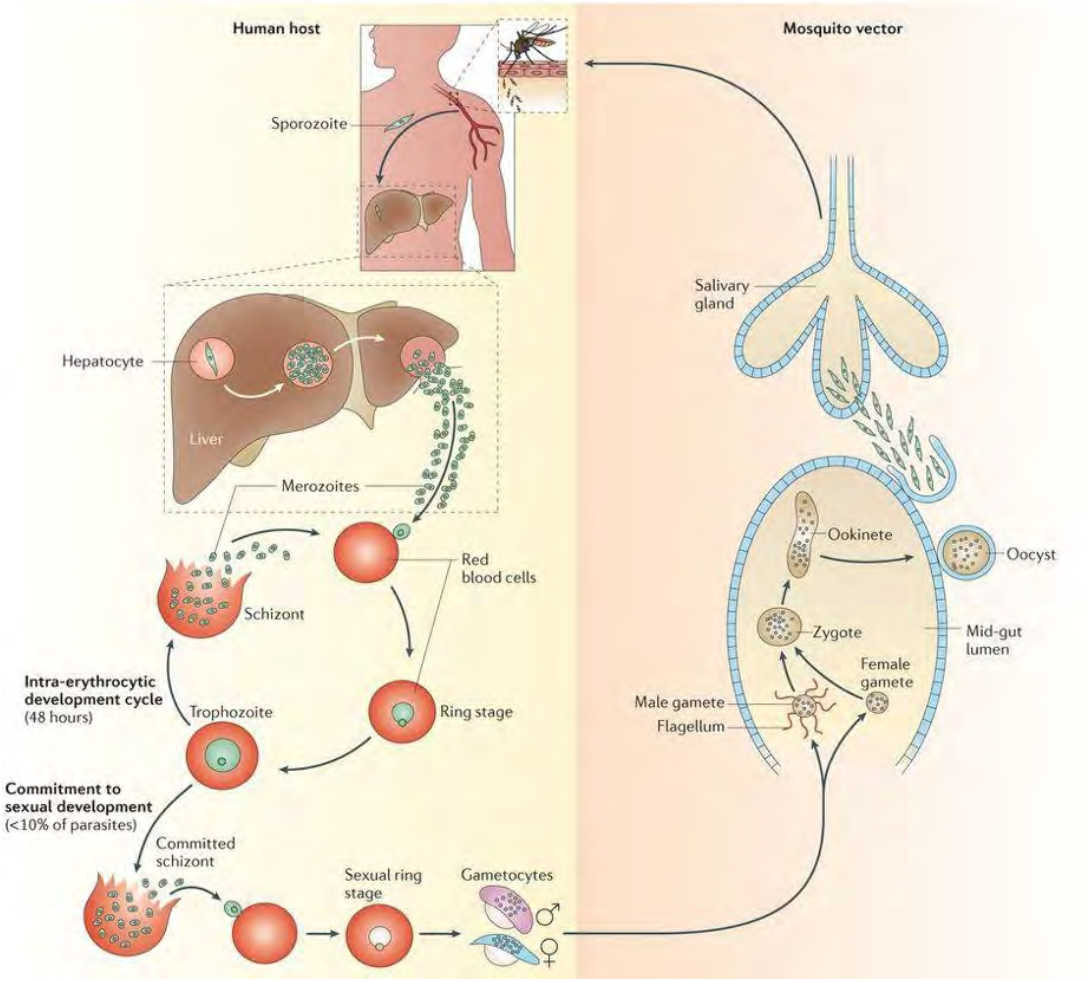

Figure 4.2: Figure depicting the life cycle of plasmodium parasites. Adapted with permission from Josling and Llinás.[186] Sporozoites invade hepatocytes in 30-60 minutes following injection by the mosquito. 6-7 days after initial infection, merozoites are released from the liver and inhabit red blood cells, causing the symptomatic stage of the disease. 36-72 h later, infected red blood cells are destroyed, and parasitic endotoxins are released. The erythrocytic cycle is propagated by the released merozoites, and a small percentage (< 10%) of released cells can also mature into gametocytes. Gametocytes gather in skin capillaries and can be uptaken by a mosquito during a blood meal. A subsequent sexual reproduction of the gametes then generates the next round of oocysts, which replicate and develop into mobile sporozoites. Following the introduction of gametocytes into a previously healthy mosquito, sporozoites require 7-10 days to develop. Therefore, the entire cycle of malaria propagation requires only a few weeks under desirable conditions.[181]

High temperatures are also needed for development of the malarial parasites. In warm conditions (30 °C), parasites require their mosquito hosts to survive for at least 9 days in order for the cells to mature into sporozoites for transmission. This process is drastically decelerated in colder climates, and when temperatures are too cool (under 20 °C for *Plasmodium falciparum* and under 15 °C for *Plasmodium vivax*), the parasites cannot survive, and malaria cannot be transmitted. As a result, this climate-related necessity for the parasite helps explain the geographical distribution of the tropical disease (**Figure 4.1**).[185]

Following maturation into sporozoites, the parasites are injected, along with anti-coagulating saliva, into humans during a blood meal. Sporozoites move through the dermis to the bloodstream using gliding motility, a random movement which allows some of the cells to traverse into blood vessels and enter the host's circulation.

Parasites which successfully invade the bloodstream then travel to the liver, where they are capable of infecting hepatocytes. Specific proteins present within the parasite allow them to form temporary vacuoles within cells, facilitating their rapid movement through the cellular framework.[187]

Once established within a hepatocyte, the sporozoites generate a parasitophorous vacuole membrane (PVM), within which they develop into liver stage forms of the parasite, and subsequently undergo schizogony (a phase of asexual reproduction) until tens of thousands of daughter merozoites are produced within the cell. These daughter cells are released in membrane-bound packets into the vasculature, known as merosomes.[187]

The immune cell evasion exhibited by the parasites during the liver-stage of infection is not completely understood, but may be related to the inhibition of Kupffer cells, which otherwise behave as resident macrophages in the liver.[181]

During hepatocyte infection, sporozoites caused by *P. vivax* and *P. ovale* parasitic strains can also lay dormant in a form known as hypnozoites. Hypnozoites may emerge from the liver months or years after the initial infection, resulting in relapsing malarial cases when not treated properly.[188]

The merozoites present within the circulation then invade erythrocytes or reticulytes (immature red blood cells, usually seen in *P. vivax* infections) in a multi-step process, which only takes 2 minutes. For *P. falc*, two essential red blood cell receptors, basigin and CD55, are essential for the invasion process.[189,190]

Following invasion, a period of echinocytosis (the formation of a red blood cell with an abnormally shaped cell membrane) is observed, following the loss of water in the cell, before the infected cell re-establishes homeostatic control over time.

Red blood cells are specifically targeted by merozoites for their haemoglobin, the protein responsible for oxygen-complexation in erythrocytes; a vital process for oxygen delivery to tissues during respiration. *Plasmodium* parasites are auxotrophic, which means that they cannot generate their own amino acids, and must source them from host cell components. All essential amino acids except isoleucine can be derived from haemoglobin metabolism within the food vacuole of the host cell. The haem protein is actually toxic to the parasite, and is resultantly polymerized as an insoluble crystalline structure called haemozoin by the organism.[191,192]

Inside the erythrocyte, the parasite releases a large number of proteins, to transform the red blood cell into a host cell capable of supporting rapid parasitic division and evading the immune system. These proteins are also involved in the restructuring of the cellular cytoskeleton to improve its resilience to temperature and shear stress changes. Included in these proteins is the major virulence factor PfEMP1 (*Plasmodium falciparum* erythrocyte membrane protein 1).

After various points of the cellular membrane around the circumference of the host cell (known as dots) have been raised outward by the KAHRP protein (knob-associated histidine-rich protein), PfEMP1 is presented at each dot to the extracellular environment. PfEMP1 controls adhesion to host cell receptors and interacts with host antibodies. The parasitic erythrocytes can express different isoforms of the protein in a transient fashion in order to avoid recognition and destruction by the immune system.[187,193]

After infecting an erythrocyte, the merozoite will perform rapid cell division over the following 48 h to afford 16-32 merozoite cells. On a collective scale, during the symptomatic stage of the disease, the parasite may reproduce exponentially to > 10^{12} parasites per patient.[181] The produced cells egress following schizogony, causing cellular destruction of the erythrocyte, and the release of many more parasites capable of invading red blood cells.

Haemozoin formed by the parasite, which is thought to be present as a complex with parasite DNA, is also released following erythrocyte rupture, and acts as an endotoxin, activating the host immune system through interactions with Toll-like receptor 9 (TLR9). This results in early clinical symptoms such as fever and shaking chills.[181]

A small proportion of the merozoites released from erythrocyte rupture do not further propagate the blood-stage cycle, but rather mature into male and female gametocytes (**Figure 4.2**). Expression of the transcription factor AP2-G has been shown to regulate commitment of the parasite to gametocytogenesis.[181] Gametocytes are haploid cells which accumulate in capillaries close to the surface of the skin. Following another blood meal, gametocytes enter the lumen of the mosquito, and reproduce to make oocysts, primordial forms of the parasite that can develop and replicate to form the next round of sporozoites.[181]

4.3 Active malarial immunity

Within endemic malarial areas, many people display active immunity against rapid progression of the disease. Many Africans are negative for the Duffy antigen (also called atypical chemokine receptor 1), a cell surface protein on red blood cells which is believed to be important for the cell's invasion by *P. vivax* parasites. As such, this natural genetic variation offers benefits for African populations in preventing *P. vivax* derived malaria and helps explain the relatively low abundance of malaria cases caused by this parasite, compared to *P. falc.* in these regions.[194]

Surprisingly, another study found that individuals with naturally occurring iron deficiency were also less susceptible to the severe malaria caused by *P. falc*.[195] This was an unexpected result, especially since malaria patients with iron deficiency have previously been dosed with iron supplements in an attempt to decelerate their clinical progression to severe anaemia.[196]

According to the study, those with natural iron deficiencies were actually both less likely contract the disease, and their parasitaemia took longer to deteriorate. On the other hand, according to further review, when administered alongside appropriate antimalarial treatments, iron supplements do not increase the risk of developing malaria.[195,196]

Many evolutionary selection pressures have been induced on individuals living in areas with large numbers of reported malaria cases. Various genetic disorders are prevalent, which reduce the incidence of severe malaria by physiological mechanisms, such as increased red blood cell phagocytosis and turnover by the spleen, reduced parasite invasion of red blood cells, reduced intracellular parasitic growth rates and reduced cytoadherence of infected cells, which can otherwise result in blood vessel blockages.[181,197]

Crucially, in areas of frequent malaria transmission, many people develop partial protective immunity through the formation and circulation of immunoglobin class G (IgG) antibodies as a result of past exposure to the parasites. The antibodies produced are able to recognise cell-surface proteins on sporozoites and merozoites, therefore lessening the extent of hepatocyte and erythrocyte invasion, and slowing down progression of the disease *via* the immune system-orchestrated destruction of parasitic cells.[181]

Typically, in areas with low levels of malaria transmission, protective immunity is rarer, and patients often suffer more severe symptomatic developments following infection.

As a result, work towards eradication of the disease could lead to a smaller fraction of the patient population having active immunity, and a concurrent rise in the reported cases of severe malaria in the affected region. Asymptomatic carriers of the disease also represent another difficult challenge in the resilience and re-emergence of malarial infections following antimalarial therapeutic intervention in an endemically affected area. As such, even in successful treatment programmes, efficient surveillance of the patient population may be required for long periods to ensure eradication of the parasite.[181]

4.4 Malaria screening and detection

Microscopic diagnosis is usually utilised to determine the presence of a malarial infection. Under microscopic analysis of a patient's blood smear and following treatment with a staining dye (usually the Giemsa stain), parasites can be observed. Visual criteria of the parasites can be used to elucidate the parasitic species present within the blood sample. The technique is

relatively simple and offers a quick and effective way of determining both the presence and extent of parasitaemia in the blood.[198]

Alternatively, a rapid diagnostic test (RDT) can also be used to identify a malarial infection. RDTs detect the presence of species-specific antigens in the blood and can therefore be used to find the parasite responsible for malaria within an affected patient. The test is immediately available, even in places where access to microscopic blood analysis may be limited, or where large delays are experienced in laboratory-based blood testing methods. However, RDTs suffer from sensitivity issues in patients with low parasitaemia (< 50 parasites/1 µL of blood), and the less common malaria-causing parasite strains (such as *P. ovale* and *P. malariae*) are more difficult to detect. Therefore, their use does not necessarily dismiss further diagnostic analysis.[198]

A serological method allows for the diagnosis of malaria in patients with low parasitaemia, who have developed a partial protective immunity. Indirect fluorescent antibody (IFA) testing uses an immobilised antigen from a selected *plasmodium* species. The antigens used are isolated blood stage parasitic cells, which are responsible for the production of daughter merozoites during the life cycle. If the patient's blood contains relevant antibodies capable of recognising the parasitic antigens, a complex is formed, which can be determined by fluorescence analysis. The technique is not suitable for most cases of acute malaria, as the method requires relatively long timescales.[198]

Nevertheless, the screening can be valuable in accurately testing blood samples for malarial parasites, even in cases where the parasitaemia is too low to be determined by blood smear analysis. This has uses in the prior screening of blood donors for transfusion, as well as in patients with tropical splenomegaly syndrome (also called hyperreactive malarial splenomegaly). For these patients, repeated bouts of malaria may activate the immune system to produce antimalarial antibodies, as well as causing an enlargement of the spleen and liver. Often, the obtained partial immunity of patients with tropical splenomegaly syndrome keeps the level of cellular parasites low in the blood, and microscopic diagnosis may not be conclusive.[198,199]

Finally, studies using polymerase chain reaction (PCR) based methods of analysis have been explored to determine parasitaemia. Though still in their infancy, new developments may allow for the technique to determine multiple pathogenic infections at once, and even identify the presence of drug-resistant malaria.[181,200-202]

4.5 Vector approaches to malaria

Various approaches have been made towards the eradication of malaria. The first revolves around the modulation or elimination of anopheline mosquitoes, the vectors for malaria.

The first WHO (World Health Organisation) Global Malaria Eradication Programme was initiated in 1955 and employed the industrial use of the insecticide dichlorodiphenyltrichloroethane (DDT, **319**, **Figure 4.3**).[203]

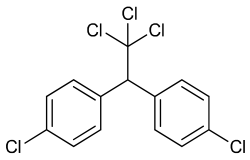

319

Figure 4.3: Dichlorodiphenyltrichloroethane (DDT, 319), an insecticide employed in early antimalarial programmes.

The programme was largely successful in areas of infestation, and some of the areas treated with the insecticide have remained malaria-free to this date. Unfortunately, emerging mosquito resistance to the insecticide, along with growing issues over its cost, safety and bioaccumulation in the environment, meant that the technique was unsustainable.[181]

A more recent controlled approach to insecticide use has involved the indoor coating of living spaces with insecticidal agents to prevent transmission from infected mosquitoes. The use of insecticide-coated bed nets has granted malarial protection for many people while sleeping in malaria-troubled environments. The combination of these two approaches have drastically reduced malaria transmission and are estimated to be responsible for two thirds of the malaria cases avoided between 2000 and 2015.[204]

On the other hand, the effectiveness of this method may be waning. Behavioural changes in mosquitoes have meant that they have begun to feed more often in the day, and insecticide resistance is becoming an increasing threat.[205] Though new chemical agents are in production, many are still multiple years away from deployment.[181]

Lastly, gene editing approaches have been considered for vector control. Using CRISPR-Cas9 (clustered regularly interspaced short palindromic repeats-CRISPR associated protein-9) technology, mosquitoes can be modified such that either their progeny are sterile, or they are refractory to parasitic infection.[206,207]

The subsequent release of gene-edited mosquitoes into the wild may allow for the eradication of malaria. However, the uncertain environmental impact of this approach, as well as the extensive regulatory hurdles involved have thus far limited the application of gene editing in mosquito control.[181]

4.6 Malaria vaccines

The development of an effective vaccine for malaria is a difficult challenge, since cellular and humoral immune responses are involved in fighting the disease but are not usually able to

entirely destroy it. Moreover, typical vaccine strategies have focused on targeting specific surface proteins expressed by individual *Plasmodium* species. This is not ideal, as it limits the scope of vaccine application and also enables the possibility of arising resistance from the affected strain.

Nevertheless, the most successful vaccine to date, RTS,S/AS01 (trade name Mosquirix™) has been employed in phase III studies of young African children and has displayed an efficacy of between 26% and 55% in reducing malaria contraction.[208,209] Though not optimal in preventing parasitaemia (a long-lasting efficacy of ≥ 75% against *P. falc.* and *P. vivax* is ideally targeted for vaccines), this still represents a ground-breaking development in the fight against malaria, and Mosquirix™ is currently under investigation in a large scale study in Ghana, Kenya and Malawi prior to determining treatment recommendations for its use.[210]

The vaccine, which was developed in a joint venture between GlaxoSmithKline and the Program for Appropriate Technology in Health (PATH) Malaria Vaccine Initiative (MVI), is a recombinant protein comprising parts of the *P. falc.* circumsporozoite protein, the most prevalent antigen present on sporozoite cell surfaces; a viral envelope protein of the hepatitis B virus, and chemical adjuvant AS01 to further activate an immune response.[208] Within the parasite life cycle (**Figure 4.2**), the vaccine therefore targets *in vivo* parasites prior to (and during) hepatocyte invasion.

Various vaccine-based approaches are currently in the pipeline, which may contain a number of different parasitic targets. Sporozoites displaying a wide variety of presented antigens after irradiation were introduced into malaria-infected patients in one study, and found to work as an effective, and potentially robust, vaccine.[211]

Subunit vaccines are also under development, and may be combined, in multi-stage and multi-antigen formulations, depending on the application. Transmission-blocking vaccines and monoclonal antibodies are two alternative approaches which have also been proposed in the drive to eliminate malaria, although further pre-clinical development is required in these areas.[181]

Vaccines are primarily designed for children, but the active malarial immunity that can be acquired in areas devastated by the disease is rapidly lost (taking 3-5 years) following successful treatment and non-sustained interaction with the parasites.[212] As such, vaccinations may prove to be useful alongside antimalarial drug regimens to ensure the lasting removal of the disease from troublesome regions.

4.7 Antimalarial pharmaceuticals

While research behind other preventative measures is still ongoing, effective treatment of malaria (both prophylactically and during the disease) through chemotherapy remains the

main strategy for reducing the mortality and morbidity associated with the disease. Some examples of commercial antimalarials, along with their parent chemical class, related commercial drugs, and their proposed mechanism of action are provided in **Figure 4.4**.

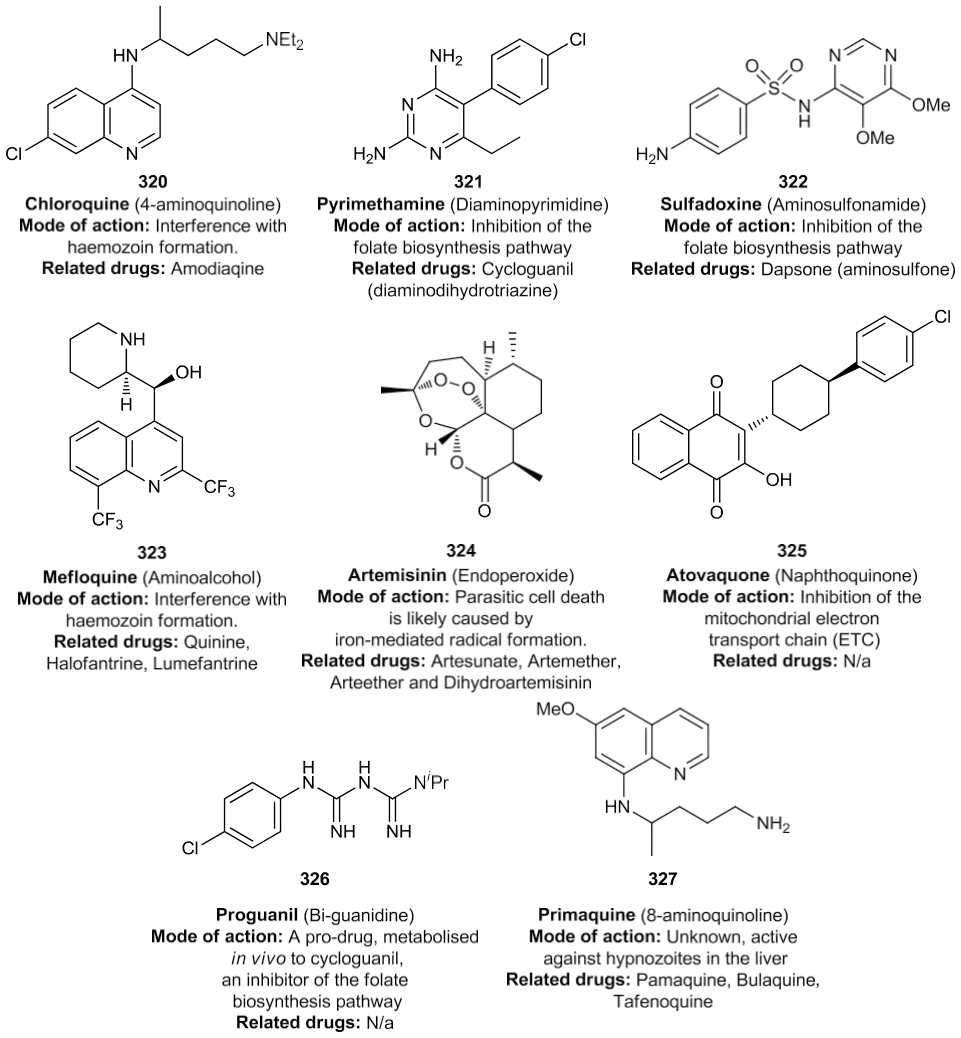

Figure 4.4 Examples of antimalarial medications which have successfully reached the market. In each case, the structural class of the molecule is shown in parenthesis, and the mode of therapeutic action (if known) as well as related pharmaceuticals are also highlighted. Antibiotics such as doxycycline and clindamycin also exhibit antimalarial activity, but their slow rate of parasite elimination is not sufficient, especially for first-line antimalarial treatments.[213] Adapted from Calderon and co-workers.[214]

Since such a large volume of antimalarials have been discovered historically, the following sections will only report some of the aforementioned medications, details behind their therapeutic mode of action, any relevant developments, and any resultant resistance arising from the clinical use of such drugs.

4.7.1 Quinine

Quinine (**Figure 4.5**, **328**) was both the first antimalarial to be isolated, in 1820, and the first reported successful use of a chemical compound in the treatment of disease. Records of using

cinchona bark extracts (which contain quinine) to cure fever date back to as early as the 1630's.[214,215] Quinine is a naturally-occurring alkaloid derived from the bark of the cinchona (or quinaquina) tree, and the ingredient responsible for the bitter taste in tonic water.

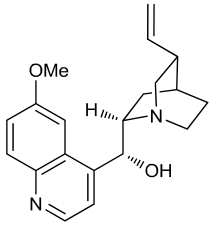

328
Quinine

Figure 4.5: Quinine, the first antimalarial, first isolated as quinine sulfate in 1820.

The origin of the antimalarial activity of quinine remained a mystery for several centuries, and still may not be fully understood. Originally, quinine was believed to be involved in interruption of the process of haemoglobin metabolism, leading to parasitic cell death.[214]

Though this cannot yet be entirely ruled out as a contributing mechanism of action, new research suggests that *P. falc.* purine nucleoside phosphorylase (PfPNP) is actually the principal binding target for the compound within the *Plasmodium falciparum* parasite, as determined through MS-CETSA (mass spectrometry coupled-cellular thermal shift assay) analysis.[216] PfPNP has already been investigated as a potential antimalarial target, and is a vital enzyme within the parasite, having an essential function within purine salvaging for the assembly of genetic material.[217]

In the publication, both quinine (**328**) and mefloquine (**323**) were shown to form strong binding complexes with (and inhibit the action of) the protein, even at low concentrations. However, mefloquine also displayed binding affinity to other cellular proteins, suggesting that the mode of action may be more complex. Interestingly, antimalarials with structural similarities to quinine, such as chloroquine and lumefantrine, were ineffective at binding to PfPNP, suggesting that the mode of action may be a complicated mechanism to derive, even for similar structures.[216]

Quinine is still used in some antimalarial applications, such as cases of uncomplicated malaria within women during the first trimester of pregnancy, but otherwise remained in prominent clinical use until the 1920's, at which point more effective related antimalarials were discovered.[214,216] Of these, chloroquine (**320**) has undoubtedly had the most significant effect on malarial care practices.

4.7.2 Chloroquine

Until the emergence of widespread resistance (see **Section 4.7.8 Parasite resistance**), chloroquine (**Figure 4.6**, **320**) remained the safest, most tested and most utilised antimalarial drug. Its high efficacy and low cost of production made the compound ideal for the treatment of acute malaria.[214]

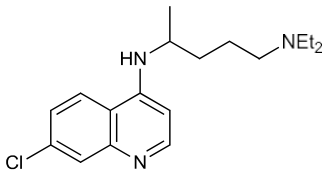

320
Chloroquine

Figure 4.6: Chloroquine, an antimalarial working through the interruption of haemoglobin digestion.

Between antimalarial medications, it has one of the better understood modes of action. During the intraerythrocytic stage of the parasitic cycle, chloroquine is believed to interrupt the haemoglobin digestion process necessary for the continued growth and viability of the plasmodium parasites. Within the acidic environment of the digestive vacuole, the compound is doubly protonated, and can interact in this form with the haem protein (also called ferriprotoporphyrin IX) derived from haemoglobin degradation.[214]

This interaction prevents the sequestration of the otherwise toxic haem protein dimers into insoluble haemozoin crystals, thereby generating a toxic environment for the plasmodium parasites.[218]

Various structural modifications of chloroquine have been attempted, in order to improve the safety profile of the drug and mitigate against developing resistance mutations. These approaches have led to the development of compounds capable of killing chloroquine-resistant parasite strains (such as **329**-**331**, **Figure 4.7**).[214,219]

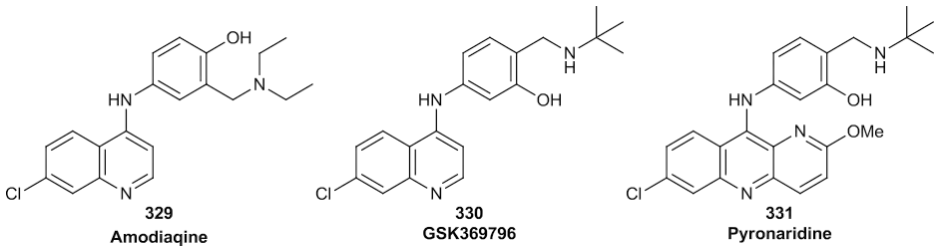

329
Amodiaqine

330
GSK369796

331
Pyronaridine

Figure 4.7: Examples of chloroquine derivates which have displayed activity against chloroquine-resistance parasite strains.

However, in most cases, application of these derivatives is often limited by unpleasant or toxic side-effects. Pyronaridine (brand name Pyramax®, **331**) is one of the more promising

developments from this work and has been widely employed as part of a combination therapy for the blood-stage treatment of *P. falc.* and *P. vivax* infection.[220]

4.7.3 Folate biosynthesis inhibitors

Another successful tactic for the development of antimalarial medication has been adopted through targeting the *Plasmodium* folate biosynthesis pathway. Folate, which is present in various forms, is a B vitamin, that is essential for nucleic acid formation and normal metabolism. *P. falc.* is capable of acquiring reduced folates from cells, but still needs to produce folate cofactors in order to survive.[221]

Various enzymes are involved within the folate biosynthetic pathway. Dihydrofolate reductase (DHFR) reduces dihydrofolate into tetrahydrofolate, an essential cofactor involved in the transfer of one carbon units during biological processes.[214] Pyrimethamine (**321**) and cycloguanil (**332**) are examples of classic inhibitors of DHFR, used in malarial treatment. Proguanil (**326**) is another commercial antimalarial, which generates cycloguanil following *in vivo* metabolism.

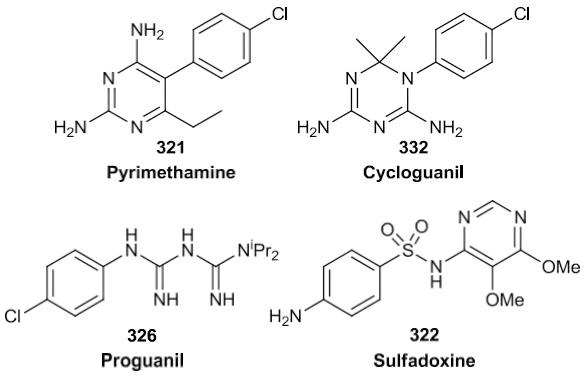

Figure 4.8: Antimalarials which interact with the parasitic folate biosynthesis pathway.

Pyrimethamine has been widely employed in combination therapy alongside sulfadoxine (**322**). Sulfadoxine is another inhibitor of the pathway, but targets dihydropteroate synthase (DHPS), an enzyme involved at an early stage than DHFR in folate biosynthesis.

Significant structural and regulatory differences between the enzymes involved in human and parasitic folate biosynthesis result in these drugs being extremely effective and safe for antimalarial treatment.[222] Nevertheless, arising resistance against them has favoured artemisinin-based combination therapies (ACTs) as a first-line treatment option (See **Section 4.7.6 Artemisinin-based combination therapies (ACTs)**).[214]

4.7.4 8-Aminoquinolines

One of the most difficult challenges facing the malarial community involves the treatment of hypnozoites. As mentioned earlier, some species of malarial parasite (*P. vivax* and *P. ovale* in

humans) are able to arrest their cellular activity and exist as dormant forms during the hepatocyte-based stage of infection. In order to fully remove all parasitaemia associated with an infected patient, therapeutics capable of recognising and eradicating these inactive forms are hence required.

8-Aminoquinolines deliver on this therapeutic target, displaying activity against hypnozoite-forming strains of the parasite and, as such, prevent the disease from relapsing with high levels of efficacy. Until recently, primaquine (**327**) was the gold standard treatment in combination therapies for *P. vivax* and *P. ovale* derived malarial infections, and studies evaluating its effectiveness found higher than 95% efficiency in its suppression of relapsing *P. vivax* derived malaria.[223]

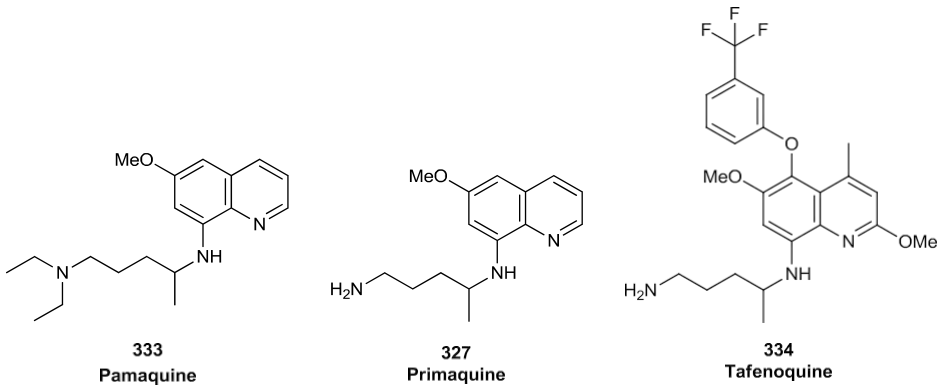

Figure 4.9: Antimalarial drugs containing an 8-aminoquinoline motif.

Primaquine was developed following the initial use of the structurally related analogue pamaquine (**333**) as an antimalarial medication. Unfortunately, pamaquine suffered from various toxicity issues and was ineffective against blood stage forms of the disease. As a result, primaquine became the slow-acting treatment of choice following its development.

Yet, the use of primaquine is also associated with severe side-effects. Within Asian and African populations, a deficiency of glucose-6-phosphate dehydrogenase (G6PD) is commonly observed, as a form of partial active immunity against malaria. G6PD deficiency is a genetic disorder which leaves erythrocytes vulnerable to oxidative stress and haemolysis. G6PD is an essential enzyme, which is involved in a pathway solely responsible for the maintenance of a sufficient level of nicotinamide adenine dinucleotide phosphate (NADPH) within erythrocytes.

NADPH is required as a co-factor in the reduction of the oxidised form of glutathione, made as a result of oxidised stress on the molecule. As such, when a deficiency of G6PD is observed, red blood cells become susceptible to haemolysis *via* oxidative damage.[224]

In the use of primaquine, bouts of acute haemolytic anaemia have been observed in patients with the deficiency.

A more recent development was achieved in the research behind tafenoquine (**334**). While tafenoquine (marketed as Krintafel) still suffers from the same drawback of haemolytic anaemia, it has been shown to be active against all life cycle stages of *P. vivax* infection and has a vastly improved half-life. As such, Krintafel is sold as a single-dose cure of *P. vivax* derived malarial infection, an advantage which is likely to vastly improve patient compliance.[225]

The precise mechanism of action for these antimalarials has still not been fully elucidated. Indeed, studies have shown that several different biological targets are involved in their anti-parasitic activity.[226-229]

4.7.5 Atovaquone

In contrast to those therapeutic agents mentioned above, the mechanism of atovaquone is fairly well understood. Atovaquone interrupts the mitochondrial electron transport chain (ETC) within the parasites. Specifically, its inhibition of the cytochrome (CYT) bc_1 protein complex prevents the normal performance of various dehydrogenase enzymes present within the mitochondria. One such enzyme, dihydroorotate dehydrogenase (DHODH), is essential for parasitic development, because of its involvement within pyrimidine biosynthesis. Consequently, inhibition of the CYT bc_1 protein complex prevents nucleic acid and protein synthesis within the parasite, and is resultantly toxic for the organism.[214]

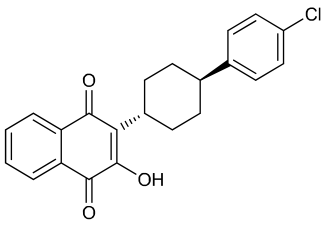

325
Atovaquone

Figure 4.10: Atovaquone, an antimalarial working through interruption of the parasitic mitochondrial ETC.

The antimalarial is usually given for treatment and prophylactic antimalarial regimes and is often administered in combination with proguanil (**326**) under the brand name Malarone®.

4.7.6 Artemisinin-based combination therapies (ACTs)

Currently, the majority of treatment methods rely on the use of artemisinin-based combination therapies (ACTs) for malarial indications. ACTs produce the fastest parasite-killing activity of currently discovered antimalarials, boast a relatively safe toxicity profile, show a broad range of antimalarial activity between Plasmodium strains, and act during the early erythrocytic stage of infection.[214] Artemisinin (**324**) is a natural product derived from *Artemisia annua* (sweet wormwood), a herb used in traditional Chinese medicine for the treatment of fever.

Artemisinin was first isolated in 1972 by Chinese scientist Tu Youyou, a discovery which was later awarded the 2015 Nobel prize in medicine due to its importance.[230,231] The structure of

the product was determined by X-ray analysis in 1979, and artemisinin was found to be as effective as quinine and chloroquine in early clinical trials.[214] Since its discovery, total synthetic, semi-synthetic and biosynthetic routes have been devised to produce artemisinin, and large scale cultivation and biosynthetic productions of the drug are used industrially.[232-235]

Artemisinin is a sesquiterpene lactone containing an endoperoxide functionality which is believed to be critical to its antimalarial activity. Though its precise mechanism of action is unknown, the peroxide bridge functionality is thought to be activated by haem-derived iron, forming oxidising free radical species. These species may interfere with *P. Falc.* phosphatidylinositol-3-phosphate (PfP13K) metabolism, which is involved in the transport of haemoglobin to the digestive vacuole. Consequently, parasitic growth is arrested and the cell is exposed to lysis following oxidative damage.[181,236,237]

Despite the high activity of artemisinin, the compound is extremely lipophilic, therefore limiting its solubility, and use within oral and intravenous (IV) formulations. As a result of this, numerous similar semi-synthetic derivatives of artemisinin have been found which offer similar activity alongside improved physicochemical characteristics.

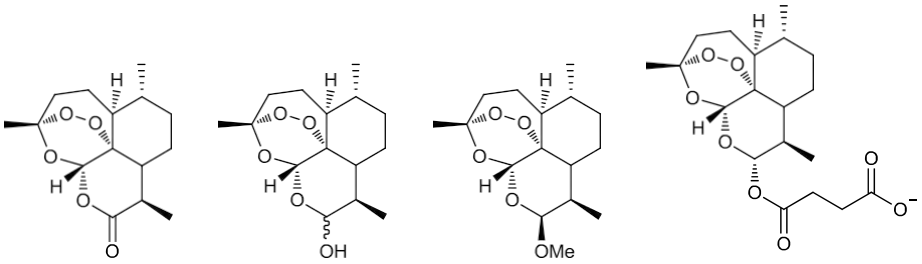

324 Artemisinin | **335** Dihydroartemisinin | **336** Artemether | **337** Artesunate

Figure 4.11: Artemisinin (324) and its related semi-synthetic derivatives (335-337), used as antimalarials.

Dihydroartemisinin (**335**) is the active metabolite to which artemisinin is reduced *in vivo*. Compound **335** is the most efficient artemisinin derivative because of this but is also rapidly metabolised in the body. Artemether (**336**) and artesunate (**337**) are methyl ether and succinate prodrugs of **335**, respectively. Artesunate displays vastly improved solubility over other fast-acting ACT drugs and, as such, is preferred for the treatment of very severe malaria cases, including in comatose patients, since **337** remains > 90% effective in even unconscious patients.[181]

Despite the high therapeutic efficiencies related to the use of artemisinin and its related derivatives, the antimalarial drugs are always administered along with another long-acting antimalarial medication (usually of the 4-aminoquinoline or aminoalcohol drug class) in order to maximise their effectiveness, and lessen the risk of emerging malarial resistance, especially within endemic regions.

4.7.7 Common treatment regimens

Where widespread resistance is yet to develop, as well as in the treatment of malarial cases not caused by *P. falc.* infections, combined treatment regimens not involving artemisinin (or a similar derivative thereof) can still be employed. Chloroquine is often chosen in such infections, owing to its high efficiency, low cost and excellent safety profile. In species capable of forming hypnozoites, primaquine or similar medication which targets hypnozoites may be combined within the course of treatment.[181]

A range of other combinations of non-ACT treatments have also previously been effective but are now seldom seen because of the resultant resistance pathways observed, especially within *P. falc.* parasites.

All ACT therapies are widely used to treat malaria, although artesunate is favoured clinically. The high solubility of the compound lends itself to various routes of administration, and treatment formulas comprising artesunate with either amodiaquine (4-aminoquinoline; **329**) or lumefantrine (aminoalcohol) are the most popular.[181]

4.7.8 Parasite resistance

Parasitic resistance to established antimalarial drugs has historically driven research around finding new, effective compounds with fast-killing profiles for the eradication of the disease.

After decades of the successful implementation of chloroquine in antimalarial regimens, resistance began to emerge and is now widespread. Resistance to chloroquine is mediated through the formation of an efflux pump (the chloroquine resistance transporter; PfCRT) between the digestive vacuole and the surrounding cytoplasm. The efflux pump prevents chloroquine from reaching the cellular compartment where haemoglobin is digested, thereby negating the pharmacological effect of the drug.[238]

In attempts to delay resistance and maximize the effectiveness of antimalarial medications, treatment regimens usually combine a fast-acting antimalarial such as artemisinin (or a similar derivative thereof), chloroquine or occasionally quinine, with another slower acting antimalarial compound. However, resistance to the slower-acting antimalarial has also been observed in many cases, and this therefore makes combined formulations redundant in clinical application.

In fact, cross-resistance profiling has even determined that parasites resistant to either 4-aminoquinolines or amino alcohols are also less sensitive to the other class.

As previously mentioned, the dual-application of pyrimethamine (**321**) and sulfadoxine (**322**) used to be a viable antimalarial drug treatment. However, various point mutations in genes responsible for transcribing DHFR and DHPS enzymes have resulted in these treatments becoming an increasingly ineffective option in reducing parasitaemia in recent times.[214]

The extent of primaquine resistance within parasite populations is not precisely known, especially within hypnozoite cells. Currently, reports largely describe the extent of resistance present within different populations around the globe, as opposed to how the resistance manifests itself. It also may involve an unclear, and perhaps complex mode of action. Nevertheless, the threat of resistance favours the use of the newly approved tafenoquine to reduce the amount of recrudescence in malarial cases.[239]

The action of atovaquone is also largely affected by mutations around the binding site of the drug. In this case, modifications are made to the CYT bc_1 complex to inhibit the action of the antimalarial medication. In one study, atovaquone-resistant *P. falc.* strains were grown from the treatment of different cultures of the parasite to gradually increasing concentrations of antimalarial.[240] Conserved base changes within the genome of the parasite were seen in the region encoding the proposed binding site of atovaquone following treatment with the drug. These mutations, led to a cumulative increase of ~900 × the IC_{50} (the concentration required for 50% inhibition of the protein, or in this case, the concentration required for a 50% reduction in the viable parasite population) in comparison to non-mutated strains.[240]

As a result of wide-spreading resistance, ACTs are now most often used to treat malaria infections. However, artemisinin itself is not invulnerable to rising resistance mechanisms, and some partial resistance (defined as a reduced rate of parasite clearance) has been associated with the use of artemisinin (and its related semi-synthetic analogues) within the Greater Mekong sub region of Southeast Asia.[181]

Although artemisinin may elicit its antimalarial effect through an interaction with PfPI3K, other research suggests that it may interact with the β-propeller shaped Kelch protein 13 within the parasite. Natural polymorphisms present within the gene sequences encoding this protein have provided resistance to the action of artemisinin, and insertions of these mutations into the native K13 locus have also triggered antimalarial resistance in parasites.[241-243]

However, other research has described strains without these mutations which still display artemisinin resistance and, as a result, the complete picture of developing resistance to ACTs remains a complicated, and potentially multi-faceted one, but is still an increasingly urgent challenge for the medicinal chemistry community.[244]

Novel antimalarials are currently in development which tackle resistance issues, targeting both current and novel antimalarial modes of action. For example, new research includes the synthesis of ferroquine (**338**), a next-generation 4-aminoquinoline which does not display cross-resistance to approved compounds, KAF156 (**339**), which has an unknown mode of action, as well as other drug candidates thought to work through their interaction with PfATP4 (*P. falc.* adenosine triphosphatase 4), PfPI4K (*P. falc.* phosphatidylinositol-4-OH kinase), PfEF2 (*P. falc.* translation elongation factor 2), or other unknown biological targets.[181,245-249]

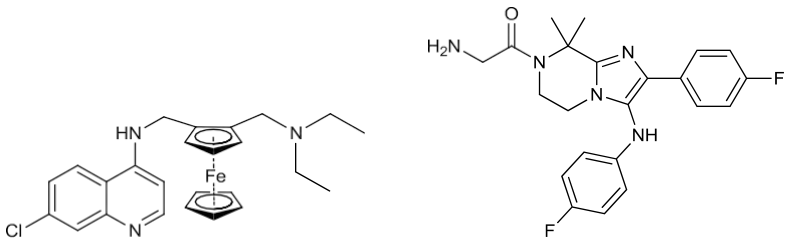

Figure 4.12: Two example antimalarial drugs currently under investigation.

Nonetheless, due to the severity of the disease, the different strains of malarial parasites present, and their rapid evolution to generate resistance mechanisms, a significant co-operative effort is required with the aim of fully preventing and eradicating malaria.

4.8 Identification of a series of novel antimalarials at GSK Tres Cantos

In line with this aim, following expansion from a high throughput screening (HTS) protocol, workers at GSK's infectious diseases site in Tres Cantos, Madrid, identified GSK2656864 (**340**, **Figure 4.13**) as a novel antimalarial, albeit with a physicochemical profile which required further optimisation.

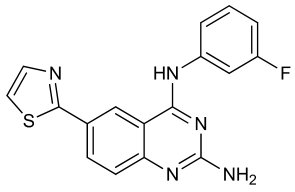

Pf_{3D7} pIC_{50}	7.35
LLE_{AT} (kcal mol^{-1} HA^{-1})	0.28
Property Forecast Index (PFI)	7.9
Chemiluminescent Nitrogen Detection (CLND) solubility (μg/mL)	5
HepG2 pIC_{50}	5.48
hERG pIC_{50}	5.50

Figure 4.13: GSK2656864 (340), an effective diaminoquinazoline antimalarial discovered following a HTS programme at GSK.

The compound displayed a sub-micromolar killing potency for *Plasmodium falciparum*, as represented by its pIC_{50} value. The IC_{50} in this case represents the concentration of antimalarial required to reduce the viable parasitic population (that is the number of parasitic cells capable of producing a continuous culture) by half. The pIC_{50} is the negative logarithm of the IC_{50} and is used to condense large differences in drug potencies into a manageable scale.

For this work, an IC_{50} of < 100 nM is targeted, which corresponds to a pIC_{50} of > 7. The IC_{50} (from which the pIC_{50} is derived) is determined using a tritium-labelled hypoxanthine assay with intra-erythrocytic stage *P. Falc.* cultures.

Hypoxanthine is an essential purine derivative used by viable parasites for nucleic acid synthesis. As such, following treatment with an antimalarial compound, live cells will incorporate the radiolabelled hypoxanthine, and the extent of this incorporation in the

population can be determined using a scintillation counter, once light has been emitted from fluorescent materials which are activated through radioactivity. For more information, see **Section 7.7 Appendix 7 – [^{3}H] Hypoxanthine Scintillation Proximity Assay procedure**.

Cross-resistance can also be determined using this assay. When comparing the ratio between the $PfIC_{50}$ obtained for *P.Falc.* strains resistant to known antimalarials:wild-type (antimalarial-sensitive) *P. Falc.* strains, a ratio of > 10 is indicative of resistance present. This may also help to identify the mode of action of novel antimalarials, since resistance pathways in these strains are well understood. When GSK2656864 was tested, no cross-resistance was observed. Moreover, when parasitic cultures were grown under a constant drug pressure for 10 weeks, very little resistant strains emerged. Therefore, the structure has a low propensity to cause resistance through parasite evolution.

A more complete picture of the mode of action can be determined when this data is combined with data from another *in vitro* tool, a parasite reduction ratio (PRR) assay (**Figure 4.14**).

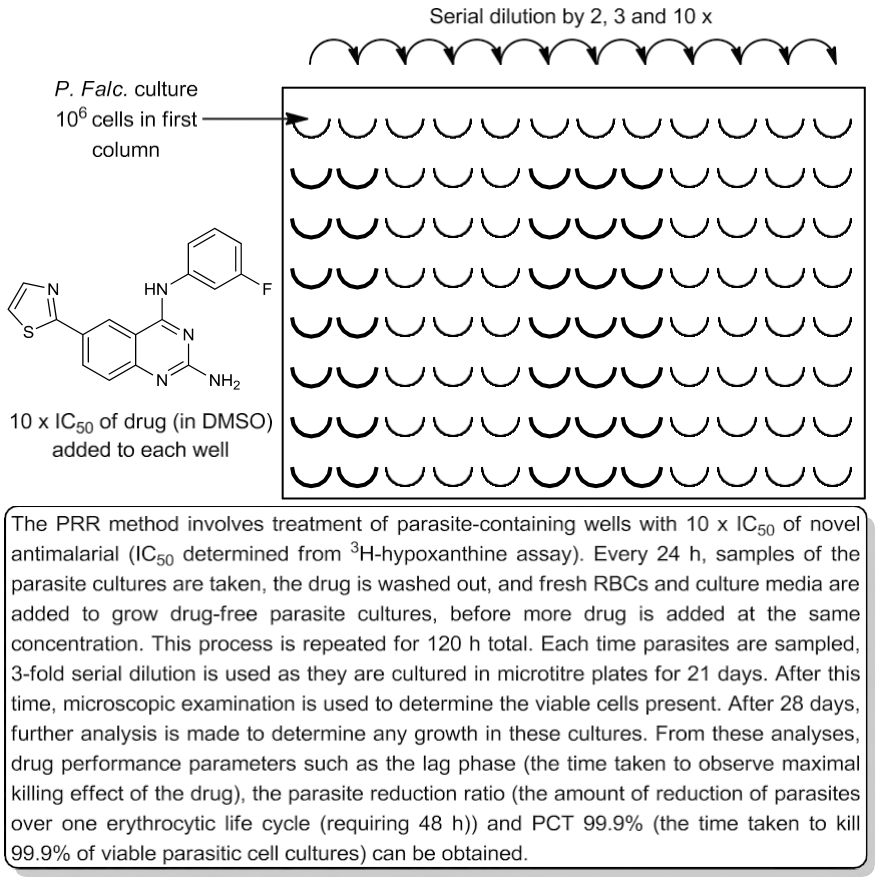

Figure 4.14: PRR Assay for antimalarial development.

In this assay, a 96-well plate is filled with 12 columns of infected red blood cells (iRBCs). The leftmost column has the highest concentration of parasites (10^6 per mL), and parasite concentration is diluted in each successive column. This assay is important, as antimalarials

work at different rates, depending on their mechanism, and arresting hypoxanthine metabolism of a parasite does not guarantee a reduction of parasite viability (and *vice versa*).

Together, these assays determined that GSK2656864 likely displays a mode of action similar to chloroquine, in preventing the haem biocrystallisation to form haemozoin. However, the compound also remains active against strains known to be resistant against established antimalarials. GSK2656864 has a rapid parasite-killing profile comparable to that seen for first-line antimalarials such as artemisinin, and therefore the eventual use of a compound containing a diaminoquinazoline motif is feasible.

Indeed, *In vivo* studies were performed in order to prove the activity of the compound within SCID (severe combined immunodeficiency) humanised mouse models infected with *P. Falc.* For more information, see **Section 7.8 Appendix 8 – *Plasmodium falciparum* humanised mouse model procedure**. Data from this model supported results obtained from the assays, showing the entire elimination of detectable *P. Falc.* parasites within 3 days following treatment.

Nevertheless, sub-optimal physicochemical parameters (measurable characteristics affecting the distribution and longevity of the drug in the body), as well as the safety profile of the compound mean that further optimisation of the initial hit was required.

The ligand efficiency (LE) is an *in vitro* metric used to quantify the potency with respect to the number of heavy atoms (HA; not hydrogen) present within the molecule. The ligand efficiency of a drug candidate can be determined through use of **Equation 4.1**.

$$LE = \left(\frac{1.37}{\text{No. of HAs}}\right) \times pIC_{50}$$

Equation 4.1: Equation used to derive the ligand efficiency of drug compounds. pIC_{50} is the negative logarithm of the IC_{50}, the concentration of the drug required to inhibit a biological process by half. In this case, the pIC_{50} is the negative logarithm of the concentration of drug required to reduce parasitaemia by half. Generally, higher values of LE represent a more significant contribution of binding to the target throughout the drug structure and values of > 0.3 kcal mol^{-1} HA^{-1} are typically targeted for drug discovery programmes.

Derived from the ligand efficiency, the lipophilic ligand efficiency (LLE) also takes the lipophilicity of the drug molecule into account with respect to its potency. The lipophilicity measurement used within LLE derivation is either cLog P or Log D, which describe the calculated partition coefficient of a drug molecule when partitioned between an organic phase (usually 1-octanol) and water, or the distribution coefficient of the molecule in the same situation, respectively.

A cLog P (or Log D) value between 2 and 3 represents a typical drug-like characteristic for oral medications, to compromise between sufficient cellular permeability and an extended

half-life within the body. Values of LLE between 5 and 7 are usually targeted for drug discovery programmes, and the equation to determine LLE is given in **Equation 4.2**.[250,251]

$$\mathrm{LLE} = \mathrm{pIC_{50}} - \mathrm{cLogP}$$

Equation 4.2: Equation used to derive the LLE from pIC_{50}.

Within GSK, the attenuated lipophilic ligand efficiency (LLE_{AT}) is used as a principal metric for drug development. LLE_{AT} essentially combines the ideas of LE and LLE, providing a lipophilic ligand efficiency value that is adjusted for heavy atom count. In this way, both the molecular weight and "greasiness" of prospective molecules are encapsulated in the measurement. The LLE_{AT} is similar in scale to LE, where values > 0.3 kcal mol^{-1} HA^{-1} are desired within drug molecules.[252] With an LLE_{AT} of 0.28, GSK2656864 is just below the targeted value. An equation used to calculate LLE_{AT} is shown below, and LLE_{AT} will be the primary parameter used to consider ligand efficiency throughout this work.

$$\mathrm{LLE_{AT}} = 0.111 + 1.37\,(\frac{\mathrm{LLE}}{\mathrm{HA}})$$

Equation 4.3: Equation used to calculate the LLE_{AT} parameter.

The property forecast index (PFI) is a compound physicochemical property, summing the lipophilicity (log $D_{pH7.4}$ is used) and the aromatic ring count (including heterocycles) as shown in **Equation 4.4**. Log $D_{pH7.4}$ describes the distribution coefficient of the molecule when partitioned between 1-octanol and water at physiological pH (7.4). It is affected by the acidity of the system. Most frequently, the distribution coefficient is now determined through chromatographic (termed Chrom Log D) methods.[253]

$$\mathrm{PFI} = \mathrm{Chrom\ Log\ D_{pH7.4}} + \mathrm{No.\ Aromatic\ rings}$$

Equation 4.4: Equation used to determine the property forecast index (PFI) of a potential drug candidate.

Drug discovery programmes within GSK often use PFI as a parameter to determine the drug-likeness of compounds within physicochemical space, and when using Chrom log $D_{pH7.4}$ as the measure of lipophilicity, a PFI value of < 7 is usually targeted, as this often corresponds to compounds with desirable solubility and permeability data, reduced promiscuous binding and increased stability to oxidative metabolism.[253] As a result, a PFI of 7.9 is higher than desired and increasing the polarity or reducing the number of aromatic rings during optimisation may help to develop the series further.

Solubility was also sub-optimal at this stage. Chemiluminescent nitrogen detection (CLND) is used in a measurement of the kinetic aqueous solubility of molecules and involves using an automated shake-flask method to encourage the dissolution of the drug-like candidates (present as samples in DMSO) into an aqueous solution, which is kept at pH 7.4 with

phosphate buffered saline. The aqueous solution is then injected into a nebulizer, where it is mixed with helium and oxygen, and resultantly sprayed as a fine aerosol into a pyrolysis tube (maintained at 1050 °C). The harsh conditions of pyrolysis form nitric oxide from all nitrogen atoms present within the sample, and its subsequent decay can be analysed computationally to provide an equimolar description for the amount of nitrogen (and therefore compound) present within the solution.[254] For drug-like compounds, an aqueous solubility of > 100 µg/mL at least is targeted to ensure the compound is suitable for oral formulation, allowing the drug to dissolve in sufficient quantity within the systemic circulation in order to exert the desired therapeutic effect. As such, further structural optimisation of GSK2656864A was required to improve the observed solubility.

Finally, off-target effects were another challenge initially, as the hit compound displayed some interactions with Hep G2 and hERG proteins. Hep G2 are epithelial liver cells, whose cell lines are used to identify cytotoxic and genotoxic compounds. Therefore, the interaction of GSK2656864A with Hep G2 suggests toxicological issues for use of the compound.

Moreover, hERG toxicity is also undesired. The hERG (human ether-à-go-go related gene) encodes a protein which constitutes a potassium-ion channel protein complex (sometimes called by the same name). The hERG ion channel plays an important role in regulating the normal electrical activity of the heart, and its inhibition by therapeutic agents can result in fatal arrythmia.

Research has shown that drugs which display lipophilic character, are positively charged, contain a low proportion of sp^3 hybridized atoms or have basic amines within their structure and/or have many aromatic rings are more likely to exhibit hERG binding.[255-257] As such, these safety issues must too be considered in the development of a safe antimalarial drug. At GSK, an electrophysiological assay is used to determine hERG inhibition and there should be at least a 3 log units (1000 x) preference of binding for the desired target rather than the hERG complex for early stage lead optimisation.[258]

With these goals in mind, workers at Tres Cantos performed hit-to-lead (H2L) optimisation to eventually identify GSK3190260 (**341**, **Figure 4.15**).

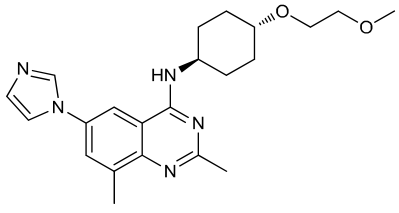

341
GSK3190260

Pf_{3D7} pIC_{50}	6.5
LLE_{AT} (kcal mol^{-1} HA^{-1})	0.26
Property Forecast Index (PFI)	7.1
CAD solubility (µg/mL)	160
AMP (nm s^{-1})	436
HepG2 pIC_{50}	4.10
hERG pIC_{50}	5.13

Figure 4.15: GSK3190260, developed as a result of a hit-to-lead programme at GSK Tres Cantos.

Although hERG activity was still observed, off-targets affects related to Hep G2 interaction were greatly reduced, and GSK3190260 possessed improved solubility and PFI parameters.

A procedural change within our laboratories led to the adoption of high-throughput CAD (charged aerosol detection) as the preferred method of solubility testing, since issues can be observed within the use of CLND solubility when molecules without nitrogen atoms or those with connected nitrogen atoms are pyrolyzed.[254,259]

The CAD method uses a similar method as CLND. After the sample (present as a solution in DMSO), is agitated in an aqueous solution buffered at physiological pH, the resultant solution is passed through a HPLC column before being nebulized with pressurized gas. The solvent is then removed in an evacuation chamber, before charged aerosol particulates are made through the interaction of the analyte molecules with a gaseous stream of charged nitrogen. The charged analyte particles are directed to an electrometer, which plots detection of the analyte material onto a chromatogram.[259]

Interpretation of this data provides an approximate solubility for the molecule, which is affected by the acidity (determined by the pKa; a negative log of the Ka parameter, the acid dissociation constant, which determines the extent at which a molecule donates protons (H^+ ions) in solution) and the surface area of the molecule.[259] Within drug discovery programmes, a CAD solubility of < 30 µg/mL is regarded as poorly soluble. Conversely, compounds with CAD values of > 200 µg/mL are highly soluble. GSK3190260 has a CAD solubility of 160 µg/mL, and is hence classified as being moderately soluble.

Finally, membrane permeability is another vital parameter governing therapeutic activity. In order for pharmaceutical compounds to exert beneficial treatment for a patient, they must successfully traverse cell membranes in order to reach the desired biological targets, which are often intracellular. At GSK, an artificial cell membrane assay is used to determine the permeability of synthesised compounds. The artificial membrane permeability (AMP) assay comprises a lipid-infused artificial membrane which is partitioned between two reservoirs containing aqueous solutions. A prospective drug compound can be dissolved in one of the aqueous solutions and, following a period of agitation, the amount of compound which has permeated into the adjacent aqueous solution can be measured.[260] Since AMP is determined through a cell membrane of particular width and over a specific period of time, the units of nm s^{-1} are used, where a cellular permeability of < 30 is insufficient, values of 30-200 are considered to describe intermediately permeable compounds, and values over 200 nm s^{-1} represent highly permeable compounds. As such, excellent permeability was observed for GSK3190260, and a similar permeability profile would ideally be retained throughout further optimisation.

4.9 Project aims – Chapter 2: A telescoped, continuous flow synthesis of diaminoquinazoline antimalarials

As outlined previously, malaria is still a huge global health issue, affecting hundreds of millions of people, predominantly within under-developed areas. The discovery of quinazolinamine antimalarial GSK3190260 (**341**), derived following early parameter optimisation of its predecessor GSK2656864 (**340**) has identified a novel class of antimalarial active within both cellular assays and mouse-modelled malarial infections, and therefore represents a potentially rewarding area for further research.

The aim of this chapter is based on first probing SAR exploration around the quinazoline motif, to determine the changes in biological data observed when introducing various functionalities in different positions of the quinazoline scaffold. Then, microfluidic flow technology will be applied within the synthesis of functionalised quinazolines in order to increase the efficiency of their preparation, and allow for an array-like procedure for late-stage derivatisation of the products, to further elucidate SAR data.

It was thought that following the synthesis of 2,4-dichloro-8-methylquinazoline **342**, a tandem S_NAr approach could be established within a flow setup to produce 2,4-disubstituted quinazoline analogues in a single process (**343**, **Figure 4.19**). Computational methods would be incorporated to select appropriate nucleophiles to introduce at these positions of the ring, based on predictions of common physicochemical parameters of the resultant adducts. Subsequent derivatisation at the 6-position of the afforded quinazoline products through cross-coupling methods may allow for further optimisation of the produced materials.

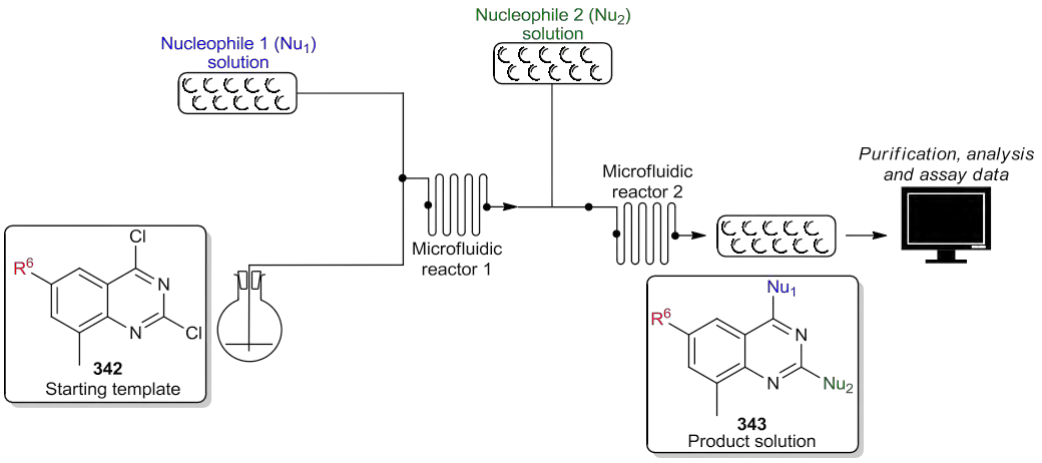

Figure 4.19: General design for a tandem S_NAr setup in flow to produce functionalised quinazolines.

If successful, the flow procedure would facilitate the rapid generation of structures for assay evaluation, probe yet-to-be explored chemical space around the quinazoline, and help to drive forward lead optimisation along with the continuing work of the Tres Cantos team.

Moreover, if an ideal candidate was eventually identified, the establishment of a continuous flow procedure for its synthesis might enable easier access to a method of large scale production of the antimalarial in the future, which could be of utility, for example, in enabling *in vivo* studies.

Ultimately, the goal of the collaborative antimalarial research effort is based on the discovery of an effective (IC_{50} < 100 nM (pIC_{50} > 7)), single-dose *P. falc.* antimalarial medication which possesses rapid parasiticidal activity, no observed cross-resistance in *Plasmodium* species resistant to clinically-established antimalarials, desirable physicochemical and safety profiles, and which also prevents malarial recrudescence. Ideally, the drug would be affordable, and simple to produce, formulate and administer, to benefit as many people as possible with the disease.

5. Results and discussion – Chapter 2: A telescoped, continuous flow synthesis of diaminoquinazoline antimalarials

5.1 Formation of a 2-amido-substituted quinazoline analogue

Initially, some thought was given towards making slight modifications of the structure of GSK3190260 in order to probe SAR data with respect to the lead compound. Interestingly, in the development of the lead from GSK2656864, a 10 fold reduction in potency for *P. falc*$_{3D7}$ was observed (*P. falc.* strain *3D7A* was typically used in the biological assay as it displays no resistance to currently known antimalarials. For more information, see **Section 7.7 Appendix 7 - ^{3}H-Hypoxanthine Scintillation Proximity Assay (SPA) procedure**). Amongst the structural changes adopted during the hit-to-lead optimisation was the substitution of the 2-amino functionality in GSK2656864 for a methyl group in its successor.

Based on pre-existing assay data, the presence of the basic amine in this position may have contributed to the antimalarial potency. However, and as discussed previously, it was also likely responsible for issues regarding hERG safety. Though carboxamide **344** (**Figure 5.1**) had shown to be inactive in the assay,[261] targets **345** and **346** were selected to determine the effect of amine substitution at the 2-position, where an amide nitrogen lone pair would be less available for promiscuous (or desired) binding interactions due to resonance into the carbonyl C=O π* orbital. As a result, amide derivatives **345** and **346** were expected to have reduced basicity, and thus reduced hERG potency in comparison to diaminoquinazoline antimalarial compounds.

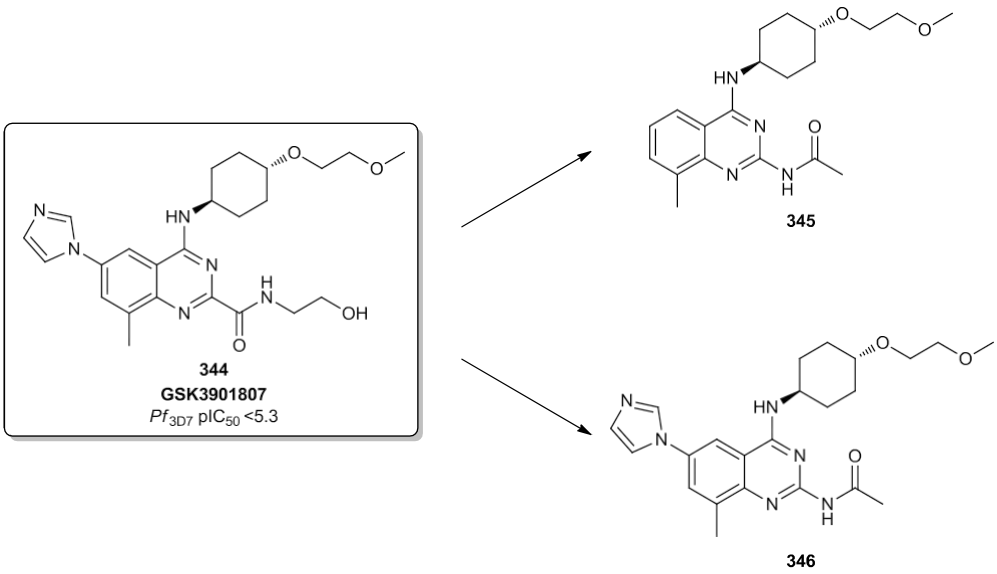

Figure 5.1: GSK3901807, an analogous compound to the lead (GSK3190260), but with a carboxamide functionality present within the 2-position. In this case, no activity for *P. falc.* was observed. As a result of previously established data, thought was given towards making 2-amidoanalogues 345 and 346 for evaluation as antimalarials.

The synthesis of compounds **345** and **346** began using the route shown in **Scheme 5.1**. Common intermediate compounds used throughout the remainder of the project were required for initial formation of the quinazoline motif. In order to introduce the required substitution at the 6-position for **346**, an iodination using *N*-iodosuccinimide (NIS) afforded **350** cleanly and in high yield. A neat cyclisation of either **347** or **350** with urea then gave access to quinazolinone structures **348** and **351**, respectively which could be dehydrated with phosphorus(V)oxychloride to generate 2,4-dichloroquinazoline compounds **349** and **352**.

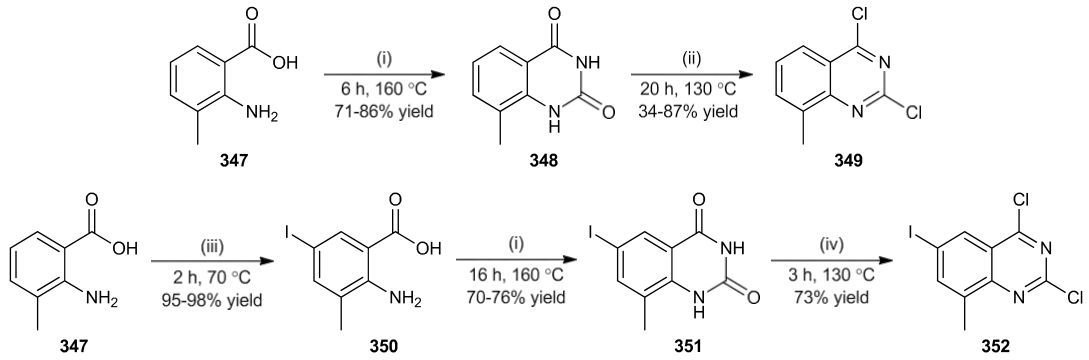

Scheme 5.1: Formation of chloro-substituted quinazoline structures for further derivation. Conditions used: (i) Urea (10 eq.; neat), (ii) $POCl_3$ (excess; neat), (iii) NIS (1.05 eq.) in DMF (iv) DIPEA (272, 2 eq.), $POCl_3$ (excess; neat).

Having synthesised the relevant precursors to **345** and **346**, the (*trans*)-4-(2-methoxyethoxy)cyclohexanamine **356**, was made using a synthetic strategy developed within our laboratories.[262] From the commercially available (*trans*)-4-(amino)cyclohexan-1-ol (**353**), a benzylation, ether formation and hydrogenation sequence afforded the desired nucleophile in a facile manner. This reaction sequence is shown below.

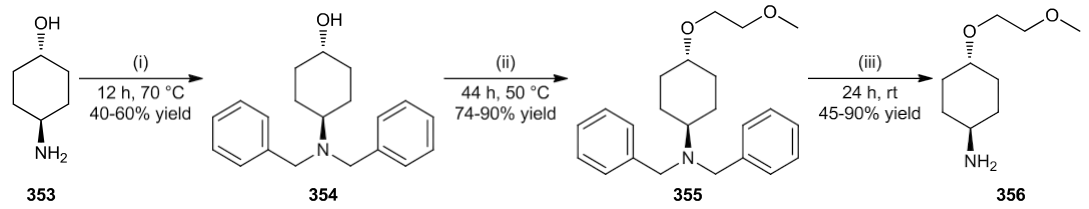

Scheme 5.2: Reaction sequence used to generate amine (356) required for the downstream formation of 345 and 346. Conditions used: (i) Benzyl bromide (2.2 eq.), K_2CO_3 (5 eq.) in MeCN (ii) 1 bromo-2-methoxyethane (7.5 eq.), sodium hydride (60 % wt. in mineral oil, 5.2 eq.) in THF (iii) H_2 (1 atm.), 20% wt. $Pd(OH)_2/C$ (5 mol%) in EtOH.

Finally, the products from the two routes could be combined. For **345**, after an S_NAr process to introduce the amine functionality regioselectively in the 4-position, a direct cross-coupling

of acetamide was performed using conditions reported by Vimolratana *et al*.[263] and successfully delivered the desired product in good yield (69%, **Scheme 5.3**).

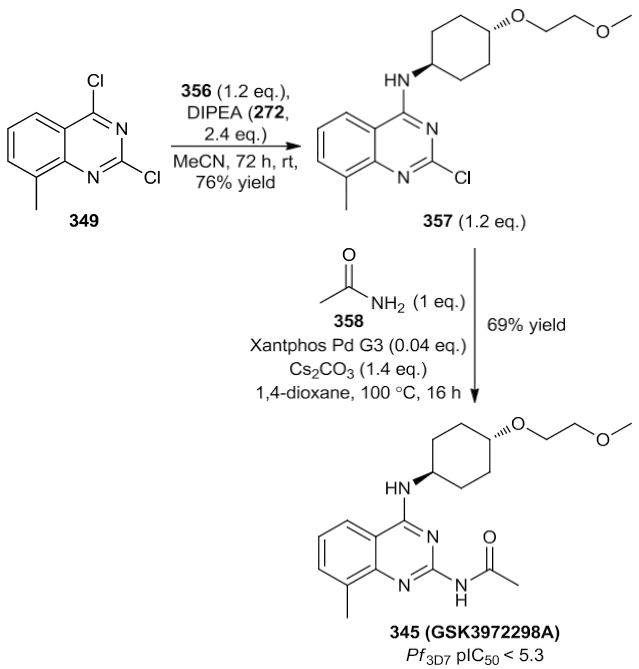

Scheme 5.3: Synthesis of 345 *via* an S_NAr and direct amide coupling reaction pathway.

Assay data for **345** determined the compound to be inactive against a *P. falc.* 3D7 culture. In the synthesis of **346**, issues were observed whilst attempting to introduce the amide group with the presence of the C6-iodo functionality. The reaction was first attempted through the introduction of the imidazole group at position 6 prior to testing the direct amidation reaction. Unfortunately, under conditions using both palladium and copper catalysis to perform the cross coupling, the desired intermediate (**360**) could not be isolated.

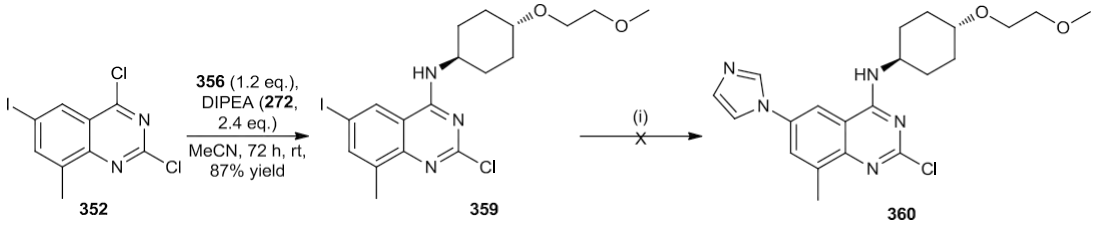

(i) Attempted conditions:
(1) *1H*-imidazole (2. eq.), Xantphos Pd G3 (0.10 eq.), Cs_2CO_3 (1.4 eq.), 1,4-dioxane, 100 °C, 96 h. *No reaction.*
(2) *1H*-imidazole (2. eq.), copper(I) iodide (0.3 eq.), K_2CO_3 (2 eq.), NMP, 160 °C, 96 h *Unclean, disubstituted product formed.*

Scheme 5.4: Attempted synthesis of intermediate 360 en-route to compound 346. As a result of preparative difficulties of the target molecule, as well as the inactivity of compound 345, synthetic efforts to produce 346 were ultimately abandoned.

Moreover, performing the cross-coupling at earlier stages in the route, for instance by attempting the reaction on compounds **350** or **351** were both unfruitful. Nevertheless, and

largely due to the complete inactivity exhibited by **345**, formation of **346** was not pursued further.

5.2 Variation of the quinazoline C6-functionality

Substitution in the C6-position was investigated next to determine the importance of this area of the molecule for target binding. In both the hit and lead compounds (**Figures 4.13** and **4.15**, respectively) small heteroaromatic groups are present at the 6-position of the quinazoline.

Therefore, whilst maintaining other substitution patterns around the ring, a small number of analogous compounds which had either a small heterocycle (both aromatic and non-aromatic heterocycles), an alkyl amine substituent, or a hydrogen atom as their C6-functionality were synthesised to examine their antimalarial activity.

Since lead compound GSK3190260 has a methyl group in position 2 of the quinazoline, previously synthesised intermediates **349** and **351** were not employed here. Instead, compound **365** (H in position 6) was generated through a cyclisation of **347** with acetic anhydride (**361**), and a subsequent condensation with ammonium acetate (**Scheme 5.5**).

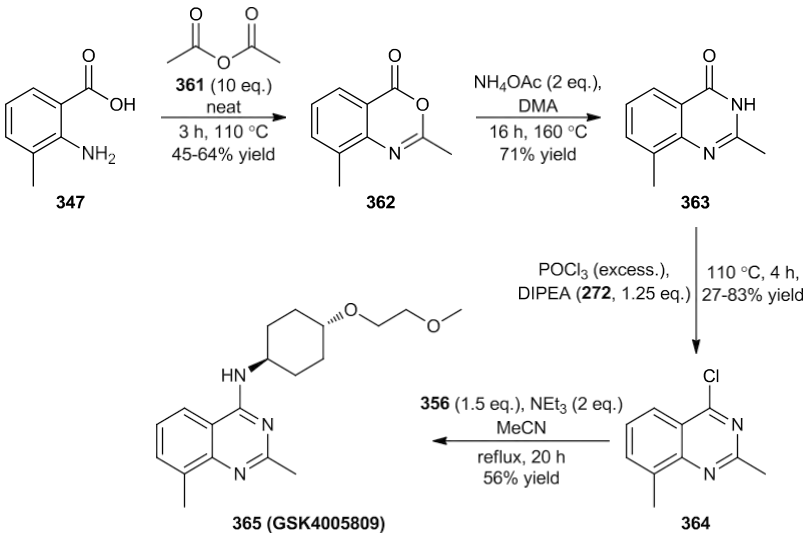

Scheme 5.5: The synthesis of the C6-unsubstituted analogue 365.

The 4-position of the quinazoline was then activated once more with phosphorus oxychloride, to afford **364**, with which amine **356** could combine in an S_NAr procedure to deliver **365** in an efficient synthetic sequence.

A similar approach was taken for targets derivatised in the C6-position using **350** as an appropriate starting material (**Scheme 5.6**).

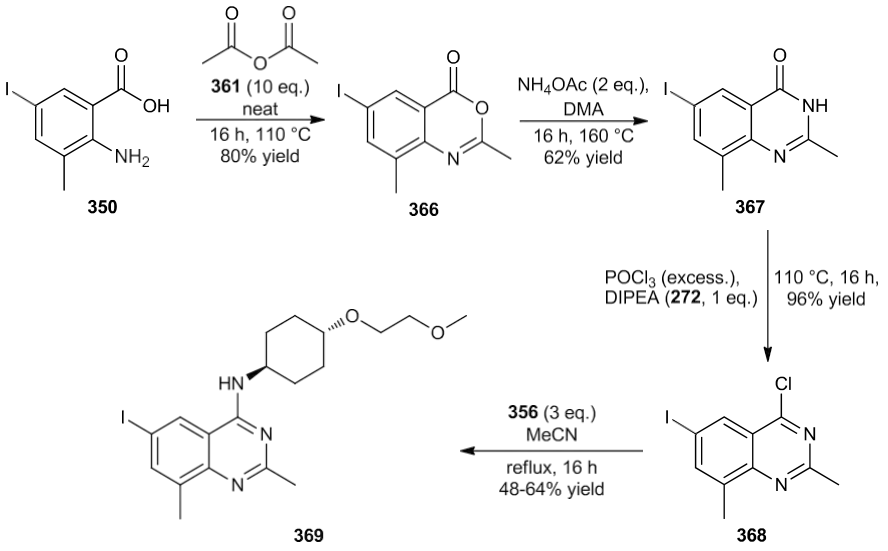

Scheme 5.6: Synthetic route for the formation of intermediate 369, for derivatisation at the 6-position.

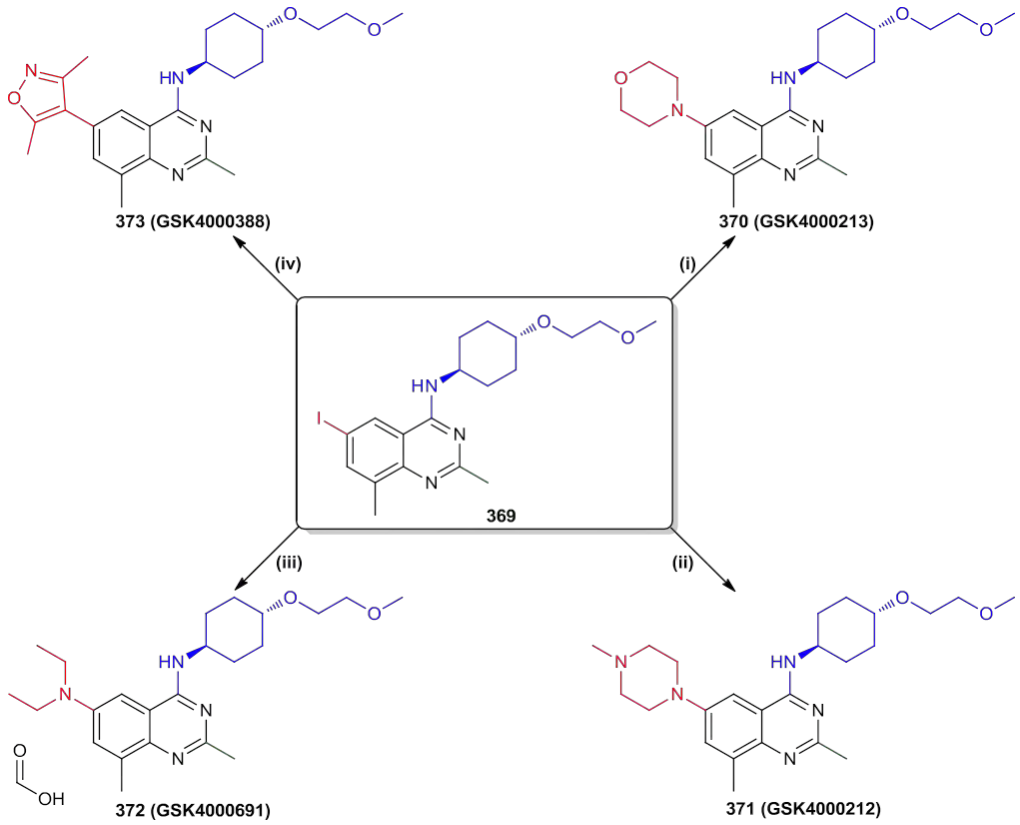

Scheme 5.7: Derivatisation of compound 369 to introduce a small number of different functionalities at the C6-position of the quinazoline scaffold. Conditions: (i) morpholine (2.5 eq.), RuPhos Pd G2 (20 mol%), RuPhos (20 mol%), Cs_2CO_3 (2 eq.) in 1,4-dioxane, 100 °C, 2 h, 20-41% yield; (ii) *N*-methylpiperazine (2.5 eq.), RuPhos Pd G2 (20 mol %), RuPhos (20 mol%), Cs_2CO_3 (2 eq.) in 1,4-dioxane, 100 °C, 2 h, 45% yield; (iii) diethylamine (2.5 eq.), copper(I) iodide (1 eq.), *L*-proline (20 mol%), K_2CO_3 (2 eq.) in CH_2Cl_2, 60 °C, 96 h, 13% yield; (iv) (3,5-dimethylisoxazol-4-yl)boronic acid (1.5 eq.), Pd(dppf)Cl_2·CH_2Cl_2 (10 mol%), K_2CO_3 (3 eq.) in DMSO:H_2O (2:1), 100 °C, 2 h, 52% yield.

At this point, coupling **369** with various nucleophiles under transition metal catalysis facilitated the synthesis of materials **370**-**373** (**Scheme 5.7**). Using conditions established elsewhere in our laboratory for the coupling of aryl halides with nitrogen nucleophiles, compounds **370** and **371** were afforded efficiently.[264]

The synthesis of the diethylamino-functionalised quinazoline, compound **372**, proved unsuccessful under these previously established conditions, but use of a mild Ullmann-based literature procedure from Ma *et al*. gave facile access to **372**, which was isolated as a formate salt following low pH reverse phase purification.[265]

Finally, 3,5-dimethylisoxazole-substituted quinazolinamine **373** was formed through a Suzuki reaction using the dimethylisoxazole boronic acid precursor. Once again, reaction conditions which had been applied on similar targets within our laboratories were applied to effectively deliver the desired product in good yield.[264]

Assay data for the compounds prepared is shown in **Figure 5.2**.

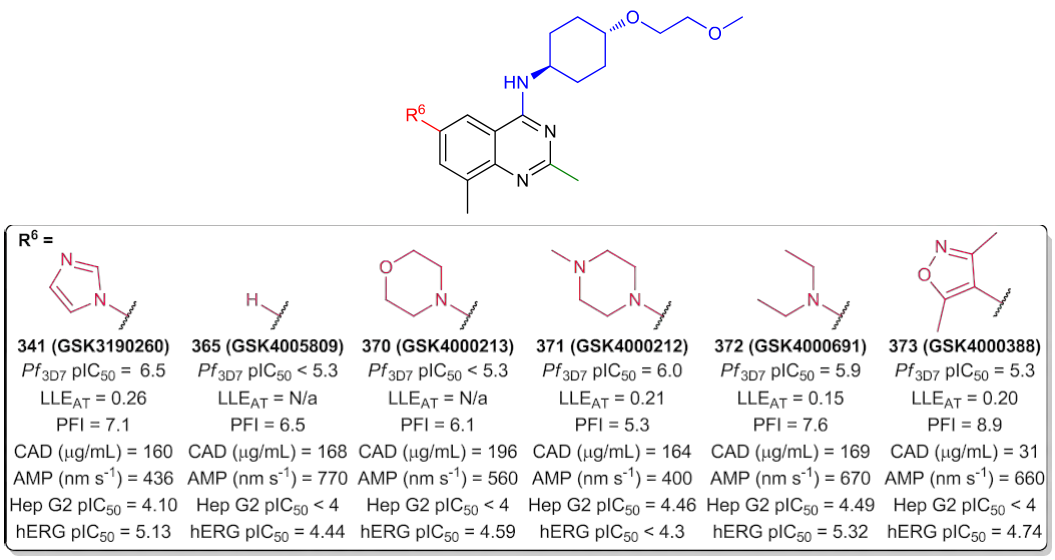

Figure 5.2: Assay data for lead compound 341 and analogous quinazolines with various C6-substituents.

As shown from the assay data above, C6-substitution clearly has some beneficial effect on potency, as **365** is entirely inactive in the assay, despite significantly improving the safety, permeability and PFI profile when compared to the lead compound (**341**).

The presence of an oxygen atom within functionality at the 6-position also appeared to be detrimental on the cellular activity, since morpholine (**370**) and dimethylisoxazole (**373**) functionalised quinazolines exhibited significant decreases in cellular potency.

Interestingly, compounds **371** and **372** offered the most promising results. Compound **371** had almost sub-micromolar potency, but showed no off-target activity for hERG, likely due to the

introduction of two nitrogen atoms in this position, causing a reduction in the lipophilicity of the compound. This data suggests that a late-stage substitution of the imidazole fragment for a methyl piperazine may be hugely advantageous to mitigate against safety concerns which could otherwise prevent drug developability.

Diethylamine **372** also showed a similar potency but was less favourable because of its higher hERG risk, and increased PFI, likely to be an effect of the increased lipophilicity of the compound.

As such, though the C6-functionality had been examined with a few different groups; some of which benefitted from increasing physicochemical properties, none were observed to be as potent as the imidazole group utilised in the lead compound.

5.3 Synthesis of the alternative stereoisomer of GSK3190260

As a result of the outputs from the study described above, the focus of synthetic efforts then moved to the 4-position of the quinazoline. Despite hit-to-lead optimisation affording GSK3190260 after trialling different functional groups, especially in C2- and C4-positions, the analogous *cis*-stereoisomer had never been synthesised during the course of the programme.

Thus, from the commercially available (*cis*)-4-(amino)cyclohexan-1-ol (**374**), (*cis*)-4-(2-methoxyethoxy)cyclohexylamine (**377**) was formed through the analogous synthetic route as previously discussed (**Scheme 5.8**).

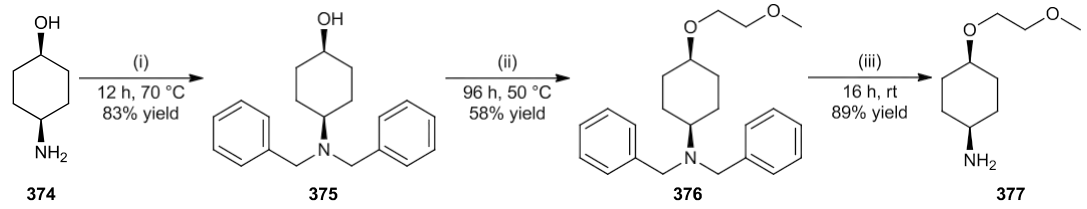

Scheme 5.8: Synthetic route to generate (*cis*)-4-(2-methoxyethoxy)cyclohexanamine (377) for comparative SAR analysis. Conditions: (i) Benzyl bromide (2.2 eq.), K_2CO_3 (5 eq.) in MeCN. (ii) 1-Bromo-2-methoxyethane (excess), sodium hydride (60 % wt. in mineral oil, 5.2 eq.) in THF. (iii) H_2 (1 atm.), 20% wt. $Pd(OH)_2/C$ (5 mol%) in EtOH.

The S_NAr procedure to couple **377** to 4-chloro-6-iodo-2,8-dimethylquinazoline (**368**) then followed cleanly to afford intermediate **378** in 69% yield. A mild Ullmann coupling employing *D*-glucosamine as an organic ligand led to the formation of the desired product,[266] albeit in a low yield due to problems encountered during purification. Nevertheless, *cis*-stereoisomer **379** was submitted to testing, and displayed similar biological activity to the lead compound, suggesting that the stereochemistry of the aminoalcohol appendage at the C4-position is not essential in orchestrating the mode of action of the antimalarial (**Scheme 5.9**).

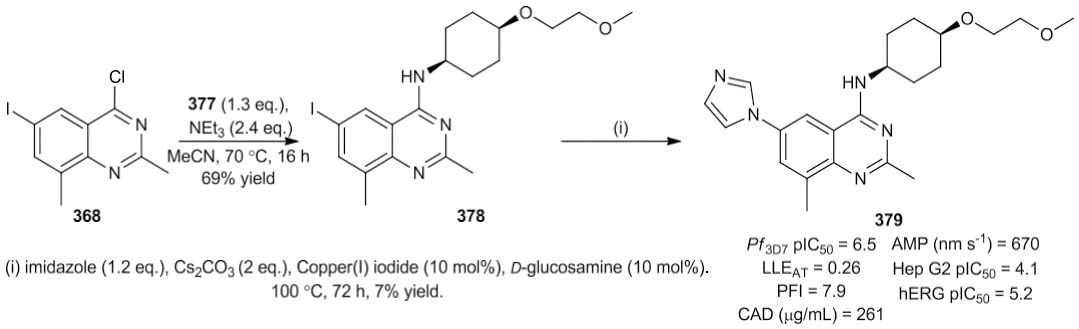

Scheme 5.9: Preparation of the *cis*-diastereoisomer (379) of the lead compound.

5.4 Batch optimisation of the tandem S_NAr procedure

Together with work from early hit development in Tres Cantos, derivatisation around the quinazoline core of the lead compound had indicated that the relationship between the substituents present and the potency observed was non-trivial. Since the programme has relied on a phenotypic route to antimalarial discovery, and thus was not facilitated by protein crystallography, a flow-based process for the synthesis of a range of quinazoline derivatives was targeted, as outlined in **Figure 4.19**. The method would be developed without a specific target in mind, but rather as a proof-of-concept, and with a potential future application of increasing the efficiency and scalability of the route to afford functionalised quinazoline antimalarials.

As such, using 1-propylamine (**380**), propane-1-thiol (**381**) or 1-propanol (**382**) as model reactants, the coupling of various nucleophiles to 2,4-dichloro-8-methylquinazoline (**349**) would be optimised in batch reactions to determine the conditions required for performing the tandem S_NAr procedure within a flow system (**Scheme 5.10**).

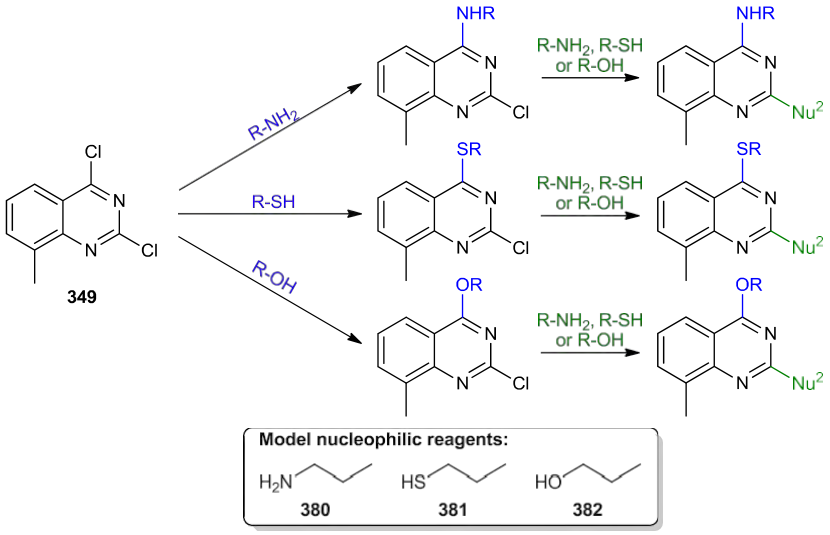

Scheme 5.10: General strategy for making difunctionalised quinazoline structures through a tandem S_NAr procedure.

Initially, literature conditions associated with the reactions were investigated. Kanuma *et al*. showed that the regioselective addition of an amine nucleophile to the C4-position of 2,4-dichloroquinazoline (**383**) was possible in under 2 h at ambient conditions, during their synthesis of melanin-concentrating hormone receptor 1 antagonist molecules.[267]

Conversely, in order to subsequently introduce amine functionality at the 2-position of the quinazoline, the second reaction step required refluxing temperatures in isopropanol to overcome the higher activation barrier associated with addition to the more deactivated site (**Scheme 5.11**).[267]

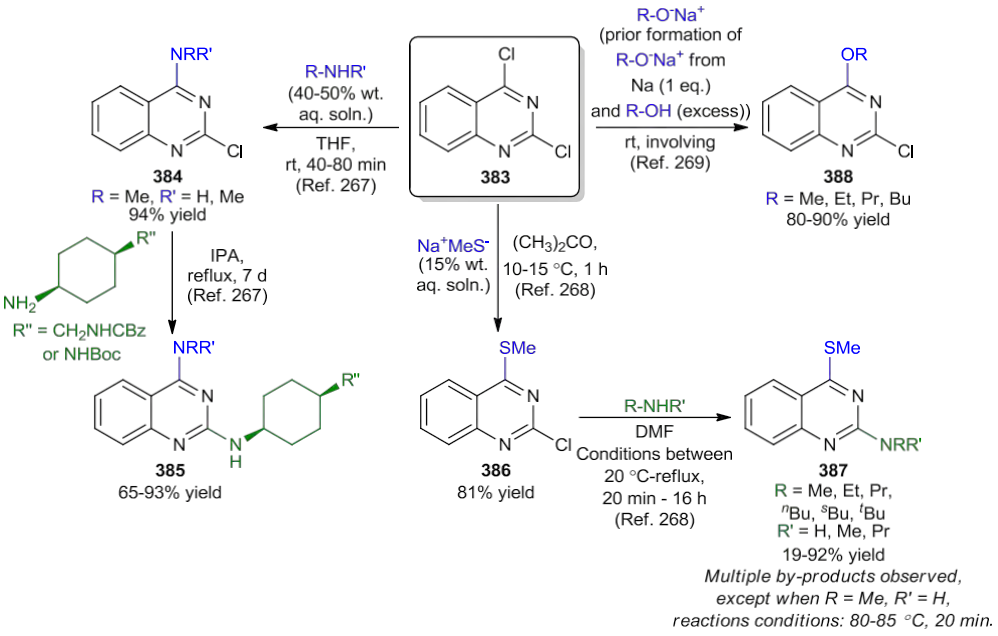

Scheme 5.11: Example literature conditions for the functionalisation of 2,4-dichloroquinazoline compound 383 with amine, thiol and alcohol nucleophiles.

The addition of thiol reagents to chlorinated quinazolines was reported to be readily achieved according to a literature example[268] (**Scheme 5.11**). Miki and a co-worker described the C4-selective coupling of methylmercaptan sodium salt (15% wt. in water) with 2,4-dichloroquinazoline (**383**) at 15 °C in 1 h.[268]

Following attempts to introduce amine functionality to the 2-position of the resultant intermediate (**386**) were successful, but also liberated a range of by-products, due to the lability of the thioether functionality in nucleophilic substitution reactions.[268]

The regioselective addition of alcohol reagents to dichlorinated quinazoline scaffolds is seldom reported in the literature, likely owing to the reduced nucleophilicity of the alcohol in comparison to amine-containing systems. Base-mediated activation of the alcohol may be possible to generate a reactive alkoxide species, but subsequent control of the regioselectivity of addition may be a challenge and would require further investigation.

Within the literature, a C4-regioselective addition of sodium alkoxide nucleophiles to dichloroquinazolines can occur following their *in situ* preparation from alcohols and sodium metal. Therefore, highly activating conditions are required to drive nucleophilicity of the alcohol reagent, although the S_NAr reaction does proceed at room temperature under these conditions (**Scheme 5.11**).[269]

In order for the S_NAr procedures to be amenable to a continuous flow setup, the following aims were targeted in the development of the tandem S_NAr method:

- Full conversion to the desired (C4-functionalised) intermediate, in order to limit by-product formation in the second step.
- Ideally avoiding the super-stoichiometric additions of the nucleophiles for the first S_NAr method in the route, in order to prevent subsequent addition of the first nucleophile in the second synthetic step.
- Fast reaction times. In an effort to develop a highly efficient library synthesis of a range of quinazoline molecules, a target of ~5 minutes reaction time was chosen for the first step, and ~15 minutes for the second, based on information attained from the literature described in **Scheme 5.11**, and the consideration that high temperatures could be utilised safely in flow to accelerate reaction processes.
- The use of a stable, high-boiling, polar, and water-miscible solvent. The quinazoline starting materials used are extremely polar, and therefore, in order to produce homogenous reaction solutions, a polar solvent was likely to be required for the method. As mentioned above, high temperatures would be needed to access fast reaction times (especially in the second nucleophile addition). Therefore, the chosen solvent would have to be stable to heating, and ideally have a high boiling point to reduce the otherwise demanding requirements for pressure containment within the flow reactor. Finally, it was thought that an array-amenable MDAP (mass-directed auto purification) LCMS method (See **Section 6.1.4 Array MDAP** for more information), which uses a reverse-phase column purification in an automated setup, would be used to further enhance the throughput of the synthesis. Hence, use of a water-miscible solvent would be essential in the tandem reaction process, to facilitate use of the array MDAP equipment in isolation of the compounds.

With these objectives in mind, the addition of the model nucleophiles to **349** was initially attempted in batch.

5.4.1 C4-Regioselective addition of propylamine

The use of 1-propylamine (**380**) as a model nucleophilic reagent was first studied (**Scheme 5.12**). In 10 different boiling tubes were added solutions of 2,4-dichloro-8-methylquinazoline (**349**) in DMSO. The tubes were placed into an

Electrothermal® STEM Integrity 10™ machine, which allows ten reactions to be run independently and in parallel.[270] For more information see **6.1.21 Integrity 10 Reactions**. The conditions of all 10 reactions and the LCMS conversions seen in each case, are shown in **Table 5.1**.

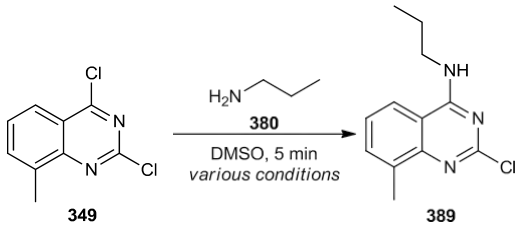

Scheme 5.12: General synthetic scheme for the formation of 2-chloro-8-methyl-*N*-propylquinazolin-4-amine (389) from 349.

Entry	Base (amount)	Temperature	Appearance of reaction mixture	By-products[a]	Conversion[b]
1	NEt_3 (0.5 eq.)	70 °C	Homogenous, crystallisation observed upon cooling.	Absent	71%
2	DBU (0.5 eq.)	70 °C	Homogenous, crystallisation observed upon cooling.	2%	78%
3	4-DMAP (0.5 eq.)	70 °C	Homogenous, crystallisation observed upon cooling.	53%	90%
4	KO^{t}Bu (0.5 eq.)	70 °C	Heterogenous mixture.	4%	66%
5	NEt_3 (0.5 eq.)	80 °C	Homogenous, crystallisation observed upon cooling.	Absent	69%
6	NEt_3 (0.5 eq.)	90 °C	Homogenous, crystallisation observed upon cooling.	Absent	58%
7	NEt_3 (0.5 eq.)	100 °C	Homogenous, crystallisation observed upon cooling.	1%	57%
8	No base	70 °C	Homogenous, crystallisation observed upon cooling.	Absent	54%
9	NEt_3 (0.1 eq.)	70 °C	Homogenous, crystallisation observed upon cooling.	Absent	45%
10	NEt_3 (1.0 eq.)	70 °C	Homogenous, crystallisation observed upon cooling.	Absent	85%

Table 5.1: Preliminary conditions for the S_NAr reaction between 349 and 380. All reactions were performed for 5 minutes in the Electrothermal® STEM Integrity 10™ machine, using 0.4 mmol 2,4-dichloro-8-methylquinazoline (349) in 2 mL DMSO. (a) By-product formation is determined here through % composition of the total LCMS AUC data which is not related to the SM or product. (b) Conversion in each case is based on % SM (349) remaining in the reaction mixture composition by LCMS AUC data. Products were not isolated.

Entries 1-4 tested the effect of changing the base present within the reaction mixture. Typical bases used in S_NAr reactions, namely triethylamine (NEt_3), 1,8-diaza bicyclo[5.4.0]undec-7-ene (DBU), 4-dimethylaminopyridine (4-DMAP) and potassium *tert*-butoxide (KO^{t}Bu) were employed in initial reactions to introduce the amine functionality. In

Entries 1-3, homogenous reaction mixtures were observed, which precipitated following cooling to ambient conditions. The use of potassium *tert*-butoxide resulted in the presence of a heterogenous mixture, which is unsuitable for adaptation to use within a flow procedure.

Triethylamine (**Entry 1**) proved the most suitable base for the transformation, since no observable by-products were detected by LCMS analysis in its use.

Nevertheless, **Entries 1-4** all displayed incomplete conversion after 5 minutes by LCMS analysis. Therefore, using these same conditions, **Entries 5-7** tested the effect of an incrementally increasing reaction temperature on the observed reaction profile. The effect was non-obvious with respect to the change of conversion observed in the reaction. Increasing the reaction temperature to 80 °C (**Entry 5**) gave a similar reaction profile to **Entry 1**, and the yield deteriorated when heated further (**Entries 6** and **7**).

The role of base stoichiometry in the reaction mixture was then considered in **Entries 8-10**. Conversion was reduced to 54% without the addition of triethylamine base, and an improvement was seen when a stoichiometric amount of base was added (**Entry 10**).

Having obtained preliminary data for the substitution reaction, another set of reactions were then performed in a similar manner. In each case, the stoichiometric use of triethylamine was employed and temperatures between 90-130 °C were tested. (**Table 5.2**).

Entry	Base (amount)	Temperature	By-products[a]	Conversion[b]
1	NEt_3 (1.0 eq.)	90 °C	Absent	98%
2	NEt_3 (1.0 eq.)	100 °C	Absent	98%
3	NEt_3 (1.0 eq.)	110 °C	Absent	97%
4	NEt_3 (1.0 eq.)	120 °C	Absent	98%
5	NEt_3 (1.0 eq.)	130 °C	Absent	98%

Table 5.2: Effect of temperature on the S_NAr reaction between 349 and 380. (a) By-product formation is determined here through % composition of the total LCMS AUC data which is not related to the SM or product. (b) Conversion in each case is based on % SM (349) remaining in the reaction mixture composition by LCMS AUC data. Products were not isolated.

In all cases, exceptionally high conversion (> 97%) was seen after 5 minutes reaction time. As a result, the reaction conditions described in **Entry 1** of **Table 5.2** were taken forward as optimal, as the increasing intensity of the conditions used in **Entries 2-5** offered little benefit on the reaction composition.

In order to provide material **389** for analysis and further derivatisation, the aforementioned reaction of 1-propylamine with **349** was also performed using conditions similar to those encountered in the synthesis of **357** (**Scheme 5.3**). This preparative method is shown below (**Scheme 5.13**).

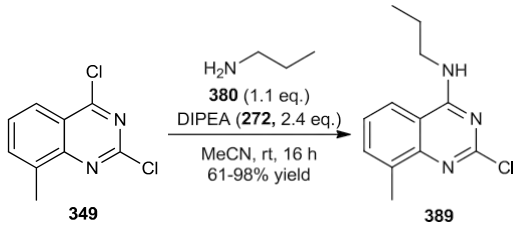

Scheme 5.13: Preparative method for the isolation of compound 389.

5.4.2 C2-Functionalisation of compound 389 with octylamine

Following the formation and isolation of compound **389**, conditions to subsequently introduce functionality in the 2-position of the quinazoline intermediate were investigated. 1-Octylamine (390) was chosen as a non-volatile model nucleophile for this purpose.

The optimal conditions identified for the introduction of the second nucleophile in batch are shown in **Scheme 5.14**. The super-stoichiometric use of triethylamine (2 eq.) and 1-octylamine (2 eq., **390**) afforded the desired product in 88% conversion after 5 minutes, and 98% conversion after 15 minutes. Furthermore, both the starting material and products of the reaction were soluble in DMSO, which would also be compatible with subsequent MDAP purification.

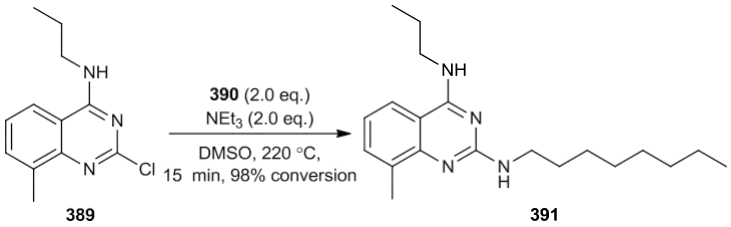

Scheme 5.14: Batch coupling of 1-octylamine with 389.

As a result, both substitution reactions could be performed readily, in timescales appropriate for the flow chemistry setup when using amine nucleophiles.

5.4.3 C4-Regioselective addition of propane-1-thiol

Thiol nucleophiles were next targeted in regioselective substitution reactions. As mentioned earlier, the addition of a thiol reagent to a dichloroquinazoline had been reported to proceed in 1 h at 15 °C in the literature.[268] Therefore, a similar synthetic procedure to earlier (**Table 5.1**) was applied in the reaction between propane-1-thiol (**381**) and quinazoline starting material **349** (**Scheme 5.15**).

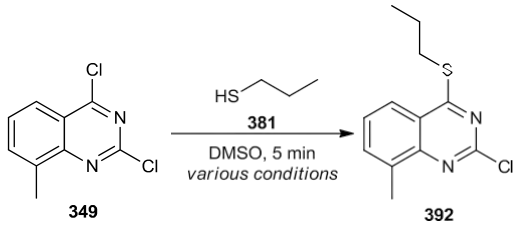

Scheme 5.15: General scheme for the reaction between propane-1-thiol (381) and 2,4-dichloro-8-methylquinazoline (349).

Once again, a reaction time of 5 minutes was targeted for complete conversion to ensure a rapid transition to application in flow chemistry. The results in **Table 5.3** show the effect of increasing reaction temperature on the conversion of starting material observed (by LCMS AUC analysis).

Entry	Temperature	Appearance of reaction mixture	Conversion[a]
1	20 °C	Homogenous.	90%
2	30 °C	Homogenous.	89%
3	40 °C	Homogenous.	98%
4	50 °C	Homogenous.	98%
5	60 °C	Homogenous.	89%

Table 5.3: Reaction conditions used in the batch optimisation reactions coupling compounds 349 and 381 to form 2-chloro-8-methyl-4-(propylthio)quinazoline (392). All reactions were performed for 5 minutes in the Electrothermal® STEM Integrity 10™ machine, using 0.2 mmol 2,4-dichloro-8-methylquinazoline (349) in 2 mL DMSO. In all cases, 1 eq. of both propane-1-thiol (381) and NEt_3 were used in the reaction. No by-products were observed in any reaction. (a) Conversion in each case is based on % SM (349) remaining in the reaction mixture composition by LCMS AUC data. Products were not isolated.

As observed in the screening results for amine addition to **349**, thiol addition was also most efficient at the intermediate temperatures tested. **Entries 3** and **4** in **Table 5.3** delivered the most promising results, with both having near quantitative conversion of the starting material to compound **392**. However, in all cases, high conversion was observed, under mild heating conditions.

Therefore, a second equivalent of both propane-1-thiol and triethylamine was added to each of the reaction mixtures, and the formal tandem S_NAr process was attempted *in situ*.

The second substitution reactions were performed at temperatures between 110-150 °C (in the same order as above, for example: reaction entry 1, which reacted at 20 °C for the first substitution was subjected to a temperature of 110 °C in the following reaction). These results are shown in **Table 5.4**.

Entry	Temperature (first reaction)	Conversion[a] (first reaction)	Temperature (second reaction)	Conversion[a] (second reaction)
1	20 °C	90%	110 °C	N/a
2	30 °C	89%	120 °C	N/a
3	40 °C	98%	130 °C	N/a
4	50 °C	98%	140 °C	N/a
5	60 °C	89%	150 °C	4%

Table 5.4: Conditions for the *in situ* batch reaction of 392 with another equivalent of propane-1-thiol and triethylamine, following its formation from 349. (a) Conversion in each case is based on the % total LCMS AUC of the reaction mixture corresponding to the MW of the desired product. Entry 5 was the only reaction conditions to show formation of the desired material (albeit in a low percentage conversion).

In **Entries 1-4** of **Table 5.4**, the formation of the desired product was not seen under the reaction conditions. For **Entry 5**, the desired material was formed, but only in 4% conversion by LCMS AUC data.

As a result, forcing conditions would be required to successfully couple thiol reagents to the C2-position of the quinazoline in an S_NAr reaction. As previously discussed, within the literature, the addition of a nucleophile to a 2-chloro-4-thioquinazoline intermediate often results in a variety of by-products.[268] Therefore, it was thought that rather than exploring a likely capricious and energy-intensive S_NAr procedure, an alternative method would be sought for the application of thiol reagents as potential 2-position substituents. For more information on this work, see **Section 5.5 Palladium-mediated *O*- and *S*-functionalisation at C2**.

5.4.4 C4-Regioselective addition of 1-propanol

The regioselective addition of 1-propanol (**382**) to 2,4-dichloro-8-methylquinazoline (**349**), shown in **Scheme 5.16**, proved to be far more challenging. When previous conditions using a stoichiometric amount of triethylamine were attempted, no conversion was observed in 5 minutes, even when at high reaction temperatures (**Entries 1-4**, **Table 5.5**).

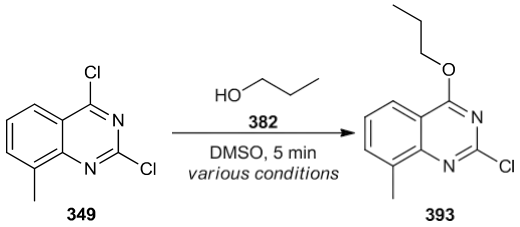

349 **393**

Scheme 5.16: General scheme for the reaction between 1-propanol (382) and 2,4-dichloro-8-methylquinazoline (349).

Entry	Temperature	Base	By-product formation[a]	Conversion[b]
1	80 °C	NEt_3	17%	N/a
2	90 °C	NEt_3	39%	N/a
3	100 °C	NEt_3	39%	N/a
4	110 °C	NEt_3	41%	N/a
5	90 °C	DBU	55%	5%
6	110 °C	DBU	72%	6%
7	130 °C	DBU	78%	6%
8	150 °C	DBU	89%	7%
9	50 °C	BTTP	19%	26%
10	60 °C	BTTP	26%	25%
11	70 °C	BTTP	18%	24%
12	80 °C	BTTP	27%	22%
13	90 °C	BTTP	24%	26%
14[c]	50 °C	BTTP	14%	27%
15	110 °C	BTTP	38%	27%
16	120 °C	BTTP	47%	21%
17	130 °C	BTTP	58%	16%
18	140 °C	BTTP	68%	20%
19	150 °C	BTTP	77%	20%

Table 5.5: Conditions for optimisation of the reaction between 349 and 1-propanol. All reactions were performed for 5 minutes in the Electrothermal® STEM Integrity 10™ machine, using 0.2 mmol 2,4-dichloro-8-methylquinazoline (349) and 1 eq. of both 1-propanol (382) and the selected base in 2 mL DMSO. (a) Conversion in each case is based on the % total LCMS AUC of the reaction mixture corresponding to the MW of the desired product (393). (b) By-product formation is determined here through % composition of the total LCMS AUC data which is not related to the SM or product. (c) Reaction was performed for an extended reaction time of 15 min. BTTP = *tert*-butylimino-tri(pyrrolidino)phosphorane.

As a result, stronger bases were considered for the reaction. The use of DBU (**Entries 5-8**) was accompanied with the formation of a wide range of by-products in the reaction, as well as a discolouration of the reaction solution which was suggestive of degradation.

Consequently, phosphazene base BTTP was used in an attempt to drive the reaction towards the desired product (**Entries 9-19**). At moderate reaction temperatures (50-90 °C), modest conversion of **349** to the desired product was observed after 5 minutes by LCMS analysis (**Entries 9-13**). However, these results were insufficient to be applied in a clean and fast formation of **393** in flow, especially since ~20% degradation was observed in all cases.

Extending the reaction time to 15 minutes (**Entry 14**) seemed to limit the amount of by-product formation seen in the reaction, but also offered no advantage with respect to conversion to the desired product. Finally, in case an energy barrier limited the extent of product formation, BTTP-containing reactions using higher temperatures were performed (**Entries 15-19**).

Unfortunately, the use of high temperature conditions caused a substantial increase in degradation of the reaction material, and no significant benefit on the efficiency of **393** production.

Consequently, conditions for the regioselective addition of alcohol reagents to dichloroquinazoline structures *via* an S_NAr reaction were not pursued further, due to the

difficulty in performing the desired reaction whilst maintaining the integrity of the reaction components.

However, it was thought that coupling of alcohol nucleophiles to the C2-position of 2-chloroquinazoline intermediates, such as **389**, may be possible. This approach was investigated using a palladium-catalysed coupling procedure and is explored in the following section.

5.5 Palladium-mediated *O*- and *S*-functionalisation at C2

Due to the difficulties faced in introducing thiol and alcohol reagents, especially at the C2-position of the quinazoline motif, another approach was targeted. In order to quickly find any active catalyst systems for coupling the reagents, plates holding 24 x 1 mL vials, which in total, contained 2 sets of 12 pre-weighed catalyst complexes (known to enable heteroatom arylation reactions in the literature) were used.[271,272] For the setup of the plate, including the catalyst complexes used, see **Section 7.9 Appendix 9 – Buchwald-Hartwig screening plate procedure**.

Due to its ease of synthesis, and in order to remove any issues of regioselectivity in the reaction, intermediate **389** was selected as an ideal scaffold for further functionalisation.

5.5.1 C2-Functionalisation of compound 389 with propane-1-thiol and 1-propanol

Initially, using 1-propanol (**382**) as a model alcohol reagent, the reaction between **382** and 2-chloro-8-methyl-*N*-propylquinazolin-4-amine (**389**) was performed using the method described in **Section 7.9 Appendix 9 – Buchwald-Hartwig screening plate procedure**, where the plate was heated at a reaction temperature of 100 °C for 18 h under an anhydrous atmosphere (**Scheme 5.17**).

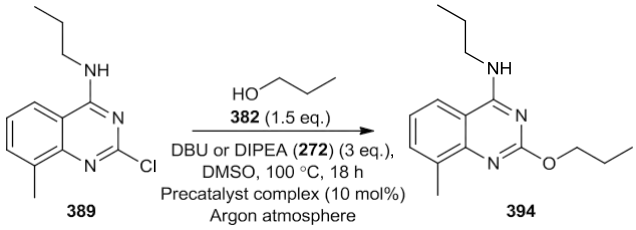

Scheme 5.17: General scheme for the array plate reaction tested with 12 palladium precatalysts. In all cases, reaction solutions were present in DMSO, 10 mol% catalyst loading was used, and the reactions were performed under an anhydrous atmosphere for 18 h.

After 18 h, the plate was cooled, and the materials were quenched according to **Section 6.3.1.2 General procedure F (Use of the Buchwald-Hartwig screening plate)**. The quench solution used contained triphenylamine, for use as an internal standard for LCMS analysis. As a result, following the reaction, rapid analysis of the reaction profiles of all array plate wells could be achieved.

The results for the coupling reaction shown in **Scheme 5.17** are shown in **Section 7.10 Appendix 10 – Buchwald-Hartwig screening plate LCMS profiles**. Gratifyingly, the reaction reached full conversion of the starting material when using DBU as base and RockPhos Pd G3 catalyst, and was highly efficient, since 87% of the reaction composition was the desired material by LCMS analysis.

Due to a later solvent change to *N*-butylpyrrolidone (NBP; trade name Tamisolve®) to increase the solubility of the reactants for the S_NAr procedure (See **Section 5.6 Tandem flow S_NAr procedure**), the array plate method was also repeated in Tamisolve®. Unfortunately, very poor conversion was observed in all cases when Tamisolve® was employed as the reaction solvent. Therefore, further optimisation of the reaction was performed in DMSO.

To ensure that the reaction was reproducible under standard batch conditions, it was repeated on larger scale using the optimised catalyst complex identified from the array plate procedure, RockPhos Pd G3 (**Scheme 5.18**). For the batch method, the reaction was performed at 100 °C for 24 h, affording the desired product in good yield (68%) following purification.

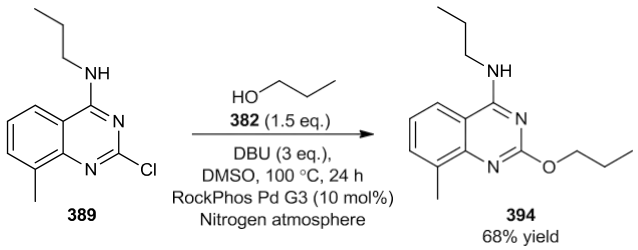

Scheme 5.18: The synthesis of 394 in batch using the optimised conditions from the array plate procedure. Following purification, compound 394 was isolated in 68% yield.

Using these optimised conditions, the analogous thiol coupling was then performed. Propane-1-thiol (**381**) was utilised in a reaction with **389** to produce 8-methyl-*N*-propyl-2-(propylthio)quinazolin-4-amine (**395**) in good yield.

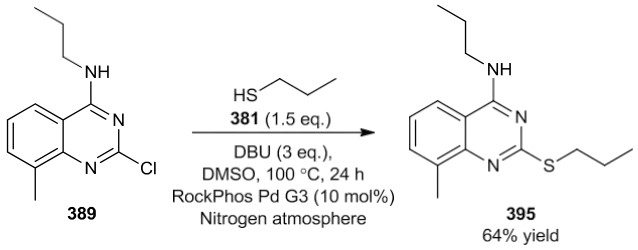

Scheme 5.19: The application of the optimised conditions from the array plate using propane-1-thiol (381).

The success of the batch coupling reactions offered a facile method for the C2-functionalisation of quinazoline intermediates with alcohol and thiol reagents, where S_NAr procedures had failed.

However, although useful within a standalone synthetic route, the reactions were deemed too inefficient to be useful within the flow reactor. Therefore, the coupling shown in **Scheme 5.18** was repeated under more temperature-intensive conditions, in order to accelerate formation of the desired product (**394**). Entries within **Table 5.6** describe the efforts made to achieve the complete conversion of **389** in a reaction time similar to that seen for the second S_NAr in the formation of diaminoquinazolines seen earlier ~15 mins (**Scheme 5.14**).

Entry	Catalyst loading	Extra additives	Reaction time	Reaction appearance	Temperature	Conversion[a]
1	2.5 mol%	N/a	24 h	Homogenous	100 °C	13%
2	5 mol%	N/a	24 h	Homogenous	100 °C	51%
3	5 mol%	N/a	15 min	Heterogenous mixture	170 °C	29%
4	2.5 mol%	1-propanol (3 eq. rather than 1.5 eq.)	15 min	Homogenous	170 °C	27%
5	5 mol%	1-propanol (3 eq. rather than 1.5 eq.), RockPhos (10 mol%)	15 min	Heterogenous mixture	170 °C	34%
6	5 mol%	1-propanol (3 eq. rather than 1.5 eq.), RockPhos (5 mol%)	15 min	Heterogenous mixture	170 °C	32%
7	5 mol%	1-propanol (3 eq. rather than 1.5 eq.)	15 min	Heterogenous mixture	150 °C	44%
8	5 mol%	1-propanol (3 eq. rather than 1.5 eq.)	15 min	Homogenous	120 °C	36%
9	5 mol%	1-propanol (3 eq. rather than 1.5 eq.), only 1 eq. DBU used	15 min	Minimal precipitation	140 °C	39%
10	5 mol%	1-propanol (3 eq. rather than 1.5 eq.), only 1 eq. DBU used	15 min	Homogenous	130 °C	44%
11	10 mol%	1-propanol (3 eq. rather than 1.5 eq.), only 1 eq. DBU used	15 min	Heterogenous mixture	130 °C	47%

Table 5.6: Tested conditions to accelerate the formation of compound 394 through a palladium-mediated coupling procedure. All reactions were performed under a nitrogen atmosphere at a concentration of 0.1 M with respect to 389, using the optimised stoichiometries determined in Scheme 5.18, unless stated in the catalyst loading or extra additives columns. (a) Conversion in each case is based on the % total LCMS AUC of the reaction mixture corresponding to the MW of the desired product (394).

Initial attempts were made to reduce the catalyst loading in the system, in order to improve solubility (**Entries 1** and **2**). Pleasingly, decreasing the catalyst loading led to homogenous reaction solutions, which would be less prone to blockage when performed in flow. However, when reduced to 2.5 mol% (**Entry 1**), insufficient activity was observed, resulting in only 13% conversion after 24 h reaction time. When 5 mol% catalyst was used under the otherwise optimised conditions (**Entry 2**), a conversion of 51% was seen in the reaction.

To accelerate the efficiency of **394** production in the system, reactions using raised temperatures were examined. In **Entry 3**, a conversion of 29% was seen after only 15 minutes at 170 °C, although this was also accompanied with the formation of an insoluble precipitate during the course of the reaction. It was thought that at such high temperatures, the precipitate made may be a result of palladium aggregation in the system.

The use of less catalyst (2.5 mol%) prevented the extent of aggregation observed in the reaction, but also reduced product formation. In **Entry 4**, for example, 27% conversion was seen using the same reaction time and temperature, even with 3 eq. of the 1-propanol (**382**) nucleophile.

In another approach to counteract palladium aggregation whist maintaining desirable reactivity, extra uncoordinated RockPhos ligand was added to the system (**Entries 5-6**). Unfortunately, the RockPhos ligand itself was not soluble in the reaction solution, and the reaction was still present as a heterogenous mixture.

A slightly reduced reaction temperature of 150 °C was applied in **Entry 7**, to successfully deliver a conversion of 44%. On the other hand, a heterogenous reaction mixture was still seen, and so milder conditions were required to allow for downstream flow application.

In **Entry 8**, a reaction temperature of 120 °C for a system containing 5 mol% catalyst was present as a homogenous solution. Though promising, the result also involved a reduced amount of starting material conversion (36%) seen and, thus, these conditions demonstrate the challenge between balancing reactivity and solubility for the metal-catalysed C2-functionalisation method.

Due to the presence of by-product **396** (**Figure 5.3**) in all of the earlier reactions, the amount of base used was reduced to avoid by-product formation (for more information, see **Section 6.3.2. Specific synthetic procedures for Chapter 2**). **Entries 9-11** show the beneficial effect observed in terms of the product formation observed.

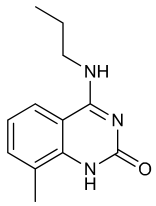

396

Figure 5.3: By-product 396, formed during the high temperature C2-functionalisation reactions. The by-product was not isolated but observed by LCMS analysis. For information on the % by-product observed for each entry in Table 5.6, see the *Experimental* section (specifically Section 6.3.2. Specific synthetic procedures for Chapter 2).

With consideration for both the extent of the by-product and desired product formation observed, **Entry 10** represents the most optimal conditions found. On the other hand, none of the conditions were sufficiently reactive to generate the desired products cleanly and fast enough to be directly applied in the flow procedure. As a result of the unpredictable solubility of the systems, especially when considering the future application of a range of potential alcohol and thiol nucleophiles, these problems may also have been exacerbated further.

Consequently, the continuous flow formation of diaminoquinazolines were prioritised for the antimalarial programme, although the developments seen within the C2-functionalisation research may outline an area for future work, for further exploration of SAR within the series.

5.5.2 C2-Functionalisation of compound 389 with octylamine

In order to compare the efficiency of the S_NAr procedure to the palladium-mediated coupling, the C2-functionalisation of **389** with 1-octylamine (**390**) was attempted (**Scheme 5.20**).

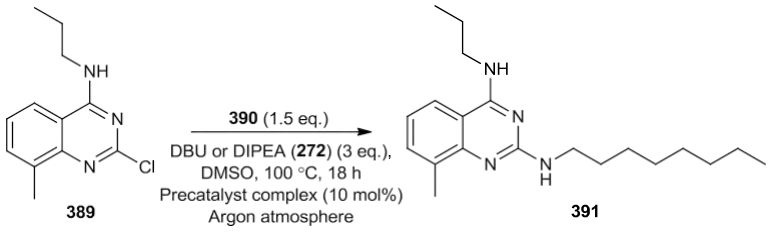

Scheme 5.20: The Buchwald-Hartwig array plate conditions used in the synthesis of 391.

Under the same conditions used for the array plate coupling involving 1-propanol (**382**), the best results were obtained in the use of XantPhos Pd G3 with DBU. However, even in the most optimised conditions (vial D6, see **Section 7.10 Appendix 10 – Buchwald-Hartwig screening plate LCMS profiles** for more information) only 25% desired product was observed by LCMS analysis, along with a range of by-products.

Thus, the reaction was inferior to the S_NAr procedure for the introduction of amine reagents in the C2-position of the quinazoline. Considering the combined findings from the research in both areas, the tandem S_NAr procedure was subsequently applied in flow.

5.6 Tandem flow S_NAr procedure

In order to ensure that the tandem S_NAr reaction could be performed in flow, the synthesis of **391** was repeated using the bespoke microfluidic flow setup (**Scheme 4.19**). For information on the reaction procedure used, see **Section 6.3.1.3 General procedure G (tandem flow synthesis of diaminoquinazolines)**. Following purification *via* a low pH automated reverse phase column chromatography, **397**, the formate salt of **391** was afforded.

The reactions were performed in *N*-butylpyrrolidone (NBP). Initially, application of the DMSO conditions had been attempted in flow. However, though the intermediate **389** was observed to be soluble in DMSO following earlier optimisation, the starting material (**349**) was insufficiently soluble in the solvent. A solvent change to Tamisolve® ensured the complete dissolution of the starting materials at the required concentrations (0.2 M used in the first reaction, 0.1 M in the second reaction following combination of the input lines) but still retained the high boiling point (241 °C) and polar nature of DMSO, with a safer profile relative to its methyl analogue, NMP.[273]

Nevertheless, solubility issues were faced when trying to dissolve the base into the reaction mixture. It was found that a substitution of the originally employed triethylamine base to the less polar tributylamine (**273**) base allowed for the formation of a homogenous reaction mixture for the tandem procedure (**Scheme 5.21**).

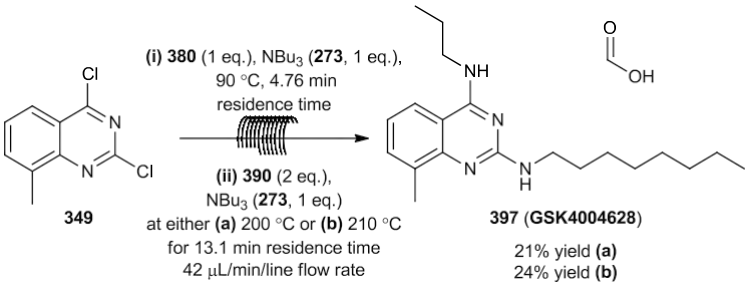

Scheme 5.21: The tandem S_NAr flow synthesis of diaminoquinazoline formate salt 397.

5.6.1 Monomer selection and enumeration

Having established conditions for the synthesis of diaminoquinazoline compounds in a tandem flow S_NAr procedure, small nucleophilic monomers were selected using the GSK TIMS building block inventory. TIMS (Tool for Interactive Monomer Selection) is a database for small monomers, which can be examined for compounds containing a selected functionality (i.e. primary amines) and containing specific physical or physicochemical property (e.g. a certain number of aromatic rings in the chemical structure of the molecule, or a specific cLogP value *etc*). The database catalogue comprises of ~40,000 molecules present within GSK stores and can allow for the rapid acquisition of small monomers for lead molecule enumeration to probe SAR ideas.

Using the TIMS database, 37 monomers (comprising of compounds with amine, thiol and alcohol functionalities) were selected for enumeration with the 8-methylquinazoline scaffold. Due to the difficulties described earlier in synthesising ether and thiol-ether quinazoline adducts, amine additions to the scaffold were prioritised (**Figure 5.4**). All of the monomers were chosen based on simplistic desirable drug-like parameters (MW < 175, cLogP < 5, HBA < 5, HBD < 5).

The hydrogen bond donor (HBD) and hydrogen bond acceptor (HBA) numbers for compounds are useful parameters for considering potential dangers of promiscuous binding in drug-like molecules. While introducing more heteroatoms in structures can reduce their lipophilicity, it also increases the number of reactive atoms capable of making non-covalent bonds (bridged by a hydrogen atom) with proteins and other large biological components, leading to off-site toxicity. As a result, Lipinski's rule of five,[274] a classic model in the literature predicting the desired physicochemical parameters of successful orally-administered drugs, suggests that

aiming for a HBD number of < 5 and HBA number of < 10 is likely to reduce the attrition often observed in drug development.[274]

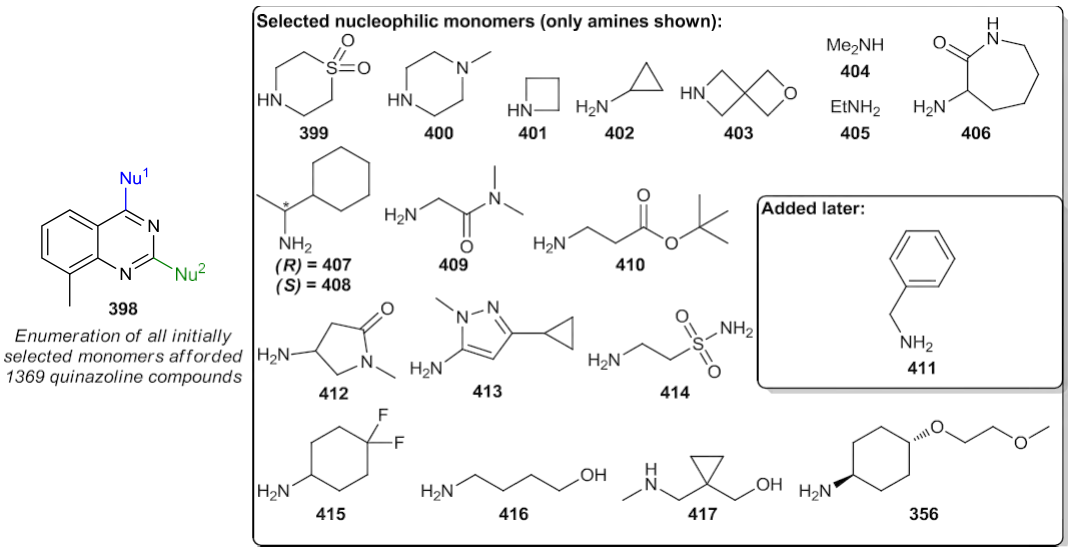

Figure 5.4: The selection of small amines, and their enumeration within the 2,4-disubstituted quinazoline structure to generate many possible synthetic targets. Benzylamine was later added to the initially selected monomers in order to probe SAR data surrounding amines substituted with α-aromatic functionality.

Monomers within these search parameters were chosen at random and enumerated with the quinazoline scaffold to afford 1369 (37^2) possible structures for synthesis when considering the selected amine, thiol and alcohol monomers. The amine monomers, which were initially prioritised, are shown in **Figure 5.4**.

Computational predictions of all of the enumerated molecules were then performed on LiveDesign™,[275] an online platform used to cumulate a vast amount of data for drug discovery programmes, based on both the computationally calculated properties of prospective molecule ideas for synthesis, as well as gathered physical data for tested compounds.

A multi-parameter optimisation (MPO)[276] calculation was then applied to all of the virtual molecules. The bespoke MPO combined many calculated physical properties (with equal weighting) to determine how drug-like the enumerated quinazoline structures were, and therefore how likely they were to have desirable physicochemical profiles. Though potent compounds were targeted, this would be difficult to predict due to the phenotypic nature of the study, and the synthesis of less potent compounds would still facilitate understanding of the SAR for the series. The parameters considered (as well as the values determining of their classification as bad (red), moderate (yellow) or good (green) profiles for that parameter) in the MPO are shown in **Table 5.7**

Parameter	Bad value	Moderate value	Good value
Predicted likeliness of hERG toxicity	Low	Medium	High
Prediction of sufficient cellular permeability	Fail, high confidence	Borderline fail	(1) Pass, high confidence (2) Borderline pass
Calculated PFI (cPFI)	> 8	≥ 4, ≤ 8	< 4
No. rotatable bonds	> 11	≥ 7, ≤ 11	< 7
Predicted plasma protein binding (logarithmic value)	> 1.99	≥ 1.28, ≤ 1.99	< 1.28
No. HBD	> 6	≥ 2, ≤ 6	< 2
No. HBA	> 11	≥ 6, ≤ 11	< 6
cLogP	> 5	≥ 3, ≤ 5	< 3
Topological polar surface area (TPSA)	(1) < 60 (2) > 140	(1) ≥ 60, < 80 (2) > 120, ≤ 140	≥ 80, ≤ 120

Table 5.7: The physicochemical parameters considered for the enumerated compounds, and the value limits to determine whether those compounds displayed bad (red), moderate (yellow) or good (green) physical and predicted properties in each case. The combination of all of the metrics provided an MPO score for each compound of between 0 and 1, where 1 represents the most optimal drug-like compound possible based the physicochemical properties, and 0 represents the least optimal.

The number of rotatable bonds within a compound gives structure-specific information regarding the molecular rigidity of compounds, which may affect their oral bioavailability (the fraction of unchanged administered drug which reaches the systemic circulation in the patient, and thereby may achieve a pharmacological effect). A previous study of over 1100 drug candidates has shown that high numbers of rotatable bonds (> 10) are often associated with the undesirable effect of reducing the amount of bioavailability observed for therapeutic compounds, thereby diminishing their activity *in vivo*.[277] Though rotatable bond number usually increases with respect to the size of the molecule, the study showed that regardless of their molecular weight, the majority of compounds containing equal to or less than 7 rotatable bonds achieved a bioavailability of at least 20%. Conversely, 75% of molecules with more than 10 rotatable bonds did not attain the same minimal value.[277]

Even if compounds can reach the systemic circulation, they may not subsequently permeate through to the desired site of action or may be metabolised rapidly. For the former consideration, plasma protein binding (PPB) determines the extent that drug compounds are restricted to the bloodstream through binding to proteins within the blood. Specifically, the most abundant protein in the blood is human serum albumin (HSA). If the drug binding to HSA and other blood proteins is very high, the compound may not be able to exert a desired pharmacological effect. However, it is also less likely to be metabolised quickly, giving the drug an extended time of action within the body.

On the other hand, although programme-dependent, lead optimisation strategies are often focused on lowering plasma protein binding, since lipophilic molecules (LogP > 4) are known to be limited by blood protein binding in drug development.[278] The measurement given here is based on the logarithmic function of the % protein binding observed in the blood plasma.

Lastly, the topological polar surface area (TPSA) gives an idea of the permeability of drug molecules and encompasses all surfaces of a drug compound which contain polar atoms (mainly nitrogen and oxygen seen within medicinal chemistry). The TPSA can be constructed from the PSA of fragments to accelerate drug discovery programmes, and high TPSA values (> 140 Å^2) often result in poor accompanying permeability data.[277,279] Molecules with TPSA values (< 60-70 Å^2) are more likely to cross the blood-brain barrier, a highly selective semi-permeable membrane responsible for controlling entry of blood-borne substances into the brain. As a result, molecules with low TPSA values often display clinical neurotoxicity issues.[280] Therefore, an intermediate range of values for the TPSA (80-120) was targeted as part of the MPO design.

The combination of all of the predicted values (outlined in **Table 5.7**) afforded each virtual molecule with an MPO score from 0 (least drug-like parametric profile possible) to 1 (most drug-like parametric profile possible), and an assortment of diaminoquinazoline molecules were subsequently selected for synthesis. The compounds targeted for synthesis were chosen due to the broad variety in chemical space and MPO score predictions that they exhibited. Henceforth, along with any computed or collected physical data on the compounds, their MPO score will also be provided for reference.

5.6.2 Synthesised diaminoquinazolines and associated data

Though many examples were synthesised using the optimised tandem S_NAr process described earlier, some of the targeted diaminoquinazolines were not made due to either their insolubility in the reaction mixture, or their lability within the reaction conditions or during reverse phase purification. The structures of these targets are shown in Section **7.11 Appendix 11 – Unattainable products from tandem flow S_NAr experiments**.

Nevertheless, for the successful isolation of diaminoquinazoline products, the general flow reaction represented in **Scheme 5.22** was used.

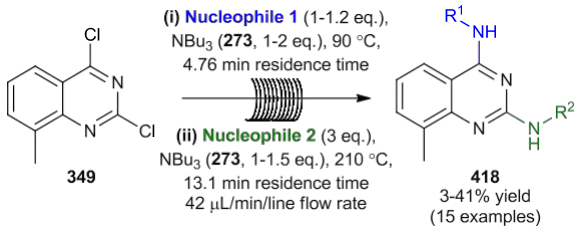

Scheme 5.22: General procedure used to synthesise 2,4-diaminoquinazolines (418) in flow. Variable yields were afforded due to the rapid throughput of reactions, and capricious solubility and reactivity of the monomeric nucleophiles used. Nevertheless, sufficient material was afforded in each case for assay testing.

Fifteen examples of diaminoquinazolines were assembled rapidly using the flow method. As a consequence of the different solubility and nucleophilicity of the monomers used, variable yields were observed in the process. However, in each case, products were rapidly

synthesised in sufficient amounts for assay testing to probe SAR data, and the procedure is easy to manipulate in the future, for the production of specific compounds. For instance, alteration of the residence time for each reaction, or the channel size of the flow reactor vessels could alleviate any issues related to incomplete conversion, or tube blockages seen in the use of the standard conditions described here.

A small number of compounds were selected for synthesis but proved unsuitable for the flow procedure. Therefore, these molecules are highlighted below prior to discussion on the biological activity and physicochemical profiles of compounds prepared. Though compound **420** was isolated in low yield (3%) from the flow process, further material was required for analytical data.

As such, the product was made in batch using the procedure outlined in **Scheme 5.23**. This afforded the desired material (**420**) in sufficient yield following an extended reaction time. Following the first S_NAr reaction between 2,4-dichloro-8-methylquinazoline (**349**) and 4,4-difluorocyclohexan-1-amine (**415**), compound **419** was produced as a regioisomeric mixture with the undesired C2-functionalised by-product. As such, the crude reaction mixture was taken on without further purification into a second S_NAr reaction with an excess of azetidine (**401**). The desired material was isolated in a 46% yield (with respect to the amount of crude starting material mixture used).

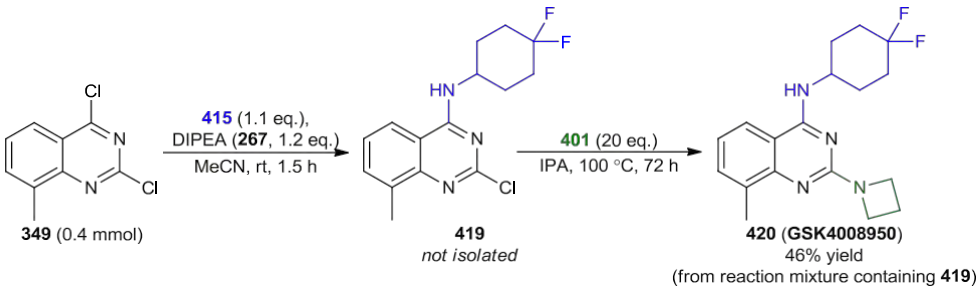

Scheme 5.23: The batch synthesis of 420, to afford sufficient product for analysis. Compound 419 was not isolated; the crude reaction mixture was taken into the next reaction due to the presence of regioisomers following the first S_NAr reaction.

The remainder of crude product **419** was used to synthesise compound **421**, since the difluorocyclohexylamine functionality displayed limited solubility in Tamisolve®, and so compounds (such as **420** and **421**) containing the motif were typically susceptible to precipitation, and therefore failure, in the flow process. Compound **421** was synthesised in batch using a similar method to the one shown in **Scheme 5.23**, using 4-aminobutan-1-ol (**416**) as the nucleophilic monomer (**Scheme 5.24**).

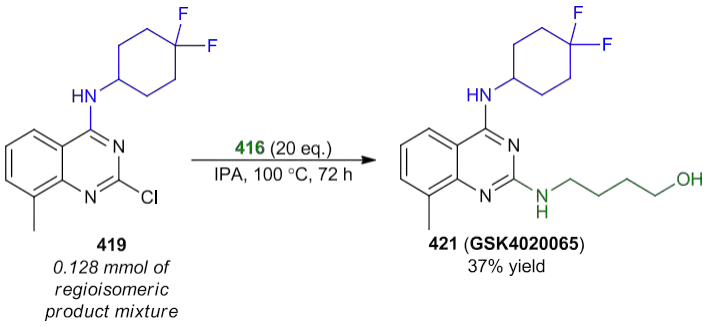

Scheme 5.24: The batch synthesis of compound 421.

2-Chloro-substituted intermediate **422** was prepared serendipitously, as the use of ethanamine (**405**; 70% wt. in H_2O) did not lead the formation of any discernible product (**Scheme 5.25**). However, since the (*trans*)-4-(2-methoxyethoxy)cyclohexan-1-amine (**356**) functionality in position 4 represented the substitution used in lead molecule **341**, the compound was still submitted for assay testing to ensure that no activity was observed prior to the introduction of C2-functionality.

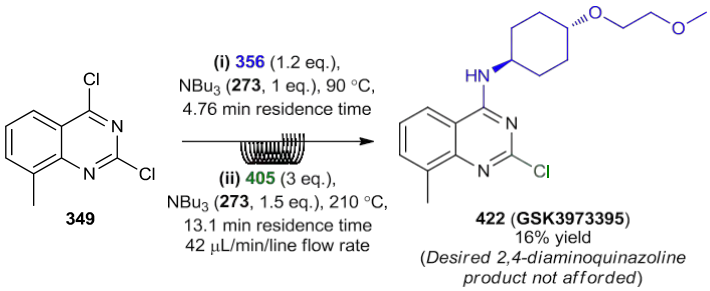

Scheme 5.25: The isolation of intermediate 422 from attempted flow procedure using 356 and 405 as nucleophilic monomers.

Finally, the synthetic preparation of molecule **423** was also unsuccessful using the flow method but was still targeted through an alternative batch method. When placed under flow conditions, nucleophilic monomer **407** was insufficiently reactive to form bis-substituted quinazoline **423**. Therefore, the reaction was reattempted in a single formal reaction step under forcing conditions using microwave irradiation, to afford the formate salt of **423** in good yield (57%) following purification (**Scheme 5.26**).

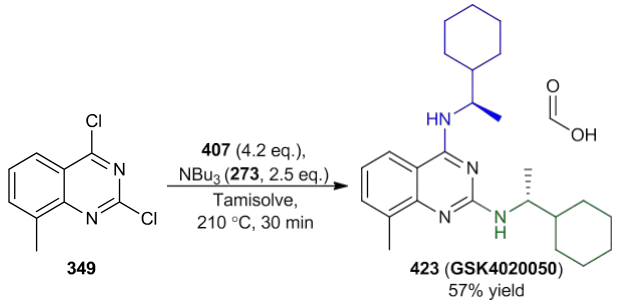

Scheme 5.26: Forcing microwave conditions for the synthesis of compound 423.

Synthetic yields and data for all of the aforementioned structures, along with those produced in the tandem S_NAr flow procedure are shown in **Figures 5.5-5.7**.

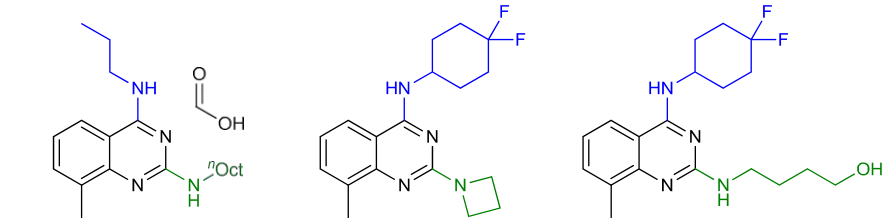

397 (**GSK4004628**)
24% yield
***Pf*$_{3D7}$ pIC$_{50}$ = 6.1**
hERG pIC$_{50}$ = N/a
HepG2 pIC$_{50}$ = 5.2
ChromLogD = 7.6
LLE$_{AT}$ = 0.01 kcal mol^{-1} HA^{-1}
CAD = 3 μg/mL, AMP = N/a
PFI = 9.6, MPO = 0.12

420 (**GSK4008950**)
46% yield[a]
***Pf*$_{3D7}$ pIC$_{50}$ = 5.3**
hERG pIC$_{50}$ = 5.7
HepG2 pIC$_{50}$ = 4.4
ChromLogD = 6.9
LLE$_{AT}$ = 0.17 kcal mol^{-1} HA^{-1}
CAD = 98 μg/mL, AMP = 270 nm s^{-1}
PFI = 8.9, MPO = 0.35

421 (**GSK4020065**)
37% yield[a]
***Pf*$_{3D7}$ pIC$_{50}$ = 5.6**
hERG pIC$_{50}$ = 6.0
HepG2 pIC$_{50}$ = 4.5
ChromLogD = 3.6
LLE$_{AT}$ = 0.18 kcal mol^{-1} HA^{-1}
CAD = 137 μg/mL, AMP = 460 nm s^{-1}
PFI = 5.6, MPO = 0.59

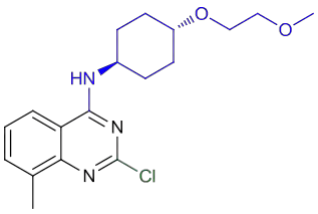

422 (**GSK3973395**)
16% yield
***Pf*$_{3D7}$ pIC$_{50}$ < 5.3**
hERG pIC$_{50}$ < 4.3
HepG2 pIC$_{50}$ < 4.0
ChromLogD = 6.1
LLE$_{AT}$ < 0.20 kcal mol^{-1} HA^{-1}
CAD = 147 μg/mL, AMP = 630 nm s^{-1}
PFI = 8.1, MPO = 0.45

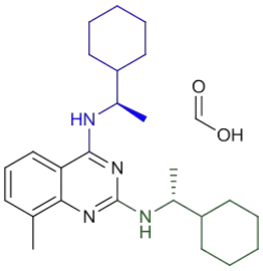

423 (**GSK4020050**)
57% yield
***Pf*$_{3D7}$ pIC$_{50}$ = 6.5**
hERG pIC$_{50}$ = 5.5
HepG2 pIC$_{50}$ = 5.5
ChromLogD = 9.3
LLE$_{AT}$ = -0.01 kcal mol^{-1} HA^{-1}
CAD = 0 μg/mL, AMP = N/a
PFI = 11.3, MPO = 0.12

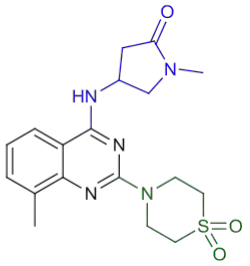

424 (**GSK4007058**)
21% yield
***Pf*$_{3D7}$ pIC$_{50}$ < 5.3**
hERG pIC$_{50}$ < 4.3
HepG2 pIC$_{50}$ < 4.0
ChromLogD = 3.6
LLE$_{AT}$ < 0.29 kcal mol^{-1} HA^{-1}
CAD = 64 μg/mL, AMP = 380 nm s^{-1}
PFI = 5.6, MPO = 0.89

Figure 5.5: Synthesised compounds tested in the *P.falc.* assay (set 1 of 3). (a) Yield determined from second synthetic step, as explained in Scheme 5.23. Data was not attained for parameters where the N/a denotation is used.

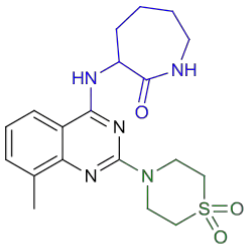

425 (GSK4005808)
7% yield
***Pf*$_{3D7}$ pIC$_{50}$ < 5.3**
hERG pIC$_{50}$ = 4.4
HepG2 pIC$_{50}$ < 4.0
ChromLogD = 4.5
LLE$_{AT}$ < 0.29 kcal mol^{-1} HA^{-1}
CAD = 9 μg/mL, AMP = 480 nm s^{-1}
PFI = 6.5, MPO = 0.85

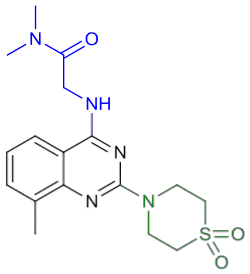

426 (GSK4006627)
12% yield
***Pf*$_{3D7}$ pIC$_{50}$ < 5.3**
hERG pIC$_{50}$ < 4.3
HepG2 pIC$_{50}$ < 4.0
ChromLogD = 3.7
LLE$_{AT}$ < 0.34 kcal mol^{-1} HA^{-1}
CAD = 86 μg/mL, AMP = 540 nm s^{-1}
PFI = 5.7, MPO = 0.89

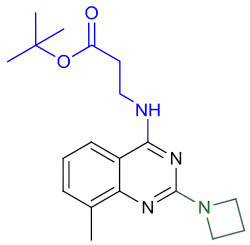

427 (GSK4020050)
10% yield
***Pf*$_{3D7}$ pIC$_{50}$ < 5.3**
hERG pIC$_{50}$ = 6.2
HepG2 pIC$_{50}$ = 4.5
ChromLogD = 6.9
LLE$_{AT}$ < 0.17 kcal mol^{-1} HA^{-1}
CAD = 91 μg/mL, AMP = 610 nm s^{-1}
PFI = 8.9, MPO = 0.53

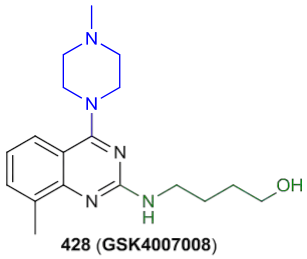

428 (GSK4007008)
23% yield
***Pf*$_{3D7}$ pIC$_{50}$ < 5.3**
hERG pIC$_{50}$ = 5.3
HepG2 pIC$_{50}$ = 4.6
ChromLogD = 2.4
LLE$_{AT}$ < 0.25 kcal mol^{-1} HA^{-1}
CAD = 135 μg/mL, AMP = 640 nm s^{-1}
PFI = 4.4, MPO = 0.69

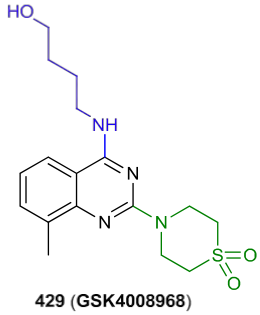

429 (GSK4008968)
41% yield
***Pf*$_{3D7}$ pIC$_{50}$ < 5.3**
hERG pIC$_{50}$ = 4.6
HepG2 pIC$_{50}$ < 4.0
ChromLogD = 2.4
LLE$_{AT}$ < 0.33 kcal mol^{-1} HA^{-1}
CAD = 164 μg/mL, AMP = 440 nm s^{-1}
PFI = 6.1, MPO = 0.84

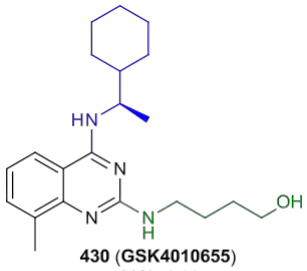

430 (GSK4010655)
20% yield
***Pf*$_{3D7}$ pIC$_{50}$ = 5.4**
hERG pIC$_{50}$ = 6.1
HepG2 pIC$_{50}$ = 4.5
ChromLogD = 4.8
LLE$_{AT}$ = 0.09 kcal mol^{-1} HA^{-1}
CAD = 18 μg/mL, AMP = 440 nm s^{-1}
PFI = 6.8, MPO = 0.40

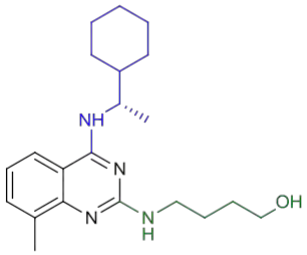

431 (GSK4010841)
16% yield
***Pf*$_{3D7}$ pIC$_{50}$ = 6.2**
hERG pIC$_{50}$ > 6.3
HepG2 pIC$_{50}$ = 4.9
ChromLogD = 4.7
LLE$_{AT}$ = 0.13 kcal mol^{-1} HA^{-1}
CAD = 116 μg/mL, AMP = 580 nm s^{-1}
PFI = 6.7, MPO = 0.40

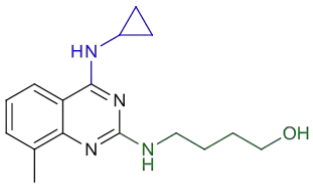

432 (GSK4011319)
35% yield
***Pf*$_{3D7}$ pIC$_{50}$ = 5.8**
hERG pIC$_{50}$ = 5.9
HepG2 pIC$_{50}$ = 4.5
ChromLogD = 2.4
LLE$_{AT}$ = 0.26 kcal mol^{-1} HA^{-1}
CAD = 263 μg/mL, AMP = 480 nm s^{-1}
PFI = 4.4, MPO = 0.68

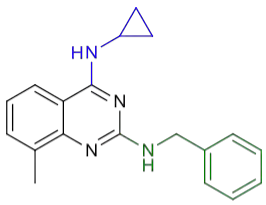

433 (GSK4018665)
13% yield
***Pf*$_{3D7}$ pIC$_{50}$ = 6.0**
hERG pIC$_{50}$ = 5.9
HepG2 pIC$_{50}$ = 4.9
ChromLogD = 5.5
LLE$_{AT}$ = 0.16 kcal mol^{-1} HA^{-1}
CAD = 54 μg/mL, AMP = N/a
PFI = 8.5, MPO = 0.30

Figure 5.6: Synthesised compounds tested in the *P.falc.* assay (set 2 of 3). Data was not attained for parameters where the N/a denotation is used.

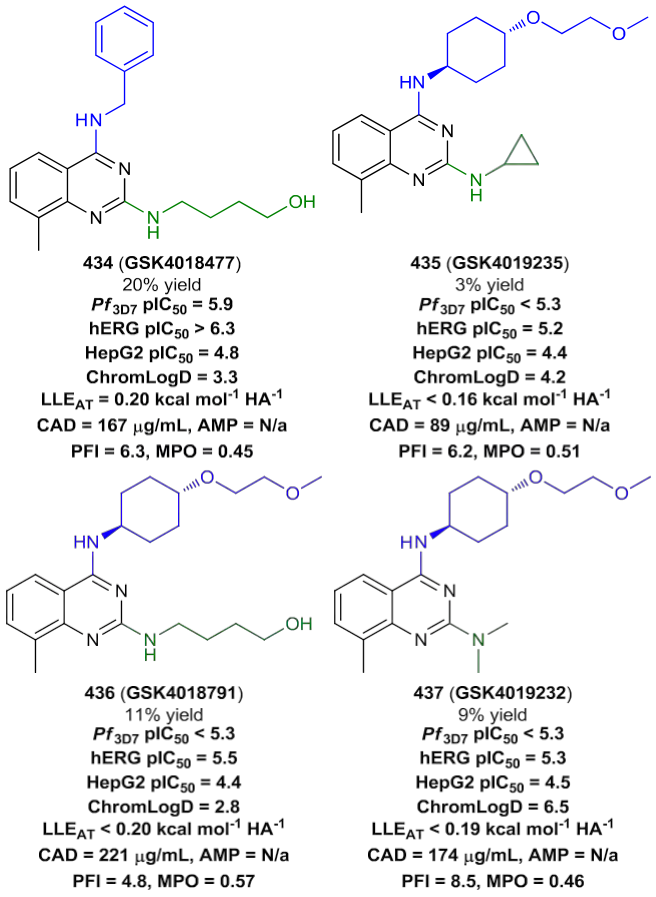

Figure 5.7: Synthesised compounds tested in the *P.falc.* assay (set 3 of 3). Data was not attained for parameters where the N/a denotation is used.

Due to the nature of the library synthesis, only 9 of the 19 compounds were active within the malaria assay. Nevertheless, interesting information was obtained from the acquired data. Though lacking a desirable physicochemical profile, due to its low solubility and high lipophilicity (ChromLogD), compound **397** still displayed sub-micromolar antimalarial potency (pIC_{50} = 6.1, **Figure 5.5**). The lipophilic nature of the compound resulted in it having an undesirable MPO score (0.12), LLE_{AT} (0.01 kcal mol^{-1} HA^{-1}) and CAD solubility (3 µg/mL), as well as exhibiting the potential for Hep G2-related toxicity.

Indeed, when the more polar, and linear nucleophilic monomer 4-aminobutan-1-ol (**416**) was utilised in the C2-position of the quinazoline scaffold, 5 of the 7 compounds containing the functionality remained active within the assay, suggesting that the use of linear structures, in the C2-position of the quinazoline, may be well tolerated with respect to compound potency. Curiously, one of the inactive compounds containing **416** in the C2-position of the quinazoline was **436** (**Figure 5.7**), which also contained the C4-functionality present in the lead molecule, GSK3190260 (**341**, **Figure 4.15**). Moreover, when the lead C4-functionality was retained and small non-linear groups were introduced into the scaffold (as seen in compounds **435** and **437**)

no activity was observed in the assay. As a result, when considering SAR data for diaminoquinazoline structures, substitution of **356** in the C4-position may offer further benefits in SAR data, especially when a linear nucleophile (which is more sterically demanding than a methyl functionality) is introduced at the C2-position of the quinazoline.

Further information about the size of the group that could be accommodated in this part of the molecule was provided by compound **433** (**Figure 5.6**), which demonstrated micromolar potency, whilst possessing an *N*-benzyl substituent at the C2-position.

Excellent physicochemical properties were observed in almost all cases when aminosulfone **399** was used as the C2-functionality of the molecule. In compounds **424**-**426** and **429**, very high MPO scores (0.84-0.89) accompanied the use of the monomer, and with the exception of the low solubility of **424** (possibly due to the presence of 4-position functionality **412**; *cf.* compound **425** which contains a slightly larger amide appendage in the C4-position, and much improved solubility (64 µg/mL compared to 9 µg/mL for **424**)), the MPO scores largely agreed with the attractive drug-like properties seen in the molecules. However, all compounds containing this functionality are also inactive as antimalarials, perhaps as a result of the size and branched nature of the C2-motif, as highlighted above.

As previously mentioned, early structural optimisation at GSK Tres Cantos determined that the use of α-cycloalkyl amine substituents in the C4-position of the quinazoline afforded mostly active antimalarial compounds, leading to the eventual finding of GSK3190260 from aniline-containing molecule GSK2656864 (**340**, **Figure 4.13**). Though not definitive, some of these findings were mirrored within this study.

For instance, the combination of 1-methylpiperazine (**400**) and 4-aminobutan-1-ol (**416**) monomers in the procedure led to the formation of inactive compound **428**. Conversely, when monomer **416** was tested as a functionality in the C2-position alongside other ring-containing monomers in the C4-position, as seen for molecules **421**, **430**-**432** and **434**, antimalarial activity was observed. In all of these cases, the C4-functionality is comprised of a secondary nitrogen attached to either a lipophilic aliphatic or benzylic appendage. The size of the ring may not drastically impact on potency, since both cyclopropyl and cyclohexyl rings, despite being of greatly differing sizes, exhibit antimalarial activity (consider data for molecules **421** and **430**-**432**).

The difference in potency between enantiomeric compounds **430** and **431** is also significant (± 0.7 pIC_{50}) and indicates that stereochemistry within the C4-functionality may be another important factor regarding the biological activity of the quinazolines. These results, together with the inactivity of compound **428** infer that 4-position functionality may have an important role in determining compound potency, and that the presence of tertiary amines in the C4-position may be undesirable, though further research would be necessary to elucidate this.

Since benzylamine derivative **434** also displays antimalarial activity, when this consideration is taken together with the results above, the use of functionality in the 4-position of the quinazoline, which is able to interact with hydrophobic moieties may be beneficial for potency.

Although a proof-of-concept was attained in the use of the flow methodology to generate diaminoquinazoline compounds in an effective manner, when compared to the lead compound GSK3190260, which had a pIC_{50} of 6.5, limited progress had been made in increasing cellular activity. It was thought that due to limited remaining scope for further research, the most optimal discovered compound would be derivatised, to more closely mimic the current lead compound, and further probe SAR data.

In order to decide which compound represented the best starting point for further derivatisation, active antimalarial compounds (**397**, **420**, **421**, **423** and **430**-**434**) were compared by considering their MPO score (for drug-likeness) and LLE_{AT} (for potency with respect to their molecular size, number of heavy atoms, and lipophilicity. These results are visualised in **Graph 5.1**.

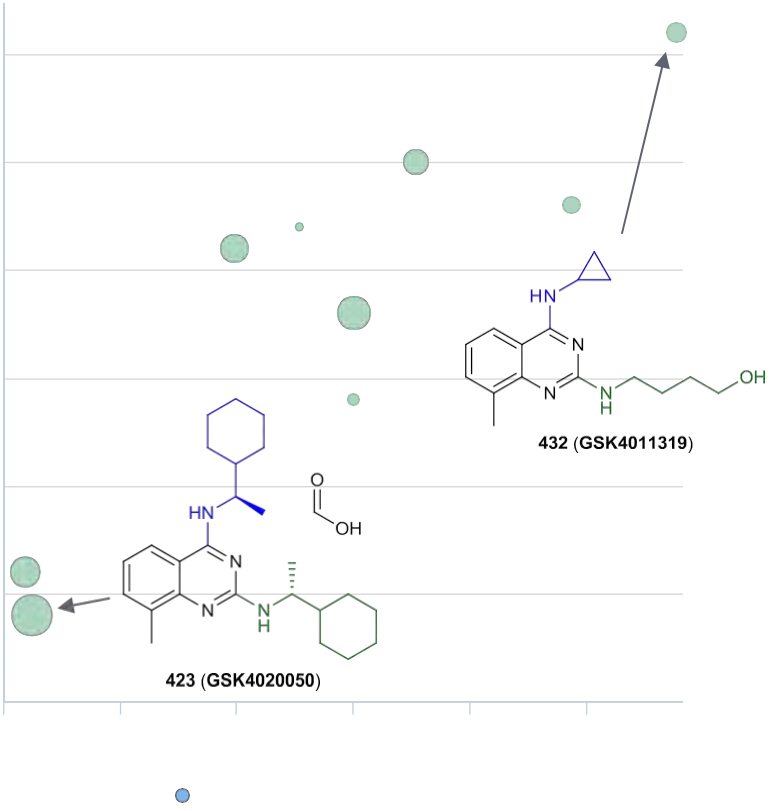

Graph 5.1: Comparison of active diaminoquinazoline antimalarials, considering their LLE_{AT} and MPO values. In each case, the size of the point is representative of the *Pf_{3D7}* assay potency.

As shown in the graph, compound **432** presented an interesting profile for further development. Though not the most potent synthesised compound, **432** retains near micromolar potency in the *P. Falc.* assay, and boasts superior ligand efficiency metrics compared to other synthesised compounds. The high MPO score of 0.68 is indicative of the compound displaying good drug-like physicochemical properties, and further evidence of this is provided in **Figure 5.6**, in the excellent solubility (263 µg/mL) and permeability (480 nm s^{-1}) data associated with **432**.

Therefore, the final work outlined in **Section 5.7. Final derivatives** describes the design of 2 derivative compounds of **432**, whose synthesis consider learnings from throughout this body of work in order to produce antimalarial compounds with more optimised drug-like profiles.

5.7 Final derivatives

The two compounds shown in **Figure 5.8** were targeted for synthesis as structurally-related analogues to compound **432**.

As shown in **Scheme 5.7**, C6-substitution can drastically affect the observed antimalarial potency of the quinazoline structures. It was thought that implementing the imidazole functionality present as the C6-moiety for lead compound **341** in targeted molecules **438** and **439** may provide advantages in both potency and physicochemical properties.

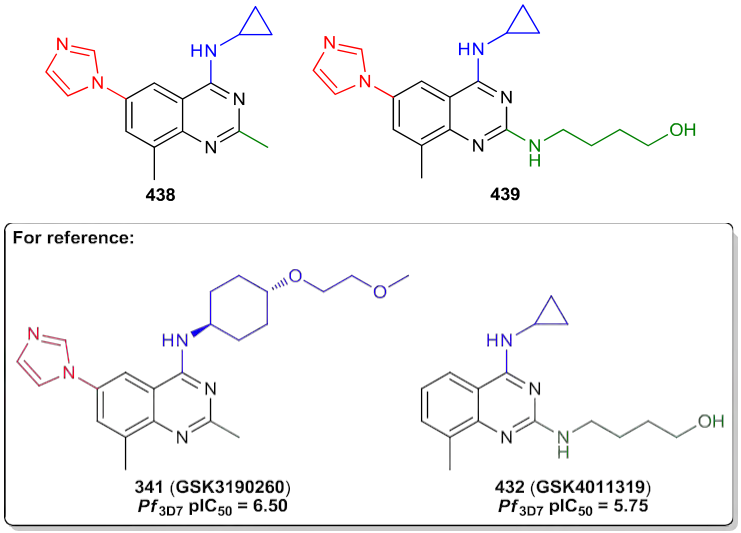

Figure 5.8: Targeted quinazoline compounds 438 and 439, which were derived from compound 432, and the previously discussed lead antimalarial, 341.

Finally, in order to further evaluate C2- and C4-substitution following the work described in the previous section, cyclopropylamine (**402**) would be used in both targets as a smaller active cyclic monomer to the lead motif in the 4-position (**356**). Its use in the formation of **438** would provide a direct comparison to lead compound GSK3190260, whilst the use of

4-aminobutan-1-ol (**416**) as an alternative C2-adduct of the quinazoline in **432** would help to expand SAR knowledge around the use of extended linear fragments in this position.

Compound **438** was synthesised in a two-step procedure from **368**, using starting material prepared elsewhere in our laboratory.[264] This route is shown in **Scheme 5.27** below.

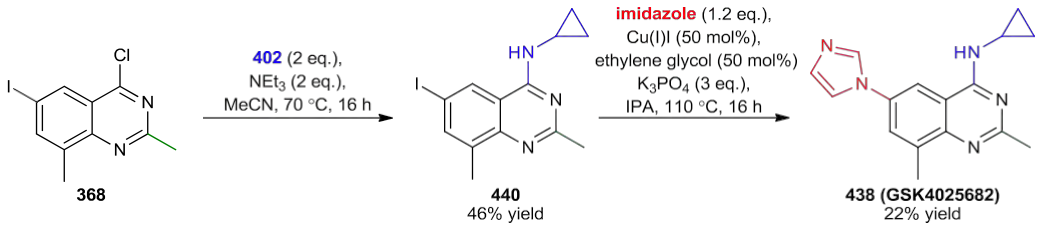

Scheme 5.27: Synthesis of compound 438 from quinazoline intermediate 368 in two steps.

Intermediate **440** was afforded following the S_NAr reaction between **402** and **368** under basic conditions. At this point, the introduction of the imidazole functional group was to be attempted *via* Ullmann conditions previously utilised in the synthesis of compound **379** (**Scheme 5.9**).[266] However, degradation of **440** was observed when the material was dissolved in DMSO-d_6 for NMR analysis. As a result, alternative reaction conditions were sought, and compound **438** was afforded in 22% yield following an Ullmann coupling procedure in isopropanol.[281]

For **439**, the tandem S_NAr procedure was used to afford intermediate **441** following the reaction. Unfortunately, due to the insolubility of **352** in Tamisolve® (NBP), a low yield of 9% was observed from the tandem S_NAr method, indicating the requirement for further optimisation of this process to accommodate this more lipophilic starting material. However, this material was successfully employed in the Ullmann coupling to form product **439** in sufficient quantity for biological screening. (**Scheme 5.28**).

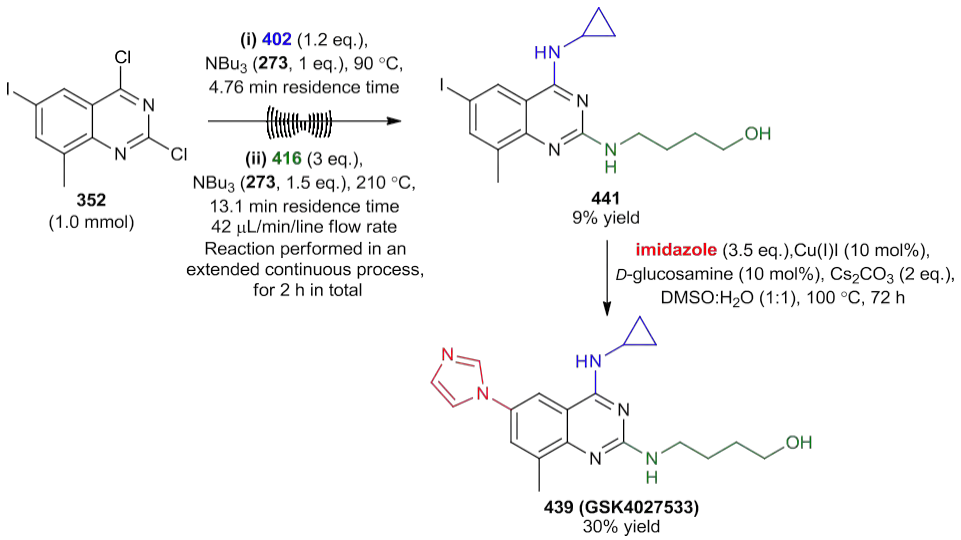

Scheme 5.28: Synthetic preparation of compound 439, including the use of the tandem flow S_NAr procedure.

The biological data for compounds **438** and **439** is shown in **Figure 5.9**.

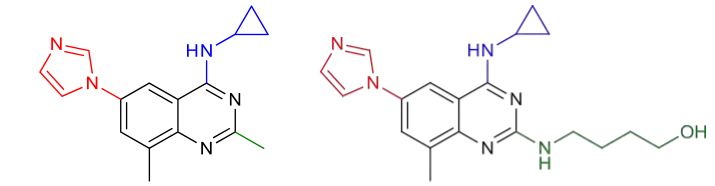

438 (GSK4025682)
Pf_{3D7} pIC_{50} = 5.8
hERG pIC_{50} = N/a
HepG2 pIC_{50} < 4.0
ChromLogD = 3.4
LLE_{AT} = 0.26 kcal mol^{-1} HA^{-1}
CAD = 98 μg/mL, AMP = 510 nm s^{-1}
PFI = 6.4, MPO = 0.58

439 (GSK4027533)
Pf_{3D7} pIC_{50} = 7.4
hERG pIC_{50} = N/a
HepG2 pIC_{50} = 4.8
ChromLogD = 2.5
LLE_{AT} = 0.32 kcal mol^{-1} HA^{-1}
CAD = 118 μg/mL, AMP = 180 nm s^{-1}
PFI = 5.5, MPO = 0.56

Figure 5.9: Biological data for compounds 438 and 439. Data for hERG toxicity was not available at the time of writing.

Both derivatives proved to have antimalarial activity within the cellular assay. For compound **438**, although no cytotoxicity was observed, a pIC_{50} of only 5.8 was observed, suggesting that use of the cyclopropylamine (**402**) functionality in the C4-position of the quinazoline resulted in inferior cellular activity in comparison to the lead compound GSK3190260 (**341**), which instead contains amine **356** in the C4-position.

On the other hand, synthesised derivative **439** proved to be extremely potent within the assay, having greater cellular activity than compound **341**. In comparison to its related predecessor molecule, **432**, a very significant potency gain of 1.6 in pIC_{50} was observed. This highlights the significance of the imidazole functionality in the C6-position of the quinazoline.

Unfortunately, a low level of activity was observed within the HepG2 assay for **439**, meaning that the molecule may induce some cytotoxicity. As a result, the compound is not suitable for further progression at this stage, but its LLE_{AT} value of 0.32 is in a promising area for further derivatisation, which could lead to future antimalarial molecules which retain or improve the potency of **439**, whilst offering a safer physicochemical profile.

5.8 Chapter 2 conclusions

In conclusion, a robust and flexible tandem flow methodology has been developed for the synthesis of quinazoline-containing antimalarial compounds, and the resultant exploration of SAR. Conditions were optimised for the addition of thiol and amine nucleophiles onto the core quinazoline scaffold in an S_NAr methodology. Thiol and alcohol nucleophiles could also be introduced *via* metal-mediated coupling practices, although further research would be required to make this method suitable for flow application.

Use of the bespoke flow apparatus led to the rapid synthesis of a range of quinazoline derivatives, and computational compound enumeration determined the calculated

physicochemical properties of the molecules, potentially allowing for early-stage monitoring of drug-like characteristics to help guide drug discovery programmes.

Compound **432**, containing cyclopropylamine (**402**) and aminobutanol (**416**) groups, was found to retain activity within the malarial assay and showed desirable drug-like characteristics, as determined by its MPO score, and measured physicochemical parameters. Derivatisation of **432** involved the synthesis of structurally related compounds **438** and **439**, to further explore structural space around the scaffold. Of these derivatives, compound **439** validated the tandem flow approach, by exhibiting excellent antimalarial potency, which was even superior to the herein discussed lead compound, **341**. This work has thus demonstrated the potential efficiency benefit of introducing computational enumeration and continuous reaction processing into a phenotypic study, in order to rapidly generate a library of potential drug candidates. This is especially notable, since the C4-functionality of compound **439** is structurally disparate to that used for the lead compound **341**, and thus would likely not be targeted for synthesis using a traditional strategy to optimise the lead compound in a series.

The flow process reported herein has been shown to work in the synthesis of a variety of different quinazoline structures, and can be modified further, facilitating a rapid transition from lead optimisation to scale-up for safety studies, following the selection of an ideal candidate.

5.9 Future work for Chapter 2

Various possible avenues have been highlighted for future work within this programme. Firstly, although further optimisation is needed, an efficient tandem flow S_NAr/Buchwald coupling procedure may be utilised to access ether and thio-ether derived quinazoline products. Early optimisation reactions described in **Section 5.5 Palladium-mediated *O*- and *S*-functionalisation at C2** showed that the formation of such compounds was possible in an accelerated procedure but was limited by instances of insoluble catalyst and palladium aggregation. Therefore, the use of a catalyst cartridge within a flow system may allow for the desired transformation without permitting leaching of the catalyst mixture. This approach could consequently allow for further SAR investigation in the use of different alcohol and thiol nucleophiles, which is an area that has yet to be explored thoroughly.

Having identified compound **439** as a potent antimalarial, further structural derivatisation may lead to advantages in the observed potency and safety profile of the resultant targets. Specifically, due to the marked benefit in introducing an imidazole functionality at the C6-position of the quinazoline (which can be proven through the comparison of the pIC_{50} data for compounds **432** and **439**), structural analogues which made small functional changes to the cyclopropylamine (**402**) and aminobutanol (**416**) groups would initially be targeted.

Moreover, having proven the utility of the flow system for the tandem S_NAr procedure in **Section 5.6 Tandem flow S_NAr procedure**, further work could revolve around testing a larger

range of amine nucleophiles. The enumeration discussed herein may have found compound **432** as a potential scaffold for further derivatisation, and subsequently, led to synthesis of the **439** (**Figure 5.9**), but implementation of the method over a much larger range of diaminoquinazoline products may facilitate the discovery of an alternative ideal drug-like candidate in an extremely effectual manner.

Following the identification of an optimised quinazoline antimalarial, use of either of the aforementioned tandem flow methodologies could significantly improve the efficiency of synthesis for the compound. Furthermore, the introduction of automated equipment such as an auto sampling machine would lend itself to self-maintenance of the process, thereby allowing industrial scale processes to use similar methods for maximum productivity downstream in the programme.

However, when considering the future scaled-up applications of the flow procedure, additional work may also be needed to adapt the flow procedure. Though use of this flow method may accelerate the transition from early stage research to scale-up practices, issues may still need to be overcome in the variable solubility and reactivity of starting materials in solution. Adaptation of the size of the flow reactor, as well as the solvent and residence times involved in the process, may all contribute to evolution of the flow method for process chemistry development and beyond.

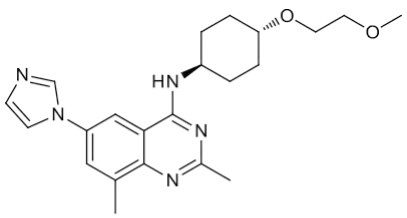

341 (GSK3190260)
***Pf*$_{3D7}$ pIC$_{50}$ = 6.5**
hERG pIC$_{50}$ = 5.1
HepG2 pIC$_{50}$ = 4.1
ChromLogD = 4.1
LLE$_{AT}$ = 0.26 kcal mol^{-1} HA^{-1}
CAD = 160 μg/mL, AMP = 436 nm s^{-1}
PFI = 7.1

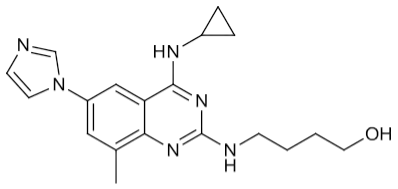

439 (GSK4027533)
***Pf*$_{3D7}$ pIC$_{50}$ = 7.4**
hERG pIC$_{50}$ = N/a
HepG2 pIC$_{50}$ = 4.8
ChromLogD = 2.5
LLE$_{AT}$ = 0.32 kcal mol^{-1} HA^{-1}
CAD = 118 μg/mL, AMP = 180 nm s^{-1}
PFI = 5.5, MPO = 0.56

Figure 5.9: Hit to lead compound 341, and its comparison to compound 439, discovered from this work.

Based on the lead compound (**341**, **Figure 5.9**), the development of a tandem S$_N$Ar/Suzuki reaction using trimethylboroxine (**443**) may allow for the formation of analogous products. This hypothesis is supported by the synthesis of compound **445**, which was generated elsewhere within our laboratory as a potential antimalarial target. Though product **445** was inactive, the synthesis of **444** from **442** and trimethylboroxine en route to the formation of **445** proceeded smoothly, potentially supporting future application of similar reaction conditions in flow (**Scheme 5.29**). Some consideration would have to be given to the order of synthetic steps when C6-substitution was also employed.

GSK CONFIDENTIAL INFORMATION – DO NOT COPY

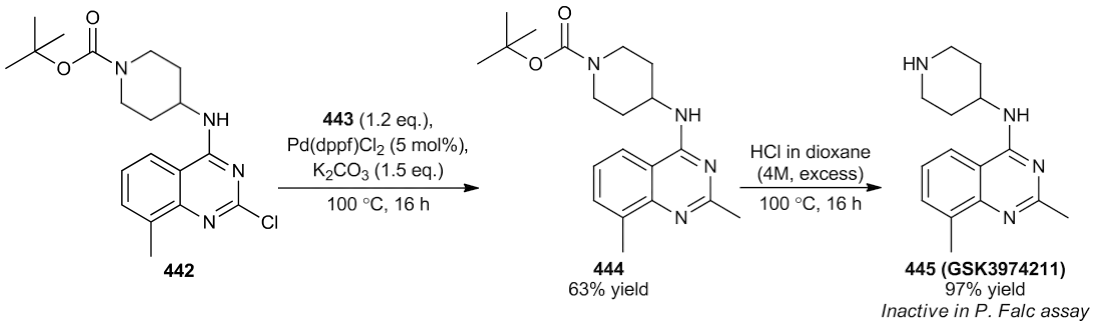

Scheme 5.29: The introduction of methyl functionality at the C2-position of the quinazoline is possible using trimethylboroxine (443) in a Suzuki-mediated strategy, as explored en-route to the synthesis of GSK3974211.

Thus, the application of flow chemistry equipment in the ongoing development of antimalarial quinazolines is believed to hold great promise. Ideally, the work described herein, will contribute to current efforts to identify an effective, single-dose antimalarial treatment for millions with the disease.

6. Experimental

6.1 General experimental information and equipment used

6.1.1 Solvents and reagents

Unless otherwise stated:

- Anhydrous solvents were not required, and glassware was not dried prior to use.
- All solvents and reagents were obtained from commercial suppliers, or from within GlaxoSmithKline's internal chemical storage system, and were used without further purification.
- Reactions were monitored by a combination of High Performance Liquid Chromatography (HPLC), Liquid Chromatography-Mass Spectrometry (LCMS), Gas Chromatography (GC) and Nuclear Magnetic Resonance (NMR) analysis techniques.

Where intermediates have been synthesised in-house, all written procedures have been provided.

6.1.2 Chromatography

Thin layer chromatography (TLC) was carried out with plastic-backed 50 precoated silica plates as the stationary phase (particle size 0.2 mm). Spots were visualized by ultraviolet (UV) light (λ max = 254 nm or 365 nm) in all cases. Normal phase silica gel chromatography was carried out using the Teledyne® ISCO CombiFlash Rf+™ apparatus with RediSep® silica cartridges. Reverse phase chromatography was carried out using Teledyne® ISCO CombiFlash Rf+ ™ apparatus with Biotage® SNAP KPC18-HS ™ cartridges. In each case, the size of the cartridge, and gradient of the eluent mixture used for purification is mentioned within the procedure.

For reverse phase conditions, Biotage® KP-C18-HS SNAP ™ cartridges were used, with an initial solvent ratio of 95:5 H_2O:MeCN. High pH conditions used a 10 mM aq. ammonium bicarbonate solution as the aqueous phase, whilst low pH conditions used a solution of water doped with 0.1% v/v formic acid or trifluoroacetic acid. In each case, the size of the column, solvent gradient and modifier used is specified.

6.1.3 Mass-directed auto purification (MDAP)

MDAP was carried out using a Waters® ZQ MS™, using an Xselect C18™ column (150 mm x 30 mm, 5 µm packing diameter) and a 40 mL/min flow rate with alternate-scan positive and negative electrospray ionisation and a summed UV wavelength of 210–350 nm. Two liquid phase methods were used:

Formic: Gradient elution occurred at ambient temperature with the eluents as (A) H_2O containing 0.1% volume/volume (v/v) formic acid and (B) acetonitrile containing 0.1% (v/v) formic acid.

High pH: Gradient elution occurred at ambient temperature with the eluents as (A) 10 mM aqueous ammonium bicarbonate solution, adjusted to pH 10 with aqueous ammonia and (B) acetonitrile.

The elution gradients used were at a flow rate of 40 mL/min over 20 or 30 min depending on separation:

Method A	5-30% B
Method B	15-55% B
Method C	30-85% B
Method D	50-99% B
Method E	80-99% B

6.1.4 Array MDAP

The purification was performed on an Agilent® 1260 Infinity II UPLC™ instrument using an ATLANTIS® dC18™ column (19 x 100 mm, 5.0 µm packing diameter) and either an Agilent® Infinity lab LC/MSD ™ or Agilent® 6120 single quadrupole LC/MS™ machine using alternative-scan positive and negative electrospray. Analytes were detected at a selected UV wavelength, generally 210, 230 or 254 nm. Two liquid phase methods were used:

Formic: Gradient elution occurred at ambient temperature with the eluents as (A) H_2O containing 0.1% volume/volume (v/v) formic acid and (B) acetonitrile containing 0.1% (v/v) formic acid.

High pH: Gradient elution occurred at ambient temperature with the eluents as (A) 10 mM aqueous ammonium bicarbonate solution, adjusted to pH 10 with aqueous ammonia and (B) acetonitrile.

The elution gradients used were at a flow rate of 20 mL/min over 20 or 30 min, and either standard or focused purification methods were used depending on the separation required (see below).

Standard Methods	Composition	Focused Methods	Composition
Method A	20-32.5% B	Focused Method A	15-37.5% B
Method B	32.5-45% B	Focused Method B	30-55% B
Method C	45-58% B	Focused Method C	40-65% B
Method D	58-70% B	Focused Method D	50-75% B
Method E	70-100% B	Focused Method E	60-85% B
Method F	N/a	Focused Method F	75-100% B

6.1.5 Liquid chromatography mass spectrometry (LCMS)

LCMS analysis was performed on an Acquity® UPLC instrument equipped with a CSH C18™ column (50 mm × 2.1 mm, 1.7 µm packing diameter) and micromass ZQ MS™ machine using

alternate-scan positive and negative electrospray. Analytes were detected as a summed UV wavelength of 210–350 nm using Acquity 2998 photodiode array (PDA) and Acquity QDA mass detectors. Two liquid phase methods were used:

- **Method A – High Ph (ammonium bicarbonate)**: 40 °C, 1 mL/min flow rate. Gradient elution between (A) 10 mM aqueous ammonium bicarbonate solution, adjusted to pH 10 with 0.88 M aqueous ammonia, and (B) acetonitrile. Gradient conditions began at 1% B, and increased linearly to 97% B over 1.5 min, before remaining at 97% B for 0.4 min, and then increasing to 100% B over 0.1 min.
- **Method B – Low pH (formic acid)**: 40 °C, 1 mL/min flow rate. Gradient elution between (A) a 0.1% volume/volume (v/v) formic acid aqueous solution and (B) acetonitrile containing 0.1% volume/volume (v/v) formic acid. Gradient conditions began at 1% B, and increased linearly to 97% B over 1.5 min, before remaining at 97% B for 0.4 min, and then increasing to 100% B over 0.1 min.

6.1.6 Nuclear magnetic resonance (NMR) spectroscopy

^{1}H, ^{13}C and ^{19}F NMR spectra were recorded in commercially supplied deuterated solvents at ambient temperature using standard pulse methods with the following spectrometers, and associated signal frequencies: Bruker® AV-400™ (^{1}H = 400 MHz, ^{13}C = 101 MHz, ^{19}F = 376 MHz) and Bruker® AV-600 ™ (^{1}H = 600 MHz, ^{13}C = 151 MHz). Chemical shifts (δ) are reported to the nearest 0.01 ppm for ^{1}H NMR and ^{19}F NMR signals, and 0.1 ppm for ^{13}C NMR signals, and are relative to tetramethylsilane (TMS) reference, where δ (TMS) = 0.00 ppm. For ^{13}C NMR analyses where no distinct TMS peak was observed, solvent references of 49.00 (CD_3OD), 39.52 (DMSO-d_6) and 77.16 ($CDCl_3$) were used, according to the published literature.[282] All NMR analysis were performed in commercially supplied deuterated solvents chloroform-*d*, methanol-d_4 and dimethyl sulfoxide-d_6. Peak assignments were made based on data provided from ^{1}H, ^{13}C, COSY, DEPT, HSQY, HMBC and NOESY analysis, where necessary. Coupling constants (*J*) are reported to the nearest 0.1 Hz for ^{1}H NMR and ^{19}F NMR analyses, and the multiplicities of signals are described as singlet (s), doublet (d), triplet (t), quartet (q), quintet (quin), sextet (sxt), broad (br.) and multiplet (m), or a combination of these descriptors for extended coupling patterns. In a case where more than one signal is observed as a single multiplicity (including when overlapping splitting patterns are observed), an apparent (app.) descriptor is used. The number of hydrogen, carbon or fluorine atoms (n) responsible for a signal is indicated by nH, nC or nF respectively.

6.1.7 Infra-red (IR) spectroscopy

Infra-red (IR) spectroscopy was performed using a Perkin Elmer ® Spectrum 1™ machine. All absorption maxima (v_{max}) are reported in wavenumbers (cm^{-1}).

6.1.8 High resolution mass spectrometry (HRMS)

The HRMS method combined an Ultra high-performance liquid chromatography (UPLC) method using an Acquity® UPLC BEH C18™ column with column dimensions of 100 mm x 2.1 mm (1.7 µm packing diameter), with a Waters® XEVO G2-XS™ QTof mass spectrometer, using a positive electrospray ionisation, and a scan range of 100–1200 Atomic Mass Units (AMU). The UPLC separation was performed using one of two liquid phase methods:

- **Method A – High pH:** 50 °C, 0.8 mL/min flow rate. Gradient elution between (A) 10 mM aqueous ammonium bicarbonate solution, adjusted to pH 10 with 0.88 M aqueous ammonia, and (B) acetonitrile. Gradient conditions began at 1% B and were maintained at this composition for 0.5 min. The gradient eluent then increased linearly to 90% B over 16.5 min, before remaining at 90% B for 1.5 min, and then the gradient returned to 99% A over 0.5 min and was held at this gradient for a further minute. The entire process required 20 minutes.
- **Method B – Low pH:** 50 °C, 0.8 mL/min flow rate. Gradient elution between (A) a 0.1% volume/volume (v/v) solution of formic acid in H_2O, and (B) a 0.1% volume/volume (v/v) solution of formic acid in acetonitrile. Gradient conditions began at 3% B, before the gradient increased linearly to 100% B over 8.5 min. The gradient remained at 100% B for 0.5 min, and then returned to 3% B over 0.5 min and was held at this gradient for a further 0.5 min. The entire process required 10 min.

In all cases, the UV detection used a summed signal from a wavelength range of 210–350 nm and an injection volume of 0.2 µL was used.

6.1.9 High performance liquid chromatography (HPLC)

HPLC analysis was carried out on an Agilent® Zorbax SB-C18™ machine, with column dimensions 50 x 3.0 mm (1 µm packing diameter). Analytes were measured at a UV wavelength of 220 nm. HPLC analysis was performed at 60 °C, at a 1.5 mL/min flow rate using a gradient elution between (A) 0.05% volume/volume (v/v) trifluoroacetic acid (TFA) in H_2O, and (B) 0.05% volume/volume (v/v) trifluoroacetic acid (TFA) in acetonitrile. Gradient conditions began at 100% A and eluted to 95% B and 5% A over a time frame of 2.5 min. The elution composition is then maintained for 0.2 min, before increasing to 100% B over 0.01 min. The elution gradient is maintained at 100% B for a further 1.29 min. The whole gradient process required 4.0 min. The injected volume of analyte solution was 1.0 µL.

6.1.10 Gas chromatography (GC)

Gas chromatography was performed using an Agilent® 7890B GC™ system equipped with an Agilent® 7693 autosampler™. A fast GC method (10 min run time) using an Agilent® DB-5 HT™ column (15.0 m x 250 µm, 0.10 µm film) with an injection volume of 1.0 µL and injection temperature of 275 °C was used. A constant pressure of 30 psi was applied during the GC separation. A flame ionisation detector (FID) was used at 320 °C to afford the resultant spectra.

6.1.11 Melting points

Melting points were recorded using a Büchi® Melting Point M-565™ machine. A melting point range of 40°C–300 °C was measured, with a 5 °C/min ramp rate.

6.1.12 Specific rotation

The rotation of 589 nm polarised light by enantiomers was measured using an Optical Activity Ltd® AA-10R™ polarimeter.

6.1.13 Microwave (MW) reactions

Reactions using microwave conditions were performed in a Biotage® initiator+™ microwave.

6.1.14 Karl Fischer (KF) analysis

Karl Fischer analysis was performed on commercial solvents and crude reaction solutions using the Mettler Toledo® V10S Compact Volumetric KF Titrator™ apparatus. For the titration, commercial hydranal composite 5K solution was used (containing iodine, imidazole and 2-methylimidazole components).

6.1.15 Cyclic voltammetry (CV)

The CV experiment was performed using an IKA® Electrosyn 2.0™ machine. The reference electrode was submerged in 3 M KCl solution, and a standard electrolyte solution of 0.1 M tetraethylammonium tetrafluoroborate in acetonitrile was used. A reference solution of 0.01 M ferrocene in the electrolyte solution was used as a control experiment. The experiment was performed at 0.01 M concentration. Voltage limits of 0.0 and 2.0 V were used, with a voltage sweep of 100 mV/s.

6.1.16 Flow reactions (GBBR work)

Flow reactions involving the GBBR work were performed in a bespoke flow reactor made through the combination of a Syrris® Asia™ syringe pump module, which utilised Syrris® Asia™ green syringes (250 µL/500 µL volume syringes, which can facilitate a flow rate between 5 µL to 1.25 mL/minute/channel) with a Vapourtec® RS-200™ machine using a 10 mL sample loop (2 x 10 mL sample loops were used in the scale-up example). PFA tubing of outer diameter 1/8” (inner diameter 1/16”) was used for the input tubing for the Syrris® module, whilst PFA tubing of 1/16” outer diameter and 1/32” inner diameter was used for the output tubing of the Syrris® module, and throughout the rest of the reactor. The tubing passed through two back

pressure regulators of 75 and 40 psi (*c.* 8.0 bar total back pressure was applied in the system). A picture of the flow setup is provided below (**Figure 6.1**), and this setup is also represented in the electronic line diagram (ELD) shown below (**Figure 6.2**).

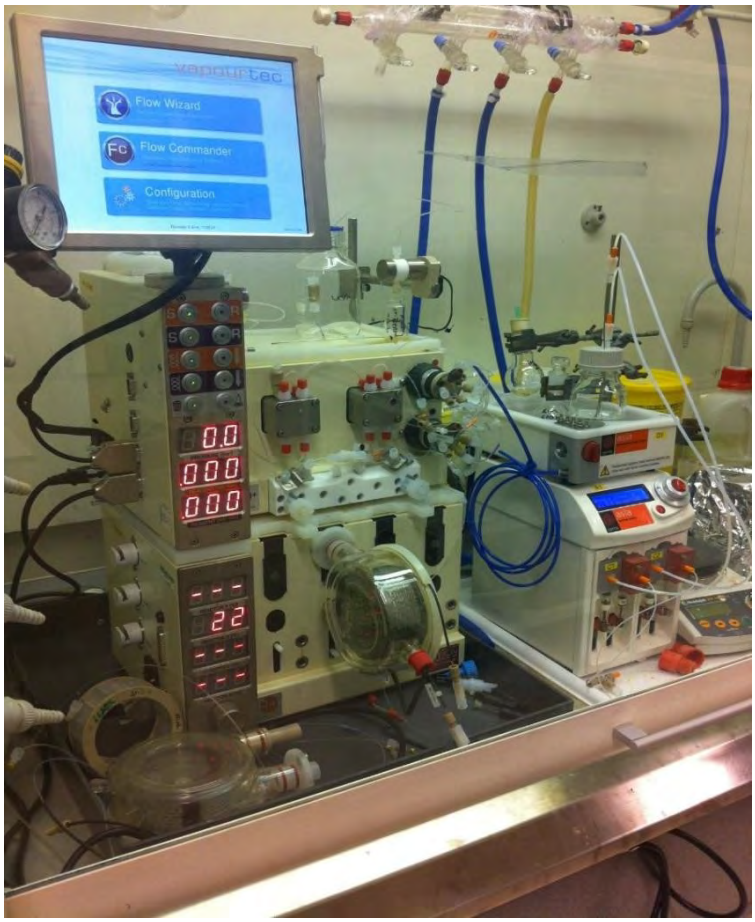

Figure 6.1: Picture of the bespoke flow reactor used in the GBBR work.

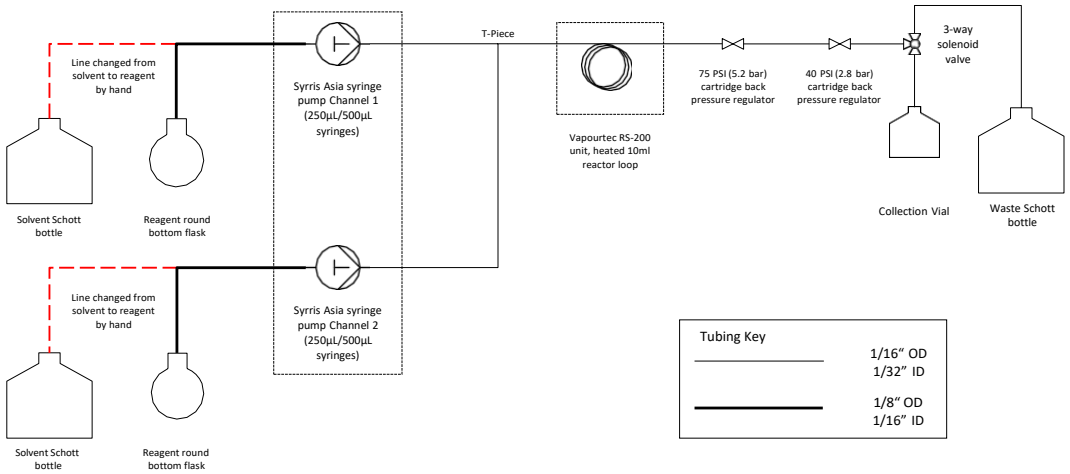

Figure 6.2: Electronic line diagram (ELD) of the flow equipment setup used in the GBBR work.

6.1.17 Flow reactor volumes (GBBR work)

Calculations of the approximate reactor volume of the flow setup were made by filling the flow reactor with toluene, before pumping a fluorescent Rose Bengal aqueous solution (0.1 M) into the reactor and observing the residence times in different parts of the reactor at a flow rate of 0.100 mL/min/channel. Schematics detailing these reactor volumes are shown below for both the usual setup of the reactor (using 1 x 10 mL reaction loop, **Figure 6.3**) as well as for the scale-up example (using 2 x 10 mL reaction loops, **Figure 6.4**).

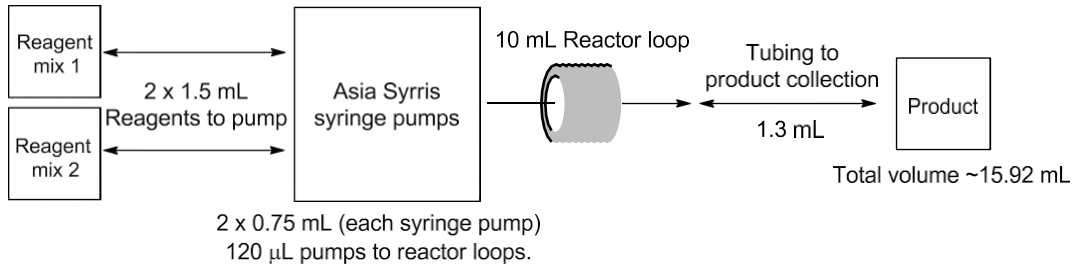

Figure 6.3: Schematic of the bespoke flow reactor setup used in the GBBR work (scope examples, Section 3).

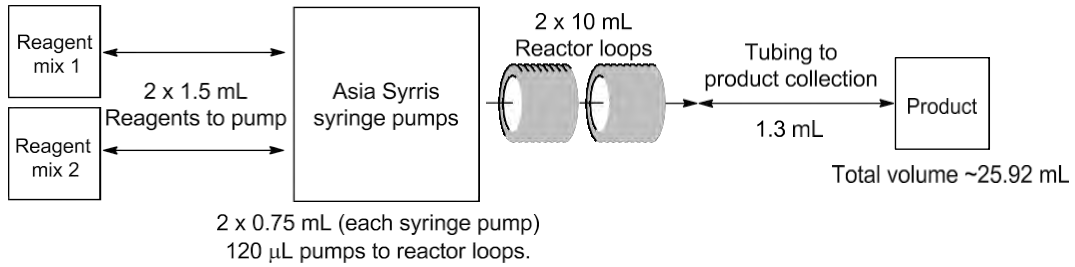

Figure 6.4: Schematic of the bespoke flow reactor setup used in the GBBR work (scale-up example, Scheme 3.11).

6.1.18 Flow reactions (tandem reactions)

Flow reactions involving the tandem isocyanide formation/GBBR were attempted in a bespoke flow reactor made through the combination of a double-channelled Vapourtec® RS-200™ machine, used for pumping starting materials for the formamide dehydration reaction (the dehydrating agents were always pumped in a separate channel to the other starting materials). The Vapourtec® machine used a 10 mL sample loop to accommodate the dehydration reaction, from which the crude product mixture was combined (in a T-mixer) with an aqueous solution (consisting of either deionised water, a 0.1 M aq. brine solution or a 0.1 M aq. hydrochloric acid solution) supplied from a from a Vapourtec® RS-100™ machine. The biphasic mixture was then pumped through a Zaiput® Sep-10™ liquid-liquid phase separator, which had either a hydrophilic or hydrophobic PTFE membrane of 0.5 nm or 1.0 nm pore size equipped. The organic-phase containing output channel of this separation was collected in an intermediate vial, before being fed *via* a Syrris® Asia™ syringe pump module, which utilised Syrris® Asia™ yellow syringes (50 µL/100 µL volume syringes, which can facilitate a flow rate between 1 µL to 250 µL/min/channel) into another double-channelled Vapourtec® RS-200™

machine using a 10 mL sample loop. The other channel of this Vapourtec® reactor would thus contain the remaining GBBR reactants. PFA tubing of outer diameter 1/8" (inner diameter 1/16") was used for the immediate input and output of the Zaiput® separator, whilst PFA tubing of 1/16" outer diameter and 1/32" inner diameter was used throughout the rest of the reactor. The tubing passed through two back pressure regulators of 75 and 40 psi (*c.* 8.0 bar total back pressure was applied in the system). In later attempts to perform the tandem reaction, a Harvard Apparatus® standard infuse/withdraw PHD ULTRA™ syringe pump was used instead of the first Vapourtec® reactor, to provide more accurate low flow rates of the starting materials. Pictures of the initial flow setup are provided below (**Figure 6.5**).

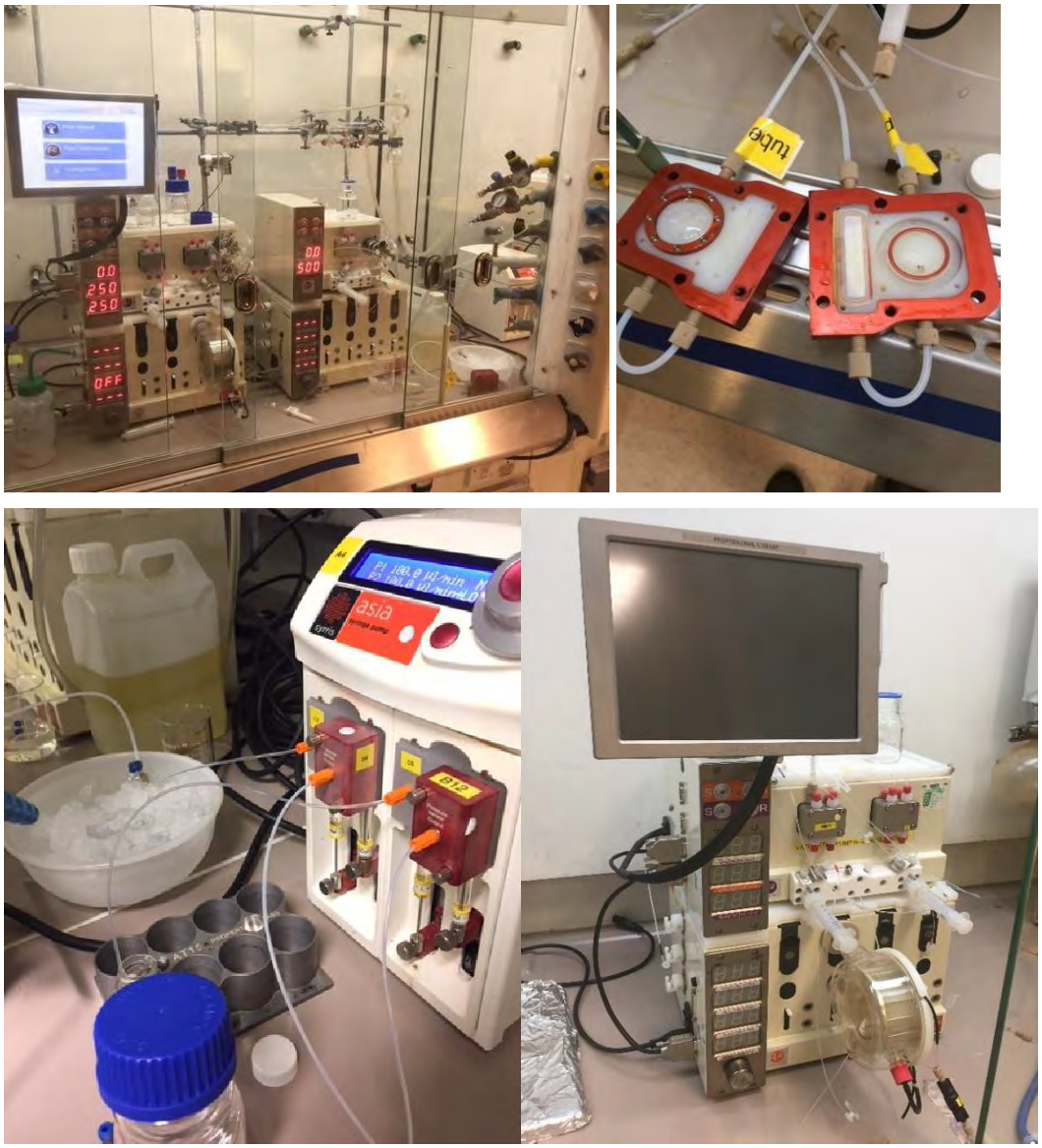

Figure 6.5: Pictures of the flow reactor setup used in attempts to perform the tandem isocyanide formation/GBBR work.

6.1.19 Flow reactions (malaria work)

Flow reactions used for the malaria work were performed using a bespoke flow reactor combining a Syrris® Asia™ syringe pump module, which utilised Syrris® Asia™ yellow syringes (50 µL/100 µL volume syringes, which can facilitate a flow rate between 1 µL to 250 µL/min/channel) with two Little Things Factory® (LTF) chips. The first chip (heated at 90 °C in the procedure) is the LTF-MS™ model, with an internal volume of 0.2 mL, while the second chip (heated at 210 °C in the procedure) is the LTF-VS™ model, with an internal volume of 1.1 mL. PFA tubing of outer diameter 1/16” and 1/32” inner diameter was used for the whole reactor. The tubing passed through two 75 psi back pressure regulators (*c.* 10.4 bar total back pressure was applied in the system). A picture of the flow setup is provided below (**Figure 6.6**), and this setup is also represented in the electronic line diagram (ELD) shown below (**Figure 6.7**).

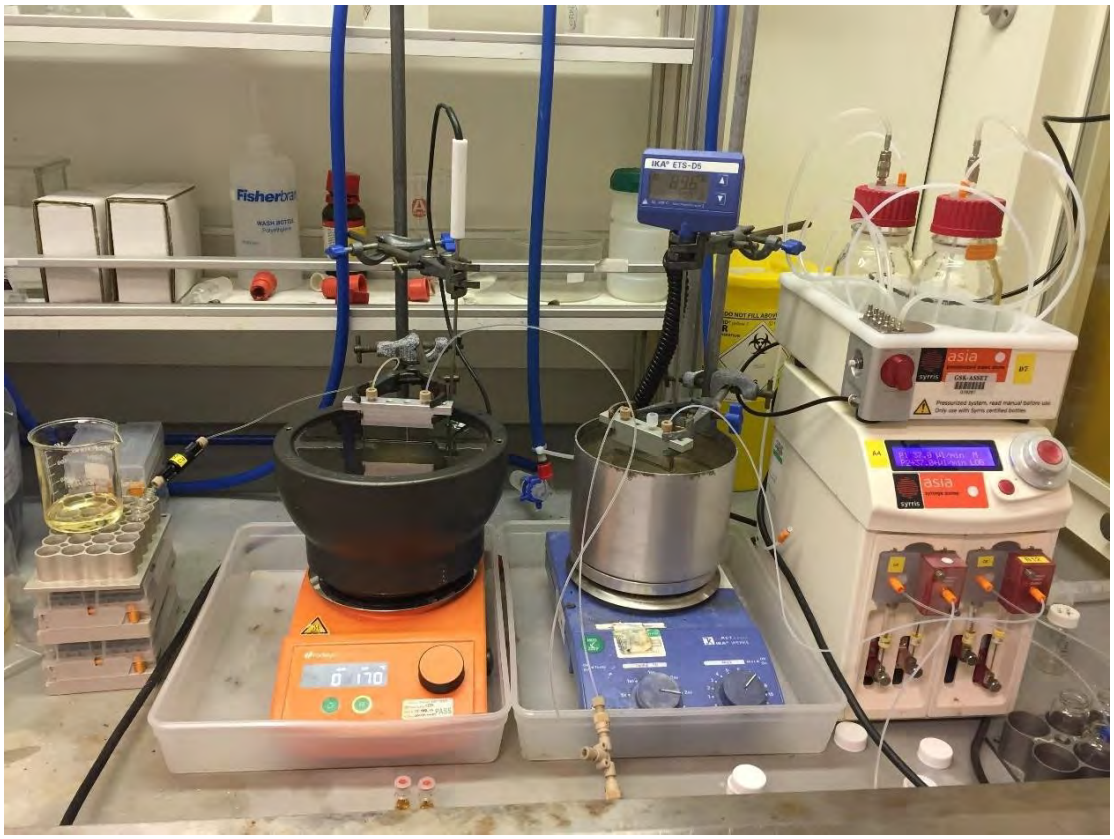

Figure 6.6: Picture of the bespoke flow reactor setup used in the malaria work.

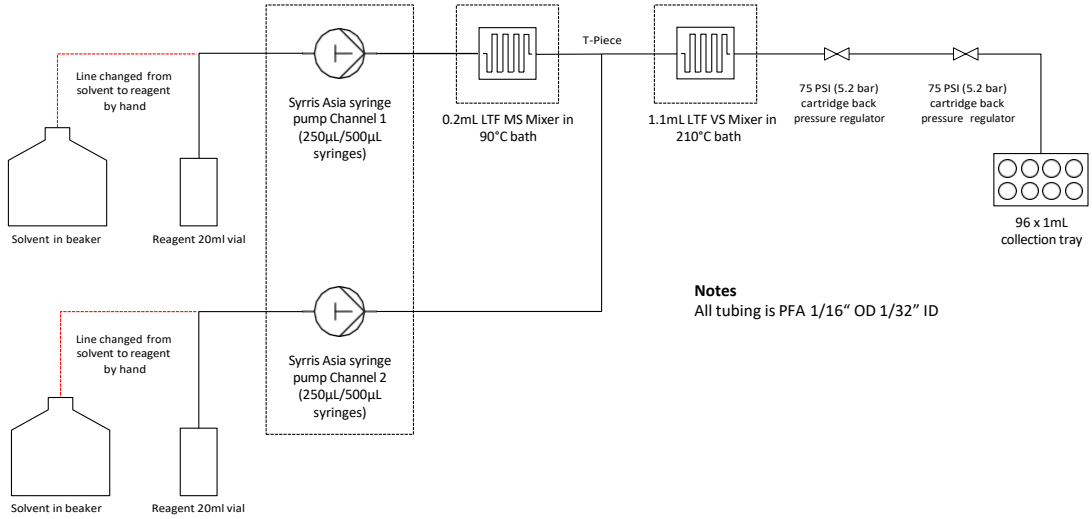

Figure 6.7: Electronic line diagram (ELD) representation of the flow reactor setup used in the malaria work.

6.1.20 Flow reactor volumes (malaria work)

Calculations of the approximate reactor volume of the flow setup were made by filling the flow reactor with toluene, before pumping a 0.1 M fluorescent Rose Bengal aq. solution into the reactor and observing the residence times in different parts of the reactor at a flow rate of 0.100 mL/min/channel. A picture showing the use of the Rose Bengal dye within the LTF-VS™ microreactor chip is shown in **Figure 6.8**, and schematics detailing the reactor volumes are shown in **Figure 6.9**.

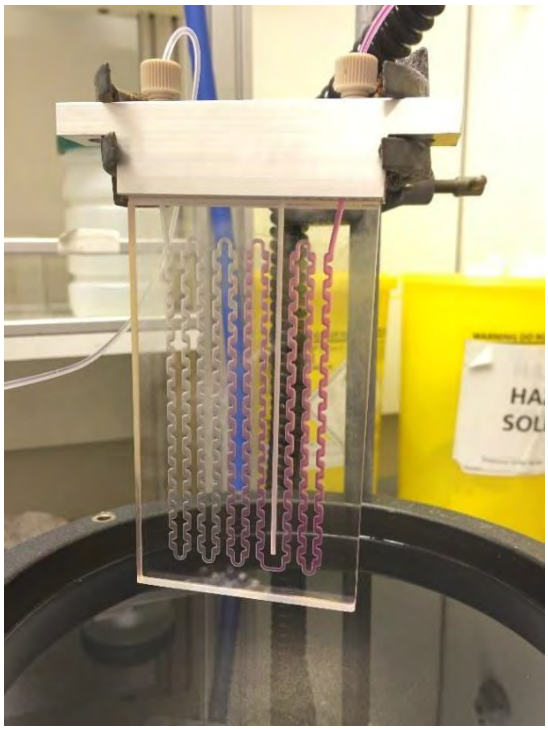

Figure 6.8: Picture showing the Rose Bengal solution within the LTF-VS™ chip.

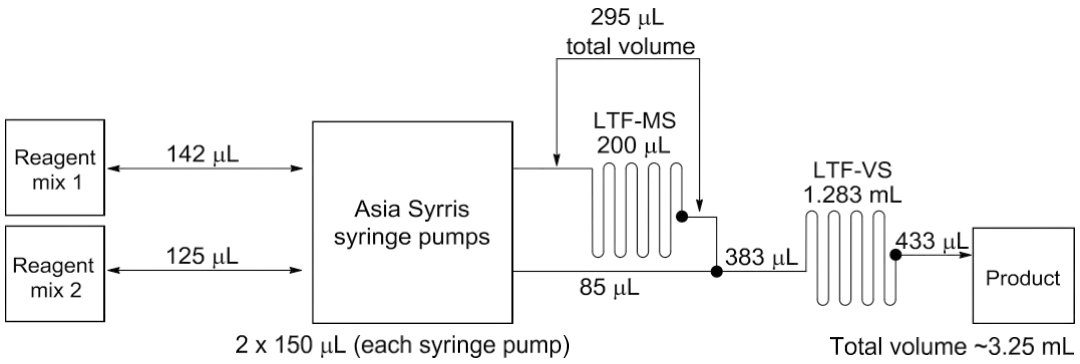

Figure 6.9: Schematic of the bespoke flow reactor setup used in the malaria work.

6.1.21 Integrity 10 reactions

For S_NAr optimisation reactions discussed in **Section 5.4: Batch optimisation of the tandem S_NAr procedure**, an Electrothermal® STEM Integrity 10™ machine was used. The machine contains 10 individual controllable cells, which can be stirred and heated independently between temperatures of -30 °C and 150 °C and stirring rates of 350-1200 rpm.

6.2. Experimental – Chapter 1: Extension of the GBBR: a green, robust, scalable and efficient continuous flow process to synthesise 3-aminoimidazoheterocycles.

6.2.1 General synthetic procedures for Chapter 1

6.2.1.1 General procedure A: optimisation of the synthesis of *N*-(*tert*-butyl)-2-phenylimidazo[1,2-*a*]pyridin-3-amine, thermal conditions (Table 3.1, Entries 1-16, Table 3.2, Entries 1-4):

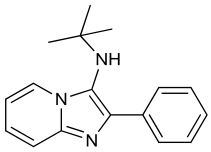

205

In a 5 mL Radleys® Carousel 12 Plus™ reaction tube was prepared a solution of 2-aminopyridine **202** (100 mg, 1.06 mmol) and benzaldehyde **203** (0.108 mL, 1.06 mmol) in 3 mL of the chosen solvent. 10 mol% (0.106 mmol) of the relevant catalyst was added to each reaction, before *N*-*tert*-butylisocyanide **204** (0.120 mL, 1.06 mmol) was added to each reaction tube, and the reaction mixtures were heated to 50 °C for either 21 h or 24 h. The reactions were sampled (a 20 μL aliquot was taken and diluted to 1 mL with methanol) and analysed by LCMS (**Entries 1-16, Table 3.1**) or according to the HPLC method described (see **Appendix 1, procedure for attaining conversion estimates from HPLC concentration gradients**) at time points of 1 h, 2 h and 20 h (**Entries 1-4, Table 3.2**). For these entries, after 24 h, the final aliquot was removed and analysed using the same HPLC method to determine the final conversion. The products were not isolated.

GSK CONFIDENTIAL INFORMATION – DO NOT COPY

Table 3.1, Entry 1: Methanol solvent, HCl catalyst (4 M in dioxane, 27 µL, 0.106 mmol), 97% LCMS conversion observed after 21 h reaction time, homogenous reaction mixture.

Table 3.1, Entry 2: Methanol solvent, $Sc(OTf)_3$ catalyst (52.3 mg, 0.106 mmol), 97% LCMS conversion observed after 21 h reaction time, partially soluble reaction mixture.

Table 3.1, Entry 3: Methanol solvent, $ZrCl_4$ catalyst (24.8 mg, 0.106 mmol), 97% LCMS conversion observed after 21 h reaction time, partially soluble reaction mixture.

Table 3.1, Entry 4: Methanol solvent, $HClO_4$ catalyst (70% wt. solution in H_2O, 9 µL, 0.106 mmol), 98% LCMS conversion observed after 21 h reaction time, homogenous reaction mixture.

Table 3.1, Entry 5: Acetonitrile solvent, HCl catalyst (4 M in dioxane, 27 µL, 0.106 mmol), 94% LCMS conversion observed after 21 h reaction time, initially a homogenous reaction mixture before precipitation of the product was observed after cooling to ambient temperature.

Table 3.1, Entry 6: Acetonitrile solvent, $Sc(OTf)_3$ catalyst (52.3 mg, 0.106 mmol), 98% LCMS conversion observed after 21 h reaction time, partially soluble reaction mixture.

Table 3.1, Entry 7: Acetonitrile solvent, $ZrCl_4$ catalyst (24.8 mg, 0.106 mmol), 91% LCMS conversion observed after 21 h reaction time, partially soluble reaction mixture.

Table 3.1, Entry 8: Acetonitrile solvent, $HClO_4$ catalyst (70% wt. solution in H_2O, 9 µL, 0.106 mmol), 96% LCMS conversion observed after 21 h reaction time, homogenous reaction mixture.

Table 3.1, Entry 9: Toluene solvent, HCl catalyst (4 M in dioxane, 27 µL, 0.106 mmol), 92% LCMS conversion observed after 21 h reaction time, insoluble reaction mixture.

Table 3.1, Entry 10: Toluene solvent, $Sc(OTf)_3$ catalyst (52.3 mg, 0.106 mmol), quantitative LCMS conversion observed after 21 h reaction time, partially soluble reaction mixture.

Table 3.1, Entry 11: Toluene solvent, $ZrCl_4$ catalyst (24.8 mg, 0.106 mmol), 95% LCMS conversion observed after 21 h reaction time, partially soluble reaction mixture.

Table 3.1, Entry 12: Toluene solvent, $HClO_4$ catalyst (70% wt. solution in H_2O, 9 µL, 0.106 mmol), 96% LCMS conversion observed after 21 h reaction time, partially soluble reaction mixture.

Table 3.1, Entry 13: 2-MeTHF solvent, HCl catalyst (4 M in dioxane, 27 µL, 0.106 mmol), 92% LCMS conversion observed after 21 h reaction time, insoluble reaction mixture.

Table 3.1, Entry 14: 2-MeTHF solvent, $Sc(OTf)_3$ catalyst (52.3 mg, 0.106 mmol), 97% LCMS conversion observed after 21 h reaction time, partially soluble reaction mixture.

Table 3.1, Entry 15: 2-MeTHF solvent, $ZrCl_4$ catalyst (24.8 mg, 0.106 mmol), 93% LCMS conversion observed after 21 h reaction time, partially soluble reaction mixture.

Table 3.1, Entry 16: 2-MeTHF solvent, $HClO_4$ catalyst (70% wt. solution in H_2O, 9 µL, 0.106 mmol), 96% LCMS conversion observed after 21 h reaction time, homogenous reaction mixture.

Table 3.2, Entry 1: Toluene solvent, $Sc(OTf)_3$ catalyst (52.3 mg, 0.106 mmol), quantitative HPLC conversion observed after 24 h, heterogenous mixture.

Table 3.2, Entry 2: Methanol solvent, $HClO_4$ catalyst (70% wt. in H_2O, 9 µL, 0.106 mmol), 92% HPLC conversion observed after 24 h.

Table 3.2, Entry 3: Acetonitrile solvent, 4 M HCl (solution in dioxane) catalyst (27 µL, 0.106 mmol), 77% HPLC conversion observed after 24 h.

Table 3.2, Entry 4: Ethanol solvent, 4 M HCl (solution in dioxane) catalyst (27 µL, 0.106 mmol), 91% HPLC conversion observed after 24 h.

6.2.1.2 General procedure B: optimisation of the synthesis of *N*-(*tert*-butyl)-2-phenylimidazo [1,2-*a*]pyridin-3-amine, microwave conditions (Table 3.2,Entries 6-9):

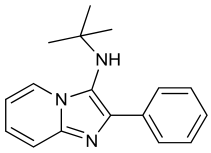

205

Into a 5 mL microwave vial was added a solution of 2-aminopyridine (**202**, 100 mg, 1.06 mmol), benzaldehyde (**203**, either **(a)** 0.108 mL, 1.06 mmol or **(b)** 0.216 mL, 2.13 mmol), *N-tert*-butylisocyanide (**204**, either **(c)** 0.120 mL, 1.06 mmol or **(d)** 0.240 mL, 2.13 mmol) and either 4 M HCl (solution in dioxane, either **(e)** 0.266 mL, 1.06 mmol **(f)** 27 µL, 0.106 mmol), 1.25 M HCl (solution in ethanol **(g)** 85 µL, 0.106 mmol) or no catalyst was added **(h)** in ethanol solvent (3 mL). The reaction mixture was irradiated at 130 °C for 50 min, before an aliquot (of either **(i)** 5 µL or **(j)** 10 µL) was taken and analysed according to the HPLC method described (see **Appendix 1, procedure for attaining conversion estimates from HPLC concentration gradients**) to determine SM consumption. The products were not isolated.

Table 1, Entry 6: Conditions used: **(a)**, **(c)**, **(e)**, **(i)**, 75% Conversion observed.

Table 1, Entry 7: Conditions used: **(a)**, **(c)**, **(h)**, **(i)**, 36% Conversion observed.

Table 1, Entry 8: Conditions used: **(b)**, **(d)**, **(f)**, **(j)**, Quantitative conversion observed.

Table 1, Entry 9: Conditions used: **(b)**, **(d)**, **(g)**, **(j)**, Quantitative conversion observed.

6.2.1.3 General procedure C: flow GBBR method using aryl and heteroaryl aldehydes:

A stock solution of the aminoazine (2.00 mmol), aryl or heteroaryl aldehyde (4.00 mmol or 2.00 mmol), and 1.25 M HCl (solution in ethanol, 0.160 mL, 0.200 mmol) was prepared in ethanol (10 mL total solution volume). Then, a solution of the relevant isocyanide (4.00 mmol) was prepared in ethanol (10 mL total solution volume). The flow reactor was heated to 130 °C whilst pumping clean ethanol through the system at a flow rate of 0.100 mL/min/line. Once at temperature, each of the two input lines was placed into one of the two stock solutions, and the reagents were pumped at 0.100 mL/min/line for 50 min (5 mL removed from each solution). The input lines were then changed back to the solvent reservoir and pumped to waste for 25 min to account for the dead volume in the reactor. The product solution was then collected for 61.75 min (12.4 mL collected), after which time the flow reactor was cooled and turned off. The reaction solutions were then analysed by the HPLC method described (see **Appendix 1, procedure for attaining conversion estimates from HPLC concentration gradients**) to determine starting material consumption. The remaining crude material was isolated either by passage through an Isolute® 5 g aminopropyl cartridge followed by drying *in vacuo*, or direct concentration *in vacuo*, and, if required, purification by flash column chromatography.

6.2.1.4 General procedure D: flow GBBR method using alkyl aldehydes:

A stock solution of the aminoazine (2.00 mmol), and isocyanide (4.00 mmol) was prepared in ethanol (10 mL total solution volume). Then, a solution of the alkyl aldehyde (2.24 mmol or 4.00 mmol), and 1.25 M HCl (solution in ethanol, 0.160 mL, 0.200 mmol) was prepared in ethanol (10 mL total solution volume). The flow reactor was heated to 130 °C whilst pumping clean ethanol through the system at a flow rate of 0.100 mL/min/line. Once at temperature, each of the two input lines was placed into one of the two stock solutions, and the reagents were pumped at 0.100 mL/min/line for 50 min (5 mL removed from each solution). The input lines were then changed back to the solvent reservoir and pumped to waste for 25 min to account for the dead volume in the reactor. The desired product solution was then collected for 61.75 min (12.4 mL collected), after which time the flow reactor was cooled and turned off. The reaction solutions were then analysed by the HPLC method described (see **Appendix 1, procedure for attaining conversion estimates from HPLC concentration gradients**) to determine starting material consumption. The remaining crude material was isolated by concentration *in vacuo*, and, if required, purified by flash column chromatography.

6.2.2 Specific synthetic procedures for Chapter 1

***N*-(*tert*-Butyl)-2-phenylimidazo[1,2-*a*]pyridin-3-amine:**

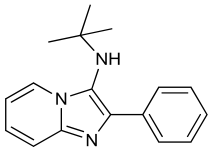

205

Preparation under flow conditions:

The reaction was performed according to **General procedure C**, using 2-aminopyridine (**202**, 94.0 mg, 1.00 mmol,), benzaldehyde (**203**, 0.203 mL, 2.00 mmol) and *N*-*tert*-butylisocyanide **204**, 0.226 mL, 2.00 mmol) as the reaction components. Following the reaction, a 50 µL aliquot of the crude product solution was taken, diluted with 0.950 mL methanol, and analysed according to the HPLC method described (see **Appendix 1, procedure for attaining conversion estimates from HPLC concentration gradients**), which showed that 97% of the starting material had been consumed in the reaction. The crude mixture was passed through an Isolute® 5 g aminopropyl cartridge with 20 mL methanol, before solvent removal *in vacuo* afforded *N*-(*tert*-butyl)-2-phenylimidazo[1,2-*a*]pyridin-3-amine (**205**, 256 mg, 0.965 mmol, 96% yield) as an off-white solid.

Preparation under MW conditions (batch synthesis):

To a 5 mL microwave vial was added a solution of 2-aminopyridine (**202**,100 mg, 1.06 mmol), benzaldehyde (**203**, 0.108 mL, 1.06 mmol), *N*-*tert*-butylisocyanide (**204**, 0.120 mL, 1.06 mmol) and 1.25 M HCl (solution in ethanol, 27 µL, 0.106 mmol) in ethanol (3 mL). The reaction mixture was irradiated at 130 °C for 50 min. After cooling, 10 µL was removed from the reaction mixture and analysed according to the HPLC method described (see **Appendix 1, procedure for attaining conversion estimates from HPLC concentration gradients**), which showed that 93% of the starting material had been consumed in the reaction. The remaining reaction mixture was dried *in vacuo* and purified by flash column chromatography using a 40 g RediSep silica cartridge, with an elution gradient of cyclohexane to 40% ethyl acetate in cyclohexane. The product-containing fractions were combined, and solvent was removed *in vacuo* to afford *N*-(*tert*-butyl)-2-phenylimidazo[1,2-*a*]pyridin-3-amine (**205**, 236 mg, 0.889 mmol, 84% yield) as an off-white solid.

Batch preparation using ethyl acetate as solvent:

To a 20 mL microwave vial was added a solution of 2-aminopyridine (**202**,94 mg, 1.00 mmol), benzaldehyde (**203**, 0.102 mL, 1.00 mmol), *N*-*tert*-butylisocyanide (**204**, 0.113 mL, 1.00 mmol) and 1.25 M HCl (solution in ethanol, 80 µL, 0.100 mmol) in ethyl acetate (10 mL). The reaction

mixture was irradiated at 130 °C for 50 min. After cooling, the reaction mixture was analysed by LCMS analysis, which determined that 95% conversion to the desired product had been observed in the reaction mixture. The product was not purified further.

Batch preparation using TFT (doped with 0.65% wt. water) as solvent:

To a 20 mL microwave vial was added a solution of 2-aminopyridine (**202**,94 mg, 1.00 mmol), benzaldehyde (**203**, 0.102 mL, 1.00 mmol), *N-tert*-butylisocyanide (**204**, 0.113 mL, 1.00 mmol) and 1.25 M HCl (solution in ethanol, 80 µL, 0.100 mmol) in TFT (10 mL, doped with 0.65% wt. water (77.4 µL)). The reaction mixture was irradiated at 130 °C for 50 min. After cooling, the reaction mixture was analysed by LCMS analysis, which determined that 64% conversion to the desired product had been observed in the reaction mixture. The product was not purified further.

One-pot synthesis of 205 from *N-tert*-butyl formamide (271):

Into a 50 mL RBF was added *N-tert*-butylformamide (**271**, 0.224 mL, 2 mmol) and tributylamine (**273**, 5.72 mL, 24.00 mmol) in ethyl acetate (10 mL overall volume) and the solution was stirred. To this mixture was added phosphorus oxychloride (0.373 mL, 4.00 mmol). Both effervescence and a gradual colour change from colourless to dark orange were observed for 30 min following the addition of phosphorus oxychloride. After 30 min, no further effervescence was observed. No precipitation was seen, but the reaction mixture was present as a biphasic mixture. The organic material was washed with water (20 mL), and then brine (10 mL). The organic phase was extracted, made up to 10 mL with ethyl acetate, and added to a 20 mL MW vial containing 2-aminopyridine (**202**, 0.188 g, 2.000 mmol), benzaldehyde (**203**, 0.205 mL, 2.000 mmol) and HCl in ethanol (0.160 mL, 0.200 mmol). The mixture was irradiated at 130 °C for 50 min. Following irradiation, LCMS analysis of the reaction mixture indicated that a conversion of 20% to the desired material was observed. The product was not purified further.

mp: 167-168 °C.

ν_{max} (neat, cm^{-1}): 3319, 2968, 1443, 1362, 1331, 1209, 757, 701.

^{1}H NMR (400 MHz, $CDCl_3$): δ 8.23 (app. dt, *J* = 6.9, 1.1 Hz, 1H), 7.92-7.89 (m, 2H), 7.53 (app. dt, *J* = 9.1, 1.0 Hz, 1H), 7.45-7.40 (m, 2H), 7.32 (tt, *J* = 7.6, 1.3 Hz, 1H), 7.12 (ddd, *J* = 9.1, 7.1, 1.0 Hz, 1H), 6.76 (td, *J* = 6.8, 1.0 Hz, 1H), 3.10 (br. s, 1H), 1.04 (s, 9H).

^{13}C NMR (101 MHz, $CDCl_3$): δ 142.1, 139.6, 135.4, 128.3 (2C), 128.2 (2C), 127.3, 123.9, 123.5 (2C), 117.4, 111.2, 56.4, 30.3 (3C).

LCMS (High pH, UV, ESI): t_{ret} = 1.16 min, $[M+H]^+$ m/z 266.2, 100.0% purity.

HRMS (TOF, ESI, formic acid): $C_{17}H_{20}N_3$ $[M+H]^+$ m/z = 266.1657 found m/z = 266.1667 (Δ = 3.8 ppm).

Spectroscopic data is in accordance with that reported in the literature.[140]

***N*-(2,6-Dimethylphenyl)-2-(p-tolyl)imidazo[1,2-*a*]pyridin-3-amine:**

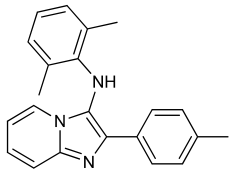

210

The reaction was performed according to **General procedure C**, using 2-aminopyridine (**202**, 94.0 mg, 1.00 mmol), 4-methylbenzaldehyde (0.236 mL, 2.00 mmol) and 2,6-dimethylphenylisocyanide (262 mg, 2.00 mmol) as the reaction components. Following the reaction, a 10 µL aliquot of the crude product solution was taken and analysed according to the HPLC method described (see **Appendix 1, procedure for attaining conversion estimates from HPLC concentration gradients**), which showed that 83% of the starting material had been consumed in the reaction. The crude mixture was passed through an Isolute® 5 g aminopropyl cartridge with 20 mL methanol, before solvent removal *in vacuo* afforded a crude material, which was purified by flash column chromatography using a 40 g RediSep silica cartridge, with an elution gradient from cyclohexane to 30% ethyl acetate in cyclohexane. The product-containing fractions were combined, and solvent was removed *in vacuo* to afford *N*-(2,6-dimethylphenyl)-2-(*p*-tolyl)imidazo[1,2-*a*]pyridin-3-amine (**210**, 267 mg, 0.815 mmol, 82% yield) as an off-white solid.

mp: 189-190 °C (dec.).

ν_{max} (neat, cm^{-1}): 3364, 1562, 1470, 1231, 825, 747.

^{1}H NMR (400 MHz, $CDCl_3$): δ 8.00 (br. d, 2H), 7.58-7.53 (m, 2H), 7.16 (d, *J* = 8.1 Hz, 2H), 7.11 (ddd, *J* = 9.1, 6.5, 1.0 Hz, 1H), 6.96 (d, *J* = 7.6 Hz, 2H), 6.78 (t, *J* = 7.6 Hz, 1H), 6.65 (td, *J* = 6.5, 1.0 Hz, 1H), 5.37 (br. s, 1H), 2.35 (s, 3H), 2.00 (s, 6H).

^{13}C NMR (101 MHz, $CDCl_3$): δ 141.3, 140.3, 139.4, 137.4, 129.9 (2C), 129.2 (2C), 127.0 (2C), 125.3 (2C), 124.1, 122.2, 121.0, 120.4, 119.6, 117.5, 112.2, 21.3, 18.5 (2C).

LCMS (High pH, UV, ESI): t_{ret} = 1.30 min, $[M+H]^+$ m/z 328.1, 100.0% purity.

HRMS (TOF, ESI, formic acid): $C_{22}H_{22}N_3$ $[M+H]^+$ m/z = 328.1808, found m/z = 328.1798 (Δ = -3.3 ppm).

2-(3-Bromophenyl)-*N*-(2-chloro-6-methylphenyl)imidazo[1,2-*a*]pyridin-3-amine:

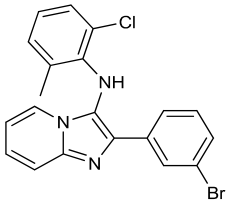

211

The reaction was performed according to **General procedure C**, using 2-aminopyridine (**202,** 94.0 mg, 1.00 mmol), 3-bromobenzaldehyde (0.233 mL, 2.00 mmol) and 2-chloro-6-methylphenylisocyanide (303 mg, 2.00 mmol) as the reaction components. Following the reaction, a 10 µL aliquot of the crude product solution was taken and analysed according to the HPLC method described (see **Appendix 1, procedure for attaining conversion estimates from HPLC concentration gradients**), which showed that 88% of the starting material had been consumed in the reaction. The crude mixture was passed through an Isolute® 5 g aminopropyl cartridge with 30 mL methanol, before solvent removal *in vacuo* afforded a crude material, which was purified by flash column chromatography using a 40 g RediSep silica cartridge, with an elution gradient from cyclohexane to 30% ethyl acetate in cyclohexane. The product-containing fractions were combined, and solvent was removed *in vacuo* to afford 2-(3-bromophenyl)-*N*-(2-chloro-6-methylphenyl)imidazo[1,2-*a*] pyridin-3-amine (**211**, 345 mg, 0.836 mmol, 84% yield) as a white powder.

mp: 188-189 °C (dec.).

ν_{max} (neat, cm^{-1}): 3309, 1596, 1466, 1351, 753, 681.

^{1}H NMR (400 MHz, $CDCl_3$): δ 8.16 (t, *J* = 1.5 Hz, 1H), 7.96 (dt, *J* = 7.6, 1.5 Hz, 1H), 7.86 (dt, *J* = 6.6, 1.0 Hz, 1H), 7.62 (br. d, *J* = 9.1 Hz, 1H), 7.36 (ddd, *J* = 8.1, 2.0, 1.0 Hz, 1H), 7.28 (dd, *J* = 8.1, 1.5 Hz, 1H), 7.24-7.17 (m, 2H), 6.85 (d, *J* = 7.1 Hz, 1H), 6.81 (td, *J* = 6.6, 1.0 Hz, 1H), 6.77 (t, *J* = 7.6 Hz, 1H), 6.12 (br. s, 1H), 1.56 (s, 3H).

^{13}C NMR (101 MHz, $CDCl_3$): δ 141.7, 138.5, 136.9, 135.1, 131.2, 130.6, 130.1, 129.8, 127.6, 127.5, 125.7, 125.1, 123.1, 122.6, 122.5, 121.7, 120.0, 117.7, 112.8, 18.2.

LCMS (High pH, UV, ESI): t_{ret} = 1.36 min, $[M+H]^+$ m/z 412.1, 100.0% purity.

HRMS (TOF, ESI, formic acid): $C_{20}H_{16}BrClN_3$ $[M+H]^+$ m/z = 412.0211, found m/z = 412.0206 (Δ = -1.2 ppm). Other m/z observed with heavier isotopes = 414.0181, 416.0163.

2-(4-Nitrophenyl)-*N*-(2,4,4-trimethylpentan-2-yl)imidazo[1,2-*a*]pyridin-3-amine:

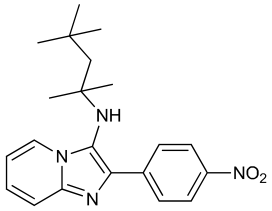

212

The reaction was performed according to **General procedure C**, using 2-aminopyridine (**202**, 94.0 mg, 1.00 mmol), 4-nitrobenzaldehyde (302 mg, 2.00 mmol) and 1,1,3,3-tetramethylbutylisocyanide (**268**, 0.351 mL, 2.00 mmol) as the reaction components. Following the reaction, a 10 µL aliquot of the crude product solution was taken and analysed according to the HPLC method described (see **Appendix 1, procedure for attaining conversion estimates from HPLC concentration gradients**), which showed that 91% of the starting material had been consumed in the reaction. The crude mixture was dried *in vacuo*, before the desired product was purified by flash column chromatography using a 40 g RediSep silica cartridge, with an elution gradient from 10% ethyl acetate in cyclohexane to 40% ethyl acetate in cyclohexane. The product-containing fractions were combined, and solvent was removed *in vacuo* to afford 2-(4-nitrophenyl)-*N*-(2,4,4-trimethylpentan-2-yl) imidazo[1,2-*a*]pyridin-3-amine (**212**, 267 mg, 0.729 mmol, 73% yield) as a bright orange powder.

Analytically pure sample prepared *via* MDAP isolation (High pH), Method D, 30 min run.

mp: 159-160 °C.

ν_{max} (neat, cm^{-1}): 2946, 1588, 1497, 1330, 752.

^{1}H NMR (400 MHz, $CDCl_3$): δ 8.31-8.27 (m, 2H), 8.22-8.17 (m, 3H), 7.55 (dt, *J* = 8.9, 1.0 Hz, 1H), 7.19 (ddd, *J* = 8.8, 6.9, 1.5 Hz, 1H), 6.83 (td, *J* = 6.4, 1.5 Hz, 1H), 3.13 (br. s, 1H), 1.64 (2H, s), 1.07 (9H, s), 1.00 (6H, s).

^{13}C NMR (101 MHz, $CDCl_3$): δ 146.8, 142.6, 142.3, 137.5, 128.7, 124.9, 124.6, 123.6, 123.5, 117.8, 112.0, 61.1, 57.3, 31.9 (3C), 31.8, 29.2 (2C).

LCMS (High pH, UV, ESI): t_{ret} = 1.44 min, $[M+H]^+$ m/z 367.3, 98.3% purity.

HRMS (TOF ESI, formic acid): $C_{21}H_{27}N_4O_2$ $[M+H]^+$ m/z = 367.2129, found m/z = 367.2118 (Δ = -2.8 ppm).

8-Methyl-*N*-((trimethylsilyl)methyl)imidazo[1,2-*a*]pyridin-3-amine:

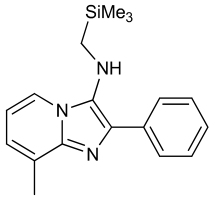

213

The reaction was performed according to **General procedure C**, using 3-methyl-2-aminopyridine (0.101 mL, 1.00 mmol), benzaldehyde (**203**, 0.203 mL, 2.00 mmol) and (isocyanomethyl)trimethylsilane (0.282 mL, 2.00 mmol) as the reaction components. Following the reaction, a 10 µL aliquot of the crude product solution was taken and analysed according to the HPLC method described (see **Appendix 1, procedure for attaining conversion estimates from HPLC concentration gradients**), which showed that 64% of the starting material had been consumed in the reaction. The crude mixture was dried *in vacuo*, before the desired product was purified by flash column chromatography using an 80 g RediSep silica cartridge, with an elution gradient from cyclohexane to 10% TBME in cyclohexane. The product-containing fractions were combined, and solvent was removed *in vacuo* to afford 8-methyl-*N*-((trimethylsilyl)methyl)imidazo[1,2-*a*]pyridin-3-amine (**213**, 169 mg, 0.546 mmol, 55% yield) as a white crystalline solid.

Analytically pure sample prepared *via* MDAP isolation (High pH), Method D, 30 min run.

mp: 80-81 °C.

ν_{max} (neat, cm^{-1}): 2952, 1494, 1349, 1246, 844.

^{1}H NMR (400 MHz, CD_3Cl): δ 7.99-7.94 (m, 2H), 7.86 (d, *J* = 6.9 Hz, 1H), 7.48-7.43 (m, 2H), 7.31 (tt, *J* = 7.4 Hz, 1.5 Hz, 1H), 6.92 (dt, *J* = 6.8, 1.1 Hz, 1H), 6.71 (t, *J* = 6.9 Hz, 1H), 2.92 (br. s, 1H), 2.64 (s, 3H), 2.56 (s, 2H), 0.16 (s, 9H).

^{13}C NMR (101 MHz, CD_3Cl): δ 141.6, 134.7, 134.3, 129.1, 128.6 (2C), 127.4, 127.1 (3C), 122.4, 120.1, 111.6, 38.6, 16.7, -2.78 (3C).

LCMS (High pH, UV, ESI): t_{ret} = 1.41 min, $[M+H]^+$ m/z 310.2, 98.8% purity.

HRMS (TOF ESI, formic acid): $C_{18}H_{24}N_3Si$ $[M+H]^+$ m/z = 310.1739, found m/z = 310.1740 (Δ = 0.3 ppm).

(3-(Butylamino)-2-(thiazol-2-yl)imidazo[1,2-*a*]pyridin-6-yl)methanol:

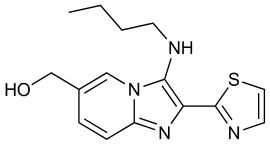

214

The reaction was performed according to **General procedure C**, using (6-aminopyridin-3-yl)methanol (124 mg, 1.00 mmol), thiazole-2-carbaldehyde (88.0 µL, 1.00 mmol) and 1-isocyanobutane (0.209 mL, 2.00 mmol) as the reaction components. Following reaction, a 10 µL aliquot of the crude product solution was taken and analysed according to the HPLC method described (see **Appendix 1, procedure for attaining conversion estimates from HPLC concentration gradients**), which showed that 78% of the starting material had been consumed in the reaction. The crude mixture was dried *in vacuo*, before the desired product was purified by reverse phase flash column chromatography using a 60 g Biotage SNAP KPC18-HS cartridge, with an elution gradient from 5% acetonitrile and 95% 10 mM aqueous ammonium bicarbonate solution (adjusted to pH 10 with 0.88 M aqueous ammonia) to 50% acetonitrile. The product-containing fractions were combined, and solvent was removed *in vacuo* to afford (3-(butylamino)-2-(thiazol-2-yl)imidazo[1,2-*a*] pyridin-6-yl)methanol (**214**, 154 mg, 0.509 mmol, 51% yield) as a viscous, yellow oil.

ν_{max} (neat, cm^{-1}): 3159, 2845, 2371, 1575, 1268, 1059, 787.

^{1}H NMR (400 MHz, $CDCl_3$): δ 7.92-7.89 (m, 1H), 7.83 (d, *J* = 3.4 Hz, 1H), 7.41 (d, *J* = 9.3 Hz, 1H), 7.28 (d, *J* = 3.4 Hz, 1H), 7.06 (dd, *J* = 9.3, 1.5 Hz, 1H), 5.34 (br. s, 1H), 4.66 (d, *J* = 1.0 Hz, 2H), 3.10 (t, *J* = 7.3 Hz, 2H), 2.91 (br. s, 1H), 1.62-1.54 (m, 2H), 1.42 (sxt, *J* = 7.4 Hz, 2H), 0.90 (t, *J* = 7.4 Hz, 3H).

^{13}C NMR (101 MHz, $CDCl_3$): δ 163.9, 143.2, 140.4, 131.1, 126.2, 126.0, 124.8, 120.4, 117.6, 117.3, 62.5, 47.0, 32.6, 20.1, 13.8.

LCMS (High pH, UV, ESI): t_{ret} = 0.96 min, $[M+H]^+$ m/z 303.2, 100.0% purity.

HRMS (TOF ESI, formic acid): $C_{15}H_{19}N_4OS$ $[M+H]^+$ m/z = 303.1280, found m/z = 303.1279 (Δ = 0.3 ppm).

(3-((2-Morpholinoethyl)amino)-2-(pyridin-2-yl)imidazo[1,2-*a*]pyridin-6-yl)methanol:

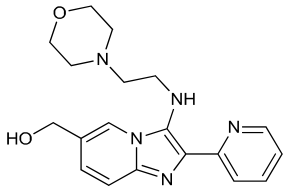

215

The reaction was performed according to **General procedure C**, using (6-aminopyridin-3-yl)methanol (124 mg, 1.00 mmol), picolinaldehyde (190 µL, 2.00 mmol) and 4-(2-isocyanoethyl)morpholine (**264**, 0.276 mL, 2.00 mmol) as the reaction components. Following the reaction, a 10 µL aliquot of the crude product solution was taken and analysed according to the HPLC method described (see **Appendix 1, procedure for attaining conversion estimates from HPLC concentration gradients**), which showed that 92% of the starting material had been consumed in the reaction. The crude mixture was dried *in vacuo*, before the desired product was purified by flash column chromatography using an 80 g Biotage RediSep silica cartridge, with an elution gradient from 5% to 30% ethyl acetate in cyclohexane. The product-containing fractions were combined, and solvent was removed *in vacuo* to afford (3-((2-morpholinoethyl)amino)-2-(pyridin-2-yl)imidazo[1,2-*a*]pyridin-6-yl)methanol (**215**, 309 mg, 0.874 mmol, 87% yield) as a beige powder.

mp: 143-144 °C.

ν_{max} (neat, cm^{-1}): 3164, 2803, 1896, 1113, 1018, 793.

^{1}H NMR (400 MHz, $CDCl_3$): δ 8.55-8.52 (m, 1H), 8.14 (br. d, *J* = 7.9 Hz, 1H), 7.97-7.93 (m, 1H), 7.74 (td, *J* = 7.8, 1.7 Hz, 1H), 7.41 (br. d, *J* = 9.4 Hz, 1H), 7.14 (ddd, *J* = 7.95, 4.8, 1.0 Hz, 1H), 7.02 (dd, *J* = 9.4, 2.0 Hz, 1H), 6.43 (br. s, 1H), 4.64 (s, 2H), 3.69 (br. t, *J* = 4.4 Hz, 4H), 3.15 (t, *J* = 5.9 Hz, 2H), 2.57 (t, *J* = 5.9 Hz, 2H), 2.45 (br. t, *J* = 4.4 Hz, 4H), 2.45 (br. s, 1H).

^{13}C NMR (101 MHz, $CDCl_3$): δ 154.9, 148.5, 140.4, 136.7, 132.2, 130.0, 125.4, 123.9, 121.2, 120.3 (2C), 117.6, 67.0 (2C), 62.7, 58.4, 53.6 (2C), 43.6.

LCMS (High pH, UV, ESI): t_{ret} = 0.73 min, $[M+H]^+$ m/z 354.3. Product unstable to LCMS analysis.

HRMS (TOF ESI, formic acid): $C_{19}H_{24}N_5O_2$ $[M+H]^+$ m/z = 354.1930, found m/z = 354.1941 (Δ = 3.1 ppm).

4-(6-Methoxy-3-(((trimethylsilyl)methyl)amino)imidazo[1,2-*a*]pyridin-2-yl)phenol:

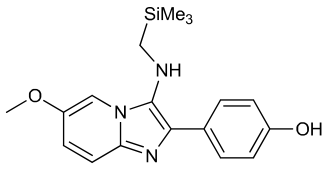

216

The reaction was performed according to **General procedure C**, using 5-methoxy-2-amino pyridine (124 mg, 1.00 mmol), 4-hydroxybenzaldehyde (244 mg, 2.00 mmol) and (isocyanomethyl)trimethylsilane (0.282 mL, 2.00 mmol) as the reaction components. Following the reaction, a 10 µL aliquot of the crude product solution was taken and analysed according to the HPLC method described (see **Appendix 1, procedure for attaining conversion estimates from HPLC concentration gradients**), which showed that 92% of the starting material had been consumed in the reaction. The crude mixture was dried *in vacuo*, before the desired product was purified by flash column chromatography using a 40 g Biotage RediSep silica cartridge, with an elution gradient from 10% to 40% ethyl acetate in cyclohexane. The product-containing fractions were combined, and solvent was removed *in vacuo* to afford 4-(6-methoxy-3-(((trimethylsilyl)methyl)amino)imidazo[1,2-*a*]pyridin-2-yl) phenol (**216**, 261 mg, 0.764 mmol, 76% yield) as a red-orange powder.

mp: 196-197 °C (dec.).

ν_{max} (neat, cm^{-1}): 1609, 1505, 1242, 837, 526.

^{1}H NMR (400 MHz, DMSO-*d*$_6$): δ 9.41 (br. s, 1H), 7.93-7.88 (m, 2H), 7.68 (d, *J* = 1.5 Hz, 1H), 7.36 (dd, *J* = 9.4, 1.0 Hz, 1H), 6.93 (dd, *J* = 9.4, 2.5 Hz, 1H), 6.83-6.78 (d, *J* = 7.9 Hz, 2H), 4.27 (t, *J* = 5.9, 1H), 3.82 (s, 3H), 2.44 (d, *J* = 5.9 Hz, 2H), 0.08 (s, 9H).

^{13}C NMR (101 MHz, DMSO-*d*$_6$): δ 156.3, 147.9, 137.1, 134.9, 128.6, 127.6 (2C), 125.9, 117.7, 116.9, 115.0 (2C), 104.4, 55.9, 37.3, -2.55 (3C).

LCMS (High pH, UV, ESI): t_{ret} = 1.14 min, $[M+H]^+$ m/z 342.2, 94.3% purity.

HRMS (TOF ESI, formic acid): $C_{18}H_{24}N_3O_2Si$ $[M+H]^+$ m/z = 342.1638, found m/z = 342.1638 (Δ = 0.0 ppm).

Ethyl-2-((8-bromo-2-(pyridin-2-yl)imidazo[1,2-*a*]pyridin-3-yl)amino)acetate:

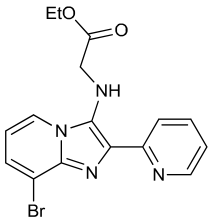

217

The reaction was performed according to **General procedure C**, using 3-bromo-2-amino pyridine (174 mg, 1.00 mmol), picolinaldehyde (0.190 mL, 2.00 mmol) and ethyl 2-isocyanoacetate (0.219 mL, 2.00 mmol) as the reaction components. Following the reaction, a 10 µL aliquot of the crude product solution was taken and analysed according to the HPLC method described (see **Appendix 1, procedure for attaining conversion estimates from HPLC concentration gradients**), which showed that 44% of the starting material had been consumed in the reaction. The crude mixture was dried *in vacuo*, before the desired product was purified by flash column chromatography using a 40 g Biotage RediSep silica cartridge, with an elution gradient of cyclohexane to 40% ethyl acetate in cyclohexane. The product-containing fractions were combined, and solvent was removed *in vacuo* to afford ethyl-2-((8-bromo-2-(pyridin-2-yl)imidazo[1,2-*a*]pyridin-3-yl)amino)acetate (**217**, 159 mg, 0.424 mmol, 42% yield) as a pale yellow solid.

Analytically pure sample prepared *via* MDAP isolation (High pH), Method C, 20 min run. This afforded the desired product as a pale yellow solid.

mp: 90-91 °C

ν_{max} (neat, cm^{-1}): 1609, 1505, 1242, 837, 526.

^{1}H NMR (400 MHz, CD_3Cl): δ 8.60-8.56 (m, 1H), 8.30 (dt, *J* = 8.0, 1.2 Hz, 1H), 8.09 (dd, *J* = 6.9, 1.0 Hz, 1H), 7.76 (td, *J* = 7.4, 2.0 Hz, 1H), 7.39 (dd, *J* = 6.9, 1.0 Hz, 1H), 7.17 (ddd, *J* = 7.4, 4.9, 1.2 Hz, 1H), 6.67 (t, *J* = 7.1 Hz, 1H), 6.55 (br s, 1H), 4.16 (q, *J* = 7.4 Hz, 2H), 3.88 (s, 2H), 1.20 (t, *J* = 7.4 Hz, 3H).

^{13}C NMR (101 MHz, CD_3Cl): δ 170.7, 154.2, 148.7, 138.5, 136.6, 131.8, 131.7, 126.0, 122.1, 121.7, 121.1, 112.2, 112.0, 61.2, 48.7, 14.1.

LCMS (High pH, UV, ESI): t_{ret} = 1.10 min, [M] m/z 374.9, 97.4% purity.

HRMS (TOF ESI, formic acid): Calculated for $C_{16}H_{16}BrN_4O_2$ $[M+H]^+$ m/z = 375.0451, found m/z = 375.0449 (Δ = -0.5 ppm). Other m/z observed with heavier isotope = 377.0427.

7-Bromo-*N*-(2,6-dimethylphenyl)-2-(thiazol-2-yl)imidazo[1,2-*a*]pyridin-3-amine:

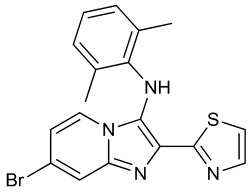

218

The reaction was performed according to **General procedure C**, using 4-bromo-2-amino pyridine (173 mg, 1.00 mmol), thiazole-2-carbaldehyde (0.176 mL, 2.00 mmol) and 2,6-dimethylphenylisocyanide (262 mg, 2.00 mmol) as the reaction components. Following the reaction, a 10 µL aliquot of the crude product solution was taken and analysed according to the HPLC method described (see **Appendix 1, procedure for attaining conversion estimates from HPLC concentration gradients**), which showed that 65% of the starting material had been consumed in the reaction. The crude mixture was passed through an Isolute® 5 g aminopropyl cartridge with 20 mL methanol and dried *in vacuo*, before the desired product was purified by flash column chromatography using a 40 g Biotage RediSep silica cartridge, with an elution gradient from cyclohexane to 40% ethyl acetate in cyclohexane. The product-containing fractions were combined, and solvent was removed *in vacuo* to afford 7-bromo-*N*-(2,6-dimethylphenyl)-2-(thiazol-2-yl)imidazo[1,2-*a*]pyridin-3-amine (**218**, 185 mg, 0.463 mmol, 46% yield) as a beige powder.

mp: 208-209 °C (dec.).

ν_{max} (neat, cm^{-1}): 3273, 2917, 1616, 1570, 1524, 1472.

^{1}H NMR (400 MHz, $CDCl_3$): δ 7.93 (br. s, 1H), 7.82 (d, *J* = 3.0 Hz, 1H), 7.66 (br. d, *J* = 2.0 Hz, 1H), 7.27 (d, *J* = 3.0 Hz, 1H), 7.11 - 7.08 (m, 3H), 6.86 (dd, *J* = 7.6, 1.0 Hz, 1H), 6.50 (dd, *J* = 7.6, 2.0 Hz, 1H), 2.14 (s, 6H).

^{13}C NMR (101 MHz, $CDCl_3$): δ 164.3, 143.0, 139.6, 136.7, 135.3 (2C), 129.6, 129.0 (2C), 126.3, 122.5 (2C), 120.1, 116.9, 116.2, 116.0, 18.7 (2C).

LCMS (High pH, UV, ESI): t_{ret} = 1.42 min, $[M+H]^+$ m/z 401.0, 100.0% purity.

HRMS (TOF ESI, formic acid): $C_{18}H_{16}BrN_4S$ $[M+H]^+$ m/z = 399.0274, found m/z = 399.0262 (Δ = -2.8 ppm). Other m/z observed with heavier isotope = 401.0341.

Ethyl-2-phenyl-3-((2,4,4-trimethylpentan-2-yl)amino)imidazo[1,2-*a*] pyridine-6-carboxylate:

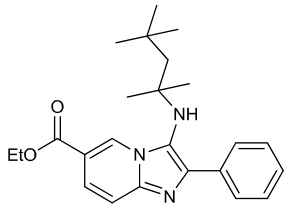

219

The reaction was performed according to **General procedure C**, using ethyl-6-amino nicotinate (**262**, 166 mg, 1.00 mmol), benzaldehyde (**203**, 0.203 mL, 2.00 mmol) and 1,1,3,3-tetramethylbutylisocyanide (**268**, 0.351 mL, 2.00 mmol) as the reaction components. Following the reaction, a 10 µL aliquot of the crude product solution was taken and analysed according to the HPLC method described (see **Appendix 1, procedure for attaining conversion estimates from HPLC concentration gradients**), which showed that 67% of the starting material had been consumed in the reaction. The crude mixture was dried *in vacuo*, before the desired product was purified by flash column chromatography using a 40 g Biotage RediSep silica cartridge, with an elution gradient from 5% to 30% ethyl acetate in cyclohexane. The product-containing fractions were combined, and solvent was removed *in vacuo* to afford ethyl-2-phenyl-3-((2,4,4-trimethylpentan-2-yl)amino)imidazo[1,2-*a*]pyridine-6-carboxylate (**219**, 247 mg, 0.628 mmol, 63% yield) as yellow flakes.

mp: 118-119 °C (dec.).

ν_{max} (neat, cm^{-1}): 3327, 2958, 1715, 1291, 1102, 695.

^{1}H NMR (400 MHz, $CDCl_3$): δ 9.05-9.03 (m, 1H), 7.87-7.83 (m, 2H), 7.69 (dd, *J* = 9.3, 1.5 Hz, 1H), 7.52 (d, *J* = 9.3 Hz, 1H), 7.45 (t, *J* = 7.5, 2H), 7.35 (br. t, *J* = 7.5, 1H), 4.43 (q, *J* = 7.2, 2H), 3.28 (br. s, 1H), 1.60 (s, 2H), 1.43 (t, *J* = 7.2 Hz, 3H), 1.06 (s, 9H), 0.96 (s, 6H).

^{13}C NMR (101 MHz, $CDCl_3$): δ 165.3, 142.5, 141.5, 134.9, 128.4 (4C), 128.0, 127.8, 124.4, 123.6, 116.6, 115.7, 61.3, 60.8, 57.0, 31.9 (3C), 31.8, 29.1 (2C), 14.4.

LCMS (High pH, UV, ESI): t_{ret} = 1.53 min, $[M+H]^+$ m/z 394.4, 100.0% purity.

HRMS (TOF ESI, formic acid): $C_{24}H_{32}N_3O_2$ $[M+H]^+$ m/z = 394.2495, found m/z = 394.2492 (Δ = -0.8 ppm).

***N*-(*tert*-Butyl)-6-phenylimidazo[2,1-*b*]thiazol-5-amine:**

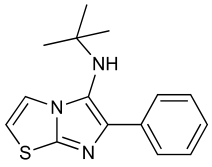

224

The reaction was performed according to **General procedure C**, using 2-aminothiazole (100 mg, 1.00 mmol), benzaldehyde (**203**, 0.203 mL, 2.00 mmol) and *N*-*tert*-butylisocyanide (**204**, 0.226 mL, 2.00 mmol) as the reaction components. Following the reaction, a 10 µL aliquot of the crude product solution was taken and analysed according to the HPLC method described (see **Appendix 1, procedure for attaining conversion estimates from HPLC concentration gradients**), which showed that 51% of the starting material had been consumed in the reaction. The crude mixture was dried *in vacuo*, before the desired product was purified by flash column chromatography using an 80 g Biotage RediSep silica cartridge, with an elution gradient from cyclohexane to 10% ethyl acetate in cyclohexane. The product-containing fractions were combined, and solvent was removed *in vacuo* to afford *N*-(*tert*-butyl)-6-phenylimidazo[2,1-*b*]thiazol-5-amine (**224**, 122 mg, 0.450 mmol, 45% yield) as a white powder.

mp: 159-160 °C.

ν_{max} (neat, cm^{-1}): 3329, 2963, 1441, 1359, 1179, 645.

^{1}H NMR (400 MHz, CD_3Cl): δ 7.90-7.86 (m, 2H), 7.41-7.37 (m, 2H), 7.37-7.35 (m, 1H), 7.25 (tt, *J* = 7.4, 1.3 Hz, 1H), 6.72 (d, *J* = 4.4 Hz, 1H), 3.05 (br. s, 1H), 1.07 (s, 9H).

^{13}C NMR (101 MHz, $CDCl_3$): δ 145.5, 140.2, 135.3, 128.2 (2C), 127.2 (2C), 126.7, 125.5, 117.8, 111.4, 55.8, 30.2 (3C).

LCMS (High pH, UV, ESI): t_{ret} = 1.16 min, $[M+H]^+$ m/z 272.1, 100.0% purity.

HRMS (TOF ESI, formic acid): $C_{15}H_{18}N_3S$ $[M+H]^+$ m/z = 272.1221, found m/z = 272.1221 (Δ = 0.0 ppm).

6-(3-Bromophenyl)-*N*-(2,4,4-trimethylpentan-2-yl)imidazo[2,1-*b*]thiazol-5-amine:

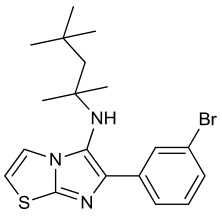

225

The reaction was performed according to **General procedure C**, using 2-aminothiazole (100 mg, 1.00 mmol), 3-bromobenzaldehyde (0.233 mL, 2.00 mmol) and 1,1,3,3-tetramethylbutylisocyanide (**268**, 0.351 mL, 2.00 mmol) as the reaction components. Following the reaction, a 10 µL aliquot of the crude product solution was taken and analysed according to the HPLC method described (see **Appendix 1, procedure for attaining conversion estimates from HPLC concentration gradients**), which showed that 87% of the starting material had been consumed in the reaction. The crude mixture was dried *in vacuo*, before the desired product was purified by flash column chromatography using an 80 g Biotage RediSep silica cartridge, with an elution gradient from cyclohexane to 20% ethyl acetate in cyclohexane. The product-containing fractions were combined, and solvent was removed *in vacuo* to afford *N*-(*tert*-butyl)-6-phenylimidazo[2,1-*b*]thiazol-5-amine (**225**, 279 mg, 0.687 mmol, 69% yield) as a colourless oil.

ν_{max} (neat, cm^{-1}): 3273, 2951, 1595, 1476, 1365, 693.

^{1}H NMR (400 MHz, CD_3Cl): δ 8.12 (t, *J* = 2.0 Hz, 1H), 7.82 (dt, *J* = 7.9, 1.5 Hz, 1H), 7.39-7.36 (m, 2H), 7.24 (t, *J* = 7.9 Hz, 1H), 6.75 (d, *J* = 4.4 Hz, 1H), 3.03 (br. s, 1H), 1.57 (s, 2H), 1.05 (s, 9H), 1.04 (s, 6H).

^{13}C NMR (101 MHz, CD_3Cl): δ 145.8, 139.0, 137.5, 130.3, 129.7, 129.6, 125.8, 125.6, 122.3, 117.8, 111.8, 60.1, 57.0, 31.9 (2C), 31.8, 29.2 (3C).

LCMS (High pH, UV, ESI): t_{ret} = 1.55 min, $[M+H]^+$ m/z 406.2, 100.0% purity.

HRMS (TOF ESI, formic acid): $C_{19}H_{25}BrN_3S$ $[M+H]^+$ m/z = 406.0947, found m/z = 406.0947 (Δ = -0.3 ppm). Other m/z observed with heavier isotope = 408.0930.

4-(3-(*tert*-Butylamino)imidazo[1,2-*a*]pyrimidin-2-yl)phenol:

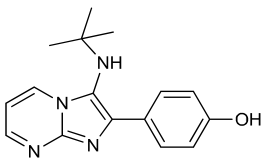

226

The reaction was performed according to **General procedure C**, using 2-aminopyrimidine (**163**, 95 mg, 1.00 mmol), 4-hydroxybenzaldehyde (244 mg, 2.00 mmol) and *N-tert*-butyl isocyanide (**204**, 0.226 mL, 2.00 mmol) as the reaction components. Following the reaction, a 10 µL aliquot of the crude product solution was taken and analysed according to the HPLC method described (see **Appendix 1, procedure for attaining conversion estimates from HPLC concentration gradients**), which showed that 32% of the starting material had been consumed in the reaction. The crude mixture was dried *in vacuo*, before the desired product was purified by flash column chromatography using a 55 g aminopropyl RediSep silica cartridge, with an elution gradient from cyclohexane to neat ethyl acetate. The product-containing fractions were combined, and solvent was removed *in vacuo* to afford 4-(3-(*tert*-butylamino)imidazo[1,2-*a*]pyrimidin-2-yl)phenol (**226**, 93 mg, 0.329 mmol, 33% yield) as a yellow-orange powder.

The product was formed as a mixture of 2 regioisomers, along with **248** (see **Section 7.2 Appendix 2 – NMR data of regioisomeric mix for compounds 226 and 248** for more information; *ca.* 8% (~7 mg) of material **248** was observed by ^{1}H and 1D NOESY NMR analysis).

Analysis for desired material (226):

mp: 185-186 °C (dec.).

ν_{max} (neat, cm^{-1}): 3116, 2966, 1611, 1506, 1365, 848, 759.

^{1}H NMR (400 MHz, CD_3OD): δ 8.76 (dd, *J* = 6.8, 2.0 Hz, 1H), 8.45 (dd, *J* = 4.3, 2.0 Hz, 1H), 7.88-7.83 (m, 2H), 7.00 (dd, *J* = 6.8, 4.0 Hz, 1H), 6.89-6.85 (m, 2H), 1.03 (s, 9H).

^{13}C NMR (101 MHz, CD_3OD): δ 158.7, 150.8, 146.1, 142.0, 133.3, 131.1 (2C), 126.8, 123.4, 116.1 (2C), 109.4, 57.0, 30.6 (3C).

LCMS (High pH, UV, ESI): t_{ret} = 0.83 min, $[M+H]^+$ m/z 283.2, 97.6% purity.

HRMS (TOF ESI, formic acid): $C_{16}H_{19}N_4O$ $[M+H]^+$ m/z = 283.1545, found m/z = 283.1555 (Δ = 3.5 ppm).

Undesired regioisomer (248):

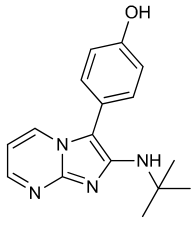

226

^{1}H NMR (400 MHz, CD_3OD): δ 8.39 (dd, *J* = 6.6, = 2.0 Hz, 1H), 8.20 (dd, *J* = 4.5, 2.0 Hz, 1H), 7.34-7.29 (m, 2H), 6.99-6.97 (m, 2H), 6.82-6.79 (m, 1H), 1.42 (s, 9H).

Complete ^{13}C NMR assignment (and other supporting data) could not be acquired due to an insufficient amount of material.

2-Phenyl-*N*-(2,4,4-trimethylpentan-2-yl)benzo[*d*]imidazo[2,1-*b*]thiazol-3-amine:

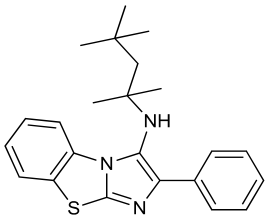

227

The reaction was performed according to **General procedure C**, using 2-aminobenzothiazole (150 mg, 1.00 mmol), benzaldehyde (**203**, 0.203 mL, 2.00 mmol) and 1,1,3,3-tetramethylbutylisocyanide (**268**, 0.351 mL, 2.00 mmol) as the reaction components. Following the reaction, a 10 µL aliquot of the crude product solution was taken and analysed according to the HPLC method described (see **Appendix 1, procedure for attaining conversion estimates from HPLC concentration gradients**), which showed that 39% of the starting material had been consumed in the reaction. The crude mixture was dried *in vacuo*, before the desired product was purified by flash column chromatography using an 80 g RediSep silica cartridge, with an elution gradient from 10% to 25% ethyl acetate in cyclohexane. The product-containing fractions were combined, and solvent was removed *in vacuo* to afford 2-phenyl-*N*-(2,4,4-trimethylpentan-2-yl)benzo[*d*]imidazo[2,1-*b*] thiazol-3-amine (**227**, 149 mg, 0.395 mmol, 40% yield) as a white crystalline solid.

mp: 132-133 °C.

ν_{max} (neat, cm^{-1}): 3272, 2950, 1487, 1191, 753, 697.

^{1}H NMR (400 MHz, DMSO-d_6): δ 8.40 (br. dd, *J* = 8.0, 0.8 Hz, 1H), 7.97 (dd, *J* = 8.0, 1.0 Hz, 1H), 7.95-7.92 (m, 2H), 7.54 (ddd, *J* = 8.3, 7.3, 1.3 Hz, 1H), 7.41-7.36 (m, 3H), 7.26 (tt, *J* = 7.3, 1.8 Hz, 1H), 4.60 (s, 1H), 1.57 (s, 2H), 0.95 (s, 6H), 0.89 (s, 9H).

^{13}C NMR (101 MHz, DMSO-d_6): δ 142.6, 140.6, 135.3, 133.1, 129.1, 128.2, 127.8 (2C), 127.7 (2C), 126.6, 125.7, 124.6, 124.4, 114.5, 59.8, 56.0, 31.5 (3C), 30.9, 28.0 (2C).

LCMS (High pH, UV, ESI): t_{ret} = 1.61 min, $[M+H]^+$ m/z 378.3, 100.0% purity.

HRMS (TOF ESI, formic acid): $C_{23}H_{28}N_3S$ $[M+H]^+$ m/z = 378.2004, found m/z = 378.2003 (Δ = -0.3 ppm).

4-(3-(Cyclohexylamino)imidazo[1,2-*a*]pyrazin-2-yl)phenol:

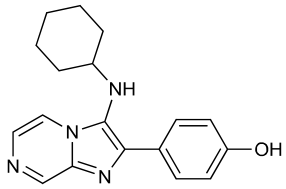

228

The reaction was performed according to **General procedure C**, using aminopyrazine (95 mg, 1.00 mmol), 4-hydroxybenzaldehyde (244 mg, 2.00 mmol) and cyclohexylisocyanide (0.249 mL, 2.00 mmol) as the reaction components. Following the reaction, a 10 µL aliquot of the crude product solution was taken and analysed according to the HPLC method described (see **Appendix 1, procedure for attaining conversion estimates from HPLC concentration gradients**), which showed that 60% of the starting material had been consumed in the reaction. The crude mixture was passed through an Isolute® 5 g aminopropyl frit with 20 mL methanol and dried *in vacuo*, before the desired product was purified by flash column chromatography using a 40 g RediSep silica cartridge, with an elution gradient from 20% to 90% ethyl acetate in cyclohexane. The product-containing fractions were combined, and solvent was removed *in vacuo* to afford 4-(3-(cyclohexylamino)imidazo[1,2-*a*] pyrazin-2-yl)phenol (**228**, 166 mg, 0.539 mmol, 54% yield) as a pale-yellow powder.

mp: 284-285 °C (dec.).

ν_{max} (neat, cm^{-1}): 3298, 2921, 1611, 1495, 1283, 832, 796.

^{1}H NMR (400 MHz, DMSO-*d*$_6$): δ 9.59 (br. s, 1H), 8.84 (d, *J* = 1.5 Hz, 1H), 8.31 (dd, *J* = 4.9, 1.5 Hz, 1H), 8.06-8.02 (m, 2H), 7.81 (d, *J* = 4.4 Hz, 1H), 6.87-6.82 (m, 2H), 4.89 (d, *J* = 6.4 Hz, 1H), 2.91-2.80 (m, 1H), 1.73-1.60 (m, 4H), 1.53-1.47 (m, 1H), 1.33-1.21 (m, 2H), 1.16-1.02 (m, 3H).

^{13}C NMR (101 MHz, DMSO-*d*$_6$): δ 157.2, 141.8, 137.3, 135.7, 128.3, 128.1 (2C), 126.1, 124.7, 116.1, 115.2 (2C), 56.2, 33.6 (2C), 25.3, 24.5 (2C).

LCMS (High pH, UV, ESI): t_{ret} = 0.96 min, $[M+H]^+$ m/z 309.3, 100.0% purity.

HRMS (TOF ESI, formic acid): $C_{18}H_{21}N_4O$ $[M+H]^+$ m/z = 309.1710, found m/z = 309.1697 (Δ = -4.3 ppm).

(*E*)-*N*-Benzyl-2-styrylimidazo[1,2-*a*]pyrazin-3-amine:

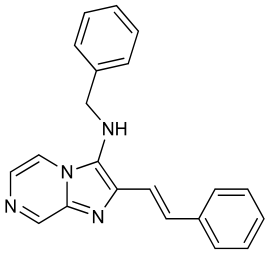

229

The reaction was performed according to **General procedure C**, using aminopyrazine (95 mg, 1.00 mmol), cinnamaldehyde (0.252 mL, 2.00 mmol) and *N*-benzylisocyanide (0.244 mL, 2.00 mmol) as the reaction components. Following the reaction, a 10 µL aliquot of the crude product solution was taken and analysed according to the HPLC method described (see **Appendix 1, procedure for attaining conversion estimates from HPLC concentration gradients**), which showed that 56% of the starting material had been consumed in the reaction. The crude mixture was dried *in vacuo*, before the desired product was purified by flash column chromatography using an 80 g RediSep silica cartridge, with an elution gradient from 20% to 80% ethyl acetate in cyclohexane. The product-containing fractions were combined, and solvent was removed *in vacuo* to afford (*E*)-*N*-benzyl-2-styrylimidazo[1,2-*a*] pyrazin-3-amine (**229**, 149 mg, 0.457 mmol, 46% yield) as a yellow powder.

Analytically pure sample prepared *via* MDAP isolation (High pH), Method B, 20 min run.

mp: 148-149 °C (lit.[283] 149-150 °C (Hexane/ethyl acetate)).

ν_{max} (neat, cm^{-1}): 3312, 1526, 1350, 966, 784, 748, 685.

^{1}H NMR (400 MHz, CD_3Cl): δ 8.94 (d, *J* = 1.5 Hz, 1H), 7.79 (dd, *J* = 4.4, 1.5 Hz, 1H), 7.76 (d, *J* = 4.9, 1H), 7.59 (d, *J* = 16.2 Hz, 1H), 7.49-7.45 (m, 2H), 7.38-7.33 (m, 4H), 7.32-7.27 (m, 4H), 6.92 (d, *J* = 16.2 Hz, 1H), 4.26 (s, 2H).

^{13}C NMR (101 MHz, CD_3Cl): δ 143.1, 138.9, 138.2, 137.4, 137.1, 132.0, 129.1 (2C), 129.0, 128.8 (2C), 128.4 (2C), 128.2 (2C), 128.0, 126.9 (2C), 117.3, 115.2, 53.3.

LCMS (High pH, UV, ESI): t_{ret} = 1.13 min, $[M+H]^+$ m/z 327.1, 97.9% purity.

HRMS (TOF ESI, formic acid): $C_{21}H_{19}N_4$ $[M+H]^+$ m/z = 327.1604, found m/z = 327.1588 (Δ = -5.0 ppm).

Spectroscopic data is in accordance with that reported in the literature.[283]

2-Phenyl-*N*-(2,4,4-trimethylpentan-2-yl)imidazo[1,2-*b*]pyridazin-3-amine:

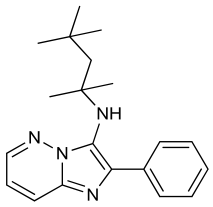

230

To a solution of pyridazin-3-amine (95 mg, 1 mmol) and benzaldehyde (**203**, 0.203 mL, 2.00 mmol) in ethanol (10 mL) was added 1,1,3,3-tetramethylbutylisocyanide (**268**, 0.351 mL, 2.00 mmol), and then HCl in ethanol (0.0800 mL, 0.100 mmol). The reaction was irradiated for 50 min at 130 °C. Following the reaction, the crude mixture was dried *in vacuo*, before the desired product was purified by flash column chromatography using an 80 g RediSep silica cartridge, with an elution gradient from 20% to 35% ethyl acetate in cyclohexane. The product-containing fractions were combined, and solvent was removed *in vacuo* to afford 2-phenyl-*N*-(2,4,4-trimethylpentan-2-yl)imidazo[1,2-*b*]pyridazin-3-amine (**230**, 266 mg, 0.825 mmol, 83% yield) as a bright yellow powder.

mp: 112-113 °C.

ν_{max} (neat, cm^{-1}): 2954, 1524, 1272, 1198, 766, 696.

^{1}H NMR (400 MHz, CD_3OD): δ 8.42 (dd, *J* = 4.4, 1.5 Hz, 1H), 8.10-8.06 (m, 2H), 7.89 (dd, *J* = 9.0, 1.7 Hz, 1H), 7.43 (tt, *J* = 7.3, 1.5 Hz, 2H), 7.33 (tt, *J* = 7.3, 1.5 Hz, 1H), 7.14 (dd, *J* = 9.3, 4.4 Hz, 1H), 1.64 (s, 2H), 1.05 (s, 9H), 0.99 (s, 6H).

^{13}C NMR (101 MHz, CD_3OD): δ 144.2, 139.3, 137.2, 136.1, 129.8, 129.5 (2C), 129.3 (2C), 128.9, 125.4, 118.1, 62.1, 57.5, 32.6, 32.3 (3C), 29.9 (2C).

LCMS (High pH, UV, ESI): t_{ret} = 1.50 min, $[M+H]^+$ m/z 323.1, 98.6% purity.

HRMS (TOF ESI, formic acid): $C_{20}H_{27}N_4$ $[M+H]^+$ m/z = 323.2236, found m/z = 323.2231 (Δ = -1.5 ppm).

***N*-(*tert*-Butyl)imidazo[1,2-*a*]pyridin-3-amine:**

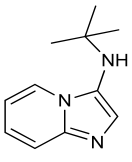

235

Preparation under MW conditions (batch synthesis):

To a solution of 2-aminopyridine (**202**, 42.4 mg, 0.45 mmol) and formaldehyde (**234**, 37% wt. solution in H_2O, 73 µL, 0.900 mmol) in ethanol (10 mL) was added *tert*-butylisocyanide (**204**, 0.102 mL, 0.900 mmol), and then HCl in ethanol (36 µL, 45.0 µmol). The reaction was irradiated for 50 min at 130 °C. Following the reaction, a 10 µL aliquot of the crude product solution was taken and analysed according to the HPLC method described (see **Appendix 1, procedure for attaining conversion estimates from HPLC concentration gradients**), which showed that 99% of the starting material had been consumed in the reaction. The crude mixture was dried *in vacuo*, before the desired product was purified using MDAP isolation (high pH), method B, 30 min run. The product-containing fractions were combined, and solvent was removed under a stream of nitrogen afford *N*-(*tert*-butyl)imidazo[1,2-*a*]pyridin-3-amine (**235**, 48 mg, 0.254 mmol, 56% yield) as an off-white powder.

Preparation under flow conditions:

The reaction was performed according to **General procedure D**, using 2-aminopyridine (**202**, 94 mg, 1.00 mmol), formaldehyde (**234**, 37% wt. solution in H_2O, 0.0830 mL, 1.12 mmol) and *N-tert*-butylisocyanide (**204**, 0.226 mL, 2.00 mmol) as the reaction components. Following the reaction, a 10 µL aliquot of the crude product solution was taken and analysed according to the HPLC method described (see **Appendix 1, procedure for attaining conversion estimates from HPLC concentration gradients**), which showed that 94% of the starting material had been consumed in the reaction. the crude mixture was dried *in vacuo*, before the desired product was purified by flash column chromatography using a 40 g RediSep silica cartridge, with an elution gradient from neat ethyl acetate to 20% ethanol in ethyl acetate. The product-containing fractions were combined, and solvent was removed *in vacuo* to afford *N*-(*tert*-butyl)imidazo[1,2-*a*]pyridin-3-amine (**235**, 155 mg, 0.819 mmol, 82% yield) as an off-white powder.

mp: 119-120 °C (lit.[159] 118-120 °C).

ν_{max} (neat, cm^{-1}): 3230, 2969, 1630, 1548, 1503, 1336, 1229, 758.

^{1}H NMR (400 MHz, $CDCl_3$): δ 8.22 (br. d, *J* = 6.9 Hz, 1H), 7.52 (br. dd, *J* = 7.5, 1.0 Hz, 1H), 7.32 (s, 1H), 7.14-7.09 (m, 1H), 6.77 (t, *J* = 6.6 Hz, 1H), 2.59 (br. s, 1H), 1.20 (s, 9H).

^{13}C NMR (101 MHz, $CDCl_3$): δ 142.7, 128.7, 127.1, 123.6, 123.0, 117.5, 111.4, 53.9, 29.7 (3C).

LCMS (Low pH, UV, ESI): t_{ret} = 0.37 min, $[M+H]^+$ m/z 190.1, 96.0% purity.

HRMS (TOF ESI, formic acid): $C_{11}H_{16}N_3$ $[M+H]^+$ m/z = 190.1344, found m/z = 190.1347 (Δ = 1.6 ppm).

Spectroscopic data is in accordance with that reported in the literature.[159]

(3-(*tert*-Butylamino)imidazo[1,2-*a*]pyridin-6-yl)methanol:

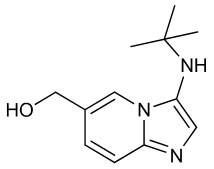

240

The reaction was performed according to **General procedure D**, using (6-aminopyridin-3-yl) methanol (124 mg, 1.00 mmol), formaldehyde (**234**, 37% wt. solution in H_2O, 83 µL, 1.12 mmol) and *N*-*tert*-butylisocyanide (**204**, 0.226 mL, 2.00 mmol) as the reaction components. Following the reaction, a 10 µL aliquot of the crude product solution was taken and analysed according to the HPLC method described (see **Appendix 1, procedure for attaining conversion estimates from HPLC concentration gradients**), which showed that 94% of the starting material had been consumed in the reaction. The crude mixture was dried *in vacuo*, before the desired product was purified by flash column chromatography using a 40 g RediSep silica cartridge, with an elution gradient from neat ethyl acetate to 10% ethanol in ethyl acetate. The product-containing fractions were combined, and solvent was removed *in vacuo* to afford (3-(*tert*-butylamino)imidazo[1,2-*a*]pyridin-6-yl) methanol (**240**, 192 mg, 0.876 mmol, 88% yield) as a white crystalline solid.

mp: 111-112 °C.

ν_{max} (neat, cm^{-1}): 3314, 3149, 2968, 2844, 1213, 1049, 822.

^{1}H NMR (400 MHz, CD_3OD): δ 8.34-8.31 (m, 1H), 7.41 (dd, *J* = 9.1, 1.0 Hz, 1H), 7.23 (dd, *J* = 9.1, 2.0 Hz, 1H), 7.20 (s, 1H), 4.64 (d, *J* = 1.0 Hz, 2H), 1.20 (s, 9H).

^{13}C NMR (101 MHz, CD_3OD): δ 143.1, 129.9, 127.7, 127.3, 126.1, 122.1, 117.1, 62.7, 54.4, 29.8 (3C).

LCMS (High pH, UV, ESI): t_{ret} = 0.68 min, $[M+H]^+$ 220.2 m/z, 95.7% purity.

HRMS (TOF ESI, formic acid): $C_{12}H_{18}N_3O$ $[M+H]^+$ m/z = 220.1450, found m/z = 220.1454 (Δ = 1.8 ppm).

***N*-(*tert*-Butyl)-8-methylimidazo[1,2-*a*]pyridin-3-amine:**

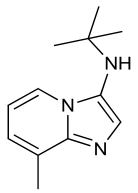

241

The reaction was performed according to **General procedure D**, using 3-methyl-2-amino pyridine (108 mg, 1.00 mmol), formaldehyde (**234**, 37% wt. solution in H_2O, 83 µL, 1.12 mmol) and *N*-*tert*-butylisocyanide (**204**, 0.226 mL, 2.00 mmol) as the reaction components. Following the reaction, a 10 µL aliquot of the crude product solution was taken and analysed according to the HPLC method described (see **Appendix 1, procedure for attaining conversion estimates from HPLC concentration gradients**), which showed that 94% of the starting material had been consumed in the reaction. The crude mixture was dried *in vacuo*, before the desired product was purified by flash column chromatography using a 40 g RediSep silica cartridge, with an elution gradient from 50% ethyl acetate in cyclohexane to neat ethyl acetate. The product-containing fractions were combined, and solvent was removed *in vacuo* to afford *N*-(*tert*-butyl)-8-methylimidazo[1,2-*a*]pyridin-3-amine (**241**, 177 mg, 0.871 mmol, 87% yield) as a white crystalline solid.

Analytically pure sample prepared *via* MDAP isolation (High pH), Method B, 30 min run.

mp: 90-91 °C.

ν_{max} (neat, cm^{-1}): 3217, 2972, 1542, 1354, 750.

^{1}H NMR (400 MHz, $CDCl_3$): δ 8.09 (br. d, *J* = 6.8 Hz, 1H), 7.31 (s, 1H), 6.94-6.91 (m, 1H), 6.70 (t, *J* = 6.8 Hz, 1H), 2.77 (br. s, 1H), 2.59 (s, 3H), 1.19 (s, 9H).

^{13}C NMR (101 MHz, $CDCl_3$): δ 142.9, 127.9, 127.5, 127.0, 122.6, 121.0, 111.6, 53.8, 29.7 (3C), 16.5.

LCMS (High pH, UV, ESI): t_{ret} = 0.93 min, $[M+H]^+$ 204.2 m/z, 100.0% purity.

HRMS (TOF ESI, formic acid): $C_{12}H_{18}N_3$ $[M+H]^+$ m/z = 204.1501, found m/z = 204.1501 (Δ = 0.0 ppm).

5-Bromo-*N*-(2-chloro-6-methylphenyl)-2-methylimidazo[1,2-*a*]pyridin-3-amine:

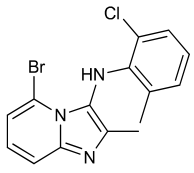

242

A stock solution of the 6-bromo-2-aminopyridine (346 mg, 2.00 mmol), and acetaldehyde (0.336 mL, 6.00 mmol) was prepared in ethanol (10 mL total solution volume). Then, a solution of the 2-chloro-6-methylphenylisocyanide (2.24 mmol), and 1.25 M HCl (solution in ethanol, 0.160 mL, 0.200 mmol) was prepared in ethanol (10 mL total solution volume). The flow reactor was heated to 130 °C whilst pumping clean ethanol through the system at a flow rate of 0.100 mL/min/line. Once at temperature, each of the two input lines was placed into one of the two stock solutions, and the reagents were pumped at 0.100 mL/min/line for 50 min (5 mL removed from each solution). The input lines were changed back to the solvent reservoir and pumped to waste for 25 minutes to account for the dead volume in the reactor. The desired product solution was then collected for 61.75 min (12.4 mL collected), after which time the flow reactor was cooled and turned off. Following the reaction, a 10 µL aliquot of the crude product solution was taken and analysed according to the HPLC method described (see **Appendix 1, procedure for attaining conversion estimates from HPLC concentration gradients**), which showed that 96% of the starting material had been consumed in the reaction. The crude mixture was dried *in vacuo*, before the desired product was purified by flash column chromatography using an 80 g RediSep silica cartridge, with an elution gradient from 15% to 30% ethyl acetate in cyclohexane. The product-containing fractions were combined, and solvent was removed *in vacuo* to afford 5-bromo-*N*-(2-chloro-6-methyl phenyl)-2-methylimidazo[1,2-*a*]pyridin-3-amine (**242**, 227 mg, 0.647 mmol, 65% yield) as a brown powder.

mp: 158-159 °C.

ν_{max} (neat, cm^{-1}): 3359, 3239, 1591, 1466, 1305, 1119, 756.

^{1}H NMR (400 MHz, $CDCl_3$): δ 7.50 (dd, *J* = 7.8, 2.5 Hz, 1H), 7.24 (dd, *J* = 7.8, 1.0 Hz, 1H), 7.03-6.97 (m, 2H), 6.94 (br. d, *J* = 7.8 Hz, 1H), 6.76 (t, *J* = 7.8 Hz, 1H), 5.88 (br. s, 1H), 2.10 (d, *J* = 1.0 Hz, 3H), 1.66 (s, 3H).

^{13}C NMR (101 MHz, $CDCl_3$): δ 143.7, 140.3, 139.8, 131.0, 127.6, 126.8, 124.4, 122.6, 122.5, 120.8, 118.6, 116.4, 112.2, 18.7, 12.8.

LCMS (High pH, UV, ESI): t_{ret} = 1.23 min, $[M+H]^+$ 350.1 m/z, 98.9% purity.

HRMS (TOF ESI, formic acid): $C_{15}H_{14}BrClN_3$ $[M+H]^+$ m/z = 350.0060, found m/z = 350.0061 (Δ = 0.3 ppm). Other m/z observed with heavier isotopes = 352.0041, 354.0014.

***N*-(*tert*-Butyl)-2-cyclopropylimidazo[1,2-*a*]pyridin-3-amine:**

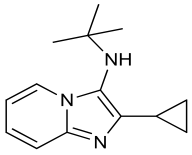

243

The reaction was performed according to **General procedure D**, using 2-aminopyridine (**202**, 124 mg, 1.00 mmol), cyclopropanecarbaldehyde (0.149 mL, 2.00 mmol) and *N*-*tert*-butylisocyanide (**204**, 0.226 mL, 2.00 mmol) as the reaction components. Following the reaction, a 10 µL aliquot of the crude product solution was taken and analysed according to the HPLC method described (see **Appendix 1, procedure for attaining conversion estimates from HPLC concentration gradients**), which showed that > 99% of the starting material had been consumed in the reaction. The crude mixture was dried *in vacuo* to afford *N*-(*tert*-butyl)-2-cyclopropylimidazo[1,2-*a*]pyridin-3-amine (**243**, 206 mg, 0.898 mmol, 90% yield) as a white crystalline solid.

mp: 56-57 °C.

ν_{max} (neat, cm^{-1}): 3253, 2966, 1329, 1205, 754.

^{1}H NMR (400 MHz, CD_3OD): δ 8.32-8.28 (m, 1H), 7.34-7.29 (m, 1H), 7.19 (ddd, *J* = 9.1, 6.6, 1.0 Hz, 1H), 6.85 (td, *J* = 6.6, 1.5 Hz, 1H), 2.20-2.12 (m, 1H), 1.22 (s, 9H), 1.00-0.94 (m, 4H). NH peak not observed.

^{13}C NMR (101 MHz, CD_3OD): δ 142.6, 142.2, 125.8, 124.6, 120.8, 116.0, 112.6, 56.5, 30.6 (3C), 9.63, 8.73 (2C).

LCMS (High pH, UV, ESI): t_{ret} = 1.04 min, $[M+H]^+$ 230.2 m/z, 98.7% purity.

HRMS (TOF ESI, formic acid): $C_{14}H_{20}N_3$ $[M+H]^+$ m/z = 230.1657, found m/z = 230.1662 (Δ = 2.2 ppm).

6-Cyclopropyl-*N*-(2,4,4-trimethylpentan-2-yl)imidazo[2,1-*b*]thiazol-5-amine:

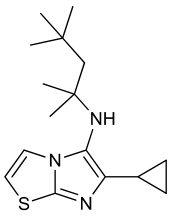

244

The reaction was performed according to **General procedure D**, using 2-aminothiazole (100 mg, 1.00 mmol), cyclopropanecarbaldehyde (0.149 mL, 2.00 mmol) and 1,1,3,3-tetramethylbutylisocyanide (**268**, 0.351 mL, 2.00 mmol) as the reaction components. Following the reaction, a 10 µL aliquot of the crude product solution was taken and analysed according to the HPLC method described (see **Appendix 1, procedure for attaining conversion estimates from HPLC concentration gradients**), which showed that > 99% of the starting material had been consumed in the reaction. The crude mixture was dried *in vacuo*, before the desired product was purified by flash column chromatography using a 40 g RediSep silica cartridge, with an elution gradient from 10% to 30% ethyl acetate in cyclohexane. The product-containing fractions were combined, and solvent was removed *in vacuo* to afford 6-cyclopropyl-*N*-(2,4,4-trimethylpentan-2-yl)imidazo[2,1-*b*]thiazol-5-amine (**244**, 246 mg, 0.844 mmol, 84% yield) as a clear, brown oil.

Preparation under batch (MW) conditions:

To a solution of 2-aminothiazole (501 mg, 5.00 mmol) and cyclopropanecarbaldehyde (0.747 mL, 10.0 mmol) in ethanol (10 mL) was added 1,1,3,3-tetramethylbutylisocyanide (**268**, 1.75 mL, 10.0 mmol), and then HCl in ethanol (0.400 mL, 0.500 mmol). The reaction was irradiated under MW conditions for 50 min at 130 °C. Following the reaction, the crude mixture was dried *in vacuo*, before the desired product was purified by flash column chromatography using an 80 g RediSep silica cartridge, with an elution gradient from 10% to 30% ethyl acetate in cyclohexane. The product-containing fractions were combined, and solvent was removed *in vacuo* to afford 6-cyclopropyl-*N*-(2,4,4-trimethylpentan-2-yl)imidazo[2,1-*b*]thiazol-5-amine (**244**, 1.22 mg, 4.19 mmol, 81% yield) as a clear, brown oil.

ν_{max} (neat, cm^{-1}): 2951, 1683, 1464, 1365, 653

^{1}H NMR (400 MHz, CD_3OD): δ 7.52 (br. d, *J* = 4.5 Hz, 1H), 6.94 (br. d, *J* = 4.5 Hz, 1H), 2.02-1.90 (m, 1H), 1.67 (s, 2H), 1.21 (s, 6H), 1.08 (s, 9H), 0.88 - 0.78 (m, 4H).

^{13}C NMR (101 MHz, CD_3OD): δ 146.0, 143.2, 127.3, 119.7, 112.0, 60.1, 57.2, 32.5, 32.4 (3C), 29.6 (2C), 9.91, 7.93 (2C).

LCMS (High pH, UV, ESI): t_{ret} = 1.35 min, $[M+H]^+$ 292.3 m/z, 96.6% purity.

HRMS (TOF ESI, formic acid): $C_{16}H_{26}N_3S$ $[M+H]^+$ m/z = 292.1847, found m/z = 292.1846 (Δ = -0.1 ppm).

***N*-Benzyl-2-cyclopropyl-6-methoxyimidazo[1,2-*a*]pyrimidin-3-amine:**

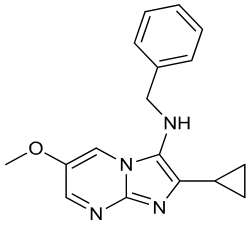

245

The reaction was performed according to **General procedure D**, using 5-methoxy-2-amino pyrimidine (125 mg, 1.00 mmol), cyclopropanecarbaldehyde (0.149 mL, 2.00 mmol) and *N*-benzylisocyanide (0.244 mL, 2.00 mmol) as the reaction components. Following the reaction, a 10 µL aliquot of the crude product solution was taken and analysed according to the HPLC method described (see **Appendix 1, procedure for attaining conversion estimates from HPLC concentration gradients**), which showed that 75% of the starting material had been consumed in the reaction. The crude mixture was dried *in vacuo*, before the desired product was purified by flash column chromatography using an 80 g RediSep silica cartridge, with an elution gradient from 30% to 60% ethyl acetate in cyclohexane. The product-containing fractions were combined, and solvent was removed *in vacuo* to afford *N*-benzyl-2-cyclopropyl-6-methoxyimidazo[1,2-*a*]pyrimidin-3-amine (**245**, 176 mg, 0.598 mmol, 60% yield) as a yellow-orange powder.

mp: 136-137 °C.

ν_{max} (neat, cm^{-1}): 3268, 3004, 2922, 1569, 1466, 1209, 698.

^{1}H NMR (600 MHz, DMSO-*d*$_6$): δ 8.11 (d, *J* = 2.9 Hz, 1H), 7.88 (d, *J* = 2.9 Hz, 1H), 7.30 (br. d, *J* = 7.3 Hz, 2H), 7.27 (br. t, *J* = 7.7 Hz, 2H), 7.22 (br. t, *J* = 7.3 Hz, 1H), 5.26 (t, *J* = 5.9 Hz, 1H), 4.16 (d, *J* = 5.9 Hz, 2H), 3.74 (s, 3H), 2.03-1.98 (m, 1H), 0.84-0.80 (m, 4H).

^{13}C NMR: (151 MHz, DMSO-*d*$_6$): δ 144.3, 140.6, 140.5, 140.4, 140.3, 128.3 (2C), 128.1 (2C), 126.9, 125.5, 111.2, 56.3, 51.9, 8.0 (2C), 7.9.

LCMS (High pH, UV, ESI): t_{ret} = 0.95 min, $[M+H]^+$ 295.2 m/z, 95.5% purity.

HRMS (TOF ESI, formic acid): $C_{17}H_{19}N_4O$ $[M+H]^+$ m/z =295.1559, found m/z = 295.1559 (Δ = 0.0 ppm).

Only regioisomer observed by ^{15}N HMBC (See **Section 7.3 Appendix 3 – NMR data for compound 245** for more information).

Ethyl 2-((2-propylimidazo[1,2-*a*]pyridin-3-yl)amino)acetate:

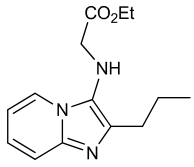

246

Preparation under flow conditions:

The reaction was performed according to **General procedure D**, using 2-aminopyridine (**202**, 94 mg, 1.00 mmol), butyraldehyde (**249**, 0.180 mL, 2.00 mmol) and ethyl 2-isocyanoacetate (**250**, 0.219 mL, 2.00 mmol) as the reaction components. Following the reaction, a 10 µL aliquot of the crude product solution was taken and analysed according to the HPLC method described (see **Appendix 1, procedure for attaining conversion estimates from HPLC concentration gradients**), which showed that 93% of the starting material had been consumed in the reaction. The crude mixture was dried *in vacuo*, before the desired product was purified by flash column chromatography using an 80 g RediSep silica cartridge, with an elution gradient from 20% to 70% ethyl acetate in cyclohexane. The product-containing fractions were combined, and solvent was removed *in vacuo* to afford ethyl-2-((2-propylimidazo[1,2-*a*]pyridin-3-yl)amino)acetate (**246**, 215 mg, 0.823 mmol, 82% yield) as a yellow oil.

ν_{max} (neat, cm^{-1}): 3217, 2959, 2929, 1738, 1181, 753, 737.

^{1}H NMR (400 MHz, $CDCl_3$): δ 8.11 (dt, *J* = 6.8, 1.5 Hz, 1H), 7.45 (dt, *J* = 8.8, 1.0 Hz, 1H), 7.08 (ddd, *J* = 8.8, 6.9, 1.5 Hz, 1H), 6.75 (td, *J* = 6.9, 1.0 Hz, 1H), 4.23 (q, *J* = 7.2 Hz, 2H), 3.76 (d, *J* = 5.9 Hz, 2H), 3.49 (br. t, *J* = 5.9 Hz, 1H), 2.74 (dd, *J* = 7.3, 7.3 Hz, 2H), 1.82-1.74 (m, 2H), 1.28 (t, *J* = 7.2 Hz, 3H), 0.99 (t, *J* = 7.3 Hz, 3H).

^{13}C NMR: (101 MHz, $CDCl_3$): δ 171.9, 141.5, 139.4, 124.9, 123.2, 122.4, 117.0, 111.3, 61.3, 50.3, 29.2, 22.9, 14.2 (2C).

LCMS (High pH, UV, ESI): t_{ret} = 0.90 min, $[M+H]^+$ 262.3 m/z.

HRMS (TOF ESI, formic acid): $C_{14}H_{20}N_3O_2$ $[M+H]^+$ m/z = 262.1556, found m/z = 262.1555 (Δ = -0.4 ppm), 98.0% LC-HRMS purity.

Preparation under batch conditions:

The reaction was performed using conditions found in the literature.[169] To a 5 mL microwave vial was added a solution of 2-aminopyridine (**202**, 0.094 g, 1.00 mmol), butyraldehyde (**249**, 0.0990 mL, 1.10 mmol), ethyl 2-isocyanoacetate (**250**, 0.131 mL, 1.20 mmol) and scandium(III)trifluoromethanesulfonate (24.6 mg, 0.050 mmol) in a mixture of methanol (1 mL) and dichloromethane (2 mL). The reaction mixture was stirred under ambient conditions for 144 h. During the reaction, 10 µL aliquots were removed from the reaction mixture at 50 min, 24 h and 144 h time points, and analysed according to the HPLC method described (see **procedure for attaining conversion estimates from HPLC concentration gradients**), which showed that 28% of the starting material had been consumed in the reaction after 50 min, 38% consumption was observed after 24 h, and 68% was observed after 144 h. The reaction mixture was dried *in vacuo*, and purified by MDAP (High pH, Method B, 20 min run). The product-containing fractions were combined, and solvent was removed under reduced pressure to afford ethyl-2-((2-propylimidazo[1,2-*a*]pyridin-3-yl)amino)acetate (**246**, 22 mg, 0.084 mmol, 8% yield) as a pale-yellow oil.

251 (4 mg, 1% yield) was also isolated as a yellow-brown oil from the same purification method. A mechanism for its formation is postulated in **Scheme 3.7**. The precise stereochemistry of the by-product could not be determined (See **Section 7.4 Appendix 4 – NMR data for by-product, compound 251** for NMR data).

Ethyl 2-((2-(4-hydroxyheptan-3-yl)imidazo[1,2-*a*]pyridin-3-yl)amino)acetate:

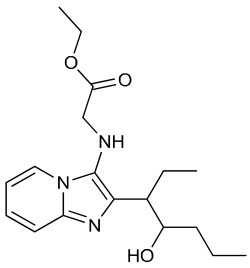

251

ν_{max} (neat, cm^{-1}): 3315, 2959, 2935, 2877, 1741, 1202.

^{1}H NMR (600 MHz, $CDCl_3$): δ 8.15 (dt, *J* = 6.8, 1.1 Hz, 1H), 7.45 (dt, *J* = 8.9, 1.1 Hz, 1H), 7.13 (ddd, *J* = 8.9, 6.8, 1.1 Hz, 1H), 6.80 (td, *J* = 6.8, 1.1 Hz, 1H), 4.25 (q, *J* = 7.2 Hz, 2H), 3.93-3.83 (m, 1H), 3.76 (dd, *J* = 5.5, 3.7 Hz, 2H), 3.58 (t, *J* = 5.5 Hz, 1H), 2.84-2.80 (m, 1H), 1.96-1.87 (m, 2H), 1.52-1.45 (m, 1H), 1.39-1.33 (m, 1H), 1.29 (t, *J* = 7.2 Hz, 3H), 1.25-1.14 (m, 2H), 0.86 (t, *J* = 7.3 Hz, 6H).

^{13}C NMR: (151 MHz, $CDCl_3$): δ 171.9, 141.5, 139.7, 126.6, 123.8, 122.5, 117.2, 111.6, 74.0, 61.4, 50.4, 43.4, 39.2, 26.1, 19.4, 14.1, 13.2, 12.5.

LCMS (High pH, UV, ESI): t_{ret} = 1.06 min, $[M+H]^+$ 334.2 m/z. Product unstable to LCMS analysis.

HRMS (TOF ESI, formic acid): $C_{18}H_{28}N_3O_3$ $[M+H]^+$ m/z = 334.2131, found m/z = 334.2129 (Δ = -0.6 ppm), 97.2% LC-HRMS purity.

2-(*tert*-Butyl)-*N*-cyclohexylimidazo[1,2-*a*]pyrazin-3-amine:

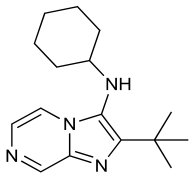

247

The reaction was performed according to **General procedure D**, using aminopyrazine (95 mg, 1.00 mmol), pivaldehyde (0.217 mL, 2.00 mmol) and cyclohexylisocyanide (0.249 mL, 2.00 mmol) as the reaction components. Following the reaction, a 10 µL aliquot of the crude product solution was taken and analysed according to the HPLC method described (see **procedure for attaining conversion estimates from HPLC concentration gradients**), which showed that 61% of the starting material had been consumed in the reaction. The crude mixture was dried *in vacuo*, before the desired product was purified by flash column chromatography using an 80 g RediSep silica cartridge, with an elution gradient from 20% to 50% ethyl acetate in cyclohexane. The product-containing fractions were combined, and solvent was removed *in vacuo* to afford ethyl 2-((2-propylimidazo[1,2-*a*]pyridin-3-yl) amino)acetate (**247**, 139 mg, 0.510 mmol, 51% yield) as off-white flakes.

mp: 126-127 °C.

ν_{max} (neat, cm^{-1}): 3313, 3260, 2925, 2853, 1528, 1344, 801.

^{1}H NMR (400 MHz, CD_3OD): δ 8.74 (d, *J* = 1.0 Hz, 1H), 8.26 (dd, *J* = 4.5, 1.5 Hz, 1H), 7.79 (d, *J* = 4.5 Hz, 1H), 3.03 (tt, *J* = 10.5, 3.5 Hz, 1H), 1.82-1.72 (m, 4H), 1.67-1.60 (m, 1H), 1.49 (s, 9H), 1.38-1.21 (m, 5H). NH peak not observed.

^{13}C NMR: (101 MHz, CD_3OD): δ 150.8, 142.2, 136.9, 129.1, 127.7, 118.1, 59.5, 35.2 (2C), 34.5 (2C), 30.8 (3C), 26.9, 26.2.

LCMS (High pH, UV, ESI): t_{ret} = 1.20 min, $[M+H]^+$ 273.3 m/z, 97.4% purity.

HRMS (TOF ESI, formic acid): $C_{16}H_{25}N_4$ $[M+H]^+$ m/z =273.2079, found m/z = 273.2082 (Δ = 1.1 ppm).

2-Bromo-2-phenylacetaldehyde:

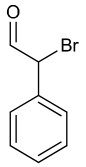

254

The reaction was performed using conditions found in the literature.[284]

To a solution of 2-phenylacetaldehyde (**253**, 1.93 mL, 16.7 mmol) in DCM (10 mL) was added a solution of bromine (0.853 mL, 16.7 mmol) in DCM (20 mL) dropwise at -10 °C over 2 h. The reaction was present as a dark-red solution following the addition. The reaction mixture was warmed to ambient conditions, before being heated to reflux for 24 h. After heating, a colour change to generate a blue-green solution was observed. The reaction mixture was washed with sat. aq. sodium bicarbonate solution (50 mL), and the organic layer was separated. The aqueous layer was extracted with dichloromethane (2 x 20 mL), before the organic layers were combined, washed with aq. sodium bicarbonate solution (30 mL), passed through a 70 mL Isolute® hydrophobic fritted reservoir, and solvent was removed *in vacuo* to afford the crude product as a viscous green oil (2.96 g, 14.9 mmol). The product mixture was used in the next reaction without further purification.

5-Phenyloxazol-2-amine:

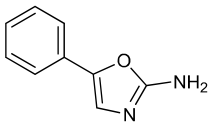

255

The reaction was performed following a literature procedure.[285]

To a solution of 2-bromo-2-phenylacetaldehyde (**254**, 2.96 g, 14.9 mmol) in ethanol (40 mL) was added urea (0.893 mL, 14.9 mmol). The reaction mixture was heated, with stirring, to reflux (80 °C) for 5.5 h under nitrogen. The reaction was cooled, and solvent was removed *in vacuo* to afford a crude green residue, which was purified using reverse phase flash column chromatography, under high pH conditions, using a 120 g Biotage KP-C18-HS SNAP cartridge, with a solvent ratio gradient of 95:5 to 65:35 (H_2O:MeCN). The product-containing fractions were combined, and solvent was removed *in vacuo* to afford the desired product, at insufficient purity. As such, the desired product was re-purified by flash column chromatography on a 40 g RediSep silica cartridge using an eluent from 40% ethyl acetate in cyclohexane to neat ethyl acetate. The product-containing fractions were combined, and

solvent was removed *in vacuo* to afford 5-phenyloxazol-2-amine (**255**, 341 mg, 2.13 mmol, 14% yield (*this represents a 13% yield over 2 steps*)) as a white powder.

mp: 193-194 °C (dec.).

ν_{max} (neat, cm^{-1}): 3423, 3343, 3122, 1637, 1169, 739, 689.

^{1}H NMR (400 MHz, DMSO-*d*$_6$): δ 7.48-7.44 (m, 2H), 7.36 (br. t, *J* = 7.5 Hz, 2H), 7.22-7.15 (m, 2H), 6.80 (br. s, 2H).

^{13}C NMR (101 MHz, DMSO-*d*$_6$): δ 161.3, 142.9, 128.8 (2C), 128.7, 126.2, 122.9, 121.8 (2C).

LCMS (High pH, UV, ESI): t_{ret} = 0.77 min, $[M+H]^+$ m/z 161.1, 93.7% purity.

HRMS (TOF ESI, formic acid): $C_9H_9N_2O$ $[M+H]^+$ m/z = 161.0715, found m/z = 161.0713 (Δ = -1.2 ppm).

Spectroscopic data is in accordance with that reported in the literature.[285]

Ethyl-2-(2,6-dimethylphenyl)-3-((2-morpholinoethyl)amino)imidazo[1,2-*a*] pyridine-6-carboxylate:

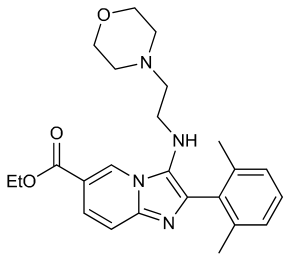

265

The reaction was performed according to **General procedure C**, ethyl 6-aminonicotinate (**262**, 166 mg, 1.00 mmol), 2,6-dimethylbenzaldehyde (**263**, 268 mg, 2.00 mmol) and 4-(2-iso cyanoethyl)morpholine (**264**, 0.276 mL, 2.00 mmol) as the reaction components. Following the reaction, the crude mixture was passed through an Isolute® 5 g aminopropyl cartridge with 20 mL methanol and dried *in vacuo*, before the desired product was purified by flash column chromatography using an 80 g RediSep silica cartridge, with an elution gradient from 20% to 90% ethyl acetate in cyclohexane. The product-containing fractions were combined, and solvent was removed *in vacuo* to afford ethyl-2-(2,6-dimethylphenyl)-3-((2-morpholino ethyl)amino)imidazo[1,2-*a*]pyridine-6-carboxylate (**265**, 40 mg, 0.0950 mmol, 9% yield) as a yellow oil.

ν_{max} (neat, cm^{-1}): 2964, 2850, 2806, 1716, 1276, 1116.

^{1}H NMR (400 MHz, DMSO-*d*$_6$): δ 9.05-8.98 (m, 1H), 7.55-7.46 (m, 2H), 7.20 (dd, *J* = 8.1, 6.8 Hz, 1H), 7.13-7.10 (m, 2H), 4.94 (t, *J* = 5.9 Hz, 1H), 4.38 (q, *J* = 7.1 Hz, 2H), 3.43 (br. t, *J* = 4.5 Hz, 4H), 2.77 (q, *J* = 6.0 Hz, 2H), 2.20 (t, *J* = 6.3 Hz, 2H), 2.11 (br. t, *J* = 4.5 Hz, 4H), 2.07 (s, 6H), 1.36 (t, *J* = 7.1 Hz, 3H).

^{13}C NMR (101 MHz, DMSO-*d*$_6$): δ 164.8, 139.8, 137.4, 133.7, 132.6, 128.9, 127.8, 127.2, 127.0, 120.9, 119.1, 116.2 (2C), 114.3, 66.0 (2C), 60.9, 57.8, 53.0 (2C), 43.3, 20.1 (2C), 14.2.

LCMS (High pH, UV, ESI): t_{ret} = 1.14 min, $[M+H]^+$ m/z 309.3, 95.2% purity.

HRMS (TOF ESI, formic acid): $C_{24}H_{31}N_4O_3$ $[M+H]^+$ m/z = 423.2391, found m/z = 423.2372 (Δ = -4.5 ppm).

(*E*)-6-Methoxy-2-styryl-*N*-((trimethylsilyl)methyl)imidazo[1,2-*a*]pyridin-3-amine:

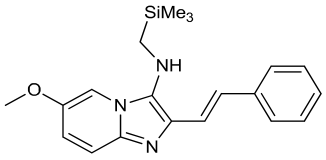

266

The reaction was performed according to **General procedure C**, using 5-methoxy-2-amino pyridine (124 mg, 1.00 mmol), cinnamaldehyde (0.252 mL, 2.00 mmol) and (isocyanomethyl)trimethylsilane (0.282 mL, 2.00 mmol) as the reaction components. Following the reaction, the crude mixture was dried *in vacuo*, before the desired product was purified by flash column chromatography using an 80 g RediSep silica cartridge, with an elution gradient from neat cyclohexane to 20% ethyl acetate in cyclohexane. The product-containing fractions were combined, and solvent was removed *in vacuo* to afford (*E*)-6-methoxy-2-styryl-*N*-((tri methylsilyl)methyl)imidazo[1,2-*a*]pyridin-3-amine (**266**, 120 mg, 0.341 mmol, 34% yield) as a cream coloured powder.

mp: 125-126 °C.

ν_{max} (neat, cm^{-1}): 3276, 2950, 1640, 1277, 839, 693.

^{1}H NMR (400 MHz, CD$_3$OD): δ 7.63 (br. d, *J* = 2.0 Hz, 1H), 7.54 (br. d, *J* = 8.1 Hz, 2H), 7.37-7.32 (m, 2H), 7.32-7.29 (m, 3H), 7.25-7.18 (m, 1H), 7.01 (dd, *J* = 9.6, 2.5 Hz, 1H), 3.86 (s, 3H), 2.61 (s, 2H), 0.16 (s, 9H).

^{13}C NMR (101 MHz, CD$_3$OD): δ 150.6, 140.1, 139.2, 134.5, 133.5, 129.7 (2C), 129.4, 128.4, 127.3 (2C), 121.2, 119.8, 117.3, 105.3, 56.7, 39.9, -2.57 (3C).

LCMS (High pH, UV, ESI): t_{ret} = 1.38 min, $[M+H]^+$ m/z 352.3. Product unstable to LCMS analysis.

HRMS (TOF ESI, formic acid): $C_{20}H_{26}N_3OSi$ $[M+H]^+$ m/z = 352.1832, found m/z = 352.1842 (Δ = 2.8 ppm).

6-Bromo-*N*-(2,4,4-trimethylpentan-2-yl)imidazo[1,2-*a*]pyridin-3-amine:

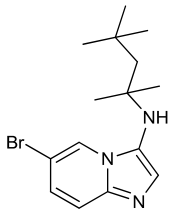

269

The scale-up synthesis of **269** was performed using the bespoke flow reactor outlined earlier (See **Section 6.1.16 Flow Reactions (GBBR work)** for more information). A stock solution of 5-bromo-2-aminopyridine (**267**, 3.46 g, 20.0 mmol) and 1,1,3,3-tetramethylbutylisocyanide (**268**, 7.01 mL, 40.0 mmol) was prepared in ethanol (100 mL total solution volume). Then, a solution of formaldehyde (**234**, 37% wt. solution in H_2O, 1.67 mL, 22.4 mmol), and 1.25 M HCl (solution in ethanol, 1.60 mL, 2.00 mmol) was prepared in ethanol (100 mL total solution volume). The bespoke flow reactor (with 2 x 10 mL loop reactors attached) was heated to 130 °C whilst pumping clean ethanol through the system at a flow rate of 0.200 mL/min/line. Once at temperature, each of the two input lines was placed into one of the two stock solutions, and the reagents were pumped at 0.200 mL/min/line. The reaction mixture was pumped to waste for 12.5 min to account for the dead volume (5 mL) in the reactor. The desired product solution was then collected for 400 min, before the input lines were changed to solvent, and the remainder of the reaction mixture was collected for 74.25 min to account for both dilution and dead volume in the reactor (189.7 mL collected in total), after which time the flow reactor was cooled and turned off. *This equates to a total of 90% of the volume of each stock solution being used in the reactor. Therefore, assuming an equal distribution within the solution, 18 mmol of the amidine reagent (1 eq.) was utilised during the reaction.* Following the reaction, a 10 µL aliquot of the crude product solution was taken and analysed according to the HPLC method described (see **procedure for attaining conversion estimates from HPLC concentration gradients**), which showed that 86% of the starting material had been consumed in the reaction. The crude mixture was dried *in vacuo*, before the desired product was purified by flash column chromatography using a 330 g RediSep silica cartridge, with an elution gradient from 40% to 60% TBME in cyclohexane. The product-containing fractions were combined, and solvent was removed *in vacuo*. The product was dissolved in acetonitrile (*c.* 20 mL) and recrystallised using an anti-solvent cold crystallisation with water. Following

filtration, 6-bromo-*N*-(2,4,4-trimethyl pentan-2-yl)imidazo[1,2-*a*]pyridin-3-amine (**269**, 4.09 g, 12.6 mmol, 70% yield) was isolated as a light brown powder.

Note: The reaction is not limited by further scalability. The starting materials and product are soluble up to at least 5 times the concentration used (0.5 M), and further modification of the flow equipment is facile for larger scale syntheses.

Preparation under batch conditions:

The reaction was performed using conditions found in the literature.[169] To a solution of 5-bromo-2-aminopyridine (**267**, 3.11 g, 18.0 mmol) and formaldehyde (**234**, 37% wt. solution in H_2O, 1.49 mL, 19.8 mmol) in a mixture of methanol (16.4 mL) and dichloromethane (32.7 mL) was added 1,1,3,3-tetramethylbutylisocyanide (**268**, 3.79 mL, 21.6 mmol) and scandium(III)trifluoromethanesulfonate (443 mg, 0.900 mmol). The reaction mixture was stirred under ambient conditions for 20 h. During the reaction, 10 µL aliquots were removed from the reaction mixture at 50 min and 20 h time points and analysed according to the HPLC method described (see **procedure for attaining conversion estimates from HPLC concentration gradients**), which showed that 65% of the starting material had been consumed in the reaction after 50 min, and 88% had been consumed after 24 h. The reaction mixture was dried *in vacuo*, and purified by flash column chromatography, using a 330 g RediSep silica cartridge, with an elution gradient from 20% to 40% ethyl acetate in cyclohexane. The product-containing fractions were combined, and solvent was removed *in vacuo* to afford 6-bromo-*N*-(2,4,4-trimethyl pentan-2-yl)imidazo[1,2-*a*]pyridin-3-amine (**269**, 3.63 g, 11.2 mmol, 62% yield) as a light brown powder.

mp: 67-68 °C.

ν_{max} (neat, cm^{-1}): 3324, 2956, 1534, 1322, 1108, 795.

^{1}H NMR (400 MHz, DMSO-*d_6*): δ 8.50-8.48 (m, 1H), 7.40 (d, *J* = 9.5 Hz, 1H), 7.14 (dd, *J* = 9.5, 1.8 Hz, 1H), 7.14 (s, 1H), 4.60 (s, 1H), 1.64 (s, 2H), 1.23 (s, 6H), 1.00 (s, 9H).

^{13}C NMR (101 MHz, DMSO-*d_6*): δ 138.5, 129.2, 124.5, 123.8, 122.8, 118.0, 105.1, 55.9, 53.0, 31.4, 31.3 (3C), 29.0 (2C).

LCMS (High pH, UV, ESI): t_{ret} = 1.39 min, $[M+H]^+$ 324.2 m/z, 100.0% purity (N62340-38-P1).

HRMS (TOF ESI, formic acid): $C_{15}H_{23}BrN_3$ $[M+H]^+$ m/z = 324.1075, found m/z = 324.1074 (Δ = -0.3 ppm). Other m/z observed with heavier isotope = 326.1076.

No analysis given in literature synthesis.[158]

6-Bromoimidazo[1,2-*a*]pyridin-3-amine:

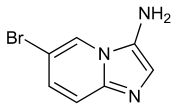

270

A solution of 6-bromo-*N*-(2,4,4-trimethylpentan-2-yl)imidazo[1,2-*a*]pyridin-3-amine **269** (4.00 g, 12.3 mmol) in 6 M HCl in isopropanol (50 mL, 300 mmol) was stirred at room temperature for 24 h under nitrogen. The reaction mixture was concentrated *in vacuo*, and the crude material was washed with diethyl ether (50 mL) and filtered. The resultant residue was dissolved in a mixture of methanol (30 mL) and water (20 mL), before being passed through an Isolute® 2 g aminopropyl cartridge, and solvent was removed *in vacuo* to afford 6-bromoimidazo[1,2-*a*]pyridin-3-amine (**270**, 2.62 g, 12.4 mmol, 100% yield) as an off-white powder.

mp: 215-216 °C (dec.).

ν_{max} (neat, cm^{-1}): 3482, 3410, 2816, 1655, 1510, 827, 772.

^{1}H NMR (400 MHz, DMSO-*d*$_6$): δ 9.00 (dd, *J* = 1.8, 1.0 Hz, 1H), 7.87-7.79 (m, 2H), 7.28 (s, 1H), 4.60 (br. s, 2H).

^{13}C NMR (101 MHz, DMSO-*d*$_6$): δ 133.4, 133.0, 132.4, 124.4, 113.2, 109.3, 102.8.

LCMS (High pH, UV, ESI): t_{ret} = 0.62 min, $[M]^-$ 210.0 m/z, 84.9% purity. Product unstable to LCMS analysis.

HRMS (TOF ESI, formic acid): $C_7H_7BrN_3$ $[M+H]^+$ m/z = 211.9823, found m/z = 211.9824 (0.5 ppm). Other m/z observed with heavier isotope = 213.9806.

8-Methoxy-2-phenyl-*N*-(2,4,4-trimethylpentan-2-yl)imidazo[1,2-*a*]pyridin-3-amine:

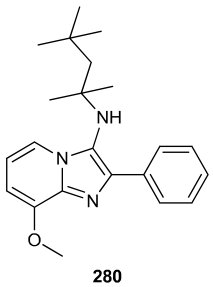

280

To a solution of 3-methoxy-2-aminopyridine (**279**, 248 mg, 2.00 mmol) and benzaldehyde (**203**, 0.407 mL, 4.00 mmol) in ethanol (10 mL) was added 1,1,3,3-tetramethylbutylisocyanide (**268**, 0.701 mL, 4.00 mmol), and then HCl in ethanol (0.0800 mL, 0.100 mmol). The reaction

was irradiated under MW conditions for 50 minutes at 130 °C. Following the reaction, the crude mixture was dried *in vacuo*, before the desired product was purified by flash column chromatography using an 80 g RediSep silica cartridge, with an elution gradient from neat cyclohexane to 65% ethyl acetate in cyclohexane. The product-containing fractions were combined, and solvent was removed *in vacuo* to afford 8-methoxy-2-phenyl-N-(2,4,4-tri methylpentan-2-yl)imidazo[1,2-*a*]pyridin-3-amine (**280**, 627 mg, 1.78 mmol, 89% yield) as a pale yellow solid.

mp: 120-121 °C.

ν_{max} (neat, cm^{-1}): 2945, 2900, 1549, 1271, 1057, 699.

^{1}H NMR (400 MHz, DMSO-*d*$_6$): δ 8.07 (br. dd, *J* = 8.3, 1.3 Hz, 2H), 8.01 (dd, *J* = 7.0, 1.0 Hz, 1H), 7.43-7.36 (m, 2H), 7.28 (tt, *J* = 7.3, 2.0 Hz, 1H), 6.78 (t, *J* = 7.3 Hz, 1H), 6.59 (dd, *J* = 7.5, 0.8 Hz, 1H), 4.38 (br. s, 1H), 3.94 (s, 3H), 1.58 (s, 2H), 0.97 (s, 9H), 0.91 (s, 6H).

^{13}C NMR (101 MHz, DMSO-*d*$_6$): δ 148.7, 138.2, 136.2, 135.8, 128.4 (2C), 128.2 (2C), 127.2, 124.9, 117.5, 111.2, 101.2, 60.3, 56.5, 56.0, 32.1 (3C), 31.7, 29.2 (2C).

LCMS (High pH, UV, ESI): t_{ret} = 1.47 min, $[M+H]^+$ m/z 352.2, 100.0% purity.

HRMS (TOF ESI, formic acid): $C_{22}H_{30}N_3O$ $[M+H]^+$ m/z = 352.2389, found m/z = 352.2385 (Δ = -1.1 ppm).

8-Methoxy-2-phenylimidazo[1,2-*a*]pyridin-3-amine:

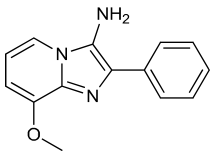

281

A solution of 8-methoxy-2-phenyl-*N*-(2,4,4-trimethylpentan-2-yl)imidazo[1,2-*a*]pyridin-3-amine (**280**, 4.00 g, 1.14 mmol) in 6 M HCl in isopropanol (5 mL, 30.0 mmol) was stirred at room temperature for 18 h under nitrogen. The reaction mixture was concentrated *in vacuo*, and the resultant material was dissolved in methanol (20 mL) and passed through an Isolute® 5 g amino propyl cartridge. Solvent was removed *in vacuo* to afford 8-methoxy-2-phenylimidazo[1,2-*a*]pyridin-3-amine (**281**, 272 mg, 1.14 mmol, 100% yield) as a cream coloured solid.

mp: 142-143 °C (melted and recrystallised), 202-203 °C (dec.).

ν_{max} (neat, cm^{-1}): 3300, 3144, 1572, 1291, 1052, 763.

^{1}H NMR (400 MHz, CD_3OD): δ 8.24 (dd, *J* = 6.7, 0.9 Hz, 1H), 7.85-7.80 (m, 2H), 7.60-7.55 (m, 2H), 7.49 (tt, *J* = 7.5, 1.3 Hz, 1H), 7.38 (dd, *J* = 6.8, 7.8 Hz, 1H), 7.31 (dd, *J* = 8.0, 0.8 Hz, 1H), 4.17 (s, 3H).

^{13}C NMR (101 MHz, CD_3OD): δ 146.4, 131.3, 130.3 (3C), 129.6, 128.7 (2C), 128.5, 120.0, 117.8, 117.6, 109.6, 57.6.

LCMS (Low pH, UV, ESI): t_{ret} = 0.42 min, $[M+H]^+$ m/z 240.1, 100.0% purity.

HRMS (TOF ESI, formic acid): $C_{14}H_{14}N_3O$ $[M+H]^+$ m/z = 240.1137, found m/z = 240.1132 (Δ = -2.1 ppm).

6-Cyclopropylimidazo[2,1-*b*]thiazol-5-amine:

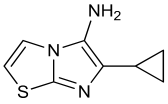

283

A solution of 6-cyclopropyl-*N*-(2,4,4-trimethylpentan-2-yl)imidazo[2,1-b] thiazol-5-amine-3-amine (**244**, 230 mg, 0.789 mmol) in 6 M HCl in isopropanol (3 mL, 18.0 mmol) was stirred at 50 °C for 72 h under nitrogen. The reaction mixture was concentrated *in vacuo*, and to the resultant residue was added diethyl ether (20 mL). The mixture was then filtered, and the precipitate was dissolved in methanol (20 mL) and passed through an Isolute® 5 g amino propyl cartridge. Solvent was removed *in vacuo* to afford a crude product mixture containing 6-cyclopropylimidazo[2,1-*b*]thiazol-5-amine (**283**, 115 mg, 0.642 mmol, 81% yield (*c.* 90% purity (NMR)). The product was not isolated in sufficient purity for analysis and was taken on without further purification.

Phenyliodine(III)di(pent-4-ynoate):

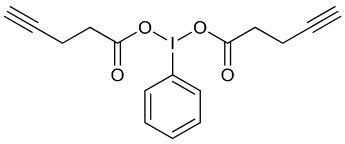

285

The reaction was performed using conditions found in the literature.[175]

To a solution of (diacetoxyiodo)benzene (**284**, 985 mg, 3.06 mmol) in toluene (50 mL) was added pent-4-ynoic acid (600 mg, 6.12 mmol). The flask was attached to a rotary evaporator and heated to 55 °C under vacuum. This process was repeated 4 times, by sequential additions of toluene (20 mL) following each drying cycle for a total reaction time of ~1 h. After

the fourth addition of toluene, the reaction mixture was dried *in vacuo* to afford bis(pent-4-ynoic-acetoxy)iodobenzene (**285**, 1.18 g, 2.96 mmol, 97% yield) as a white powder.

mp: 118-119 °C.

ν_{max} (neat, cm^{-1}): 3291, 1658, 1371, 1292, 1197, 743, 709.

^{1}H NMR (400 MHz, $CDCl_3$): δ 8.11-8.07 (m, 2H), 7.59 (tt, *J* = 7.3, 1.3 Hz, 1H), 7.52-7.47 (m, 2H), 2.52-2.47 (m, 4H), 2.45-2.40 (m, 4H), 1.95 (t, *J* = 2.5 Hz, 2H).

^{13}C NMR (101 MHz, $CDCl_3$): δ 176.5 (2C), 134.9 (2C), 131.8 (2C), 131.0, 121.9, 82.9 (2C), 68.8 (2C), 33.0 (2C), 15.1 (2C).

LCMS: Product unstable to LCMS analysis. No ionisation observed.

HRMS: Product unstable to HRMS analysis. No ionisation observed.

(*E*)-3-Phenylprop-2-enenitrile:

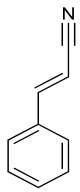

292

To a mixture of 2-aminopyridine (**202**, 188 mg, 2.00 mmol) and sodium sulfate (*c.* 200 mg) was added benzaldehyde (**203**, 203 µL, 2.00 mmol). The reaction vial was sealed, evacuated under vacuum, and filled with nitrogen, before anhydrous acetonitrile (5 mL) was added and the reaction mixture was stirred under ambient conditions for 30 min. In a separate vial, to a nitrogen-purged mixture of trimethylsulfonium bromide (**291**, 314 mg, 2.00 mmol) and potassium *tert*-butoxide (224 mg, 2.00 mmol) was added anhydrous acetonitrile (5 mL) at 0 °C, and the reaction mixture was stirred for 10 min. The vials were opened, and the contents of the second vial were added to the first. The reaction mixture was heated to 50 °C for 18 h. The crude reaction mixture was dried *in vacuo*, and partitioned between DCM (20 mL), and water (20 mL). The organic layer was collected, and the aqueous layer was extracted with DCM (2 x 20 mL). The organic layers were combined and passed through an Isolute® hydrophobic fritted reservoir (70 mL volume). Solvent was removed *in vacuo* to afford (*E*)-3-phenylprop-2-enenitrile (**292**, 30.0 mg, 0.232 mmol, 12% yield) as a colourless oil.

ν_{max} (neat, cm^{-1}): 3054, 2216, 1617, 964, 746, 685.

^{1}H NMR (600 MHz, $CDCl_3$): δ 7.47-7.37 (m, 6H), 5.88 (d, *J* = 16.9 Hz, 1H).

^{13}C NMR (151 MHz, $CDCl_3$): δ 150.5, 133.5, 131.2, 129.1 (2C), 127.3 (2C), 118.1, 96.3.

LCMS (High pH, UV, ESI): t_{ret} = 0.96 min, 100.0% purity, mass ion not observed.

HRMS (TOF ESI, formic acid): C_9H_8N $[M+H]^+$ m/z = 130.0657, found m/z = 130.0653 (Δ = -3.1 ppm).

Spectroscopic data is in accordance with that reported in the literature.[286]

***N*-(*tert*-Butyl)-2-(*1H*-pyrazol-1-yl)imidazo[1,2-*a*]pyridin-3-amine:**

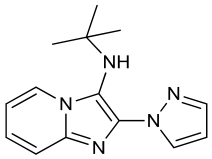

309

Synthesis using photoredox catalysis:

The reaction was performed using conditions found in the literature.[177]

To a 3 mL vial was added *N*-(*tert* butyl)imidazo[1,2-*a*]pyridin-3-amine (**235**, 57 mg, 0.300 mmol), 1H-pyrazole (**312**, 40.8 mg, 0.600 mmol), TEMPO (**314**, 9.38 mg, 0.0600 mmol) and 9-mesityl-3, 6-di-*tert*-butyl-10-phenylacridiniumtetrafluoroborate (**302**, 8.60 mg, 0.0150 mmol) in EDC (3 mL). The resultant bronze solution was heated, with stirring to 50 °C, and irradiated between two A160WE tuna blue polychromatic (350-600 nm) Kessil lamps, whilst using an accompanying cooling fan for 24 h. Solvent was removed *in vacuo* to afford a crude product which was purified by flash column chromatography on a 40 g RediSep silica cartridge, using an eluent gradient from 10% to 30% ethyl acetate in cyclohexane. Product-containing fractions were combined, and solvent was removed *in vacuo* to afford *N*-(*tert*-butyl)-2-(*1H*-pyrazol-1-yl)imidazo[1,2-*a*]pyridin-3-amine (**309**, 15.0 mg, 59 µmol, 20% yield) as a white crystalline solid.

Synthesis under thermal conditions (in the dark):

To a solution of *N*-(*tert*-butyl)imidazo[1,2-*a*]pyridin-3-amine (**235**, 57 mg, 0.300 mmol), *1H*-pyrazole (**312**, 40.8 mg, 0.600 mmol) and TEMPO (**314**, 9.38 mg, 0.0600 mmol) in EDC (3 mL) was added 9-mesityl-3,6-di-*tert*-butyl-10-phenylacridinium tetrafluoroborate (**302**, 8.60 mg, 0.015 mmol). The vial was sealed, and heated, in the dark at 120 °C for 24 h. Solvent removal *in vacuo* afforded a crude brown oil, which was purified by flash column chromatography, on a 40 g RediSep silica cartridge, using an eluent gradient from 10% to 30% ethyl acetate in cyclohexane. Product-containing fractions were combined, and solvent

was removed *in vacuo* to afford *N*-(*tert*-butyl)-2-(*1H*-pyrazol-1-yl)imidazo[1,2-*a*] pyridin-3-amine (**309**, 12.0 mg, 47 µmol, 16% yield) as a white crystalline solid.

mp: 101-102 °C (dec.).

ν_{max} (neat, cm^{-1}): 3332, 2971, 1596, 1402, 1049, 749.

^{1}H NMR (400 MHz, $CDCl_3$): δ 8.31 (dt, *J* = 6.8, 1.2 Hz, 1H), 8.21 (dd, *J* = 2.5, 0.8 Hz, 1H), 7.70 (dd, *J* = 1.8, 0.8 Hz, 1H), 7.49 (dt, *J* = 9.0, 1.3 Hz, 1H), 7.17 (ddd, *J* = 9.0, 6.8, 1.3 Hz, 1H), 6.82 (td, *J* = 7.0, 1.0 Hz, 1H), 6.44 (dd, *J* = 2.5, 1.8 Hz, 1H), 1.04 (s, 9H). NH peak not observed.

^{13}C NMR (101 MHz, $CDCl_3$): δ 140.5, 139.3, 136.4, 128.6, 124.3, 123.9, 117.8, 116.8, 111.7, 106.6, 56.3, 29.4 (3C).

LCMS (High pH, UV, ESI): t_{ret} = 1.07 min, $[M+H]^+$ m/z 256.2, 100.0% purity.

HRMS (TOF ESI, formic acid): $C_{14}H_{18}N_5$ $[M+H]^+$ m/z = 256.1562, found m/z = 256.1556 (Δ = -2.3 ppm).

6.3 Experimental – Chapter 2: A telescoped, continuous flow synthesis of diaminoquinazoline antimalarials

6.3.1 General synthetic procedures for Chapter 2

6.3.1.1 General procedure E: Use of Electrothermal® STEM Integrity 10™ machine in substitution reactions:

For each reaction: to an Electrothermal® Integrity 10™ small volume (3 mL) reaction tube was added 2,4-dichloro-8-methylquinazoline (**349**, either **(a)** 43 mg, 0.200 mmol, or **(b)** 86 mg, 0.400 mmol) and base (either **(c)** 0.1 eq., **(d)** 0.5 eq. or **(e)** 1 eq. of **(f)** triethylamine **(g)** DBU, **(h)** 4-DMAP, **(i)** KO^{t}Bu or **(j)** BTTP; or no base was added **(k)**. To the resultant solution was added either **(l)** 1-propylamine (**380**), **(m)** propane-1-thiol (**381**) or **(n)** 1-propanol (**382**) in 1 eq. with respect to **347**. The reaction was then heated to the stated temperature **(o)** for either **(p)** 5 min or **(q)** 15 min with a stirring rate of 500 rpm, before an aliquot was removed, and the reaction mixture was analysed by LCMS. The conversion observed in each reaction is provided by **(r)**. % composition of LCMS mixture which is not related to the starting materials or the desired product is given by **(s)** (if mentioned within the associated table within the text). The products were not isolated. The conditions used for each reaction are stated below.

Table 5.1, Entry 1: (b), **(d)**, **(f)** 28 µL, 0.200 mmol, **(l)** 33 µL, 0.400 mmol, **(o)** 70 °C, **(p)**, **(r)** 71%, **(s)** N/a.

Table 5.1, Entry 2: (b), **(d)**, **(g)** 30 µL, 0.200 mmol, **(l)** 33 µL, 0.400 mmol, **(o)** 70 °C, **(p)**, **(r)** 78%, **(s)** 2%.

Table 5.1, Entry 3: (b), **(d)**, **(h)** 24 mg, 0.200 mmol, **(l)** 33 µL, 0.400 mmol, **(o)** 70 °C, **(p)**, **(r)** 90%, **(s)** 53%.

Table 5.1, Entry 4: (b), **(d)**, **(i)** 22 mg, 0.200 mmol, **(l)** 33 µL, 0.400 mmol, **(o)** 70 °C, **(p)**, **(r)** 66% , **(s)** 4%.

Table 5.1, Entry 5: (b), **(d)**, **(f)** 28 µL, 0.200 mmol, **(l)** 33 µL, 0.400 mmol, **(o)** 80 °C, **(p)**, **(r)** 68%, **(s)** N/a.

Table 5.1, Entry 6: (b), **(d)**, **(f)** 28 µL, 0.200 mmol, **(l)** 33 µL, 0.400 mmol, **(o)** 90 °C, **(p)**, **(r)** 58%, **(s)** N/a.

Table 5.1, Entry 7: (b), **(d)**, **(f)** 28 µL, 0.200 mmol, **(l)** 33 µL, 0.400 mmol, **(o)** 100 °C, **(p)**, **(r)** 57%, **(s)** 1%.

Table 5.1, Entry 8: (b), **(k)**, **(l)** 33 µL, 0.400 mmol, **(o)** 70 °C, **(p)**, **(r)** 54%, **(s)** N/a.

Table 5.1, Entry 9: (b), **(c)**, **(f)** 6 µL, 40 µmol, **(l)** 33 µL, 0.400 mmol, **(o)** 70 °C, **(p)**, **(r)** 45%, **(s)** N/a.

Table 5.1, Entry 10: (b), **(e)**, **(f)** 56 µL, 0.400 mmol, **(l)** 33 µL, 0.400 mmol, **(o)** 70 °C, **(p)**, **(r)** 85%, **(s)** N/a.

Table 5.2, Entry 1: (a), **(e)**, **(f)** 28 µL, 0.200 mmol, **(l)** 16 µL, 0.200 mmol, **(o)** 90 °C, **(p)**, **(r)** 98%, **(s)** N/a.

Table 5.2, Entry 2: (a), **(e)**, **(f)** 28 µL, 0.200 mmol, **(l)** 16 µL, 0.200 mmol, **(o)** 100 °C, **(p)**, **(r)** 98%, **(s)** N/a.

Table 5.2, Entry 3: (a), **(e)**, **(f)** 28 µL, 0.200 mmol, **(l)** 16 µL, 0.200 mmol, **(o)** 110 °C, **(p)**, **(r)** 97%, **(s)** N/a.

Table 5.2, Entry 4: (a), **(e)**, **(f)** 28 µL, 0.200 mmol, **(l)** 16 µL, 0.200 mmol, **(o)** 120 °C, **(p)**, **(r)** 98%, **(s)** N/a.

Table 5.2, Entry 5: (a), **(e)**, **(f)** 28 µL, 0.200 mmol, **(l)** 16 µL, 0.200 mmol, **(o)** 130 °C, **(p)**, **(r)** 98%, **(s)** N/a.

Table 5.3, Entry 1: (a), **(e)**, **(f)** 28 µL, 0.200 mmol, **(m)** 19 µL, 0.200 mmol, **(o)** 20 °C, **(p)**, **(r)** 90%.

Table 5.3, Entry 2: (a), **(e)**, **(f)** 28 µL, 0.200 mmol, **(m)** 19 µL, 0.200 mmol, **(o)** 30 °C, **(p)**, **(r)** 89%.

Table 5.3, Entry 3: (a), **(e)**, **(f)** 28 µL, 0.200 mmol, **(m)** 19 µL, 0.200 mmol, **(o)** 40 °C, **(p)**, **(r)** 98%.

Table 5.3, Entry 4: (a), **(e)**, **(f)** 28 µL, 0.200 mmol, **(m)** 19 µL, 0.200 mmol, **(o)** 50 °C, **(p)**, **(r)** 98%.

Table 5.3, Entry 5: (a), **(e)**, **(f)** 28 µL, 0.200 mmol, **(m)** 19 µL, 0.200 mmol, **(o)** 60 °C, **(p)**, **(r)** 89%.

Table 5.4, Entries 1-5 all involved the addition of a further 1 eq. of **(f)** and **(n)** to the preceding product solutions obtained from reactions reported in **Table 5.3**. Each reaction tube was subsequently heated to the temperature shown in **Table 5.4** for 15 min, before an aliquot was removed and analysed by LCMS. **Entries 1-4** exhibited no conversion to the desired product. A conversion of 4% was observed in **Entry 5**.

Table 5.5, Entry 1: (a), **(e)**, **(f)** 28 µL, 0.200 mmol, **(n)** 15 µL, 0.200 mmol, **(o)** 80 °C, **(p)**, **(r)** No conversion observed, **(s)** 17%.

Table 5.5, Entry 2: (a), **(e)**, **(f)** 28 µL, 0.200 mmol, **(n)** 15 µL, 0.200 mmol, **(o)** 90 °C, **(p)**, **(r)** No conversion observed, **(s)** 39%.

Table 5.5, Entry 3: (a), **(e)**, **(f)** 28 µL, 0.200 mmol, **(n)** 15 µL, 0.200 mmol, **(o)** 100 °C, **(p)**, **(r)** No conversion observed, **(s)** 39%.

Table 5.5, Entry 4: (a), **(e)**, **(f)** 28 µL, 0.200 mmol, **(n)** 15 µL, 0.200 mmol, **(o)** 110 °C, **(p)**, **(r)** No conversion observed, **(s)** 41%.

Table 5.5, Entry 5: (a), **(e)**, **(g)** 30 µL, 0.200 mmol, **(n)** 15 µL, 0.200 mmol, **(o)** 90 °C, **(p)**, **(r)** 5%, **(s)** 55%.

Table 5.5, Entry 6: (a), **(e)**, **(g)** 30 µL, 0.200 mmol, **(n)** 15 µL, 0.200 mmol, **(o)** 110 °C, **(p)**, **(r)** 6%, **(s)** 72%.

Table 5.5, Entry 7: (a), **(e)**, **(g)** 30 µL, 0.200 mmol, **(n)** 15 µL, 0.200 mmol, **(o)** 130 °C, **(p)**, **(r)** 6%, **(s)** 78%.

Table 5.5, Entry 8: (a), **(e)**, **(g)** 30 µL, 0.200 mmol, **(n)** 15 µL, 0.200 mmol, **(o)** 150 °C, **(p)**, **(r)** 7%, **(s)** 89%.

Table 5.5, Entry 9: (a), **(e)**, **(j)** 61 µL, 0.200 mmol, **(n)** 15 µL, 0.200 mmol, **(o)** 50 °C, **(p)**, **(r)** 26%, **(s)** 19%.

Table 5.5, Entry 10: (a), **(e)**, **(j)** 61 µL, 0.200 mmol, **(n)** 15 µL, 0.200 mmol, **(o)** 60 °C, **(p)**, **(r)** 25%, **(s)** 26%.

Table 5.5, Entry 11: (a), **(e)**, **(j)** 61 µL, 0.200 mmol, **(n)** 15 µL, 0.200 mmol, **(o)** 70 °C, **(p)**, **(r)** 24%, **(s)** 18%.

Table 5.5, Entry 12: (a), **(e)**, **(j)** 61 µL, 0.200 mmol, **(n)** 15 µL, 0.200 mmol, **(o)** 80 °C, **(p)**, **(r)** 22%, **(s)** 27%.

Table 5.5, Entry 13: (a), **(e)**, **(j)** 61 µL, 0.200 mmol, **(n)** 15 µL, 0.200 mmol, **(o)** 90 °C, **(p)**, **(r)** 26%, **(s)** 24%.

Table 5.5, Entry 14: (a), **(e)**, **(j)** 61 µL, 0.200 mmol, **(n)** 15 µL, 0.200 mmol, **(o)** 50 °C, **(q)**, **(r)** 27%, **(s)** 14%.

Table 5.5, Entry 15: (a), **(e)**, **(j)** 61 µL, 0.200 mmol, **(n)** 15 µL, 0.200 mmol, **(o)** 110 °C, **(p)**, **(r)** 27%, **(s)** 38%.

Table 5.5, Entry 16: (a), **(e)**, **(j)** 61 µL, 0.200 mmol, **(n)** 15 µL, 0.200 mmol, **(o)** 120 °C, **(p)**, **(r)** 21%, **(s)** 47%.

Table 5.5, Entry 17: (a), **(e)**, **(j)** 61 µL, 0.200 mmol, **(n)** 15 µL, 0.200 mmol, **(o)** 130 °C, **(p)**, **(r)** 16%, **(s)** 58%.

Table 5.5, Entry 18: (a), **(e)**, **(j)** 61 µL, 0.200 mmol, **(n)** 15 µL, 0.200 mmol, **(o)** 140 °C, **(p)**, **(r)** 20%, **(s)** 68%.

Table 5.5, Entry 19: (a), **(e)**, **(j)** 61 µL, 0.200 mmol, **(n)** 15 µL, 0.200 mmol, **(o)** 150 °C, **(p)**, **(r)** 20%, **(s)** 77%.

6.3.1.2 General procedure F (use of the Buchwald-Hartwig screening plate):

Using the prepared Buchwald-Hartwig screening plate shown in **Section 7.9 Appendix 9 – Buchwald-Hartwig screening plate procedure**, the following procedure was used in attempting metal catalysed N, O and S-arylation procedures.

In a glovebox, a solution of 2-chloro-*N*-propylquinazolin-4-amine (**389**, 27 mg, 0.120 mmol) and the nucleophile (denoted as **(a)**) was dissolved in 960 µL DMSO or 1-butyl-2-pyrrolidinone (Tamisolve®). Two basic solutions were also prepared, in each case containing 0.240 or 0.360 mmol of the base (base 1, used for vials A1-B6, denoted as **(b1)** or base 2, used for vials C1-D6, denoted as **(b2)**) in 240 µL DMSO or 1-butyl-2-pyrrolidinone (Tamisolve®). In all cases, 0.1 M reactions were used with respect to the 2-chloro-*N*-propylquinazolin-4-amine (**389**) starting material, and a catalyst loading of 10 mol% was used for the palladium precatalyst complexes.

80 µL of the reagent solution was then added to vials A1 to D6. Of the solution containing **(b1)**, 20 µL was added to each of the vials A1-B6. The same process was repeated for the **(b2)** solution to each of the vials C1-D6.

The plate was sealed in the glove box and heated on a stirrer hotplate at 100 °C for a time point as denoted by **(c)**.

After cooling, 500 µL of a quench solution of 0.2 mM triphenylamine in acetonitrile:DMSO (3:1) was added to each vial. A 25 µL aliquot was then removed from each vial and diluted in 750 µL acetonitrile. LCMS analysis of the reaction composition then provided the conversion data for the reactions. The triphenylamine added in the neutral quench was used as the internal standard in each case. See **Section 7.10 Appendix 10 – Buchwald-Hartwig screening plate LCMS profiles** for the data from the plates.

6.3.1.3 General procedure G (tandem flow synthesis of diaminoquinazolines):

Using the bespoke flow reactor setup shown in **Figures 6.6-6.9**, the following general process was used for the synthesis of diaminoquinazoline targets through a double S_NAr procedure.

A solution of 2,4-dichloro-8-methylquinazoline (**349**, 85 mg, 0.400 mmol), tributylamine (**273**, amount denoted by **(a)**) and the first nucleophile (denoted as **(b)**) was made up in 1-butyl-2-pyrrolidinone (Tamisolve®, 2 mL total volume). This solution was pumped through the first reactor (heated at 90 °C) at a flow rate of 42.0 µL/min. Meanwhile, a second solution was made up, containing tributylamine (**273**, amount denoted by **(c)**) and the second nucleophile (denoted by **(d)**) and) in Tamisolve® (2 mL total volume). After 10 min 9 s reaction time, the second solution was pumped into the reactor using the other line at the same flow rate (42.0 µL/min) for the two streams to converge after the T-piece after 18 min 44 s total reaction time.

The materials were then pumped through the rest of the reactor, including a second heated reactor (held at either 200 °C or 210 °C, as denoted by **(e)**) at a combined flow rate of 84.0 µL/min for another 24 min 59 s (43 min 43 s total reaction time). After which time, the pumps were temporarily stopped, and their input lines were placed into clean Tamisolve®, which was pumped into the reactor at the same flow rate (42.0 µL/min/line). The crude product solution was collected in a HPLC vial for analysis for a length of time denoted by **(f)** in each case, and this material was diluted in Tamisolve® (~500 µL) and analysed by LCMS analysis, using the pH method denoted by **(g)**.

Thereafter, the remaining crude product solution was collected in 3 x 1 mL vials suitable for array MDAP purification (3 x 11 min 54 s collection time, 35 min 42 s total). Finally, the reactors were cooled as clean solvent was continually pumped through the system to waste for a further 5 min before the pumps were switched off.

The crude product solutions were then purified using either MDAP or array MDAP isolations, using the optimal method determined from the sampled aliquot. The purification method used in each case is denoted by **(h)**. Product-containing fractions were combined, and solvent was removed under a stream of nitrogen to afford the title compound in an appearance and yield as denoted by **(i)**.

6.3.2 Specific synthetic procedures for Chapter 2

8-Methylquinazoline-2,4(*1H*,*3H*)-dione:

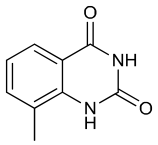

348

The reaction was performed using conditions found in the literature.[287]

To 2-amino-3-methylbenzoic acid (**347**, 7.50 g, 49.6 mmol) was added urea (29.8 g, 496 mmol). The mixture was heated neat, with stirring, to reflux (160 °C) for 6 h. The reaction was cooled to 100 °C, water (20 mL) was added, and the heterogenous solution was stirred for 5 min. The mixture was filtered, and the filter cake was washed with water (10 mL). The resultant brown precipitate was suspended in 0.5 M aq. sodium hydroxide solution (120 mL). Concentrated hydrochloric acid was added until pH 2 (*c.* 15 mL added). The suspension was filtered, and the resultant precipitate was washed with water:methanol (1:1) solution (20 mL). Following drying under vacuum, 8-methylquinazoline-2,4(*1H*,*3H*)-dione (**348**, 6.72 g, 38.1 mmol, 77% yield) was afforded as a white-grey powder.

mp: 269-270 °C (dec.; lit.[288] > 250 °C).

ν_{max} (neat, cm^{-1}): 3512, 3422, 3017, 1714, 1684, 1417, 751.

^{1}H NMR (400 MHz, DMSO-*d*$_6$): δ 11.30 (s, 1H), 10.37 (s, 1H), 7.77 (d, *J* = 7.8 Hz, 1H), 7.51-7.44 (m, 1H), 7.09 (t, *J* = 7.6 Hz, 1H), 2.34 (s, 3H).

^{13}C NMR (101 MHz, DMSO-*d*$_6$): δ 163.4, 150.9, 139.7, 136.4, 125.2, 124.5, 122.5, 115.0, 17.6.

LCMS (High pH, UV, ESI): t_{ret} = 0.59 min, $[M]^-$ m/z 175.1, 100.0% purity.

HRMS (TOF ESI, formic acid): $C_9H_9N_2O_2$ $[M+H]^+$ m/z = 177.0664, found m/z = 177.0672 (Δ = 4.5 ppm).

Spectroscopic data is in accordance with that reported in the literature.[288]

The product was synthesised a further three times under similar conditions, with yields of 71% (52.9 mmol scale), 79% (20.3 mmol scale) and 86% (49.6 mmol scale).

2,4-Dichloro-8-methylquinazoline:

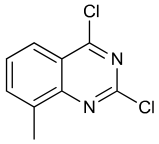

349

The reaction was performed using conditions found in the literature.[289]

8-Methylquinazoline-2,4(*1H*,*3H*)-dione (**348**, 5.00 g, 28.4 mmol) was dissolved in phosphoryl trichloride (60.0 mL, 644 mmol), and the mixture was heated, with stirring to 130 °C for 20 h. Toluene (20 mL) was added, and the reaction mixture was dried *in vacuo*. This process was repeated three times, after which the resultant residue was dissolved in ethyl acetate (50 mL) and triethylamine (10 mL) was added. The reaction mixture was stirred for 5 min. The reaction mixture was washed with water (20 mL), and the organic phase was collected. The aqueous phase was extracted with ethyl acetate (2 x 20 mL), and the organic phases were combined, washed with sat. aq. brine solution (20 mL) and passed through an Isolute® hydrophobic fritted reservoir (70 mL volume). Solvent was removed *in vacuo* to afford 2,4-dichloro-8-methylquinazoline (**349**, 4.97 g, 23.3 mmol, 82% yield) as a white powder.

mp: 139-140 °C.

ν_{max} (neat, cm^{-1}): 1543, 1445, 1328, 1270, 1144, 881, 766.

^{1}H NMR (400 MHz, $CDCl_3$): δ 8.14-8.10 (m, 1H), 7.87-7.79 (m, 1H), 7.63 (dd, *J* = 8.5, 7.3 Hz, 1H), 2.77 (s, 3H).

^{13}C NMR (101 MHz, $CDCl_3$): δ 163.4, 150.9, 139.7, 136.4, 125.2, 124.5, 122.5, 115.0, 17.6.

LCMS (High pH, UV, ESI): t_{ret} = 1.28 min, 96.9% purity, mass ion not observed.

HRMS (TOF ESI, single mass analysis): $C_9H_7Cl_2N_2$ $[M+H]^+$ m/z = 212.9986, found m/z = 212.9991 (Δ = 2.3 ppm). Other m/z observed with heavier isotopes = 214.9904, 216.9937.

Spectroscopic data is in accordance with that reported in the literature.[290]

The product was synthesised a further four times under similar conditions, with yields of 34% (12.8 mmol scale), 47% (14.2 mmol scale), 65% (22.7 mmol scale) and 87% (14.2 mmol scale).

2-Amino-5-iodo-3-methylbenzoic acid:

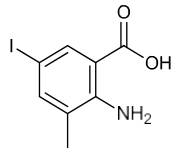

350

To a solution of 2-amino-3-methylbenzoic acid (**347**, 5 g, 33.1 mmol) in DMF (30 mL) was added *N*-iodosuccinimide (8.93 g, 39.7 mmol). The reaction mixture was heated, with stirring, to 70 °C for 2 h. The reaction mixture was concentrated under reduced pressure, suspended in water (20 mL) and filtered. Following drying, 2-amino-5-iodo-3-methylbenzoic acid (**350**, 8.82 g, 31.8 mmol, 96% yield) was afforded as a dark brown powder.

mp: 190-191 °C.

ν_{max} (neat, cm^{-1}): 3505, 3373, 1664, 1562, 1224, 681.

^{1}H NMR (400 MHz, DMSO-*d*$_6$): δ 7.86 (d, *J* = 2.4 Hz, 1H), 7.46-7.43 (m, 1H), 2.08 (s, 3H).

^{13}C NMR (101 MHz, DMSO-*d*$_6$): δ 168.7, 149.3, 141.6, 136.7, 126.4, 111.7, 74.4, 17.0.

LCMS (High pH, UV, ESI): t_{ret} = 0.62 min, $[M]^-$ m/z 275.9, 94.1% purity.

HRMS (TOF ESI, formic acid): $C_8H_9INO_2$ $[M+H]^+$ m/z = 277.9678, found m/z = 277.9683 (Δ = 1.8 ppm).

The product was not purified further, used directly in the next reaction.

Spectroscopic data is in accordance with that reported in the literature.[291]

The product was synthesised a further four times under similar conditions, with yields of 95% (3.31 mmol scale), 95% (6.62 mmol scale), 96% (3.31 mmol scale) and 98% (16.5 mmol scale).

6-Iodo-8-methylquinazoline-2,4(*1H*,*3H*)-dione:

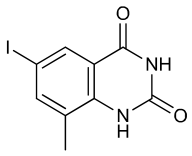

351

2-Amino-5-iodo-3-methylbenzoic acid (**350**, 800 mg, 2.89 mmol) and urea (1.73 g, 28.9 mmol) were combined, and heated, with stirring, to 160 °C under a nitrogen atmosphere for 16 h. The reaction mixture was cooled to 100 °C, and water (25 mL) was added. The reaction mixture

was stirred for 5 min. The heterogenous mixture was filtered, and the filter cake was washed with water (10 mL). The formed precipitate was then suspended in 0.5 M aq. NaOH solution (10 mL) and heated, with stirring, to reflux for 5 min. After cooling, the reaction mixture was acidified with concentrated HCl until pH 2 (*c.* 2 mL), and the precipitate was filtered, and the filter cake washed with a solution of water:methanol (10 mL; 1:1). The product was dried *in vacuo* to afford 6-iodo-8-methylquinazoline-2,4(*1H*,*3H*)-dione (**351**, 664 mg, 2.20 mmol, 76% yield) as brown flakes.

mp: Product stable up to 300 °C.

ν_{max} (neat, cm^{-1}): 3173, 3055, 1681, 1373, 761, 509, 474.

^{1}H NMR (400 MHz, DMSO-*d*$_6$): δ 11.43 (s, 1H), 10.50 (s, 1H), 7.99 (d, *J* = 2.0 Hz, 1H), 7.83-7.78 (m, 1H), 2.31 (s, 3H).

^{13}C NMR (101 MHz, DMSO-*d*$_6$): δ 161.6, 150.2, 143.4, 139.0, 132.6, 127.1, 116.5, 85.0, 16.7.

LCMS (High pH, UV, ESI): t_{ret} = 0.77 min, $[M]^-$ m/z 301.0, 95.9% purity.

HRMS (TOF ESI, formic acid): $C_9H_8IN_2O_2$ $[M+H]^+$ m/z = 302.9630, found m/z = 302.9633 (Δ = 1.0 ppm).

The product was synthesised on one other occasion under similar conditions, with a yield of 70% (21.7 mmol scale).

2,4-Dichloro-6-iodo-8-methylquinazoline:

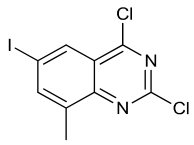

352

The reaction was performed using conditions found in the literature.[292]

To a mixture of 6-iodo-8-methylquinazoline-2,4(*1H*,*3H*)-dione (**351**, 1 g, 3.31 mmol) and DIPEA (**272**, 1.15 mL, 6.62 mmol) was added phosphoryl trichloride (4.00 mL, 42.9 mmol). The vial was sealed, and irradiated, with stirring, to 130 °C for 3 h in the MW reactor. After cooling, the reaction mixture was cautiously poured over crushed ice (50 g) and stirred vigorously for 5 minutes. The mixture was then separated into DCM (50 mL), and the aqueous layer was extracted with DCM (2 x 20 mL). The organic layers were combined, washed with brine (20 mL) and solvent was removed *in vacuo* to afford 2,4-dichloro-6-iodo-8-methyl quinazoline (**352**, 818 mg, 2.41 mmol, 73% yield) as a dark brown powder.

mp: 167-168 °C.

ν_{max} (neat, cm^{-1}): 1533, 1392, 1157, 858, 825, 789.

^{1}H NMR (400 MHz, $CDCl_3$): δ 8.47 (br. d, *J* = 2.0 Hz, 1H), 8.12-8.09 (m, 1H), 2.70 (s, 3H).

^{13}C NMR (101 MHz, $CDCl_3$): δ 162.5, 154.5, 150.9, 144.5, 139.0, 132.4, 123.7, 94.5, 16.9.

LCMS (Low pH, UV, ESI): t_{ret} = 1.43 min, $[M+H]^+$ m/z 338.7, 92.5% purity. Product unstable to LCMS analysis.

HRMS: Product unstable to LC-HRMS analysis.

(*trans*)-4-(Dibenzylamino)cyclohexanol:

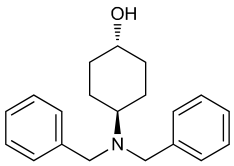

354

To a mixture of (*trans*)-4-(amino)cyclohexan-1-ol (**353**, 2.89 mL, 26.0 mmol) and potassium carbonate (18.0 g, 130 mmol) in acetonitrile (150 mL) was added benzyl bromide (6.82 mL, 57.3 mmol). The reaction mixture was heated, with stirring to 70 °C for 12 h. The crude reaction mixture was filtered, and the filter cake was washed with acetonitrile (10 mL). The filtrate was concentrated *in vacuo* and the crude product was purified by flash column chromatography on a 330 g RediSep silica cartridge using an eluent gradient from 10% to 30% ethyl acetate in cyclohexane. The product-containing fractions were combined, and solvent was removed *in vacuo* to afford (*trans*)-4-(dibenzylamino)cyclohexan-1-ol (**354**, 4.07 g, 13.8 mmol, 53% yield) as white flakes.

mp: 109-110 °C.

ν_{max} (neat, cm^{-1}): 3257, 2931, 1493, 1452, 1060, 737, 695.

^{1}H NMR (400 MHz, $CDCl_3$): δ 7.35 (br. d, *J* = 7.3 Hz, 4H), 7.30-7.25 (m, 4H), 7.20 (tt, *J* = 7.3, 1.5 Hz, 2H), 3.61 (s, 4H), 3.53 (tt, *J* = 10.8, 4.4 Hz, 1H), 2.52 (tt, *J* = 11.9, 3.5 Hz, 1H), 2.03-1.95 (m, 2H), 1.92-1.86 (m, 2H), 1.48-1.37 (m, 3H), 1.24-1.13 (m, 2H).

^{13}C NMR (101 MHz, $CDCl_3$): δ 140.1 (2C), 128.4 (4C), 128.1 (4C), 126.6 (2C), 70.9, 56.9, 54.1 (2C), 35.0 (2C), 26.0 (2C).

LCMS (High pH, UV, ESI): t_{ret} = 1.34 min, $[M+H]^+$ m/z 296.2, 100.0% purity.

HRMS (TOF ESI, formic acid): $C_{20}H_{26}NO$ $[M+H]^+$ m/z = 296.2014, found m/z = 296.2018 (Δ = 1.4 ppm).

Spectroscopic data is in accordance with that reported in the literature.[293]

The product was synthesised a further two times under similar conditions, with yields of 40% (17.4 mmol scale) and 60% (65.1 mmol scale).

(*trans*)-*N*,*N*-Dibenzyl-4-(2-methoxyethoxy)cyclohexanamine:

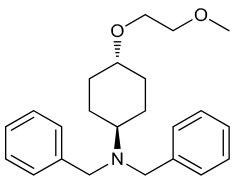

355

To a mixture of (*trans*)-4-(dibenzylamino)cyclohexanol (**354**, 4.00 g, 13.5 mmol) and 1-bromo-2-methoxyethane (6.36 mL, 67.7 mmol) in THF (20 mL) was added sodium hydride (60% wt. in mineral oil, 2.82 g, 70.4 mmol). The reaction mixture was heated, with stirring to 50 °C for 20 h. Further 1-bromo-2-methoxyethane (3.18 mL, 33.9 mmol) was added, and the reaction mixture was heated for a further 24 h. The reaction was cooled to 0 °C, before IPA (2 mL) was added. Solvent was removed *in vacuo* to afford a crude yellow oil, which was partitioned between ethyl acetate (20 mL) and water (20 mL). The organic phase was collected, and the aqueous phase was extracted with ethyl acetate (2 x 20 mL). The organic phases were combined, washed with brine (20 mL), passed through an Isolute® hydrophobic fritted reservoir (70 mL volume) and solvent was removed *in vacuo* to afford a crude residue which was purified using flash column chromatography on a 120 g RediSep silica cartridge, using an eluent gradient from 5% to 20% ethyl acetate in cyclohexane. Product-containing fractions were combined, and solvent was removed *in vacuo* to afford (*trans*)-*N*,*N*-dibenzyl-4-(2-methoxyethoxy)cyclohexanamine (**355**, 4.30 g, 12.2 mmol, 90% yield) as a pale yellow, clear oil.

ν_{max} (neat, cm^{-1}): 2931, 2858, 1452, 1101, 735, 697.

^{1}H NMR (400 MHz, $CDCl_3$): δ 7.34 (d, *J* = 6.8 Hz, 4H), 7.27 (t, *J* = 7.3 Hz, 4H), 7.19 (tt, *J* = 7.3, 2.0 Hz, 2H), 3.60 (s, 4H), 3.59-3.56 (m, 2H), 3.51-3.47 (m, 2H), 3.36 (s, 3H), 3.23-3.14 (m, 1H), 2.52 (tt, *J* = 11.7, 3.4 Hz, 1H), 2.11-2.04 (m, 2H), 1.94-1.87 (m, 2H), 1.43-1.32 (m, 2H), 1.22-1.10 (m, 2H).

^{13}C NMR (101 MHz, $CDCl_3$): δ 140.9 (2C), 128.4 (4C), 128.1 (4C), 126.6 (2C), 78.5, 72.3, 67.3, 59.1, 57.2 (2C), 54.1, 31.5 (2C), 26.1 (2C).

LCMS (High pH, UV, ESI): t_{ret} = 1.52 min, $[M+H]^+$ m/z 354.3, 89.2% purity. Product unstable to LCMS analysis.

HRMS (TOF ESI, formic acid): $C_{23}H_{32}NO_2$ $[M+H]^+$ m/z = 354.2433, found m/z = 354.2437 (Δ = 1.1 ppm).

The product was synthesised on one other occasion under similar conditions, with a yield of 74% (2.20 mmol scale).

(*trans*)-4-(2-Methoxyethoxy)cyclohexylamine:

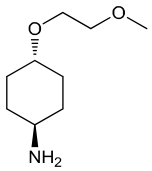

356

(*trans*)-*N*,*N*-Dibenzyl-4-(2-methoxyethoxy)cyclohexanamine (**355**, 1.00 g, 2.83 mmol) was dissolved in ethanol (10 mL). To the solution was added palladium hydroxide on carbon (20% wt.; 99.0 mg, 0.141 mmol), and the reaction was evacuated and placed under an atmosphere of hydrogen. The reaction mixture was stirred at rt for 24 h. The reaction mixture was filtered through celite (5 g), and the filter cake washed with ethanol (10 mL). Solvent removal *in vacuo* afforded (*trans*)-4-(2-methoxyethoxy)cyclohexanamine (**356**, 440 mg, 2.54 mmol, 90% yield) as a colourless oil.

ν_{max} (neat, cm^{-1}): 3385, 3338, 2928, 2858, 1596, 1452, 1099, 622.

^{1}H NMR (400 MHz, $CDCl_3$): δ 3.64-3.58 (m, 2H), 3.55-3.50 (m, 2H), 3.38 (s, 3H), 3.24 (tt, *J* = 10.8, 4.4 Hz, 1H), 2.69 (tt, *J* = 10.8, 3.9 Hz, 1H), 2.07-2.00 (m, 2H), 1.91-1.84 (m, 2H), 1.38-1.25 (m, 2H), 1.18-1.06 (m, 2H). 2 x NH peaks not observed.

^{13}C NMR (101 MHz, $CDCl_3$): δ 78.0, 72.3, 67.4, 59.1, 50.0, 34.5 (2C), 30.7 (2C).

LCMS (High pH, UV, ESI): Desired mass ion not observed, product contains no chromophore.

HRMS (TOF ESI, formic acid): $C_9H_{20}NO_2$ $[M+H]^+$ m/z = 174.1494, found m/z = 174.1500 (Δ = 3.4 ppm).

The product was synthesised a further three times under similar conditions, with yields of 45% (0.750 mmol scale), 86% (4.53 mmol scale) and 90% (2.83 mmol scale).

2-Chloro-*N*-(*trans*-4-(2-methoxyethoxy)cyclohexyl)-8-methylquinazolin-4-amine:

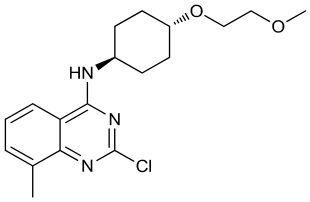

357

To a solution of 2,4-dichloro-8-methylquinazoline (**349**, 200 mg, 0.939 mmol) in acetonitrile (3 mL), was added (*trans*)-4-(2-methoxyethoxy)cyclohexanamine (**356**, 195 mg, 1.13 mmol) and DIPEA (**272**, 307 µL, 2.25 mmol). The reaction mixture was stirred at rt for 72 h. Solvent was removed *in vacuo* to afford a bronze crude oil, which was partitioned between ethyl acetate (20 mL) and water (20 mL), and the organic phase was collected. The aqueous phase was extracted with ethyl acetate (2 x 20 mL), the organic phases were combined, washed with brine (20 mL), passed through an Isolute® hydrophobic fritted reservoir (70 mL volume), and solvent was removed *in vacuo* to afford 2-chloro-*N*-((*trans*-4-(2-methoxy ethoxy)cyclohexyl)-8-methylquinazolin-4-amine (**357**, 248 mg, 0.709 mmol, 76% yield) as white flakes.

mp: 143-144 °C.

ν_{max} (neat, cm^{-1}): 3354, 2938, 2866, 1531, 1265, 1108, 755.

^{1}H NMR (400 MHz, $CDCl_3$): δ 7.56 (app. dt, *J* = 7.2, 0.9 Hz, 1H), 7.45 (br. d, *J* = 8.0 Hz, 1H), 7.31 (dd, *J* = 8.2, 7.2 Hz, 1H), 5.55 (br. d, *J* = 7.5 Hz, 1H), 4.30-4.20 (m, 1H), 3.66-3.62 (m, 2H), 3.58-3.53 (m, 2H), 3.40 (s, 3H), 3.38-3.30 (m, 1H), 2.63 (s, 3H), 2.29-2.20 (m, 2H), 2.17-2.08 (m, 2H), 1.58-1.48 (m, 2H), 1.37-1.24 (m, 2H).

^{13}C NMR (101 MHz, $CDCl_3$): δ 160.6, 157.1, 150.1, 136.7. 133.5, 125.4, 118.0, 113.0, 77.5, 72.4, 67.6, 59.1, 49.3, 30.7 (2C), 30.4 (2C), 17.7.

LCMS (High pH, UV, ESI): t_{ret} = 1.20 min, $[M+H]^+$ m/z 350.1, 100.0% purity.

HRMS (TOF ESI, formic acid): $C_{18}H_{25}ClN_3O_2$ $[M+H]^+$ m/z = 350.1635, found m/z = 350.1636 (Δ = 0.3 ppm). Other m/z observed with heavier isotope = 352.1612.

***N*-(4-(((*trans*)-4-(2-Methoxyethoxy)cyclohexyl)amino)-8-methylquinazolin-2-yl) acetamide:**

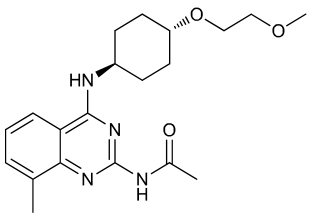

345

The reaction was performed using conditions found in the literature.[263]

A solution of 2-chloro-*N*-((*trans*)-4-(2-methoxyethoxy)cyclohexyl)-8-methyl quinazolin-4-amine (**357**, 84.0 mg, 0.240 mmol) in 1,4-dioxane (1 mL) was made up. To this solution was added acetamide (**358**, 11.8 mg, 0.200 mmol), caesium carbonate (91.0 mg, 0.280 mmol) and XantPhos Pd G3 (9.21 mg, 10.0 µmol). The reaction was heated, with stirring, to 100 °C for 16 h. The reaction was diluted with DCM (20 mL) and passed through a celite frit. Solvent removal *in vacuo* afforded a crude white solid, which was purified by flash column chromatography on a 12 g RediSep silica cartridge using an eluent of 40% ethyl acetate in cyclohexane. Product-containing fractions were combined, and solvent was removed *in vacuo* to afford *N*-(4-(((*trans*)-4-(2-methoxyethoxy)cyclohexyl)amino)-8-methylquinazolin-2-yl) acetamide (**345**, 51.0 mg, 0.137 mmol, 69% yield) as a white, crystalline solid.

mp: 161-162 °C.

ν_{max} (neat, cm^{-1}): 3324, 2927, 2856, 1661, 1591, 1301, 763.

^{1}H NMR (400 MHz, $CDCl_3$): δ 7.79 (br. s, 1H), 7.51 (app. dt, *J* = 7.0, 1.2 Hz, 1H), 7.41 (br. d, *J* = 8.0 Hz, 1H), 7.19 (dd, *J* = 8.3, 7.0 Hz, 1H), 5.48 (br. d, *J* = 7.3 Hz, 1H), 4.15-4.04 (m, 1H), 3.67-3.63 (m, 2H), 3.58-3.53 (m, 2H), 3.40 (s, 3H), 3.35 (tt, *J* = 10.5, 4.0 Hz, 1H), 2.73 (s, 3H), 2.57 (s, 3H), 2.28-2.18 (m, 2H), 2.18-2.10 (m, 2H), 1.55-1.42 (m, 2H), 1.38-1.26 (m, 2H).

^{13}C NMR (101 MHz, $CDCl_3$): δ 172.6, 160.2, 153.2, 149.6 135.9, 133.0, 123.4, 117.9, 111.8, 77.5, 72.3, 67.6, 59.1, 49.6, 30.6 (2C), 30.5 (2C), 25.3, 17.8.

LCMS (High pH, UV, ESI): t_{ret} = 1.04 min, $[M+H]^+$ m/z 373.2, 95.6% purity.

HRMS (TOF ESI, formic acid): $C_{20}H_{29}N_4O_3$ $[M+H]^+$ m/z = 373.2240, found m/z = 373.2243 (Δ = 0.8 ppm).

2-Chloro-6-iodo-*N*-((*trans*)-4-(2-methoxyethoxy)cyclohexyl)-8-methyl quinazolin-4-amine:

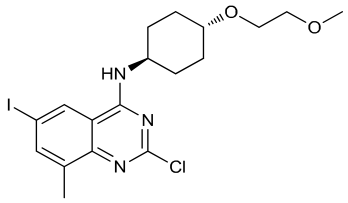

359

A solution of 2,4-dichloro-6-iodo-8-methylquinazoline (**352**, 200 mg, 0.590 mmol), DIPEA (**272**, 193 µL, 1.42 mmol) and (*trans*)-4-(2-methoxyethoxy)cyclohexan-1-amine (**356**, 123 mg, 0.708 mmol) in acetonitrile (2 mL) was made up. The reaction mixture was stirred at rt for 72 h. The solution was concentrated *in vacuo*, before being partitioned between ethyl acetate (20 mL) and water (20 mL). The organic phase was collected, and the aqueous phase was extracted with ethyl acetate (2 x 20 mL). The organic phases were combined and passed through an Isolute® hydrophobic fritted reservoir (70 mL volume), before solvent removal *in vacuo* afforded a crude oil, which was purified by flash column chromatography on a 12 g RediSep silica cartridge, using an eluent gradient from 10% to 40% ethyl acetate in cyclohexane. Product-containing fractions were combined, and solvent was removed *in vacuo* to afford 2-chloro-6-iodo-*N*-((*trans*)-4-(2-methoxyethoxy)cyclohexyl)-8-methyl quinazolin-4-amine (**359**, 245 mg, 0.515 mmol, 87% yield) as a white powder.

mp: 199-200 °C.

ν_{max} (neat, cm^{-1}): 3309, 2907, 1574, 1525, 1103, 853.

^{1}H NMR (400 MHz, $CDCl_3$): δ 7.84-7.82 (m, 1H), 7.80-7.78 (m, 1H), 5.51 (br. d, *J* = 7.8 Hz, 1H), 4.28-4.17 (m, 1H), 3.66-3.63 (m, 2H), 3.58-3.52 (m, 2H), 3.40 (s, 3H), 3.34 (tt, *J* = 10.5, 4.0 Hz, 1H), 2.58 (s, 3H), 2.27-2.19 (m, 2H), 2.17-2.08 (m, 2H), 1.57-1.46 (m, 2H), 1.39-1.28 (m, 2H).

^{13}C NMR (101 MHz, $CDCl_3$): δ 159.1, 157.3, 149.5, 141.9, 138.9, 127.2, 114.8, 89.8, 77.5, 72.4, 67.6, 59.1, 49.6, 30.6 (2C), 30.4 (2C), 17.3.

LCMS (High pH, UV, ESI): t_{ret} = 1.50 min, 98.9% purity, mass ion not observed.

HRMS (TOF ESI, formic acid): $C_{18}H_{24}ClIN_3O_2$ $[M+H]^+$ m/z = 476.0602, found m/z = 476.0609 (Δ = 1.6 ppm). Other m/z observed with heavier isotope = 478.0585.

2,8-Dimethyl-*4H*-benzo[*d*][1,3]oxazin-4-one:

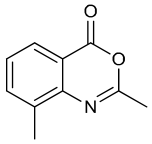

362

Acetic anhydride (**361**, 18.8 mL, 198 mmol) was added to 2-amino-3-methylbenzoic acid (**347**, 3.00 g, 19.9 mmol) and the solution was heated, with stirring to 110 °C for 3 h. The reaction was cooled, and filtered, and the filter cake was washed with diethyl ether (20 mL). The resultant precipitate was dried under reduced pressure to afford 2,8-dimethyl-*4H*-benzo[*d*][1,3] oxazin-4-one (**362**, 1.57 g, 8.96 mmol, 45% yield) as a white, crystalline solid.

mp: 137-138 °C (lit.[294] 136-137 °C (benzene, petroleum ether)).

ν_{max} (neat, cm^{-1}): 1742, 1645, 1463, 773, 714.

^{1}H NMR (400 MHz, $CDCl_3$): δ 8.02 (dd, *J* = 7.8, 1.0 Hz, 1H), 7.64-7.61 (m, 1H), 7.36 (t, *J* = 7.6 Hz, 1H), 2.54 (s, 3H), 2.47 (s, 3H).

^{13}C NMR (101 MHz, $CDCl_3$): δ 160.3, 158.7, 144.9, 137.3, 135.4, 127.5, 126.0, 116.6, 21.5, 17.0.

LCMS (High pH, UV, ESI): t_{ret} = 0.99 min, $[M+H]^+$ m/z 176.1, 100.0% purity.

HRMS (TOF ESI, formic acid): $C_{10}H_{10}NO_2$ $[M+H]^+$ m/z = 176.0712, found m/z = 176.0719 (Δ = 4.0 ppm).

Spectroscopic data is in accordance with that reported in the literature.[291]

The product was synthesised on one other occasion, under similar conditions, with a yield of 64% (9.92 mmol scale).

2,8-Dimethylquinazolin-4(*3H*)-one:

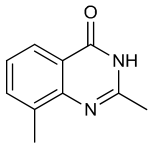

363

To a solution of 2,8-dimethyl-*4H*-benzo[*d*][1,3]oxazin-4-one (**362**, 1.2 g, 6.85 mmol) in DMA (3 mL) was added ammonium acetate (1.06 g, 13.7 mmol), and the reaction mixture was heated to 160 °C for 16 h. The reaction was cooled, and filtered, and the filter cake was washed with acetonitrile (10 mL). The precipitate was dried under reduced pressure to afford

2,8-dimethylquinazolin-4(*3H*)-one (**363**, 842 mg, 4.83 mmol, 71% yield) as a white crystalline solid.

mp: 249-250 °C (lit.[295] 250-252 °C).

ν_{max} (neat, cm^{-1}): 2861, 1682, 1622, 1291, 905, 764.

^{1}H NMR (400 MHz, $CDCl_3$): δ 11.99 (br. s, 1H), 8.13 (br. d, *J* = 7.9 Hz, 1H), 7.62-7.58 (m, 1H), 7.34 (t, *J* = 7.6 Hz, 1H), 2.62 (s, 3H), 2.60 (s, 3H).

^{13}C NMR (101 MHz, $CDCl_3$): δ 164.7, 151.9, 148.2, 135.6, 135.4, 125.8, 123.8, 120.2, 22.3, 17.6.

LCMS (Low pH, UV, ESI): t_{ret} = 0.62 min, $[M+H]^+$ m/z 175.1, 100.0% purity.

HRMS (TOF ESI, formic acid): $C_{10}H_{11}N_2O$ $[M+H]^+$ m/z = 175.0871, found m/z = 175.0875 (Δ = 2.3 ppm).

Spectroscopic data is in accordance with that reported in the literature.[296]

The product was synthesised on one other occasion, under similar conditions, with a yield of 60% (2.28 mmol scale).

4-Chloro-2,8-dimethylquinazoline:

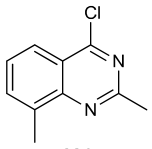

364

To a mixture of 2,8-dimethylquinazolin-4(*3H*)-one (**363**, 800 mg, 4.57 mmol) and DIPEA (**272**, 1.00 mL, 5.73 mmol) was added phosphoryl trichloride (10.0 mL, 107 mmol). The reaction mixture was heated, with stirring, to 110 °C for 4 h. The reaction was cooled, and the reaction was concentrated under reduced pressure. The resultant residue was dissolved in DCM (20 mL) and poured into sat. aq. sodium carbonate solution (50 mL). The organic phase was collected, and the aqueous phase was extracted with DCM (2 x 20 mL). The organic phases were combined and passed through an Isolute® hydrophobic fritted reservoir (70 mL volume), before solvent removal *in vacuo* afforded a crude product, which was isolated by flash column chromatography on an 80 g RediSep silica cartridge using an eluent of 20% ethyl acetate in cyclohexane. The product-containing fractions were combined, and solvent was removed *in vacuo* to afford 4-chloro-2,8-dimethylquinazoline (**364**, 734 mg, 3.81 mmol, 83% yield) as a white powder.

mp: 87-88 °C.

ν_{max} (neat, cm^{-1}): 1568, 1391, 1323, 1110, 822, 760.

^{1}H NMR (400 MHz, $CDCl_3$): δ 8.05 (br. d, *J* = 8.5 Hz, 1H), 7.75-7.71 (m, 1H), 7.51 (dd, *J* = 8.3, 7.0 Hz, 1H), 2.86 (s, 3H), 2.75 (s, 3H).

^{13}C NMR (101 MHz, $CDCl_3$): δ 162.4, 162.2, 150.8, 136.8, 134.6, 127.4, 123.4, 121.7, 26.3, 17.5.

LCMS (Low pH, UV, ESI): t_{ret} = 1.16 min, $[M+H]^+$ m/z 193.1, 100.0% purity.

HRMS (TOF ESI, formic acid): $C_{10}H_{10}ClN_2$ $[M+H]^+$ m/z = 193.0533, found m/z = 193.0530 (Δ = -1.6 ppm). Other m/z observed with heavier isotope = 195.0499.

The product was synthesised on one other occasion under similar conditions, with a yield of 27% (0.574 mmol scale).

***N*-((*trans*)-4-(2-Methoxyethoxy)cyclohexyl)-2,8-dimethylquinazolin-4-amine:**

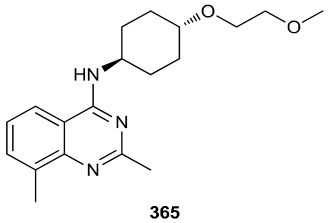

365

To a solution of 4-chloro-2,8-dimethylquinazoline (**364**, 20 mg, 0.104 mmol) in acetonitrile (2 mL) was added triethylamine (36 µL, 0.208 mmol) and (*trans*)-4-(2-methoxyethoxy) cyclohexan-1-amine (**356**, 27 mg, 0.156 mmol). The reaction mixture was irradiated, with stirring to reflux (70 °C) for 20 h in the MW reactor. The reaction was concentrated under reduced pressure, before the residue was partitioned between DCM (20 mL) and water (20 mL). The organic phase was collected, and the aqueous phase was extracted with DCM (2 x 20 mL). The organic phases were combined, washed with sat. aq. brine solution (20 mL) and passed through an Isolute® hydrophobic fritted reservoir (70 mL volume), before solvent was removed *in vacuo* to afford *N*-((*trans*)-4-(2-methoxyethoxy)cyclohexyl)-2,8-di methylquinazolin-4-amine (**365**, 19 mg, 58 µmol, 56% yield) as an amorphous white gum.

ν_{max} (neat, cm^{-1}): 3323, 2911, 1580, 1523, 1114, 775.

^{1}H NMR (400 MHz, $CDCl_3$): δ 7.54-7.49 (m, 1H), 7.44 (br. d, *J* = 7.9 Hz, 1H), 7.26-7.22 (m, 1H), 5.31 (br. d, *J* = 7.4 Hz, 1H), 4.31-4.19 (m, 1H), 3.69-3.61 (m, 2H), 3.60-3.52 (m, 2H), 3.40 (s, 3H), 3.34 (tt, *J* = 10.8, 4.0 Hz, 1H), 2.66 (s, 3H), 2.64 (s, 3H), 2.29-2.21 (m, 2H), 2.16-2.08 (m, 2H), 1.59-1.46 (m, 2H), 1.36-1.23 (m, 2H).

^{13}C NMR (101 MHz, $CDCl_3$): δ 163.6, 159.0, 149.2, 136.2, 132.4, 124.1, 117.7, 112.6, 77.8, 72.4, 67.5, 59.1, 48.9, 30.8 (2C), 30.6 (2C), 27.1, 17.8.

LCMS (High pH, UV, ESI): t_{ret} = 1.05 min, $[M+H]^+$ m/z 330.2, 100.0% purity.

HRMS (TOF ESI, formic acid): $C_{19}H_{28}N_3O_2$ $[M+H]^+$ m/z = 330.2182, found m/z = 330.2182 (Δ = 0.0 ppm).

6-Iodo-2,8-dimethyl-*4H*-benzo[*d*][1,3]oxazin-4-one:

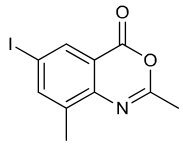

366

2-Amino-5-iodo-3-methylbenzoic acid (**350**, 4.35 g, 15.7 mmol) and acetic anhydride (**361**, 14.8 mL, 157 mmol) were combined, and heated, with stirring to 110 °C for 16 h. The reaction was cooled and filtered. The resultant precipitate was washed with diethyl ether (30 mL), and then dried under reduced pressure to afford 6-iodo-2,8-dimethyl-*4H*-benzo[*d*][1,3] oxazin-4-one (**366**, 3.80 g, 12.6 mmol, 80% yield) as a beige powder.

mp: 177-178 °C.

ν_{max} (neat, cm^{-1}): 1736, 1649, 1311, 1238, 966, 790, 768.

^{1}H NMR (400 MHz, $CDCl_3$): δ 8.36-8.33 (m, 1H), 7.95-7.92 (m, 1H), 2.48 (s, 3H), 2.45 (s, 3H).

^{13}C NMR (101 MHz, $CDCl_3$): δ 159.4, 158.7, 145.7, 144.1, 137.8, 134.6, 118.1, 91.7, 21.5, 16.6.

LCMS (High pH, UV, ESI): t_{ret} = 1.23 min, 98.8% purity, mass ion not observed.

HRMS (TOF ESI, formic acid): $C_{10}H_9INO_2$ $[M+H]^+$ m/z = 301.9678, found m/z = 301.9683 (Δ = 1.7 ppm).

Spectroscopic data is in accordance with that reported in the literature.[291]

6-Iodo-2,8-dimethylquinazolin-4(*3H*)-one:

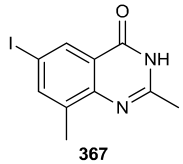

367

To a solution of 6-iodo-2,8-dimethyl-*4H*-benzo[*d*][1,3]oxazin-4-one (**366**, 3.7 g, 12.3 mmol) in DMA (30 mL) was added ammonium acetate (1.90 g, 24.6 mmol). The reaction mixture was heated, with stirring, to 160 °C for 16 h. The reaction was cooled, and filtered, and the filter cake was washed with acetonitrile (30 mL). The product was dried *in vacuo* to afford 6-iodo-2,8-dimethylquinazolin-4(*3H*)-one (**367**, 2.28 g, 7.60 mmol, 62% yield) as a cream coloured solid.

mp: The product recrystallised at 254-255 °C, and was subsequently stable to 300 °C.

ν_{max} (neat, cm^{-1}): 3070, 2874, 1677, 1621, 1297, 782, 627.

^{1}H NMR (400 MHz, DMSO-*d*$_6$): δ 12.30 (br. s, 1H), 8.17 (d, *J* = 1.5 Hz, 1H), 7.95-7.92 (m, 1H), 2.45 (s, 3H), 2.35 (s, 3H).

^{13}C NMR (101 MHz, DMSO-*d*$_6$): δ 160.6, 154.0, 146.8, 142.4, 137.5, 131.6, 122.3, 90.2, 21.8, 16.7.

LCMS (High pH, UV, ESI): t_{ret} = 0.98 min, $[M+H]^+$ m/z = 301.0, 98.8% purity.

HRMS (TOF ESI, formic acid): $C_{10}H_{10}IN_2O$ $[M+H]^+$ m/z = 300.9838, found m/z = 300.9845 (Δ = 2.3 ppm).

4-Chloro-6-iodo-2,8-dimethylquinazoline:

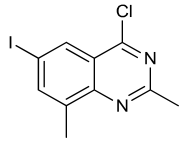

368

To a solution of 6-iodo-2,8-dimethylquinazolin-4(*3H*)-one (**367**, 200 mg, 0.666 mmol) dissolved in phosphoryl trichloride (5 mL, 53.6 mmol), was added DIPEA (**272**, 116 µL, 0.666 mmol). The reaction mixture was heated, with stirring, to 110 °C for 16 h. The reaction was cooled, and concentrated twice *in vacuo*, using toluene as a co-solvent each time (2 x 20 mL). The resultant red-brown residue was then dissolved in DCM (40 mL), poured into a solution of aq. sat. sodium carbonate (50 mL) and stirred for 20 min. The organic phase was separated, and the aqueous phase was extracted with DCM (2 x 30 mL). The organic phases were combined, and solvent was removed *in vacuo* to afford 4-chloro-6-iodo-2,8-dimethyl quinazoline (**368**, 203 mg, 0.637 mmol, 96% yield) as an orange powder.

mp: 183-185 °C (dec.).

ν_{max} (neat, cm^{-1}): 2914, 1560, 1408, 1285, 1120, 861, 794, 565.

^{1}H NMR (400 MHz, $CDCl_3$): δ 8.42 (br. d, *J* = 2.0 Hz, 1H), 8.01-7.97 (m, 1H), 2.83 (s, 3H), 2.69 (s, 3H).

^{13}C NMR (101 MHz, $CDCl_3$): δ 163.0, 160.6, 149.9, 143.1, 139.0, 132.1, 123.1, 92.9, 26.3, 17.0.

LCMS (Low pH, UV, ESI): t_{ret} = 1.42 min, $[M+H]^+$ m/z = 318.8, 98.7% purity.

HRMS (TOF ESI, formic acid): $C_{10}H_9ClIN_2$ $[M+H]^+$ m/z = 318.9499, found m/z = 318.9504 (Δ = 1.6 ppm). Other m/z observed with heavier isotope = 320.9474.

The product was synthesised on one other occasion under similar conditions, with a yield of 68% (3.00 mmol scale).

6-Iodo-*N*-((*trans*)-4-(2-methoxyethoxy)cyclohexyl)-2,8-dimethylquinazolin-4-amine:

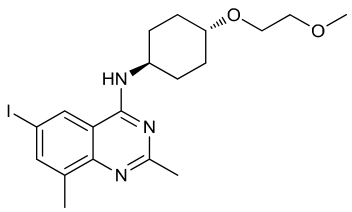

369

To a solution of 4-chloro-6-iodo-2,8-dimethylquinazoline (**368**, 120 mg, 0.377 mmol) in acetonitrile (5 mL) was added (*trans*)-4-(2-methoxyethoxy) cyclohexan-1-amine (**356**, 200 mg, 1.15 mmol). The reaction mixture was heated, with stirring to reflux (70 °C) for 16 h. The reaction was cooled to rt and concentrated *in vacuo*. The resultant residue was separated between DCM (20 mL) and water (20 mL). The organic layer was collected, and the aqueous layer was extracted with DCM (2 x 20 mL). The organic layers were combined, washed with sat. aq. brine solution (15 mL) and passed through an Isolute® hydrophobic fritted reservoir (70 mL volume). Solvent was removed *in vacuo* to afford 6-iodo-*N*-((*trans*)-4-(2-methoxy ethoxy)cyclo hexyl)-2,8-di methylquinazolin-4-amine (**369**, 252 mg, 0.553 mmol, 48% yield) as an off-white powder.

mp: 155-156 °C.

ν_{max} (neat, cm^{-1}): 3345, 2930, 1573, 1527, 1101, 800.

^{1}H NMR (400 MHz, $CDCl_3$): δ 7.80 (br. s, 1H), 7.78 (br. d, *J* = 1.0 Hz, 1H), 5.30 (br. s, 1H), 4.29-4.18 (m, 1H), 3.67-3.63 (m, 2H), 3.57-3.54 (m, 2H), 3.40 (s, 3H), 3.38-3.30 (m, 1H), 2.62 (s, 3H), 2.61 (s, 3H), 2.26-2.19 (m, 2H), 2.16-2.09 (m, 2H), 1.56-1.45 (m, 2H), 1.36-1.25 (m, 2H).

^{13}C NMR (101 MHz, $CDCl_3$): δ 164.1, 157.7, 141.4, 140.8, 138.6, 127.1, 114.5, 88.4, 77.7, 72.4, 67.6, 59.1, 49.1, 30.7 (2C), 30.6 (2C), 27.0, 17.4.

LCMS (High pH, UV, ESI): t_{ret} = 1.33 min, $[M+H]^+$ m/z = 456.1, 98.6% purity.

HRMS (TOF ESI, formic acid): $C_{19}H_{27}IN_3O_2$ $[M+H]^+$ m/z = 456.1148, found m/z = 456.1149 (Δ = 0.2 ppm).

The product was synthesised on one other occasion under similar conditions, with a yield of 64% (0.377 mmol scale).

***N*-((*trans*)-4-(2-Methoxyethoxy)cyclohexyl)-2,8-dimethyl-6-morpholino quinazolin-4-amine:**

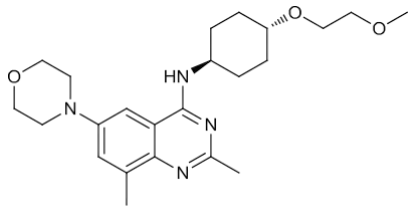

370

6-Iodo-*N*-((*trans*)-4-(2-methoxyethoxy)cyclohexyl)-2,8-dimethylquinazolin-4-amine (**369**, 40 mg, 88.0 µmol), caesium carbonate (57 mg, 0.176 mmol), RuPhos Pd G2 (14 mg, 18 µmol), RuPhos (8 mg, 18 µmol) and morpholine (19 µL, 0.220 mmol) were added to a 5 mL MW vial. The vial was sealed, evacuated and placed under a nitrogen atmosphere, before anhydrous 1,4-dioxane (1 mL) was added. The reaction mixture was irradiated, with stirring, to 100 °C for 2 h in the MW reactor. The reaction mixture was separated between ethyl acetate (10 mL) and water (10 mL). The organic layer was collected, and the aqueous layer was extracted with ethyl acetate (2 x 10 mL). The organic phases were combined, passed through an Isolute® hydrophobic fritted reservoir (70 mL volume). Solvent was removed *in vacuo*, and the crude product was purified by MDAP (High pH) isolation using method C, 30 min run. Product-containing fractions were combined, and solvent was removed under a stream of nitrogen to afford *N*-((*trans*)-4-(2-methoxyethoxy)cyclohexyl)-2,8-dimethyl-6-morpholino quinazolin-4-amine (**370**, 7 mg, 17 µmol, 20% yield) as a beige, crystalline solid.

mp: 159-160 °C.

ν_{max} (neat, cm^{-1}): 2857, 1560, 1528, 1449, 1374, 1112, 876.

^{1}H NMR (400 MHz, $CDCl_3$): δ 7.29-7.27 (m, 1H), 6.69-6.65 (m, 1H), 5.28 (br. s, 1H), 4.31-4.19 (m, 1H), 3.89 (dd, *J* = 4.4, 3.0 Hz, 4H), 3.67-3.64 (m, 2H), 3.58-3.54 (m, 2H), 3.40 (s, 3H), 3.38-3.30 (m, 1H), 3.22 (dd, *J* = 5.7, 4.2 Hz, 4H), 2.65 (s, 3H), 2.63 (s, 3H), 2.28-2.22 (m, 2H), 2.16-2.10 (m, 2H), 1.57-1.47 (m, 2H), 1.39-1.27 (m, 2H).

^{13}C NMR (101 MHz, $CDCl_3$): δ 166.1, 161.2, 158.4, 148.0, 145.0, 124.5, 113.0, 101.1, 77.9, 72.4, 67.5, 66.9 (2C), 59.1, 49.9 (2C), 49.1, 30.9 (2C), 30.7 (2C), 26.5, 18.2.

LCMS (High pH, UV, ESI): t_{ret} = 1.03 min, $[M+H]^+$ m/z = 415.3, 96.4% purity.

HRMS (TOF ESI, formic acid): $C_{23}H_{35}N_4O_3$ $[M+H]^+$ m/z = 415.2709, found m/z = 415.2705 (Δ = -1.0 ppm).

The product was synthesised on one other occasion under similar conditions, with a yield of 41% (88 µmol scale).

***N*-((*trans*)-4-(2-Methoxyethoxy)cyclohexyl)-2,8-dimethyl-6-(4-methylpiperazin-1-yl) quinazolin-4-amine:**

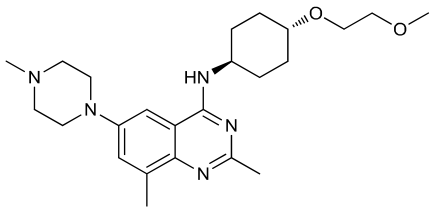

371

A mixture of 6-iodo-*N*-((*trans*)-4-(2-methoxyethoxy)cyclohexyl)-2,8-dimethyl quinazolin-4-amine (**369**, 40 mg, 0.088 mmol), caesium carbonate (57 mg, 0.176 mmol), RuPhos Pd G2 (14 mg, 18 µmol), RuPhos (8 mg, 18 µmol) and 1-methylpiperazine (24 µL, 0.220 mmol) were added to a 5 mL MW vial. The vial was sealed, evacuated and placed under a nitrogen atmosphere, before anhydrous 1,4-dioxane (1 mL) was added. The reaction mixture was irradiated, with stirring, to 100 °C for 2 h in the MW reactor. Solvent was removed *in vacuo* to afford a residue which was partitioned between ethyl acetate (10 mL) and water (10 mL). The organic phase was collected, and the aqueous phase was extracted with ethyl acetate (2 x 10 mL). The organic layers were combined, passed through an Isolute® hydrophobic fritted reservoir (25 mL volume) and solvent was removed *in vacuo* to produce a crude product residue, which was purified by MDAP (High pH) isolation using method C, 30 min run. Product-containing fractions were combined, and solvent was removed under a stream of nitrogen to afford *N*-((*trans*)-4-(2-methoxyethoxy)cyclohexyl)-2,8-dimethyl-6-(4-methyl piperazin-1-yl) quinazolin-4-amine (**371**, 17 mg, 40 µmol, 45% yield) as a yellow crystalline solid.

mp: 70-72 °C.

ν_{max} (neat, cm^{-1}): 2933, 1580, 1526, 1370, 1101, 1002, 798.

^{1}H NMR (400 MHz, $CDCl_3$): δ 7.28 (br. d, *J* = 2.0 Hz, 1H), 6.82-6.71 (m, 1H), 5.52 (br. s, 1H), 4.33-4.21 (m, 1H), 3.66-3.63 (m, 2H), 3.57-3.54 (m, 2H), 3.40 (s, 3H), 3.37-3.31 (m, 1H), 3.28

(t, *J* = 4.9 Hz, 4H), 2.64 (s, 6H), 2.64-2.60 (m, 4H), 2.38 (s, 3H), 2.27-2.20 (m, 2H), 2.15-2.09 (m, 2H), 1.56-1.45 (m, 2H), 1.42-1.31 (m, 2H).

^{13}C NMR (101 MHz, $CDCl_3$): δ 161.0, 153.4, 148.0 (2C), 136.3, 124.8, 113.0, 101.5, 77.9, 72.4, 67.5, 59.1, 55.0 (2C), 49.4 (2C), 49.2, 46.0, 30.9 (2C), 30.8 (2C), 26.4, 18.3.

LCMS (High pH, UV, ESI): t_{ret} = 1.01 min, $[M+H]^+$ m/z = 428.4, 98.7% purity.

HRMS (TOF ESI, formic acid): $C_{24}H_{38}N_5O_2$ $[M+H]^+$ m/z = 428.3026, found m/z = 428.3021 (Δ = -1.2 ppm).

***N*^{6},*N*^{6}-Diethyl-*N*^{4}-((*trans*)-4-(2-methoxyethoxy)cyclohexyl)-2,8-dimethyl quinazoline-4,6-diamine formate:**

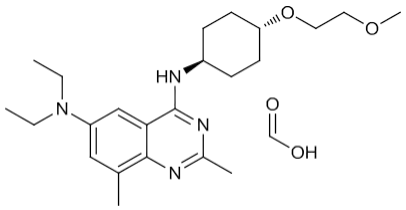

372

The reaction was performed using conditions found in the literature.[265]

A mixture of 6-iodo-*N*-((*trans*)-4-(2-methoxyethoxy)cyclohexyl)-2,8-dimethyl quinazolin-4-amine (**369**, 40 mg, 88 µmol), potassium carbonate (24 mg, 0.176 mmol), diethylamine (23 µL, 0.220 mmol), copper(I)iodide (17 mg, 88 µmol) and L-proline (2 mg, 18 µmol) were added to a 5 mL MW vial. The vial was sealed, evacuated and placed under a nitrogen atmosphere, before DCM (2 mL) was added. The reaction mixture was heated, with stirring, to 60 °C for 96 h. The reaction was cooled and partitioned between ethyl acetate (20 mL) and water (20 mL). The organic phase was collected, and the aqueous phase was extracted with ethyl acetate (2 x 10 mL). The organic layers were combined, passed through an Isolute® hydrophobic fritted reservoir (25 mL volume) and solvent was removed *in vacuo* to produce a crude product residue, which was purified by MDAP (Low pH) isolation using method B, 30 min run. Product-containing fractions were combined, and solvent was removed under a stream of nitrogen to afford *N*^{6},*N*^{6}-diethyl-*N*^{4}-((*1R,4R*)-4-(2-methoxyethoxy) cyclohexyl)-2,8-dimethylquinazoline-4,6-diamine formate (**372**, 5 mg, 11 µmol, 13% yield) as a yellow oil.

ν_{max} (neat, cm^{-1}): 2930, 1577, 1524, 1345, 1094, 781.

^{1}H NMR (400 MHz, $CDCl_3$): δ 8.72-8.44 (m, 2H), 6.99 (d, *J* = 2.5 Hz, 1H), 6.84 (d, *J* = 2.5 Hz, 1H), 6.77 (br. s, 1H), 4.19-4.02 (m, 1H), 3.67-3.62 (m, 2H), 3.57-3.53 (m, 2H), 3.47-3.40 (m,

4H), 3.40 (s, 3H), 3.36-3.28 (m, 1H), 2.53 (s, 3H), 2.50 (s, 3H), 2.12 (br. t, *J* = 10.3 Hz, 4H), 1.56-1.35 (m, 4H), 1.19 (t, *J* = 6.9 Hz, 6H).

^{13}C NMR (101 MHz, $CDCl_3$): δ 167.5, 158.7, 157.6, 146.2, 130.5, 121.6, 113.7, 99.1, 77.5, 72.3, 67.5, 59.1, 51.0, 44.3 (2C), 30.9 (2C), 29.7 (2C), 22.6, 18.6, 12.5 (2C).

LCMS (Low pH, UV, ESI): t_{ret} = 0.76 min, $[M+H]^+$ m/z = 401.2.

HRMS (TOF ESI, formic acid): $C_{23}H_{37}N_4O_2$ $[M+H]^+$ m/z = 401.2917, found m/z = 401.2907 (Δ = -2.5 ppm).

6-(3,5-Dimethylisoxazol-4-yl)-*N*-((*trans*)-4-(2-methoxyethoxy)cyclohexyl)-2,8-dimethyl quinazolin-4-amine:

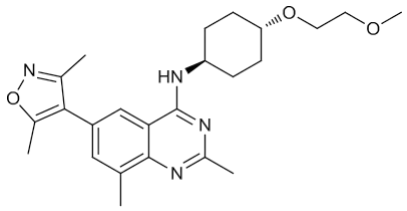

373

A mixture of 6-iodo-*N*-((*trans*)-4-(2-methoxyethoxy)cyclohexyl)-2,8-dimethyl quinazolin-4-amine (**369**, 50 mg, 0.110 mmol), (3,5-dimethylisoxazol-4-yl)boronic acid (23 mg, 0.165 mmol), Pd(dppf)Cl_2·DCM (9 mg, 11 µmol), and potassium carbonate (46 mg, 0.329 mmol) in DMSO (1 mL) and water (0.5 mL) was made up. The reaction mixture was irradiated, with stirring, at 100 °C for 2 h in the MW reactor. The crude reaction mixture was partitioned between ethyl acetate (15 mL) and water (20 mL). The organic phase was collected, and the aqueous phase was extracted with ethyl acetate (2 x 20 mL). The organic phases were combined, passed through an Isolute® hydrophobic fritted reservoir (25 mL volume), and solvent was removed *in vacuo* to afford a crude brown oil which was purified by MDAP (High pH) isolation using method C, 30 min run. Product-containing fractions were combined, and solvent was removed *in vacuo* to afford 6-(3,5-dimethyl isoxazol-4-yl)-*N*-((*trans*)-4-(2-methoxyethoxy)cyclohexyl)-2,8-dimethylquinazolin-4-amine (**373**, 24 mg, 57 µmol, 52% yield) as an off-white crystalline solid.

mp: 199-200 °C (dec.).

ν_{max} (neat, cm^{-1}): 3375, 2934, 2860, 1581, 1539, 1102.

^{1}H NMR (400 MHz, $CDCl_3$): δ 7.39-7.35 (m, 1H), 7.30-7.27 (m, 1H), 5.41 (br. d, *J* = 7.4 Hz, 1H), 4.34-4.23 (m, 1H), 3.68-3.53 (m, 4H), 3.40 (s, 3H), 3.38-3.30 (m, 1H), 2.69 (s, 3H), 2.66 (s, 3H), 2.39 (s, 3H), 2.31-2.24 (m, 2H), 2.23 (s, 3H), 2.18-2.09 (m, 2H), 1.59-1.48 (m, 2H), 1.39-1.28 (m, 2H). NH peak not observed.

^{13}C NMR (101 MHz, $CDCl_3$): δ 165.4, 164.1, 158.9, 158.7, 148.7, 137.0, 133.4, 126.1, 118.6, 116.6, 112.7, 77.8, 72.4, 67.5, 59.1, 49.1, 30.8 (2C), 30.7 (2C), 27.1, 17.9, 11.5, 10.7.

LCMS (High pH, UV, ESI): t_{ret} = 1.18 min, $[M+H]^+$ m/z = 425.3, 100.0% purity.

HRMS (TOF ESI, formic acid): $C_{24}H_{33}N_4O_3$ $[M+H]^+$ m/z = 425.2553, found m/z = 425.2546 (Δ = -1.6 ppm).

(*cis*)-4-(Dibenzylamino)cyclohexanol:

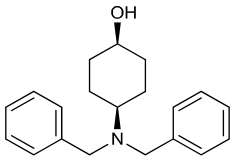

375

To a mixture of (*cis*)-4-(amino)cyclohexan-1-ol (**374**, 415 µL, 3.73 mmol) and potassium carbonate (2.58 g, 18.7 mmol) in acetonitrile (20 mL) was added benzyl bromide (977 µL, 8.21 mmol). The reaction mixture was heated, with stirring to 70 °C for 12 h. The reaction was cooled and filtered, and the filter cake was washed with acetonitrile (10 mL). The filtrate was concentrated *in vacuo* and the crude product was purified by flash column chromatography on an 80 g RediSep silica cartridge using an eluent gradient from 10% to 30% ethyl acetate in cyclohexane. The product-containing fractions were combined, and solvent was removed *in vacuo* to afford (*cis*)-4-(dibenzylamino)cyclohexan-1-ol (**375**, 913 mg, 3.09 mmol, 83% yield) as white flakes.

mp: 103-104 °C.

ν_{max} (neat, cm^{-1}): 3308, 2926, 1493, 960, 728, 693.

^{1}H NMR (400 MHz, $CDCl_3$): δ 7.36 (d, *J* = 7.4 Hz, 4H), 7.31-7.24 (m, 4H), 7.19 (tt, *J* = 7.4, 2.5 Hz, 2H), 3.96 (br. s, 1H), 3.66 (s, 4H), 2.51 (tt, *J* = 11.3, 3.4 Hz, 1H), 1.87-1.73 (m, 4H), 1.71-1.63 (m, 2H), 1.46-1.33 (m, 2H), 1.18 (br. s, 1H).

^{13}C NMR (101 MHz, $CDCl_3$): δ 141.1 (2C), 128.4 (4C), 128.1 (4C), 126.5 (2C), 65.8, 57.2, 53.8 (2C), 32.4 (2C), 22.1 (2C).

LCMS (High pH, UV, ESI): t_{ret} = 1.37 min, $[M+H]^+$ m/z 296.2, 100.0% purity.

HRMS (TOF ESI, formic acid): $C_{20}H_{26}NO$ $[M+H]^+$ m/z = 296.2014, found m/z = 296.2018 (Δ = 1.4 ppm).

(*cis*)-*N*,*N*-Dibenzyl-4-(2-methoxyethoxy)cyclohexanamine:

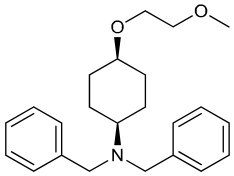

376

To a mixture of (*cis*)-4-(dibenzylamino)cyclohexanol (**375**, 750 mg, 2.54 mmol) and 1-bromo-2-methoxyethane (1.19 mL, 12.7 mmol) in THF (5 mL) was added sodium hydride (60% wt. in mineral oil, 528 mg, 13.2 mmol). The reaction mixture was heated, with stirring to 50 °C for 72 h. Further 1-bromo-2-methoxyethane (1.00 mL, 10.6 mmol) was added, and the reaction mixture was heated for a further 24 h. The reaction was cooled to 0 °C, before water (4 mL) was added. The aqueous solution was extracted into ethyl acetate (10 mL), and the organic layer was collected. The aqueous phase was extracted with ethyl acetate (2 x 20 mL). The organic phases were combined, washed with sat. aq. brine solution (20 mL), passed through an Isolute® hydrophobic fritted reservoir (70 mL volume) and solvent was removed *in vacuo* to afford a crude residue which was purified using flash column chromatography on a 120 g RediSep silica cartridge, using an eluent gradient from 5% to 20% ethyl acetate in cyclohexane. Product-containing fractions were combined, and solvent was removed *in vacuo* to afford (*cis*)-*N*,*N*-dibenzyl-4-(2-methoxyethoxy)cyclohexanamine (**376**, 523 mg, 1.48 mmol, 58% yield) as a pale yellow, clear oil, which later crystallised as an off-white solid.

mp: 40-41 °C.

ν_{max} (neat, cm^{-1}): 2927, 2860, 1452, 1095, 734, 697.

^{1}H NMR (400 MHz, $CDCl_3$): δ 7.39-7.33 (m, 4H), 7.30-7.24 (m, 4H), 7.18 (tt, *J* = 6.9, 2.0 Hz, 2H), 3.64 (s, 4H), 3.54-3.51 (m, 4H), 3.48 (t, *J* = 3.0 Hz, 1H), 3.38 (s, 3H), 2.51 (tt, *J* = 11.8, 3.9 Hz, 1H), 2.03-1.95 (m, 2H), 1.80-1.67 (m, 2H), 1.66-1.59 (m, 2H), 1.29-1.18 (m, 2H).

^{13}C NMR (101 MHz, $CDCl_3$): δ 141.2 (2C), 128.4 (4C), 128.1 (4C), 126.5 (2C), 73.2, 72.4, 67.0, 59.1, 57.1, 53.9 (2C), 29.5 (2C), 22.4 (2C).

LCMS (High pH, UV, ESI): t_{ret} = 1.60 min, $[M+H]^+$ m/z 354.2, 97.4% purity.

HRMS (TOF ESI, formic acid): $C_{23}H_{32}NO_2$ $[M+H]^+$ m/z = 354.2433, found m/z = 354.2449 (Δ = 4.5 ppm).

(*cis*)-4-(2-Methoxyethoxy)cyclohexanamine:

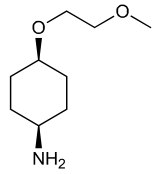

377

(*cis*)-*N*,*N*-Dibenzyl-4-(2-methoxyethoxy)cyclohexanamine (**376**, 50 mg, 1.27 mmol) was dissolved in ethanol (10 mL). To the solution was added palladium hydroxide on carbon (20% wt.; 45 mg, 64 µmol), and the reaction was evacuated and placed under an atmosphere of hydrogen. The reaction mixture was stirred at rt for 16 h. The reaction mixture was filtered through celite (5 g), and the filter cake washed with ethanol (10 mL). Solvent removal *in vacuo* afforded (*cis*)-4-(2-methoxyethoxy)cyclohexanamine (**377**, 196 mg, 1.13 mmol, 89% yield) as a colourless oil.

ν_{max} (neat, cm^{-1}): 2928, 2859, 1447, 1345, 1087.

^{1}H NMR (400 MHz, $CDCl_3$): δ 3.58-3.52 (m, 4H), 3.49-3.44 (m, 1H), 3.39 (s, 3H), 2.79-2.69 (m, 3H), 1.94-1.80 (m, 2H), 1.66-1.56 (m, 2H), 1.55-1.44 (m, 4H).

^{13}C NMR (101 MHz, $CDCl_3$): δ 73.9, 72.3, 67.1, 59.1, 49.0, 30.6 (2C), 28.2 (2C).

LCMS (High pH, UV, ESI): Desired mass ion not observed, product contains no chromophore.

HRMS (TOF ESI, formic acid): $C_9H_{20}NO_2$ $[M+H]^+$ m/z = 174.1494, found m/z = 174.1497 (Δ = 1.7 ppm).

6-Iodo-*N*-((*cis*)-4-(2-methoxyethoxy)cyclohexyl)-2,8-dimethylquinazolin-4-amine:

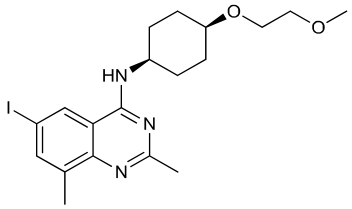

378

To a solution of (*cis*)-4-(2-methoxyethoxy)cyclohexan-1-amine (**377**, 85 mg, 0.490 mmol) in acetonitrile (5 mL), was added 4-chloro-6-iodo-2,8-dimethylquinazoline (**368**, 120 mg, 0.377 mmol) and triethylamine (132 µL, 0.753 mmol). The reaction mixture was heated, with stirring, to reflux (70 °C) for 16 h. The reaction mixture was cooled, concentrated *in vacuo*, and the resultant residue was separated between DCM (20 mL) and water (20 mL). The organic phase was collected, and the aqueous phase was extracted with DCM (2 x 20 mL). The organic layers were combined, washed with sat. aq. brine solution (20 mL) and passed through an

Isolute® hydrophobic fritted reservoir (70 mL volume). Solvent was removed *in vacuo* to afford 6-iodo-*N*-((*cis*)-4-(2-methoxyethoxy)cyclohexyl)-2,8-dimethylquinazolin-4-amine (**378**, 119 mg, 0.261 mmol, 69% yield) as a colourless oil, which later crystallised as a white powder.

mp: 59-60 °C.

ν_{max} (neat, cm^{-1}): 3361, 2928, 2865, 1572, 1526, 1086.

^{1}H NMR (400 MHz, $CDCl_3$): δ 7.80-7.78 (m, 1H), 7.78-7.76 (m, 1H), 5.41 (br. d, *J* = 7.9 Hz, 1H), 4.39-4.29 (m, 1H), 3.63-3.60 (m, 2H), 3.59-3.54 (m, 3H), 3.41 (s, 3H), 2.60 (s, 6H), 1.94-1.82 (m, 4H), 1.81-1.67 (m, 4H).

^{13}C NMR (101 MHz, $CDCl_3$): δ 164.0, 157.5, 148.6, 140.7, 138.7, 127.1, 114.6, 88.4, 73.9, 72.4, 67.3, 59.2, 47.9, 28.4 (2C), 27.4 (2C), 27.1, 17.3.

LCMS (High pH, UV, ESI): t_{ret} = 1.40 min, $[M+H]^+$ m/z 456.1, 98.9% purity.

HRMS (TOF ESI, single mass analysis): $C_{19}H_{27}IN_3O_2$ $[M+H]^+$ m/z = 456.1148, found m/z = 456.1156 (Δ = 1.8 ppm).

6-(*1H*-Imidazol-1-yl)-*N*-((*cis*)-4-(2-methoxyethoxy)cyclohexyl)-2,8-dimethyl quinazolin-4-amine:

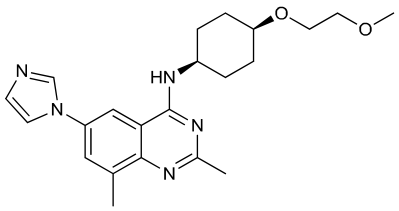

379

The reaction was performed following a literature procedure.[266]

To a mixture of 6-iodo-*N*-((*cis*)-4-(2-methoxyethoxy)cyclohexyl)-2,8-dimethyl quinazolin-4-amine (**378**, 100 mg, 0.220 mmol), imidazole (18 mg, 0.264 mmol), *D*-glucosamine (5 mg, 22 µmol) and caesium carbonate (143 mg, 0.439 mmol) in water (2 mL) and DMSO (2 mL) was added copper(I)iodide (4 mg, 22 µmol). The reaction mixture was heated, with stirring, to 100 °C for 72 h. A colour change was observed in the solution from blue-grey to brown during the reaction. The reaction mixture was partitioned between ethyl acetate (10 mL) and water (10 mL). The organic phase was collected, and the aqueous phase was extracted with ethyl acetate (2 x 10 mL). The organic layers were combined, passed through an Isolute® hydrophobic fritted reservoir (25 mL volume). Solvent was removed *in vacuo* to afford a crude product which was isolated using MDAP purification (High pH, method C), 20 min run. During the run, the MDAP machine suffered a mechanical failure. As

such, the waste stream was collected, concentrated *in vacuo*, and the resultant residue was purified using the same MDAP method. Solvent removal under a stream of nitrogen afforded 6-(*1H*-imidazol-1-yl)-*N*-((*cis*)-4-(2-methoxyethoxy)cyclohexyl)-2,8-dimethylquinazolin 4 amine (**379**, 6.40 mg, 16 µmol, 7% yield) as a pale pink powder.

mp: 217-218 °C (dec.).

ν_{max} (neat, cm^{-1}): 3284, 2928, 2859, 2440, 1520, 1087.

^{1}H NMR (600 MHz, CD_3OD): δ 8.24 (br. s, 1H), 8.19 (d, *J* = 2.6 Hz, 1H), 7.80-7.78 (m, 1H), 7.69 (br. s, 1H), 7.18 (br. s, 1H), 4.39-4.29 (m, 1H), 3.64-3.61 (m, 1H), 3.61-3.59 (m, 2H), 3.59-3.55 (m, 2H), 3.39 (s, 3H), 2.66 (s, 3H), 2.57 (s, 3H), 2.06-2.00 (m, 2H), 1.86-1.80 (m, 4H), 1.66-1.59 (m, 2H). NH peak not observed.

^{13}C NMR (151 MHz, CD_3OD): δ 165.6, 160.9, 149.1, 138.9, 137.1, 134.4, 130.3, 127.0, 119.7, 114.6, 112.4, 74.5, 73.5, 68.2, 59.2, 50.4, 29.7 (2C), 27.6 (2C), 26.4, 18.3.

LCMS (High pH, UV, ESI): t_{ret} = 1.07 min, $[M+H]^+$ m/z 396.1, 100.0% purity.

HRMS (TOF ESI, formic acid): $C_{22}H_{30}N_5O_2$ $[M+H]^+$ m/z = 396.2400, found m/z = 396.2403 (Δ = 0.8 ppm).

2-Chloro-8-methyl-*N*-propylquinazolin-4-amine:

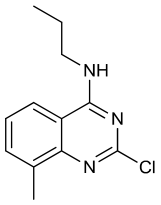

389

Batch synthesis (ambient conditions, Scheme 5.13): To a solution of 2,4-dichloro-8-methyl quinazoline (**349**, 600 mg, 2.82 mmol) in acetonitrile (10 mL) was added diisopropylethylamine (0.922 mL, 6.76 mmol) and 1-propylamine (**380**, 0.255 mL, 3.10 mmol). The reaction mixture was stirred at rt for 16 h. Solvent was removed *in vacuo* to afford an orange oil, which was partitioned between ethyl acetate (20 mL) and water (20 mL). The organic phase was collected, and the aqueous phase was extracted with ethyl acetate (2 x 20 mL), the organic phases were combined and passed through an Isolute® hydrophobic fritted reservoir (70 mL volume), and solvent was removed *in vacuo* to an orange crude oil, which was purified by flash column chromatography on a 40 g RediSep silica cartridge using an eluent gradient from cyclohexane to 40% TBME in cyclohexane. Product-containing fractions were combined, and solvent was removed *in vacuo* to afford 2-chloro-8-methyl-*N*-propylquinazolin-4-amine (**389**, 578 mg, 2.45 mmol, 87% yield) as a pale yellow crystalline solid.

mp: 109-110 °C.

ν_{max} (neat, cm^{-1}): 3344, 2964, 2927, 1558, 1532, 1331, 953, 759.

^{1}H NMR (400 MHz, $CDCl_3$): δ 7.58-7.54 (m, 1H), 7.49 (br. d, *J* = 8.0 Hz, 1H), 7.32 (dd, *J* = 8.2, 7.2 Hz, 1H), 5.81 (br. s, 1H), 3.66-3.59 (m, 2H), 2.63 (s, 3H), 1.74 (sxt, *J* = 7.3 Hz, 2H), 1.03 (t, J = 7.4 Hz, 3H).

^{13}C NMR (101 MHz, $CDCl_3$): δ 161.3, 157.1, 150.0, 136.6, 133.5, 125.5, 118.1, 113.0, 43.3, 22.5, 17.7, 11.5.

LCMS (High pH, UV, ESI): t_{ret} = 1.22 min, $[M+H]^+$ m/z 236.1, 100.0% purity.

HRMS (TOF ESI, formic acid): $C_{12}H_{15}ClN_3$ $[M+H]^+$ m/z = 236.0955, found m/z = 236.0959 (Δ = 1.7 ppm). Other m/z observed with heavier isotope = 238.0931.

The product was synthesised a further four times under similar conditions, with yields of 61% (1.88 mmol scale), 92% (2.35 mmol scale), 96% (4.69 mmol scale) and 98% (2.35 mmol scale).

8-Methyl-*N*^{2}-octyl-*N*^{4}-propylquinazoline-2,4-diamine:

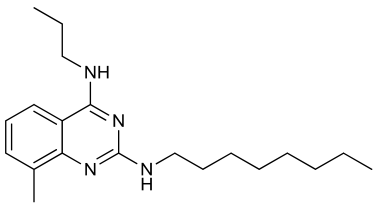

391

Optimal synthesis in MW reaction (batch):

2-Chloro-8-methyl-*N*-propylquinazolin-4-amine (**389**, 47 mg, 0.200 mmol) was dissolved in DMSO (0.4 mL). To this solution was added 1-octylamine (**390**, 66 µL, 0.400 mmol), and triethylamine (56 µL, 0.400 mmol). The reaction mixture was irradiated to 220 °C for 5 min in the MW reactor. The product mixture was analysed by LCMS analysis, and then irradiated for a further 10 min at 220 °C. LCMS analysis was also taken at the end of the reaction. LCMS analysis after 5 minutes showed 88% conversion to the desired product. 98% conversion to the desired product was observed after 15 minutes. The product was not purified further.

Synthesis in Buchwald plate procedure

The reaction was performed according to **General procedure F**, using the following conditions:

(a) 1-Octylamine (**390**, 30 µL, 0.180 mmol) **(b1)** DBU (36 µL, 0.240 mmol) **(b2)** DIPEA (**272**, 42 µL, 0.240 mmol) **(c)** 24 h reaction time using DMSO as solvent.

Full consumption of the 2-chloro-8-methyl-*N*-propylquinazolin-4-amine (**349**) starting material was observed in the use of **(b1)**, with XantPhos Pd G3 (vial A5, 16% desired product observed + by-products) or **(b2)** with SL-J009-1 Pd G3 (Vial D6, 25% desired product, various by-products observed).

The product was not purified further.

2-Chloro-8-methyl-4-(propylthio)quinazoline:

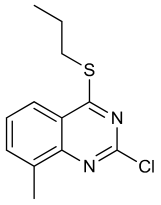

392

Example batch synthesis (Table 5.3, Entry 3): A solution of 2,4-dichloro-8-methylquinazoline (**349**, 43 mg, 0.200 mmol), triethylamine (28 µL, 0.200 mmol) and 1-propanethiol (**381**, 19 µL, 0.200 mmol) in dimethyl sulfoxide (2 mL) was prepared. The reaction mixture was heated to 40 °C for 5 min. LCMS analysis of the reaction mixture showed 98% conversion to the desired product, which was not purified further.

8-Methyl-2-propoxy-*N*-propylquinazolin-4-amine:

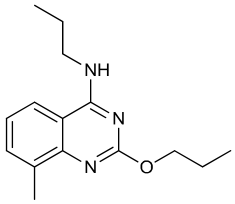

394

Synthesis in Buchwald plate procedure:

The reaction was performed according to **General procedure F**, using the following conditions:

(a) 1-Propanol (**382**, 14 µL, 0.180 mmol) **(b1)** DBU (54 µL, 0.360 mmol) **(b2)** DIPEA (**272**, 63 µL, 0.360 mmol) **(c)** 18 h reaction time using DMSO as solvent.

Full consumption of the 2-chloro-8-methyl-*N*-propylquinazolin-4-amine (**389**) starting material was observed in the use of **(b1)**, with RockPhos Pd G3 (vial A5, 87% desired product observed).

The product was not purified further.

Synthesis in Buchwald plate procedure (in Tamisolve®):

The reaction was performed according to **General procedure F**, using the following conditions:

(a) 1-Propanol (**382**, 9 µL, 0.120 mmol) **(b1)** Triethylamine (33 µL, 0.240 mmol) **(b2)** DBU (36 µL, 0.240 mmol) **(c)** 17 h reaction time using Tamisolve® as solvent.

Very poor conversion was observed in all cases. The most optimal conditions were observed in the use of **(b2)** with RockPhos Pd G3 (vial C5, 6% desired product observed) or with SL-J009-1 Pd G3 (vial D1, 8% desired product observed). The product was not purified further.

Batch Buchwald-Hartwig synthesis:

2-Chloro-8-methyl-*N*-propylquinazolin-4-amine (**389**, 47 mg, 0.200 mmol) and RockPhos Pd G3 (17 mg, 20.0 µmol) were combined in a reaction vessel. The vial was degassed and placed under a nitrogen atmosphere. In a separate vessel, a solution of DBU (90 µL, 0.600 mmol) and 1-propanol (**382**, 22 µL, 0.300 mmol), was degassed and placed under a nitrogen atmosphere, before anhydrous DMSO (2 mL) was added to the mixture. The contents of the second vial were added to the first vial, and the reaction was heated, with stirring, to 100 °C for 24 h. The reaction was cooled, the solution was separated into two batches, and the crude product solution was purified by MDAP isolation (Low pH), method A, 30 min run. Product-containing fractions were combined, and solvent was removed under a stream of nitrogen to afford 8-methyl-2-propoxy-*N*-propylquinazolin-4-amine (**394**, 35.0 mg, 0.135 mmol, 68% yield) as an orange oil.

ν_{max} (neat, cm^{-1}): 2967, 1573, 1174, 1128, 759.

^{1}H NMR (400 MHz, $CDCl_3$): δ 7.99 (br. s, 1H), 7.47 (br. d, *J* = 7.3, 1H), 7.21 (t, *J* = 7.7 Hz, 1H), 4.23 (t, *J* = 6.7 Hz, 2H), 3.46-3.28 (m, 2H), 2.56 (s, 3H), 1.83 (sxt, J = 7.1 Hz, 2H), 1.67 (sxt, *J* = 7.4 Hz, 2H), 1.06 (t, *J* = 7.5 Hz, 3H), 0.96 (t, *J* = 7.4 Hz, 3H).

^{13}C NMR (101 MHz, $CDCl_3$): δ 183.0, 162.5, 162.2, 161.5, 135.4, 124.6, 124.5, 110.8, 70.3, 43.9, 21.9, 21.8, 17.8, 11.5, 10.3.

LCMS (Low pH, UV, ESI): t_{ret} = 0.66 min, $[M+H]^+$ m/z 260.1, 100.0% purity.

HRMS (TOF ESI, formic acid): $C_{15}H_{22}N_3O$ $[M+H]^+$ m/z = 260.1763, found m/z = 260.1755 (Δ = -3.1 ppm).

Buchwald-Hartwig syntheses (Table 5.6, Entries 1-11):

For each reaction: Into a 5 mL MW vial was added 2-chloro-8-methyl-*N*-propyl quinazolin-4-amine (**389**, 47 mg, 0.200 mmol) RockPhos Pd G3 (either **(a)** 4 mg, 5 µmol, **(b)** 9 mg, 10 µmol, or **(c)** 17 mg, 20 µmol). In some cases, RockPhos (either **(d)** 9 mg, 20 µmol or **(e)** 5 mg, 10 µmol) was also added. The vial was degassed and placed under a nitrogen atmosphere. In a separate 5 mL MW vial, a solution of DBU (either **(f)** 90 µL, 0.600 mmol or **(g)** 30 µL, 0.200 mmol) and 1-propanol (**382**, either **(h)** 22 µL, 0.300 mmol or **(i)** 45 µL, 0.600 mmol), was degassed and placed under a nitrogen atmosphere, before anhydrous DMSO (2 mL) was added to the mixture. The contents of the second vial were added to the first vial, and the reaction was heated, either under thermal conditions **(j)**, or under microwave irradiation **(k)**, with stirring, to a temperature **(l)** for either 24 h **(m)** or 15 min **(n)**. The reaction was cooled, and an aliquot was removed and analysed by LCMS analysis (low pH), which showed **(o)** conversion to the desired product (according to the LCMS AUC composition which related to product **394**). The LCMS AUC composition which related to by-product **396** is denoted by **(p)** in each case. A general statement detailing the solubility of the reaction mixture in each case is provided by **(q)**. The products were not purified further in all cases. The conditions used for each reaction are stated below.

Table 5.6, Entry 1: (a), **(f)**, **(h)**, **(j)**, **(l)** 100 °C, **(m)**, **(o)** 13%, **(p)** 4%, **(q)** homogenous reaction mixture.

Table 5.6, Entry 2: (b), **(f)**, **(h)**, **(j)**, **(l)** 100 °C, **(m)**, **(o)** 51%, **(p)** 11%, **(q)** homogenous reaction mixture.

Table 5.6, Entry 3: (b), **(f)**, **(h)**, **(k)**, **(l)** 170 °C, **(n)**, **(o)** 29%, **(p)** 16%, **(q)** heterogenous reaction mixture.

Table 5.6, Entry 4: (a), **(f)**, **(i)**, **(k)**, **(l)** 170 °C, **(n)**, **(o)** 27%, **(p)** 15%, **(q)** homogenous reaction mixture.

Table 5.6, Entry 5: (b), **(d)**, **(f)**, **(i)**, **(k)**, **(l)** 170 °C, **(n)**, **(o)** 34%, **(p)** 29%, **(q)** heterogenous reaction mixture.

Table 5.6, Entry 6: (b), **(e)**, **(f)**, **(i)**, **(k)**, **(l)** 170 °C, **(n)**, **(o)** 32%, **(p)** 20%, **(q)** heterogenous reaction mixture.

Table 5.6, Entry 7: (b), **(f)**, **(i)**, **(k)**, **(l)** 150 °C, **(n)**, **(o)** 44%, **(p)** 16%, **(q)** heterogenous reaction mixture.

Table 5.6, Entry 8: (b), **(f)**, **(i)**, **(k)**, **(l)** 120 °C, **(n)**, **(o)** 36%, **(p)** 12%, **(q)** homogenous reaction mixture.

Table 5.6, Entry 9: (b), **(g)**, **(i)**, **(k)**, **(l)** 140 °C, **(n)**, **(o)** 39%, **(p)** 16%, **(q)** only minimal precipitation of reaction mixture observed.

Table 5.6, Entry 10: (b), **(g)**, **(i)**, **(k)**, **(l)** 130 °C, **(n)**, **(o)** 44%, **(p)** 11%, **(q)** homogenous reaction mixture.

Table 5.6, Entry 11: (c), **(g)**, **(i)**, **(k)**, **(l)** 130 °C, **(n)**, **(o)** 47%, **(p)** 12%, **(q)** heterogenous reaction mixture.

8-Methyl-*N*-propyl-2-(propylthio)quinazolin-4-amine:

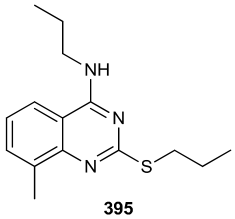

395

2-Chloro-8-methyl-*N*-propylquinazolin-4-amine (**389**, 47 mg, 0.200 mmol) and RockPhos Pd G3 (17 mg, 20.0 µmol) were combined in a reaction vessel. The vial was degassed and placed under a nitrogen atmosphere. In a separate vessel, a solution of DBU (90 µL, 0.600 mmol) and 1-propanethiol (**381**, 28 µL, 0.300 mmol) was degassed and placed under a nitrogen atmosphere, before anhydrous DMSO (2 mL) was added to the mixture. The contents of the second vial were added to the first vial, and the reaction was heated, with stirring, to 100 °C for 24 h. The reaction was cooled, the solution was separated into two batches, and the crude product solution was purified by MDAP isolation (Low pH), Method B, 30 min run. Product-containing fractions were combined, and solvent was removed under a stream of nitrogen to afford 8-methyl-2-propoxy-*N*-propylquinazolin-4-amine (**395**, 35 mg, 0.127 mmol, 64% yield) as a colourless oil.

ν_{max} (neat, cm^{-1}): 3327, 2962, 1672, 1532, 1329, 756.

^{1}H NMR (400 MHz, $CDCl_3$): δ 7.57 (br. s, 1H), 7.47 (br. dd, *J* = 7.3, 0.8 Hz, 1H), 7.19 (t, *J* = 7.7 Hz, 1H), 3.57-3.49 (m, 2H), 3.14 (t, *J* = 7.3 Hz, 2H), 2.60 (s, 3H), 1.81 (sxt, *J* = 7.3 Hz, 2H), 1.70 (sxt, *J* = 7.4 Hz, 2H), 1.06 (t, *J* = 7.3 Hz, 3H), 0.99 (t, *J* = 7.4 Hz, 3H). NH peak not observed.

^{13}C NMR (101 MHz, $CDCl_3$): δ 166.5, 162.6, 162.3, 158.7, 133.4, 124.2, 119.1, 112.1, 43.3, 33.0, 23.1, 22.4, 17.7, 13.6, 11.5.

LCMS (Low pH, UV, ESI): t_{ret} = 0.83 min, $[M+H]^+$ m/z 276.1, 100.0% purity.

HRMS (TOF ESI, formic acid): $C_{15}H_{22}N_3S$ $[M+H]^+$ m/z = 276.1534, found m/z = 276.1528 (Δ = -2.2 ppm).

8-Methyl-*N*^{2}-octyl-*N*^{4}-propylquinazoline-2,4-diamine formate:

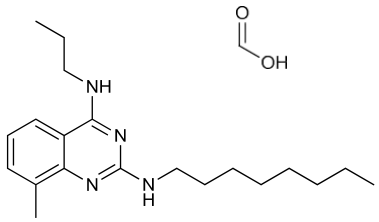

397

The reaction was performed according to **General procedure G (tandem flow synthesis of diaminoquinazolines)**, using the following conditions:

(a) 1 Eq. tributylamine was used for the first reaction (**273**, 96 µL, 0.400 mmol). **(b)** 1-Propylamine (**280**, 30 µL, 0.400 mmol) was used as the first nucleophile. **(c)** 1 Eq. tributylamine was used for the second reaction (**273**, 96 µL, 0.400 mmol). **(d)** 1-Octylamine (**390**, 0.120 mL, 0.800 mmol) was used as the second nucleophile. **(e)** The second reactor was heated to 200 °C. **(f)** An aliquot of the crude product solution was collected for 2 min 25 s. **(g)** The reaction aliquot was analysed using low pH LCMS analysis. **(h)** The product was purified using MDAP isolation (Low pH), method C, 30 min run. **(i)** 8-Methyl-*N*^{2}-octyl-*N*^{4}-propyl quinazoline-2,4-diamine formate (**397**, 32 mg, 85 µmol, 21% yield) was afforded as an off-white amorphous gum.

ν_{max} (neat, cm^{-1}): 3296, 2923, 1570, 1082, 756.

^{1}H NMR (400 MHz, $CDCl_3$): δ 8.88 (s, 1H), 7.41 (br. d, *J* = 6.4 Hz, 1H), 7.36 (br. d, *J* = 6.9 Hz, 1H), 6.96 (br. t, *J* = 7.9 Hz, 1H), 3.56-3.50 (m, 2H), 3.50-3.42 (m, 2H), 2.51 (s, 3H), 1.77-1.66 (m, 2H), 1.66-1.57 (m, 2H), 1.43-1.23 (m, 10H), 1.00 (t, *J* = 7.4 Hz, 3H), 0.88 (br. t, *J* = 7.4 Hz, 3H)

^{13}C NMR (101 MHz, $CDCl_3$): δ 169.6, 160.5, 160.4, 150.4, 133.2, 133.0, 120.5, 118.6, 110.2, 43.1, 41.5, 31.9, 29.9, 29.4, 29.3, 27.2, 22.7, 22.6, 17.7, 14.1, 11.6.

LCMS (Low pH, UV, ESI): t_{ret} = 1.06 min, $[M+H]^+$ m/z 329.3, 100.0% purity.

HRMS (TOF ESI, formic acid): $C_{20}H_{33}N_4$ $[M+H]^+$ m/z = 329.2705, found m/z = 329.2701 (Δ = -1.2 ppm).

The product was synthesised on one other occasion under similar conditions, but with a second reactor at 210 °C (condition **(e)**) with a yield of 24% (0.400 mmol scale).

2-Chloro-*N*-(4,4-difluorocyclohexyl)-8-methylquinazolin-4-amine:

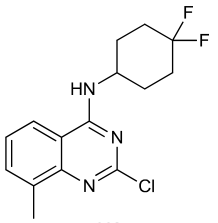

419

2,4-Dichloro-8-methylquinazoline (**349**, 85.0 mg, 0.400 mmol), 4,4-difluorocyclohexan-1-amine (**415**, 59.5 mg, 0.440 mmol) and DIPEA (**272**, 84.0 µL, 0.480 mmol) were combined in acetonitrile (3 mL). The mixture was stirred at rt for 1.5 h. The reaction mixture was concentrated *in vacuo*, and the resultant residue was partitioned between ethyl acetate (10 mL) and water (10 mL). The organic phase was collected, and the aqueous phase was extracted with ethyl acetate (2 x 10 mL). The organic phases were combined, washed with sat. aq. brine solution (10 mL) and passed through an Isolute® hydrophobic fritted reservoir (25 mL volume). Solvent was removed *in vacuo* to afford a crude mixture of regioisomers (including **419**; 92 mg, 0.295 mmol), as an off-white crystalline solid which was taken on without further purification.

2-(Azetidin-1-yl)-*N*-(4,4-difluorocyclohexyl)-8-methylquinazolin-4-amine:

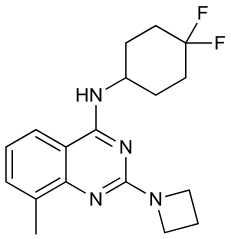

420

Batch synthesis from 2-chloro-*N*-(4,4-difluorocyclohexyl)-8-methylquinazolin-4-amine:

To a solution of the regioisomeric mixture mentioned above (**419**, 25.0 mg, 80 µmol) in IPA (1 mL) was added azetidine (**401**, 0.108 mL, 1.60 mmol). The vial was sealed, and heated to 100 °C for 72 h. The desired product was isolated using MDAP (high pH) method D purification, 20 min run. The product-containing fractions were combined, and solvent was removed under a stream of nitrogen to afford 2-(azetidin-1-yl)-*N*-(4,4-difluoro cyclohexyl)-8-methylquinazolin-4-amine (**420**, 12.3 mg, 37.0 µmol, 46% yield) as a brown oil.

Flow synthesis:

The reaction was performed according to **General procedure G (tandem flow synthesis of diaminoquinazolines)**, using the following conditions:

(a) 1 Eq. tributylamine was used for the first reaction (**273**, 96 µL, 0.800 mmol). **(b)** 4,4-difluorocyclohexan-1-amine (**415**, 65 mg, 0.480 mmol) was used as the first nucleophile. **(c)** 1.5 eq. tributylamine was used for the second reaction (**273**, 0.140 mL, 0.600 mmol). **(d)** Azetidine (**401**, 81 µL, 1.20 mmol) was used as the second nucleophile. **(e)** The second reactor was heated to 210 °C. **(f)** An aliquot of the crude product solution was collected for 1 min 10 s. **(g)** The reaction aliquot was analysed using high pH LCMS analysis. **(h)** The product was purified using MDAP isolation (high pH), method D, 20 min run. **(i)** 2-(Azetidin-1-yl)-*N*-(4,4-difluorocyclohexyl)-8-methylquinazolin-4-amine (**420**, 5 mg, 14 µmol, 3% yield) was afforded as a beige powder.

Unfortunately, during the reaction, precipitation was observed in the reactor. The material which was salvaged from the reaction prior to blockage is reported, although the product was also resynthesised in batch to generate sufficient material for all analyses.

ν_{max} (neat, cm^{-1}): 3339, 2935, 1562, 1143, 1004, 756.

^{1}H NMR (400 MHz, $CDCl_3$): δ 7.39 (d, *J* = 6.9 Hz, 1H), 7.32 (br. d, *J* = 7.9 Hz, 1H), 7.00-6.95 (m, 1H), 5.31 (br. s, 1H), 4.31-4.22 (m, 1H), 4.18 (t, *J* = 7.4 Hz, 4H), 2.53 (s, 3H), 2.33 (quin, *J* = 7.5 Hz, 2H), 2.25-2.12 (m, 4H), 2.01-1.84 (m, 2H), 1.74-1.60 (m, 2H).

^{13}C NMR (101 MHz, $CDCl_3$): δ 160.2, 159.6, 151.1, 134.3, 132.4, 122.7, 120.2, 117.9, 109.8, 50.2 (2C), 47.5, 32.3 (2C), 28.5, 28.4, 17.5, 16.2.

^{19}F NMR (376 MHz, $CDCl_3$): δ -94.85 (d, $^{2F\text{-}F}J$ = 244 Hz, 1F), -100.85 (d, $^{2F\text{-}F}J$ = 244 Hz, 1F).

LCMS (High pH, UV, ESI): t_{ret} = 1.40 min, $[M+H]^+$ m/z 333.2, 100.0% purity.

HRMS (TOF ESI, formic acid): $C_{18}H_{23}F_2N_4$ $[M+H]^+$ m/z = 333.1891, found m/z = 333.1902 (Δ = 3.3 ppm).

4-((4-((4,4-Difluorocyclohexyl)amino)-8-methylquinazolin-2-yl)amino)butan-1-ol:

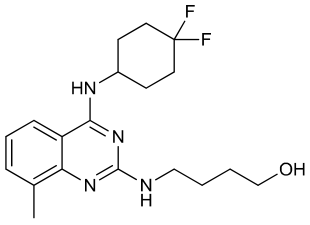

421

To a solution of 2-chloro-*N*-(4,4-difluorocyclohexyl)-8-methylquinazolin-4-amine (**419**, 40 mg, 0.128 mmol) in IPA (1 mL) was added 4-aminobutan-1-ol (**416**, 0.237 mL, 2.57 mmol). The vial was sealed, and heated to 100 °C for 72 h. The desired product was isolated using MDAP (high pH) method C purification, 20 min run. The product-containing fractions were combined, and solvent was removed under a stream of nitrogen to afford 4-((4-((4,4-difluorocyclohexyl)amino)-8-methylquinazolin-2-yl)amino)butan-1-ol (**421**, 17 mg, 47 µmol, 37% yield) as a white powder.

mp: 78-79 °C.

ν_{max} (neat, cm^{-1}): 3343, 2932, 1580, 1375, 1117, 761.

^{1}H NMR (400 MHz, $CDCl_3$): δ 7.39 (br. d, *J* = 6.8 Hz, 1H), 7.30 (d, *J* = 8.4 Hz, 1H), 6.96 (dd, *J* = 8.1, 7.1 Hz, 1H), 5.26 (br. d, *J* = 7.4 Hz, 1H), 4.97 (br. s, 1H), 4.31-4.19 (m, 1H), 3.71 (t, *J* = 5.9 Hz, 2H), 3.55 (br. t, *J* = 6.2 Hz, 2H), 2.52 (s, 3H), 2.22-2.11 (m, 4H), 2.03–1.85 (m, 2H), 1.78-1.66 (m, 6H). NH peak not observed.

^{13}C NMR (101 MHz, $CDCl_3$): δ 159.9, 159.1, 151.2, 134.1, 132.8, 122.8, 120.4, 118.1, 110.5, 62.9, 47.6, 41.3, 32.5, 30.2 (2C), 28.7 (2C), 26.7, 17.9.

^{19}F NMR (376 MHz, $CDCl_3$): δ -94.75 (d, $^{2F\text{-}F}$J = 235 Hz, 1F), -101.10 (d, $^{2F\text{-}F}$J = 235 Hz, 1F).

LCMS (High pH, UV, ESI): t_{ret} = 1.11 min, $[M+H]^+$ m/z 365.1, 100.0% purity.

HRMS (TOF ESI, formic acid): $C_{19}H_{27}F_2N_4O$ $[M+H]^+$ m/z = 365.2153, found m/z = 365.2156 (Δ = 0.8 ppm).

2-Chloro-*N*-((*trans*)-4-(2-methoxyethoxy)cyclohexyl)-8-methylquinazolin-4-amine:

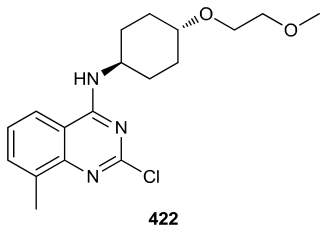

422

The reaction was performed according to **General procedure G (tandem flow synthesis of diaminoquinazolines)**, using the following conditions:

(a) 1 Eq. tributylamine was used for the first reaction (**273**, 96 mL, 0.400 mmol). **(b)** (*trans*)-4-(2-Methoxyethoxy)cyclohexan-1-amine (**356**, 83 mg, 0.480 mmol) was used as the first nucleophile. **(c)** 1.5 Eq. tributylamine was used for the second reaction (**273**, 0.140 mL, 0.600 mmol). **(d)** Ethanamine (**405**, 70% wt. solution in H_2O, 95 µL, 1.20 mmol) was used as the second nucleophile. **(e)** The second reactor was heated to 210 °C. **(f)** An aliquot of the

crude product solution was collected for 1 min 10 s. **(g)** The reaction aliquot was analysed using high pH LCMS analysis. **(h)** The product was purified using an array MDAP isolation (high pH), method C, 30 min run. **(i)** The desired product was not made in the reaction, and as such, the intermediate, 2-chloro-*N*-((*trans*)-4-(2-methoxyethoxy)cyclohexyl)-8-methyl quinazolin-4-amine (**422**, 22 mg, 63 µmol, 16% yield) was isolated a white crystalline solid.

ν_{max} (neat, cm^{-1}): 3351, 2937, 1530, 1266, 1087, 755.

^{1}H NMR (400 MHz, $CDCl_3$): δ 7.59-7.54 (m, 1H), 7.45 (d, *J* = 8.4 Hz, 1H), 7.32 (dd, *J* = 7.4, 7.4 Hz, 1H), 5.56 (br. d, *J* = 7.5 Hz, 1H), 4.31-4.19 (m, 1H), 3.67-3.62 (m, 2H), 3.58-3.53 (m, 2H), 3.40 (s, 3H), 3.38-3.29 (m, 1H), 2.64 (s, 3H), 2.30-2.21 (m, 2H), 2.16-2.08 (m, 2H), 1.59-1.46 (m, 2H), 1.38-1.26 (m, 2H).

^{13}C NMR (101 MHz, $CDCl_3$): δ 160.7, 157.2, 150.2, 136.8, 133.6, 125.6, 118.1, 113.1, 77.7, 72.5, 67.7, 59.3, 49.5, 30.8 (2C), 30.6 (2C), 17.8.

LCMS (High pH, UV, ESI): t_{ret} = 1.19 min, $[M+H]^+$ m/z 350.0, 100.0% purity.

HRMS (TOF ESI, formic acid): $C_{18}H_{25}ClN_3O_2$ $[M+H]^+$ m/z = 350.1635, found m/z = 350.1635 (Δ = 1.4 ppm). Other m/z observed with heavier isotope = 352.1613.

***N^2*,*N^4*-Bis((*R*)-1-cyclohexylethyl)-8-methylquinazoline-2,4-diamine formate:**

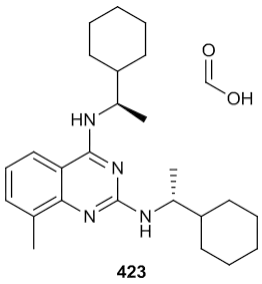

423

To a solution of 2,4-dichloro-8-methylquinazoline (**349**, 85 mg, 0.400 mmol) and tributylamine (**273**, 0.238 mL, 1.00 mmol) in Tamisolve® (2 mL total volume) was added (*R*)-1-cyclohexyl ethan-1-amine (**407**, 0.247 mL, 1.68 mmol). The reaction mixture was irradiated, with stirring, at 210 °C for 30 min in the MW reactor. The product was purified using MDAP isolation (low pH), method C, 30 min run. Product-containing fractions were combined, and solvent was removed under a stream of nitrogen to afford *N^2*,*N^4*-bis((*R*)-1-cyclohexyl ethyl)-8-methylquinazoline-2,4-diamine formate (**423**, 101 mg, 0.229 mmol, 57% yield) as an off-white crystalline solid

mp: 90-91 °C.

ν_{max} (neat, cm^{-1}): 3343, 2932, 1579, 1375, 1117, 761.

^{1}H NMR (600 MHz, $CDCl_3$): δ 9.41 (br. s, 1H), 8.90 (s, 1H), 8.47 (br. s, 1H), 8.10 (br. s, 1H), 7.35 (d, *J* = 7.3 Hz, 1H), 7.02 (t, *J* = 7.7 Hz, 1H), 4.30 (sxt, *J* = 7.3 Hz, 1H), 4.05 (sxt, *J* = 6.6 Hz, 1H), 2.51 (s, 3H), 1.84-1.74 (m, 4H), 1.74-1.51 (m, 8H), 1.29 (d, *J* = 7.0 Hz, 3H), 1.21 (d, *J* = 7.0 Hz, 3H), 1.20-0.97 (m, 10H).

^{13}C NMR (151 MHz, $CDCl_3$): δ 169.1, 159.8, 153.8, 139.2, 134.8, 126.1, 122.4, 121.0, 109.6, 52.2, 51.7, 42.3 (2C), 29.4 (2C), 29.2 (2C), 25.9 (6C), 17.5, 17.0 (2C).

LCMS (Low pH, UV, ESI): t_{ret} = 1.27 min, mass ion not observed, 97.1% purity. Broad peak. Product unstable to LCMS analysis.

HRMS (TOF ESI, formic acid): $C_{25}H_{39}N_4$ $[M+H]^+$ m/z = 395.3175, found m/z = 395.3178 (Δ = 0.8 ppm).

4-((2-(1,1-Dioxidothiomorpholino)-8-methylquinazolin-4-yl)amino)-1-methyl pyrrolidin-2-one:

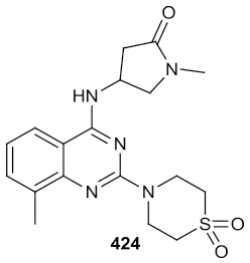

424

The reaction was performed according to **General procedure G (tandem flow synthesis of diaminoquinazolines)**, using the following conditions:

(a) 1 Eq. tributylamine was used for the first reaction (**273**, 96 µL, 0.400 mmol). **(b)** 4-Amino-1-methylpyrrolidin-2-one (**412**, 55 mg, 0.480 mmol) was used as the first nucleophile. **(c)** 1.5 eq. tributylamine was used for the second reaction (**273**, 0.140 mL, 0.600 mmol). **(d)** Thiomorpholine 1,1-dioxide (**399**, 162 mg, 1.20 mmol) was used as the second nucleophile. **(e)** The second reactor was heated to 210 °C. **(f)** An aliquot of the crude product solution was collected for 1 min 10 s. **(g)** The reaction aliquot was analysed using high pH LCMS analysis. **(h)** The product was purified using array MDAP isolation (high pH), focused method B, 20 min run. **(i)** 4-((2-(1,1-Dioxidothiomorpholino)-8-methyl quinazolin-4-yl)amino)-1-methylpyrrolidin-2-one (**424**, 32 mg, 82 µmol, 21% yield) was afforded as a white powder.

mp: 297-298 °C (dec.).

ν_{max} (neat, cm^{-1}): 3349, 1675, 1541, 1288, 1125, 756.

^{1}H NMR (400 MHz, DMSO-*d*$_6$): δ 8.12 (d, *J* = 5.9 Hz, 1H), 7.94 (d, *J* = 7.9 Hz, 1H), 7.44 (d, *J* = 6.9 Hz, 1H), 7.04 (dd, *J* = 8.1, 7.1 Hz, 1H), 4.78-4.63 (m, 1H), 4.33-4.20 (m, 4H), 3.77 (dd, *J* = 10.3, 7.4 Hz, 1H), 3.38 (dd, *J* = 10.3, 3.9 Hz, 1H), 3.17 - 3.09 (m, 4H), 2.74 (s, 3H), 2.73-2.66 (m, 1H), 2.54-2.51 (m, 1H), 2.42 (s, 3H).

^{13}C NMR (101 MHz, DMSO-*d*$_6$): δ 172.0, 160.3, 156.4, 150.1, 132.8, 132.5, 120.6, 120.5, 110.2, 54.9, 50.7 (2C), 44.0, 42.4 (2C), 36.4, 28.9, 17.3.

LCMS (High pH, UV, ESI): t_{ret} = 0.92 min, $[M+H]^+$ m/z 390.2, 100.0% purity.

HRMS (TOF ESI, formic acid): $C_{18}H_{24}N_5O_3S$ $[M+H]^+$ m/z = 390.1600, found m/z = 390.1601 (Δ = 0.3 ppm).

3-((2-(1,1-Dioxidothiomorpholino)-8-methylquinazolin-4-yl)amino)azepan-2-one:

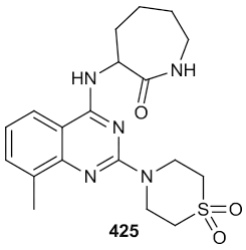

425

The reaction was performed according to **General procedure G (tandem flow synthesis of diaminoquinazolines)**, using the following conditions:

(a) 1 Eq. tributylamine was used for the first reaction (**273**, 96 µL, 0.400 mmol). **(b)** 3-Aminoazepan-2-one (**406**, 51 mg, 0.400 mmol) was used as the first nucleophile. **(c)** 1 Eq. tributylamine was used for the second reaction (**273**, 96 µL, 0.400 mmol). **(d)** Thiomorpholine 1,1-dioxide (**399**, 162 mg, 1.20 mmol) was used as the second nucleophile. **(e)** The second reactor was heated to 210 °C. **(f)** An aliquot of the crude product solution was collected for 2 min 25 s. **(g)** The reaction aliquot was analysed using low pH LCMS analysis. **(h)** The product was purified using array MDAP isolation (low pH), method A, 20 min run. **(i)** 3-((2-(1,1-Dioxidothiomorpholino)-8-methylquinazolin-4-yl)amino) azepan-2-one (**425**, 12 mg, 30 µmol, 7% yield) was afforded as a white powder.

mp: 297-298 °C (dec.).

ν_{max} (neat, cm^{-1}): 3375, 3312, 2921, 1667, 1475, 1115, 761.

^{1}H NMR (400 MHz, CDCl$_3$): δ 7.57 (d, *J* = 8.4 Hz, 1H), 7.46 (d, *J* = 7.4 Hz, 1H), 7.28-7.26 (m, 1H), 7.10 (dd, *J* = 8.1, 7.1 Hz, 1H), 6.15 (t, *J* = 6.4 Hz, 1H), 4.78-4.70 (m, 1H), 4.46 (br. t, *J* = 4.9 Hz, 4H), 3.43-3.32 (m, 2H), 3.16-3.02 (m, 4H), 2.51 (s, 3H), 2.34-2.27 (m, 1H), 2.18-2.10 (m, 1H), 1.98-1.89 (m, 1H), 1.75 (tt, *J* = 13.4, 3.1 Hz, 1H), 1.59-1.49 (m, 2H).

^{13}C NMR (101 MHz, $CDCl_3$): δ 175.7, 159.1, 156.5, 150.4, 134.3, 133.0, 121.8, 118.9, 110.5, 53.6, 51.5 (2C), 43.0 (2C), 42.4, 30.7, 29.0, 28.4, 17.6.

LCMS (Low pH, UV, ESI): t_{ret} = 0.57 min, $[M+H]^+$ m/z 404.2, 96.9% purity.

HRMS (TOF ESI, formic acid): $C_{19}H_{26}N_5O_3S$ $[M+H]^+$ m/z = 404.1756, found m/z = 404.1755 (Δ = -0.2 ppm).

2-((2-(1,1-Dioxidothiomorpholino)-8-methylquinazolin-4-yl)amino)-*N*,*N*-dimethyl acetamide:

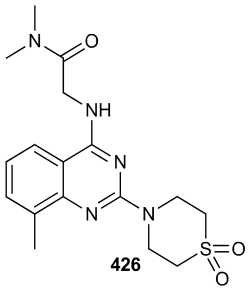

426

The reaction was performed according to **General procedure G (tandem flow synthesis of diaminoquinazolines)**, using the following conditions:

(a) 2 Eq. tributylamine was used for the first reaction (**273**, 0.191 mL, 0.800 mmol). **(b)** 2-Amino-*N*,*N*-dimethylacetamide acetate (**409**, 65 mg, 0.400 mmol) was used as the first nucleophile. **(c)** 1 Eq. tributylamine was used for the second reaction (**273**, 96 µL, 0.400 mmol). **(d)** Thiomorpholine 1,1-dioxide (**399**, 162 mg, 1.20 mmol) was used as the second nucleophile. **(e)** The second reactor was heated to 210 °C. **(f)** An aliquot of the crude product solution was collected for 2 min 25 s. **(g)** The reaction aliquot was analysed using low pH LCMS analysis. **(h)** The product was purified using MDAP isolation (high pH), method B, 20 min run. **(i)** 2-((2-(1,1-Dioxidothiomorpholino)-8-methylquinazolin-4-yl)amino)-*N*,*N*-dimethylacetamide (**426**, 17 mg, 46 µmol, 12% yield) was afforded as a white crystalline solid.

mp: 217-218 °C.

ν_{max} (neat, cm^{-1}): 3265, 2931, 1548, 1296, 1122, 765.

^{1}H NMR (400 MHz, $CDCl_3$): δ 7.58 (d, *J* = 8.4 Hz, 1H), 7.48-7.43 (m, 1H), 7.09 (dd, *J* = 8.1, 7.1 Hz, 1H), 6.97 (t, *J* = 3.9 Hz, 1H), 4.45 (br. t, *J* = 4.9 Hz, 4H), 4.25 (d, *J* = 3.9 Hz, 2H), 3.11-3.06 (m, 10H), 2.51 (s, 3H).

^{13}C NMR (101 MHz, $CDCl_3$): δ 168.2, 160.1, 156.6, 150.3, 134.3, 133.0, 121.8, 118.9, 110.3, 51.5 (2C), 43.0 (2C), 42.6, 36.0, 35.7, 17.6.

LCMS (High pH, UV, ESI): t_{ret} = 0.92 min, $[M+H]^+$ m/z 378.2, 98.7% purity.

HRMS (TOF ESI, formic acid): $C_{17}H_{24}N_5O_3S$ $[M+H]^+$ m/z = 378.1600, found m/z = 378.1602 (Δ = 0.5 ppm).

***tert*-Butyl-3-((2-(azetidin-1-yl)-8-methylquinazolin-4-yl)amino)propanoate:**

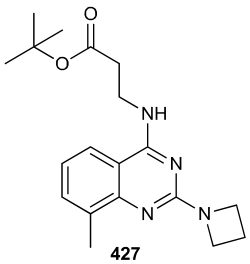

427

The reaction was performed according to **General procedure G (tandem flow synthesis of diaminoquinazolines)**, using the following conditions:

(a) 2 Eq. tributylamine was used for the first reaction (**273**, 0.191 mL, 0.800 mmol). **(b)** *tert*-Butyl-3-aminopropanoate hydrochloride (**410**, 73 mg, 0.400 mmol) was used as the first nucleophile. **(c)** 1 Eq. tributylamine was used for the second reaction (**273**, 96 µL, 0.400 mmol). **(d)** Azetidine (**401**, 81 µL, 1.20 mmol) was used as the second nucleophile. **(e)** The second reactor was heated to 210 °C. **(f)** An aliquot of the crude product solution was collected for 2 min 25 s. **(g)** The reaction aliquot was analysed using high pH LCMS analysis. **(h)** The product was purified using MDAP isolation (high pH), method D, 30 min run. **(i)** *tert*-Butyl-3-((2-(azetidin-1-yl)-8-methylquinazolin-4-yl)amino)propanoate (**427**, 14 mg, 40 µmol, 10% yield) was afforded as a beige powder.

During the reaction, precipitation was observed in the reactor. The material which was collected from the reaction prior to blockage is reported.

mp: 97-98 °C.

ν_{max} (neat, cm^{-1}): 3317, 2937, 1722, 1569, 1434, 1152, 773.

^{1}H NMR (400 MHz, $CDCl_3$): δ 7.38 (d, *J* = 6.9 Hz, 1H), 7.33 (d, *J* = 8.4 Hz, 1H), 6.96 (t, *J* = 6.9 Hz, 1H), 6.12 (br. s, 1H), 4.17 (t, *J* = 7.4 Hz, 4H), 3.84 (q, *J* = 5.9 Hz, 2H), 2.61 (t, *J* = 6.4 Hz, 2H), 2.52 (s, 3H), 2.31 (quin, *J* = 7.6 Hz, 2H), 1.45 (s, 9H).

^{13}C NMR (101 MHz, $CDCl_3$): δ 172.4, 160.2, 134.0, 132.4, 120.2, 118.3, 110.1 (2C), 110.0, 81.0, 50.3 (2C), 36.6, 34.8, 28.2 (3C), 17.5, 16.3.

LCMS (High pH, UV, ESI): t_{ret} = 1.39 min, $[M+H]^+$ m/z 343.0, 100.0% purity.

HRMS (TOF ESI, formic acid): $C_{19}H_{27}N_4O_2$ $[M+H]^+$ m/z = 313.2134, found m/z = 313.2135 (Δ = 0.3 ppm).

4-((8-Methyl-4-(4-methylpiperazin-1-yl)quinazolin-2-yl)amino)butan-1-ol:

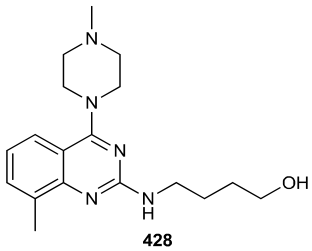

428

The reaction was performed according to **General procedure G (tandem flow synthesis of diaminoquinazolines)**, using the following conditions:

(a) 1 Eq. tributylamine was used for the first reaction (**273**, 96 µL, 0.400 mmol). **(b)** 1-Methylpiperazine (**400**, 44 mg, 0.400 mmol) was used as the first nucleophile. **(c)** 1 Eq. tributylamine was used for the second reaction (**273**, 96 µL, 0.400 mmol). **(d)** 4-aminobutan-1-ol (**416**, 0.111 mL, 1.20 mmol) was used as the second nucleophile. **(e)** The second reactor was heated to 210 °C. **(f)** An aliquot of the crude product solution was collected for 2 min 25 s. **(g)** The reaction aliquot was analysed using high pH LCMS analysis. **(h)** The product was purified using MDAP isolation (high pH), method B, 20 min run. **(i)** 4-((8-Methyl-4-(4-methylpiperazin-1-yl)quinazolin-2-yl)amino)butan-1-ol (**428**, 30 mg, 91 µmol, 23% yield) was afforded as a viscous orange oil.

ν_{max} (neat, cm^{-1}): 3339, 2935, 1562, 1143, 1004, 756.

^{1}H NMR (400 MHz, $CDCl_3$): δ 7.54 (d, *J* = 7.9 Hz, 1H), 7.37 (d, *J* = 6.9 Hz, 1H), 6.95 (t, *J* = 7.6 Hz, 1H), 5.29 (br. s, 1H), 3.70 (t, *J* = 6.2 Hz, 2H), 3.64 (br. t, *J* = 4.4 Hz, 4H), 3.55 (br. t, *J* = 5.9 Hz, 2H), 3.48 (s, 1H), 2.59 (br. t, *J* = 4.4 Hz, 4H), 2.54 (s, 3H), 2.36 (s, 3H), 1.78-1.66 (m, 4H).

^{13}C NMR (101 MHz, $CDCl_3$): δ 166.7, 158.4, 153.0, 133.8, 132.4, 122.9, 119.8, 112.2, 62.7, 55.0 (2C), 49.9 (2C), 46.2, 41.3, 30.1, 26.5, 17.8.

LCMS (High pH, UV, ESI): t_{ret} = 0.96 min, $[M+H]^+$ m/z 330.2, 100.0% purity.

HRMS (TOF ESI, formic acid): $C_{18}H_{28}N_5O$ $[M+H]^+$ m/z = 330.2294, found m/z = 330.2295 (Δ = 0.3 ppm).

4-(4-((4-Hydroxybutyl)amino)-8-methylquinazolin-2-yl)thiomorpholine-1,1-dioxide:

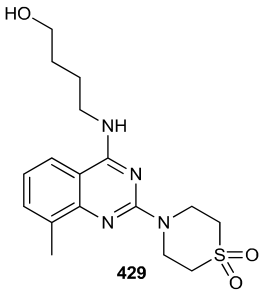

429

The reaction was performed according to **General procedure G (tandem flow synthesis of diaminoquinazolines)**, using the following conditions:

(a) 1 Eq. tributylamine was used for the first reaction (**273**, 96 µL, 0.400 mmol). **(b)** 4-Aminobutan-1-ol (**416**, 44 µL, 0.480 mmol) was used as the first nucleophile. **(c)** 1.5 Eq. tributylamine was used for the second reaction (**273**, 0.140 mL, 0.600 mmol). **(d)** Thiomorpholine-1,1-dioxide (**399**, 162 mg, 1.20 mmol) was used as the second nucleophile. **(e)** The second reactor was heated to 210 °C. **(f)** An aliquot of the crude product solution was collected for 1 min 10 s. **(g)** The reaction aliquot was analysed using high pH LCMS analysis. **(h)** The product was purified using MDAP isolation (high pH), method B, 20 min run. **(i)** 4-(4-((4-Hydroxybutyl)amino)-8-methylquinazolin-2-yl)thiomorpholine-1,1-di oxide (**429**, 59 mg, 0.162 mmol, 41% yield) was afforded as a beige powder.

mp: 173-174 °C.

ν_{max} (neat, cm^{-1}): 3418, 2906, 1575, 1281, 1121, 753.

^{1}H NMR (400 MHz, $CDCl_3$): δ 7.43 (br. d, *J* = 7.4 Hz, 1H), 7.39 (d, *J* = 7.9 Hz, 1H), 7.05 (dd, *J* = 8.1, 7.1 Hz, 1H), 6.01 (br. t, *J* = 5.4 Hz, 1H), 4.50-4.39 (m, 4H), 3.79-3.70 (m, 2H), 3.66-3.58 (m, 2H), 3.11-3.05 (m, 4H), 2.51 (s, 3H), 1.86-1.77 (m, 2H), 1.77-1.67 (m, 2H), 1.53 (br. s, 1H).

^{13}C NMR (101 MHz, $CDCl_3$): δ 160.9, 156.8, 150.5, 134.5, 132.7, 121.5, 118.2, 110.3, 62.5, 51.5 (2C), 43.0 (2C), 41.1, 30.0, 25.8, 17.6.

LCMS (High pH, UV, ESI): t_{ret} = 0.96 min, $[M+H]^+$ m/z 365.2, 100.0% purity.

HRMS (TOF ESI, formic acid): $C_{17}H_{25}N_4O_3S$ $[M+H]^+$ m/z = 365.1647, found m/z = 365.1649 (Δ = 0.5 ppm).

(*R*)-4-((4-((1-Cyclohexylethyl)amino)-8-methylquinazolin-2-yl)amino)butan-1-ol:

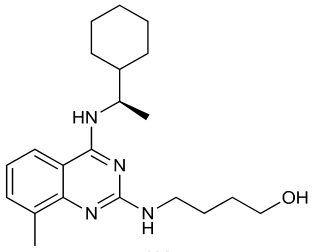

430

The reaction was performed according to **General procedure G (tandem flow synthesis of diaminoquinazolines)**, using the following conditions:

(a) 1 Eq. tributylamine was used for the first reaction (**273**, 96 mL, 0.400 mmol). **(b)** (*R*)-1-Cyclohexylethan-1-amine (**407**, 71 µL, 0.480 mmol) was used as the first nucleophile. **(c)** 1.5 Eq. tributylamine was used for the second reaction (**273**, 0.140 mL, 0.600 mmol). **(d)** 4-Aminobutan-1-ol (**416**, 0.111 mL, 1.20 mmol) was used as the second nucleophile. **(e)** The second reactor was heated to 210 °C. **(f)** An aliquot of the crude product solution was collected for 1 min 10 s. **(g)** The reaction aliquot was analysed using high pH LCMS analysis. **(h)** The product was purified using an array MDAP isolation (high pH), method D, 20 min run. **(i)** (*R*)-4-((4-((1-Cyclohexylethyl)amino)-8-methylquinazolin-2-yl)amino) butan-1-ol (**430**, 28 mg, 79 µmol, 20% yield) was afforded as a pale brown oil, which later crystallised.

mp: 58-59 °C.

$[\alpha_D]^{20\,°C}$ (c. 0.50, MeCN) + 4°.

ν_{max} (neat, cm^{-1}): 3354, 2923, 2851, 1576, 1511, 757.

^{1}H NMR (400 MHz, $CDCl_3$): δ 7.37 (d, *J* = 6.9 Hz, 1H), 7.31 (d, *J* = 7.9 Hz, 1H), 6.95 (t, *J* = 7.9 Hz, 1H), 5.29 (br. d, *J* = 7.4 Hz, 1H), 4.94 (br. s, 1H), 4.35-4.25 (m, 1H), 3.71 (t, *J* = 6.2 Hz, 2H), 3.58-3.50 (m, 2H), 2.52 (s, 3H), 1.84-1.65 (m, 11H), 1.57-1.47 (m, 1H), 1.32-1.23 (m, 1H), 1.21 (d, *J* = 6.9 Hz, 3H), 1.16-1.05 (m, 2H).

^{13}C NMR (101 MHz, $CDCl_3$): δ 160.0, 159.2, 151.1, 133.7, 132.4, 120.0, 118.0, 110.5, 62.8, 50.3, 43.3, 41.1, 30.1, 29.4, 29.0, 26.6, 26.5, 26.4, 26.3, 17.8, 17.7.

LCMS (High pH, UV, ESI): t_{ret} = 1.34 min, $[M+H]^+$ m/z 357.3, 100.0% purity.

HRMS (TOF ESI, formic acid): $C_{21}H_{33}N_4O$ $[M+H]^+$ m/z = 357.2654, found m/z = 357.2657 (Δ = 0.8 ppm).

(*S*)-4-((4-((1-Cyclohexylethyl)amino)-8-methylquinazolin-2-yl)amino)butan-1-ol:

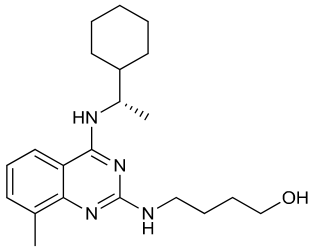

431

The reaction was performed according to **General procedure G (tandem flow synthesis of diaminoquinazolines)**, using the following conditions:

(a) 1 eq. tributylamine was used for the first reaction (**273**, 96 mL, 0.400 mmol). **(b)** (*S*)-1-cyclohexylethan-1-amine (**408**, 71 µL, 0.480 mmol) was used as the first nucleophile. **(c)** 1.5 eq. tributylamine was used for the second reaction (**273**, 0.140 mL, 0.600 mmol). **(d)** 4-Aminobutan-1-ol (**416**, 0.111 mL, 1.20 mmol) was used as the second nucleophile. **(e)** The second reactor was heated to 210 °C. **(f)** An aliquot of the crude product solution was collected for 1 min 10 s. **(g)** The reaction aliquot was analysed using high pH LCMS analysis. **(h)** The product was purified using an array MDAP isolation (high pH), method D, 20 min run. **(i)** (*S*)-4-((4-((1-Cyclohexylethyl)amino)-8-methylquinazolin-2-yl)amino)butan-1-ol (**431**, 23 mg, 63 µmol, 16% yield) was afforded as a pale brown oil, which later crystallised.

mp: 58-59 °C.

$[\alpha_D]^{20\ °C}$ (c. 0.50, MeCN) - 4°.

ν_{max} (neat, cm^{-1}): 3354, 2923, 2851, 1576, 1511, 757.

^{1}H NMR (400 MHz, $CDCl_3$): δ 7.37 (d, *J* = 6.9 Hz, 1H), 7.31 (d, *J* = 7.9 Hz, 1H), 6.95 (t, *J* = 7.9 Hz, 1H), 5.29 (br. d, *J* = 7.4 Hz, 1H), 4.94 (br. s, 1H), 4.35-4.25 (m, 1H), 3.71 (t, *J* = 6.2 Hz, 2H), 3.58-3.50 (m, 2H), 2.52 (s, 3H), 1.84-1.65 (m, 11H), 1.57-1.47 (m, 1H), 1.32-1.23 (m, 1H), 1.21 (d, *J* = 6.9 Hz, 3H), 1.16-1.05 (m, 2H). 1H peak not observed (exchangeable).

^{13}C NMR (101 MHz, $CDCl_3$): δ 160.0, 159.2, 151.1, 133.7, 132.4, 120.0, 118.0, 110.5, 62.8, 50.3, 43.3, 41.1, 30.1, 29.4, 29.0, 26.6, 26.5, 26.4, 26.3, 17.8, 17.7.

LCMS (High pH, UV, ESI): t_{ret} = 1.33 min, $[M+H]^+$ m/z 357.3, 100.0% purity.

HRMS (TOF ESI, formic acid): $C_{21}H_{33}N_4O$ $[M+H]^+$ m/z = 357.2654, found m/z = 357.2656 (Δ = 0.6 ppm).

4-((4-(Cyclopropylamino)-8-methylquinazolin-2-yl)amino)butan-1-ol:

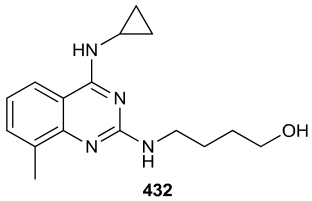

432

The reaction was performed according to **General procedure G (tandem flow synthesis of diaminoquinazolines)**, using the following conditions:

(a) 1 Eq. tributylamine was used for the first reaction (**273**, 96 mL, 0.400 mmol). **(b)** Cyclopropanamine (**402**, 33 µL, 0.480 mmol) was used as the first nucleophile. **(c)** 1.5 Eq. tributylamine was used for the second reaction (**273**, 0.140 mL, 0.600 mmol). **(d)** 4-Aminobutan-1-ol (**416**, 0.111 mL, 1.20 mmol) was used as the second nucleophile. **(e)** The second reactor was heated to 210 °C. **(f)** An aliquot of the crude product solution was collected for 1 min 10 s. **(g)** The reaction aliquot was analysed using high pH LCMS analysis. **(h)** The product was purified using an array MDAP isolation (high pH), focused method B, 20 min run. **(i)** 4-((4-(Cyclopropylamino)-8-methylquinazolin-2-yl)amino)butan-1-ol (**432**, 40 mg, 0.140 mmol, 35% yield) was afforded as a pale-yellow oil.

ν_{max} (neat, cm^{-1}): 3330, 2934, 1577, 1509, 1349, 751.

^{1}H NMR (400 MHz, DMSO-*d*$_6$): δ 7.76 (d, *J* = 7.9 Hz, 1H), 7.72-7.54 (m, 1H), 7.33 (d, *J* = 6.9 Hz, 1H), 6.86 (dd, *J* = 8.1, 7.1 Hz, 1H), 6.41 (br. t, *J* = 5.9 Hz, 1H), 4.33 (br. t, *J* = 4.9 Hz, 1H), 3.47-3.41 (m, 2H), 3.37 (q, *J* = 6.4 Hz, 2H), 3.02–2.95 (m, 1H), 2.39 (s, 3H), 1.65-1.56 (m, 2H), 1.54-1.45 (m, 2H), 0.77-0.71 (m, 2H), 0.64-0.58 (m, 2H).

^{13}C NMR (101 MHz, DMSO-*d*$_6$): δ 161.9, 159.3, 151.1, 132.5, 132.3, 120.8, 119.3, 110.8, 61.3, 41.1, 30.7, 26.5, 24.5, 18.0, 6.73 (2C).

LCMS (High pH, UV, ESI): t_{ret} = 0.95 min, $[M+H]^+$ m/z 287.2, 98.9% purity.

HRMS (TOF ESI, formic acid): $C_{16}H_{23}N_4O$ $[M+H]^+$ m/z = 287.1872, found m/z = 287.1879 (Δ = 2.4 ppm).

***N*^{2}-Benzyl-*N*^{4}-cyclopropyl-8-methylquinazoline-2,4-diamine:**

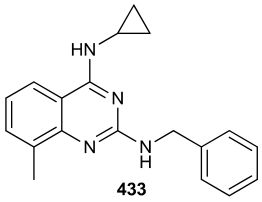

433

The reaction was performed according to **General procedure G (tandem flow synthesis of diaminoquinazolines)**, using the following conditions:

(a) 1 Eq. tributylamine was used for the first reaction (**273**, 96 mL, 0.400 mmol). **(b)** Cyclopropylamine (**402**, 33 µL, 0.480 mmol) was used as the first nucleophile. **(c)** 1.5 Eq. tributylamine was used for the second reaction (**273**, 0.140 mL, 0.600 mmol). **(d)** Benzylamine (**411**, 0.131 mL, 1.20 mmol) was used as the second nucleophile. **(e)** The second reactor was heated to 210 °C. **(f)** An aliquot of the crude product solution was collected for 1 min 10 s. **(g)** The reaction aliquot was analysed using high pH LCMS analysis. **(h)** The product was purified using MDAP isolation (high pH), method D, 30 min run. **(i)** *N*^{2}-Benzyl-*N*^{4}-cyclo propyl-8-methylquinazoline-2,4-diamine (**433**, 16 mg, 53 µmol, 13% yield) was afforded as an off-white amorphous gum.

ν_{max} (neat, cm^{-1}): 3354, 2923, 2851, 1576, 1511, 757.

^{1}H NMR (400 MHz, $CDCl_3$): δ 7.44 (br. d, *J* = 7.4 Hz, 2H), 7.40-7.36 (m, 1H), 7.33-7.28 (m, 2H), 7.28-7.25 (m, 1H), 7.25-7.21 (m, 1H), 6.95 (dd, *J* = 7.4, 7.4 Hz, 1H), 5.64 (br. s, 1H), 5.42 (br. s, 1H), 4.75 (d, *J* = 3.9 Hz, 2H), 2.96-2.89 (m, 1H), 2.53 (s, 3H), 0.86-0.81 (m, 2H), 0.61-0.56 (m, 2H).

^{13}C NMR (101 MHz, $CDCl_3$): δ 161.7, 158.7, 140.5, 134.0, 133.7, 132.5, 128.3 (2C), 128.0 (2C), 126.9, 120.3, 118.1, 110.5, 45.7, 24.2, 17.7, 7.35 (2C).

LCMS (High pH, UV, ESI): t_{ret} = 1.32 min, $[M+H]^+$ m/z 305.1. Product unstable to LCMS analysis.

HRMS (TOF ESI, formic acid): $C_{19}H_{21}N_4$ $[M+H]^+$ m/z = 305.1766, found m/z = 305.1774 (Δ = 0.6 ppm), 100.0% LC-HRMS purity.

4-((4-(Benzylamino)-8-methylquinazolin-2-yl)amino)butan-1-ol:

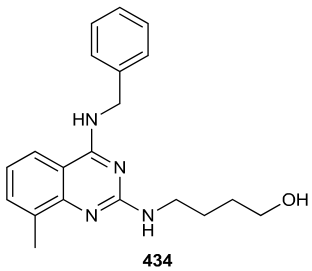

434

The reaction was performed according to **General procedure G (tandem flow synthesis of diaminoquinazolines)**, using the following conditions:

(a) 1 Eq. tributylamine was used for the first reaction (**273**, 96 mL, 0.400 mmol). **(b)** Benzylamine (**411**, 52 µL, 0.480 mmol) was used as the first nucleophile. **(c)** 1.5 Eq.

tributylamine was used for the second reaction (**273**, 0.140 mL, 0.600 mmol). **(d)** 4-Aminobutan-1-ol (**416**, 0.111 mL, 1.20 mmol) was used as the second nucleophile. **(e)** The second reactor was heated to 210 °C. **(f)** An aliquot of the crude product solution was collected for 1 min 10 s. **(g)** The reaction aliquot was analysed using high pH LCMS analysis. **(h)** The product was purified using an array MDAP isolation (high pH), method C, 20 min run. **(i)** 4-((4-(Benzylamino)-8-methylquinazolin-2-yl)amino)butan-1-ol (**434**, 26 mg, 78 µmol, 20% yield) was afforded as an off-white powder.

mp: 134-135 °C.

ν_{max} (neat, cm^{-1}): 3432 (br. w), 1575 (s), 1504 (s), 1349 (m), 755 (s).

^{1}H NMR (400 MHz, DMSO-*d*$_6$): δ 8.28 (br. s, 1H), 7.84 (d, *J* = 7.9 Hz, 1H), 7.38-7.33 (m, 3H), 7.33-7.27 (m, 2H), 7.21 (tt, *J* = 6.9, 1.5 Hz, 1H), 6.90 (dd, *J* = 7.4, 7.4 Hz, 1H), 6.40 (br. t, *J* = 5.4 Hz, 1H), 4.72 (d, *J* = 5.9 Hz, 2H), 4.32 (t, *J* = 5.2 Hz, 1H), 3.45-3.34 (m, 2H), 3.31-3.24 (m, 2H), 2.39 (s, 3H), 1.54 (br. s, 2H), 1.50-1.38 (m, 2H).

^{13}C NMR (101 MHz, DMSO-*d*$_6$): δ 160.2, 158.7, 150.9, 140.1, 132.0, 131.9, 128.1 (2C), 127.2 (2C), 126.5, 120.1, 118.9, 110.3, 60.7, 43.3, 40.6, 30.2, 26.0, 17.5.

LCMS (High pH, UV, ESI): t_{ret} = 1.11 min, $[M+H]^+$ m/z 337.2, 100.0% purity.

HRMS (TOF ESI, formic acid): $C_{20}H_{25}N_4O$ $[M+H]^+$ m/z = 337.2028, found m/z = 337.2035 (Δ = 2.1 ppm).

***N*^{2}-Cyclopropyl-*N*^{4}-((*trans*)-4-(2-methoxyethoxy)cyclohexyl)-8-methyl quinazoline-2,4-diamine:**

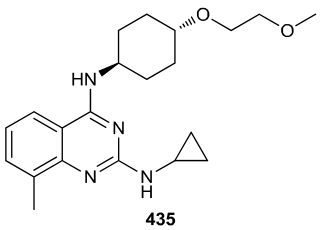

435

The reaction was performed according to **General procedure G (tandem flow synthesis of diaminoquinazolines)**, using the following conditions:

(a) 1 Eq. tributylamine was used for the first reaction (**273**, 96 mL, 0.400 mmol). **(b)** (*trans*)-4-(2-Methoxyethoxy)cyclohexan-1-amine (**356**, 83 mg, 0.480 mmol) was used as the first nucleophile. **(c)** 1.5 Eq. tributylamine was used for the second reaction (**273**, 0.140 mL, 0.600 mmol). **(d)** Cyclopropanamine (**402**, 83 µL, 1.20 mmol) was used as the second nucleophile. **(e)** The second reactor was heated to 210 °C. **(f)** An aliquot of the crude product solution was collected for 1 min 10 s. **(g)** The reaction aliquot was analysed using high pH

LCMS analysis. **(h)** The product was purified using MDAP isolation (high pH), method C, 20 min run. **(i)** *N*^{2}-Cyclopropyl-*N*^{4}-((*trans*)-4-(2-methoxyethoxy)cyclohexyl)-8-methyl quinazoline-2,4-diamine (**435**, 5 mg, 14 µmol, 3% yield) was afforded as an orange oil.

ν_{max} (neat, cm^{-1}): 3365, 2932, 1579, 1509, 1099, 761.

^{1}H NMR (600 MHz, $CDCl_3$): δ 7.39 (d, *J* = 7.0 Hz, 1H), 7.30 (br. d, *J* = 8.1 Hz, 1H), 6.96 (t, *J* = 7.3 Hz, 1H), 5.26-5.20 (m, 1H), 5.13-5.07 (m, 1H), 4.18-4.10 (m, 1H), 3.64 (dd, *J* = 5.7, 3.9 Hz, 2H), 3.55 (dd, *J* = 5.7, 3.9 Hz, 2H), 3.40 (s, 3H), 3.36-3.30 (m, 1H), 2.88-2.84 (m, 1H), 2.53 (s, 3H), 2.29-2.24 (m, 2H), 2.15-2.09 (m, 2H), 1.52-1.43 (m, 2H), 1.33-1.24 (m, 2H), 0.78-0.73 (m, 2H), 0.59-0.55 (m, 2H).

^{13}C NMR (151 MHz, $CDCl_3$): δ 160.0, 159.8, 151.1, 134.2, 132.4, 120.2, 118.0, 110.5, 77.8, 72.3, 67.6, 59.1, 49.2, 30.7 (4C), 24.1, 17.6, 7.1 (2C).

LCMS (High pH, UV, ESI): t_{ret} = 1.23 min, $[M+H]^+$ m/z 371.1, 98.8% purity.

HRMS (TOF ESI, formic acid): $C_{21}H_{31}N_4O_2$ $[M+H]^+$ m/z = 371.2447, found m/z = 371.2450 (Δ = 0.8 ppm).

4-((4-(((*trans*)-4-(2-methoxyethoxy)cyclohexyl)amino)-8-methylquinazolin-2-yl)amino) butan-1-ol:

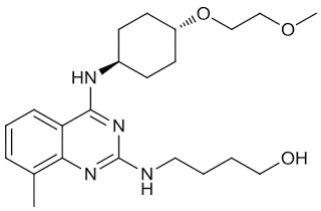

436

The reaction was performed according to **General procedure G (tandem flow synthesis of diaminoquinazolines)**, using the following conditions:

(a) 1 Eq. tributylamine was used for the first reaction (**273**, 96 mL, 0.400 mmol). **(b)** (*trans*)-4-(2-Methoxyethoxy)cyclohexan-1-amine (**356**, 83 mg, 0.480 mmol) was used as the first nucleophile. **(c)** 1.5 Eq. tributylamine was used for the second reaction (**273**, 0.140 mL, 0.600 mmol). **(d)** 4-Aminobutan-1-ol (**416**, 0.111 mL, 1.20 mmol) was used as the second nucleophile. **(e)** The second reactor was heated to 210 °C. **(f)** An aliquot of the crude product solution was collected for 1 min 10 s. **(g)** The reaction aliquot was analysed using high pH LCMS analysis. **(h)** The product was purified using an array MDAP isolation (high pH), method C, 30 min run. **(i)** 4-((4-(((*Trans*)-4-(2-methoxyethoxy)cyclohexyl)amino)-8-methyl quinazolin-2-yl)amino) butan-1-ol (**436**, 18 mg, 45 µmol, 11% yield) was afforded a colourless oil.

ν_{max} (neat, cm^{-1}): 3369, 2933, 1577, 1511, 1083, 753.

^{1}H NMR (400 MHz, $CDCl_3$): δ 7.37 (d, *J* = 6.9 Hz, 1H), 7.29 (d, *J* = 7.9 Hz, 1H), 6.94 (t, *J* = 7.4 Hz, 1H), 5.29-5.22 (m, 1H), 4.17-4.06 (m, 1H), 3.70 (t, *J* = 6.2 Hz, 2H), 3.66-3.62 (m, 2H), 3.57-3.51 (m, 4H), 3.40 (s, 3H), 3.37-3.29 (m, 1H), 2.51 (s, 3H), 2.26-2.19 (m, 2H), 2.15-2.08 (m, 2H), 1.78-1.64 (m, 4H), 1.53-1.42 (m, 2H), 1.33-1.22 (m, 2H).

^{13}C NMR (101 MHz, $CDCl_3$): δ 159.8, 159.0, 156.0, 133.7, 132.5, 120.1, 118.0, 110.4, 77.7, 72.4, 67.6, 62.8, 59.1, 49.0, 41.1, 30.7 (4C), 30.1, 26.6, 17.7.

LCMS (High pH, UV, ESI): t_{ret} = 1.02 min, $[M+H]^+$ m/z 403.1, 95.8% purity.

HRMS (TOF ESI, formic acid): $C_{22}H_{35}N_4O_3$ $[M+H]^+$ m/z = 403.2709, found m/z = 403.2725 (Δ = 4.0 ppm).

***N^4*-((*trans*)-4-(2-Methoxyethoxy)cyclohexyl)-*N^2*,*N^2*,8-trimethylquinazoline-2,4-diamine:**

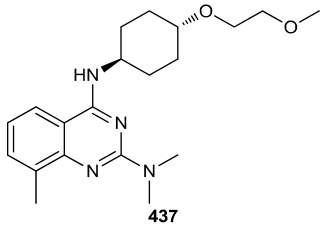

437

The reaction was performed according to **General procedure G (tandem flow synthesis of diaminoquinazolines)**, using the following conditions:

(a) 1 Eq. tributylamine was used for the first reaction (**273**, 96 mL, 0.400 mmol). **(b)** (*trans*)-4-(2-Methoxyethoxy)cyclohexan-1-amine (**356**, 83 mg, 0.480 mmol) was used as the first nucleophile. **(c)** 1.5 Eq. tributylamine was used for the second reaction (**273**, 0.140 mL, 0.600 mmol). **(d)** Dimethylamine (**404**, 40% wt. solution in H_2O, 0.152 mL, 1.20 mmol) was used as the second nucleophile. **(e)** The second reactor was heated to 210 °C. **(f)** An aliquot of the crude product solution was collected for 1 min 10 s. **(g)** The reaction aliquot was analysed using high pH LCMS analysis. **(h)** The product was purified using an array MDAP isolation (high pH), method D, 30 min run. **(i)** *N^4*-((*trans*)-4-(2-Methoxyethoxy) cyclohexyl)-*N^2*,*N^2*,8-trimethylquinazoline-2,4-diamine (**437**, 12 mg, 34 µmol, 9% yield) was afforded as off-white flakes.

mp: 129-130 °C.

ν_{max} (neat, cm^{-1}): 3387, 2911, 1573, 1515, 1133, 762.

^{1}H NMR (400 MHz, $CDCl_3$): δ 7.36 (br. d, *J* = 6.9 Hz, 1H), 7.29-7.25 (m, 1H), 6.91 (dd, *J* = 6.9, 6.9 Hz, 1H), 5.17 (d, *J* = 7.4 Hz, 1H), 4.19-4.07 (m, 1H), 3.66-3.62 (m, 2H), 3.56-3.53 (m, 2H),

3.40 (s, 3H), 3.38-3.30 (m, 1H), 3.23 (s, 6H), 2.52 (s, 3H), 2.30-2.22 (m, 2H), 2.17-2.09 (m, 2H), 1.54-1.43 (m, 2H), 1.34-1.23 (m, 2H).

^{13}C NMR (101 MHz, $CDCl_3$): δ 159.3, 159.1, 151.4, 134.0, 132.1, 119.5, 117.9, 109.2, 77.7, 72.4, 67.5, 59.1, 49.4, 36.7 (2C), 30.8 (2C), 30.6 (2C), 17.6.

LCMS (High pH, UV, ESI): t_{ret} = 1.39 min, $[M+H]^+$ m/z 359.1, 100.0% purity.

HRMS (TOF ESI, formic acid): $C_{20}H_{31}N_4O_2$ $[M+H]^+$ m/z = 359.2447, found m/z = 359.2450 (Δ = 0.8 ppm).

***N*-Cyclopropyl-6-iodo-2,8-dimethylquinazolin-4-amine:**

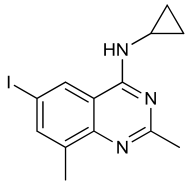

440

To a solution of 4-chloro-6-iodo-2,8-dimethylquinazoline (**368**, 76 mg, 0.239 mmol) in acetonitrile (2 mL) was added cyclopropylamine (**402**, 33 µL, 0.477 mmol) and triethylamine (83 µL, 0.477 mmol). The reaction mixture was heated, with stirring, to 70 °C for 16 h. Solvent was removed *in vacuo* to afford a yellow residue, which was partitioned between dichloromethane (20 mL) and water (20 mL). The organic phase was collected, and the aqueous phase was extracted with dichloromethane (2 x 20 mL), the organic phases were combined and washed with sat. aq. brine solution (20 mL), before the organic phase was collected and passed through an Isolute® hydrophobic fritted reservoir (70 mL volume). Solvent was then removed *in vacuo* to afford the crude product as a pale-yellow powder. The desired material was isolated by high pH MDAP separation, using method C, 30 min run. Product-containing fractions were combined, and solvent was removed under a stream of nitrogen to afford *N*-cyclopropyl-6-iodo-2,8-dimethylquinazolin-4-amine (**440**, 37 mg, 0.109 mmol, 46% yield) as a white, crystalline solid.

mp: 127-128 °C.

ν_{max} (neat, cm^{-1}): 3379, 3215, 1575, 1529, 1343, 805.

^{1}H NMR (400 MHz, CD_3OD): δ 8.29 (d, *J* = 2.0 Hz, 1H), 7.83 (app. dd, *J* = 2.0, 1.0 Hz, 1H), 3.02 (quin, *J* = 7.5, 3.4 Hz, 1H), 2.58 (s, 3H), 2.55 (s, 3H), 0.89-0.83 (m, *J* = 5.4 Hz, 2H), 0.70-0.65 (m, 2H).

^{13}C NMR (101 MHz, CD_3OD): δ 165.3, 161.8, 149.0, 142.4, 138.7, 130.1, 116.1, 89.5, 26.3, 25.2, 17.6, 7.1 (2C).

LCMS (High pH, UV, ESI): t_{ret} = 1.23 min, $[M+H]^+$ m/z 340.0, 96.9% purity.

HRMS (TOF, ESI, formic acid): $C_{13}H_{15}IN_3$ $[M+H]^+$ m/z = 340.0311, found m/z = 340.0306 (Δ = -1.5 ppm).

***N*-Cyclopropyl-6-(*1H*-imidazol-1-yl)-2,8-dimethylquinazolin-4-amine:**

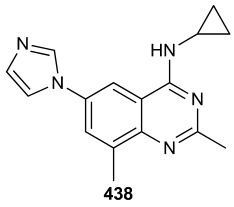

438

To a mixture of *N*-cyclopropyl-6-iodo-2,8-dimethylquinazolin-4-amine (**440**, 30 mg, 88 µmol), copper(I)iodide (8 mg, 44 µmol) ethylene glycol (3 µL, 44 µmol) and potassium phosphate tribasic (56 mg, 0.265 mmol) in IPA (1 mL) was added imidazole (7 mg, 0.106 mmol). The reaction vial was sealed, evacuated under vacuum and placed under a nitrogen atmosphere, before the reaction mixture was heated, with stirring, to 110 °C for 16 h. Solvent was removed *in vacuo* to afford a brown residue, which was purified by high pH MDAP separation, using method B, 30 min run. Product-containing fractions were combined, and solvent was removed under a stream of nitrogen to afford *N*-cyclopropyl-6-(*1H*-imidazol-1-yl)-2,8-dimethyl quinazolin-4-amine (**438**, 5 mg, 19 µmol, 22% yield) as a brown powder.

mp: 272-273 °C (dec.).

ν_{max} (neat, cm^{-1}): 3262, 1574, 1542, 1352, 1061, 801.

^{1}H NMR (600 MHz, DMSO-*d*$_6$): δ 8.24 (br. s, 1H), 8.19 (d, *J* = 2.2 Hz, 1H), 7.98 (br. d, *J* = 3.3 Hz, 1H), 7.90-7.88 (m, 1H), 7.74 (br. s, 1H), 7.13 (br. s, 1H), 3.09-3.05 (m, 1H), 2.57 (s, 3H), 2.50 (m, 3H), 0.82-0.77 (m, 2H), 0.64-0.59 (m, 2H).

^{13}C NMR (151 MHz, DMSO-*d*$_6$): δ 162.8, 160.8, 147.1, 137.2, 135.6, 132.5, 129.8, 125.2, 118.2, 112.7, 110.6, 26.7, 24.2, 17.5, 6.2 (2C).

LCMS (High pH, UV, ESI): t_{ret} = 0.87 min, $[M+H]^+$ m/z 280.1, 100% purity.

HRMS (TOF, ESI, ammonium bicarbonate): $C_{16}H_{18}N_5$ $[M+H]^+$ m/z = 280.1562, found m/z = 280.1563 (Δ = 0.4 ppm).

4-((4-(Cyclopropylamino)-6-iodo-8-methylquinazolin-2-yl)amino)butan-1-ol:

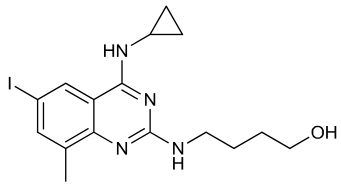

441

Using the bespoke flow reactor setup shown in **Figures 6.6-6.9**, the following general process was used for the synthesis of 4-((4-(cyclopropylamino)-6-iodo-8-methyl quinazolin-2-yl)amino)butan-1-ol (**441**).

A solution of 2,4-dichloro-6-iodo-8-methylquinazoline (**352**, 339 mg, 1.00 mmol), tributylamine (**273**, 238 µL, 1 mmol) and cyclopropylamine (**402**, 83 µL, 1.20 mmol) was made up in 1-butyl-2-pyrrolidinone (Tamisolve®, 5 mL total volume). *2,4-dichloro-6-iodo-8-methyl quinazoline (**352**) was only partially soluble in the reaction solvent, so the mixture was superheated under a hot air gun to establish homogeneity.* The resultant solution was pumped through the first reactor (heated at 90 °C) at a flow rate of 42.0 µL/min. Meanwhile, a second solution was made up, containing tributylamine (**273**, 358 µL, 1.50 mmol) and 4-aminobutan-1-ol (**416**, 277 µL, 3.00 mmol) in Tamisolve® (5 mL total volume). After 10 min 9 s reaction time, the second solution was pumped into the reactor using the other line at the same flow rate (42.0 µL/min) for the two streams to converge after the T-piece after 18 min 44 s total reaction time. The materials were then pumped through the rest of the reactor, including a second heated reactor held at 210 °C, at a combined flow rate of 84.0 µL/min for another 24 min 59 s (43 min 43 s total reaction time).

After this time, the first of the crude product solution was collected in a 1 mL HPLC vial for 1 min 10 s, and this material was diluted in Tamisolve® (~500 µL) and analysed by high pH LCMS analysis.

Thereafter, the remaining crude product solution was collected over a 75 min collection period (in 7 x 1 mL vials suitable for array MDAP purification). The pumps were temporarily stopped, and their input lines placed into clean Tamisolve®, which was pumped into the reactor at the same flow rate (42.0 µL/min/line). The crude reaction mixture was collected for another 43 min 43 s, filling 10 x 1 mL HPLC vials in all.

The crude product solutions were then purified using an array MDAP (high pH) isolations, method C, 30 min run using the optimal method determined from the sampled aliquot. Product-containing fractions were combined, and solvent was removed under a stream of nitrogen to afford 4-((4-(cyclopropylamino)-6-iodo-8-methylquinazolin-2-yl)amino)butan-1-ol (**441**, 37 mg, 90 µmol, 9% yield) as a pale orange powder.

*The partial solubility of **352** and initial heating of the reaction mixture led to the formation of a mixture of regioisomeric products following the first S_NAr reaction, and a resultantly low yield of the desired product (**441**). The identity of the desired product was elucidated through COSY and 1D ROESY NMR analysis (*See **Section 7.12 Appendix 12 – Elucidation of desired regioisomer (compound 441)** *for more information).*

mp: 193-194 °C (dec.).

ν_{max} (neat, cm^{-1}): 3370, 1575, 1511, 1033, 799, 463.

^{1}H NMR (600 MHz, DMSO-*d*$_6$): δ 8.16 (d, *J* = 1.5 Hz, 1H), 7.92-7.65 (m, 1H), 7.59 (s, 1H), 6.60 (br. s, 1H), 4.37-4.28 (m, 1H), 3.45-3.40 (m, 2H), 3.35 (q, *J* = 6.6 Hz, 2H), 3.01-2.96 (m, 1H), 2.34 (s, 3H), 1.59 (quin, *J* = 7.2 Hz, 2H), 1.47 (quin, *J* = 7.2 Hz, 2H), 0.76-0.71 (m, 2H), 0.63-0.59 (m, 2H).

^{13}C NMR (151 MHz, DMSO-*d*$_6$): δ 160.2, 158.8, 149.9, 139.5, 135.0, 128.6, 112.4, 81.8, 60.7, 40.5, 30.2, 25.7, 24.0, 16.8, 6.05 (2C).

LCMS (High pH, UV, ESI): t_{ret} = 1.19 min, $[M+H]^+$ m/z 413.0, 100.0% purity.

HRMS (TOF, ESI, formic acid): $C_{16}H_{22}IN_4O$ $[M+H]^+$ m/z = 413.0838, found m/z = 413.0835 (Δ = -0.7 ppm).

4-((4-(Cyclopropylamino)-6-(*1H*-imidazol-1-yl)-8-methylquinazolin-2-yl) amino)butan-1-ol:

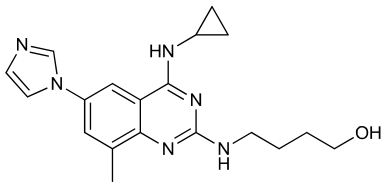

439

A mixture consisting of 4-((4-(cyclopropylamino)-6-iodo-8-methylquinazolin-2-yl)amino) butan-1-ol (**441**, 30 mg, 73 µmol), imidazole (17 mg, 0.255 mmol), copper(I)iodide (1 mg, 7 µmol), cesium carbonate (47 mg, 0.146 mmol) and *D*-glucosamine (2 mg, 7 µmol) was made using a 1:1 water:DMSO (2 mL total volume) solvent combination. The reaction vial was sealed, evacuated under vacuum and placed under a nitrogen atmosphere, before the reaction mixture was heated, with stirring, to 100 °C for 72 h. The reaction mixture was partitioned between ethyl acetate (10 mL) and water (10 mL), before the organic phase was separated. The aqueous layer was extracted with ethyl acetate (2 x 10 mL), before the organic layers were combined, passed through an Isolute® hydrophobic fritted reservoir (70 mL volume). Solvent was then removed *in vacuo* and the crude reaction mixture was purified by high pH MDAP separation, using method B, 20 min run. Product-containing fractions were combined, and

solvent was removed under a stream of nitrogen to afford 4-((4-(cyclopropylamino)-6-(*1H*-imidazol-1-yl)-8-methylquinazolin-2-yl)amino)butan-1-ol (**439**, 8 mg, 22 µmol, 30% yield) as a brown powder.

mp: 198-199 °C.

ν_{max} (neat, cm^{-1}): 3396, 3262, 3114, 1562, 1065, 796.

^{1}H NMR (400 MHz, DMSO-*d*$_6$): δ 8.13 (s, 1H), 8.00 (d, *J* = 2.5 Hz, 1H), 7.73 (br. s, 1H), 7.69-7.62 (m, 2H), 7.10 (app. s, 1H), 6.64-6.55 (m, 1H), 4.34 (br. s, 1H), 3.44 (t, *J* = 6.4 Hz, 2H), 3.38 (q, *J* = 6.7 Hz, 2H), 3.03-2.96 (m, 1H), 2.46 (s, 3H), 1.66-1.58 (m, 2H), 1.54-1.45 (m, 2H), 0.81-0.75 (m, 2H), 0.65-0.59 (m, 2H).

^{13}C NMR (101 MHz, DMSO-*d*$_6$): δ 165.3, 161.3, 159.1, 135.5, 134.1, 129.4, 128.4, 125.1, 118.3, 111.9, 111.6, 60.7, 40.6, 30.2, 26.0, 24.0, 17.4, 6.2 (2C).

LCMS (High pH, UV, ESI): t_{ret} = 0.88 min, $[M+H]^+$ m/z 353.1, 96.4% purity.

HRMS (TOF, ESI, formic acid): $C_{19}H_{25}N_6O$ $[M+H]^+$ m/z = 353.2090, found m/z = 353.2083 (Δ = -2.0 ppm).

7. Appendix

7.1 Appendix 1 – HPLC concentration gradients and associated procedure

To prepare a HPLC concentration gradient for each amidine starting material, the following procedure was performed:

HPLC concentration gradient general procedure: 50.0 mg of the amidine of interest was dissolved in methanol to generate a 50.0 mL total solution volume of 1 mg/mL concentration. From this stock solution was separately taken 1.00 mL, 0.50 mL, 0.25 mL, 125 µL and 62.5 µL samples, which were each added into separate HPLC vials. Each vial was then made up to 1 mL total volume with methanol. For each reagent, these concentration values were plotted against the observed HPLC AUC data to generate concentration gradients. Only data with an $R^2 \geq 0.99$ was accepted. If data was insufficiently uniform, the procedure was repeated.

2-Aminopyridine:

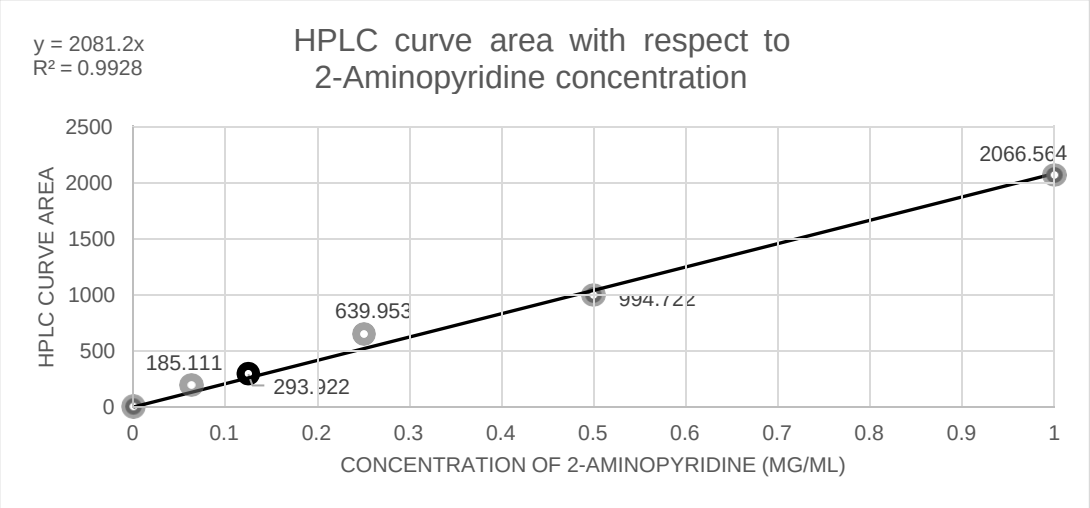

3-Methyl-2-aminopyridine:

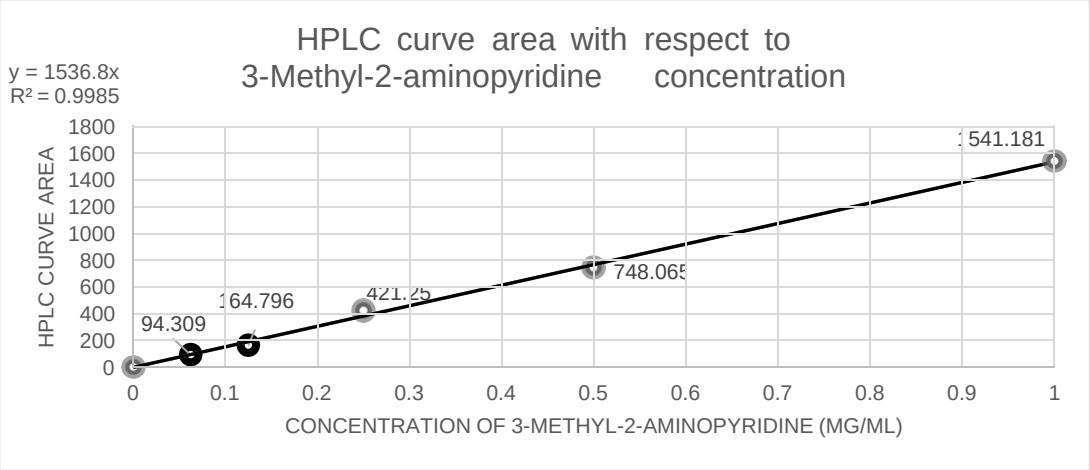

(6-aminopyridin-3-yl)methanol:

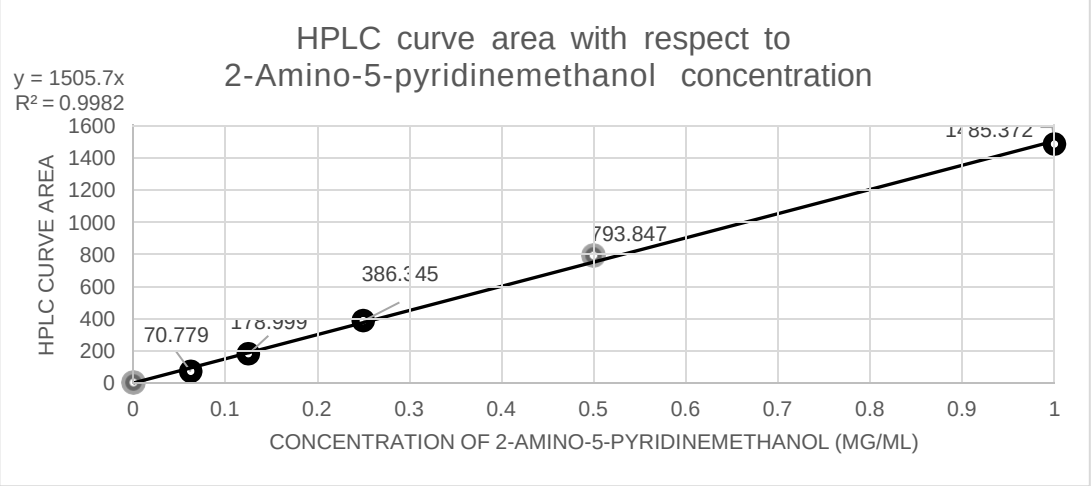

5-Methoxy-2-aminopyridine:

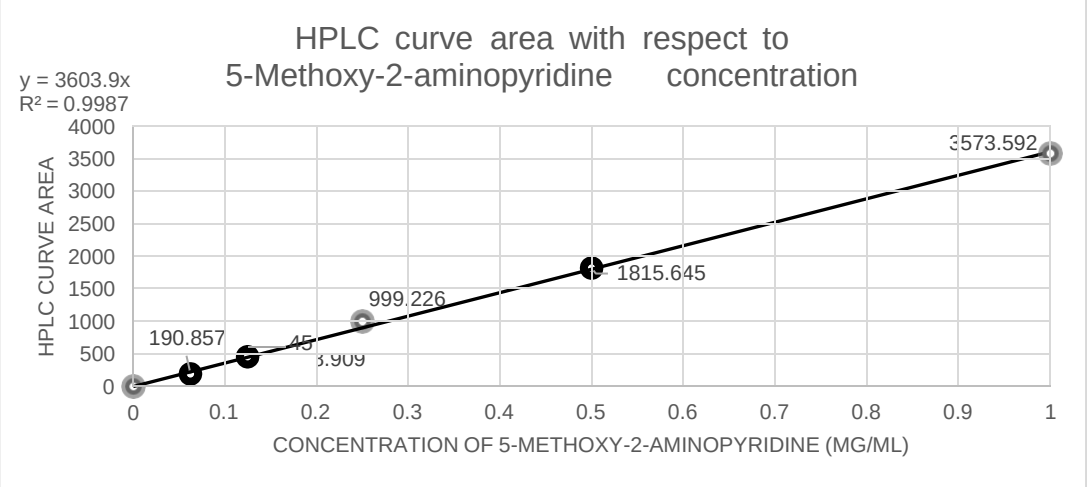

3-Bromo-2-aminopyridine:

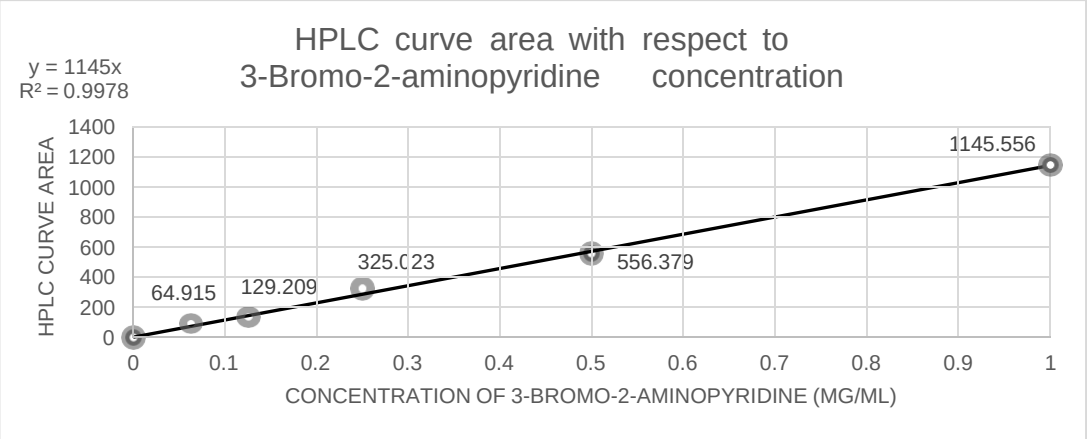

4-Bromo-2-aminopyridine:

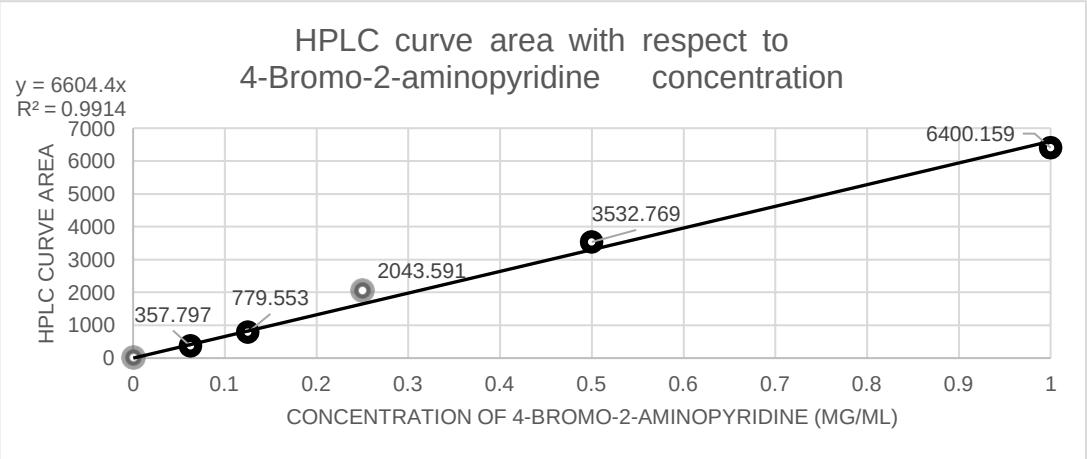

Ethyl-6-aminonicotinate:

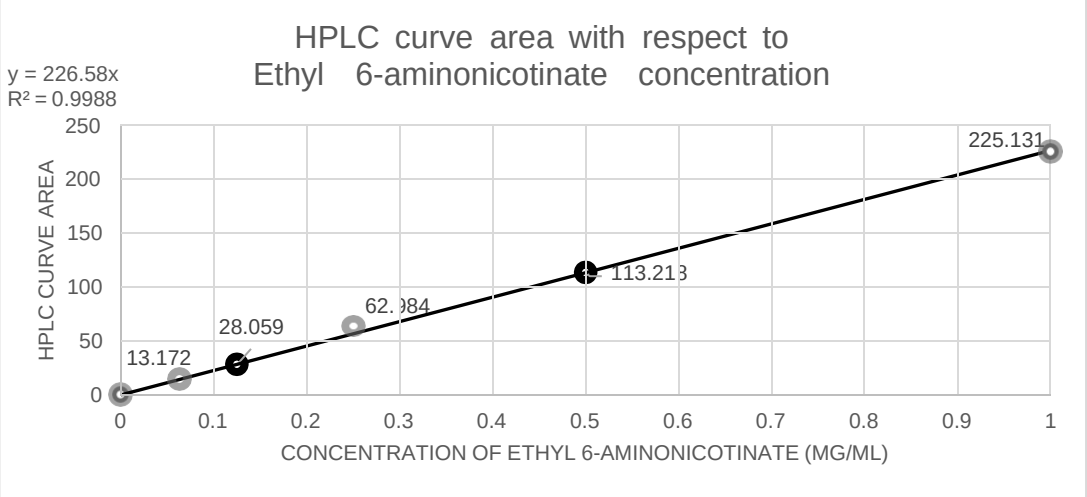

2-Aminothiazole:

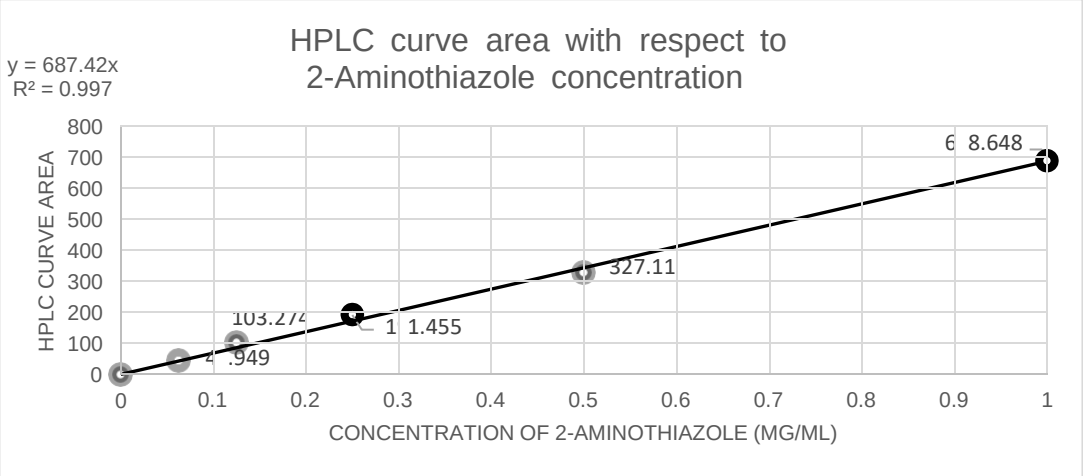

2-Aminopyrimidine:

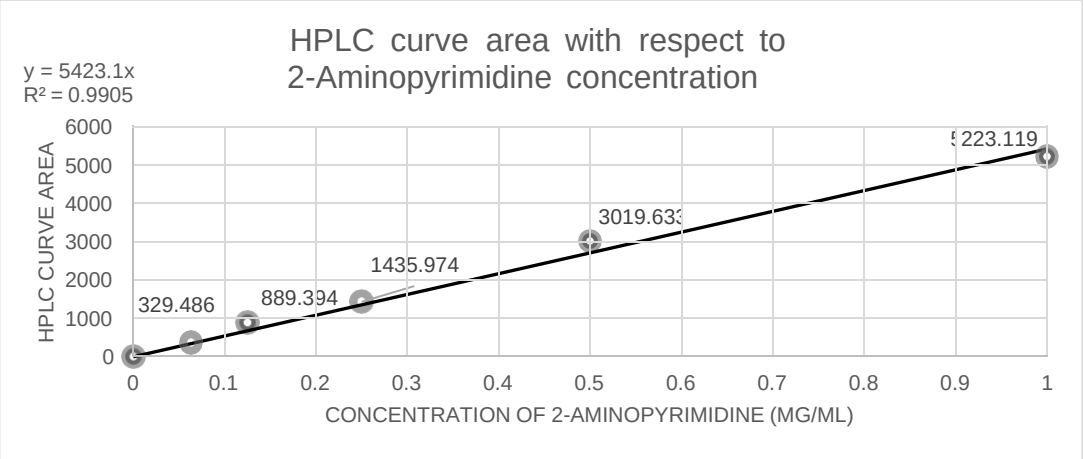

2-Aminobenzothiazole:

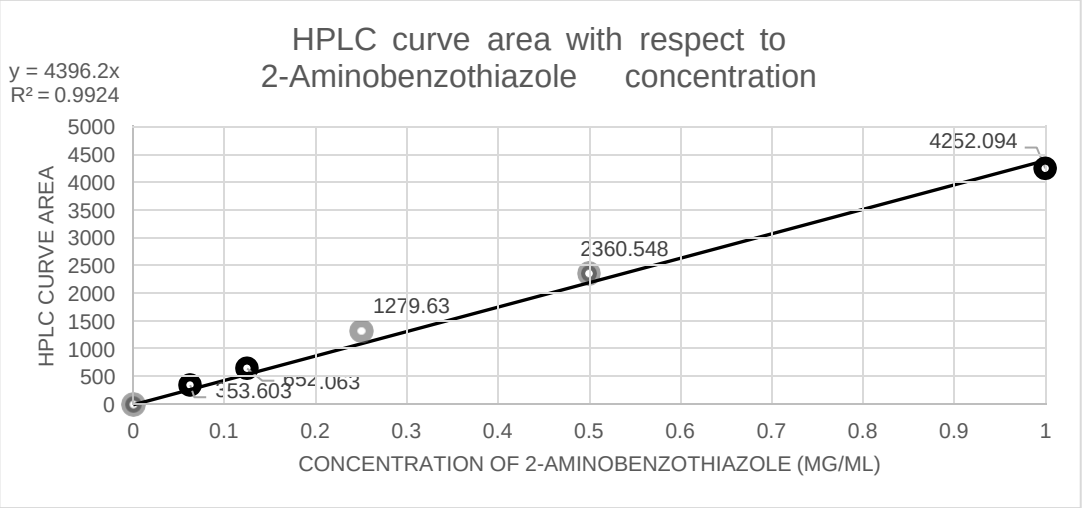

Aminopyrazine:

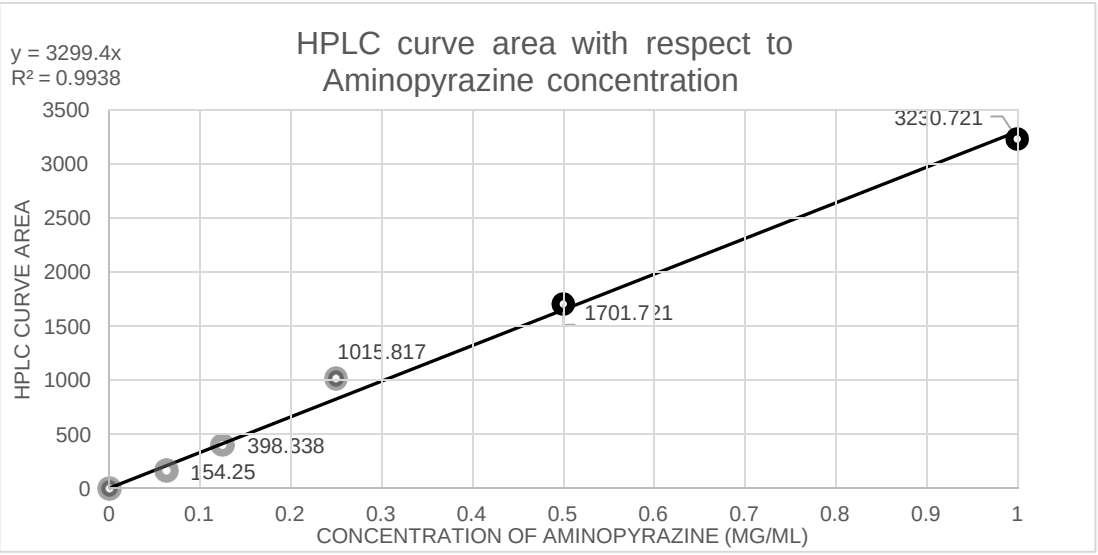

6-Bromo-2-aminopyridine:

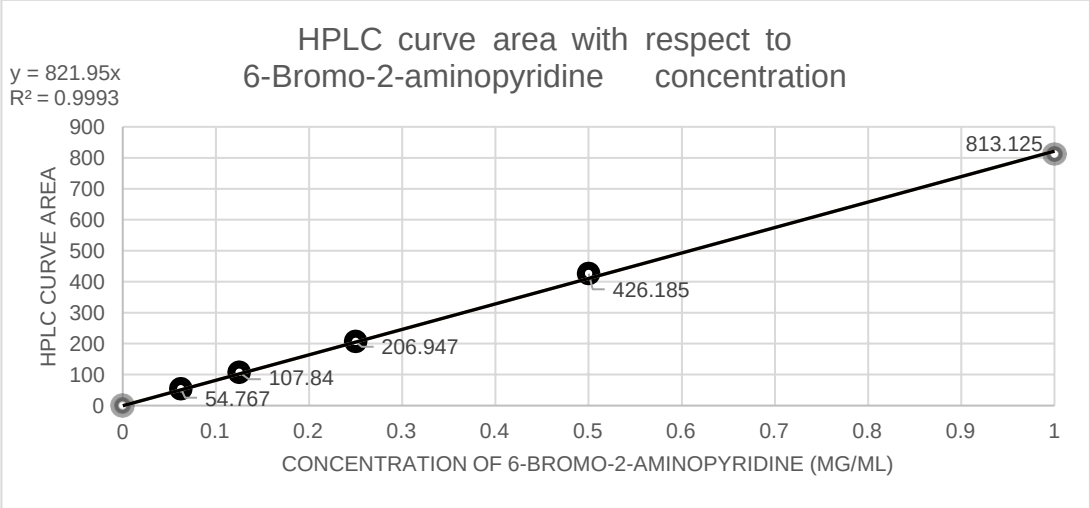

5-Methoxy-2-aminopyrimidine:

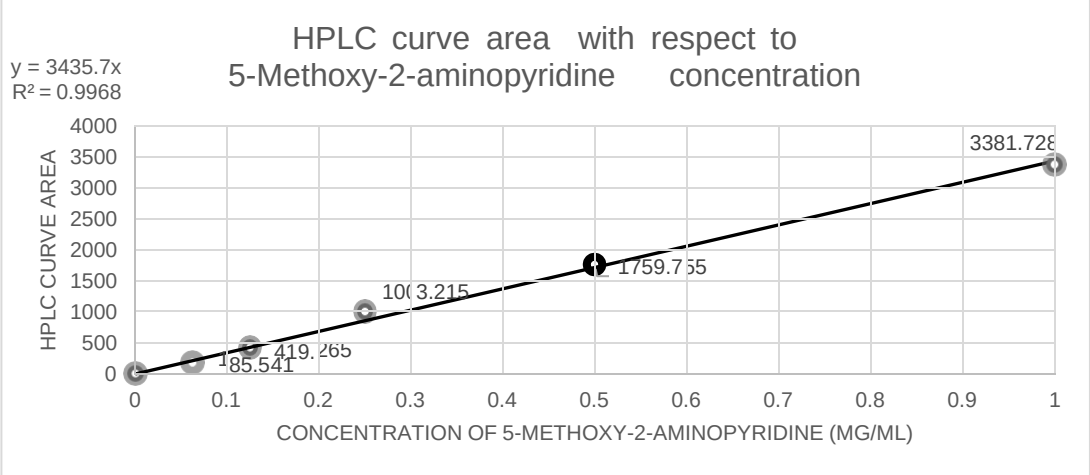

5-Bromo-2-aminopyridine:

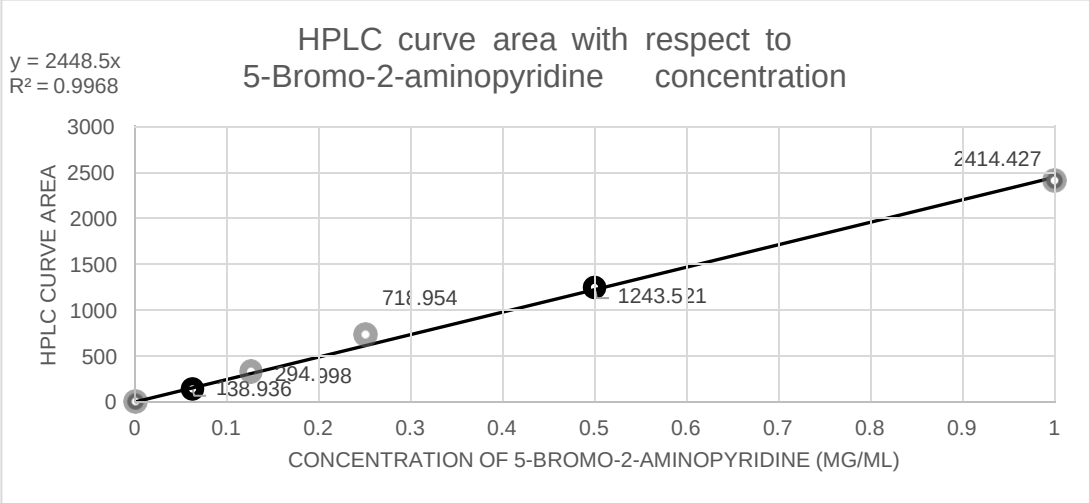

3-Aminopyridazine:

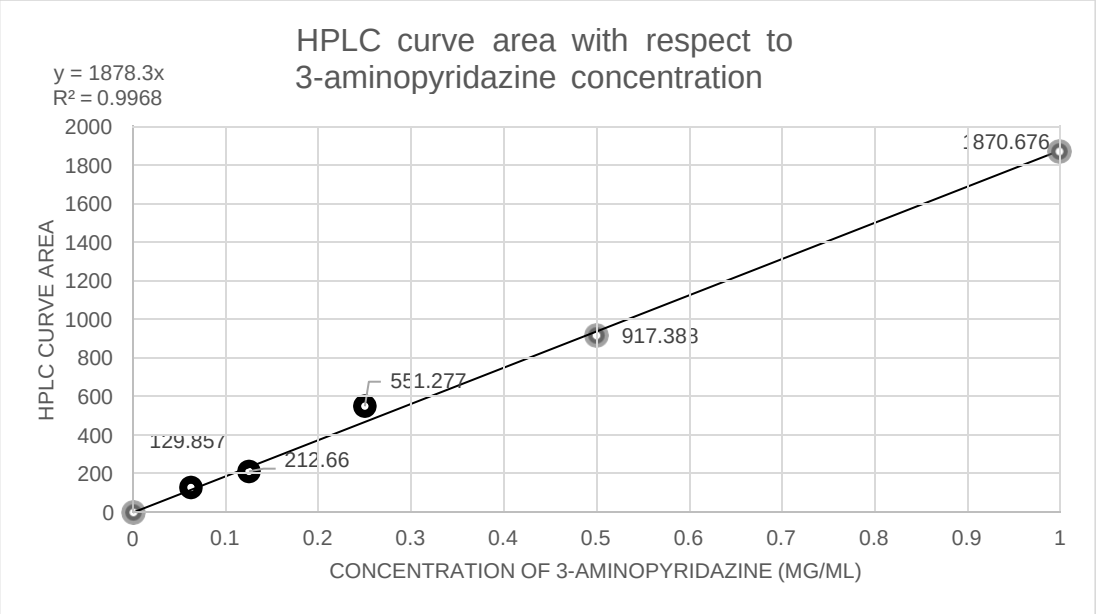

7.1.1 Procedure for attaining conversion estimates from HPLC concentration gradients: Following flow reaction procedures, x µL (See **synthetic procedures**) was removed from the crude reaction mixture and diluted with 1 mL methanol. The solution was analysed by the HPLC method described (See **General experimental information and equipment used**). The area under curve (AUC) data from the HPLC run was attained, and, using the relevant concentration gradient, calculated as a concentration of starting material (in mg/(1.00 mL + x µL)) remaining in the crude reaction mixture. As the crude reaction mixture tested was present as a solution of (1.00 mL + x µL) total volume, the value was adjusted (divided by (1.00 + x)) to provide the data as a concentration in mg/mL.

Subsequently, taking the calculated concentration value of the crude material as a proportion of the maximal starting material concentration remaining in the reaction (if no starting material had been consumed) allowed for the calculation of remaining starting material in the reaction composition. As such, the equation used to calculate HPLC conversion became:

$$\text{SM Consumption} = \left(1 - \frac{(\text{Concentration of SM left in mixture (from AUC)} \div (1.00 + \text{x}))}{\text{Maximal SM concentration in x µL reaction volume(conditions if no consumption was observed)}}\right) \times 100$$

7.1.2 HPLC data for reaction profiles

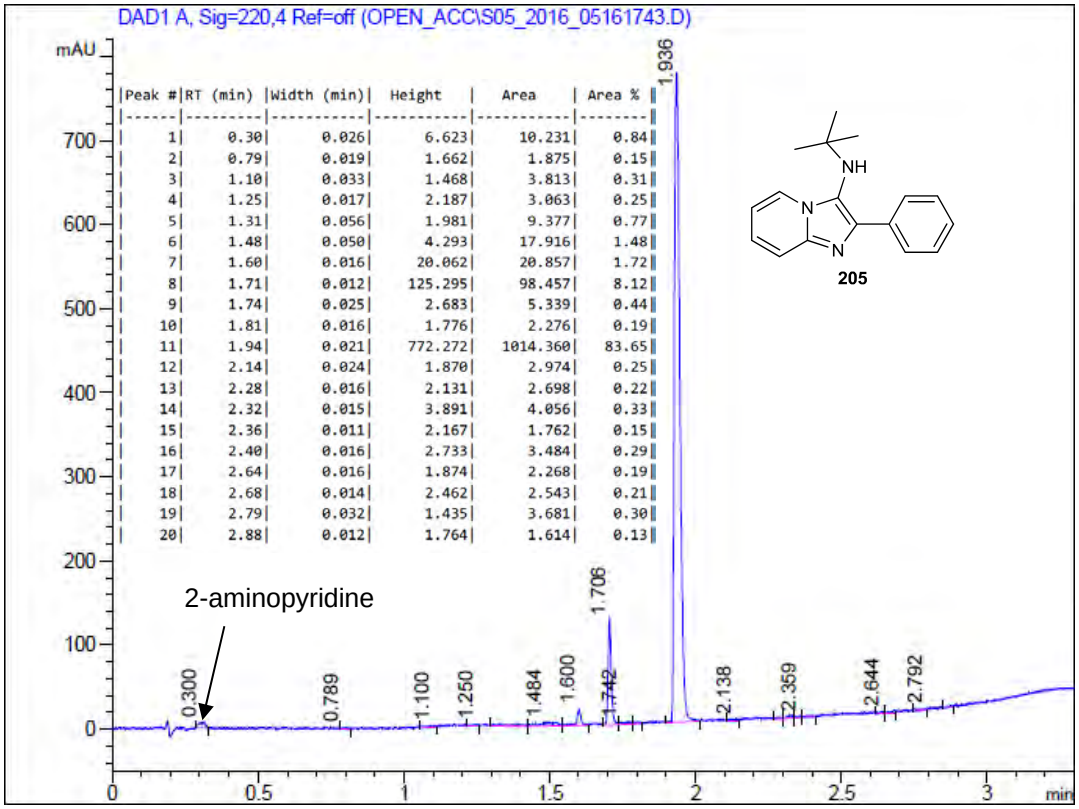

Peak #	RT (min)	Width (min)	Height	Area	Area %
1	0.30	0.026	6.623	10.231	0.84
2	0.79	0.019	1.662	1.875	0.15
3	1.10	0.033	1.468	3.813	0.31
4	1.25	0.017	2.187	3.063	0.25
5	1.31	0.056	1.981	9.377	0.77
6	1.48	0.050	4.293	17.916	1.48
7	1.60	0.016	20.062	20.857	1.72
8	1.71	0.012	125.295	98.457	8.12
9	1.74	0.025	2.683	5.339	0.44
10	1.81	0.016	1.776	2.276	0.19
11	1.94	0.021	772.272	1014.360	83.65
12	2.14	0.024	1.870	2.974	0.25
13	2.28	0.016	2.131	2.698	0.22
14	2.32	0.015	3.891	4.056	0.33
15	2.36	0.011	2.167	1.762	0.15
16	2.40	0.016	2.733	3.484	0.29
17	2.64	0.016	1.874	2.268	0.19
18	2.68	0.014	2.462	2.543	0.21
19	2.79	0.032	1.435	3.681	0.30
20	2.88	0.012	1.764	1.614	0.13

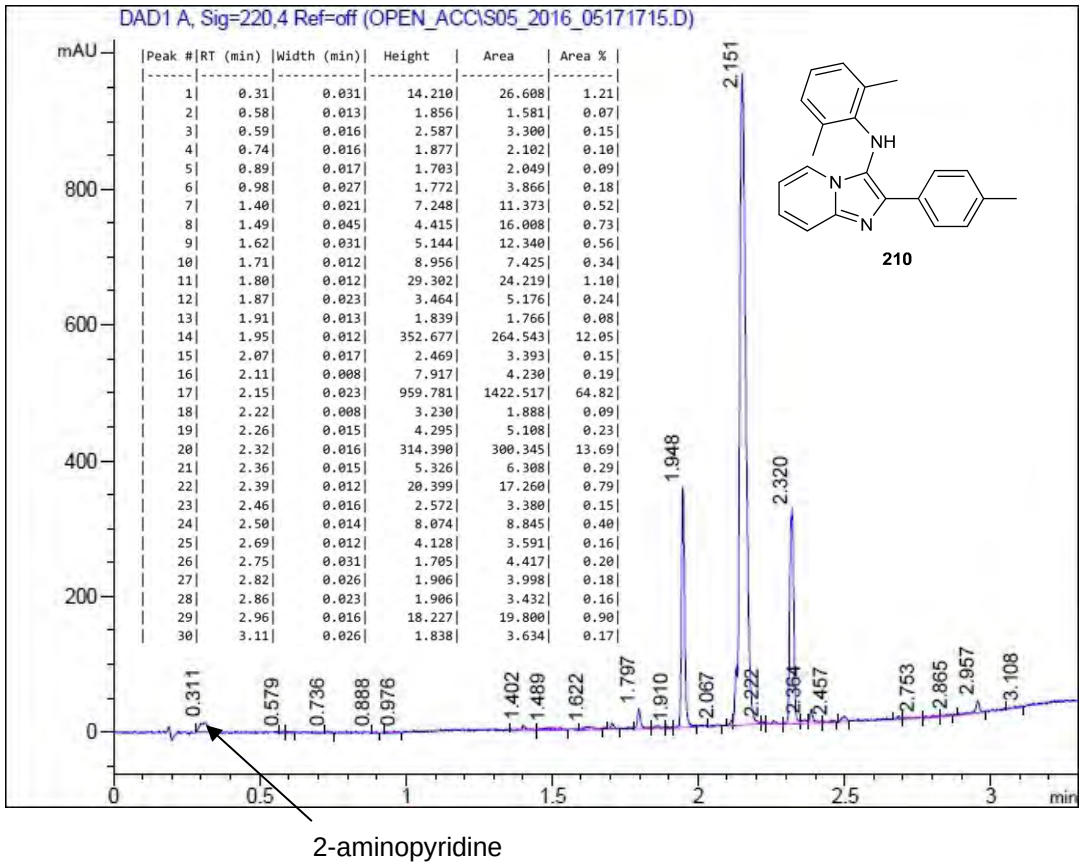

Peak #	RT (min)	Width (min)	Height	Area	Area %
1	0.31	0.031	14.210	26.608	1.21
2	0.58	0.013	1.856	1.581	0.07
3	0.59	0.016	2.587	3.300	0.15
4	0.74	0.016	1.877	2.102	0.10
5	0.89	0.017	1.703	2.049	0.09
6	0.98	0.027	1.772	3.866	0.18
7	1.40	0.021	7.248	11.373	0.52
8	1.49	0.045	4.415	16.008	0.73
9	1.62	0.031	5.144	12.340	0.56
10	1.71	0.012	8.956	7.425	0.34
11	1.80	0.012	29.302	24.219	1.10
12	1.87	0.023	3.464	5.176	0.24
13	1.91	0.013	1.839	1.766	0.08
14	1.95	0.012	352.677	264.543	12.05
15	2.07	0.017	2.469	3.393	0.15
16	2.11	0.008	7.917	4.230	0.19
17	2.15	0.023	959.781	1422.517	64.82
18	2.22	0.008	3.230	1.888	0.09
19	2.26	0.015	4.295	5.108	0.23
20	2.32	0.016	314.390	300.345	13.69
21	2.36	0.015	5.326	6.308	0.29
22	2.39	0.012	20.399	17.260	0.79
23	2.46	0.016	2.572	3.380	0.15
24	2.50	0.014	8.074	8.845	0.40
25	2.69	0.012	4.128	3.591	0.16
26	2.75	0.031	1.705	4.417	0.20
27	2.82	0.026	1.906	3.998	0.18
28	2.86	0.023	1.906	3.432	0.16
29	2.96	0.016	18.227	19.800	0.90
30	3.11	0.026	1.838	3.634	0.17

GSK CONFIDENTIAL INFORMATION – DO NOT COPY

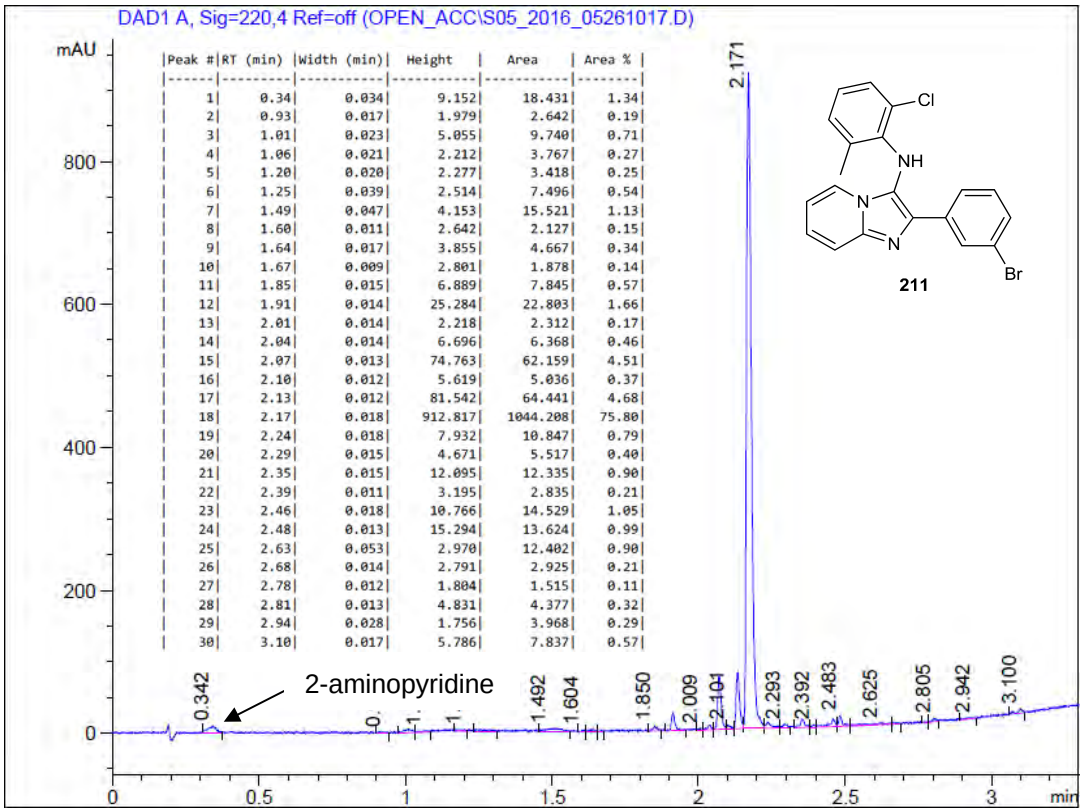

Peak #	RT (min)	Width (min)	Height	Area	Area %
1	0.34	0.034	9.152	18.431	1.34
2	0.93	0.017	1.979	2.642	0.19
3	1.01	0.023	5.055	9.740	0.71
4	1.06	0.021	2.212	3.767	0.27
5	1.20	0.020	2.277	3.418	0.25
6	1.25	0.039	2.514	7.496	0.54
7	1.49	0.047	4.153	15.521	1.13
8	1.60	0.011	2.642	2.127	0.15
9	1.64	0.017	3.855	4.667	0.34
10	1.67	0.009	2.801	1.878	0.14
11	1.85	0.015	6.889	7.845	0.57
12	1.91	0.014	25.284	22.803	1.66
13	2.01	0.014	2.218	2.312	0.17
14	2.04	0.014	6.696	6.368	0.46
15	2.07	0.013	74.763	62.159	4.51
16	2.10	0.012	5.619	5.036	0.37
17	2.13	0.012	81.542	64.441	4.68
18	2.17	0.018	912.817	1044.208	75.80
19	2.24	0.018	7.932	10.847	0.79
20	2.29	0.015	4.671	5.517	0.40
21	2.35	0.015	12.095	12.335	0.90
22	2.39	0.011	3.195	2.835	0.21
23	2.46	0.018	10.766	14.529	1.05
24	2.48	0.013	15.294	13.624	0.99
25	2.63	0.053	2.970	12.402	0.90
26	2.68	0.014	2.791	2.925	0.21
27	2.78	0.012	1.804	1.515	0.11
28	2.81	0.013	4.831	4.377	0.32
29	2.94	0.028	1.756	3.968	0.29
30	3.10	0.017	5.786	7.837	0.57

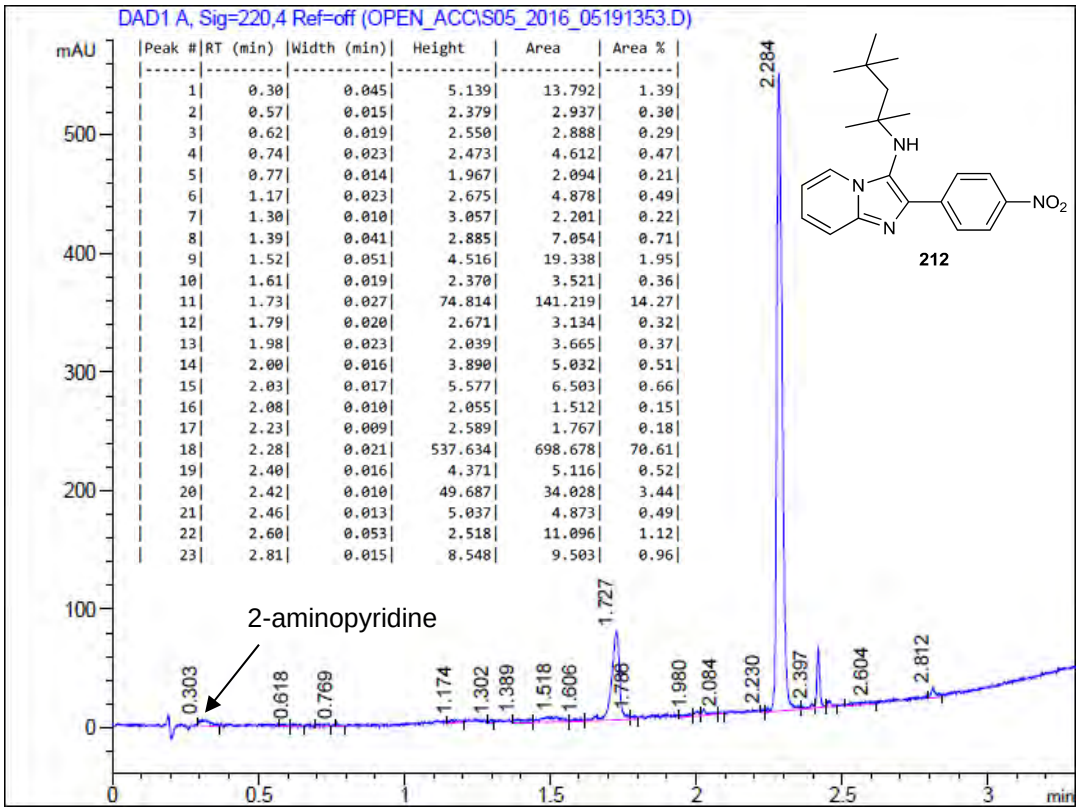

Peak #	RT (min)	Width (min)	Height	Area	Area %
1	0.30	0.045	5.139	13.792	1.39
2	0.57	0.015	2.379	2.937	0.30
3	0.62	0.019	2.550	2.888	0.29
4	0.74	0.023	2.473	4.612	0.47
5	0.77	0.014	1.967	2.094	0.21
6	1.17	0.023	2.675	4.878	0.49
7	1.30	0.010	3.057	2.201	0.22
8	1.39	0.041	2.885	7.054	0.71
9	1.52	0.051	4.516	19.338	1.95
10	1.61	0.019	2.370	3.521	0.36
11	1.73	0.027	74.814	141.219	14.27
12	1.79	0.020	2.671	3.134	0.32
13	1.98	0.023	2.039	3.665	0.37
14	2.00	0.016	3.890	5.032	0.51
15	2.03	0.017	5.577	6.503	0.66
16	2.08	0.010	2.055	1.512	0.15
17	2.23	0.009	2.589	1.767	0.18
18	2.28	0.021	537.634	698.678	70.61
19	2.40	0.016	4.371	5.116	0.52
20	2.42	0.010	49.687	34.028	3.44
21	2.46	0.013	5.037	4.873	0.49
22	2.60	0.053	2.518	11.096	1.12
23	2.81	0.015	8.548	9.503	0.96

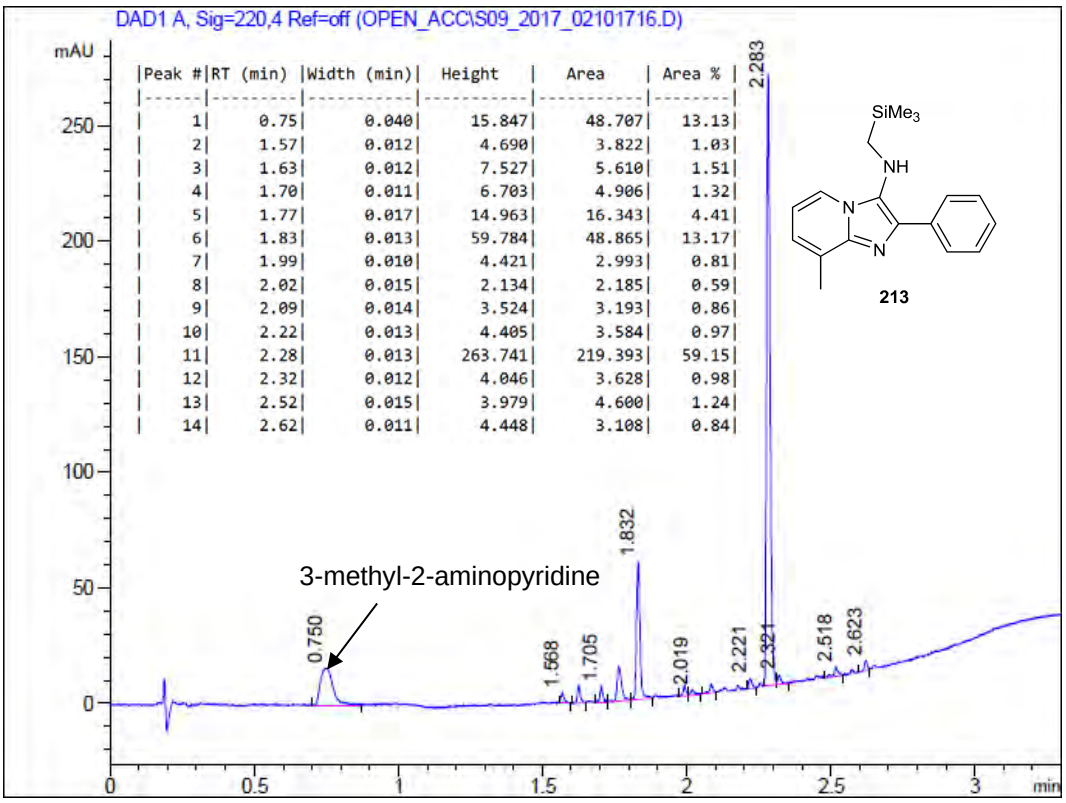
DAD1 A, Sig=220,4 Ref=off (OPEN_ACC\S09_2017_02101716.D)
mAU
Peak # | RT (min) | Width (min) | Height | Area | Area %
1 | 0.75 | 0.040 | 15.847 | 48.707 | 13.13
2 | 1.57 | 0.012 | 4.690 | 3.822 | 1.03
3 | 1.63 | 0.012 | 7.527 | 5.610 | 1.51
4 | 1.70 | 0.011 | 6.703 | 4.906 | 1.32
5 | 1.77 | 0.017 | 14.963 | 16.343 | 4.41
6 | 1.83 | 0.013 | 59.784 | 48.865 | 13.17
7 | 1.99 | 0.010 | 4.421 | 2.993 | 0.81
8 | 2.02 | 0.015 | 2.134 | 2.185 | 0.59
9 | 2.09 | 0.014 | 3.524 | 3.193 | 0.86
10 | 2.22 | 0.013 | 4.405 | 3.584 | 0.97
11 | 2.28 | 0.013 | 263.741 | 219.393 | 59.15
12 | 2.32 | 0.012 | 4.046 | 3.628 | 0.98
13 | 2.52 | 0.015 | 3.979 | 4.600 | 1.24
14 | 2.62 | 0.011 | 4.448 | 3.108 | 0.84
2.283
1.832
3-methyl-2-aminopyridine
0.750
1.568
1.705
2.019
2.221
2.321
2.518
2.623
min
SiMe3
NH
N
N
213

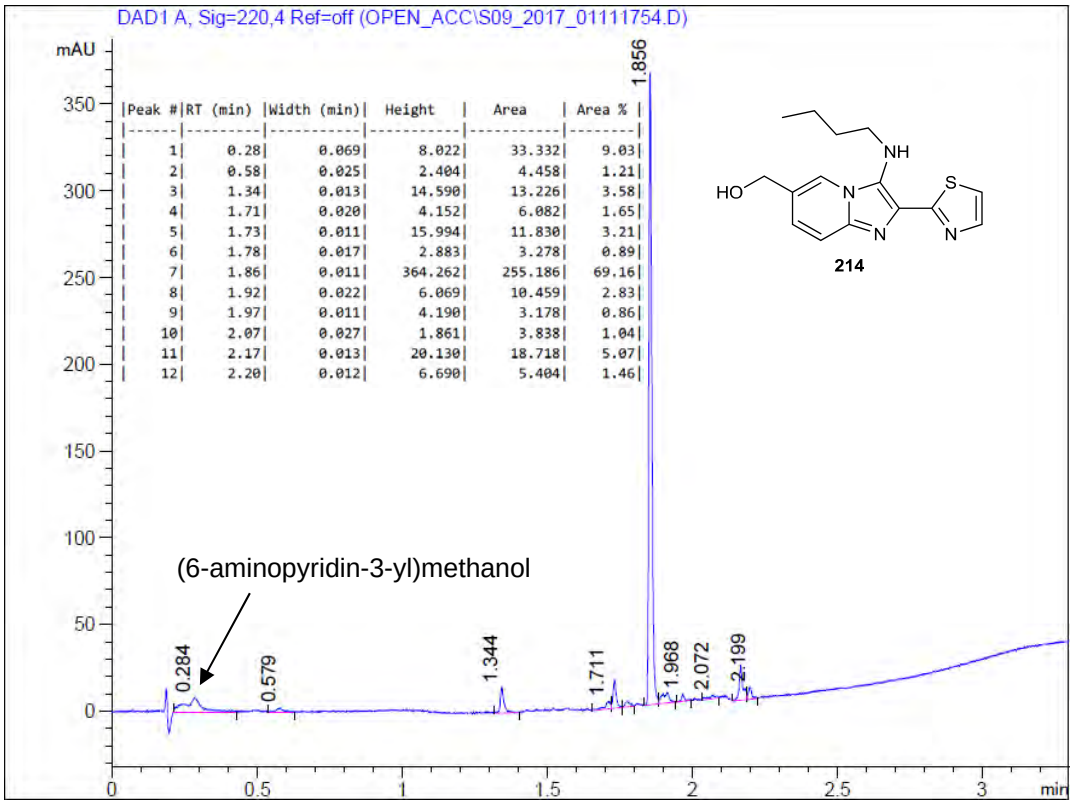
DAD1 A, Sig=220,4 Ref=off (OPEN_ACC\S09_2017_01111754.D)
mAU
Peak # | RT (min) | Width (min) | Height | Area | Area %
1 | 0.28 | 0.069 | 8.022 | 33.332 | 9.03
2 | 0.58 | 0.025 | 2.404 | 4.458 | 1.21
3 | 1.34 | 0.013 | 14.590 | 13.226 | 3.58
4 | 1.71 | 0.020 | 4.152 | 6.082 | 1.65
5 | 1.73 | 0.011 | 15.994 | 11.830 | 3.21
6 | 1.78 | 0.017 | 2.883 | 3.278 | 0.89
7 | 1.86 | 0.011 | 364.262 | 255.186 | 69.16
8 | 1.92 | 0.022 | 6.069 | 10.459 | 2.83
9 | 1.97 | 0.011 | 4.190 | 3.178 | 0.86
10 | 2.07 | 0.027 | 1.861 | 3.838 | 1.04
11 | 2.17 | 0.013 | 20.130 | 18.718 | 5.07
12 | 2.20 | 0.012 | 6.690 | 5.404 | 1.46
1.856
(6-aminopyridin-3-yl)methanol
0.284
0.579
1.344
1.711
1.968
2.072
2.199
min
NH
HO
N
S
N
N
214

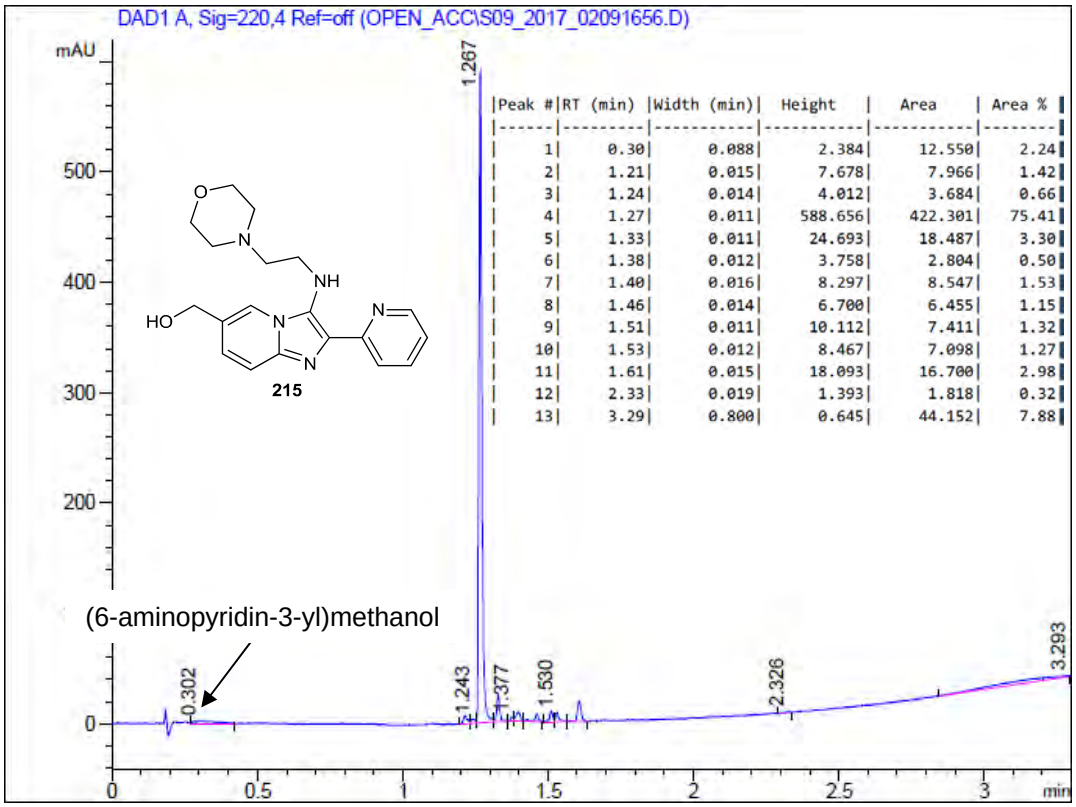

Peak #	RT (min)	Width (min)	Height	Area	Area %
1	0.30	0.088	2.384	12.550	2.24
2	1.21	0.015	7.678	7.966	1.42
3	1.24	0.014	4.012	3.684	0.66
4	1.27	0.011	588.656	422.301	75.41
5	1.33	0.011	24.693	18.487	3.30
6	1.38	0.012	3.758	2.804	0.50
7	1.40	0.016	8.297	8.547	1.53
8	1.46	0.014	6.700	6.455	1.15
9	1.51	0.011	10.112	7.411	1.32
10	1.53	0.012	8.467	7.098	1.27
11	1.61	0.015	18.093	16.700	2.98
12	2.33	0.019	1.393	1.818	0.32
13	3.29	0.800	0.645	44.152	7.88

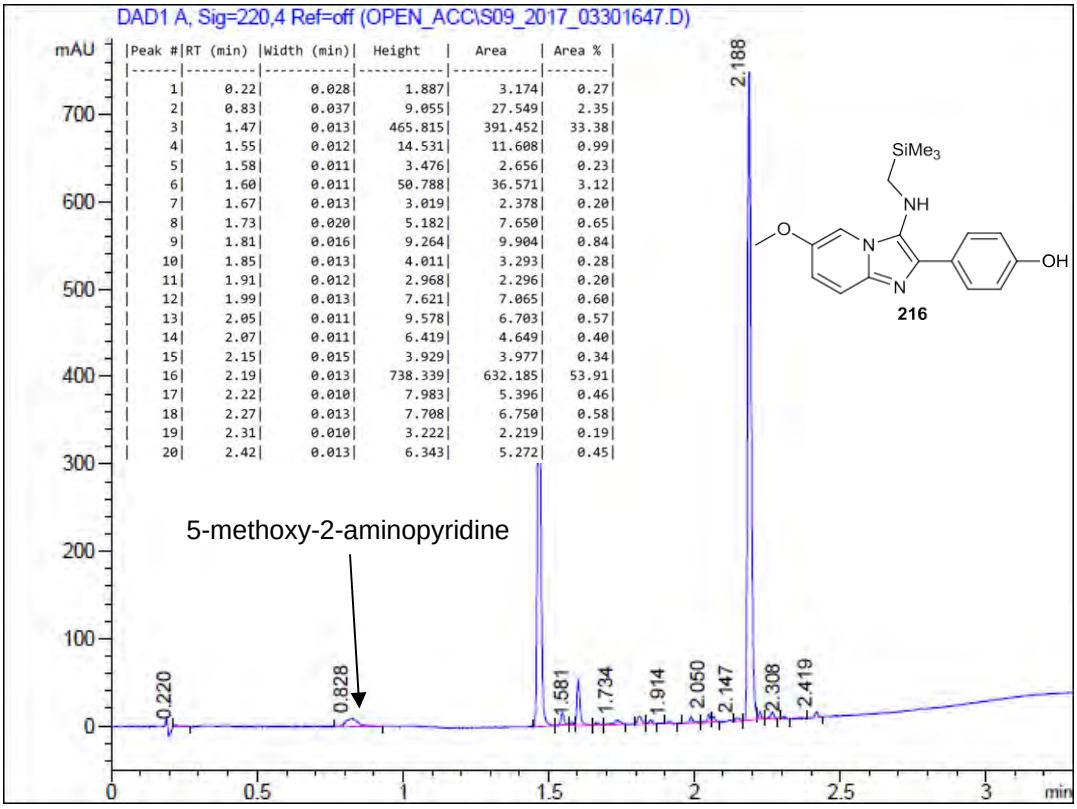

Peak #	RT (min)	Width (min)	Height	Area	Area %
1	0.22	0.028	1.887	3.174	0.27
2	0.83	0.037	9.055	27.549	2.35
3	1.47	0.013	465.815	391.452	33.38
4	1.55	0.012	14.531	11.608	0.99
5	1.58	0.011	3.476	2.656	0.23
6	1.60	0.011	50.788	36.571	3.12
7	1.67	0.013	3.019	2.378	0.20
8	1.73	0.020	5.182	7.650	0.65
9	1.81	0.016	9.264	9.904	0.84
10	1.85	0.013	4.011	3.293	0.28
11	1.91	0.012	2.968	2.296	0.20
12	1.99	0.013	7.621	7.065	0.60
13	2.05	0.011	9.578	6.703	0.57
14	2.07	0.011	6.419	4.649	0.40
15	2.15	0.015	3.929	3.977	0.34
16	2.19	0.013	738.339	632.185	53.91
17	2.22	0.010	7.983	5.396	0.46
18	2.27	0.013	7.708	6.750	0.58
19	2.31	0.010	3.222	2.219	0.19
20	2.42	0.013	6.343	5.272	0.45

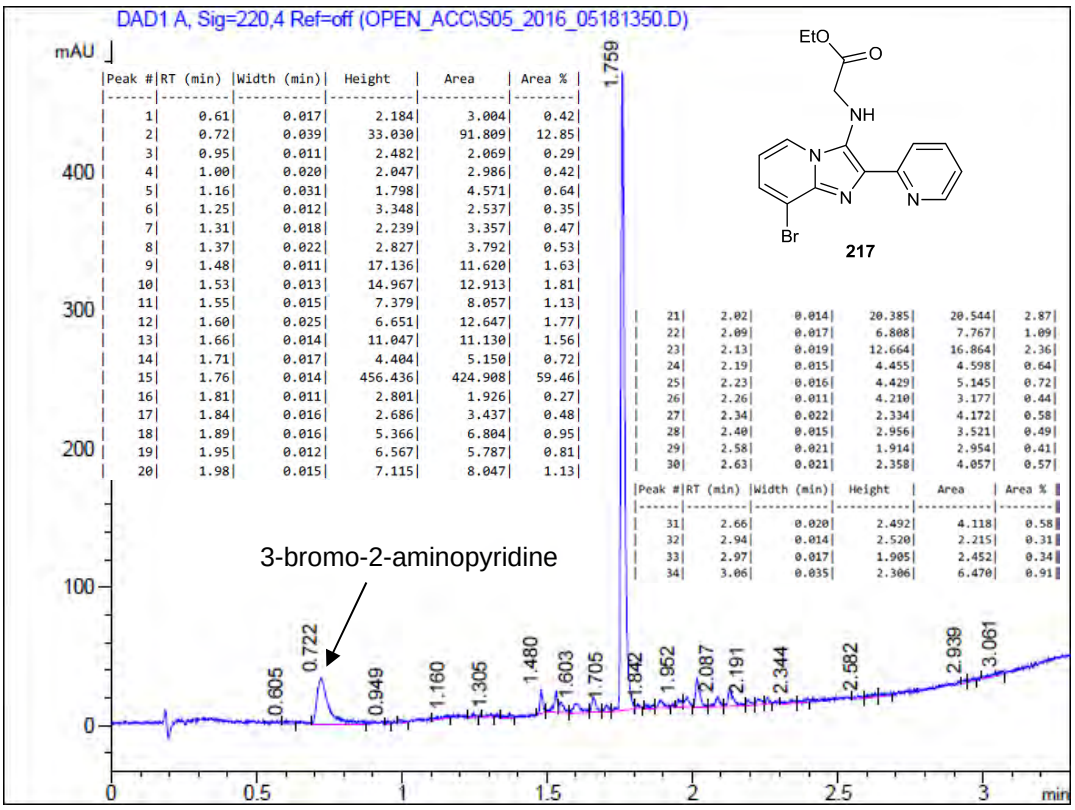

Peak #	RT (min)	Width (min)	Height	Area	Area %
1	0.61	0.017	2.184	3.004	0.42
2	0.72	0.039	33.030	91.809	12.85
3	0.95	0.011	2.482	2.069	0.29
4	1.00	0.020	2.047	2.986	0.42
5	1.16	0.031	1.798	4.571	0.64
6	1.25	0.012	3.348	2.537	0.35
7	1.31	0.018	2.239	3.357	0.47
8	1.37	0.022	2.827	3.792	0.53
9	1.48	0.011	17.136	11.620	1.63
10	1.53	0.013	14.967	12.913	1.81
11	1.55	0.015	7.379	8.057	1.13
12	1.60	0.025	6.651	12.647	1.77
13	1.66	0.014	11.047	11.130	1.56
14	1.71	0.017	4.404	5.150	0.72
15	1.76	0.014	456.436	424.908	59.46
16	1.81	0.011	2.801	1.926	0.27
17	1.84	0.016	2.686	3.437	0.48
18	1.89	0.016	5.366	6.804	0.95
19	1.95	0.012	6.567	5.787	0.81
20	1.98	0.015	7.115	8.047	1.13
21	2.02	0.014	20.385	20.544	2.87
22	2.09	0.017	6.808	7.767	1.09
23	2.13	0.019	12.664	16.864	2.36
24	2.19	0.015	4.455	4.598	0.64
25	2.23	0.016	4.429	5.145	0.72
26	2.26	0.011	4.210	3.177	0.44
27	2.34	0.022	2.334	4.172	0.58
28	2.40	0.015	2.956	3.521	0.49
29	2.58	0.021	1.914	2.954	0.41
30	2.63	0.021	2.358	4.057	0.57
31	2.66	0.020	2.492	4.118	0.58
32	2.94	0.014	2.520	2.215	0.31
33	2.97	0.017	1.905	2.452	0.34
34	3.06	0.035	2.306	6.470	0.91

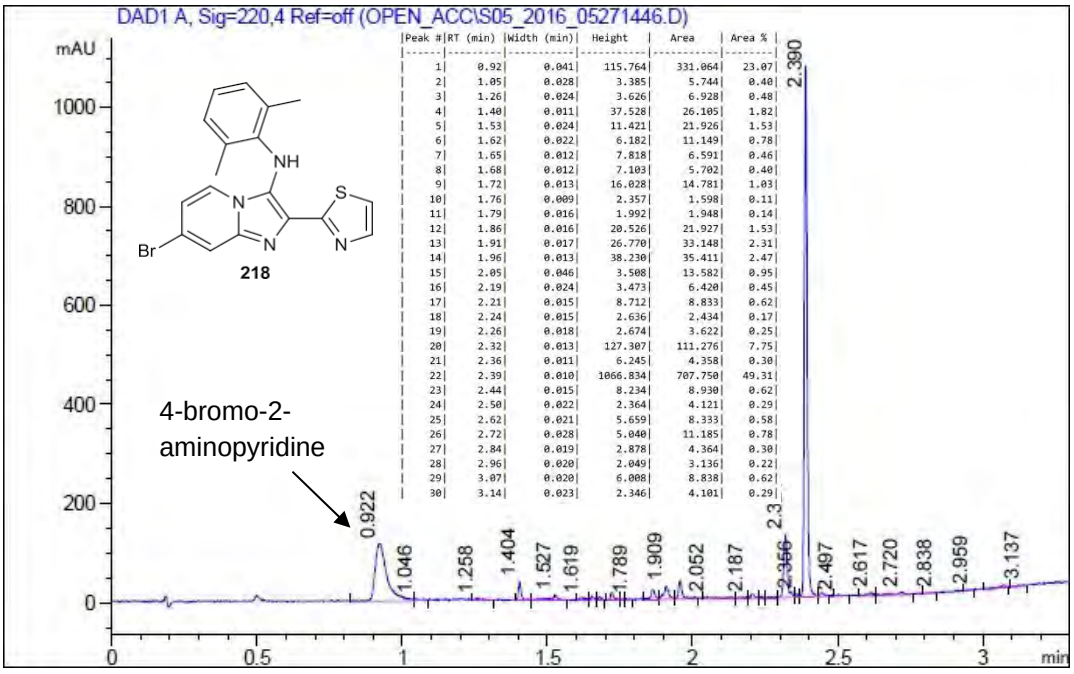

Peak #	RT (min)	Width (min)	Height	Area	Area %
1	0.92	0.041	115.764	331.064	23.07
2	1.05	0.028	3.385	5.744	0.40
3	1.26	0.024	3.626	6.928	0.48
4	1.40	0.011	37.528	26.105	1.82
5	1.53	0.024	11.421	21.926	1.53
6	1.62	0.022	6.182	11.149	0.78
7	1.65	0.012	7.818	6.591	0.46
8	1.68	0.012	7.103	5.702	0.40
9	1.72	0.013	16.028	14.781	1.03
10	1.76	0.009	2.357	1.598	0.11
11	1.79	0.016	1.992	1.948	0.14
12	1.86	0.016	20.526	21.927	1.53
13	1.91	0.017	26.770	33.148	2.31
14	1.96	0.013	38.230	35.411	2.47
15	2.05	0.046	3.508	13.582	0.95
16	2.19	0.024	3.473	6.420	0.45
17	2.21	0.015	8.712	8.833	0.62
18	2.24	0.015	2.636	2.434	0.17
19	2.26	0.018	2.674	3.622	0.25
20	2.32	0.013	127.307	111.276	7.75
21	2.36	0.011	6.245	4.358	0.30
22	2.39	0.010	1066.834	707.750	49.31
23	2.44	0.015	8.234	8.930	0.62
24	2.50	0.022	2.364	4.121	0.29
25	2.62	0.021	5.659	8.333	0.58
26	2.72	0.028	5.040	11.185	0.78
27	2.84	0.019	2.878	4.364	0.30
28	2.96	0.020	2.049	3.136	0.22
29	3.07	0.020	6.008	8.838	0.62
30	3.14	0.023	2.346	4.101	0.29

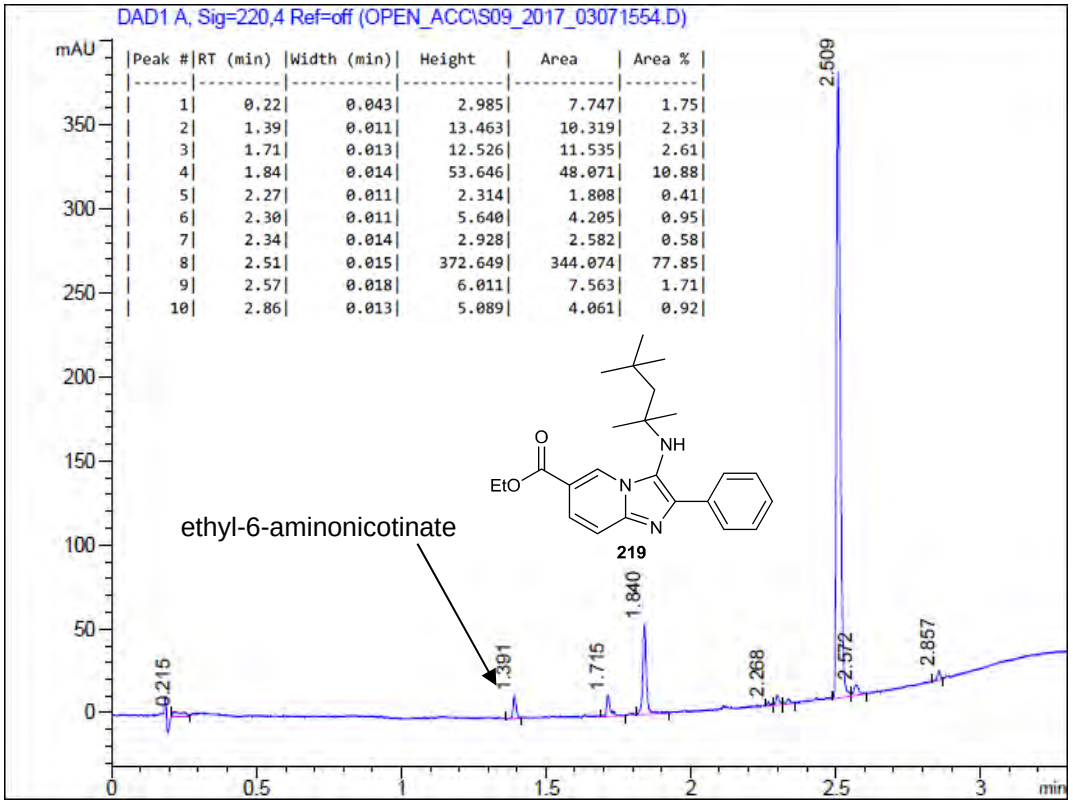
DAD1 A, Sig=220,4 Ref=off (OPEN_ACC\S09_2017_03071554.D)
mAU
Peak # | RT (min) | Width (min) | Height | Area | Area %
1 | 0.22 | 0.043 | 2.985 | 7.747 | 1.75
2 | 1.39 | 0.011 | 13.463 | 10.319 | 2.33
3 | 1.71 | 0.013 | 12.526 | 11.535 | 2.61
4 | 1.84 | 0.014 | 53.646 | 48.071 | 10.88
5 | 2.27 | 0.011 | 2.314 | 1.808 | 0.41
6 | 2.30 | 0.011 | 5.640 | 4.205 | 0.95
7 | 2.34 | 0.014 | 2.928 | 2.582 | 0.58
8 | 2.51 | 0.015 | 372.649 | 344.074 | 77.85
9 | 2.57 | 0.018 | 6.011 | 7.563 | 1.71
10 | 2.86 | 0.013 | 5.089 | 4.061 | 0.92
ethyl-6-aminonicotinate
219
0.215
1.391
1.715
1.840
2.268
2.509
2.572
2.857
min

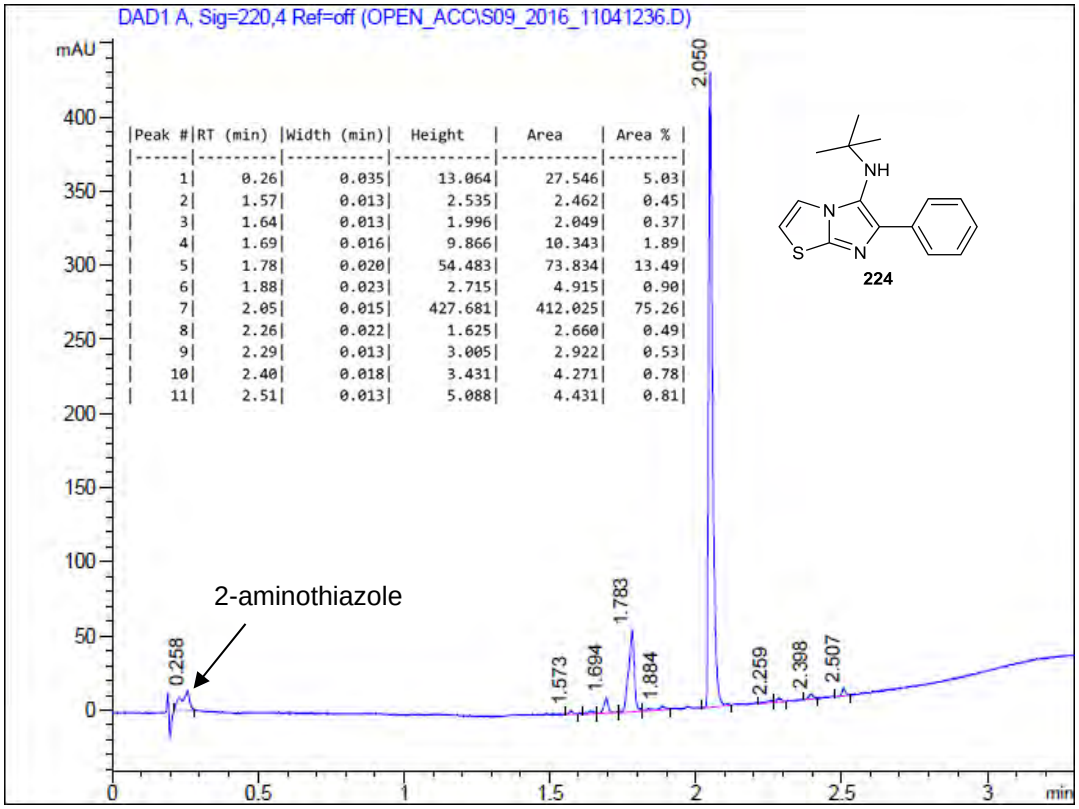
DAD1 A, Sig=220,4 Ref=off (OPEN_ACC\S09_2016_11041236.D)
mAU
Peak # | RT (min) | Width (min) | Height | Area | Area %
1 | 0.26 | 0.035 | 13.064 | 27.546 | 5.03
2 | 1.57 | 0.013 | 2.535 | 2.462 | 0.45
3 | 1.64 | 0.013 | 1.996 | 2.049 | 0.37
4 | 1.69 | 0.016 | 9.866 | 10.343 | 1.89
5 | 1.78 | 0.020 | 54.483 | 73.834 | 13.49
6 | 1.88 | 0.023 | 2.715 | 4.915 | 0.90
7 | 2.05 | 0.015 | 427.681 | 412.025 | 75.26
8 | 2.26 | 0.022 | 1.625 | 2.660 | 0.49
9 | 2.29 | 0.013 | 3.005 | 2.922 | 0.53
10 | 2.40 | 0.018 | 3.431 | 4.271 | 0.78
11 | 2.51 | 0.013 | 5.088 | 4.431 | 0.81
2-aminothiazole
224
0.258
1.573
1.694
1.783
1.884
2.050
2.259
2.398
2.507
min

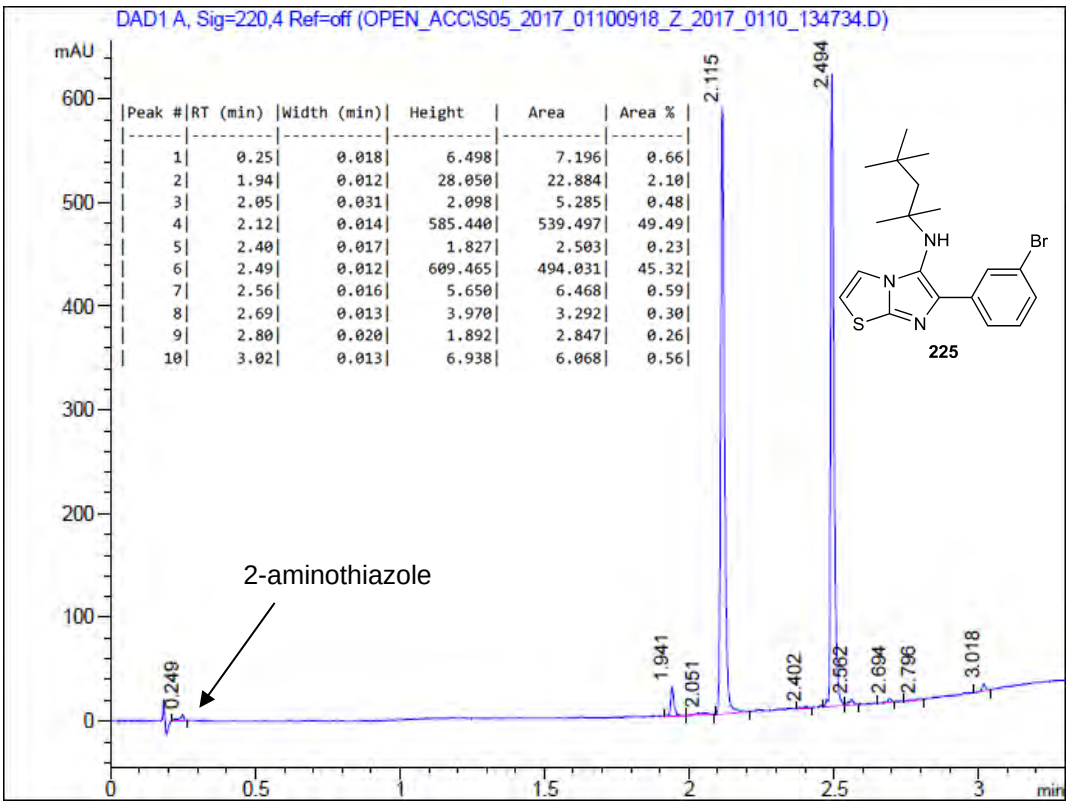

Peak #	RT (min)	Width (min)	Height	Area	Area %
1	0.25	0.018	6.498	7.196	0.66
2	1.94	0.012	28.050	22.884	2.10
3	2.05	0.031	2.098	5.285	0.48
4	2.12	0.014	585.440	539.497	49.49
5	2.40	0.017	1.827	2.503	0.23
6	2.49	0.012	609.465	494.031	45.32
7	2.56	0.016	5.650	6.468	0.59
8	2.69	0.013	3.970	3.292	0.30
9	2.80	0.020	1.892	2.847	0.26
10	3.02	0.013	6.938	6.068	0.56

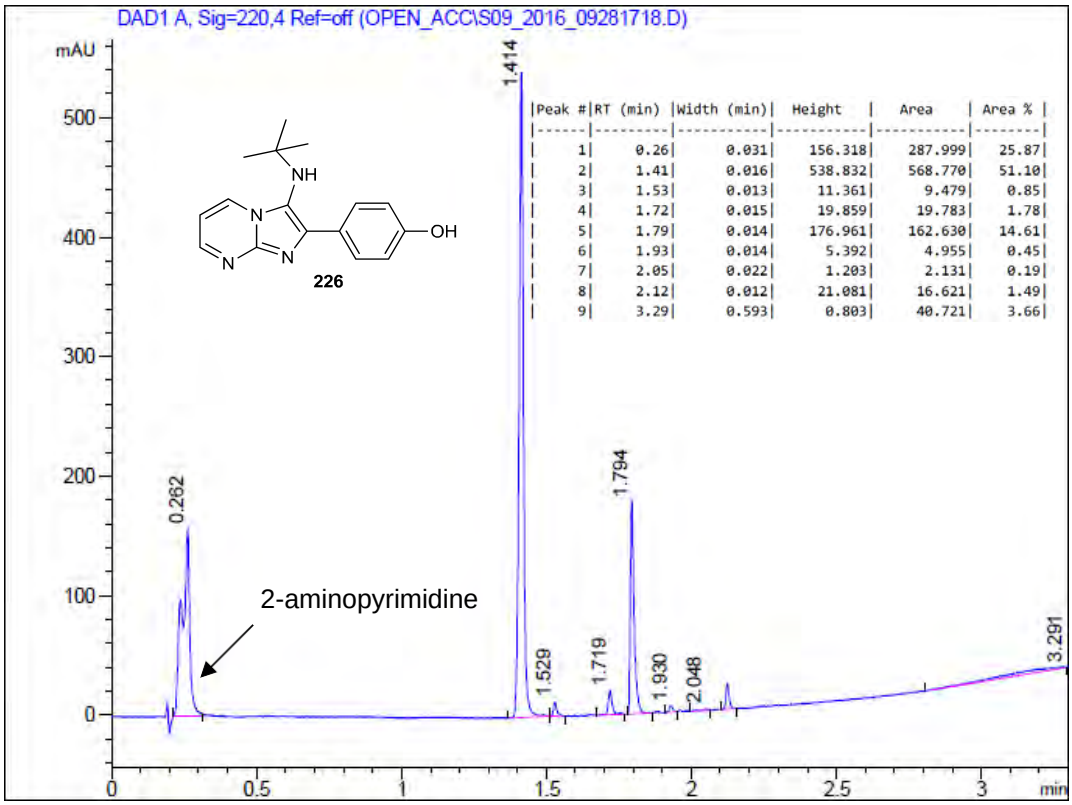

Peak #	RT (min)	Width (min)	Height	Area	Area %
1	0.26	0.031	156.318	287.999	25.87
2	1.41	0.016	538.832	568.770	51.10
3	1.53	0.013	11.361	9.479	0.85
4	1.72	0.015	19.859	19.783	1.78
5	1.79	0.014	176.961	162.630	14.61
6	1.93	0.014	5.392	4.955	0.45
7	2.05	0.022	1.203	2.131	0.19
8	2.12	0.012	21.081	16.621	1.49
9	3.29	0.593	0.803	40.721	3.66

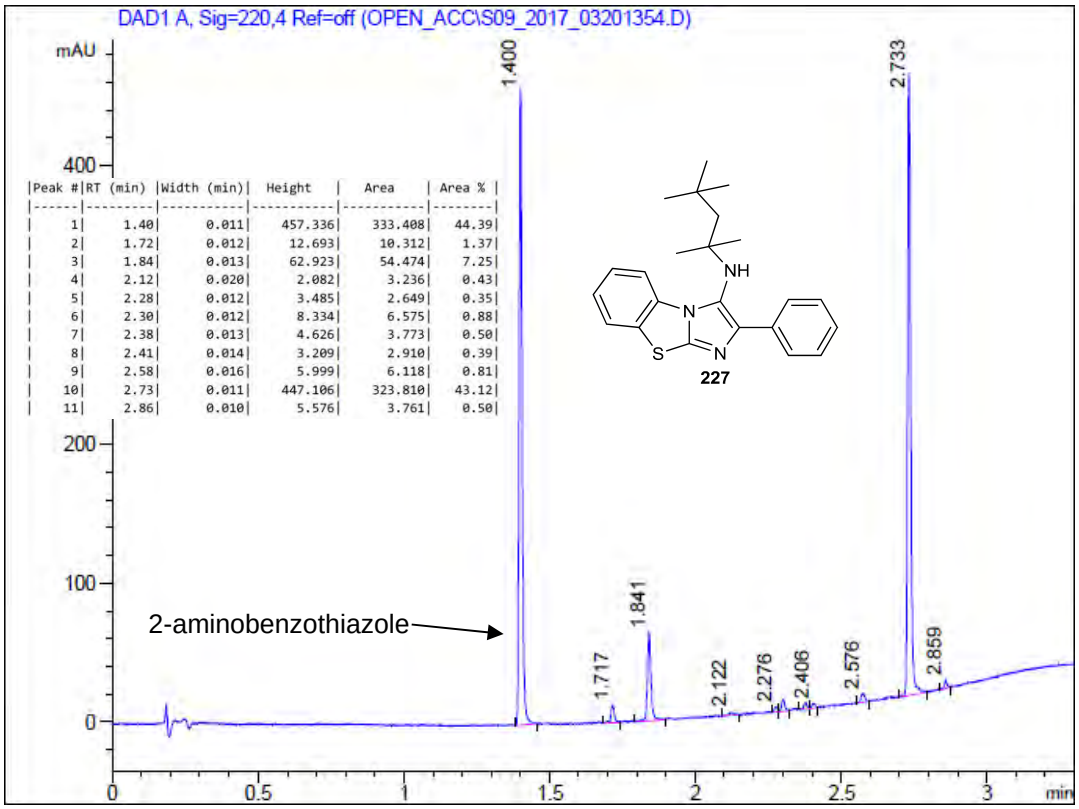

Peak #	RT (min)	Width (min)	Height	Area	Area %
1	1.40	0.011	457.336	333.408	44.39
2	1.72	0.012	12.693	10.312	1.37
3	1.84	0.013	62.923	54.474	7.25
4	2.12	0.020	2.082	3.236	0.43
5	2.28	0.012	3.485	2.649	0.35
6	2.30	0.012	8.334	6.575	0.88
7	2.38	0.013	4.626	3.773	0.50
8	2.41	0.014	3.209	2.910	0.39
9	2.58	0.016	5.999	6.118	0.81
10	2.73	0.011	447.106	323.810	43.12
11	2.86	0.010	5.576	3.761	0.50

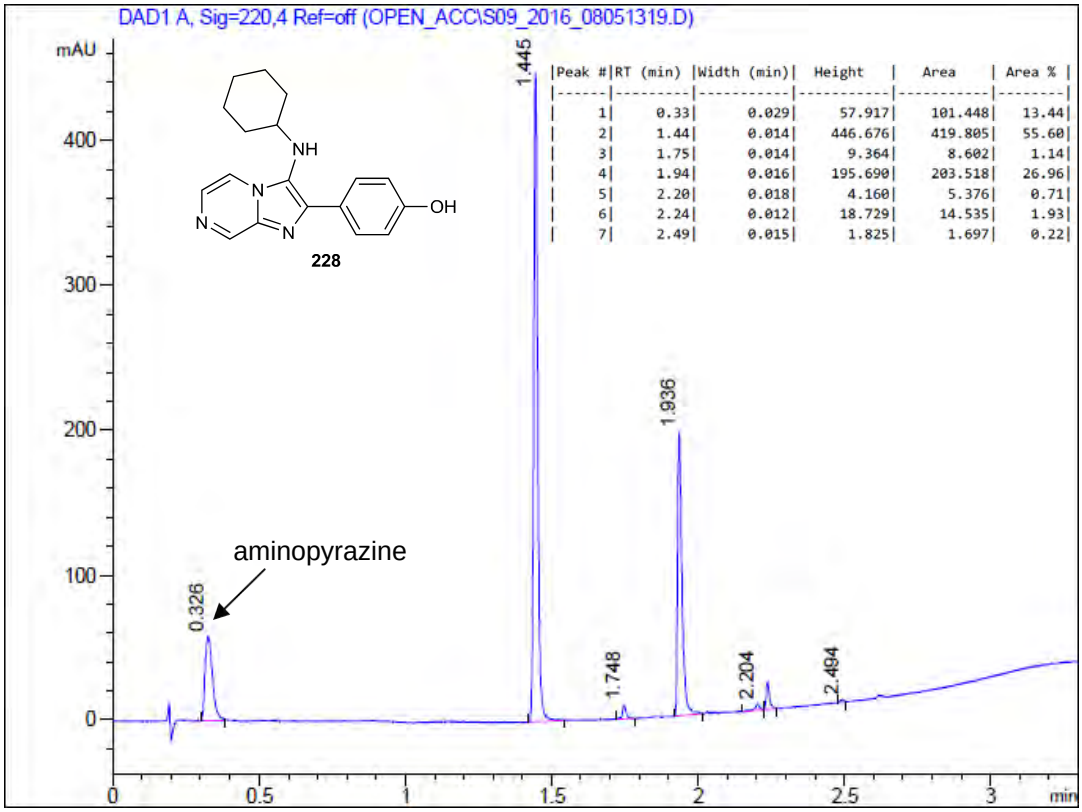

Peak #	RT (min)	Width (min)	Height	Area	Area %
1	0.33	0.029	57.917	101.448	13.44
2	1.44	0.014	446.676	419.805	55.60
3	1.75	0.014	9.364	8.602	1.14
4	1.94	0.016	195.690	203.518	26.96
5	2.20	0.018	4.160	5.376	0.71
6	2.24	0.012	18.729	14.535	1.93
7	2.49	0.015	1.825	1.697	0.22

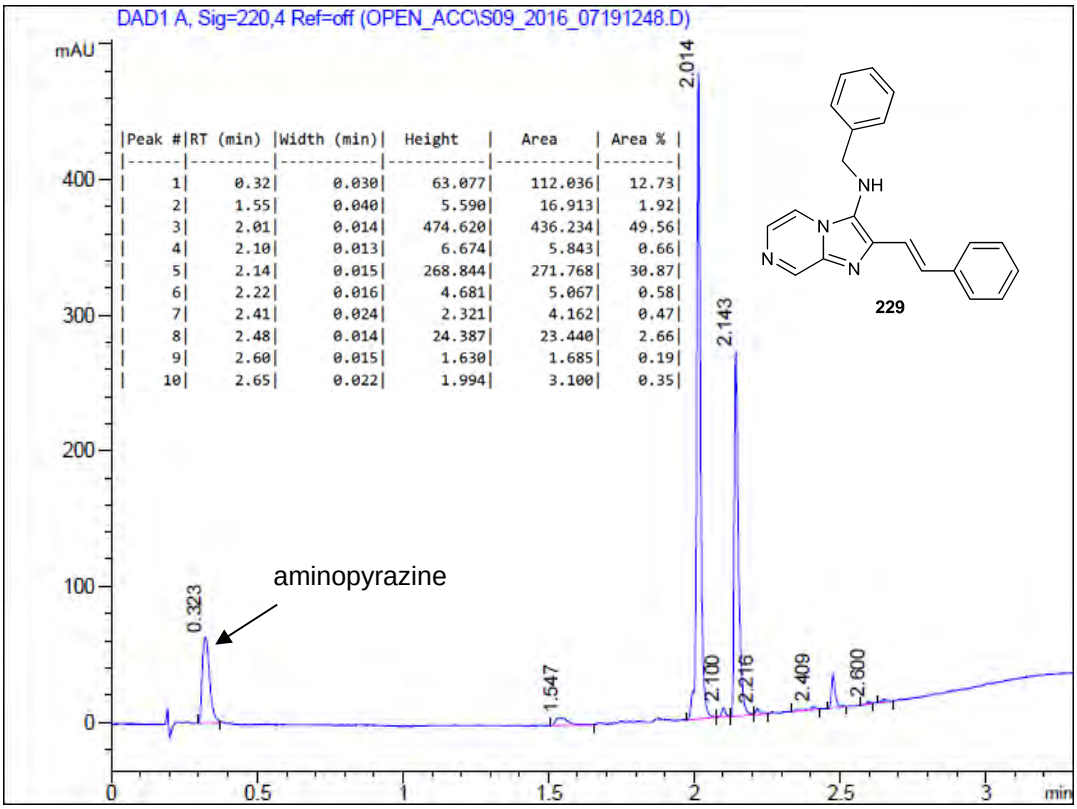

Peak #	RT (min)	Width (min)	Height	Area	Area %
1	0.32	0.030	63.077	112.036	12.73
2	1.55	0.040	5.590	16.913	1.92
3	2.01	0.014	474.620	436.234	49.56
4	2.10	0.013	6.674	5.843	0.66
5	2.14	0.015	268.844	271.768	30.87
6	2.22	0.016	4.681	5.067	0.58
7	2.41	0.024	2.321	4.162	0.47
8	2.48	0.014	24.387	23.440	2.66
9	2.60	0.015	1.630	1.685	0.19
10	2.65	0.022	1.994	3.100	0.35

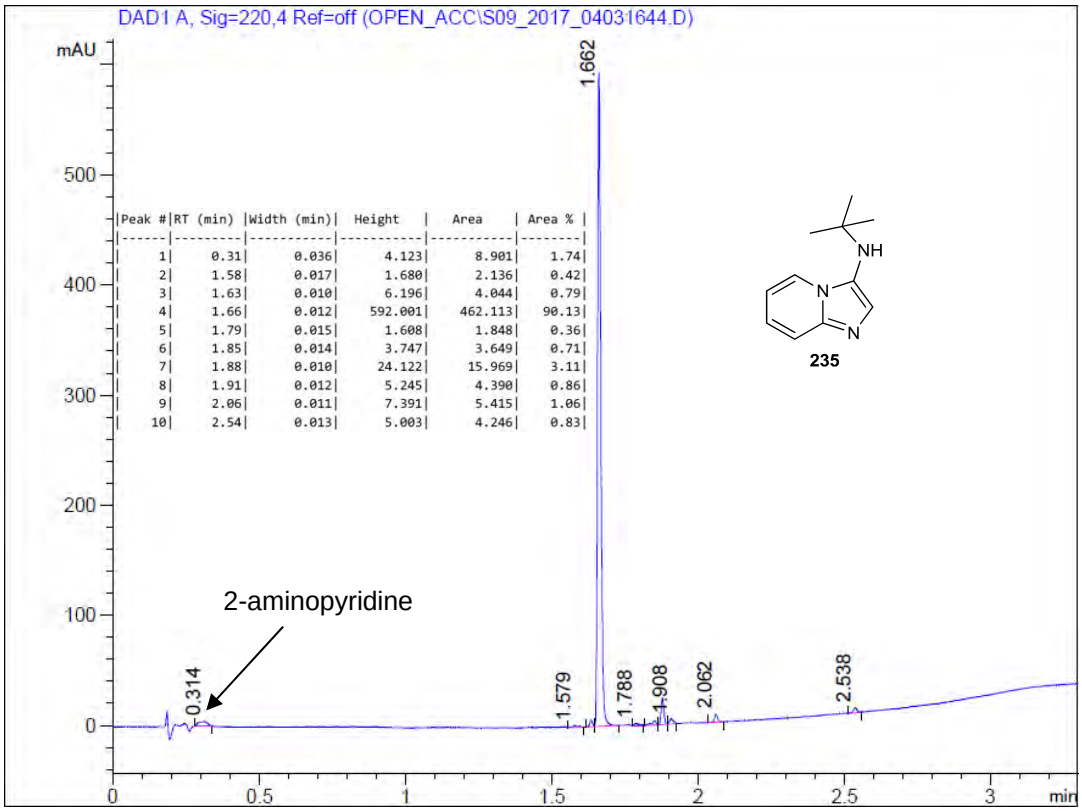

Peak #	RT (min)	Width (min)	Height	Area	Area %
1	0.31	0.036	4.123	8.901	1.74
2	1.58	0.017	1.680	2.136	0.42
3	1.63	0.010	6.196	4.044	0.79
4	1.66	0.012	592.001	462.113	90.13
5	1.79	0.015	1.608	1.848	0.36
6	1.85	0.014	3.747	3.649	0.71
7	1.88	0.010	24.122	15.969	3.11
8	1.91	0.012	5.245	4.390	0.86
9	2.06	0.011	7.391	5.415	1.06
10	2.54	0.013	5.003	4.246	0.83

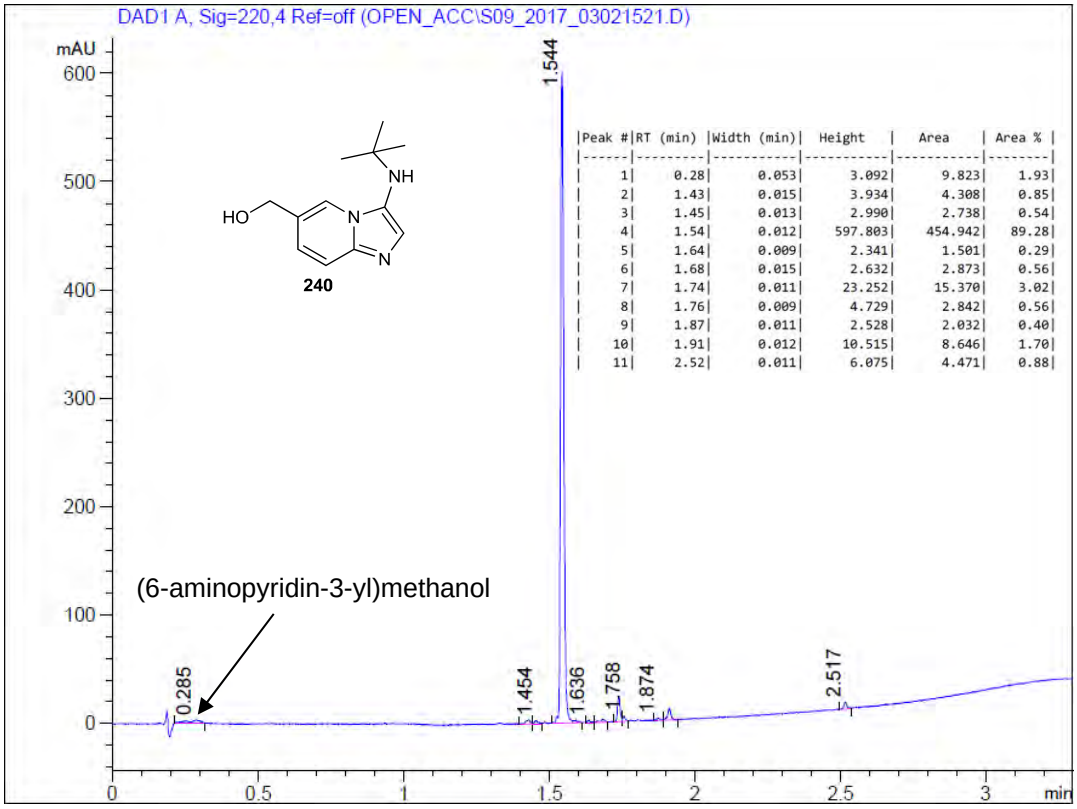

Peak #	RT (min)	Width (min)	Height	Area	Area %
1	0.28	0.053	3.092	9.823	1.93
2	1.43	0.015	3.934	4.308	0.85
3	1.45	0.013	2.990	2.738	0.54
4	1.54	0.012	597.803	454.942	89.28
5	1.64	0.009	2.341	1.501	0.29
6	1.68	0.015	2.632	2.873	0.56
7	1.74	0.011	23.252	15.370	3.02
8	1.76	0.009	4.729	2.842	0.56
9	1.87	0.011	2.528	2.032	0.40
10	1.91	0.012	10.515	8.646	1.70
11	2.52	0.011	6.075	4.471	0.88

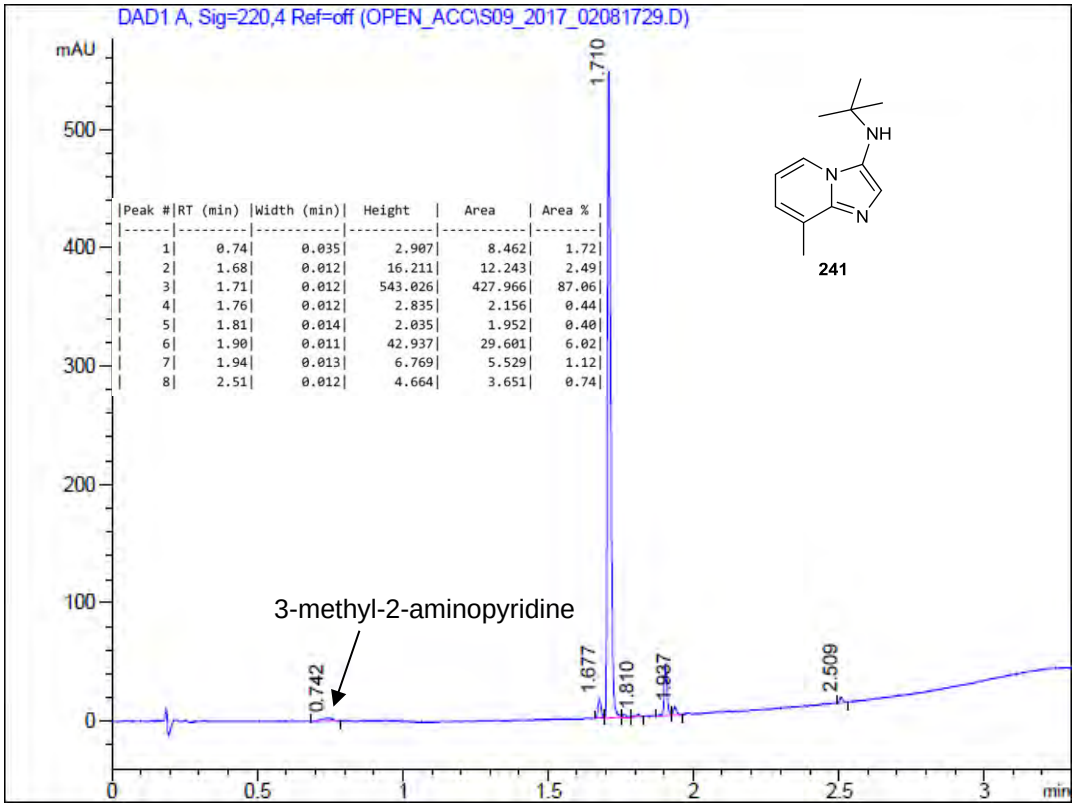

Peak #	RT (min)	Width (min)	Height	Area	Area %
1	0.74	0.035	2.907	8.462	1.72
2	1.68	0.012	16.211	12.243	2.49
3	1.71	0.012	543.026	427.966	87.06
4	1.76	0.012	2.835	2.156	0.44
5	1.81	0.014	2.035	1.952	0.40
6	1.90	0.011	42.937	29.601	6.02
7	1.94	0.013	6.769	5.529	1.12
8	2.51	0.012	4.664	3.651	0.74

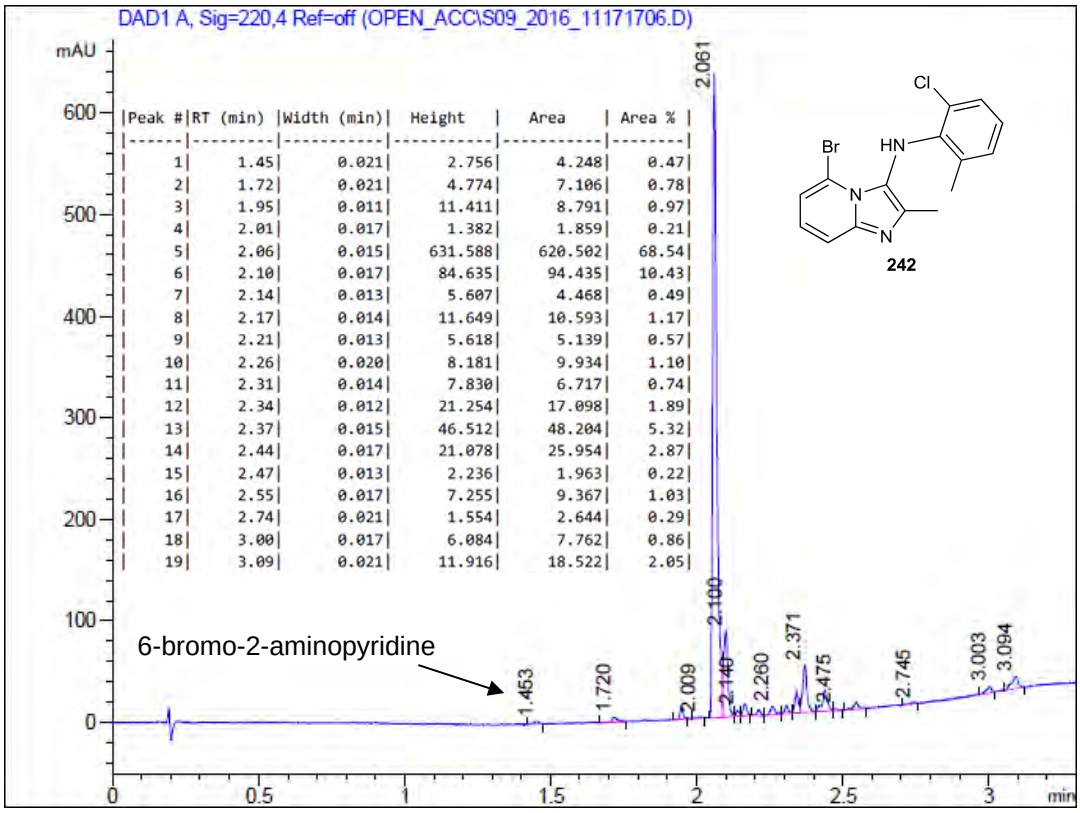

Peak #	RT (min)	Width (min)	Height	Area	Area %
1	1.45	0.021	2.756	4.248	0.47
2	1.72	0.021	4.774	7.106	0.78
3	1.95	0.011	11.411	8.791	0.97
4	2.01	0.017	1.382	1.859	0.21
5	2.06	0.015	631.588	620.502	68.54
6	2.10	0.017	84.635	94.435	10.43
7	2.14	0.013	5.607	4.468	0.49
8	2.17	0.014	11.649	10.593	1.17
9	2.21	0.013	5.618	5.139	0.57
10	2.26	0.020	8.181	9.934	1.10
11	2.31	0.014	7.830	6.717	0.74
12	2.34	0.012	21.254	17.098	1.89
13	2.37	0.015	46.512	48.204	5.32
14	2.44	0.017	21.078	25.954	2.87
15	2.47	0.013	2.236	1.963	0.22
16	2.55	0.017	7.255	9.367	1.03
17	2.74	0.021	1.554	2.644	0.29
18	3.00	0.017	6.084	7.762	0.86
19	3.09	0.021	11.916	18.522	2.05

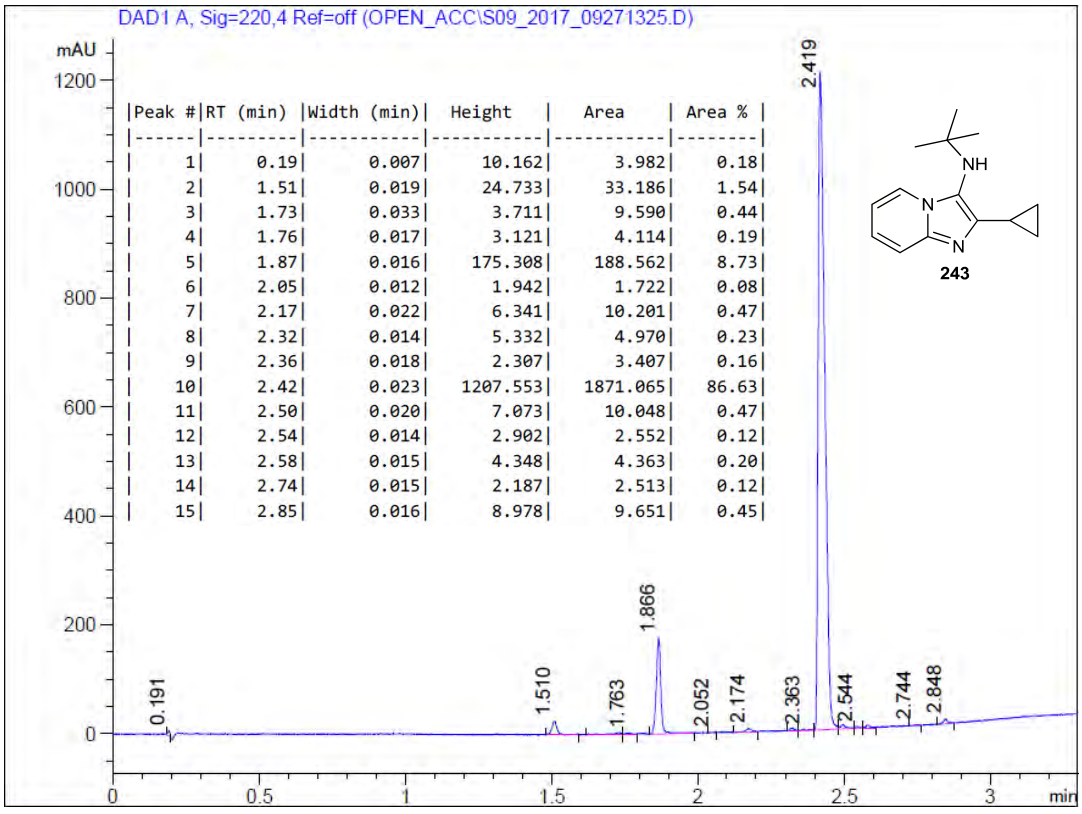

Peak #	RT (min)	Width (min)	Height	Area	Area %
1	0.19	0.007	10.162	3.982	0.18
2	1.51	0.019	24.733	33.186	1.54
3	1.73	0.033	3.711	9.590	0.44
4	1.76	0.017	3.121	4.114	0.19
5	1.87	0.016	175.308	188.562	8.73
6	2.05	0.012	1.942	1.722	0.08
7	2.17	0.022	6.341	10.201	0.47
8	2.32	0.014	5.332	4.970	0.23
9	2.36	0.018	2.307	3.407	0.16
10	2.42	0.023	1207.553	1871.065	86.63
11	2.50	0.020	7.073	10.048	0.47
12	2.54	0.014	2.902	2.552	0.12
13	2.58	0.015	4.348	4.363	0.20
14	2.74	0.015	2.187	2.513	0.12
15	2.85	0.016	8.978	9.651	0.45

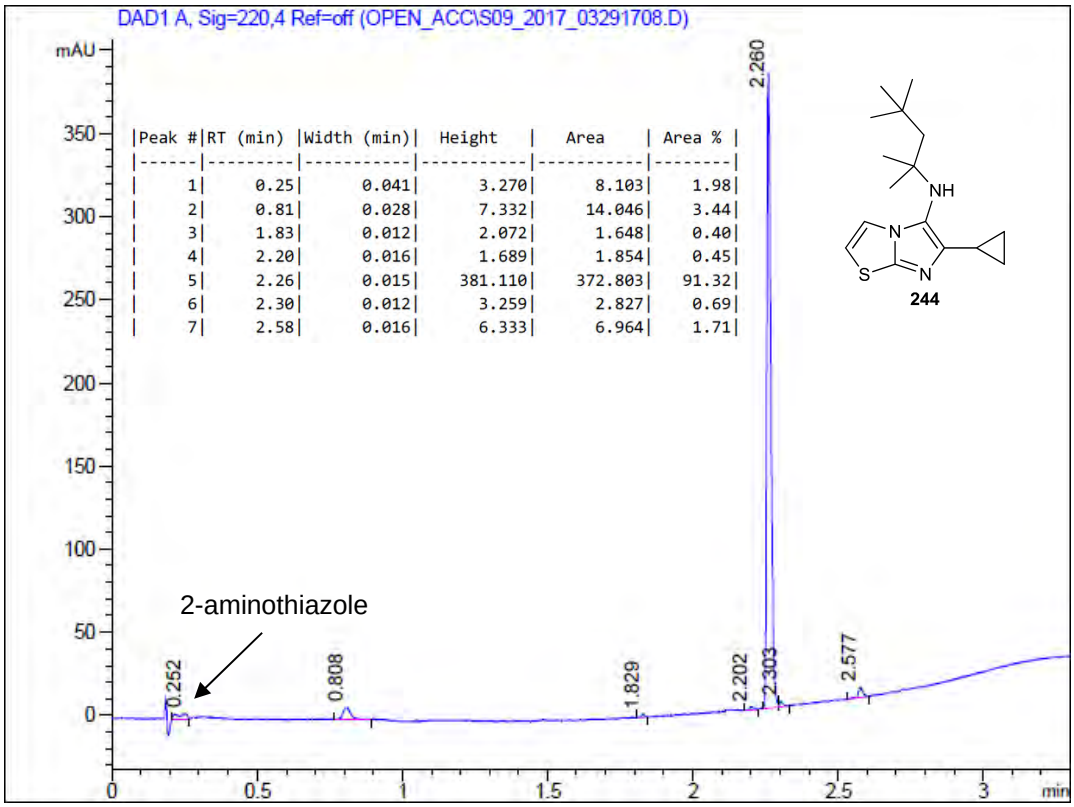

Peak #	RT (min)	Width (min)	Height	Area	Area %
1	0.25	0.041	3.270	8.103	1.98
2	0.81	0.028	7.332	14.046	3.44
3	1.83	0.012	2.072	1.648	0.40
4	2.20	0.016	1.689	1.854	0.45
5	2.26	0.015	381.110	372.803	91.32
6	2.30	0.012	3.259	2.827	0.69
7	2.58	0.016	6.333	6.964	1.71

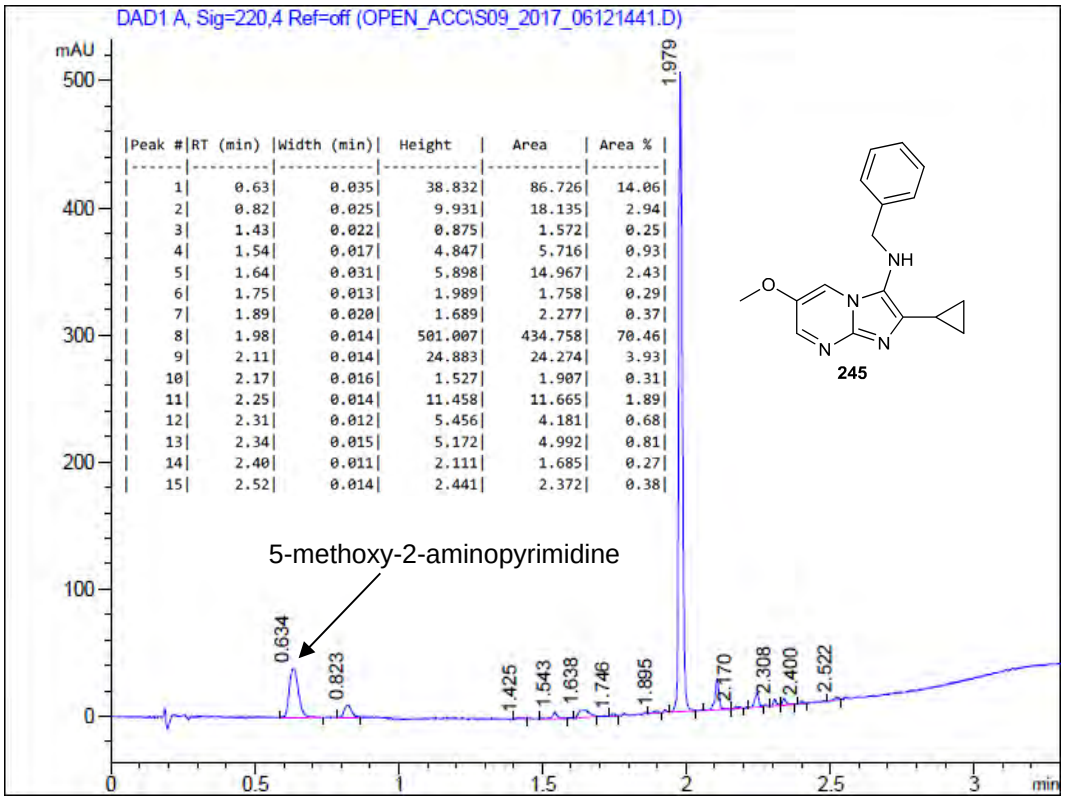

Peak #	RT (min)	Width (min)	Height	Area	Area %
1	0.63	0.035	38.832	86.726	14.06
2	0.82	0.025	9.931	18.135	2.94
3	1.43	0.022	0.875	1.572	0.25
4	1.54	0.017	4.847	5.716	0.93
5	1.64	0.031	5.898	14.967	2.43
6	1.75	0.013	1.989	1.758	0.29
7	1.89	0.020	1.689	2.277	0.37
8	1.98	0.014	501.007	434.758	70.46
9	2.11	0.014	24.883	24.274	3.93
10	2.17	0.016	1.527	1.907	0.31
11	2.25	0.014	11.458	11.665	1.89
12	2.31	0.012	5.456	4.181	0.68
13	2.34	0.015	5.172	4.992	0.81
14	2.40	0.011	2.111	1.685	0.27
15	2.52	0.014	2.441	2.372	0.38

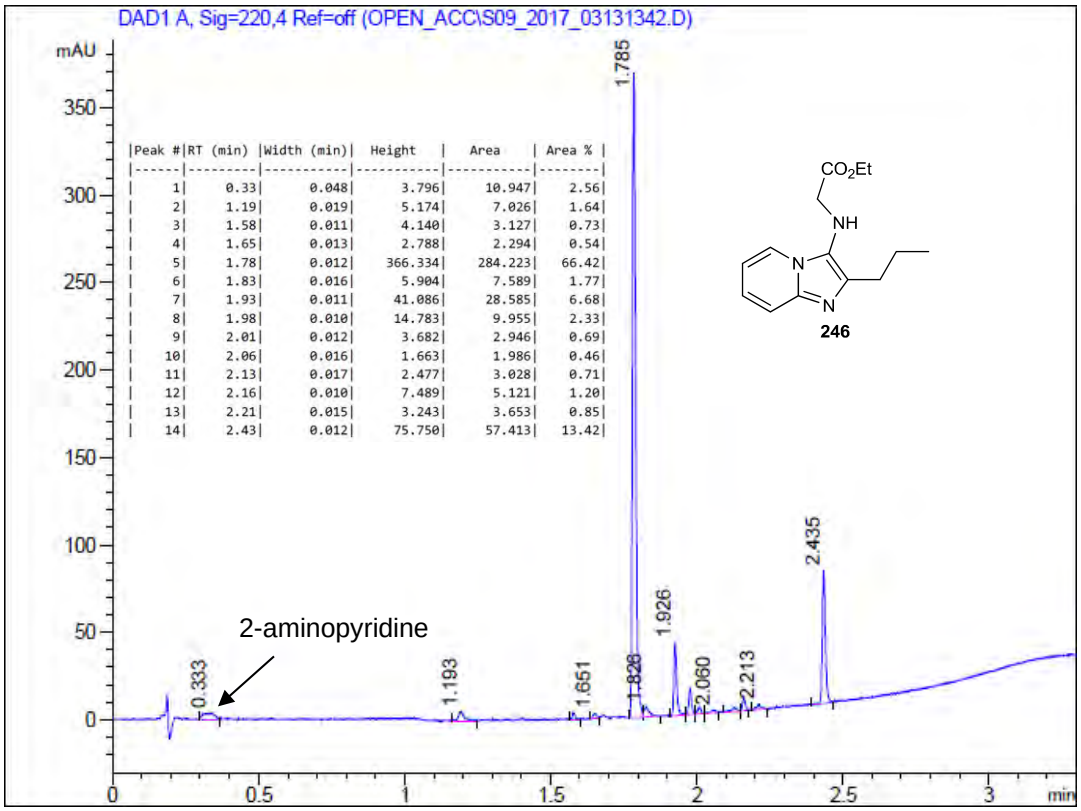

Peak #	RT (min)	Width (min)	Height	Area	Area %
1	0.33	0.048	3.796	10.947	2.56
2	1.19	0.019	5.174	7.026	1.64
3	1.58	0.011	4.140	3.127	0.73
4	1.65	0.013	2.788	2.294	0.54
5	1.78	0.012	366.334	284.223	66.42
6	1.83	0.016	5.904	7.589	1.77
7	1.93	0.011	41.086	28.585	6.68
8	1.98	0.010	14.783	9.955	2.33
9	2.01	0.012	3.682	2.946	0.69
10	2.06	0.016	1.663	1.986	0.46
11	2.13	0.017	2.477	3.028	0.71
12	2.16	0.010	7.489	5.121	1.20
13	2.21	0.015	3.243	3.653	0.85
14	2.43	0.012	75.750	57.413	13.42

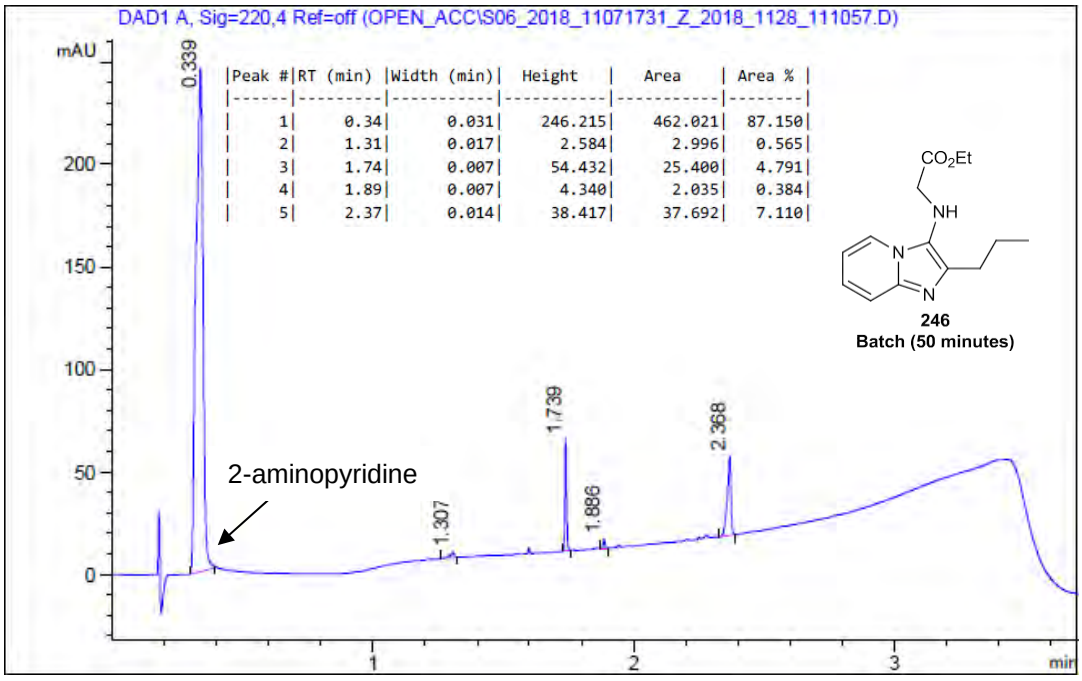

Peak #	RT (min)	Width (min)	Height	Area	Area %
1	0.34	0.031	246.215	462.021	87.150
2	1.31	0.017	2.584	2.996	0.565
3	1.74	0.007	54.432	25.400	4.791
4	1.89	0.007	4.340	2.035	0.384
5	2.37	0.014	38.417	37.692	7.110

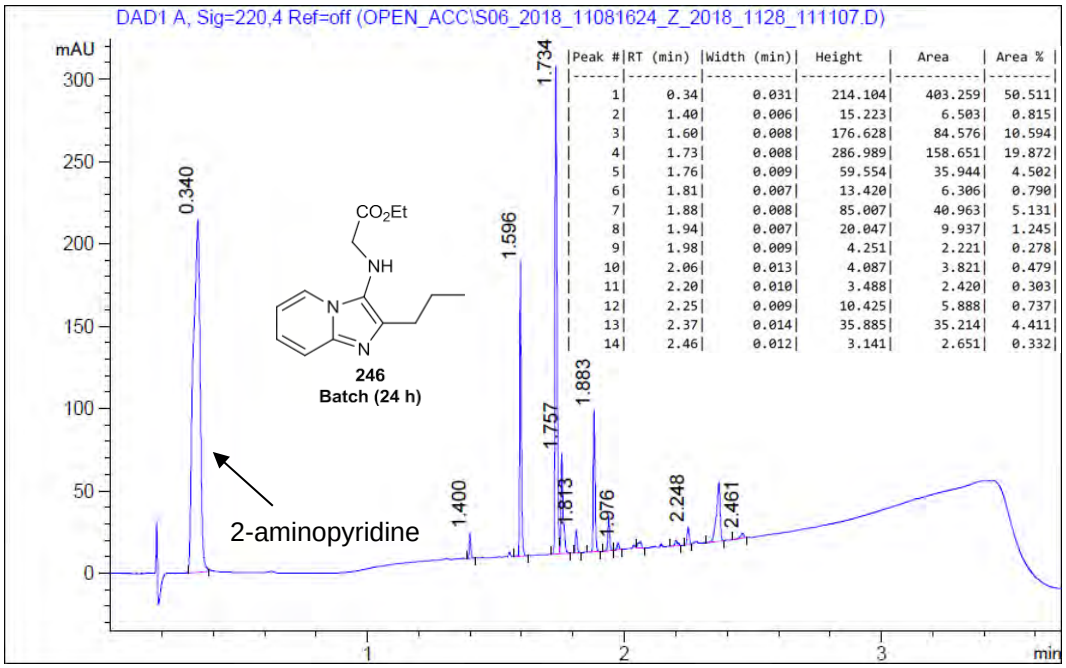

Peak #	RT (min)	Width (min)	Height	Area	Area %
1	0.34	0.031	214.104	403.259	50.511
2	1.40	0.006	15.223	6.503	0.815
3	1.60	0.008	176.628	84.576	10.594
4	1.73	0.008	286.989	158.651	19.872
5	1.76	0.009	59.554	35.944	4.502
6	1.81	0.007	13.420	6.306	0.790
7	1.88	0.008	85.007	40.963	5.131
8	1.94	0.007	20.047	9.937	1.245
9	1.98	0.009	4.251	2.221	0.278
10	2.06	0.013	4.087	3.821	0.479
11	2.20	0.010	3.488	2.420	0.303
12	2.25	0.009	10.425	5.888	0.737
13	2.37	0.014	35.885	35.214	4.411
14	2.46	0.012	3.141	2.651	0.332

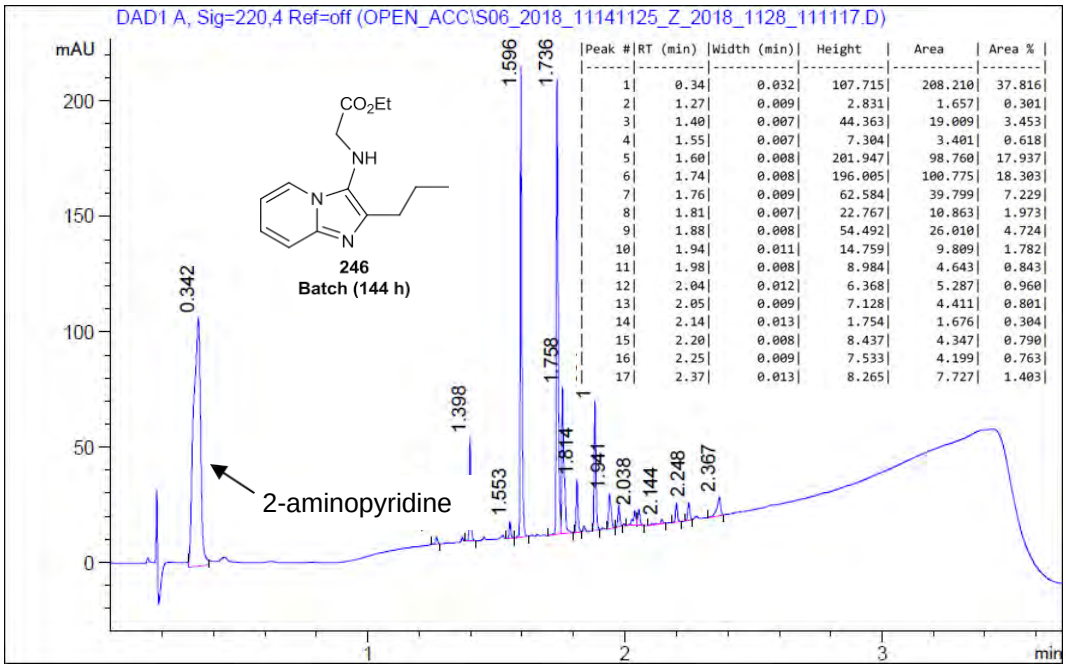

Peak #	RT (min)	Width (min)	Height	Area	Area %
1	0.34	0.032	107.715	208.210	37.816
2	1.27	0.009	2.831	1.657	0.301
3	1.40	0.007	44.363	19.009	3.453
4	1.55	0.007	7.304	3.401	0.618
5	1.60	0.008	201.947	98.760	17.937
6	1.74	0.008	196.005	100.775	18.303
7	1.76	0.009	62.584	39.799	7.229
8	1.81	0.007	22.767	10.863	1.973
9	1.88	0.008	54.492	26.010	4.724
10	1.94	0.011	14.759	9.809	1.782
11	1.98	0.008	8.984	4.643	0.843
12	2.04	0.012	6.368	5.287	0.960
13	2.05	0.009	7.128	4.411	0.801
14	2.14	0.013	1.754	1.676	0.304
15	2.20	0.008	8.437	4.347	0.790
16	2.25	0.009	7.533	4.199	0.763
17	2.37	0.013	8.265	7.727	1.403

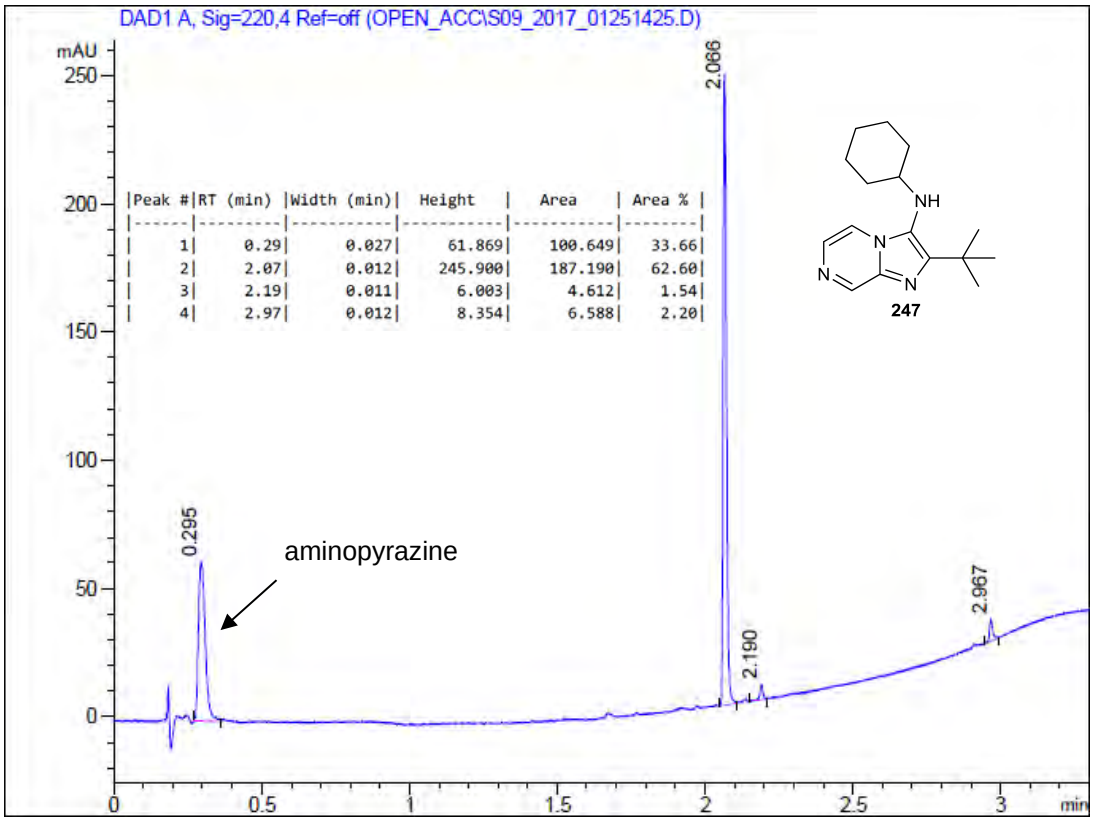

Peak #	RT (min)	Width (min)	Height	Area	Area %
1	0.29	0.027	61.869	100.649	33.66
2	2.07	0.012	245.900	187.190	62.60
3	2.19	0.011	6.003	4.612	1.54
4	2.97	0.012	8.354	6.588	2.20

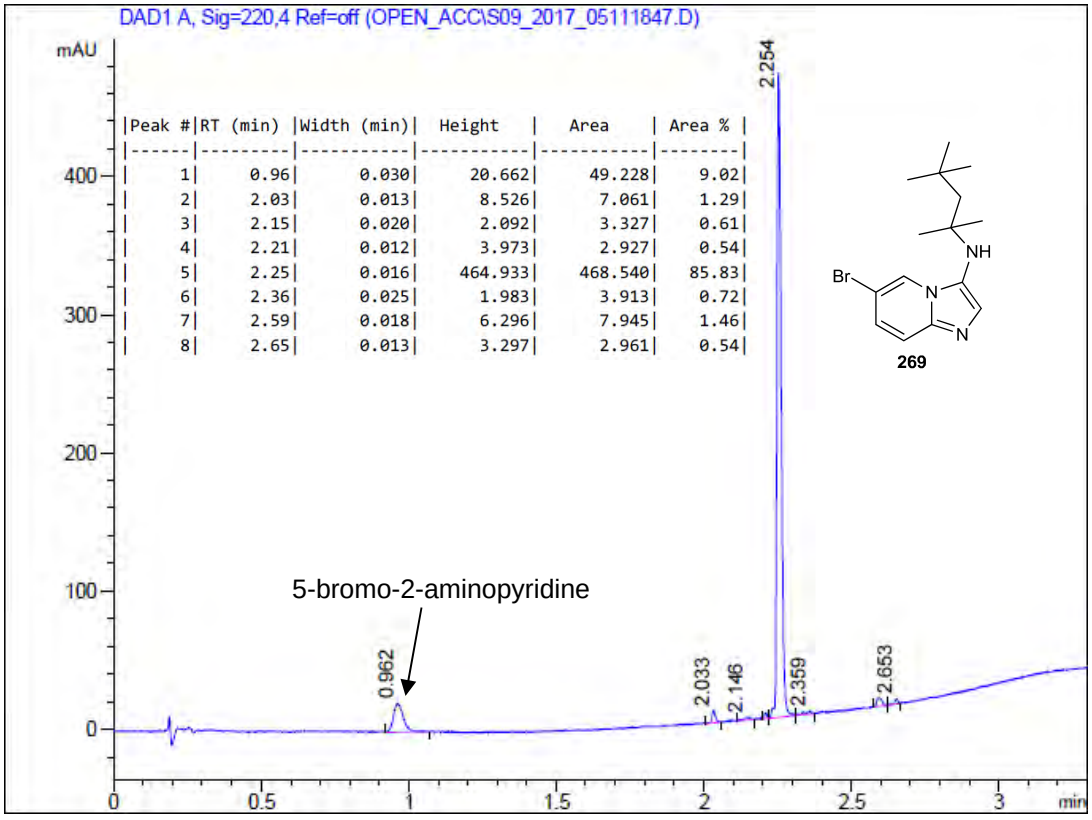

Peak #	RT (min)	Width (min)	Height	Area	Area %
1	0.96	0.030	20.662	49.228	9.02
2	2.03	0.013	8.526	7.061	1.29
3	2.15	0.020	2.092	3.327	0.61
4	2.21	0.012	3.973	2.927	0.54
5	2.25	0.016	464.933	468.540	85.83
6	2.36	0.025	1.983	3.913	0.72
7	2.59	0.018	6.296	7.945	1.46
8	2.65	0.013	3.297	2.961	0.54

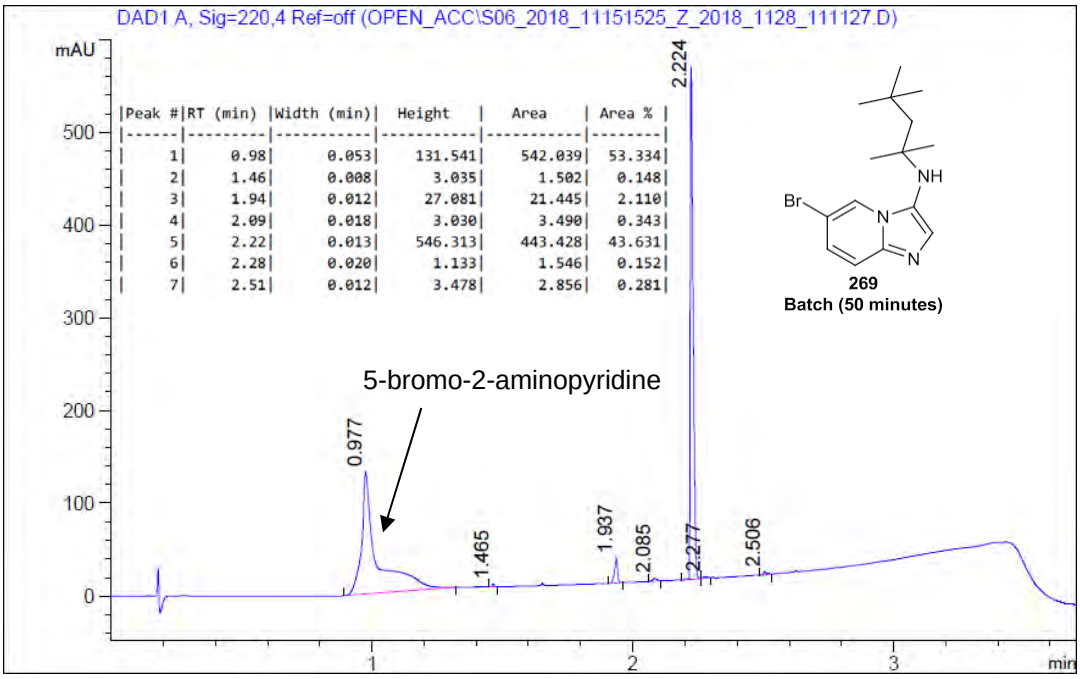
DAD1 A, Sig=220,4 Ref=off (OPEN_ACC\S06_2018_11151525_Z_2018_1128_111127.D)
mAU
Peak # | RT (min) | Width (min) | Height | Area | Area %
1 | 0.98 | 0.053 | 131.541 | 542.039 | 53.334
2 | 1.46 | 0.008 | 3.035 | 1.502 | 0.148
3 | 1.94 | 0.012 | 27.081 | 21.445 | 2.110
4 | 2.09 | 0.018 | 3.030 | 3.490 | 0.343
5 | 2.22 | 0.013 | 546.313 | 443.428 | 43.631
6 | 2.28 | 0.020 | 1.133 | 1.546 | 0.152
7 | 2.51 | 0.012 | 3.478 | 2.856 | 0.281
2.224
NH
Br
N
N
269
Batch (50 minutes)
5-bromo-2-aminopyridine
0.977
1.465
1.937
2.085
2.277
2.506
min

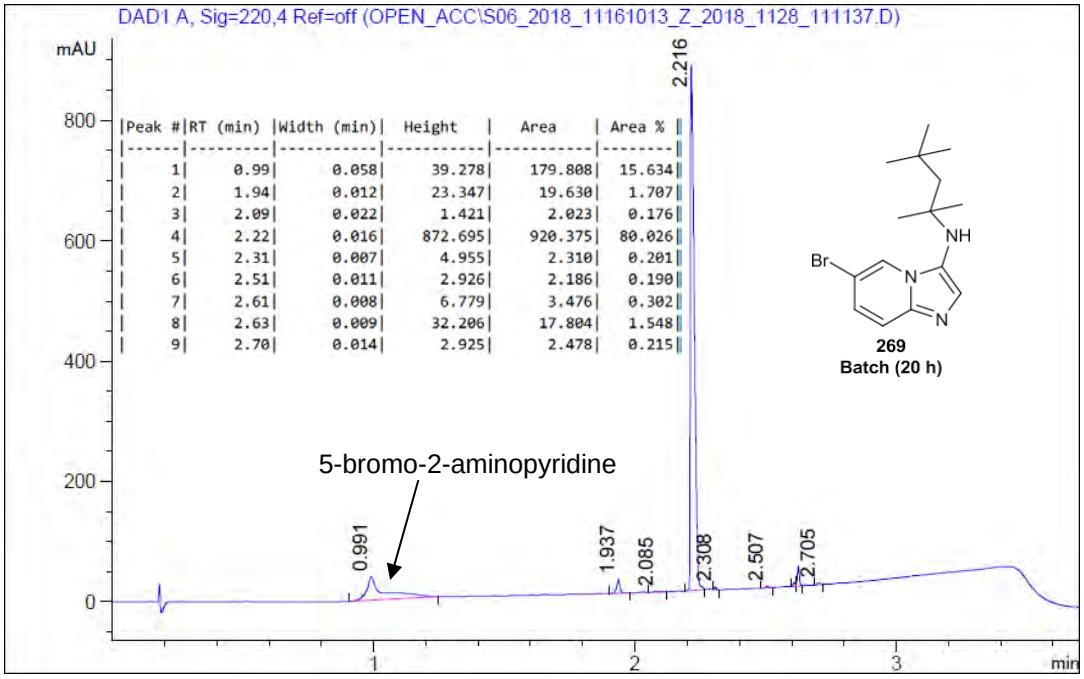
DAD1 A, Sig=220,4 Ref=off (OPEN_ACC\S06_2018_11161013_Z_2018_1128_111137.D)
mAU
Peak # | RT (min) | Width (min) | Height | Area | Area %
1 | 0.99 | 0.058 | 39.278 | 179.808 | 15.634
2 | 1.94 | 0.012 | 23.347 | 19.630 | 1.707
3 | 2.09 | 0.022 | 1.421 | 2.023 | 0.176
4 | 2.22 | 0.016 | 872.695 | 920.375 | 80.026
5 | 2.31 | 0.007 | 4.955 | 2.310 | 0.201
6 | 2.51 | 0.011 | 2.926 | 2.186 | 0.190
7 | 2.61 | 0.008 | 6.779 | 3.476 | 0.302
8 | 2.63 | 0.009 | 32.206 | 17.804 | 1.548
9 | 2.70 | 0.014 | 2.925 | 2.478 | 0.215
2.216
NH
Br
N
N
269
Batch (20 h)
5-bromo-2-aminopyridine
0.991
1.937
2.085
2.308
2.507
2.705
min

7.2 Appendix 2 – NMR data of regioisomeric mixture for compounds 226 and 248

In the synthesis of compound **226**, a mixture was afforded, likely due to the formation of another regioisomer (**248**) during the reaction. The presence of the desired isomer was confirmed by NOESY NMR analysis (see assignment below). The other material, **248**, is present in *c.* 8% in the reaction mixture.

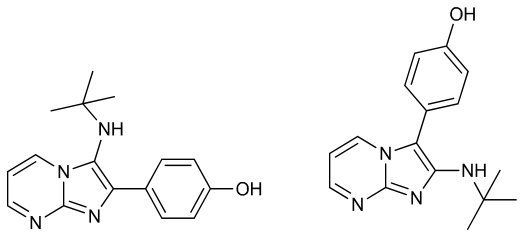

226 **248**

An assignment of **226** is shown below. Within the ^{1}H NMR spectra, smaller peaks related to **248** can be observed at ~8% signal intensity. This structure was confirmed by NOESY analysis, indicating spatial proximity between *tert*-butyl proton signals (CH_3-19, CH_3-20 and CH_3-21) with proton signals 6, 13 and 17.

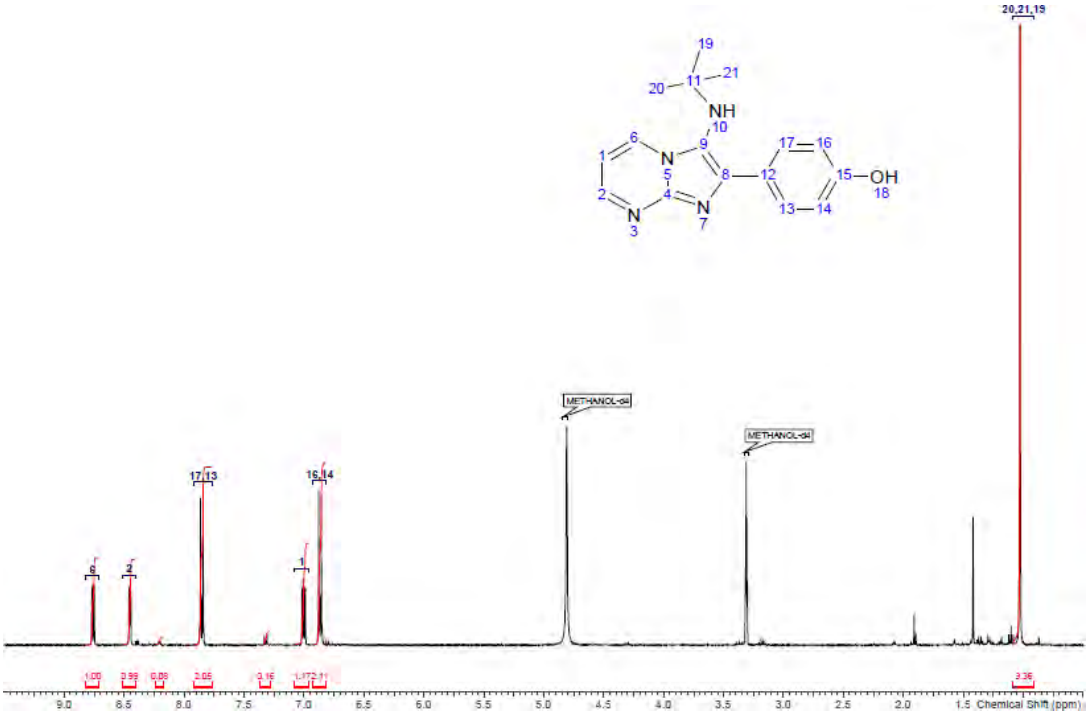

GSK CONFIDENTIAL INFORMATION – DO NOT COPY

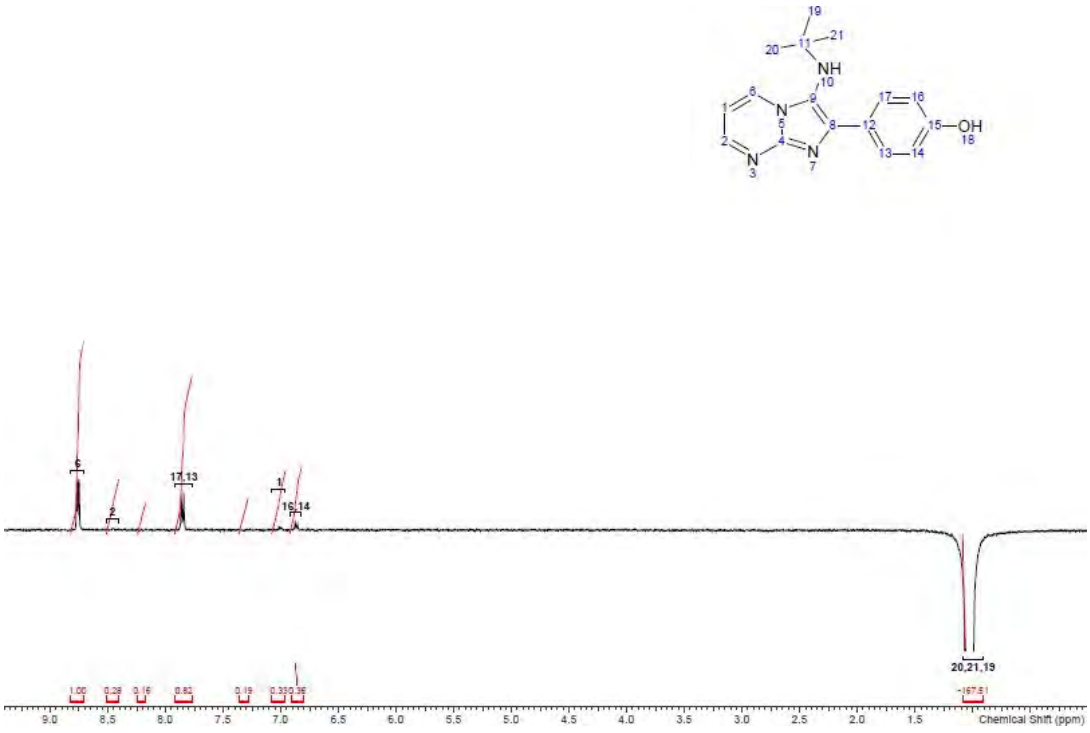

7.3 Appendix 3 – NMR data for compound 245

For compound **245**, only one regioisomer was observed in ^{1}H NMR analysis (see below). Elucidation of the structure of **245** was made through consideration of the correlations observed in ^{15}N HMBC analysis (especially CH-13 with N-3) as well as through NOESY analysis, which shows spatial proximity between benzyl proton signal CH_2-7 with aryl CH-8.

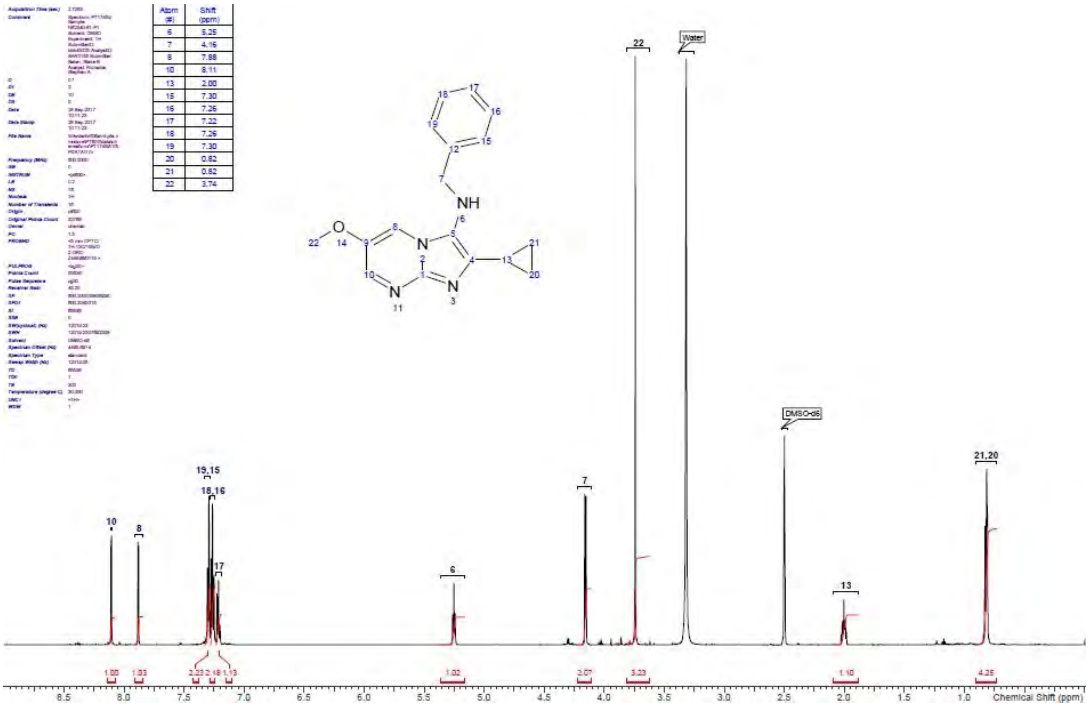

GSK CONFIDENTIAL INFORMATION – DO NOT COPY

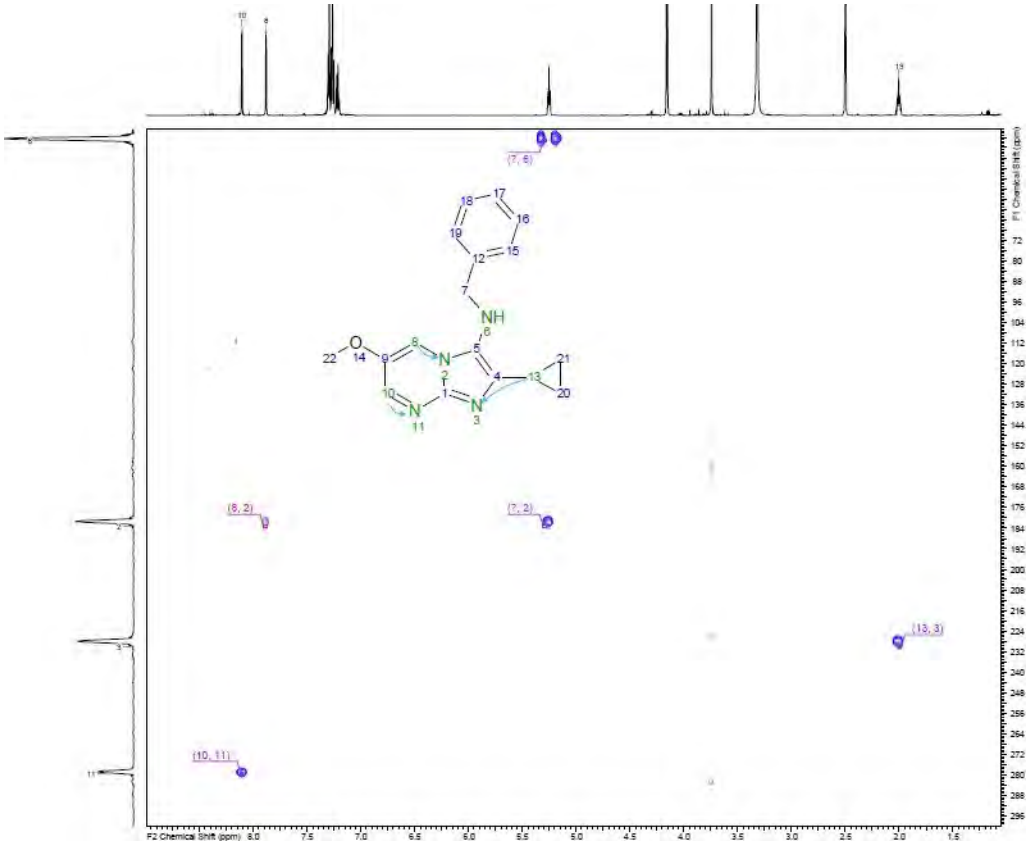

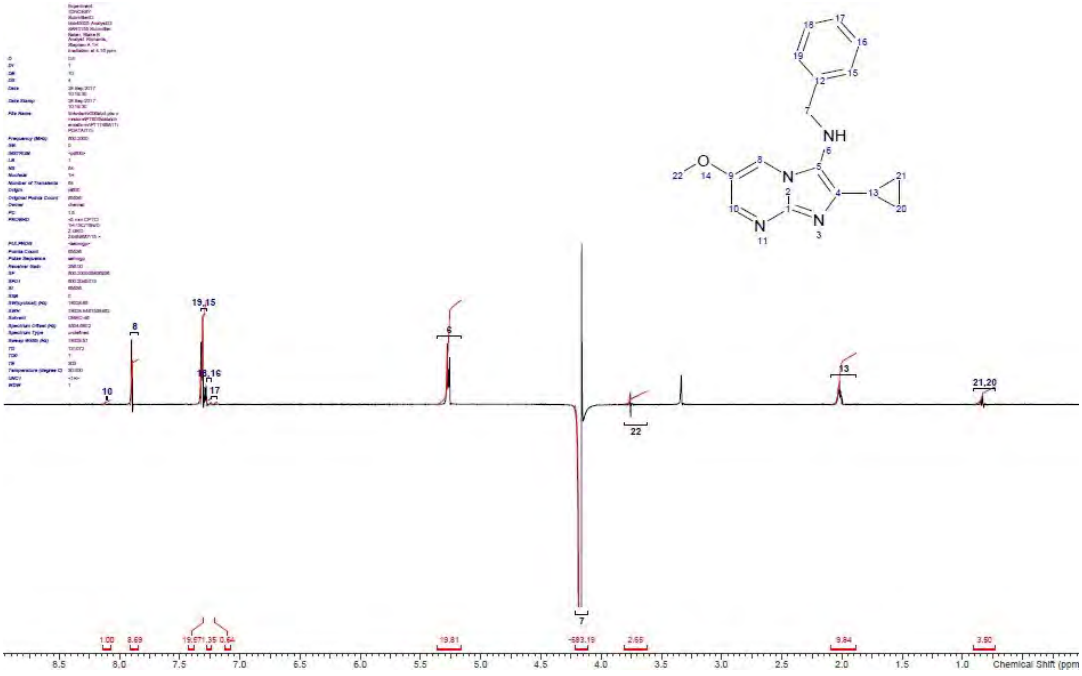

7.4 Appendix 4 – NMR data for by-product, compound 251

All collected NMR data for compound **251** suggest the structure shown. HRMS and IR analysis (observed $[M+H]^+$ m/z and a 3315 (br. w) cm^{-1} peak) both also support the structure elucidated from NMR analysis. The relative stereochemistry of the alkyl chain could not be determined.

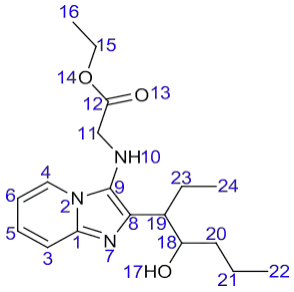

251

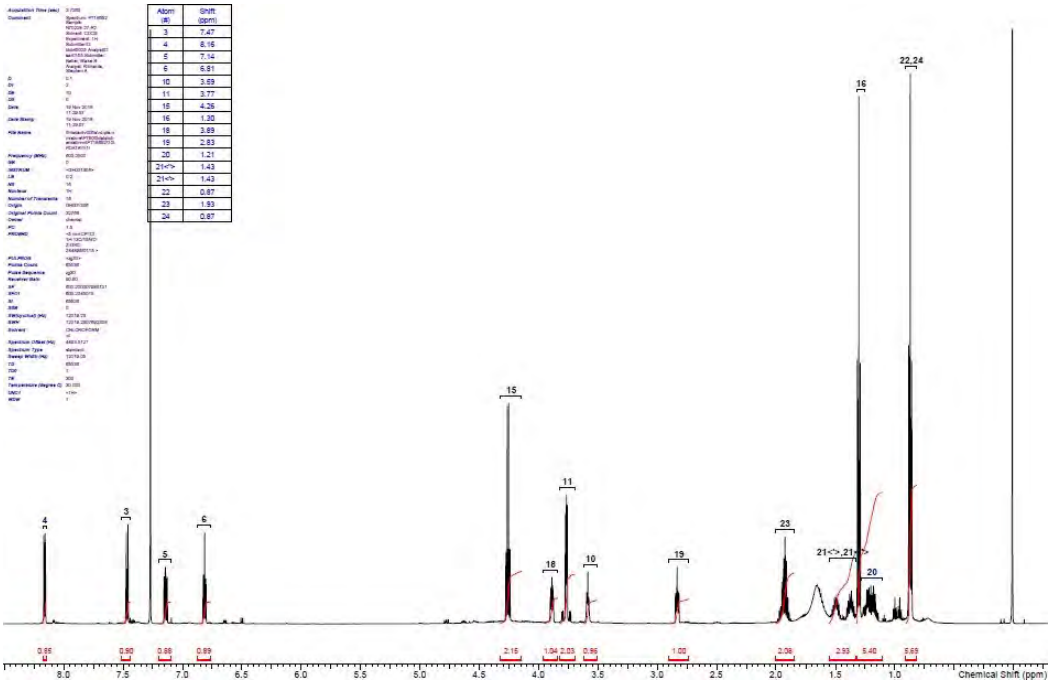

GSK CONFIDENTIAL INFORMATION – DO NOT COPY

Atom (#)	Shift (ppm)
1	141.5
3	117.2
4	122.5
5	123.8
6	111.6
8	139.7
9	126.6
11	50.4
12	171.9
15	61.4
16	14.2
18	74.0
19	43.4
20	39.2
21	19.4
22	14.1
23	26.1
24	12.5

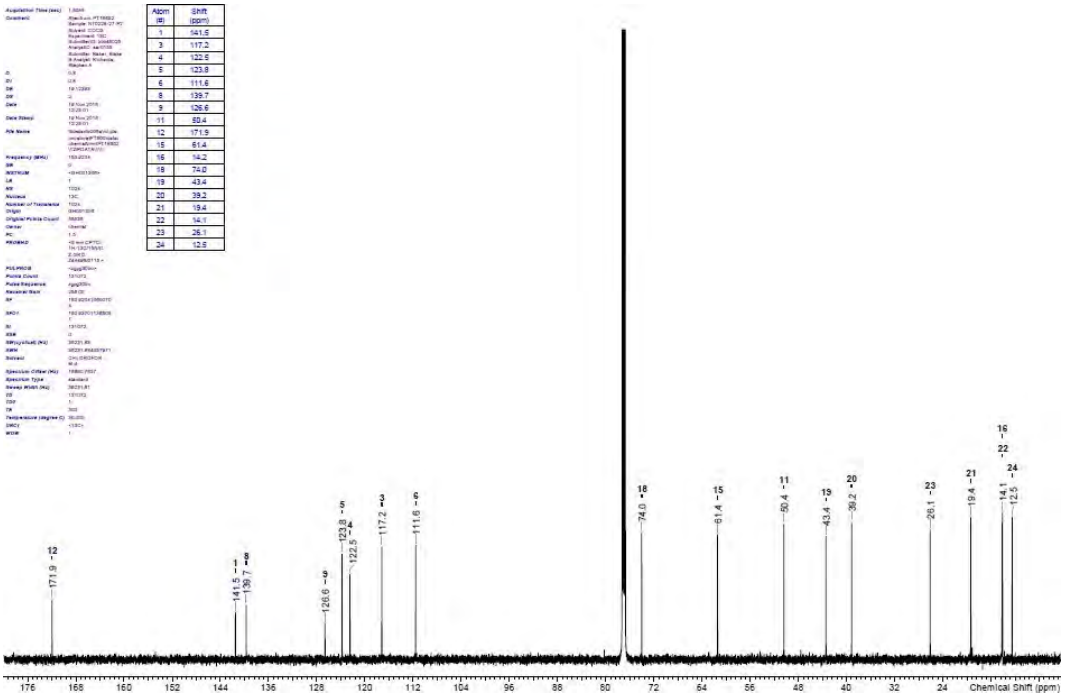

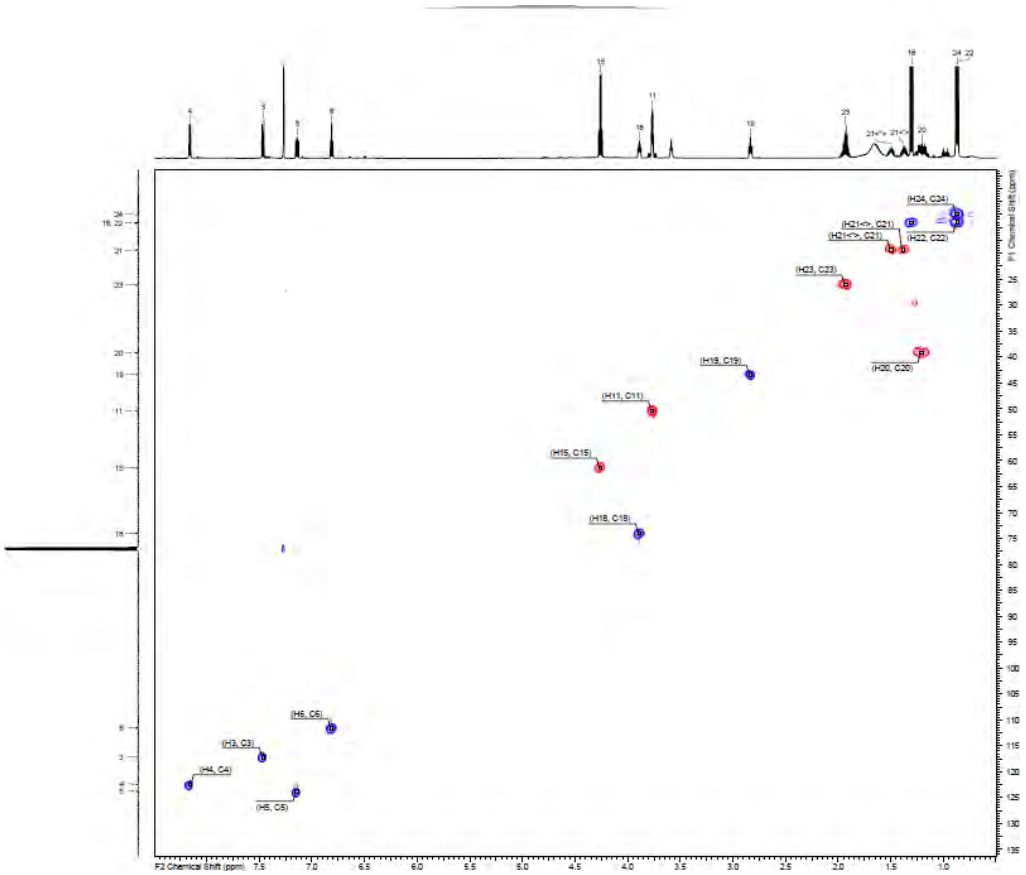

GSK CONFIDENTIAL INFORMATION – DO NOT COPY

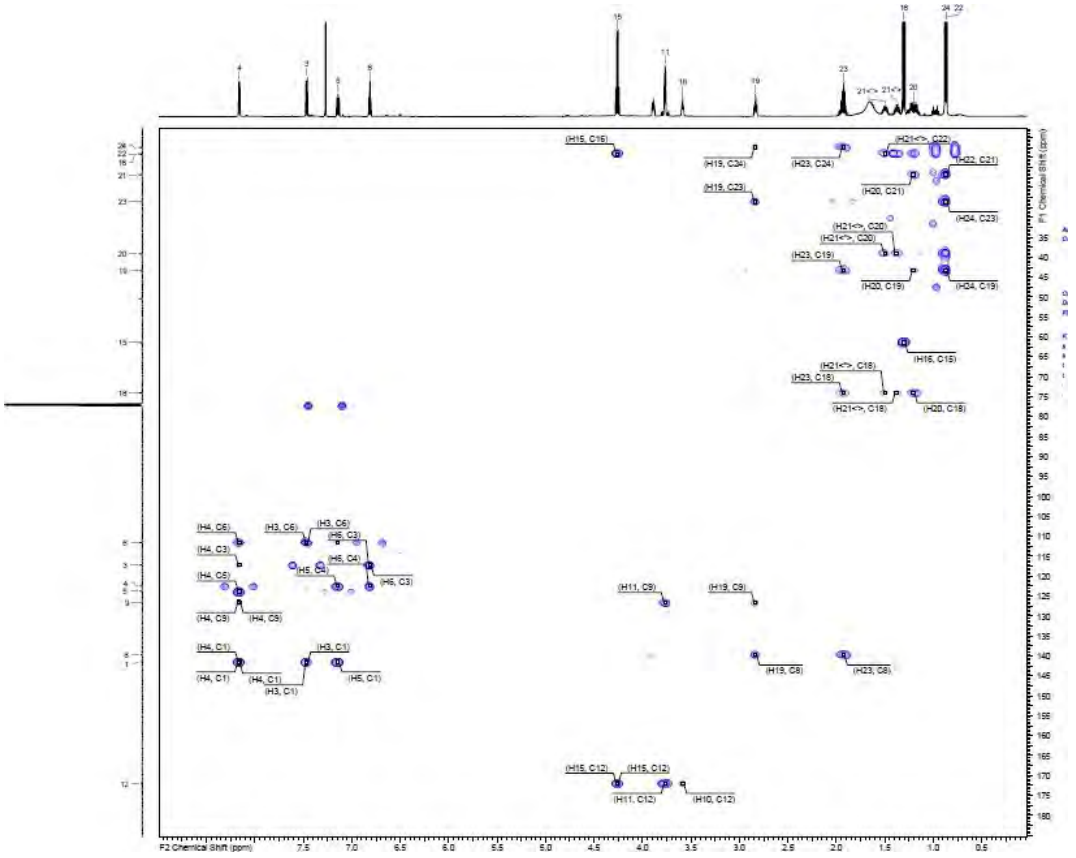

7.5 Appendix 5 – GC-MS concentration gradients with respect to naphthalene internal standard at different relative molar ratios

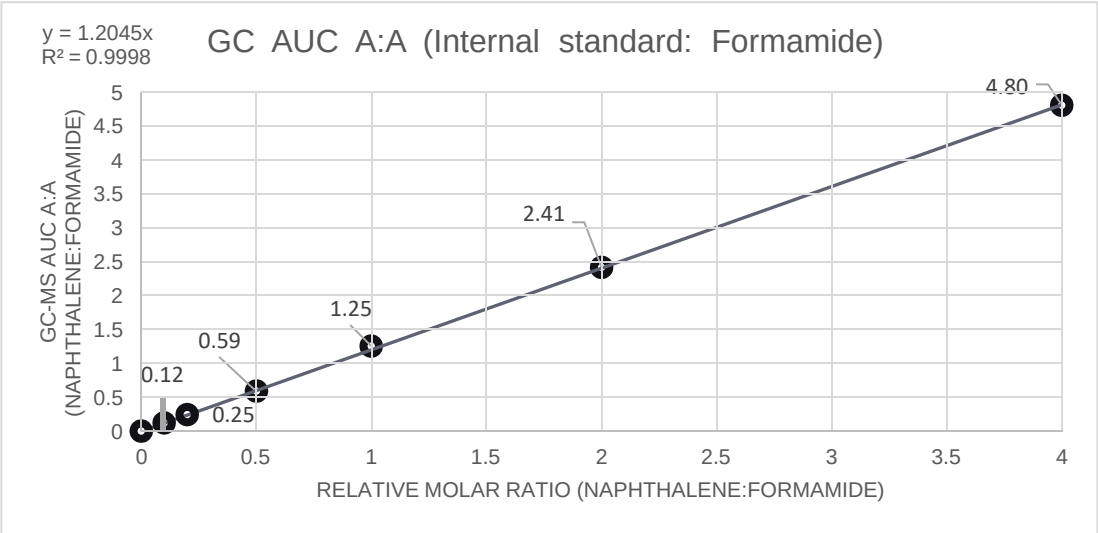

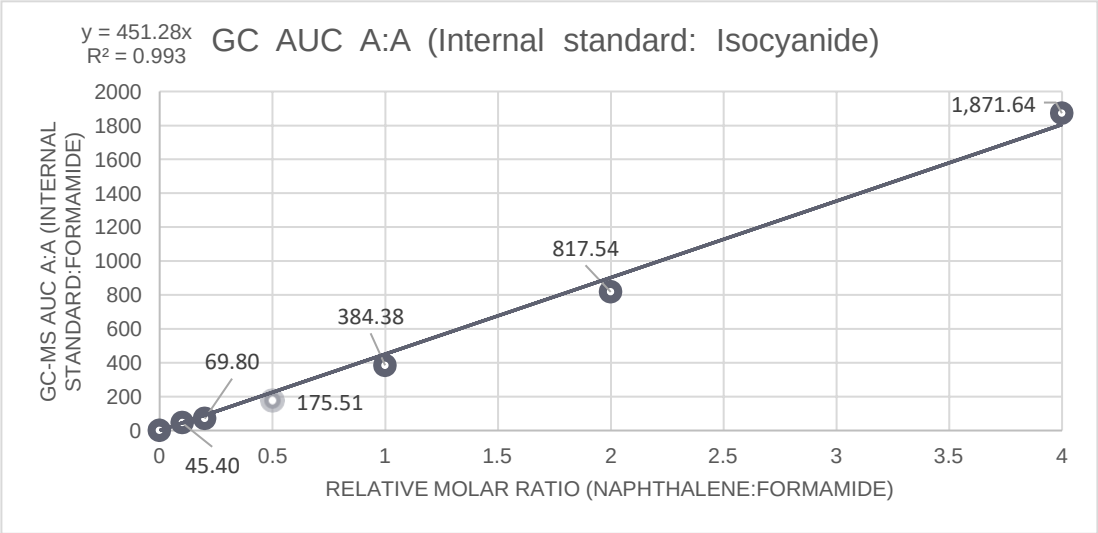

GSK CONFIDENTIAL INFORMATION – DO NOT COPY

7.6 Appendix 6 – Cyclic voltammetry data for compound 235

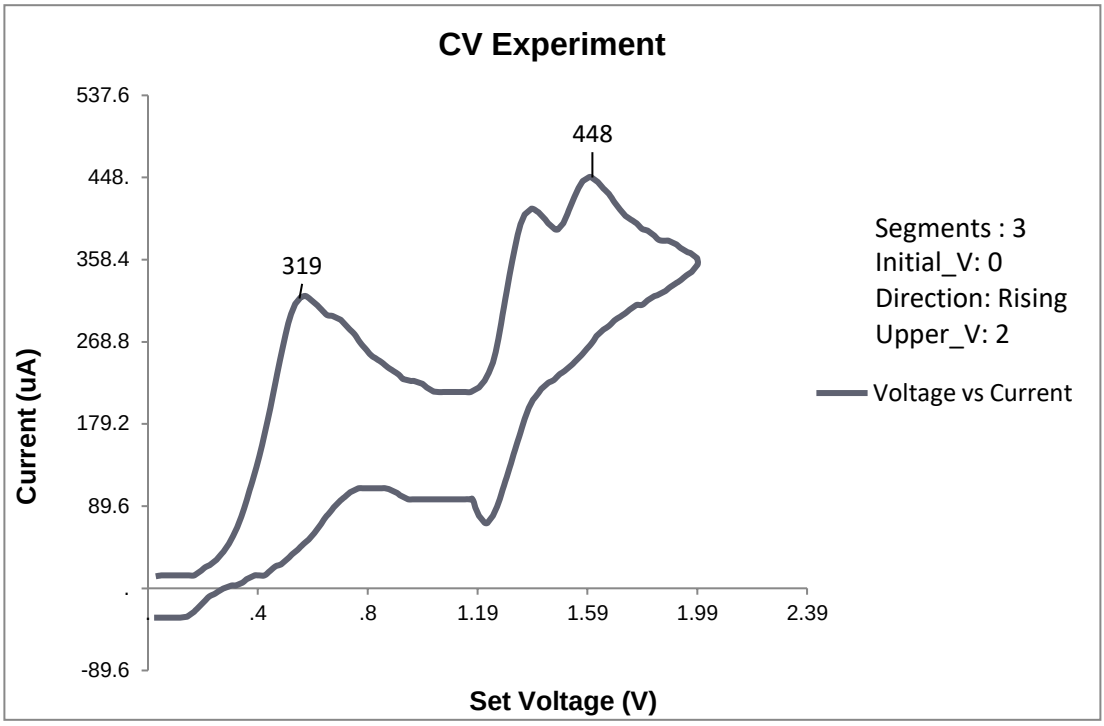

7.7 Appendix 7 – ^{3}H-Hypoxanthine scintillation proximity assay (SPA) procedure

In order to test the potency of produced antimalarial compounds against *P. Falc.* cultures, a tritium-labelled hypoxanthine assay was used. The assay can be performed in either a 96-well or 384-well plate format for rapid throughput analysis.[297]

For the 96-well plate procedure, assay plates were prepared which contained 3-fold serial dilutions of the antimalarials (made from solutions in DMSO using Multidrop Combi dispensers) from column 1 through to column 9 of the plate. Columns 10 and 11 both contained positive controls for the assay (DMSO), and column 12 contained the negative control (2 μM artesunate in DMSO). In each case, a volume of 0.5 μL was added to each well. The plates were then frozen at -20 °C overnight.

A culture of *Plasmodium falciparum* parasite-infected red blood cells (iRBCs) were then prepared using a growth medium consisting of RMPI 1640 (a commercial culture medium containing glutathione and vitamins), 1X albumax (lipid-rich bovine serum albumin) and 5 μM hypoxanthine. The prepared sample had a composition of 0.5% parasitaemia and 2% haematocrit. *P. falc.* strain *3D7A* was typically used as it displays no resistance to currently known antimalarials.

To each well was then added 100 μL of the iRBC mixture. Following combination of the assay constituents, the plates were pre-warmed to 37 °C, and incubated for 24 h at 37 °C, under a maintained atmosphere of 5% CO_2, 5% O_2, 90% N_2.

Following the incubation period, from a stock solution of ^{3}H-hypoxanthine in RMPI 1640 (0.025 μCi/μL) was added 8 μL (0.2 μCi) to each well, and the blood samples were incubated for a further 24 h under the same conditions. To determine longer antimalarial activity, plates could instead be incubated for 48 h or 72 h at this stage. After incubation with the hypoxanthine, the plates were frozen overnight at -70 °C.

Following thawing, the plates were then shaken, and parasites were harvested on a glass fibre filter using a Tomtec Cell Harvester 96. These filters were dried, and melt-on MeltiLex scintillator sheets were used to determine the extent of ^{3}H-hypoxanthine incorporation, through a microbeta radioactivity counter.

If hypoxanthine had been incorporated by these cells, the emission of β-particles from the radioactive decay of the tritium would activate the scintillant within the sheets, resulting in emission of light from the scintillant. The intensity of light emitted from the scintillant could then be quantified to facilitate its application in a biological assay.

Raw data of radioactivity (given as counts per minute) from the microbeta radioactivity counter could then be normalised using the negative and positive controls.

Raw data was normalised using the following general formula:

$$100 - (100 \frac{(\text{Novel antimalarial scintillation measurement } - \text{measurement of negative control })}{(\text{Range of scintillation intensity (positive control } - \text{ negative control}))}$$

This provided the % inhibition of parasite growth observed. From this data, IC_{50} values could then be determined using a dose-response curve produced from an XL-FIT model.

For the 384-well plate method, all columns except columns 6 and 18 were filled with 50 nL from a stock solution of 1mM of the antimalarials in neat DMSO. In column 6, only neat DMSO was added (positive control) and in column 18, a 50 nL solution of artesunate (2 μM solution in DMSO) was added.

The *Plasmodium falciparum* containing iRBCs were then cultured in the same way as described above, before 25 μL of the RBC mixture was dispensed into all of the wells, and the plates were incubated, under the same conditions as previously mentioned, for 24 h.

After incubation, to all wells was then added 4 μL (0.1 μCi) from a stock solution of ^{3}H-hypoxanthine in RMPI 1640 (0.025 μCi/μL). After incubation of the parasites with the antimalarial and radiolabelled hypoxanthine, the samples underwent freeze-thawing (-70 °C to rt as seen above, frozen overnight), before 25 μL of poly-Lys YOx SPA (polylysine Yttrium oxide scintillation proximity assay) bead solution were added to each well as a solution in deionised water (5 mg/mL concentration). The beads were kept under stirring conditions during dispensing to ensure their homogeneity in the sample solutions.

All plates were incubated (at rt) for at least 1 h to allow the beads to settle and avoid further centrifugation. The samples were also kept away from light during this incubation. The microplate was then read in a Viewlux microplate reader by recording luminescence for 10 min using a emission filter at 613 nm.[297] Assay signal resolution was optimal when the plate was sealed and maintained at a temperature of 4 °C.

For this assay method, the IC_{50} data fitted into a two-parameter model, where pulses per minute (obtained from the SPA) was plotted against drug concentration to determine the concentration required for 50% inhibition of parasite growth.

The model relating these parameters is given by the following equation:

$$y = \frac{100\%}{1 + [\frac{x}{IC_{50}}]^{S}}$$

Where y = pulses per minute from the SPA, x = concentration of the novel antimalarial and S = slope factor. The equation assumes that y falls as x increases.

7.8 Appendix 8 – *Plasmodium falciparum* humanised mouse model procedure

In order to test the *in vivo* clinical efficacy of the quinazolamine series, a SCID mouse model could be used. In this assay, selectively bred mice which lack B and T lymphocytes, as well as natural killer (NK) cells are tested as a model biological system lacking an immune response. The SCID mice used were a NOD/SCID/IL2RY^{null} strain.

New chemical entities (NCEs) for malaria were also tested against rodent forms of the parasite (namely *P. berghei*, *P. yoelii*, *P. chabaudi* and *P. vinckei*) although these studies may not be directly translatable to clinical trial results, since differences in the genome between *Plasmodium* species, as well as the proteins that they encode, could affect the effectiveness of the antimalarial.

Therefore, each of the mice were injected with human red blood cells which were suspended in an 50% haematocrit isotonic solution comprising RMPI 1640 culture medium with 25% decomplemented human serum and 3.1 mM hypoxanthine. After 25 days of blood injections, the injected human erythrocytes made up ~90% of the red blood cells within the mice.

Following this, infection of the mice with a *P. Falc.* strain capable of invading these cross-species human red blood cells, *P.Falc.* 3D7$^{0087/N9}$ allowed for the development of the disease. Since the mice are severely immunodeficient, the disease could not be controlled by the immune system, and human red blood cell eradication was observed 7 days after infection without antimalarial treatment.

Flow cytometry was used to detect mouse erythrocytes (by using a TER 119 monoclonal antibody) and parasitic cells (by using a DNA dye, Syto-16). Flow cytometry involves flowing cellular samples through an instrument containing a laser beam. Light scattering is observed when the laser comes into contact with cells, and fluorescent additives (such as those shown above) can be observed to provide information regarding the presence of particular cellular components or microorganisms (such as parasites).

The *in vivo* efficacy assay is a 4-day experiment, in which the efficacy of the novel antimalarial is tested against exponential *P. Falc.* growth over two growth cycles (2 x 48 h). 3 days after the mice are infected with malarial parasites, they are treated orally once a day for four consecutive days, with each mouse receiving different doses of the drug. The potency is determined as the average daily drug concentration required to remove 90% of parasitaemia following 4 days of treatment. Recrudescence of the malarial parasites represents failure of the drug, either due to resistance mechanisms arising from the parasitic cells, or insufficient blood solubility of the drug to exert the targeted therapeutic effect.

The model shown below is then used to determine the change in blood parasitaemia following antimalarial treatment in the mice.

GSK CONFIDENTIAL INFORMATION – DO NOT COPY

$$\frac{dP}{dt} = (K_{growth} \times P \times (1 - \frac{P}{P_{max}})) - (K_{kill} \times (\frac{C^H}{(C^H + EC_{50}^H)}) \times P)$$

Equation used to determine the change in parasitaemia observed over time, where K_{growth} is the parasite growth rate constant, P is the total number of parasites present in the mouse, P_{max} is the maximum number of parasite possible within the mouse (i.e. when no treatment is applied), K_{kill} is the maximum kill rate constant of the antimalarial, H is the hill slope (concerning the rate of changing drug concentration) and EC_{50} is the effective concentration of the drug required to reduce parasitaemia by half.

7.9 Appendix 9 – Buchwald-Hartwig screening plate procedure

Below is shown a diagram of the Buchwald-Hartwig screening plate used. Each 1 mL vial contains one of 12 pre-weighed metal catalyst complexes known to perform Buchwald-Hartwig coupling reactions in the literature.[271,272] These catalysts are also shown below.

The plate contains 24 wells, in rows A-D (reading top to bottom) and columns 1-6 (reading left to right). Since vials 1-12 and vials 13-24 contain the same catalysts in the same order, 2 different bases could be compared in the reaction under otherwise identical conditions.

Reactions were performed as described in **General procedure F (use of the Buchwald-Hartwig screening plate)**.

	1	2	3	4	5	6
A	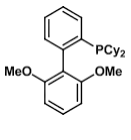 SPhos	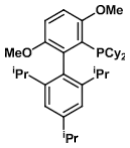 BrettPhos	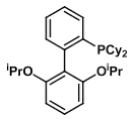 RuPhos	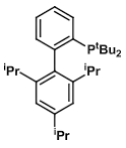 ^{t}BuXPhos	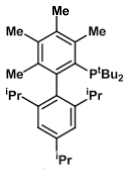 Me$_4$^{t}BuXPhos	 ^{t}Bu$_3$P
B	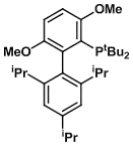 ^{t}BuBrettPhos	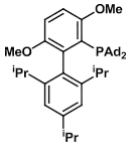 AdBrettPhos	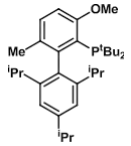 RockPhos	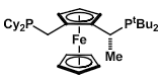 SL-J009	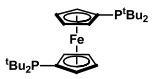 DTBPF	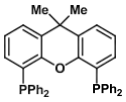 XantPhos
C	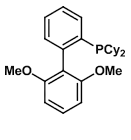 SPhos	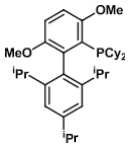 BrettPhos	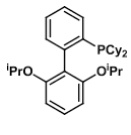 RuPhos	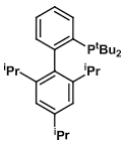 ^{t}BuXPhos	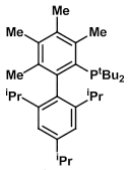 Me$_4$^{t}BuXPhos	 ^{t}Bu$_3$P
D	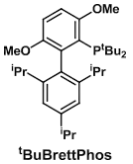 ^{t}BuBrettPhos	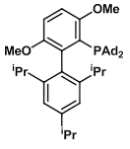 AdBrettPhos	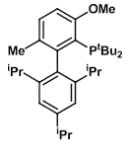 RockPhos	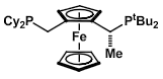 SL-J009	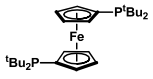 DTBPF	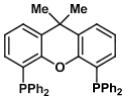 XantPhos

7.10 Appendix 10 – Buchwald-Hartwig screening plate LCMS profiles

LCMS profiles for the reactions attempted using the Buchwald-Hartwig screening plate are shown below. Triphenylamine is used as the internal standard for the reaction mixtures. The internal standard is introduced during the addition of the neutral quench solution. See **General procedure F (use of the Buchwald-Hartwig screening plate)** for more information.

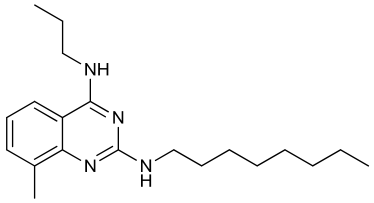

391

Vial A5, full conversion of **389**, 16% product, only one by-product observed (purple).

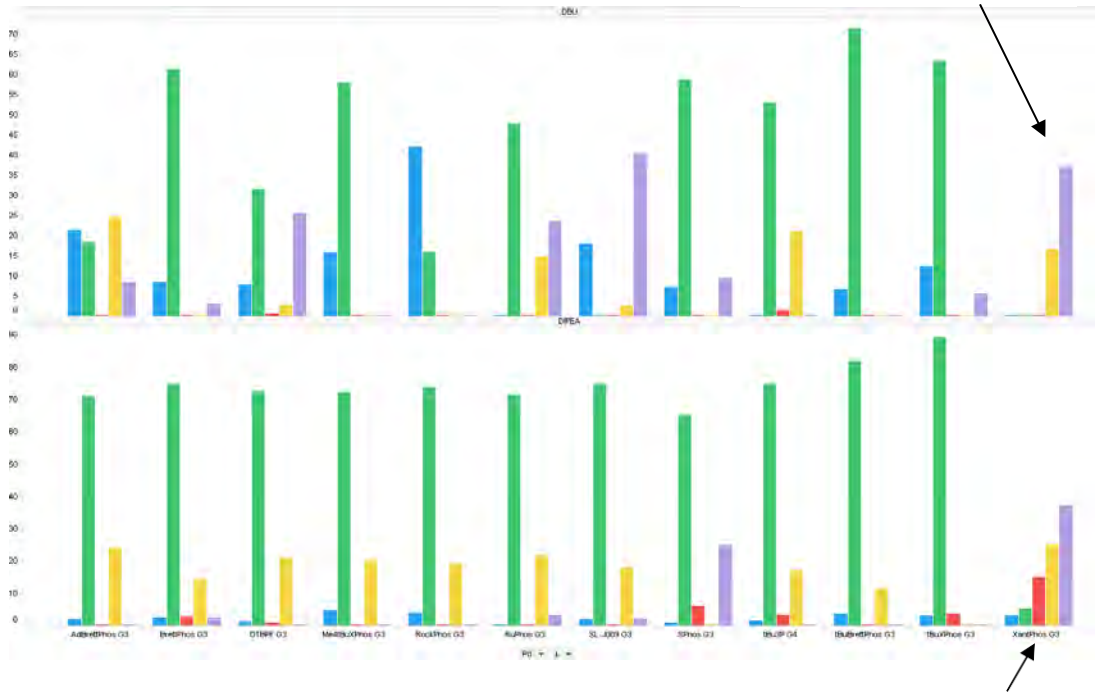

Vial D6, high conversion of **389**, 25% product, various by-products observed.

Key:

- Hydrolysed starting material (**396**)
- Starting material (**389**)
- Dimer by-product (**446**)
- Desired material (**391**)
- Unknown by-product, MW 367

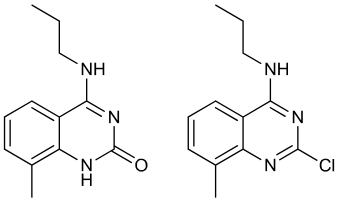

396

389

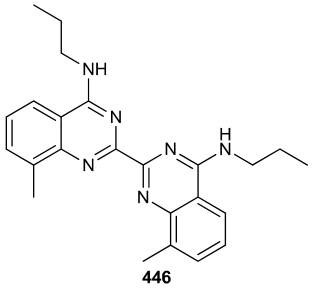

446

GSK CONFIDENTIAL INFORMATION – DO NOT COPY

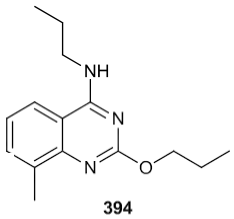

394
(DMSO)

Vial A5 (best example), high conversion of **389**, 87% product (**394**) observed.

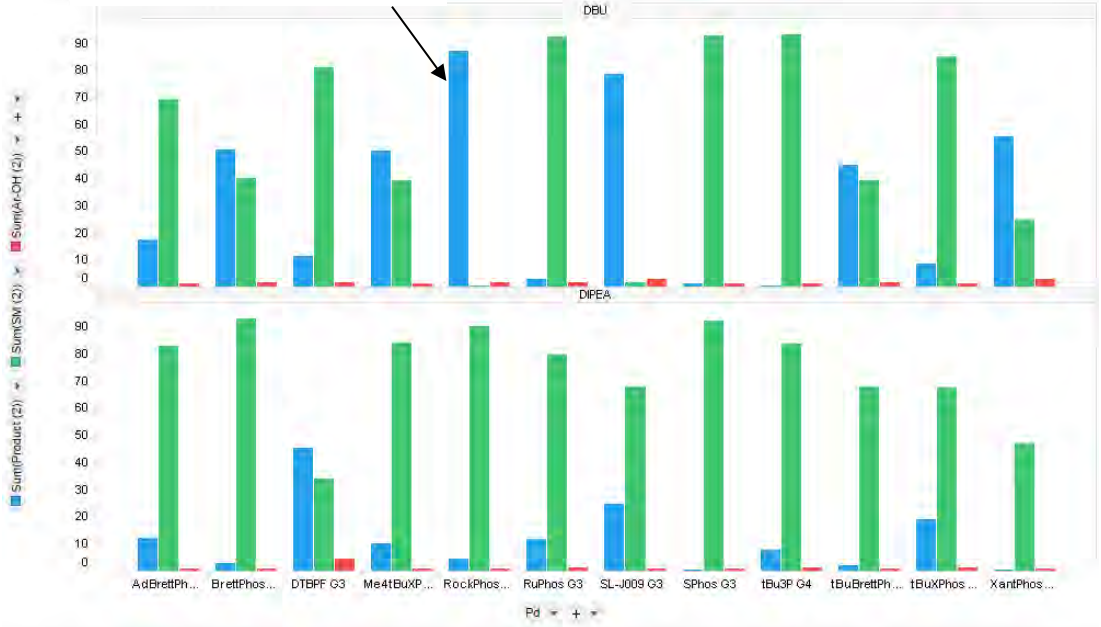

Key:

- Desired material (**394**)
- Starting material (**389**)
- Hydrolysed starting material (**396**)

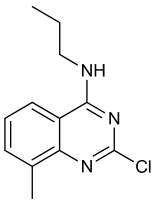

389

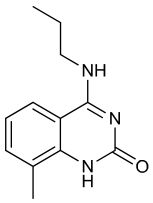

396

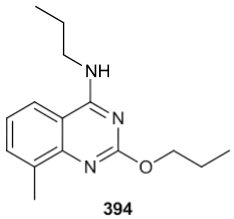

394
(Tamisolve)

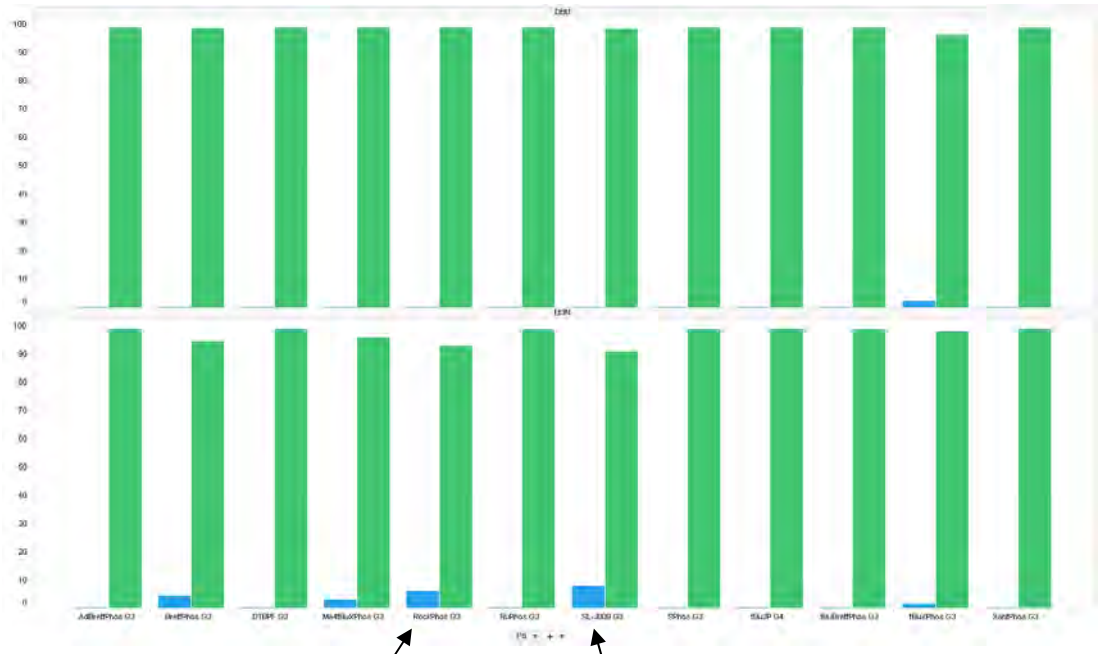

Vial C5, 6% conversion to the desired product observed.

Vial D1, 8% conversion to the desired product observed.

Low conversion seen in all cases.

Key:

Desired material (**394**)

Starting material (**389**)

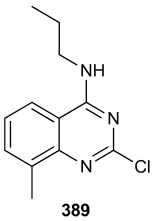

389

7.11 Appendix 11 – Unattainable products from tandem flow S_NAr experiments

The following targets were selected for synthesis but could not be made using the flow procedure described in **General procedure F (tandem flow synthesis of diaminoquinazolines)**, due to either their insolubility in Tamisolve®, their unreactivity, the hydrolytic instability of formed products or intermediates, or due to precipitation observed within the flow reactor.

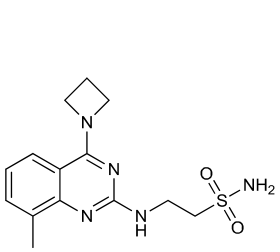

447

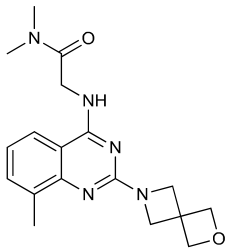

448

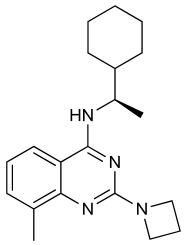

449

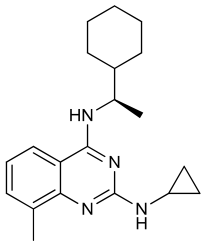

450

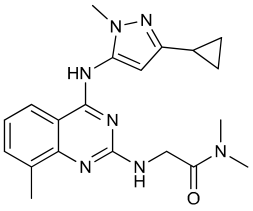

451

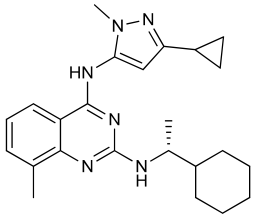

452

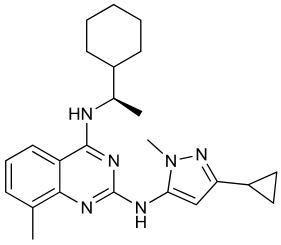

453

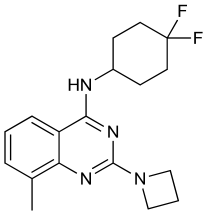

454

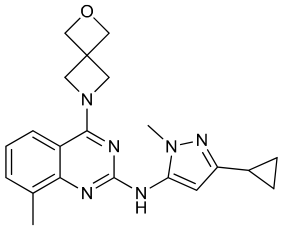

455

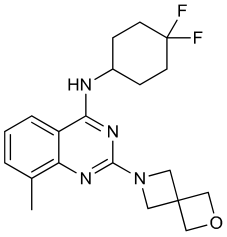

456

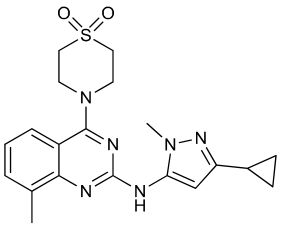

457

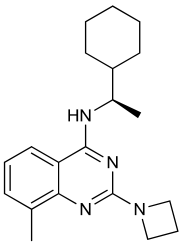

458

7.12 Appendix 12 – Elucidation of desired regioisomer (compound 441)

Following prior heating of the reaction mixture used to synthesise compound **441**, issues were presented in the formation of regioisomeric products following the tandem S_NAr procedure. In order to elucidate the precise structure of the isolated material, COSY and 1D ROESY NMR analysis was utilised.

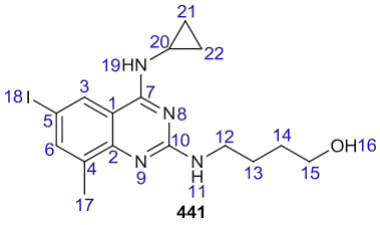

COSY analysis was first used to distinguish between the exchangeable protons in the sample (CH-11, CH-16 and CH-19). For protons 11 and 16, through-bond coupling was observed to proton signals 12 and 15 respectively, determining that the multiplet signal at 7.92-7.65 ppm was related to NH-19. (See spectra below)

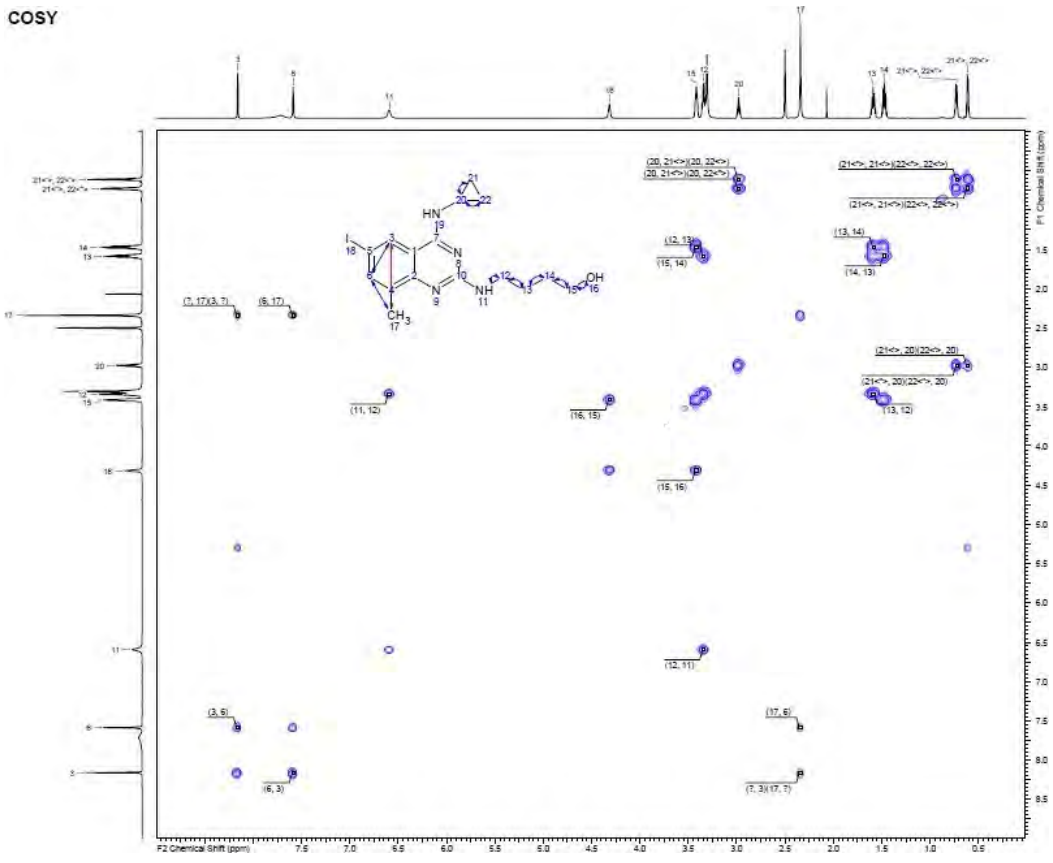

1D ROESY NMR analysis of this material then showed a spatial proximity between CH-3 and NH-19 to confirm identification of the desired product (**441**). The 1D ROESY spectra is shown below.

GSK CONFIDENTIAL INFORMATION – DO NOT COPY

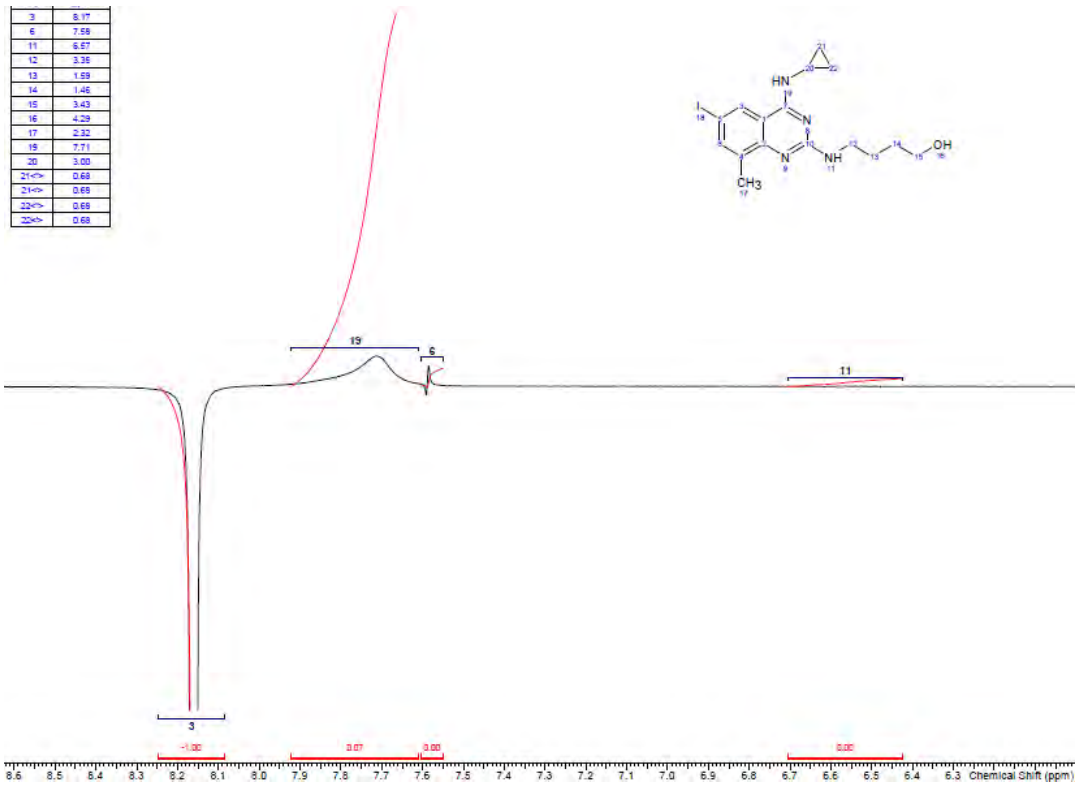

8. References

1. McQuade, D. T.; Seeberger, P. H. *J. Org. Chem.* **2013**, 78, 6384-6389.
2. *Based on a survey of Web of Science results for the topic "Flow Chemistry". **Accessed 21st January 2019.***,
3. Britton, J.; Jamison, T. F. *Nat. Protoc.* **2017**, 12, 2423-2446.
4. Gutmann, B.; Cantillo, D.; Kappe, C. O. *Angew. Chem. Int. Ed.* **2015**, 54, 6688-6728.
5. Murray, P. R. D.; Browne, D. L.; Pastre, J. C.; Butters, C.; Guthrie, D.; Ley, S. V. *Org. Process Res. Dev.* **2013**, 17, 1192-1208.
6. Cantillo, D.; Kappe, C. O. *J. Org. Chem.* **2013**, 78, 10567-10571.
7. Giraudeau, P.; Felpin, F. X. *React. Chem. Eng.* **2018**, 3, 399-413.
8. Carter, C. F.; Lange, H.; Ley, S. V.; Baxendale, I. R.; Wittkamp, B.; Goode, J. G.; Gaunt, N. L. *Org. Process Res. Dev.* **2010**, 14, 393-404.
9. Benito-Lopez, F.; Verboom, W.; Kakuta, M.; Gardeniers, J. G. E.; Egberink, R. J. M.; Oosterbroek, E. R.; Berg, A. V. D.; Reinhoudt, D. N. *Chem. Commun.* **2005**, 2857-2859.
10. Browne, D. L.; Wright, S.; Deadman, B. J.; Dunnage, S.; Baxendale, I. R.; Turner, R. M.; Ley, S. V. *Rapid Commun. Mass Spectrom.* **2012**, 26, 1999-2010.
11. Fletcher, P. D. I.; Haswell, S. J.; Zhang, X. *Electrophoresis* **2003**, 24, 3239-3245.
12. Gitlin, L.; Hoera, C.; Meier, R. J.; Nagl, S.; Belder, D. *Lab Chip* **2013**, 13, 4134-4141.
13. Wagner, J.; Tshikhudo, T. R.; Köhler, J. M. *Chem. Eng. J.* **2008**, 135, S104-S109.
14. Baumann, M.; Baxendale, I. R. *Beilstein J. Org. Chem.* **2013**, 9, 1613-1619.
15. Varas, A. C.; Noël, T.; Wang, Q.; Hessel, V. *ChemSusChem* **2012**, 5, 1703-1707.
16. Baxendale, I. R.; Deeley, J.; Griffiths-Jones, C. M.; Ley, S. V.; Saaby, S.; Tranmer, G. K. *Chem. Commun.* **2006**, 2566-2568.
17. Ley, S. V.; Schucht, O.; Thomas, A. W.; Murray, P. J. *J. Chem. Soc., Perkin Trans. 1* **1999**, 1251-1252.
18. *H-Cube™ image taken from: https://thalesnano.com/products. Permission for use granted by Thales Nano. **Accessed 23rd January 2019***.
19. *O-Cube™ image supplied by Thales Nano. Permission for use granted by Thales Nano. **Accessed 23rd January 2019.***
20. Viviano, M.; Milite, C.; Rescigno, D.; Castellano, S.; Sbardella, G. *RSC Adv.* **2015**, 5, 1268-1273.
21. Irfan, M.; Glasnov, T. N.; Kappe, C. O. *Org. Lett.* **2011**, 13, 984-987.
22. Wegner, J.; Ceylan, S.; Kirschning, A. *Chem. Commun.* **2011**, 47, 4583-4592.
23. Hartman, R. L.; McMullen, J. P.; Jensen, K. F. *Angew. Chem. Int. Ed.* **2011**, 50, 7502-7519.
24. Sarma, P.; Patowari, P. K. *J. Adv. Manuf. Syst.* **2016**, 15, 161-172.

25. Hanna, G. J.; Noble, R. D. *Chem. Rev.* **1985**, 85, 583-598.
26. Avila, K.; Moxey, D.; Lozar, A. d.; Avila, M.; Barkley, D.; Hof, B. *Science* **2011**, 333, 192-196.
27. Adapted from: Newby, J. A. *Synthesis and reactions of isocyanides using a flow reactor. PhD Thesis*. **2013**, University of Sheffield.
28. Stroock, A. D.; Dertinger, S. K. W.; Ajdari, A.; Mezić, I.; Stone, H. A.; Whitesides, G. M. *Science* **2002**, 295, 647-651.
29. Monnier, H.; Wilhelm, A. M.; Delmas, H. *Chem. Eng. Sci.* **2000**, 55, 4009-4020.
30. Volker, H.; Löwe, H.; Schönfeld, F. *Chem. Eng. Sci.* **2005**, 60, 2479-2501.
31. Zhang, Z.; Szita, N.; Boccazzi, P.; Sinskey, A. J.; Jensen, K. F. *Biotech. Bioeng.* **2006**, 93, 286-296.
32. Glasgow, I.; Aubry, N. *Lab Chip* **2003**, 3, 114-120.
33. *Information obtained at: https://syrris.com/product/asia-flow-chemistry-syringe-pump/. **Accessed 24th January 2019.***
34. *Comparisons of pumps: https://www.chemyx.com/support/knowledge-base/applications/syringe-pumps-vs-peristaltic-pumps/. **Accessed 24th January 2019.***
35. *Information obtained at: https://ltf-gmbh.com/produkte/mr_lab_en.html. **Accessed 24th January 2019.***
36. Ugi, I.; Dömling, A.; Horl, W. *Endeavour* **1994**, 18, 115-122.
37. Dömling, A.; Wang, W.; Wang, K. *Chem. Rev.* **2012**, 112, 3083-3135.
38. Alvim, H. G. O.; da Silva Júnior, E. N.; Neto, B. A. D. *RSC Adv.* **2014**, 4, 54282-54299.
39. Strecker, A. *Justus Liebigs Ann. Chem.* **1850**, 75, 27-45.
40. Kouznetsov, V. V.; Galvis, C. E. P. *Tetrahedron* **2018**, 74, 773-810.
41. Hughes, A. B., *Amino Acids, Peptides and Proteins in Organic Chemistry.* **2009**, WILEY-VCH, Weinhelm.
42. Bommarius, A. S.; Schwarm, M.; Drauz, K. *Chimia* **2001**, 55, 50-59.
43. Banphavichit, V.; Mansawat, W.; Bhanthumnavin, W.; Vilaivan, T. *Tetrahedron* **2009**, 65, 5849-5854.
44. Sigman, M. S.; Vachal, P.; Jacobsen, E. N. *Angew. Chem. Int. Ed.* **2000**, 39, 1279-1281.
45. Vachal, P.; Jacobsen, E. N. *J. Am. Chem. Soc.* **2002**, 124, 10012-10014.
46. Zuend, S. J.; Jacobsen, E. N. *J. Am. Chem. Soc.* **2009**, 131, 15358-15374.
47. Zuend, S. J.; Coughlin, M. P.; Lalonde, M. P.; Jacobsen, E. N. *Nature* **2009**, 461, 968-970.
48. Way, J. *Annu. Rev. Pharmacol. Toxicol.* **1984**, 24, 451-481.
49. Yan, H.; Oh, J. S.; Lee, J. W.; Song, C. E. *Nat. Commun.* **2012**, 3, 1212-1218.
50. Mannich, C.; Krösche, W. *Arch. Pharm. Pharm. Med. Chem.* **1912**, 250, 647-667.

51. Roman, G. *Eur. J. Med. Chem.* **2015**, 89, 743-816.
52. Alvim, H. G. O.; Bataglion, G. A.; Ramos, L. M.; de Oliveira, A. L.; de Oliveira, H. C. B.; Eberlin, M. N.; de Macedo, J. L.; da Silva, W. A.; Neto, B. A. D. *Tetrahedron* **2014**, 70, 3306-3313.
53. Lu, H.; Wu, R.; Cheng, H.; Nie, S.; Tang, Y.; Gao, Y.; Luo, Z. *Synthesis* **2015**, 47, 1447-1454.
54. Guo, Q.-X.; Liu, H.; Guo, C.; Luo, S.-W.; Gu, Y.; Gong, L.-Z. *J. Am. Chem. Soc.* **2007**, 129, 3790-3791.
55. Córdova, A.; Notz, W.; Zhong, G.; Betancort, J. M.; Barbas, C. F. *J. Am. Chem. Soc.* **2002**, 124, 1842-1843.
56. Córdova, A.; Watanabe, S. I.; Tanaka, F.; Notz, W.; Barbas, C. F. *J. Am. Chem. Soc.* **2002**, 124, 1866-1867.
57. Notz, W.; Watanabe, S.; Chowdari, N. S.; Zhong, G.; Betancort, J. M.; Tanaka, F.; Barbas III, C. F. *Adv. Synth. Catal.* **2004**, 346, 1131-1140.
58. List, B. *J. Am. Chem. Soc.* **2000**, 122, 9336-9337.
59. Zhang, H.; Mitsumori, S.; Utsumi, N.; Imai, M.; Garcia-Delgado, N.; Mifsud, M.; Albertshofer, K.; Cheong, P. H. Y.; Houk, K. N.; Tanaka, F.; Barbas, C. F. *J. Am. Chem. Soc.* **2008**, 130, 875-886.
60. Petasis, N. A.; Akritopoulou, I. *Tetrahedron Lett.* **1993**, 34, 583-586.
61. Guerrera, C. A.; Ryder, T. R., *The Petasis Borono-Mannich Multicomponent Reaction.* In A. Coca, *Boron Reagents in Synthesis.* **2016**, American Chemical Society, Washington, DC, USA.
62. Au, C. W. G.; Pyne, S. G. *J. Org. Chem.* **2006**, 71, 7097-7099.
63. Muncipinto, G.; Moquist, P. N.; Schreiber, S. L.; Schaus, S. E. *Angew. Chem. Int. Ed.* **2011**, 50, 8172-8175.
64. Gomes, G. D. P.; Loginova, Y.; Vatsadze, S. Z.; Alabugin, I. V. *J. Am. Chem. Soc.* **2018**, 140, 14272-14288.
65. Ramozzi, R.; Chéron, N.; Braïda, B.; Hiberty, P. C.; Fleurat-Lessard, P. *New. J. Chem.* **2012**, 36, 1137-1140.
66. Gordy, W.; Pauling, L. *J. Am. Chem. Soc.* **1942**, 64, 2952-2953.
67. Edwards, D. A.; Tetrick, S. M.; Walton, R. A. *J. Organomet. Chem.* **1988**, 349, 383-391.
68. Michelin, R. A.; Pombeiro, A. J. L.; Guedes da Silva, M. F. C. *Coord. Chem. Rev.* **2001**, 218, 75-112.
69. Hagedorn, I.; Tönjes, H. *Pharmazie* **1956**, 11, 409-410.
70. Hagedorn, I.; Tönjes, H. *Pharmazie* **1957**, 12, 567-580.
71. Yamaguchi, T.; Miyake, Y.; Miyamura, A.; Ishiwata, N.; Tatsuta, K. *J. Antibiot.* **2006**, 59, 729-734.

72. Lim, F. Y.; Won, T. H.; Raffa, N.; Baccile, J. A.; Wisecaver, J.; Rokas, A.; Schroeder, F. C.; Keller, N. P. *mBio* **2018**, 9(3): e00785-18.
73. Scheuer, P. J. *Acc. Chem. Res.* **1992**, 25, 433-439.
74. Pirrung, M. C.; Ghorai, S.; Ibarra-Rivera, T. R. *J. Org. Chem.* **2009**, 74, 4110-4117.
75. Lieke, W. *Justus Liebigs Ann. Chem.* **1859**, 112, 316-321.
76. Schuster, R. E.; Scott, J. E.; J. Casanova, J. *Org. Synth.* **1966**, 46, 75.
77. Ugi, I.; Meyr, R. *Angew. Chem.* **1958**, 70, 702-703.
78. Creedon, S. M.; Crowley, H. K.; McCarthy, D. G. *J. Chem. Soc., Perkin Trans. 1* **1998**, 0, 1015-1018.
79. Neochoritis, C. G.; Zarganes-Tzitzikas, T.; Stotani, S.; Dömling, A.; Herdtweck, E.; Khoury, K.; Dömling, A. *ACS Comb. Sci.* **2015**, 17, 493-499.
80. Gokel, G. W.; Widera, R. P.; Weber, W. P. *Org. Synth.* **1976**, 55, 96.
81. Pirrung, M. C.; Ghorai, S. *J. Am. Chem. Soc.* **2006**, 128, 11772-11773.
82. Curran, D. P.; Liu, H. *J. Am. Chem. Soc.* **1991**, 113, 2127-2132.
83. Curran, D. P.; Liu, H. *J. Am. Chem. Soc.* **1992**, 114, 5863-5864.
84. Cioc, R. C.; Preschel, H. D.; van der Heijden, G.; Ruijter, E.; Orru, R. V. A. *Chem. Eur. J.* **2016**, 22, 7837-7842.
85. Dömling, A. *Chem. Rev.* **2006**, 106, 17-89.
86. Passerini, M. *Gazz. Chim. Ital.* **1921**, 51, 126-129.
87. Passerini, M. *Gazz. Chim. Ital.* **1921**, 51, 181-188.
88. Carofiglio, T.; Cozzi, P. G.; Floriani, C.; Chiesi-Villa, A.; Rizzoli, C. *Organometallics* **1993**, 12, 2726-2736.
89. Passerini, M. *Gazz. Chim. Ital.* **1922**, 52, 432-435.
90. Baker, R. H.; Stanonis, D. *J. Am. Chem. Soc.* **1951**, 73, 699-702.
91. Dömling, A.; Ugi, I. *Angew. Chem. Int. Ed.* **2000**, 39, 3168-3210.
92. Ugi, I.; Meyr, R. *Chem. Ber.* **1961**, 94, 2229-2233.
93. Maeda, S.; Komagawa, S.; Uchiyama, M.; Morokuma, K. *Angew. Chem. Int. Ed.* **2011**, 50, 644-649.
94. Kürti, L.; Czakó, B., *Strategic Applications of Named Reactions in Organic Synthesis.* **2005**, Elsevier B.V., Amsterdam.
95. Bock, H.; Ugi, I. *J. Prakt. Chem.* **1997**, 339, 385-389.
96. Frey, R.; Galbraith, S. G.; Guelfi, S.; Lamberth, C.; Zeller, M. *Synlett* **2003**, 1536-1538.
97. Moni, L.; Banfi, L.; Basso, A.; Bozzano, A.; Spallarossa, M.; Wessjohann, L.; Riva, R. *Molecules* **2016**, 21, 1153-1161.
98. Berłożecki, S.; Szymanski, W.; Ostaszewski, R. *Tetrahedron* **2008**, 64, 9780-9783.
99. Denmark, S. E.; Fan, Y. *J. Am. Chem. Soc.* **2003**, 125, 7825-7827.
100. Wang, S. X.; Wang, M. X.; Wang, D. X.; Zhu, J. *Angew. Chem. Int. Ed.* **2008**, 47, 388-391.

101. Andreana, P. R.; Liu, C. C.; Schreiber, S. L. *Org. Lett.* **2004**, 6, 4231-4233.
102. Keating, T. A.; Armstrong, R. W. *J. Am. Chem. Soc.* **1996**, 118, 2574-2583.
103. Zhang, J.; Lin, S. X.; Cheng, D. J.; Liu, X. Y.; Tan, B. *J. Am. Chem. Soc.* **2015**, 137, 14039-14042.
104. Ugi, I.; Meyr, R.; Fetzer, U.; Steinbrückner, C. *Angew. Chem.* **1959**, 71, 373-388.
105. Mumm, O. *Ber. Dtsch. Chem. Ges.* **1910**, 43, 886-893.
106. Mumm, O.; Hesse, H.; Volquartz, H. *Ber. Dtsch. Chem. Ges.* **1915**, 48, 379-391.
107. Chéron, N.; Ramozzi, R.; Kaïm, L. E.; Grimaud, L.; Fleurat-Lessard, P. *J. Org. Chem.* **2012**, 77, 1361-1366.
108. Iacobucci, C.; Reale, S.; Gal, J. F.; Angelis, F. D. *Eur. J. Org. Chem.* **2014**, 2014, 7087-7090.
109. Faggi, C.; García-Valverde, M.; Marcaccini, S.; Menchi, G. *Org. Lett.* **2010**, 12, 788-791.
110. Kalinski, C.; Lemoine, H.; Schmidt, J.; Burdack, C.; Kolb, J.; Umkehrer, M.; Ross, G. *Synthesis* **2008**, 4007-4011.
111. Heublein, N.; Moore, J. S.; Smith, C. D.; Jensen, K. F. *RSC Adv.* **2014**, 4, 63627-63631.
112. Portlock, D. E.; Ostaszewski, R.; Naskar, D.; West, L. *Tetrahedron Lett.* **2003**, 44, 603-605.
113. Sharma, S.; Maurya, R. A.; Min, K. I.; Jeong, G. Y.; Kim, D. P. *Angew. Chem. Int. Ed.* **2013**, 52, 7564-7568.
114. Zhang, J.; Yu, P.; Li, S-Y.; Sun, H.; Xiang, S-H.; Wang, J.; Houk, K. N.; Tan, B. *Science* **2018**, 361, eaas8707.
115. Tanaka, Y.; Hasui, T.; Suginome, M. *Org. Lett.* **2007**, 9, 4407-4410.
116. Pan, S. C.; List, B. *Angew. Chem. Int. Ed.* **2008**, 47, 3622-3625.
117. Váradi, A.; Palmer, T. C.; Dardashti, R. N.; Majumdar, S. *Molecules* **2016**, 21, 19-40.
118. Kaïm, L. E.; Grimaud, L.; Oble, J. *Angew. Chem. Int. Ed.* **2005**, 44, 7961-7964.
119. Ugi, I.; Rosendahl, F. K.; Bodesheim, F. *Liebigs. Ann. Chem.* **1963**, 666, 54-61.
120. Groebke, K.; Weber, L.; Mehlin, F. *Synlett* **1998**, 661-663.
121. Blackburn, C.; Guan, B.; Fleming, P.; Shiosaki, K.; Tsai, S. *Tetrahedron Lett.* **1998**, 39, 3635-3638.
122. Bienaymé, H.; Bouzid, K. *Angew. Chem. Int. Ed.* **1998**, 37, 2234-2237.
123. Baviskar, A. T.; Madaan, C.; Preet, R.; Mohapatra, P.; Jain, V.; Agarwal, A.; Guchhait, S. K.; Kundu, C. N.; Banerjee, U. C.; Bharatam, P. V. *J. Med. Chem.* **2011**, 54, 5013-5030.
124. McKeown, M. R.; Shaw, D. L.; Fu, H.; Liu, S.; Xu, X.; Marineau, J. J.; Huang, Y.; Zhang, X.; Buckley, D. L.; Kadam, A.; Zhang, Z.; Blacklow, S. C.; Qi, J.; Zhang, W.; Bradner, J. E. *J. Med. Chem.* **2014**, 57, 9019-9027.

125. Shukla, N. M.; Salunke, D. B.; Yoo, E.; Mutz, C. A.; Balakrishna, R.; David, S. A. *Bioorg. Med. Chem.* **2012**, 20, 5850-5863.

126. Tazeem; Han, X.; Zhou, Q.; Wei, J.; Tien, P.; Yang, G.; Wu, S.; Dong, C. *RSC Adv.* **2016**, 6, 95177-95188.

127. Sashidhara, K. V.; Singh, L. R.; Choudhary, D.; Arun, A.; Gupta, S.; Adhikary, S.; Palnati, G. R.; Konwar, R.; Trivedi, R. *RSC Adv.* **2016**, 6, 80037-80048.

128. Azimi, S.; Zonouzi, A.; Firuzi, O.; Iraji, A.; Saeedi, M.; Mahdavi, M.; Edraki, N. *Eur. J. Med. Chem.* **2017**, 138, 729-737.

129. Flesch, D.; Cheung, S. Y.; Schmidt, J.; Gabler, M.; Heitel, P.; Kramer, J.; Kaiser, A.; Hartmann, M.; Lindner, M.; Lüddens-Dämgen, K.; Heering, J.; Lamers, C.; Lüddens, H.; Wurglics, M.; Proschak, E.; Schubert-Zsilavecz, M.; Merk, D. *J. Med. Chem.* **2017**, 60, 7199-7205.

130. Mizushige, K.; Ueda, T.; Yukiiri, K.; Suzuki, H. *Cardiovasc. Drug. Rev.* **2002**, 20, 163-174.

131. McNamara, C. W.; Lee, M. C. S.; Lim, C. S.; Lim, S. H.; Roland, J.; Nagle, A.; Simon, O.; Yeung, B. K. S.; Chatterjee, A. K.; McCormack, S. L.; Manary, M. J.; Zeeman, A-M.; Dechering, K. J.; Kumar, T. R. S.; Henrich, P. P.; Gagaring, K.; Ibanez, M.; Kato, N.; Kuhen, K. L.; Fischli, C.; Rottmann, M.; Plouffe, D. M.; Bursulaya, B.; Meister, S.; Rameh, L.; Trappe, J.; Haasen, D.; Timmerman, M.; Sauerwein, R. W.; Suwanarusk, R.; Russell, B.; Renia, L.; Nosten, F.; Tully, D. C.; Kocken, C. H. M.; Glynne, R. J.; Bodenreider, C.; Fidock, D. A.; Diagana, T. T.; Winzeler, E. A. *Nature* **2013**, 504, 248-253.

132. Berson, A.; Descatoire, V.; Sutton, A.; Fau, D.; Maulny, B.; Vadrot, N.; Feldmann, G.; Berthon, B.; Tordjmann, T.; Pessayre, D. *J. Pharmacol. Exp. Ther.* **2001**, 299, 793-800.

133. Desroy, N.; Heckmann, B.; Brys, R. C. X.; Joncour, A. Compounds and pharmaceutical compositions thereof for the treatment of inflammatory disorders. WO2014/139882 A1, **2014**.

134. Wallrapp, C.; Thoenes, E.; Geigle, P. Novel GLP-1 fusion peptides, their production and use. WO2008/16648 A2, **2008**.

135. Shaabani, A.; Rezazadeh, F.; Soleimani, E. *Monatsh. Chem.* **2008**, 139, 931-933.

136. Ireland, S. M.; Tye, H.; Whittaker, M. *Tetrahedron Lett.* **2003**, 44, 4369-4371.

137. Rousseau, A. L.; Matlaba, P.; Parkinson, C. J. *Tetrahedron Lett.* **2007**, 48, 4079-4082.

138. Shaabani, A.; Soleimani, E.; Maleki, A. *Tetrahedron Lett.* **2006**, 47, 3031-3034.

139. Chen, J. J.; Golebiowski, A.; McClenaghan, J.; Klopfenstein, S. R.; West, L. *Tetrahedron Lett.* **2001**, 42, 2269-2271.

140. Vidyacharan, S.; Shinde, A. H.; Satpathi, B.; Sharada, D. S. *Green Chem.* **2014**, 16, 1168-1175.

141. Butler, A. J. E.; Thompson, M. J.; Maydom, P. J.; Newby, J. A.; Guo, K.; Adams, H.; Chen, B. *J. Org. Chem.* **2014**, 79, 10196-10202.

142. Carballares, S.; Cifuentes, M. M.; Stephenson, G. A. *Tetrahedron Lett.* **2007**, 48, 2041-2045.

143. Reutlinger, M.; Rodrigues, T.; Schneider, P.; Schneider, G. *Angew. Chem. Int. Ed.* **2014**, 53, 582-585.

144. *Information obtained at: https://www.drs.illinois.edu/SafetyLibrary/PerchloricAcid. **Accessed 5th February 2019.***

145. Ramesha, A. B.; Raghavendra, G. M.; Nandeesh, K. N.; Rangappa, K. S.; Mantelingu, K. *Tetrahedron Lett.* **2013**, 54, 95-100.

146. Adib, M.; Sheikhi, E.; Rezaei, N. *Tetrahedron Lett.* **2011**, 52, 3191-3194.

147. Katritzky, A. R.; Xu, Y. J.; Tu, H. *J. Org. Chem.* **2003**, 68, 4935-4937.

148. Fei, Z.; Zhu, Y. P.; Liu, M. C.; Jia, F. C.; Wu, A. X. *Tetrahedron Lett.* **2013**, 54, 1222-1226.

149. Yu, C.; Chen, X.; Wu, R.; Yang, G.; Shi, J.; Pan, L. *Eur. J. Org. Chem.* **2014**, 2037-2043.

150. Shao, N.; Pang, G.-X.; Yan, C.-X.; Shi, G.-F.; Cheng, Y. *J. Org. Chem.* **2011**, 76, 7458-7465.

151. Régnier, S.; Bechara, W. S.; Charette, A. B. *J. Org. Chem.* **2016**, 81, 10348-10356.

152. Law, R. P.; Ukuser, S.; Tape, D. T.; Talbot, E. P. A. *Synthesis* **2017**, 49, 3775-3793.

153. Adiyala, P. R.; Mani, G. S.; Nanubolu, J. B.; Shekar, K. C.; Maurya, R. A. *Org. Lett.* **2015**, 17, 4308-4311.

154. Gladysz, R.; Adriaenssens, Y.; de Winter, H.; Joossens, J.; Lambeir, A-M.; Augustyns, K.; van der Veken, P. *J. Med. Chem.* **2015**, 58, 9238-9257.

155. Demjén, A.; Gyuris, M.; Wölfling, J.; Puskás, L. G.; Kanizsai, I. *Beilstein J. Org. Chem.* **2014**, 10, 2338-2344.

156. Bode, M. L.; Gravestock, D.; Moleele, S. S.; van der Westhuyzen, C. W.; Pelly, S. C.; Steenkamp, P. A.; Hoppe, H. C.; Khan, T.; Nkabinde, L. A. *Bioorg. Med. Chem.* **2011**, 19, 4227-4237.

157. Lyon, M. A.; Kercher, T. S. *Org. Lett.* **2004**, 6, 4989-4992.

158. Sharma, A.; Li, H. Y. *Synlett* **2011**, 1407-1412.

159. Surkar, P.; Kaur, T.; Sharma, A. *Synlett* **2015**, 26, 1403-1407.

160. Moro, A. M.; Brucker, N.; Charão, M.; Bulcão, R.; Freitas, F.; Baierle, M.; Nascimento, S.; Valentini, J.; Cassini, C.; Salvador, M.; Linden, R.; Thiesen, F.; Buffon, A.; Moresco, R.; Garcia, S. C. *Mutat. Res. Genet. Toxicol. Environ. Mutagen.* **2012**, 746, 42-48.

161. Gottlieb, H. E.; Graczyk-Millbrandt, G.; Inglis, G. G. A.; Nudelman, A.; Perez, D.; Qian, Y.; Shuster, L. E.; Sneddon, H. F.; Upton, R. J. *Green Chem.* **2016**, 18, 3867-3878.

162. Capello, C.; Fischer, U.; Hungerbühler, K. *Green Chem.* **2007**, 9, 927-934.

163. Dourson, M.; Reichard, J.; Nance, P.; Burleigh-Flayer, H.; Parker, A.; Vincent, M.; McConnell, E. E. *Regul. Toxicol. Pharmacol.* **2014**, 68, 387-401.

164. Blackburn, C.; Guan, B. *Tetrahedron Lett.* **2000**, 41, 1495.

165. Sandulenko, Y.; Komarov, A.; Rufanov, K.; Krasavin, M. *Tetrahedron Lett.* **2008**, 49, 5990-5993.

166. Georgieff, K. K. *J. Appl. Polym. Sci.* **1966**, 10, 1305-1313.

167. Parchinsky, V. Z.; Shuvalova, O.; Ushakova, O.; Kravchenko, D. V.; Krasavin, M. *Tetrahedron Lett.* **2006**, 47, 947-951.

168. Mandair, G. S.; Light, M.; Russell, A.; Hursthouse, M.; Bradley, M. *Tetrahedron Lett.* **2002**, 43, 4267-4269.

169. Allen, S.; Brandhuber, B. J.; Condroski, K. R.; Huang, L.; Kercher, T.; Winski, S. L. Bicyclic heteroaryl urea, thiourea, guanidine and cyanoguanidine compounds as TRKA kinase inhibitors. WO2014/78408 A1, **2014**.

170. Wang, G.; Shen, R.; Long, J.; Ma, J.; Xing, X.; He, Y.; Granger, B.; He, J.; Wang, B.; Or, Y. Apoptosis signal-regulating kinase 1 inhibitors and methods of use thereof. WO2018209354 (A1), **2018**.

171. Shuman, R. T.; Ornstein, P. L.; Paschal, J. W.; Gesellchen, P. D. *J. Org. Chem.* **1990**, 55, 738-741.

172. *Information obtained at: https://www.zaiput.com/product/liquid-liquid-gas-separators/. **Accessed 13th February 2018.***

173. Atik, Z.; Chaou, M. *J. Chem. Thermodyn.* **2007**, 39, 583-587.

174. Matheis, C.; Jouvin, K.; Goossen, L. J. *Org. Lett.* **2014**, 16, 5984-5987.

175. Liang, Y.; Zhang, X.; MacMillan, D. W. C. *Nature* **2018**, 559, 83-88.

176. Li, A. H.; Dai, L. X.; Aggarwal, V. K. *Chem. Rev.* **1997**, 97, 2341-2372.

177. Margrey, K. A.; McManus, J. B.; Bonazzi, S.; Zecri, F.; Nicewicz, D. A. *J. Am. Chem. Soc.* **2017**, 139, 11288-11299.

178. Romero, N. A.; Margrey, K. A.; Tay, N. E.; Nicewicz, D. A. *Science* **2015**, 349, 1326-1330.

179. McManus, J. B.; Nicewicz, D. A. *J. Am. Chem. Soc.* **2017**, 139, 2880-2883.

180. *Information obtained at: https://www.who.int/malaria/media/world-malaria-report-2018/en/. **Accessed 4th March 2019.***

181. Phillips, M. A.; Burrows, J. N.; Manyando, C.; Huijsduijnen, R. H. V.; Voorhis, W. C. V.; Wells, T. N. C. *Nat. Rev. Dis. Primers* **2017**, 3, 17050.

182. *Source: World Malaria Report 2018. Geneva: World Health Organization; 2018. Licence: CC BY-NC-SA 3.0 IGO, https://apps.who.int/iris/bitstream/handle/10665/275867/9789241565653-eng.pdf?ua=1. **Accessed 5th March 2019.***

183. Bernabeu, M.; Smith, J. D. *Trends Parasitol.* **2017**, 33, 295-308.

184. Mitchell, S. N.; Kakani, E. G.; South, A.; Howell, P. I.; Waterhouse, R. M.; Catteruccia, F. *Science* **2015**, 347, 985-988.

185. *Information obtained at: https://www.cdc.gov/malaria/about/biology/index.html.* ***Accessed 5th March 2019.***

186. Josling, G. A.; Llinás, M. *Nat. Rev. Microbiol.* **2015**, 13, 573-587.

187. Cowman, A. F.; Healer, J.; Marapana, D.; Marsh, K. *Cell* **2016**, 167, 610-624.

188. White, N. J. *Malar. J.* **2011**, 10, 297-331.

189. Crosnier, C.; Bustamante, L. Y.; Bartholdson, S. J.; Bei, A. K.; Theron, M.; Uchikawa, M.; Mboup, S.; Ndir, O.; Kwiatkowski, D. P.; Duraisingh, M. T.; Rayner, J. C.; Wright, G. J. *Nature* **2011**, 480, 534-537.

190. Egan, E. S.; Jiang, R. H. Y.; Moechtar, M. A.; Barteneva, N. S.; Weekes, M. P.; Nobre, L. V.; Gygi, S. P.; Paulo, J. A.; Frantzreb, C.; Tani, Y.; Takahashi, J.; Watanabe, S.; Goldberg, J.; Paul, A. S.; Brugnara, C.; Root, D. E.; Wiegand, R. C.; Doench, J. G.; Duraisingh, M. T. *Science* **2015**, 348, 711-714.

191. Istvan, E. S.; Dharia, N. V.; Bopp, S. E.; Gluzman, I.; Winzeler, E. A.; Goldberg, D. E. *Proc. Natl. Acad. Sci. USA* **2011**, 108, 1627-1632.

192. Wunderlich, J.; Rohrbach, P.; Dalton, J. P. *Front. Biosci. (Schol. Ed.)* **2012**, 4, 1424-1448.

193. Boddey, J. A.; Cowman, A. F. *Annu. Rev. Microbiol.* **2013**, 67, 243-269.

194. Miller, L. H.; Mason, S. J.; Clyde, D. F.; McGinniss, M. H. *N. Engl. J. Med.* **1976**, 295, 302-304.

195. Gwamaka, M.; Kurtis, J. D.; Sorensen, B. E.; Holte, S.; Morrison, R.; Mutabingwa, T. K.; Fried, M.; Duffy, P. E. *Clin. Infect. Dis.* **2012**, 54, 1137-1144.

196. Neuberger, A.; Okebe, J.; Yahav, D.; Paul, M. *Cochrane Database Syst. Rev.* **2016**, 2, CD006589.

197. Cholera, R.; Brittain, N. J.; Gillrie, M. R.; Lopera-Mesa, T. M.; Diakité, S. A. S.; Arie, T.; Krause, M. A.; Guindo, A.; Tubman, A.; Fujioka, H.; Diallo, D. A.; Doumbo, O. K.; Ho, M.; Wellems, T. E.; Fairhurst, R. M. *Proc. Natl. Acad. Sci.* **2008**, 105, 991-996.

198. *Information obtained at: https://www.cdc.gov/malaria/diagnosis_treatment/diagnostic_tools.html#tabs-1-1.* ***Accessed 6th March 2019.***

199. Benito, A.; Rubio, J. M.; González-Lahoz, J. M.; Subirats, M.; Puente, S. *J. Travel Med.* **2001**, 8, 322-324.

200. Imwong, M.; Stepniewska, K.; Tripura, R.; Peto, T. J.; Lwin, K. M.; Vihokhern, B.; Wongsaen, K.; von Seidlein, L.; Dhorda, M.; Snounou, G.; Keereecharoen, L.; Singhasivanon, P.; Sirithiranont, P.; Chalk, J.; Nguon, C.; Day, N. P. J.; Nosten, F.; Dondorp, A.; White, N. J. *J. Infect. Dis.* **2016**, 213, 1322-1329.

201. Sema, M.; Alemu, A.; Bayih, A. G.; Getie, S.; Getnet, G.; Guelig, D.; Burton, R.; LaBarre, P.; Pillai, D. R. *Malar. J.* **2015**, 14, 44-52.

202. Pholwat, S.; Liu, J.; Stroup, S.; Jacob, S. T.; Banura, P.; Moore, C. C.; Huang, F.; Laufer, M. K.; Houpt, E.; Guler, J. L. *Antimicrob. Agents Chemother.* **2017**, 61, e00110-17.

203. *Source: Eliminating malaria: learning from the past, looking ahead: https://www.who.int/malaria/publications/atoz/9789241502504/en/ (2011).* ***Accessed 6th March 2019.***

204. Bhatt, S.; Weiss, D. J.; Cameron, E.; Bisanzio, D.; Mappin, B.; Dalrymple, U.; Battle, K. E.; Moyes, C. L.; Henry, A.; Eckhoff, P. A.; Wenger, E. A.; Briët, O.; Penny, M. A.; Smith, T. A.; Bennett, A.; Yukich, J.; Eisele, T. P.; Griffin, J. T.; Fergus, C. A.; Lynch, M.; Lindgren, F.; Cohen, J. M.; Murray, C. L. J.; Smith, D. L.; Hay, S. I.; Cibulskis, R. E.; Gething, P. W. *Nature* **2015**, 526, 207-211.

205. Ojuka, P.; Boum, Y.; Denoeud-Ndam, L.; Nabasumba, C.; Muller, Y.; Okia, M.; Mwanga-Amumpaire, J.; Beaudrap, P. D.; Protopopoff, N.; Etard, J. F. *Malar. J.* **2015**, 14, 148-155.

206. Bert, A. *Philos. Trans. R. Soc. Lond. B. Sci.* **2014**, 369, 20130432-20130439.

207. Gantz, V. M.; Jasinskiene, N.; Tatarenkova, O.; Fazekas, A.; Macias, V. M.; Bier, E.; James, A. A. *Proc. Natl. Acad. Sci.* **2015**, 112, E6736.

208. RTS, S Clinical Trials Partnership. *The Lancet* **2015**, 386, 31-45.

209. Penny, M. A.; Verity, R.; Bever, C. A.; Sauboin, C.; Galactionova, K.; Flasche, S.; White, M. T.; Wenger, E. A.; Velde, N. V. D.; Pemberton-Ross, P.; Griffin, J. T.; Smith, T. A.; Eckhoff, P. A.; Muhib, F.; Jit, M.; Ghani, A. C. *The Lancet* **2016**, 387, 367-375.

210. *Information obtained at: https://www.malariavaccine.org/projects/vaccine-projects/rtss-as01e-pediatric-indication.* ***Accessed on 7th March 2019.***

211. Hoffman, S. L.; Goh, L. M. L.; Luke, T. C.; Schneider, I.; Le, T. P.; Doolan, D. L.; Sacci, J.; Vega, P. D. L.; Dowler, M.; Paul, C.; Gordon, D. M.; Stoute, J. A.; Church, L. W. P.; Sedegah, M.; Heppner, D. G.; Ballou, W. R.; Richie, T. L. *J. Infect. Dis.* **2002**, 185, 1155-1164.

212. Keegan, L. T.; Dushoff, J. *BMC Infect. Dis.* **2013**, 13, 428-438.

213. Dahl, E. L.; Rosenthal, P. J. *Antimicrob. Agents Chemother.* **2007**, 51, 3485-3490.

214. Calderón, F.; Wilson, D. M.; Gamo, F.-J., *Chapter Three - Antimalarial Drug Discovery: Recent Progress and Future Directions.* In *Progress in Medicinal Chemistry.* **2013**, Newnes (Elsevier inc), Oxford, UK.

215. Honigsbaum, M.; Wilcox, M., *Cinchona.* In *Traditional Medicinal Plants and Malaria.* **2004**, CRC Press (Taylor & Francis), Boca Raton, FL, USA.

216. Dziekan, J. M.; Yu, H.; Chen, D.; Dai, L.; Wirjanata, G.; Larsson, A.; Prabhu, N.; Sobota, R. M.; Bozdech, Z.; Nordlund, P. *Sci. Transl. Med.* **2019**, 11, eaau3174.

217. Cassera, M. B.; Hazleton, K. Z.; Merino, E. F.; Obaldia, N. I.; Ho, M. C.; Murkin, A. S.; DePinto, R.; Gutierrez, J. A.; Almo, S. C.; Evans, G. B.; Babu, Y. S.; Schramm, V. L. *PLoS ONE* **2011**, 6, e26916.

218. Reiling, S. J.; Krohne, G.; Friedrich, O.; Geary, T. G.; Rohrbach, P. *Sci. Rep.* **2018**, 8, 11137-11147.

219. O'Neill, P. M.; Park, B. K.; Shone, A. E.; Maggs, J. L.; Roberts, P.; Stocks, P. A.; Biagini, G. A.; Bray, P. G.; Gibbons, P.; Berry, N.; Winstanley, P. A.; Mukhtar, A.; Bonar-Law, R.; Hindley, S.; Bambal, R. B.; Davis, C. B.; Bates, M.; Hart, T. K.; Gresham, S. L.; Lawrence, R. M.; Brigandi, R. A.; Gomez-delas-Heras, F. M.; Gargallo, D. V.; Ward, S. A. *J. Med. Chem.* **2009**, 52, 1408-1415.

220. *Information obtained at: https://www.mmv.org/access/products-projects/pyramax-pyronaridine-artesunate. **Accessed 8th March 2019.***

221. Hyde, J. E. *Acta Trop.* **2005**, 94, 191-206.

222. Zhang, K.; Rathod, P. K. *Science* **2002**, 296, 545-547.

223. Goller, J. L.; Jolley, D.; Ringwald, P.; Biggs, B. A. *Am. J. Trop. Med. Hyg.* **2007**, 76, 203-207.

224. Beutler, E.; Duparc, S. *Am. J. Trop. Med. Hyg.* **2007**, 77, 779-789.

225. *Information obtained at: https://www.gsk.com/en-gb/media/press-releases/us-fda-approves-krintafel-tafenoquine-for-the-radical-cure-of-p-vivax-malaria/. **Accessed 11th March 2019.***

226. Basso, L. G. M.; Rodrigues, R. Z.; Naal, R. M. Z. G.; Costa-Filho, A. J. *BBA-Biomembranes* **2011**, 1808, 55-64.

227. Marcsisin, S. R.; Reichard, G.; Pybus, B. S. *Pharmacol. Ther.* **2016**, 161, 1-10.

228. Lalève, A.; Vallières, C.; Golinelli-Cohen, M. P.; Bouton, C.; Song, Z.; Pawlik, G.; Tindall, S. M.; Avery, S. V.; Clain, J.; Meunier, B. *Redox. Biol.* **2016**, 7, 21-29.

229. Kimura, T.; Shirakawa, R.; Yaoita, N.; Hayashi, T.; Nagano, K.; Horiuchi, H. *FEBS Lett.* **2014**, 588, 3673-3676.

230. Miller, Louis H.; Su, X. *Cell* **2011**, 146, 855-858.

231. *Information obtained at: https://www.nobelprize.org/prizes/medicine/2015/tu/facts/. **Accessed 11th March 2019.***

232. Schmid, G.; Hofheinz, W. *J. Am. Chem. Soc.* **1983**, 105, 624-625.

233. Lévesque, F.; Seeberger, P. H. *Angew. Chem. Int. Ed.* **2012**, 51, 1706-1709.

234. van Herpen, T. W. J. M.; Cankar, K.; Nogueira, M.; Bosch, D.; Bouwmeester, H. J.; Beekwilder, J. *PLoS ONE* **2010**, 5, e14222.

235. Paddon, C. J.; Westfall, P. J.; Pitera, D. J.; Benjamin, K.; Fisher, K.; McPhee, D.; Leavell, M. D.; Tai, A.; Main, A.; Eng, D.; Polichuk, D. R.; Teoh, K. H.; Reed, D. W.; Treynor, T.; Lenihan, J.; Jiang, H.; Fleck, M.; Bajad, S.; Dang, G.; Dengrove, D.; Diola, D.; Dorin, G.; Ellens, K. W.; Fickes, S.; Galazzo, J.; Gaucher, S. P.; Geistlinger, T.; Henry, R.; Hepp, M.; Horning, T.; Iqbal, T.; Kizer, L.; Lieu, B.; Melis,

D.; Moss, N.; Regentin, R.; Secrest, S.; Tsuruta, H.; Vazquez, R.; Westblade, L. F.; Xu, L.; Yu, M.; Zhang, Y.; Zhao, L.; Lievense, J.; Covello, P. S.; Keasling, J. D.; Reiling, K. K.; Renninger, N. S.; Newman, J. D. *Nature* **2013**, 496, 528-532.

236. Tilley, L.; Straimer, J.; Gnädig, N. F.; Ralph, S. A.; Fidock, D. A. *Trends Parasitol.* **2016**, 32, 682-696.

237. Vaid, A.; Ranjan, R.; Smythe, W. A.; Hoppe, H. C.; Sharma, P. *Blood* **2010**, 115, 2500-2507.

238. Bray, P. G.; Mungthin, M.; Hastings, I. M.; Biagini, G. A.; Saidu, D. K.; Lakshmanan, V.; Johnson, D. J.; Hughes, R. H.; Stocks, P. A.; O'Neill, P. M.; Fidock, D. A.; Warhurst, D. C.; Ward, S. A. *Mol. Microbiol.* **2006**, 62, 238-251.

239. Thomas, D.; Tazerouni, H.; Sundararaj, K. G. S.; Cooper, J. C. *Acta Trop.* **2016**, 160, 35-38.

240. Korsinczky, M.; Chen, N.; Kotecka, B.; Saul, A.; Rieckmann, K.; Cheng, Q. *Antimicrob. Agents Chemother.* **2000**, 44, 2100-2108.

241. Ariey, F.; Witkowski, B.; Amaratunga, C.; Beghain, J.; Langlois, A. C.; Khim, N.; Kim, S.; Duru, V.; Bouchier, C.; Ma, L.; Lim, P.; Leang, R.; Duong, S.; Sreng, S.; Suon, S.; Chuor, C. M.; Bout, D. M.; Ménard, S.; Rogers, W. O.; Genton, B.; Fandeur, T.; Miotto, O.; Ringwald, P.; Bras, J. L.; Berry, A.; Barale, J. C.; Fairhurst, R. M.; Benoit-Vical, F.; Mercereau-Puijalon, O.; Ménard, D. *Nature* **2013**, 505, 50-55.

242. Straimer, J.; Gnädig, N. F.; Witkowski, B.; Amaratunga, C.; Duru, V.; Ramadani, A. P.; Dacheux, M.; Khim, N.; Zhang, L.; Lam, S.; Gregory, P. D.; Urnov, F. D.; Mercereau-Puijalon, O.; Benoit-Vical, F.; Fairhurst, R. M.; Ménard, D.; Fidock, D. A. *Science* **2015**, 347, 428-431.

243. Miotto, O.; Amato, R.; Ashley, E. A.; MacInnis, B.; Almagro-Garcia, J.; Amaratunga, C.; Lim, P.; Mead, D.; Oyola, S. O.; Dhorda, M.; Imwong, M.; Woodrow, C.; Manske, M.; Stalker, J.; Drury, E.; Campino, S.; Amenga-Etego, L.; Thanh, T. N. N.; Tran, H. T.; Ringwald, P.; Bethell, D.; Nosten, F.; Phyo, A. P.; Pukrittayakamee, S.; Chotivanich, K.; Chuor, C. M.; Nguon, C.; Suon, S.; Sreng, S.; Newton, P. N.; Mayxay, M.; Khanthavong, M.; Hongvanthong, B.; Htut, Y.; Han, K. T.; Kyaw, M. P.; Faiz, M. A.; Fanello, C. I.; Onyamboko, M.; Mokuolu, O. A.; Jacob, C. G.; Takala-Harrison, S.; Plowe, C. V.; Day, N. P.; Dondorp, A. M.; Spencer, C. C. A.; McVean, G.; Fairhurst, R. M.; White, N. J.; Kwiatkowski, D. P. *Nat. Genet.* **2015**, 47, 226-234.

244. Mukherjee, A.; Bopp, S.; Magistrado, P.; Wong, W.; Daniels, R.; Demas, A.; Schaffner, S.; Amaratunga, C.; Lim, P.; Dhorda, M.; Miotto, O.; Woodrow, C.; Ashley, E. A.; Dondorp, A. M.; White, N. J.; Wirth, D.; Fairhurst, R.; Volkman, S. K. *Malar. J.* **2017**, 16, 195-206.

245. White, N. J.; Duong, T. T.; Uthaisin, C.; Nosten, F.; Phyo, A. P.; Hanboonkunupakarn, B.; Pukrittayakamee, S.; Jittamala, P.; Chuthasmit, K.;

Cheung, M. S.; Feng, Y.; Li, R.; Magnusson, B.; Sultan, M.; Wieser, D.; Xun, X.; Zhao, R.; Diagana, T. T.; Pertel, P.; Leong, F. J. *N. Engl. J. Med.* **2016**, 375, 1152-1160.

246. White, N. J.; Pukrittayakamee, S.; Phyo, A. P.; Rueangweerayut, R.; Nosten, F.; Jittamala, P.; Jeeyapant, A.; Jain, J. P.; Lefèvre, G.; Li, R.; Magnusson, B.; Diagana, T. T.; Leong, F. J. *N. Engl. J. Med.* **2014**, 371, 403-410.

247. Paquet, T.; Manach, C. L.; Cabrera, D. G.; Younis, Y.; Henrich, P. P.; Abraham, T. S.; Lee, M. C. S.; Basak, R.; Ghidelli-Disse, S.; Lafuente-Monasterio, M. J.; Bantscheff, M.; Ruecker, A.; Blagborough, A. M.; Zakutansky, S. E.; Zeeman, A. M.; White, K. L.; Shackleford, D. M.; Mannila, J.; Morizzi, J.; Scheurer, C.; Angulo-Barturen, I.; Martínez, M. S.; Ferrer, S.; Sanz, L. M.; Gamo, F. J.; Reader, J.; Botha, M.; Dechering, K. J.; Sauerwein, R. W.; Tungtaeng, A.; Vanachayangkul, P.; Lim, C. S.; Burrows, J.; Witty, M. J.; Marsh, K. C.; Bodenreider, C.; Rochford, R.; Solapure, S. M.; Jiménez-Díaz, M. B.; Wittlin, S.; Charman, S. A.; Donini, C.; Campo, B.; Birkholtz, L. M.; Hanson, K. K.; Drewes, G.; Kocken, C. H. M.; Delves, M. J.; Leroy, D.; Fidock, D. A.; Waterson, D.; Street, L. J.; Chibale, K. *Sci. Transl. Med.* **2017**, 9, eaad9735.

248. Baragaña, B.; Hallyburton, I.; Lee, M. C. S.; Norcross, N. R.; Grimaldi, R.; Otto, T. D.; Proto, W. R.; Blagborough, A. M.; Meister, S.; Wirjanata, G.; Ruecker, A.; Upton, L. M.; Abraham, T. S.; Almeida, M. J.; Pradhan, A.; Porzelle, A.; Martínez, M. S.; Bolscher, J. M.; Woodland, A.; Luksch, T.; Norval, S.; Zuccotto, F.; Thomas, J.; Simeons, F.; Stojanovski, L.; Osuna-Cabello, M.; Brock, P. M.; Churcher, T. S.; Sala, K. A.; Zakutansky, S. E.; Jiménez-Díaz, M. B.; Sanz, L. M.; Riley, J.; Basak, R.; Campbell, M.; Avery, V. M.; Sauerwein, R. W.; Dechering, K. J.; Noviyanti, R.; Campo, B.; Frearson, J. A.; Angulo-Barturen, I.; Ferrer-Bazaga, S.; Gamo, F. J.; Wyatt, P. G.; Leroy, D.; Siegl, P.; Delves, M. J.; Kyle, D. E.; Wittlin, S.; Marfurt, J.; Price, R. N.; Sinden, R. E.; Winzeler, E. A.; Charman, S. A.; Bebrevska, L.; Gray, D. W.; Campbell, S.; Fairlamb, A. H.; Willis, P. A.; Rayner, J. C.; Fidock, D. A.; Read, K. D.; Gilbert, I. H. *Nature* **2015**, 522, 315-320.

249. Chavchich, M.; Birrell, G. W.; Ager, A. L.; MacKenzie, D. O.; Heffernan, G. D.; Schiehser, G. A.; Jacobus, L. R.; Shanks, G. D.; Jacobus, D. P.; Edstein, M. D. *Antimicrob. Agents Chemother.* **2016**, 60, 3115-3118.

250. Hopkins, A. L.; Keserü, G. M.; Leeson, P. D.; Rees, D. C.; Reynolds, C. H. *Nat. Rev. Drug Discov.* **2014**, 13, 105-121.

251. Leeson, P. D.; Springthorpe, B. *Nature Rev. Drug Discov.* **2007**, 6, 881-890.

252. Mortenson, P. N.; Murray, C. W. *J. Comput. Aided Mol. Des.* **2011**, 25, 663-667.

253. Young, R. J.; Green, D. V. S.; Luscombe, C. N.; Hill, A. P. *Drug Discov. Today* **2011**, 16, 822-830.

254. Bhattachar, S. N.; Wesley, J. A.; Seadeek, C. *J. Pharm. Biomed. Anal.* **2006**, 41, 152-157.
255. Waring, M. J. *Expert Opin. Drug Discov.* **2010**, 5, 235-248.
256. Springer, C.; Sokolnicki, K. L. *Chem. Cent. J.* **2013**, 7, 167-174.
257. Vilums, M.; Overman, J.; Klaasse, E.; Scheel, O.; Brussee, J.; IJzerman, A. P. *ChemMedChem* **2012**, 7, 107-113.
258. Hughes, J. P.; Rees, S.; Kalindjian, S. B.; Philpott, K. L. *Br. J. Pharmacol.* **2011**, 162, 1239-1249.
259. Robinson, M. W.; Hill, A. P.; Readshaw, S. A.; Hollerton, J. C.; Upton, R. J.; Lynn, S. M.; Besley, S. C.; Boughtflower, B. J. *Anal. Chem.* **2017**, 89, 1772-1777.
260. Ottaviani, G.; Martel, S.; Carrupt, P. A. *J. Med. Chem.* **2006**, 49, 3948-3954.
261. GSK Tres Cantos Open Lab Foundation. *Unpublished work.*
262. Tape, D. *GSK, Unpublished work.*
263. Vimolratana, M.; Simard, J. L.; Brown, S. P. *Tetrahedron Lett.* **2011**, 52, 1020-1022.
264. Roberts, J. *GSK and University of Strathclyde, Unpublished work.*
265. Ma, D.; Cai, Q.; Zhang, H. *Org. Lett.* **2003**, 5, 2453-2455.
266. Wen, M.; Shen, C.; Wang, L.; Zhang, P.; Jin, J. *RSC Adv.* **2015**, 5, 1522-1528.
267. Kanuma, K.; Omodera, K.; Nishiguchi, M.; Funakoshi, T.; Chaki, S.; Nagase, Y.; Iida, I.; Yamaguchi, J. I.; Semple, G.; Tran, T. A.; Sekiguchi, Y. *Bioorg. Med. Chem.* **2006**, 14, 3307-3319.
268. Miki, H.; Yamada, J. *Chem. Pharm. Bull.* **1982**, 30, 2313-2318.
269. Kazemi, S. S.; Keivanloo, A.; Nasr-Isfahani, H.; Bamoniri, A. *RSC Adv.* **2016**, 6, 92663-92669.
270. *Information obtained at: http://www.electrothermal.com/product.asp?dsl=783.* ***Accessed 22nd March 2019.***
271. Surry, D. S.; Buchwald, S. L. *Chem. Sci.* **2011**, 2, 27-50.
272. Beletskaya, I. P.; Cheprakov, A. V. *Organometallics* **2012**, 31, 7753-7808.
273. Marino, T.; Russo, F.; Criscuoli, A.; Figoli, A. *J. Memb. Sci.* **2017**, 542, 418-429.
274. Lipinski, C. A.; Lombardo, F.; Dominy, B. W.; Feeney, P. J. *Adv. Drug Deliv. Rev.* **2001**, 46, 3-26.
275. *Information obtained at: https://www.schrodinger.com/livedesign.* ***Accessed 19th June 2019.***
276. Wage, T. T.; Hou, X.; Verhoest, P. R.; Villalobos, A. *ACS Chem. Neurosci.* **2016**, 7, 767-775.
277. Veber, D. F.; Johnson, S. R.; Cheng, H.-Y.; Smith, B. R.; Ward, K. W.; Kopple, K. D. *J. Med. Chem.* **2002**, 45, 2615-2623.
278. *Information obtained at: https://www.cambridgemedchemconsulting.com/resources/ADME/distribution.html.* ***Accessed 26th March 2019.***

279. Ertl, P.; Rohde, B.; Selzer, P. *J. Med. Chem.* **2000**, 43, 3714-3717.

280. Kelder, J.; Grootenhuis, P. D. J.; Bayada, D. M.; Delbressine, L. P. C.; Ploemen, J. P. *Pharm. Res.* **1999**, 16, 1514-1519.

281. Roy, S.; Paul, B.; Mukherjee, A.; Kundu, B.; Talukdar, A. *RSC Adv.* **2017**, 7, 44366-44370.

282. Fulmer, G. R.; Miller, A. J. M.; Sherden, N. H.; Gottlieb, H. E.; Nudelman, A.; Stoltz, B. M.; Bercaw, J. E.; Goldberg, K. I. *Organometallics* **2010**, 29, 2176.

283. Varma, R. S.; Kumar, D. *Tetrahedron Lett.* **1999**, 40, 7665.

284. Bounaud, P. Y.; Smith, C. R.; Jefferson, E. A.; Hendle, J.; Lee, P. S.; Thayer, A. M.; Hirst, G. C. Heterocyclic kinase modulators. WO2008144767 A1, **2008**.

285. Turner, W. W.; Arnold, L. D.; Maag, H.; Zlotnick, A. Hepatitis B core protein allosteric modulators. WO2015138895 A1, **2015**.

286. Rokade, B. V.; Prabhu, K. R. *J. Org. Chem.* **2012**, 77, 5364-5370.

287. Smits, R. A.; Lim, H. D.; van der Meer, T.; Kuhne, S.; Bessembinder, K.; Zuiderveld, O. P.; Wijtmans, M.; de Esch, I. J. P.; Leurs, R. *Bioorg. Med. Chem. Lett.* **2012**, 22, 461-467.

288. Wang, P. X.; Wang, Y. N.; Lin, Z. Y.; Li, G.; Huang, H.-H. *Synth. Commun.* **2018**, 48, 1183-1189.

289. Eastwood, P. R.; Jacob, G. R.; Tana, J. B.; Santacana, L. M. P.; Joan, T. M.; Javaloyes, J. F. C.; Matassa, V. G. Imidazopyridine derivatives as JAK inhibitors WO2011/76419 A1, **2011**.

290. Johannes, J. W.; Almeida, L.; Barlaam, B.; Boriack-Sjodin, A. P.; Casella, R.; Croft, R. A.; Dishington, A. P.; Gingipalli, L.; Gu, C.; Hawkins, J. L.; Holmes, J. L.; Howard, T.; Huang, J.; Ioannidis, S.; Kazmirski, S.; Lamb, M. L.; McGuire, T. M.; Moore, J. E.; Ogg, D.; Patel, A.; Pike, K. G.; Pontz, T.; Robb, G. R.; Su, N.; Wang, H.; Wu, X.; Zhang, H. J.; Zhang, Y.; Zheng, X.; Wang, T. *ACS Med. Chem. Lett.* **2015**, 6, 254-259.

291. Allendörfer, N.; Es-Sayed, M.; Nieger, M.; Bräse, S. *Tetrahedron Lett.* **2012**, 53, 388-391.

292. Smits, R. A.; Adami, M.; Istyastono, E. P.; Zuiderveld, O. P.; van Dam, C. M. E.; de Kanter, F. J. J.; Jongejan, A.; Coruzzi, G.; Leurs, R.; de Esch, I. J. P. *J. Med. Chem.* **2010**, 53, 2390-2400.

293. Deaton, D. N.; Guo, Y.; Hancock, A. P.; Schulte, C.; Shearer, B. G.; Smith, E. D.; Stewart, E. L.; Thomson, S. A. 1,3 Di-substituted cyclobutane or azetidine derivatives as hematopoietic prostaglandin D synthase inhibitors. WO2018069863 A1, **2018**.

294. Mosuke, H.; Sinzo, T.; Ikuo, M.; Hirochika, N. *Bull. Chem. Soc. Jpn.* **1936**, 11, 184-200.

295. Kulkarni, S. S.; Singh, S.; Shah, J. R.; Low, W. K.; Talele, T. T. *Eur. J. Med. Chem.* **2012**, 50, 264-273.

296. Frackenpohl, J.; Zeis, H. J.; Heinemann, I.; Willms, L.; Mueller, T.; Busch, M.; Doering-Korskull, P. V.; Hahn-Haeuser, I.; Rosinger, H. C.; Dittgen, J.; Hills, J. M.; Schmitt, M. H. Substituted fused pyrimidinones and dihydropyrimidinones. CN103228141 A, **2013**.

297. Cózar, C. D.; Caballero, I.; Colmenarejo, G.; Sanz, L. M.; Álvarez-Ruiz, E.; Gamo, F. J.; Cid, C. *Antimicrob. Agents Chemother.* **2016**, 60, 5949-5956.